Asymmetric Radiant Fields and Human Thermal Comfort

Kuskana Kubaha

This thesis is submitted to De Montfort University, in partial fulfilment of the requirement for the degree of Doctor of Philosophy

September 2005

Institute of Energy and Sustainable Development
De Montfort University, Leicester

Abstract

The main purpose of this thesis was to develop a first principles model for predicting human local thermal comfort responses to asymmetric radiation environments. The research deployed state-of-the-art computer simulation techniques to model in detail inhomogeneous short-wave and long-wave radiative heat exchanges of standing and sedentary humans. Detailed 3D human geometry models, simulation software incorporating advanced, voxel-based ray techniques and statistical regression analysis were used to accurately model human local geometry-related characteristics, i.e. projected area factors with respect to both direct and diffuse solar radiation, and view factors for individual parts of the human body.

The local projected area factors with respect to direct short-wave radiation ($f_{p,dir}$) were presented as functions of the solar azimuth angle (α) between $0° < \alpha < 360°$ and the solar altitude (β) angles between $-90° < \beta < +90°$. In case of diffuse solar radiation from the isotropic sky the local human projected area factors ($f_{p,dif}$) were modelled as a function of the ground albedo (ρ_g) ranging between $0 < \rho_g < 1$. The functions were validated against available experimental data and showed good general agreement with projected area factors measured for both the human body as a whole and for local quantities.

The view factors of individual body parts were modelled as functions of local projected area factors. This technique makes it possible to predict view factors between individual body parts and surrounding surfaces for almost any arbitrary geometrical configurations. Validation showed good agreement with available experimental data for both standing and sedentary humans.

The detailed projected area factors and view factors developed were used in conjunction with the IESD-Fiala multi-node model of human heat transfer and

thermal comfort to predict thermal responses of subjects exposed to various asymmetric radiation conditions. The extended model showed good agreement with available measured data obtained for frontal, lateral, horizontal and vertical thermal radiation asymmetries as well as for direct solar radiation.

A new comfort model was developed using physiological parameters which predicts human local responses to asymmetric radiation in terms of percentage of dissatisfied due to local discomfort. Both local cold discomfort (LCD) and local warm discomfort (LWD) which are based on different physiological principles – were modelled as two separate responses. LCD was found to be a function of the sensitivity-weighted local skin temperature as related to the actual general thermal state of the human body described by the mean skin temperature. LWD was modelled as an exclusive function of local influences, i.e. the (sensitivity-weighted) local skin temperatures and the corresponding local setpoint values (referring to skin temperatures in a thermo-neutral environment of 30°C). The new model was verified and validated using various experiments in which the subjects were exposed to different types of asymmetric radiation conditions. The test showed good/acceptable level of agreement with measured data regarding the percentage of dissatisfied due to local discomfort, the location on the body where discomfort was perceived, as well as the dynamics of the local response (i.e. time dependence).

The new comfort model was linked with a building simulation program to predict thermal comfort conditions in buildings. A computational procedure was developed to enable this in conjunction with ESP-r which is one of the most well known building simulation programs. The new link enables researchers to perform detailed thermal comfort analysis and occupant implications of the dynamic climate conditions in buildings with daily, monthly, seasonal and annual statistics, and facilitates to quantify the thermal comfort implications of different building designs and individual constructions.

Acknowledgements

This work could not been completed without the support and help of many people. I very appreciated to have a dedicated supervision team, without their supports and encouragements, the project could not have been successful.

I am the most grateful to Dr. Dusan Fiala for his valuable supervisions, encouragements throughout the whole work and for his critical review of this thesis. I would like to have a special thank to Prof. Dr. Jørn Toftum of International Centre for Indoor Environment and Energy, Technical University of Denmark and Dr. Ahmad H. Taki of School of Architecture, De Montfort University, for their fruitful advices and suggestions of this work.

The work would not be possible without financial support (GR/R03495/01) from the UK Engineering and Physical Sciences Research Council (EPSRC). The support of the EPSRC is gratefully acknowledged. I am thankful to the ThermoAnalytics Inc, for contributing to the research by providing their RadTherm software.

I am also grateful to the Thai government who gave me the opportunity to carry out my postgraduate studies in the UK and for their financial support.

I also would like to thank all of the staff and friend at the IESD for their moral support and hospitality.

Finally, I would like to thank, my wife, my children, my parents and my mother in law who always stand on my side.

Bibliography

Lists of interim reports were produced during the course of this research.

IR1: Literature survey on fundamentals and modelling techniques of the radiative heat exchange between the human body and the environment.

IR2: Validation and sensitivity analysis of numerically calculated view factors using RadTherm.

IR3: Modelling projected area factors for human body.

IR4: Modelling projected area factors of the human body, part II.

IR5: Modelling view factors for individual parts of the human body.

Two papers have been published in international refereed conference and International Journal of Biometeorology.

(1) Kubaha K., D. Fiala and K. J. Lomas (2003), Predicting human geometry-related factors for detailed radiation analysis in indoor spaces, Eighth International IBPSA Conference, Building Simulation 2003, Eindhoven, Netherlands, Vol. 2, pp 681-688.

(2) Kubaha K., D. Fiala, J. Toftum and A.H. Taki (2004), Human projected area factor for detailed direct and diffuse solar radiation analysis, International Journal of Biometeorology, Vol. 49 (2), pp. 113-129.

Contents

Chapter 3

Choice and validation of numerical radiation simulation methods

Chapter 4

Human projected area factors for detailed direct and diffuse solar radiation analysis

Chapter 7

Modelling human local thermal comfort responses to asymmetric radiation

Chapter 8

Predicting thermal comfort responses in buildings

Chapter 9

Conclusions and recommendations

Nomenclature

English symbols	Description	Unit
A	area	[m^2]
A	regression coefficient (Chapter 4)	[-]
A_{Du}	DuBois area	[m^2]
A_{eff}	effective radiation area	[m^2]
A_p	projected area	[m^2]
a	dimension (width) of plane	[-]
B	regression coefficient	[-]
b	dimension (height) of plane	[m]
C_o	regression coefficient	[-]
C_1	regression coefficient	[-]
C_{sk}	skin sensitivity	[-]
c	distance from a body to a plane (cylinder)	[m]
c_p	heat capacitance	[kJ kg^{-1} K^{-1}]
D_o	regression coefficient	[-]
D_1	regression coefficient	[-]
DBT	dry bulb temperature	[°C]
E_o	regression coefficient	[-]
E_1	regression coefficient	[-]
ERF	effective radiant flux	[Wm^{-2}]
f_{cl}	ratio of the surface area of the clothed body to the surface area of nude body	[-]
f_{eff}	effective radiation area factor	[-]
f_p	projected area factor	[-]
g_0	regression coefficient	[-]
g_1	regression coefficient	[-]
h_r	radiative heat transfer coefficient	[$Wm^{-2}K^{-1}$]

I_{cl}	overall intrinsic clothing thermal insulation from the skin to the clothing surface	[clo]
J	radiosity	[W m^{-2}]
k	thermal conductance	[W m^{-1} K^{-1}]
LCD	local cold discomfort	[%]
LCS	local cold stimuli	[K]
LWD	local warm discomfort	[%]
LWS	local warm stimuli	[K]
MRT	mean radiant temperature	[K]
$\bar{n}$	normal vector	[-]
P	perimeter of a surface	[m]
PMV	predicted mean vote	[-]
PPD	predicted percentage of dissatisfy	[%]
Q	radiative heat transfer	[W]
q	heat loss	[W m^{-2}]
q_m	metabolic rate	[W m^{-3}]
R	correlation coefficient	[-]
RH	relative humidity	[%]
r	radius, distance	[m]
S	radiant intensity	[W m^{-2}]
S_h	shading function	[-]
T	temperature, absolute temperature	[°C, K]
t	time	[s, min]
V_a	air velocity	[ms^{-1}]
X	polar coordinate	
x	independent variable	
Y	polar coordinate	
y	independent variable	
Z	polar coordinate	
z	independent variable	

Greek symbols	Description	Unit
α	azimuth angle	[deg, rad]
α_{sf}	short wave absorptivity	[-]
β	altitude angle	[deg, rad]
θ	arbitrary angle, incident angle	[deg, rad]
Φ	tilt angle	[deg, rad]
Δ	difference	
φ	view factor	[-]
ε	long wave emissivity	[-]
ρ	density	[kg m^{-3}]
ρ_g	ground albedo	[-]
σ	Stefan-Boltzmann constant (=5.67*10^{-8})	[$Wm^{-2}K^{-4}$]
ω	geometry factor of radial heat conduction	[-]
ξ	fraction of two areas	[-]

Subscripts and superscripts

0	sign of the thermal neutrality
a	air
ab	absorbed
anal	analytical solution
b	body sector
bl	blood
bla	arterial blood
dif	diffuse solar radiation
dir	direct solar radiation
c	cold, convection
cl	clothed body, clothing
Du	Dubois
e	evaporation
eff	effective
exp	exponential
i	running number
j	running number
,l	sign for local value
,m	sign for mean value
max	maximum value
min	minimum value
n	total number
o	operative
P	person, human body
RTh	numerical (RadTherm) result
sf	body surface
sk	skin
sr	surrounding surface
sR	short-wave radiation
r	radiation
re	rectal

ts	tissue
w	wall, warm

Acronyms

ASHRAE	American Society of Heating, Refrigerating and Air-Conditioning Engineers
BSPs	Building simulation programs
EPSRC	Engineering and Physical Sciences Research Council
HVAC	Heating Ventilating and Air Conditioning
IESD	Institute of Energy and Sustainable Development
ISO	International Organisation for Standardization
KSU	Kansas State University
L	left
Lo	lower
Mid	middle
Nr	near
R	right
Up	upper

Chapter 1

Introduction

1.1 Background

Thermal comfort is the primary goal of the heating and conditioning industry to create comfortable conditions. Current comfort standards, such as ASHRAE Standard 55 (2004) specify a "comfort zone" which represents the optimum range for combinations of thermal factors (air temperature, radiant temperature, air velocity, relative humidity) and personal factors (clothing and activity level) with which at least 90% of the occupants are expected to express satisfaction. Thereby, occupant comfort refers to the human body as a whole which predicted by the PMV (predicted mean vote) and PPD (predicted percentage of dissatisfied) indices (Fanger, 1970). In addition to the general (dis)comfort, however, local thermal discomfort may be perceived at different body parts under inhomogeneous environmental conditions such as enclosures with non-uniform surrounding surface temperatures, (Fanger et al.,1985; McNall and Biddison, 1970); due to draughts, (e.g. Fanger et al., 1977); or vertical air temperature gradients, (e.g. Olesen et al., 1979). Fiala (1998) and others indicated that overall thermal comfort indices cannot be used to predict local thermal (dis)comfort. The reason for this are the different physiological mechanisms which govern the perception of the general and local thermal (dis)comfort. While the overall response reflects an integration of thermal stimuli from various body sites local comfort responses appear to be associated with local cutaneous thermoreception, i.e. depend on the local skin temperature, Hensel (1979), Fiala (2003).

In real life, human beings are frequently subjected to asymmetric radiation which influences the acceptability of environmental conditions e.g. inside buildings, cars, aircraft cabins and in other artificial environments. Critical, life threatening situations arise from exposures to fire and intense heat. Outdoors and indoors, direct and diffuse solar radiation may subject parts of the human body to radiant temperature will above 50°C. Even when room or zone is maintained at a comfortable condition (temperature, humidity etc.), occupants may still experience significant discomfort due to asymmetric long-wave radiation caused by cold windows and walls, chilled panels, hot radiators, heated floors, etc. Uncomfortable environmental conditions, for example, in cars and aircraft cabins slow down the reaction times of drivers and pilots (Haghighat et al., 1998 and 1999). In buildings, asymmetric radiation makes occupied zones uncomfortable causing restrictions in the usability and functionality of spaces, and reducing occupants' performance at the workplace.

International standards define limits for local discomfort due to asymmetric thermal radiation in terms of the so called "radiant temperature asymmetry" which is the difference between "*two plane radiant temperatures measured on opposite sides of a small plane element placed 0.6m vertically or horizontally above the floor*" (ASHRAE Standard 55, 2004). These asymmetry limits have been measured for cold and warm walls and ceilings for sedentary subjects clad in a standard uniform, exposed to comfortable operative temperatures, still air, and under specific geometrical configurations (Figure 1.1).

The validity of these environmental asymmetry limits, however, becomes questionable when the boundary conditions for which they were obtained change. For example, in the presence of increased air speed elevated convective-cooling of the skin might influence the acceptability of the actual radiant asymmetry. Similarly, the acceptability of a certain radiant asymmetry (i.e. a temperature difference) will vary with the general level of the mean radiant temperature in a room.

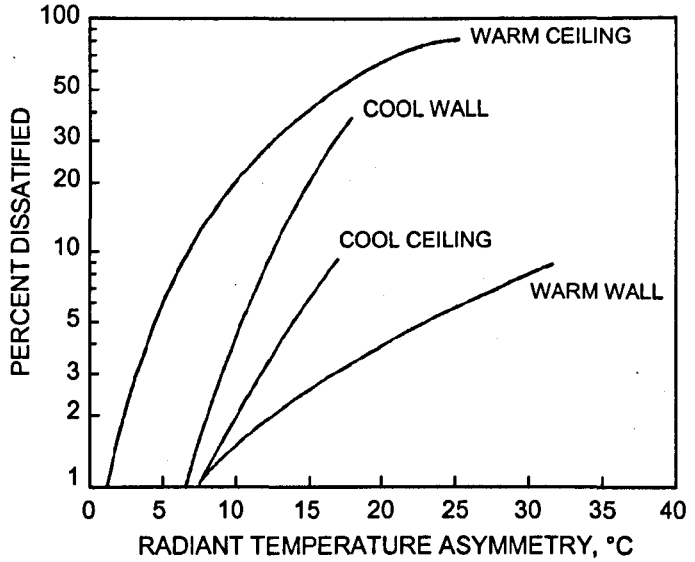

Figure 1.1 Percentage of people who expressed discomfort regarding asymmetric radiation (ASHRAE Standard 55, 2004).

Furthermore, the currently used asymmetry limits are, strictly speaking, only valid for the specific geometric situation found in the experiment. In reality, a three dimensional human body will experience (particularly in confined spaces) a different temperature asymmetry than that measured by a small plane element.

1.2 Experimental knowledge on thermal comfort in asymmetric radiation environments

The effect of asymmetric radiation on human thermal comfort has been subjected to various experimental studies over the past five decades. Chrenko (1953), for example, undertook short exposure experiments in which he found out that radiation of heat from above a person causing an increase in the mean radiant temperature of more than 2°C may result in an unpleasant sensation of temperature at upper body parts, especially the head. A significant number of the subjects complained of general warm discomfort.

Comprehensive experiments were undertaken by McNall and Biddison (1970) in which, 234 subjects were exposed to asymmetric radiation due to cold and warm surfaces of the surroundings. Thermal sensations were recorded under four series of exposure: hot ceiling, cool ceiling warm and cold spatial walls. The subjects were exposed to surface temperatures which were, in one experiment, 37°C higher and, in another experiment, 15°C lower than the balance of the chamber surface temperatures. In the third and fourth experiment the subjects were exposed spatially to wall temperatures which were 35°C higher and 11°C lower than the remaining surrounding temperatures. As a result, thermal discomfort due to radiant asymmetry was observed only in the test where the spatial wall was 35°C warmer than ambient temperature. In all other exposures local thermal discomfort due to radiant asymmetry was regarded as insignificant.

McIntyre and Griffiths (1972) studied the relative importance of air temperature and mean radiant temperature in influencing a person's sensation of warmth. One of their objectives was to identify whether a 'warm' mean radiant temperature would result in similar feelings compared to air temperatures of equivalent 'warmth'. In these trials, sixteen male subjects were exposed to twelve different combinations of mean radiant temperature (MRT) and air temperature (T_a): 19 and 22°C, 19 and 28°C, 22 and 16°C, 22 and 22°C, 22 and 28°C, 25 and 16°C, 25 and 28°C, 25 and 34 °C, 28 and 26°C, 28 and 28°C, 28 and 34°C, and 31 and 22°C. The study confirmed that the subjects did not distinguish between radiant and convective removal of heat from their body in uniform environments. The experiments were then extended for the effect of a hot ceiling on thermal comfort. Twenty four subjects (of whom eight were bald) were exposed seated to the following ceiling temperatures: 26, 30, 38 and 45°C while the wall temperatures were set at 26, 25, 20 and 15°C, respectively. It was observed that a combination of high ceiling temperature and cool walls was perceived as cooler than a uniform environment with the same mean radiant temperature (baldness and seat height were generally unimportant). However, the subjects did not rate the hot ceiling conditions as more uncomfortable or more unpleasant compared to the other cases investigated. The findings of both

Griffiths and McIntyre (1974), and McIntyre (1977) indicated that a ceiling of up to 45°C maximum temperature (view factor between the body and the ceiling was about 0.10) did not produce any significant discomfort when compared with the control uniform conditions.

Olesen et al. (1972) studied thermal comfort limits for humans exposed to horizontal radiant asymmetries while keeping the overall radiation conditions at a thermoneutral level. Sixteen subjects (eight females and eight males) were exposed to four different arrangements of surrounding surface temperatures: cold left-warm right, cold right-warm left, cold front-warm back and warm front-cold back. The subjects wore light clothing (0.1 clo) in order to maximize the sensitivity to the radiation. In the experiments, temperature of the vertical plane was changed in opposite increment of 5°C every 30 minutes (by decreasing the temperature in one of the end walls and simultaneously increasing the temperature of the opposite wall). The plane radiant temperature asymmetries investigated were 5, 10, 15 and 20°C. The findings showed that the subjects could sense the asymmetric radiation at a certain level independently of the direction they were facing. The subjects accepted the highest degree of asymmetry when facing the cold wall (having the warm wall at the back). Radiant asymmetry caused by the cold left-warm right (or cold right-warm left) was felt to be most uncomfortable followed by the warm front-cold back as the second most uncomfortable conditions. The authors also recommended the following formula for estimating the limits of acceptable temperature difference between a vertical surface and the mean radiant temperature:

$$-2.4-1.8I_{cl} \leq \Delta t_w \varphi_{pw} \leq 3.9+1.8I_{cl}$$

where I_{cl} = clo-value of clothing,

φ_{pw} = view factor between the person and radiant source,

Δt_w = temperature difference between the radiant source, and the mean radiant temperature.

Other extensive experimental trials were carried out by Fanger et al. (1980) in which sixteen college-age persons (eight males and eight females) were seated exposed to a heated ceiling. The purpose of the study was to determine the asymmetric radiation limits to which man can be exposed without feeling local discomfort. The experiments were run for the following vertical radiant temperature asymmetries: 0, 4.5, 9.2, 14.1, 20.4 and 23.6K. The subjects perceived local discomfort either at the head (uncomfortably warm) or at the feet (uncomfortably cool) or at both places at the same time (with the discomfort/sensation of cold on the feet being almost as frequent as a warm discomfort/sensation on the head).

Fanger et al. (1985) conducted three other experimental series to measure the comfort limits for asymmetric radiation due to a cool spatial wall, warm spatial wall and cool ceiling. In the cool wall series, thirty two persons were involved while sixteen persons were used as subjects in the warm wall and cool ceiling experiments. In all exposures, the overall environmental conditions were adjusted to achieve global thermal comfort of the subjects so any reported complaints were solely due to local cool or local warm discomfort. Radiant asymmetry caused by the warm ceiling was felt to be most uncomfortable followed by the cool wall as the second most uncomfortable condition. The cool ceiling and the warm wall caused only few complains.

All the experimental results obtained by Fanger et al. (1980 and 1985) are summarised in Figure 1.1. Today they form the basis for evaluating asymmetric radiation conditions and are incorporated in current thermal comfort standard (ASHRAE Standard 55, 2004). The curves for the latter two cases (i.e. cool ceiling and warm wall) provided in Figure 1.1 are based on a weak data basis.

Further experiments investigating the effect of asymmetric radiation from a cold wall on occupant comfort were conducted by Berglund and Fobelets (1987). Fifty persons (25 males and 25 females) wearing winter indoor clothing (0.86 clo) were used as subjects in the study. The study was carried out for two overall conditions: thermal neutrality (N) and for conditions 3°C (operative

temperature) lower than neutral condition (N-3). For each condition, four different surface temperatures of the cold wall (0, 5, 10 and 18°C) and four different air velocities (0.05, 0.15, 0.25 and 0.50 m/s) were used as the main factors affecting the thermal sensation of the subjects in the experiments. Air temperature was controlled to maintain a constant operative temperature of 22°C (N conditions) and 19°C (N-3 conditions), respectively. The authors showed that an average of 25% (of the test persons in the four asymmetric radiations) perceived local thermal discomfort in the N conditions compared to 50% in the N-3 conditions.

More recently, chilled ceiling experiments were undertaken by Loveday et al. (1998 and 2002) and Hodder et al. (1998). In the experiments thermal comfort responses of sedentary persons (desk-seated occupants) exposed to vertical radiant asymmetry due to a chilled ceiling were observed. Eight female subjects took part in the experiment. The subjects were exposed for three hours to four different ceiling surface temperatures: 22, 18, 14 and 12°C. The view factor between the subjects and the ceiling was about 0.12. In the experiment, the air temperature and air velocity was maintained constant at 19°C and 0.05 m/s, respectively. The subjects wore typical office clothing (0.75 clo). They were asked to report on their overall and local comfort sensations at various body parts. As a result, there was no significant effect on local discomfort due to vertical radiant asymmetry induced by the chilled ceiling.

1.3 Aim and objectives

The main aim of the research is to advance modelling of the human radiative heat transfer and to develop a first principles model for predicting human local comfort responses to asymmetric radiation. The individual objectives of the research are as follows:

1) to evaluate existing methods for predicting human radiative heat exchange including advanced methods such as the voxel-based ray tracing technique for detailed radiation analysis,
2) to model local projected area factors of individual body parts for predicting in detail the human short-wave radiative heat transfer,
3) to develop a technique for predicting local view factors of individual body parts for detailed long-wave radiation calculations,
4) to predict and validate human physiological responses in asymmetric radiation environments using a mathematical multi-node model of human heat transfer with incorporated detailed radiation models,
5) to develop a more universal, physiologically based, thermal comfort model for predicting local perceptual responses of humans to asymmetric radiation, and
6) to link the new comfort model with state-of-the-art building simulation programs to predict human comfort conditions in buildings.

1.4 Thesis contents

The thesis is divided into nine chapters. Chapter one (this chapter) provides a general background and motivations for the research with information of the current experimental knowledge on human thermal comfort under asymmetric radiation condition as well as the aims and the objectives of the work.

Chapter two is a review of literature on fundamental and available techniques for modelling human radiative heat transfer.

Chapter three provides reasons, choice and validation of the numerical tool to be used in this research for detailed radiation modelling.

Chapter four describes the development and validation of a model for predicting parameters needed for detailed human short-wave, direct and diffuse, radiation analysis.

In chapter five a technique is developed which enables detailed predictions of the human long-wave radiation heat exchange in asymmetric environments.

Chapter six described the validation of the IESD-Fiala model of human heat transfer and thermal comfort, extended for detailed radiation modelling, to predict human physiological responses to asymmetric short-wave and long-wave radiation.

Chapter seven is concerned with modelling human local comfort responses to asymmetric radiation.

In chapter eight a link of the new comfort model with a state-of-the-art building simulation program (ESP-r) is developed and demonstrated using simulations and comfort predictions performed for an existing building.

In chapter nine the main results of the research are discussed and conclusions drawn with outlook and ideas for future work.

Chapter 2

Fundamentals of radiative heat transfer

2.1 Introduction

Thermal radiation is electromagnetic radiation emitted by particles of matter as they undergo internal energy state transition (Duffie and Beckman, 1991). Thermal radiation is also a form of heat that is transfered from one body of matter to another due to a temperature difference, e.g. Brewster (1992) and Jones (2000).

Calculating of the radiant heat exchanged between two bodies requires knowledge of two basic parts, with the first part representing radiative properties of the bodies and the second part is the geometry of the considered problem. The radiative properties are a measure of the tendency of a given surface or participating medium to emit, absorb and reflect (or scatter) radiation. Once the properties have been evaluated, the geometric properties can be solved to determine the net transfer rate of radiant energy to or from a given surface element.

2.2 Long wave radiation

All bodies above a temperature of absolute zero (-273.15°C) emit and absorb thermal radiation known as long wave radiation, e.g. Brewster (1992). All physical bodies, with the exceptions of perfect reflectors or a system completely at absolute zero temperature, are therefore involved in an exchange of radiant

energy with their surroundings resulting in a net flow of energy from the hotter to the cooler bodies.

2.2.1 Radiative heat exchange between two surfaces

The amount of radiant heat exchanged between two surfaces depends upon the radiation properties and the temperature of the surfaces, Duffie and Beckman (1991). Consider two area elements dA_1 and dA_2, which may be part of two larger, finite areas A_1 and A_2, Figure 2.1.

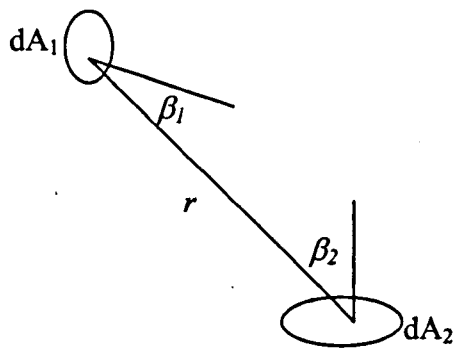

Figure 2.1
Radiative heat transfer between two area elements.

Assuming that the emitted radiation is isotropic, the rate of heat transfer (Q_{12}) between two elements can be derived from the geometry (Figure 2.1) as follows, Brewster (1992):

$$Q_{12} = \varepsilon_1 \varepsilon_2 \sigma A_1 \varphi_{12} (T_1^4 - T_2^4) \qquad (2.1)$$

where $\varepsilon_1, \varepsilon_2$ = the emittance of surface A_1 and A_2, respectively,
σ = the Stefan-Boltzmann constant = 5.67×10^{-8} [$Wm^{-2}K^{-4}$]
A_1 = area of surface 1, [m^2]
φ_{12} = view factor between surfaces A_1 and A_2,
T_1, T_2 = absolute temperature of surface 1 and 2, respectively. [K]

The view factor φ_{12} is the fraction of the radiation emitted by surface A_1 which is directly intercepted by surface A_2 and can be expressed as:

$$\varphi_{12} = \frac{1}{\pi A_1} \int_{A_1} \int_{A_2} \frac{\cos\beta_1 \cos\beta_2}{r^2} dA_1 dA_2 \qquad (2.2)$$

where β_1, β_2 = the angle between the distance vector r and the normal vectors of the area elements dA_1 and dA_2 (Figure 2.1).

2.2.2 Multi-surface problems

One particularly useful method for multi-surface problems is the use of matrix methods for sets of simultaneous equations (Ozisik, 1973 and Jones, 2000). The net radiation Q_i leaving surface i in all directions can be written as:

$$Q_i = \sum_j A_i \varphi_{ij} (J_i - J_j). \qquad (2.3)$$

The grey body approximation gives:

$$Q_i = \frac{A_i \varepsilon_i}{1 - \varepsilon_i} (\sigma T_i^4 - J_i). \qquad (2.4)$$

Equation (2.3) and (2.4) can be combined to give for any surface i:

$$\frac{A_i \varepsilon_i}{1 - \varepsilon_i} (\sigma T_i^4 - J_i) = \sum_j A_i \varphi_{ij} (J_i - J_j) \qquad (2.5)$$

where J is radiosity, [W/m²].

If the temperature is known, equation (2.5) can be used to give an equation solely in terms of radiosities of each surface; if the heat flux is known, equation (2.3) can be used to provide equations which are described solely in terms of radiosities on each surface (Ozisik, 1973 and Jones, 2000). Thus any N-surface problem can be defined by a set of N equations with N unknown radiosities:

$$\begin{aligned}
a_{11}J_1 + a_{12}J_2 + \ldots\ldots + a_{1N}J_N &= C_1 \\
a_{21}J_1 + a_{22}J_2 + \ldots\ldots + a_{2N}J_N &= C_2 \\
\vdots \quad \vdots \qquad\qquad \vdots \quad \vdots & \\
a_{N1}J_1 + a_{N2}J_2 + \ldots\ldots + a_{NN}J_N &= C_N
\end{aligned}$$

These equations can be expressed in a matrix form as:

$$\boldsymbol{AJ = C} \tag{2.6}$$

where $$A = \begin{pmatrix} a_{11} & a_{12} & \cdots & a_{1N} \\ a_{21} & a_{22} & \cdots & a_{2N} \\ \vdots & \vdots & & \vdots \\ a_{N1} & a_{N2} & \cdots & a_{NN} \end{pmatrix} \quad J = \begin{pmatrix} J_1 \\ J_2 \\ \vdots \\ J_N \end{pmatrix} \quad C = \begin{pmatrix} C_1 \\ C_2 \\ \vdots \\ C_3 \end{pmatrix}$$

The coefficients a_{ij} and C_i will be functions of the known view factors and temperatures or heat fluxes: $a_{ij} = \sum_j A_i \varphi_{ij}$ and $C_i = \frac{A_i \varepsilon_i}{1-\varepsilon_i}(\sigma T_i^4 - J_i)$.

The solution of the equations for the radiosities is obtained by inverting matrix $\boldsymbol{A}$:

$$\boldsymbol{J = A^{-1}C} \tag{2.7}$$

where $$A^{-1} = \begin{pmatrix} b_{11} & b_{12} & \cdots & b_{1N} \\ b_{21} & b_{22} & \cdots & b_{2N} \\ \vdots & \vdots & & \vdots \\ b_{N1} & b_{N2} & \cdots & b_{NN} \end{pmatrix}$$

The elements of both matrices on the right-hand side of the equation are known, so each radiosity may be calculated. Once the radiosities are known, all the unknown temperatures and heat fluxes may be calculated (Ozisik, 1973 and Jones, 2000).

2.3 View factor calculation techniques

Over many years various analytical solutions determining view factors for a variety of geometries have been developed and published in a range of reference books, e.g. McAdams (1954), Ozisik (1973), Holman (1981), Brewster (1992), ASHRAE (1993), Siegel and Howell (1992), and Jones (2000), these figures have either been presented in the form of algebraic equations or as charts, from which the view factor can be determined. For complex geometries, however, no analytical solutions are available and numerical techniques have to be used.

2.3.1 Cosine law

Consider a hemisphere of radius r, which base is centred at dA_1 (Figure 2.2). All radiation from dA_1 will land on the curved surface of the hemisphere. A thin circular strip element, dA_2, of the surface subtends an angle $d\theta_1$ at dA_1 and will have a thickness $rd\theta_1$ and the radius $r\sin\theta_1$, Jones (2000).

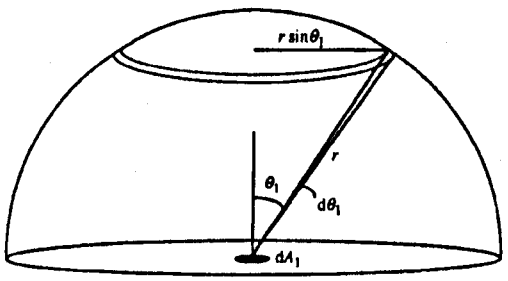

Figure 2.2
Cosine law method, Jones (2000).

Therefore:
$$dA_2 = 2\pi r \sin\theta_1 \times r d\theta_1 \tag{2.8}$$

and the view factor between surface A_1 to surface A_2 can be expressed as:

$$\varphi_{12} = \frac{1}{A_1}\int_{A_1}\int_{A_2}\frac{\cos\theta_1 \cos\theta_2 dA_1 dA_2}{\pi r^2} \tag{2.9}$$

which can be presented in numerical term as:

$$\varphi_{12} = \frac{1}{A_1}\sum_{A_1}\sum_{A_2}\frac{\cos\theta_1 \cos\theta_2 dA_1 dA_2}{\pi r^2}. \tag{2.10}$$

2.3.2 Hemisphere Method

An unit hemisphere method provides a way of using a geometric construction to determine one of the area integrals in equation (2.10). Consider the two area elements, dA_1 and dA_2 at a distance r, and imagine a hemisphere of unit radius center on dA_1, Figure 2.3. The areas of each projection:

$$dA_2' = dA_2 \cos\theta_2 \times \frac{1}{r^2} \tag{2.11}$$

and

$$dA_2'' = \frac{dA_2 \cos\theta_1 \cos\theta_2}{r^2} \tag{2.12}$$

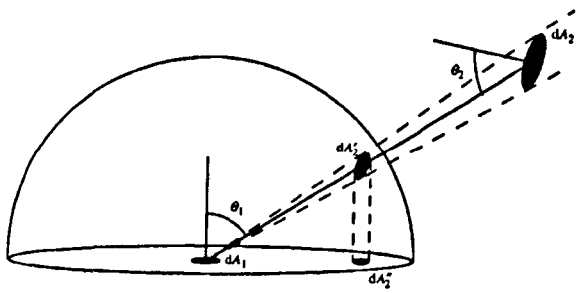

Figure 2.3
Unit hemisphere method, Jones (2000).

The area of the base of the unit hemisphere is π, so the fraction of the base occupied by dA_2'' is: $dA_2'' = \frac{dA_2 \cos\theta_1 \cos\theta_2}{\pi r^2}$; and the fraction of the base occupied by A_2'' is then: $A_2'' = \sum_{A_2} \frac{dA_2 \cos\theta_1 \cos\theta_2}{\pi r^2}$. If ξ is the fraction of the above equation, then substitution into the cosine law leads to:

$$A_1 \varphi_{12} = \sum_{A_1} \xi dA_1$$

If this sum can be evaluated, then φ_{12} can be determined. If A_1 is elemental, then no integration is required, and $\varphi_{12}=\xi$.

2.3.3 Hottel's crossed-string method

Hottel's method (Jones, 2000) can be used in systems which are essentially two-dimensional, i.e. where the surfaces are of constant cross-section, constant separation, and their length is much greater than their separation. Consider two parallel objects of infinite length (Figure 2.4) the view factor can be written as:

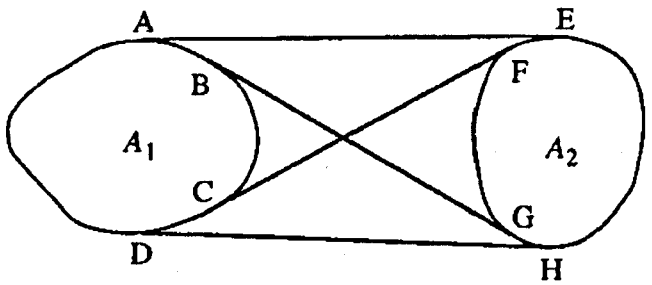

Figure 2.4
Hottel's crossed-strings method for two general surfaces, Jones (2000).

$$\varphi_{12} = \frac{1}{2P_1}[(\overline{ABGH} + \overline{DCFE}) - (\overline{AE} + \overline{DH})] \qquad (2.13)$$

where P_1 = the perimeter of surface A_1, [m]

$\overline{ABGH}$ = the length of string ABGH. [m]

The equation (2.13) can be said in words as:

$$\varphi_{12} = \frac{1}{2P_1}[\text{(sum of the crossed strong lengths)}$$

$$- \text{(sum of the uncrossed string lengths)}].$$

2.3.4 Monte Carlo method

The probably most often used numerical method for determining view factors is the Monte Carlo method e.g. Mammersley and Handscomb (1964), Fishman (1996). The basis of the Monte Carlo method is to select at random a series of beams of radiation from surface 1, and to determine the proportion which impinge on surface 2.

Consider Figure 2.5, pick any point on surface 1 at random by using a random number generator to give a number R_1 between 0 and 1, which represents the fractional distance along the surface from x_1.

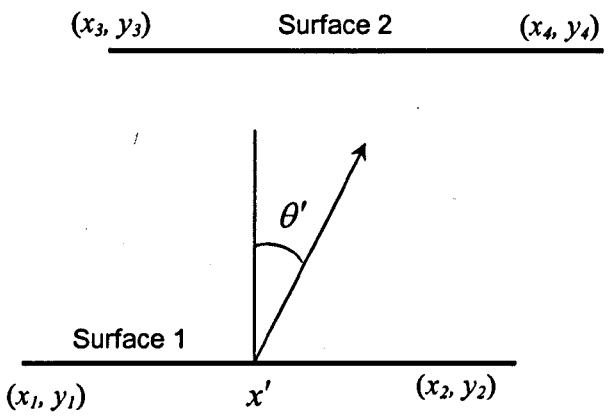

Figure 2.5 Arrangement for two parallel plates, showing a beam of radiation from a random point on surface 1 in a random direction (Jones, 2000).

The selected point x' is related algebraically to R_1:

$$R_1 = \frac{x' - x_1}{x_2 - x_1}$$

or

$$x' = x_1 + R_1(x_2 - x_1) \tag{2.14}$$

If the intensity of radiation normal to surface 1 is I, then the energy emitted in direction θ of the beam leaving surface 1 will be $I\cos\theta$. The selected angle θ' is related to R_2 by:

$$R_2 = \frac{\int_{-\pi/2}^{\theta'} I\cos\theta\, d\theta}{\int_{-\pi/2}^{+\pi/2} I\cos\theta\, d\theta} = \frac{1}{2}(\sin\theta' + 1) \tag{2.15}$$

where θ is the angle between the normal to surface 1 at x' and θ' is the direction of the beam which leaves the surface 1. The selected angle θ' can be written in term of R_2 as:

$$\theta' = \sin^{-1}(2R_2 - 1) \tag{2.16}$$

where R_2 is random number of any angle from surface 1 (between $-\pi/2$ and $+\pi/2$) and the equation of beam:

$$y = \frac{x - x'}{\tan \theta'} \tag{2.17}$$

Substituting $y=y_3$ into equation (2.17) gives us a point x where the two lines intersect. If $x_3 \leq x \leq x_4$, then the beam does impinge on surface 2 and it is recorded a hit; if $x<x_3$ or $x>x_4$, then the beam does not impinge on surface 2 and it is recorded miss. A very large number of randomly selected beams is needed to repeat the procedure. The use of computers, however, allows us to compute several thousand beams very quickly, and hence determine the view factor to a high degree of accuracy.

2.3.5 Voxel-based ray tracing method

Finally, the voxel-based ray tracing method is an advanced numerical technique in which a geometry scene is 'ray-traced' being developed into small volume elements or voxels. As each ray is cast, the voxels are visited in the sequence in which the ray passes through them and only those faces that occupy these voxels are tested for intersection (ThermoAnalytics, 2001).

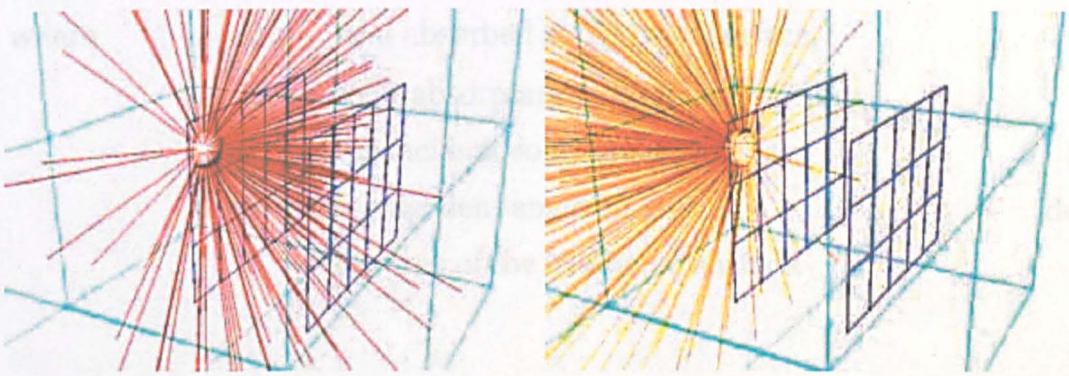

Figure 2.6 Casting rays from each element in the voxel-based ray tracing technique (ThermoAnalytics, 2001).

Thousands of rays are cast from each element centroid to determine the view factor to all other elements that are visible from the element centroid (Figure 2.6). The number of rays that intersect another element determines the relative view factor relationship. For this technique, the accuracy of the predicted view factors depend on the number of rays cast from each element.

According to ThermoAnalytics (2001), this ray tracing technique provides the fastest radiation exchange solver on the market.

2.4 Short wave radiation

Short wave radiation is generally classified as in the range of 0.3 - 3 μm (Duffie and Beckman, 1991). Solar radiation is in the wavelength range of 0.25-4 μm. It can be separated into two components: direct and diffuse beam. Direct beam is the portion of radiation that reaches the earth's surface in relatively parallel rays. The diffuse component is the portion of the radiation that has been scattered by gas molecules and suspended particles in the atmosphere and reaches the earth's surface from multiple directions.

The amount of heat absorbed on a plane surface depends upon the solar properties and the incident angle of solar beam (ASHRAE, 1993)

$$Q_{ab} = \alpha_{sf} S \cos\theta A \tag{2.18}$$

where
Q_{ab} = heat absorbed at the body surface, [W]
α_{sf} = solar absorptance of the body surface, [-]
S = the incident solar radiation, [Wm^{-2}]
θ = the incident angle on area A, [deg, rad]
A = the area of the irradiated surface. [m^2]

2.5 Human radiative heat transfer

2.5.1 Long wave radiation

The radiative heat exchange between a human body as a whole and an enclosure can be computed by means of the Stefan-Boltzmann law (Fanger, 1970).

$$Q = A_{eff}\varepsilon\sigma(T_{cl}^{4} - MRT^{4}) \tag{2.19}$$

where

Q	=	radiant heat exchange between human body and environment,	[W]
A_{eff}	=	effective radiation area of the clothed body,	[m²]
ε	=	emittance of the outer surface of the clothed body,	[-]
σ	=	Stefan-Boltzmann constant,	[Wm⁻²K⁻⁴]
T_{cl}	=	mean temperature of the outer surface of clothed body,	[K]
MRT	=	mean radiant temperature of the (asymmetric) enclosure.	[K]

The term A_{eff} is generally difficult to evaluate, due to its strong dependence on the geometric properties of the human body (i.e. the concavities generated by the irregularities of the body contour). Nevertheless, it can be defined by means provided by Fanger (1970) and using the following equation (2.20).

$$A_{eff} = f_{eff} f_{cl} A_{Du} \tag{2.20}$$

where

f_{eff}	=	effective radiation area factor,	[-]
f_{cl}	=	ratio of the surface area of the clothed body to the surface area of nude body,	[-]
A_{Du}	=	DuBois Area.	[m²]

Assume that a human body is located within an inhomogeneous enclosure of n surfaces with different surfaces temperatures T_i. The net total heat exchange between the body, A_b, and the enclosure is calculated as follows:

$$Q = \varepsilon_{sf} A \sigma \sum_{i}^{n} \varepsilon_{sr,i} \varphi_{sf-sr,i} (T_{sf}^4 - T_i^4) \qquad (2.21)$$

where

Q = heat exchange between the human body and the inhomogeneous enclosure, [W]

ε_{sf} = the emittance of the body surface, [-]

$\varepsilon_{sr,i}$ = the emittance of the surrounding surface *i* of the enclosure, [-]

A = the surface area of the human body, [m²]

$\varphi_{sf-sr,i}$ = view factor between the body surface and *i-th* surface of the enclosure, [-]

T_{sf} = the temperature of the body surface, [K]

T_i = the temperature of surrounding surface *i*. [K]

The radiative heat exchange between a human and the inhomogeneous enclosure can also be described by using a mean surface temperature $\overline{T}$, and a mean emissivity $\bar{\varepsilon}$ of the asymmetric enclosure (Michael, 1997).

$$Q = \varepsilon_{sf} \bar{\varepsilon} A \, \sigma (T_{sf}^4 - \overline{T}^4) \qquad (2.22)$$

Thereby, the mean surface temperature $\overline{T}$ results from setting equal equation (2.21) and equation (2.22), and rearranging:

$$\overline{T} = \sqrt[4]{T_{sf}^4 - \sum_{i}^{n} \varphi_{sf-sr,i} \varepsilon_{sr,i} (T_{sf}^4 - T_i^4) \cdot \frac{1}{\bar{\varepsilon}}} \qquad (2.23)$$

where $\bar{\varepsilon} = \sum_{i}^{n} \varepsilon_{sr,i} \varphi_{sf-sr,i}$.

In cases where T_i do not differ significantly from each other $\overline{T}$ may be obtained with a reasonable accuracy by weighting T_i with the corresponding view factor $\varphi_{sf-sr,i}$ (McIntyre, 1980):

$$\overline{T} = \sum_{i}^{n} T_i \, \varphi_{sf-sr,i} \tag{2.24}$$

and even more straight forward but less accurate approach is to weight T_i by the corresponding surface areas A_i, (Fanger, 1970).

or
$$\overline{T} = \frac{\sum_{i}^{n} T_i A_i}{\sum_{i}^{n} A_i} \tag{2.25}$$

where A_i is the surface area of element i.

2.5.1.1 Mean radiant temperature

The mean radiant temperature is defined as that temperature of a fictitious, uniform black (i.e. $\bar{\varepsilon} = 1$) enclosure which provides the same radiant heat exchange with a surface/body as the actual inhomogeneous enclosure, Fanger (1970), ASHRAE (1993):

$$MRT = \sqrt[4]{\sum_{i=1}^{n} T_i^4 \varphi_{sf-sr,i}} \tag{2.26}$$

The emissivity of human skin has been measured by Mitchell (1970) and found to be close to unity. The emittance of most types of clothing is about 0.95 (Fanger, 1970).

2.5.1.2 Effective radiation area

The effective radiation area is the actual area which directly affect to the radiant environment. Consider a person located in the centre of a spherical coordinate system, where any direction in relation to the person is defined by the azimuth angle (α) and altitude angle (β), Figure (2.7).

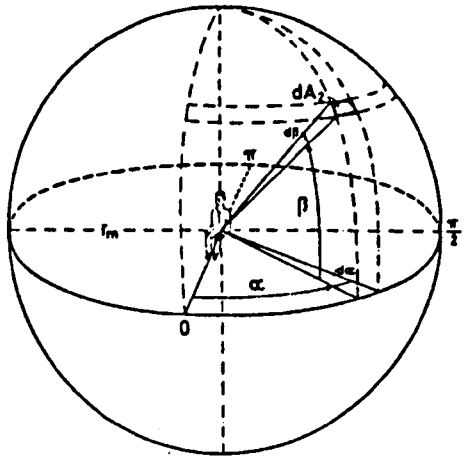

Figure 2.7
Notation pertinent to calculation of the effective radiation area (Fanger, 1970).

If the surrounding is considered as a large sphere A_2, with a radius r_m, the reciprocity theory for view factors for the area of sphere and the person can be used, assuming that the angular distribution of the radiant fluxes leaving surfaces are diffuse. The effective radiation area can be presented as follows.

$$A_{eff}\varphi_{PA_2} = A_2\varphi_{A_2P}$$

or

$$A_{eff} = \frac{4}{\pi}\int_{\alpha=0}^{\alpha=\pi}\int_{\beta=0}^{\beta=\pi/2} A_p \cos\beta d\alpha d\beta \qquad (2.27)$$

where
A_{eff} = effective radiation area
A_2 = the area of the sphere
$\varphi_{PA_2}, \varphi_{A_2P}$ = the view factor between person to the sphere and between sphere to the person
A_{eff} = effective radiation area
A_p = projected area of the human body

2.5.1.3 Effective radiation area factor

The effective radiation area factor is the ratio of effective radiation area and DuBois area (Fanger, (1970).

$$f_{eff} = \frac{A_{eff}}{A_{Du}} \tag{2.28}$$

where f_{eff} is effective radiation area factor and A_{Du} is DuBois Area.

2.5.1.4 View factor between human body and individual walls

The enclosure surfaces found in indoor spaces are usually rectangular. According to Fanger (1970) the view factors between a sedentary or standing person and the whole rectangular surfaces can be described as follows, if the orientation of the person is known:

$$\varphi_{PA} = \frac{1}{\pi} \int_{\frac{x}{y}=0}^{\frac{x}{y}=\frac{a}{c}} \int_{\frac{z}{y}=0}^{\frac{z}{y}=\frac{b}{c}} \frac{f_p}{[1+(\frac{x}{y})^2+(\frac{z}{y})^2]^{\frac{3}{2}}} d(\frac{x}{y}) d(\frac{z}{y}) \tag{2.29}$$

where

φ_{PA}	=	view factor of the human body to the vertical plane
a	=	the width of the plane
b	=	the height of the plane
c	=	the distance between the person and the corner point of the plane
f_p	=	projected area factor of the human body
x, y, z	=	the coordinate in orthogonal coordinate.

Fanger (1970) has also provided the equation for determining the mean value of a view factor when the orientation of the person in a room is unknown. It is the integral from azimuth angle from 0 to 2π.

$$\bar{\varphi}_{PA} = \frac{1}{2\pi^2} \int_{\frac{x}{y}=0}^{\frac{x}{y}=\frac{a}{c}} \int_{\frac{z}{y}=0}^{\frac{z}{y}=\frac{b}{c}} \int_{\alpha=0}^{\alpha=2\pi} \frac{f_p}{[1+(\frac{x}{y})^2+(\frac{z}{y})^2]^{\frac{3}{2}}} d(\frac{x}{y}) d(\frac{z}{y}) d\alpha \qquad (2.30)$$

where α = azimuth angle.

View factors between a person and vertical and horizontal rectangular plane areas were provided by Fanger (1970) and plotted as diagram. Each diagram portrays dimensionlessly the view factor as a function of the two length relationships *a/c* and *b/c*, where *a* and *b* are the side lengths in the rectangle and *c* is the normal distance between person (his centre) and rectangle, Figure (2.8) to (2.11).

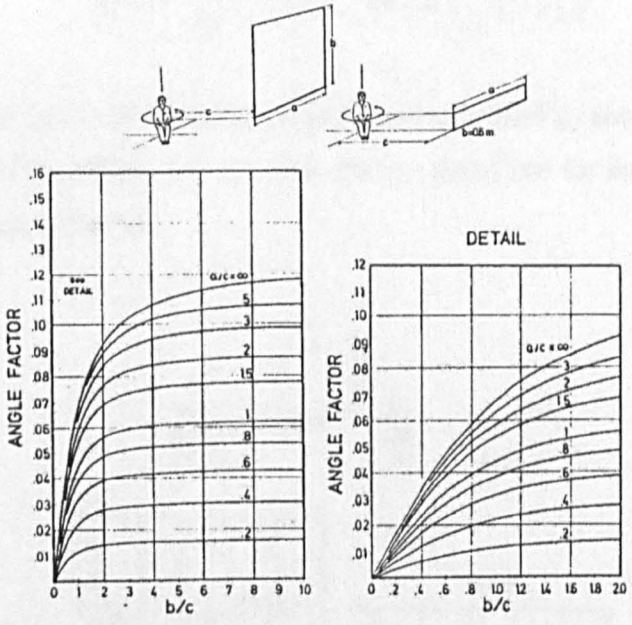

Figure 2.8 Mean value of view factor between a seated person and a vertical rectangular (*above or below his centre, location is known but not the orientation*), Fanger (1970).

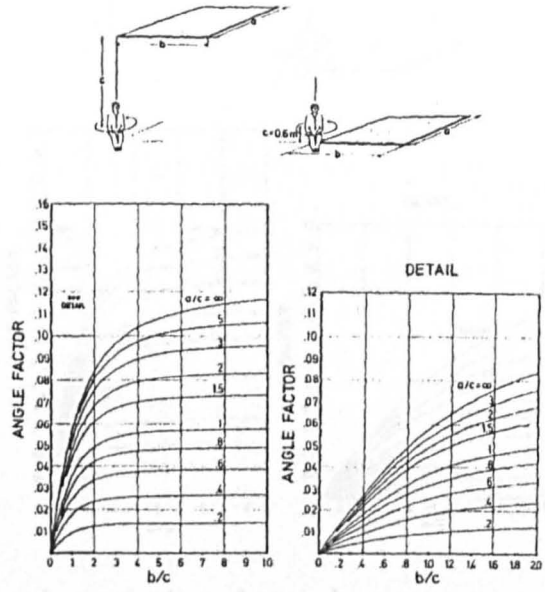

Figure 2.9 Mean value of view factor between a seated person and a horizontal rectangular (*on the ceiling or on the floor, location is known but not the orientation*), Fanger (1970).

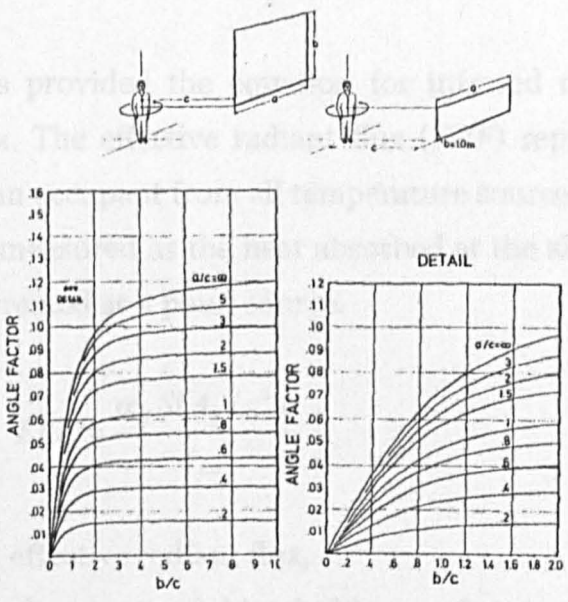

Figure 2.10 Mean value of view factor between a standing person and a vertical rectangular (*above or below his center, location is known but not the orientation*), Fanger (1970).

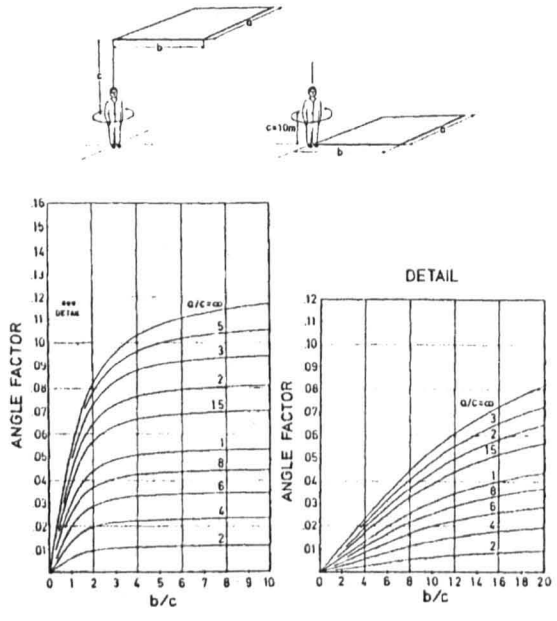

Figure 2.11 Mean value of view factor between a standing person and a horizontal rectangular (*on the ceiling or on the floor, location is known but not the orientation*), Fanger (1970).

2.5.2 Short wave radiation

ASHRAE (1996) has provided the equation for infrared radiant heat as the effective radiant flux. The effective radiant flux (*ERF*) represents the radiant energy absorbed by an occupant from all temperature sources different from the ambient and can be measured as the heat absorbed at the skin-clothing surface from a beam heater treated as a point source.

$$ERF = \frac{\alpha_{sf} S(A_p / c^2)}{A_{Du}} \tag{2.31}$$

where ERF = effective radiant flux, [Wm^{-2}]

α_{sf} = absortance of skin-clothing surface at emitter temperature

S = irradiance from beam heater or radiant intensity, [Wm^{-2}]

A_p = projected area of human body on plane normal to direction of heater beam, [m^2]

c = distance from beam heater to centre of human body, [m]

A_{Du} = DuBois area, [m²]

or $$ERF = \frac{\alpha_{sf} f_{eff} f_p S}{d^2} \quad (2.32)$$

where f_{eff} = effective radiation factor

f_p = projected area factor.

2.5.2.1 Projected area

The projected area of the human body is important for short-wave radiation calculations when assessing the effect of e.g. solar radiation on humans. The projected body area is defined as that surface area of the human body which is exposed to parallel rays and projected onto a plane perpendicular to the rays as shown in Figure 2.12.

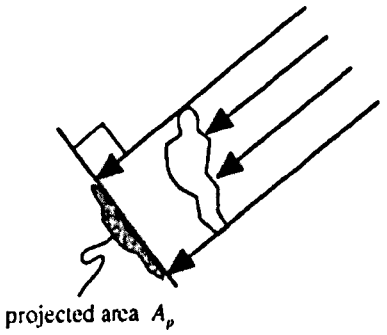

Figure 2.12
Projected area of the human body.

2.5.2.2 Projected area factor

The projected area factor is defined as the ratio of the projected area and the effective radiation area of the body as shown in equation (2.33):

$$f_p = \frac{A_p}{A_{eff}} \quad (2.33)$$

where f_p is the projected area factor of the human body. A_p is the projected area and A_{eff} is effective radiation area of human body (Fanger, 1970).

Fanger (1970) has determined experimentally the projected area factors as a function of the azimuth angle (α) and altitude angle (β) for the nude and clothed body both in seated and standing posture, Figure (2.13) and (2.14).

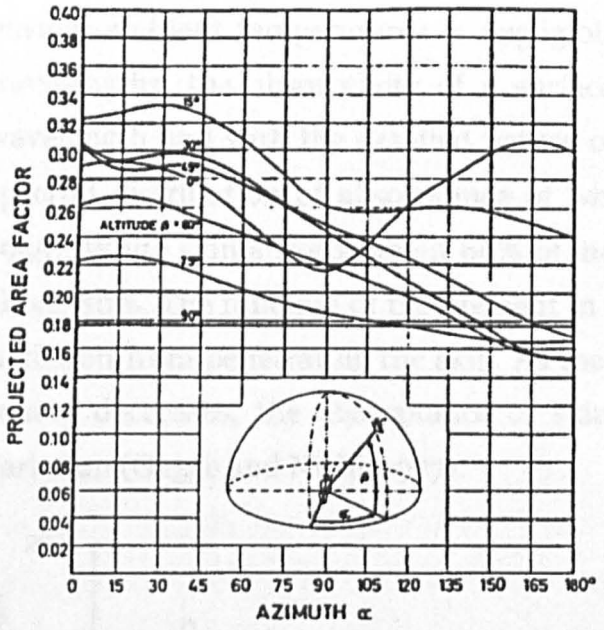

Figure 2.13 Projected area factor for seated person, nude and clothed (Fanger, 1970).

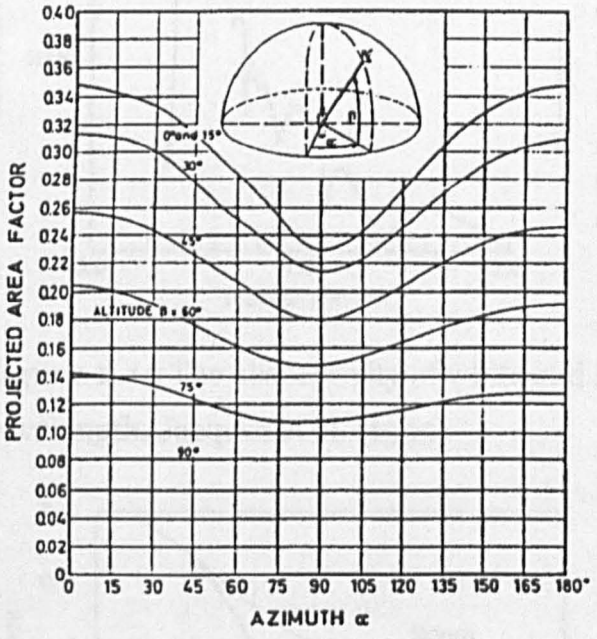

Figure 2.14 Projected area factor for standing persons, nude and clothed (Fanger, 1970).

2.5.2.3 Solar absorptivity

In the solar and near infra-red region it is more usual to speak of absorptivity than emissivity, since the actual emission at these wavelengths by a surface at normal ambient temperatures is negligible. In the visible and near infra-red wavelengths, the absorptivity of a surface is hard to predict; it varies with wavelength and with the detailed nature of the surface. Figure 2.15 shows the spectral distribution of absorptance of white and Negro skin (Jacquez et al., 1955). White skin absorbs about 60% of incident solar radiation and black skin about 80%. The function of the pigment in the black skin is to block ultra-violet radiation from penetrating the skin. As the colour temperature of the radiation source decreases, the absorptance of skin increases. Figure 2.16 shows this variation (Gagge and Nishi, 1977).

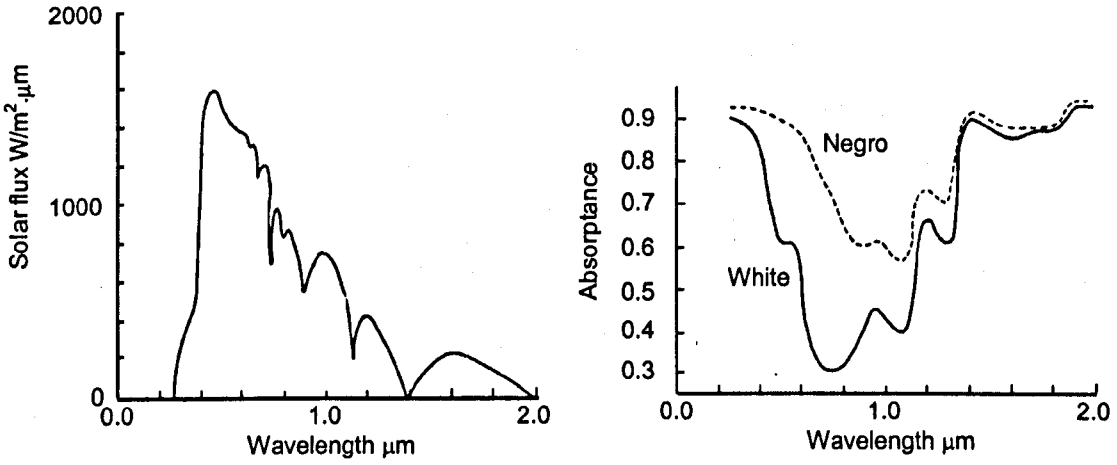

Figure 2.15 The absorptivity of white and Negro skin as a function of wavelength, Jacquez et al. (1955).

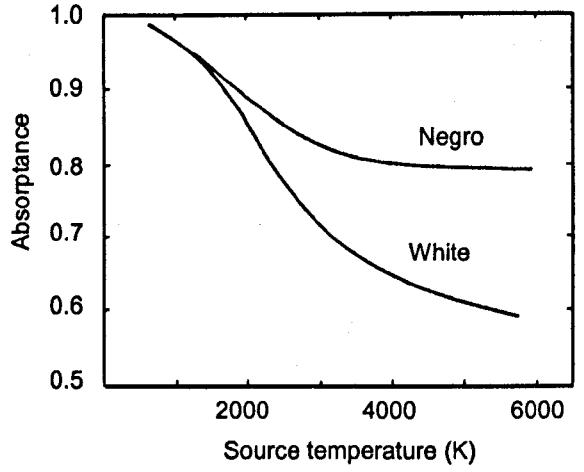

Figure 2.16
The variation of absorptivity of human skin as a function of the temperature of a black body source, Gagge and Nishi (1977).

Chapter 3

Choice and validation of numerical radiation simulation methods

3.1 Introduction

The prediction of human thermal responses to asymmetric radiant fields requires detailed modelling of the human radiation heat exchange. The direction-dependent long- and short-wave radiation heat transfer is significantly affected by the geometry of the human body. Unfortunately, the human body is too complex, so, no analytical solutions exist to calculate components of the human radiative heat exchange in detail. Instead, numerical methods have to be used to obtain view factors and projected areas for individual parts of the human body at given body postures and for different geometrical configurations of the surroundings.

Nowadays, specialist software tools such as POSER4 (Curious Labs, 2000) are available which enable the creation of detailed three-dimensional human body geometries for arbitrary body postures. The intention of this research was to use such tools in conjunction with advanced numerical simulation models to aid accurate predictions of the geometry-related radiation characteristics of the human body. Given this advance, a US software company, ThermoAnalytics (http://www.thermoanalytics.com), expressed interest in collaborating on the project and contributed their thermal analysis software RadTherm. RadTherm is a sophisticated numerical simulation tool which is capable of dealing with highly complex geometries (such as the human body) and complex boundary conditions. The software incorporates advanced, voxel-based ray tracing techniques to enable fast and accurate radiation predictions.

3.2 Aim

The aim of this chapter is to investigate the accuracy and sensitivity of the numerical radiation calculation techniques incorporated in RadTherm by comparison of predicted view factors with available analytical solutions obtained for various geometries.

3.3 Methodology

Two simplified geometries and two more complex geometries were set up to investigate the accuracy and the sensitivity of numerically calculated view factors by comparison with available analytical solutions. For this purpose the following geometrical configurations were selected: two rectangular parallel surfaces, two perpendicular plates, and cylinders facing a rectangular surface, Figure 3.1.

The distances between the plates and between the cylinders and the plates were varied to investigate the relative sensitivity of the numerical results for different magnitudes of view factors. The surfaces of the panels were subdivided into different numbers of finite surface elements to analyse the accuracy of RadTherm calculations with respect to the geometrical resolution of the scene.

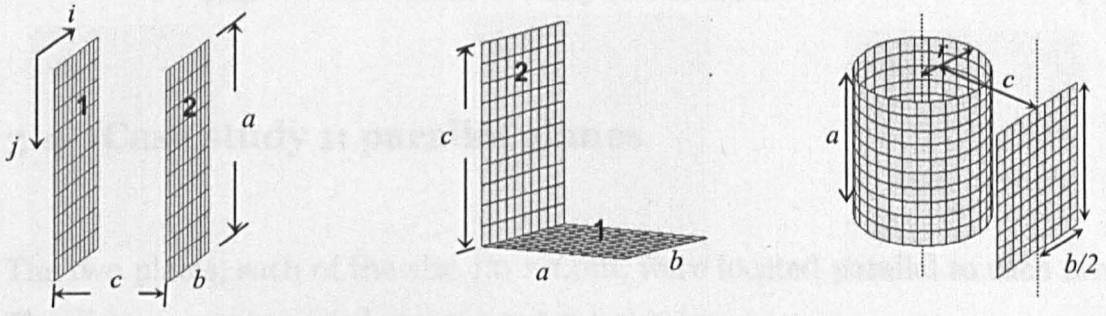

Parallel planes | Perpendicular planes | Cylinder and plate

Figure 3.1 Geometrical configurations studied.

In RadTherm, the voxel-based ray tracing technique is used to calculate view factors. The scheme subdivides the scene to be ray-traced into volume elements, or voxels. As mentioned in section 2.3.5 the accuracy of this method depends on the number of rays, which are cast from each surface element. Therefore, the effect of the number of rays cast (up to 4608) on the accuracy of the numerical results was also studied. For this purpose, five setting numbers of rays: 512 rays (1R), 1152 rays (2Rs), 2048 rays (3Rs), 3200 rays (4Rs), and 4608 rays (5Rs) were used to investigate the accuracy of the voxel-based ray tracing technique.

The numerical results were compared with analytical solutions for the above geometries. To obtain quantitative information on the accuracy of the numerical results, the relative error, Δe, was calculated for each instance investigated in the study. The relative error [in %] was defined as the quotient of the absolute difference between numerically and analytically calculated view factors and the analytical value:

$$\Delta e = \left| \frac{\varphi_{RTh} - \varphi_{anal}}{\varphi_{anal}} \right| \times 100\% \qquad (3.1)$$

where Δe = relative error, [%]

φ_{RTh} = view factor of numerical result (RadTherm), [-]

φ_{anal} = view factor of analytical solution. [-]

3.4 Case study 1: parallel planes

The two plates, each of the size 1.0 x 1.0m, were located parallel to each other. The distances were varied at 0.5, 1.0, 1.5 and 2.0m.

3.4.1 Simulation

Four resolutions were analysed classified as: low, medium, high and very high resolution (*Table 3.1*).

Table 3.1 The resolution of two parallel plates.

Geometry	Resolution	Number of elements (*Area of the surface element*, *10^{-4}m^2)	
		Plate 1 (a=1.0m; b=1.0m)	Plate 2 (a=1.0m; b=1.0m)
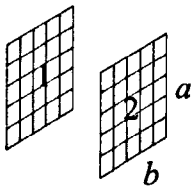	Low	5x5 (*400.0*)	5x5 (*400.0*)
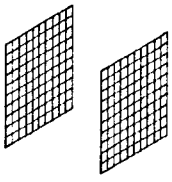	Medium	10x10 (*100.0*)	10x10 (*100.0*)
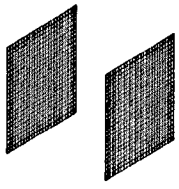	High	25x25 (*16.0*)	25x25 (*16.0*)
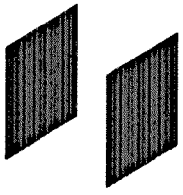	Very high	40x40 (*6.3*)	40x40 (*6.3*)

3.4.2 Analytical solution

The analytical solution for this geometrical configuration is described by the following equations (Brewster, 1992):

$$\varphi_{12} = \frac{2}{\pi XY}\left\{\ln\sqrt{\frac{(1+X^2)(1+Y^2)}{1+X^2+Y^2}} + X\sqrt{1+Y^2}\tan^{-1}\left(\frac{X}{\sqrt{1+Y^2}}\right)\right\}$$
$$+\frac{2}{\pi XY}\left\{Y\sqrt{1+X^2}\tan^{-1}\left(\frac{Y}{\sqrt{1+X^2}}\right) - X\tan^{-1}X - Y\tan^{-1}Y\right\} \qquad (3.2)$$

where φ_{12} = view factor between plate 1 and plate 2

$X = a/c$ and $Y = b/c$.

3.4.3 Results

A comparison of the numerical view factors obtain using voxel-based ray tracing technique and analytical solution are illustrated in Figure 3.2.

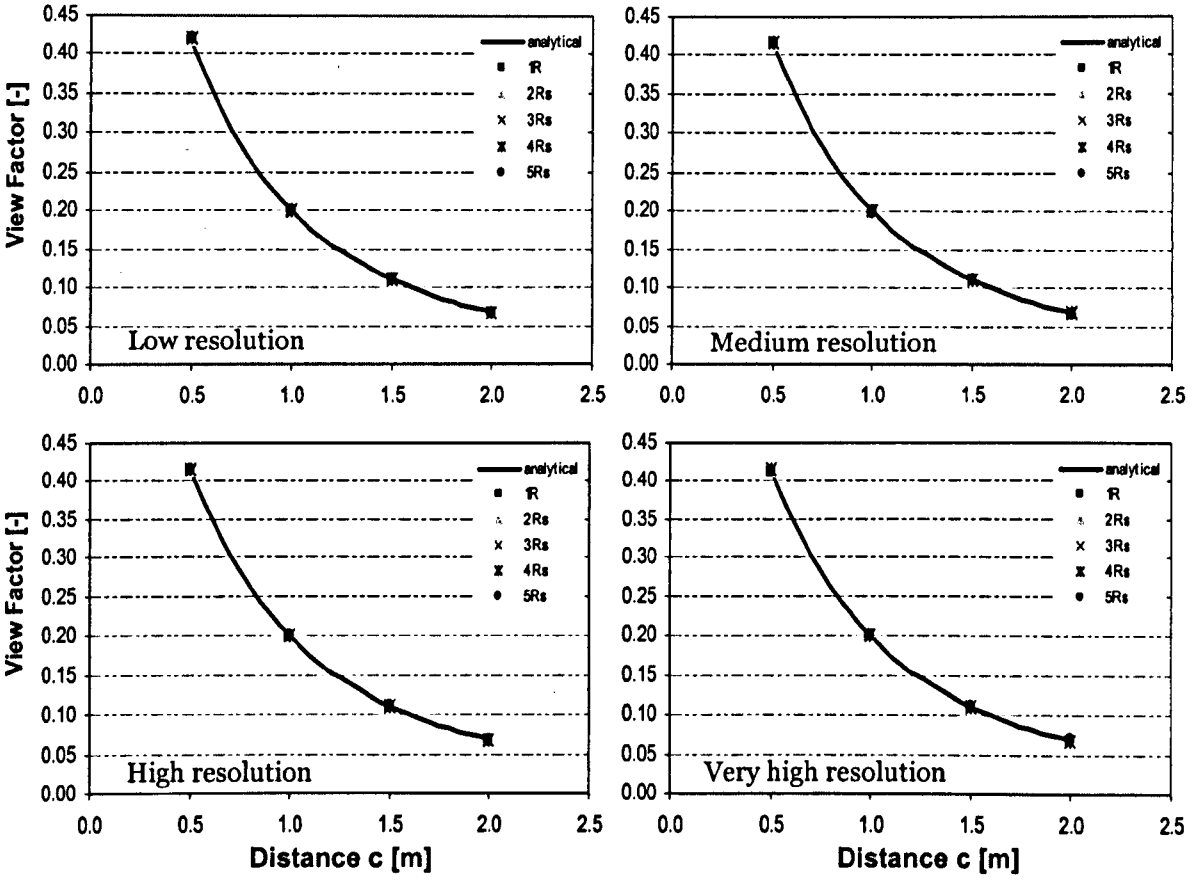

Figure 3.2 View factor between two parallel plates (φ_{12}).

There was a very good general agreement between analytically (solid lines) and numerically calculated view factors (data points) for all distances between the plates, resolutions, and numbers of rays investigated. The average relative error varied between 0.53% and 1.20% (detailed analysis in *Table A.1*). The relative error seemed to decrease slightly when the resolution of the geometrical configuration increased. An exception was the medium resolution for which the best agreement with the analytical solution was achieved. However, there was no consistent effect of the numbers of rays on the accuracy of the results.

3.5 Case study 2: perpendicular plates

Two perpendicular plates, both of the same width of 1.0m were located perpendicular to each other. The length of the first plate was 1.0m, while the length of the second plate was varied: 0.5m, 1.0m, 1.5m and 2.0m.

3.5.1 Simulation

As same as case study 1: four resolutions were analysed classified as: low, medium, high and very high resolution (*Table 3.2*).

Table 3.2 The resolution of two perpendicular plates.

Geometry	Resolution	Number of elements (*Area of the surface element*, *$10^{-4}m^2$)	
		Plate 1 (b=1.0m)	Plate 2 (b=1.0m; c=1.0m)
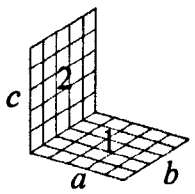	Low	a=0.5m: 5x3 (666.7) a=1.0m: 5x5 (*400.0*) a=1.5m: 5x8 (*375.0*) a=2.0m: 5x10 (*400.0*)	5x5 (*400.0*)
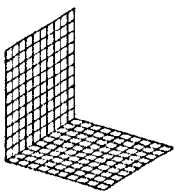	Medium	a=0.5m: 10x5 (*100.0*) a=1.0m: 10x10 (*100.0*) a=1.5m: 10x15 (*100.0*) a=2.0m: 10x20 (*100.0*)	10x10 (*100.0*)
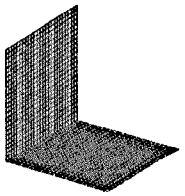	High	a=0.5m: 25x13 (*15.4*) a=1.0m: 25x25 (*16.0*) a=1.5m: 25x38 (*15.8*) a=2.0m: 25x50 (*16.0*)	25x25 (*16.3*)
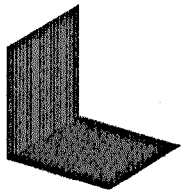	Very high	a=0.5m: 40x20 (*6.3*) a=1.0m: 40x40 (*6.3*) a=1.5m: 40x60 (*6.3*) a=2.0m: 40x80 (*6.3*)	40x40 (*6.3*)

3.5.2 Analytical solution

The analytical solution for the view factor between two perpendicular plates was obtained from, Brewster (1992) as following:

$$\varphi_{12} = \frac{1}{\pi X}\left\{X\tan^{-1}\left(\frac{1}{X}\right) + Y\tan^{-1}\left(\frac{1}{Y}\right) - \sqrt{X^2+Y^2}\tan^{-1}\left(\frac{1}{\sqrt{X^2+Y^2}}\right)\right\}$$

$$+\frac{1}{4\pi X}\left\{\ln\left[\frac{(1+X^2)(1+Y^2)}{1+X^2+Y^2}\right] + X^2\ln\left[\frac{X^2(1+X^2+Y^2)}{(1+X^2)(X^2+Y^2)}\right]\right.$$

$$\left. + Y^2\ln\left[\frac{Y^2(1+X^2+Y^2)}{(1+Y^2)(X^2+Y^2)}\right]\right\} \qquad (3.3)$$

where φ_{12} = view factor between plates 1 and 2

$X = a/c$, and $Y = b/c$.

3.5.3 Results

The numerical and analytical view factors of the perpendicular plates are presented in Figure 3.3.

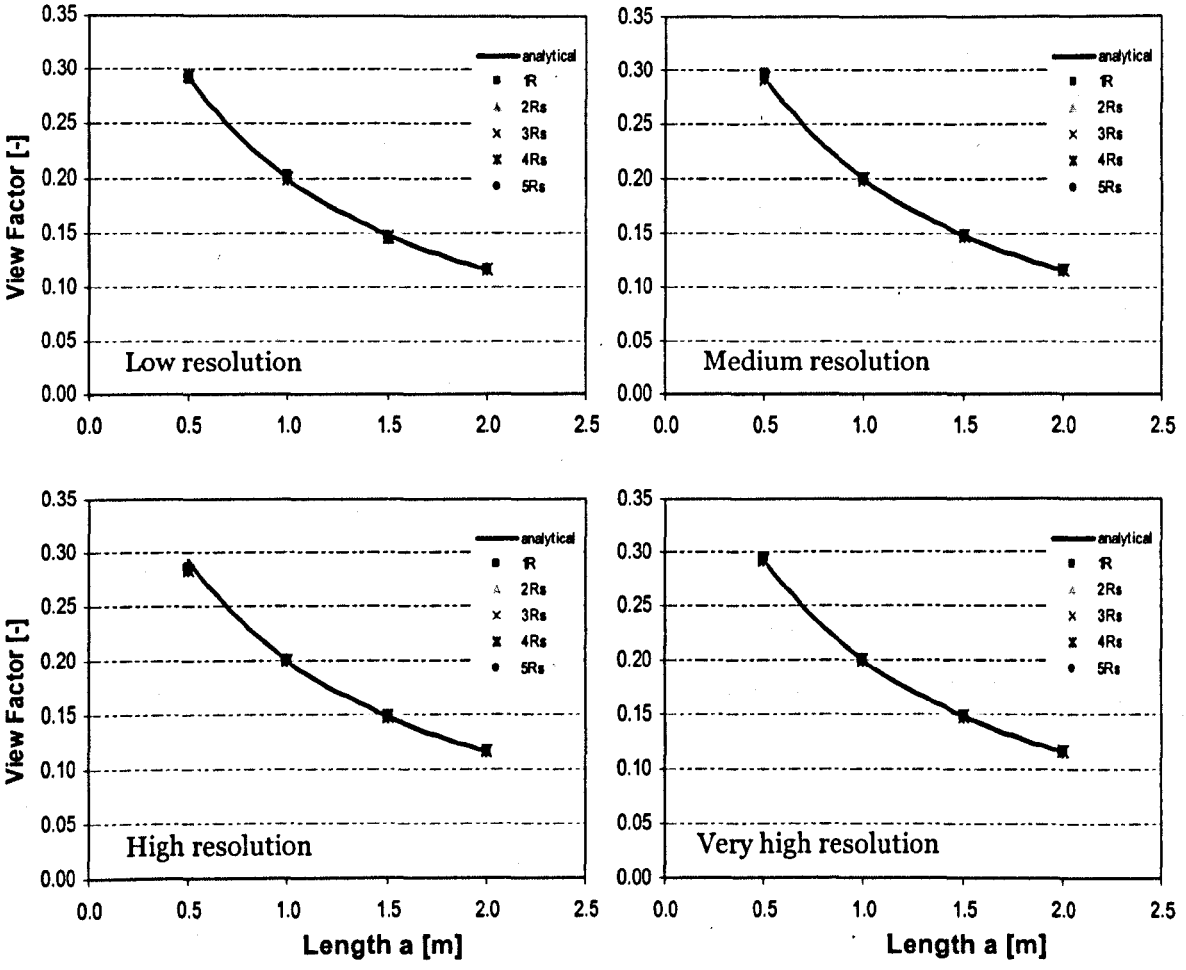

Figure 3.3 View factor of perpendicular plates (φ_{12}).

Similar to the results obtained for two parallel plates, there was a very good agreement between numerical and analytical results for all distances, resolutions and numbers of rays. The average relative error of the numerical view factors varied between 0.05% and 0.70% (Table A2). Here too, the relative error seemed to decrease slightly with a higher resolution of the geometry, but there was no consistent effect of the numbers of rays on the accuracy of the results.

3.6 Case study 3: cylinders and plates

Two sizes of the cylinder were specified. In *case a* the diameter and the height of the cylinder were defined arbitrarily. The dimensions of the cylinder in *case b* were chosen to approximate the size of human body. In both cases the plate was a square, which was centred at various distances from the cylinder and which height was equal to the height of the cylinder, *a* (*Figure 3.1*). Also the distance, *c*, was varied at 0.5, 1.0, 1.5 and 2.0m.

3.6.1 Simulation

Similarly, four resolutions (low, medium, high and very high resolution) were analysed as shown in Table 3.3 and Table 3.4.

Table 3.3. The resolution of cylinder and plane plate (*case a*).

Geometry	Resolution	Number of elements (*Area of the surface element*, $*10^{-4}m^2$)	
		Cylinder (r=0.5m; a=1.0m)	Plate (b=1.0m; a=1.0m)
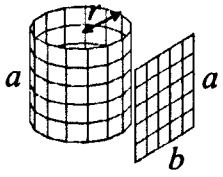	Low	15x5 (*418.9*)	5x5 (*400.0*)
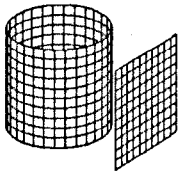	Medium	30x10 (*104.7*)	10x10 (*100.0*)
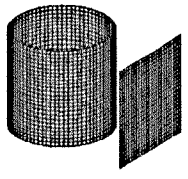	High	75x25 (*16.8*)	25x25 (*16.0*)
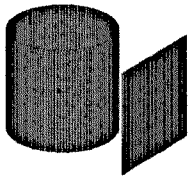	Very high	120x40 (*6.5*)	40x40 (*6.3*)

Table 3.4. The resolution of cylinder and plane plate (*case b*).

Geometry	Resolution	Number of elements (*Area of the surface element*, cm²)	
		Cylinder (r=0.3m; a=1.8m)	Plate (b=1.8m; a=1.8m)
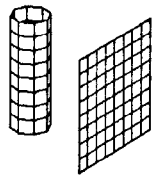	Low	8x8 (*530.1*)	8x8 (*506.3*)
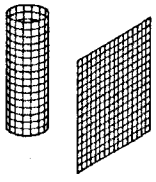	Medium	16x16 (*132.5*)	16x16 (*126.6*)
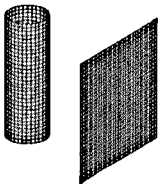	High	32x32 (*33.1*)	32x32 (*31.6*)
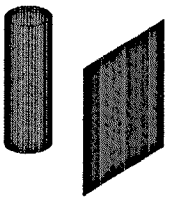	Very high	48x48 (*14.7*)	48x48 (*14.1*)

3.6.2 Analytical solution

The corresponding analytical solution for view factors is described by the following equations (Fiala, 1991):

$$\varphi_{PC} = \frac{2}{B}\int_0^{B/2} f(g)dg \tag{3.4}$$

where

$$f(g) = \frac{A}{A^2+g^2} - \frac{A}{\pi(A^2+g^2)}\left\{\cos^{-1}\left(\frac{Y}{X}\right) - \frac{1}{2C}\left[\sqrt{X^2+4C^2}\cos^{-1}\left(\frac{Y}{X\sqrt{A^2+g^2}}\right) + Y\sin^{-1}\left(\frac{1}{\sqrt{A^2+g^2}}\right) - \frac{\pi X}{2}\right]\right\} \tag{3.5}$$

and

$$A = \frac{c}{r},\ B = \frac{b}{r},\ C = \frac{a}{r}$$

$$X = A^2 + C^2 + g^2 - 1$$

$$Y = C^2 - A^2 - g^2 + 1$$

The integral in equation (3.4) was solved using the Simpson's rule (Blum, 1972). The view factor between cylinder and the plane plate, φ_{cp}, was then obtained by:

$$\varphi_{CP} = \frac{A_P \varphi_{PC}}{A_C} \tag{3.6}$$

where A_P = surface area of the plate, [m²]

A_C = surface area of the cylinder. [m²]

3.6.3 Results

A comparison of the analytical solution and the numerical view factors obtain using voxel-based ray tracing technique are presented in Figure 3.4 and 3.5.

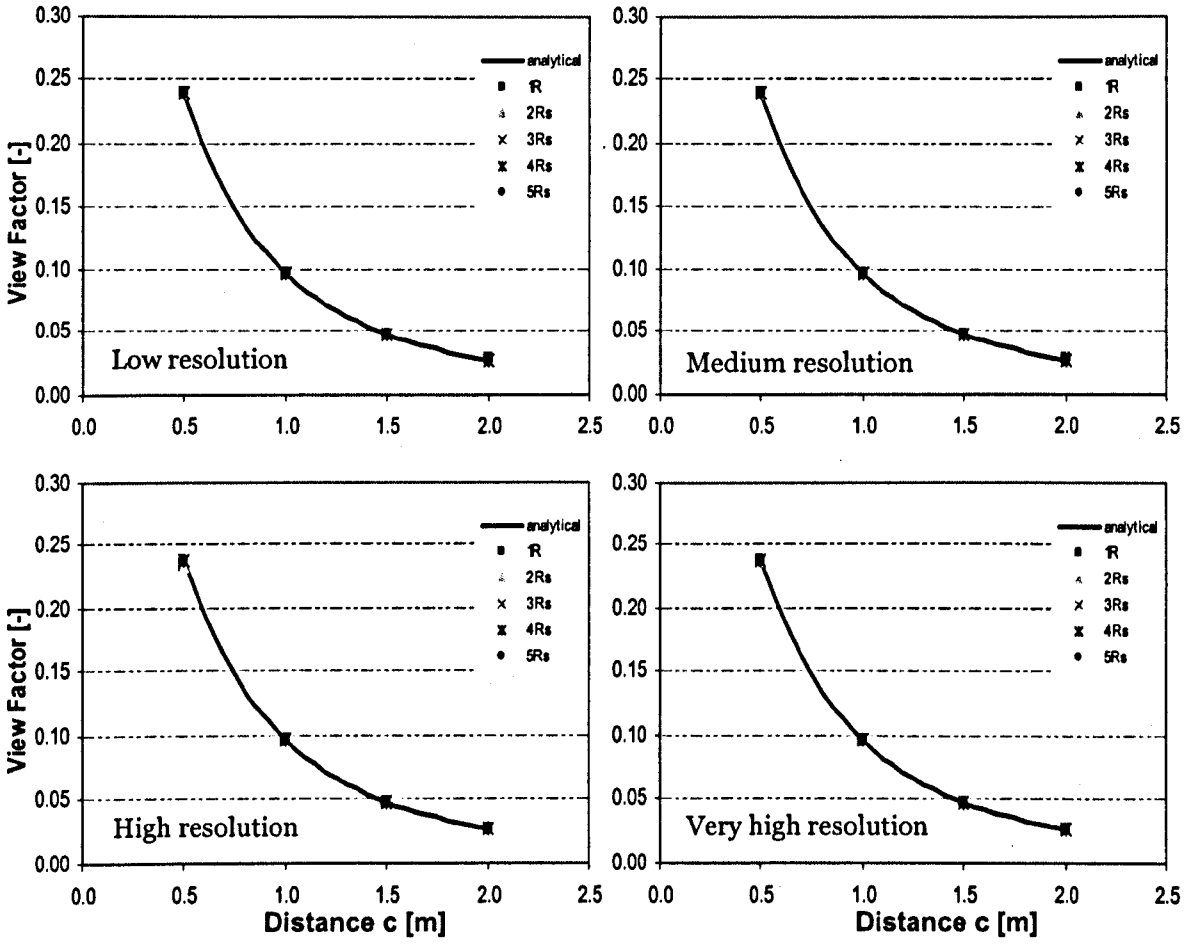

Figure 3.4 View factor between cylinder and plate (φ_{cp}), *case a*.

Also in this case, a very good agreement between analytically and numerically calculated view factors was achieved for all distances, resolutions, and numbers of rays for both, *case a* and *case b* (see *Figure 3.4 and 3.5*).

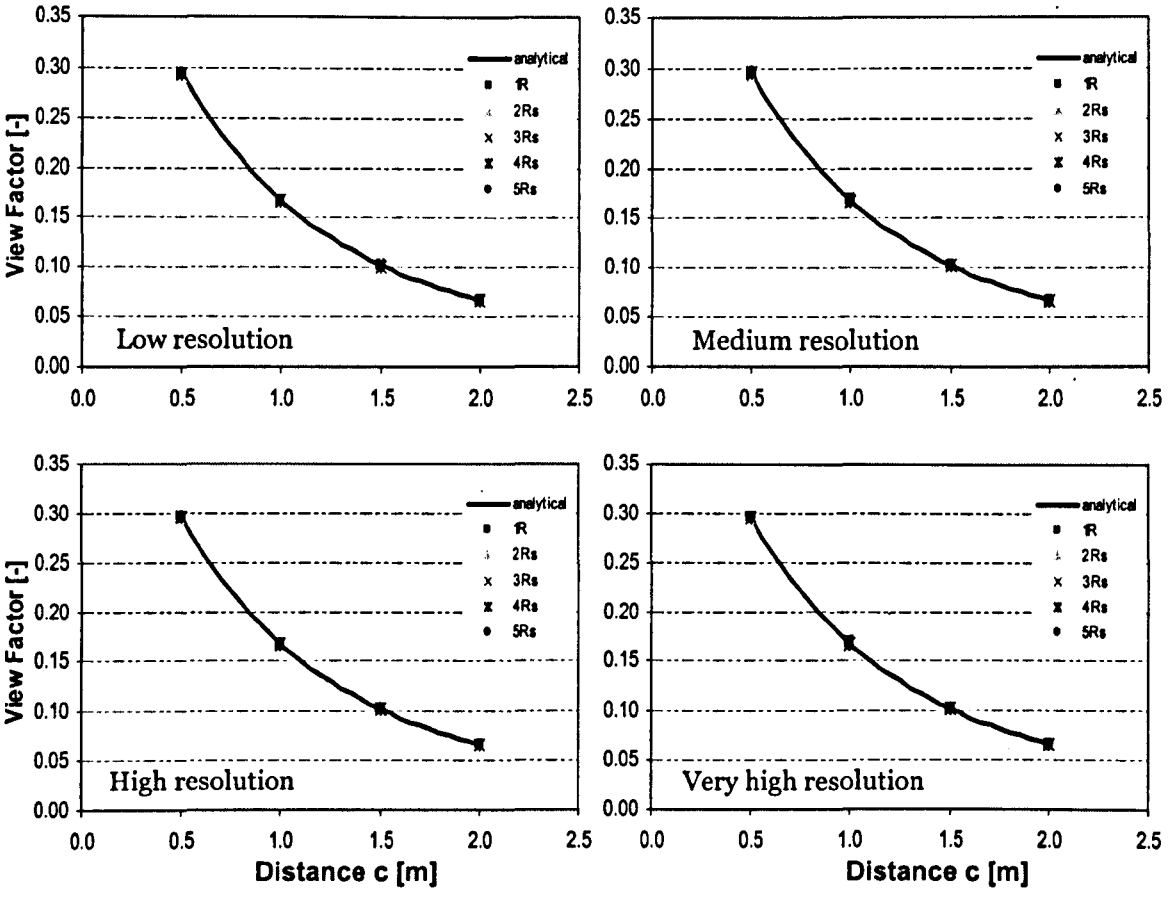

Figure 3.5 View factor between cylinder and plate (φ_{cp}), *case b*.

The average relative error varied between 0.24% and 0.71% and 0.15% and 0.75% for *case a* and *case b*, respectively (*Appendix A, Table A3 and A4*). In contrast to plates, the relative error clearly decreased when the geometrical resolution of the cylinder increased in both *case a* and *case b*. However, no effect of the resolution of the surface of the plane plate on the predicted results was observed. Furthermore, no consistent effect of the number of rays on the accuracy of the results, neither for *case a* nor *case b* was observed but the relative error rose with an increasing distance between the plate and the cylinder.

3.7 Conclusions

Based on comparisons with available analytical solutions for different geometries it could be shown that RadTherm produces sufficiently accurate predictions of view factors. In most cases the accuracy of the numerical results would exceed the accuracy of any experimental trials. Therefore, it was decided to use RadTherm as a numerical simulation tool to perform the detailed analysis of the human radiative heat exchange in the next stages of the work.

A general tendency of improved accuracy was observed for all geometries when using higher resolutions. Particularly, in the case of cylinders the higher resolutions ensured improved levels of result accuracy. There was no significant effect of the number of rays on the relative error. Excepting results obtained using setting 1 (fastest) which produced the largest relative error, the results obtained for using setting 2, 3, 4 and 5 were of a comparable accuracy and sufficient for practical use.

In order to obtain the most appropriate practical solution when using RadTherm, it seems necessary to consider both the precision of the results and the time required to obtain a solution. The highest resolutions of the geometry and the maximum number of rays required the longest computation times and were associated the highest hardware requirements. These did not justify the little gain on improved accuracy of the results. For most practical applications a 'medium resolution' combined with the voxel-based ray tracing calculations using setting 2-4 was felt to be the best compromise between accuracy, computational time and hardware requirements.

Chapter 4

Human projected area factors for detailed direct and diffuse solar radiation analysis

4.1 Introduction

Radiative heat exchange with the environment plays an important role in human heat transfer and thermal comfort. In buildings, occupants are frequently exposed to inhomogeneous radiation e.g. in the proximity of cold windows, hot radiators, or due to solar radiation transmitted through glazed façades. Such asymmetric conditions can make indoor environments thermally uncomfortable cause restrictions in the usability and functionality of spaces and reduce occupants' productivity in the work place. In cars and aircraft cabins such uncomfortable conditions can slow down the reactions of drivers and pilots. Critical, life-threatening situations arise for people such as firefighters on duty or workers in metal work factories who are exposed to thermal radiation from fire and intense heat.

Outdoors, both direct and diffuse solar radiation can reach levels at which the impact on human thermal comfort and the perceived outdoor temperature is overwhelming. Besides perceptual effects, there are various health implications of human exposure to solar radiation that require a careful consideration, Kimlin et al. (2002). Thereby, a detailed knowledge of the human radiant geometry and its local characteristics is required in cases where the risk of skin injury arises. During exposures to extremely low ambient temperatures, for example, the amount of solar irradiation at individual body parts, such as the face, needs to be considered to adequately assess the risk of frostbite and

allowable exposure times. Similarly, the risk of injury due to overdose of UV-radiation depends on the local radiation geometry of exposed body parts rather than on global quantities. Despite the need for local characteristics, however, only the overall radiation data for the human body as a whole is available.

The amount of solar radiation received by a person depends on the projected area factor (f_p) as a geometry-related, direction-dependent radiation parameter of the human body. Over decades the human projected area factors and solar heat load have been subject to various experimental investigations. Underwood and Ward (1966), for example, measured projected area factors of 25 standing male and female persons using photographic methods. The authors developed empirical formulae for predicting the f_p-factors of the human body as a whole based on measurements obtained for 7 different altitudes and 3 solar azimuth angles.

Fanger (1970) carried out extensive experimental trials to determine the projected area factors of 20 male and female subjects in the standing and sedentary position for azimuth and altitude angles between 0° to 180° and 0° to 90°, respectively. In these experiments the camera was positioned at a relatively large distance (about 7m) from the subjects to simulate the case of parallel rays from direct solar radiation. The original results were presented in form of graphs. Other authors (e.g. Steinman et al. 1988; Rizzo et al. 1991) have used Fanger's data to developed formulae for calculating the human projected area factors for use in computerised procedures. More recently, Jones et al. (1998) measured projected area factors of a full-scale manikin for a range of azimuth and altitude angles between $0° < \alpha < 180°$ and $-90° < \beta < +90°$ (referring to the centre of the body) using a similar method employed by Fanger. The distance between the camera and the manikin however was set at 4.3m and 3.7m for positive and negative altitude angles, respectively. In contrast to other experiments, Jones et al. (1998) did not only measure the overall projected area factors of the body as a whole but also provided local quantities for individual body segments. Also alternative approaches to projected area factor concept to calculate solar heat load on human body have been developed by various authors, e.g. Breckenridge and Goldman (1972), Blazejczyk et al. (1992).

Blazejczyk (1996), for example, proposed equations for assessing the amount of solar radiation absorbed by man using basic meteorological parameters.

To date, sophisticated computer simulation software tools are available which make detailed modelling of the human radiative heat exchange with the surrounding environment possible. There is a growing interest to predict human physiological and perceptual responses in various disciplines of science and technology, and, over decades, several multi-segmental models of the human thermal system (e.g. Stolwijk 1971; Fiala et al. 1999, 2001 and 2003; Huizenga et al. 2001) have emerged that enable the effect of wide-ranging environmental conditions on human beings to be quantified. In recent years also software have become available using which detailed 3D models of the human body geometry can be generated for almost any body posture. Diverse CFD packages and thermal analysis tools are capable of predicting radiation exchange dealing with highly complex and boundary conditions geometries (such as the human body).

The level of detail and the accuracy in prediction make today's numerical radiation models superior to experimental investigations in several respects. There are hardly any restrictions regarding the considered geometrical configurations; the simulations can be run with the high intensity source at an infinite distance from the human body for any solar angle that can be exactly adjusted. In addition to direct radiation, it is also possible to study diffuse solar radiation effects for which no experimental results seem to exist. Predictions include detailed information on the solar irradiation mapping over the three dimensional human body surface. Besides overall body data, it is thus possible to obtain information also on the effect of local body characteristics which is required for detailed human radiation analysis.

Over the past years, several studies of the human radiative heat exchange have been carried out using numerical methods. Miyazaki et al. (1995), for example, considered the human body as consisting of several cylindrical parts and verified measured effective radiation area factors of the human body using the Monte Carlo method. Tanabe et al. (2000) used realistic 3D geometry models and solar heat gain calculations to predict projected area factors with respect to

direct solar radiation for sedentary and standing subjects. As most experimental studies, however, overall human radiation data rather than local quantities were provided.

In this study numerical simulation techniques and detailed geometry models are used to predict projected area factors for individual segments of the human body. The aim of the work is to develop formulae for predicting local f_p–factors of standing and sedentary humans with respect to both direct and diffuse solar radiation that scientists and engineers can use to perform detailed short-wave radiation analysis e.g. in conjunction with models of human thermoregulation, facial cooling, or models for predicting the UV-dose at exposed body parts.

4.2 Methodology

4.2.1 Human body models

The human body for both the standing and sedentary posture, was modelled as having left-right symmetry and a stress-free position using commercial software (Curious Labs, 2000). The software enabled generating detailed 3D models of the human body for almost any body postures. Each model consisted of 10995 small surface elements that provided sufficient detail for the radiation simulations (*Figure 4.1*). With a height of 1.75m and a DuBois' area of 1.83 m² this body size was felt as representing an average male subject, DuBois (1916). The elements were grouped together into 19 main body parts (*Table 4.1*) subdivided into 59 spatial sectors (*Figure 4.2*) for which the local projected area factors were to be modelled.

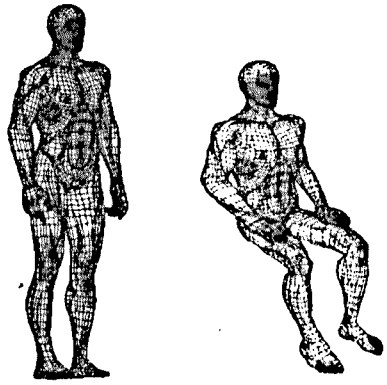

Figure 4.1 The human body geometry model used in the study.

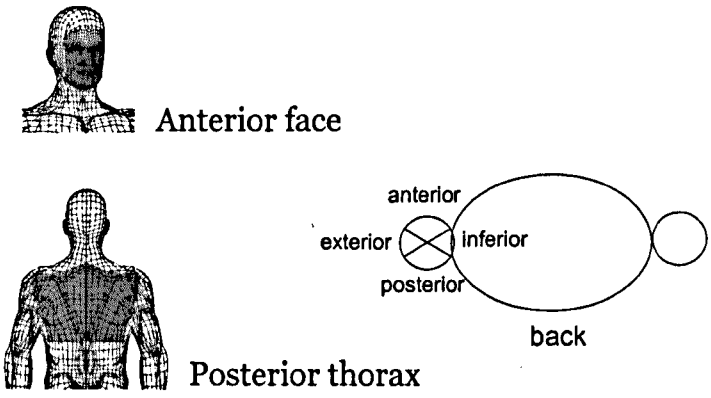

Figure 4.2 Subdivision of the humanoid into individual body sectors.

Table 4.1 Surface areas of individual body sectors.

Body parts	Body sectors	Surface area [m²]	Body parts	Body sectors	Surface area [m²]
Head	Head	0.0525	Lower arm (L/R)	Anterior	0.0092
	Forehead	0.0050		Exterior	0.0269
Face	Anterior	0.0193		Inferior	0.0268
	Exterior (L/R)	0.0110		Posterior	0.0124
Neck	Anterior	0.0050	Hand (L/R)	Handback	0.0285
	Exterior (L/R)	0.0094		Palm	0.0276
	Posterior	0.0068			
Shoulder	Left	0.0205	Upper leg (L/R)	Anterior	0.0466
	Right	0.0205		Exterior	0.0503
				Inferior	0.0407
				Posterior	0.0386
Thorax	Anterior	0.1115	Lower leg (L/R)	Lower anterior	0.0254
	Inferior (L/R)	0.0093		Lower exterior	0.0390
	Posterior	0.0916		Lower inferior	0.0335
				Lower posterior	0.0372
Abdomen	Anterior	0.1104	Foot (L/R)	Instep	0.0400
	Inferior (L/R)	0.0401		Sole	0.0203
	Posterior	0.1091			
Upper arm (L/R)	Anterior	0.0144			
	Exterior	0.0292			
	Inferior	0.0098			
	Posterior	0.0143			

4.2.2 Radiation simulations

The humanoid geometries were imported into a thermal analysis software package (ThermoAnalytics, 2001) which uses a voxel-based ray tracing technique to predict the absorbed short-wave radiation energy at each of the 10995 surface elements. The scheme subdivides the scene to be ray-traced into small volume elements, or voxels. Rays were cast from each element to all other surrounding voxels and the high intensity source and the intersections were determined. The software calculated the amount of solar flux, $Q_{a,i}$, absorbed by each surface element from the incident solar radiation using the elements' short-wave absorptivities and the apparent areas predicted by the voxel based ray-tracing scheme. At this stage the surface elements were defined as black body radiators with an absorptivity of one to simplify the subsequent calculations. The results were then postprocessed integrating the elemental fluxes to obtain projected area factors for individual body sectors. Thereby, the total amount of short-wave radiation absorbed by a body sector consisting of n surface elements was obtained as the sum of predicted nodal quantities, $Q_{a,i}$. For a group of surface nodes, the projected area factor, f_p, which is defined as the ratio between the projected area and the actual surface area of a sector, is thus presented as:

$$f_p = \frac{1}{S} \times \frac{\sum_{i=1}^{n} Q_{a,i}}{\sum_{i=1}^{n} A_i} \tag{4.1}$$

where f_p = projected area factor of an individual body sector, [-]
$Q_{a,i}$= solar radiation absorbed by surface element, i, [W]
S = incident solar radiation flux, [Wm^{-2}]
A_i = area of surface element, i. [m^2]

The projected area factors were calculated for both direct and diffuse short-wave radiation. For the direct short-wave radiation, the simulation procedure calculated the projected area factors across a range of azimuth angles, α, from

0° to 360° (due north, clockwise) and altitude angles, β, from −90° to 90° (*Figure 4.3*). For the diffuse short-wave radiation case, the projected area factors were calculated by varying the ground albedo, ρ_g, between 0 and 1 (assuming isotropic, i.e. homogeneously radiating sky).

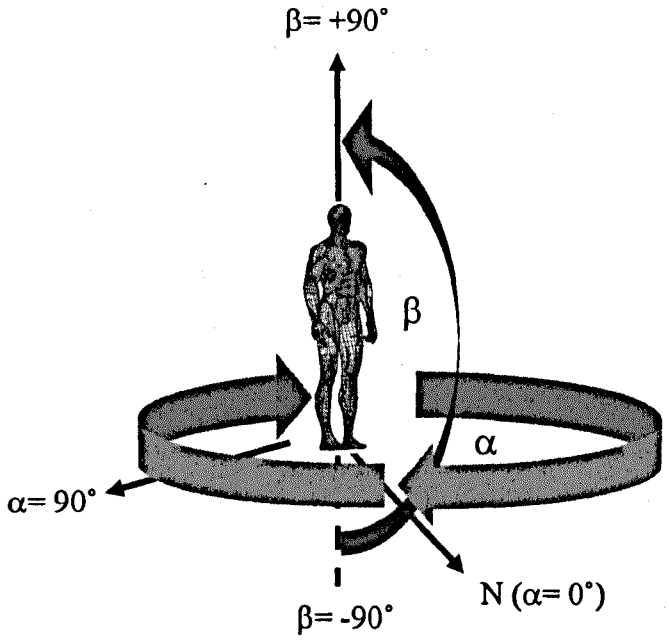

Figure 4.3 Variation of the solar altitude (β) and azimuth angle (α) in the study.

4.2.3 Regression analysis

Simple and polynomial regression was used to develop the equations. In case of direct solar radiation the f_p-factors were considered as functions of the solar azimuth and solar altitude angles α and β, and as functions of the ground albedo ρ_g in case of diffuse solar radiation. If any regression coefficient was not significantly different from zero at the 0.95 confidence level, a new regression was run without the non-significant variable. The two-tailed population *t*-test was applied to determine the significance level of the regression coefficients.

4.3 Modelling local projected area factors

4.3.1 Direct solar radiation

Analysis of the post-processed data indicated that for most parts of the human body the projected area factor curves for direct solar radiation (i.e. with respect to parallel rays) can be described as periodic, i.e. *cosine* or *sine* functions of the solar azimuth angle, α. As an example, the projected area factors predicted by the ray-tracing technique for the posterior thorax of a standing person are plotted in Figure 4.4.

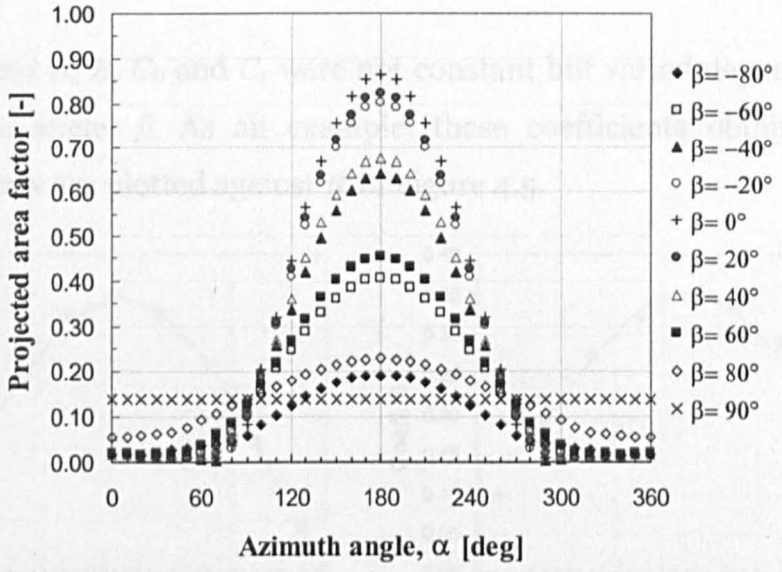

Figure 4.4 The course of projected area factors predicted for the posterior thorax of a standing person.

The trend of each curve can be commonly described using the following mathematical expression:

$$f_{p,dir} = A\cos(C_1\alpha + C_0) + B \tag{4.2}$$

where $f_{p,dir}$ = projected area factor of the body sector for a given β, [-]

α = azimuth angle, [rad]

C_1, C_0 = regression coefficients, [-]

and $$A = \frac{f_{p,\max} - f_{p,\min}}{2} \quad (4.3)$$

$$B = \frac{f_{p,\max} + f_{p,\min}}{2} \quad (4.4)$$

$f_{p,max}$ = the maximum projected area factor, [-]

$f_{p,min}$ = the minimum projected area factor. [-]

The coefficients C_1 and C_0 were determined by regression analysis using a rearranged equation (4.2):

$$\cos^{-1}\left(\frac{f_p - B}{A}\right) = C_1\alpha + C_0 \quad (4.5)$$

The coefficients A, B, C_0 and C_1 were not constant but varied depending on the solar altitude angle, β. As an example, these coefficients obtained for the posterior thorax are plotted against β in Figure 4.5.

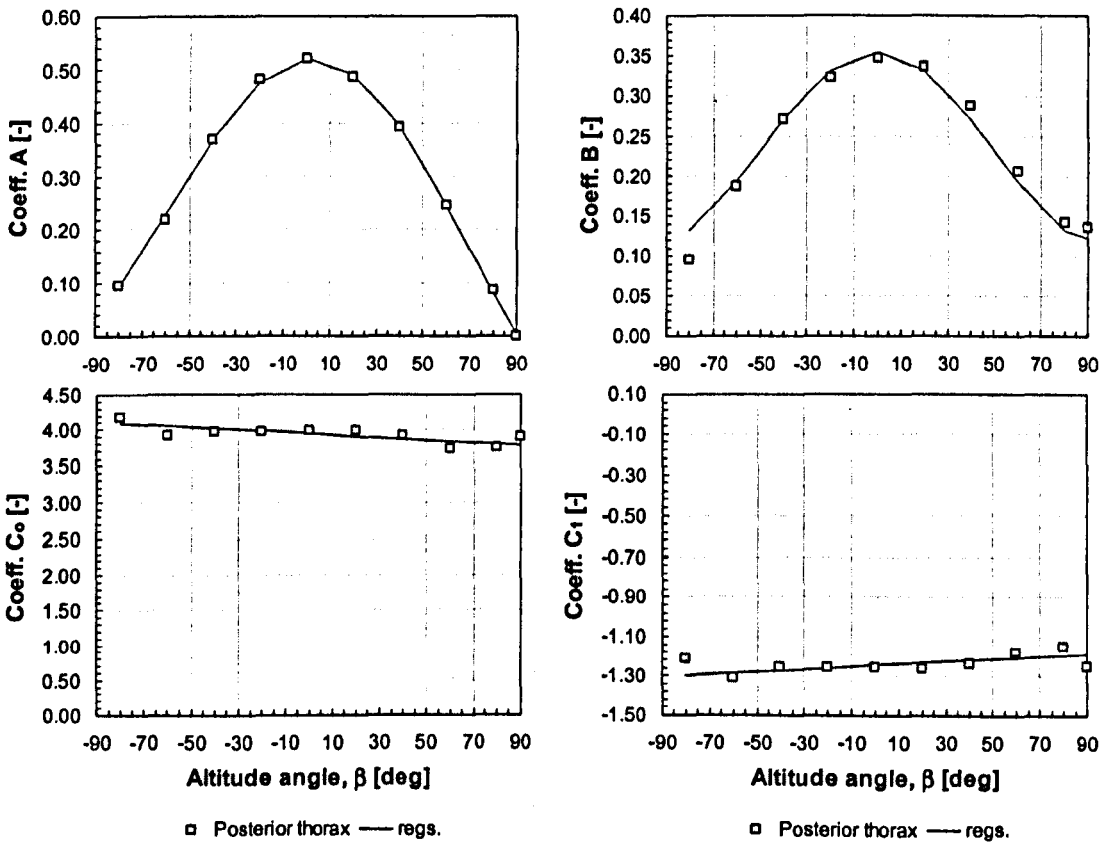

Figure 4.5 The regression coefficients for the posterior thorax body sector.

The functions of these coefficients were determined using polynomials up to an order of four (see *Appendix B, Tables B.1 to B.3*).

In contrast to body parts that were fully exposed to the beam of direct radiation, equation 4.2 did not perform well for sectors that were hidden/partly hidden by other body parts at certain solar angles. As an example, in Figure 4.6, such discrepancies between simulated data and f_p-factors predicted using equation 4.2 are apparent for azimuth angles $210° < \alpha < 350°$ where the shoulder was 'shaded' by the head.

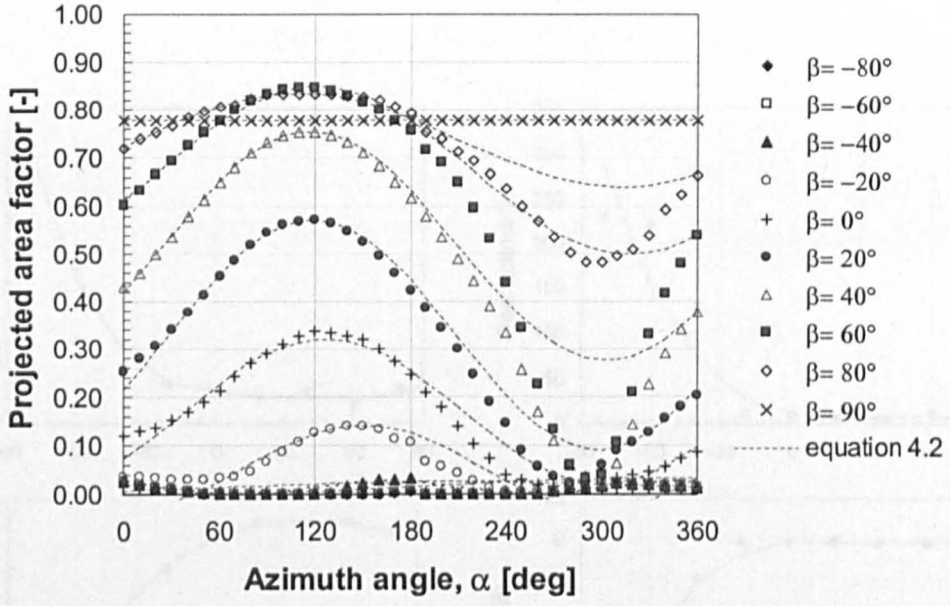

Figure 4.6 Inadequacy of equation 4.2 to predict f_p-factors for sun positions where the body sector (right shoulder, standing posture) was hidden by another body part.

It was, therefore, necessary to account for this 'shading' effect by modelling the so called 'shading-function' as a part of the final solution for each body sector. For this purpose, equation (4.2) was extended as follows:

$$f_{p,dir} = [A\cos(c_1\alpha + c_0) + B] \times S_h \qquad (4.6)$$

where S_h is the shading function.

To model S_h, a number of different concepts were developed and tested. Thereby, the use of *tanh* functions turned out to be the most suitable approach:

$$S_h = 1 + \frac{\tanh(D_1\alpha + D_0)}{2} + \frac{\tanh(E_1\alpha + E_0)}{2} \tag{4.7}$$

where D_1, D_0, E_1, and E_0 represent coefficients to be determined by regression analysis. Also these coefficients depended on the solar altitude, β, as shown for the shoulder body elements in Figure4.7. The results of the polynomial regressions for each coefficient are listed in Appendix B (*Tables B.4 to B.7*).

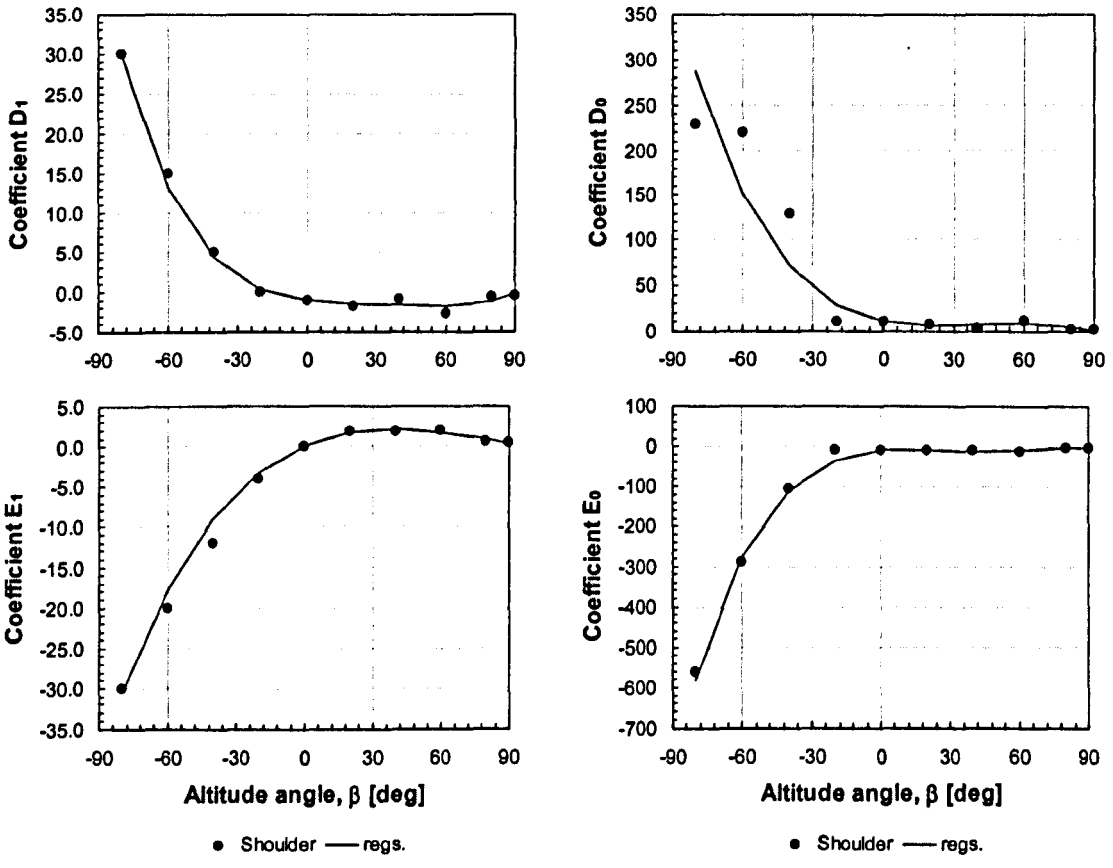

Figure 4.7 The regression coefficients of the shading function for the shoulder body sector.

Because of the symmetry of the humanoid models used in the study the results obtained for the right-hand body parts were applicable also to the left-hand side

body element. For left-hand side body sectors, however, the reverse azimuth angle $\alpha^* = 2\pi - \alpha$ has to be used with equation (4.6) and (4.7).

4.3.2 Diffuse solar radiation

In case of diffuse solar radiation the projected area factors, $f_{p,dif}$ could be described as linear functions of the ground albedo for each body part:

$$f_{p,dif} = g_1 \rho_g + g_o \qquad (4.8)$$

where $f_{p,dif}$	=	projected area factor of an individual body sector,	[-]
ρ_g	=	ground albedo,	[-]
g_0 and g_1	=	regression coefficients of individual body sector.	[-]

The results of the regression analysis are provided in Appendix B (*Table B.8*).

4.4 Results

In the verification and validation process to which the new model was subjected, the predictions of the $f_{p,dir}$-factors (equation 4.6) for each body sector of the standing and the sedentary human were first verified against simulation results obtained by the voxel-based ray tracing technique.

The results obtained for the head and the posterior thorax of the standing person exposed to the direct solar radiation are shown in Figure 4.8. The irradiation of solar rays on both sectors was not obstructed by other body parts. In both cases the $f_{p,dir}$-curves therefore exactly replicated the cosine function as described by Equation 4.2. As can be seen, the predictions agreed well with the results of the ray-tracing simulations across the whole range of the azimuth and altitude angles, α and β.

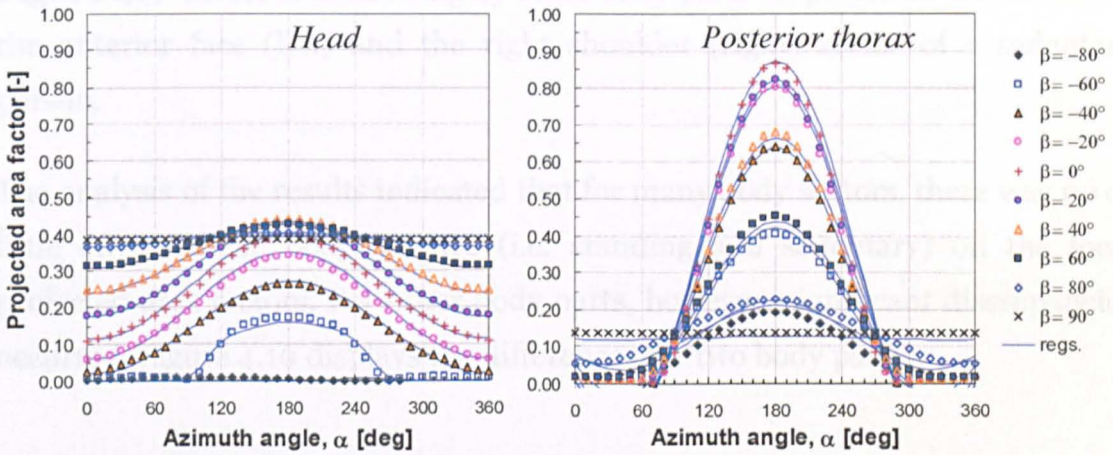

Figure 4.8 Comparison of predicted and simulated projected area factor for two 'unshaded' body parts i.e. head (left) and posterior thorax (right) of the standing person.

Some partly significant deviations from the ideal cosine-shape trend are apparent from Figure 4.9 in which the $f_{p,dir}$-factors are plotted for the anterior face and the right shoulder. For the case of anterior face the upper legs of the sedentary posture hindered a full irradiation of solar rays on this body part causing a remarkable fall in $f_{p,dir}$ at a solar altitude of β = -60°. In case of the

right shoulder the appreciable discrepancies from an ideal cosine-shape observed for $0° < \beta < 60°$ between $210° < \alpha < 330°$ were caused by the head. The shading function of the regression model accounted appropriately for these shadowing effects.

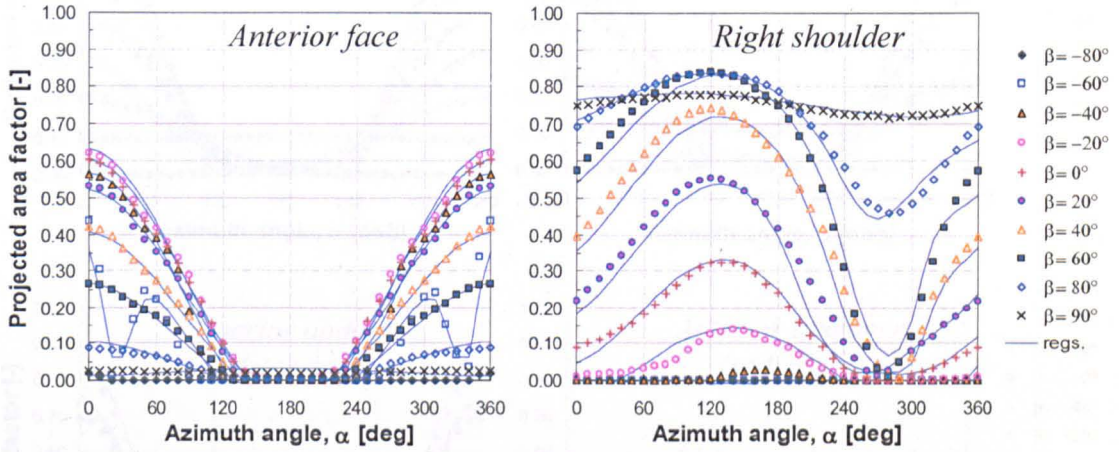

Figure 4.9 Effect of shadowing by other body parts on projected area factor of the anterior face (left) and the right shoulder (right) sector of a sedentary person.

The analysis of the results indicated that for many body sectors, there was no or little effect of the body posture (i.e. standing and sedentary) on the local projected area factors. For other body parts, however, significant discrepancies occurred. Figure 4.10 displays the differences for two body parts.

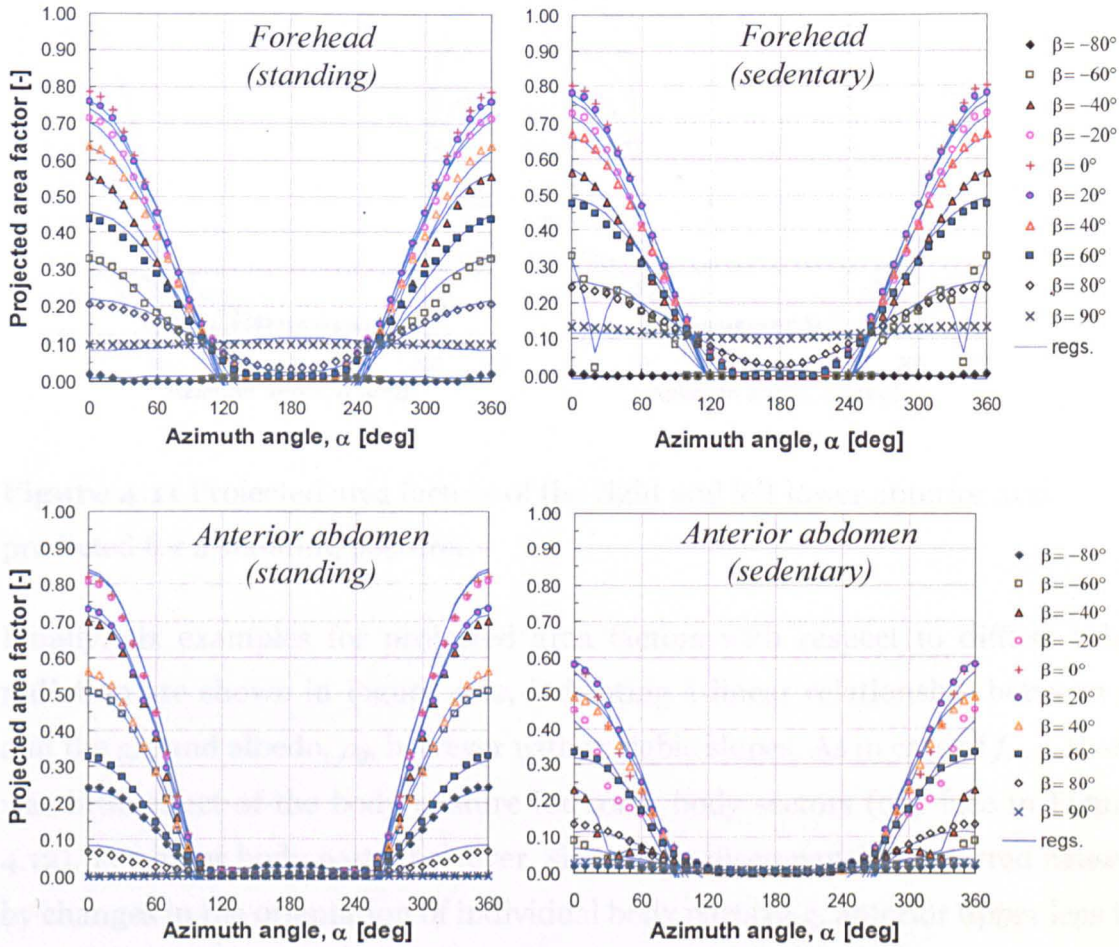

Figure 4.10 The effect of body posture on the local projected area factors of the forehead and the anterior abdomen.

For symmetry reasons, the local projected area factors were modelled explicitly only for the right-hand side body elements. The application of these regression results to both, the right and the left lower arm (anterior) is demonstrated in Figure 4.11. As described previously the reverse azimuth angle $\alpha^* = 2\pi - \alpha$ was used with equations (4.6) and (4.7) to predict the $f_{p,dir}$-factors of the left hand-side body part in Figure 4.11 (right).

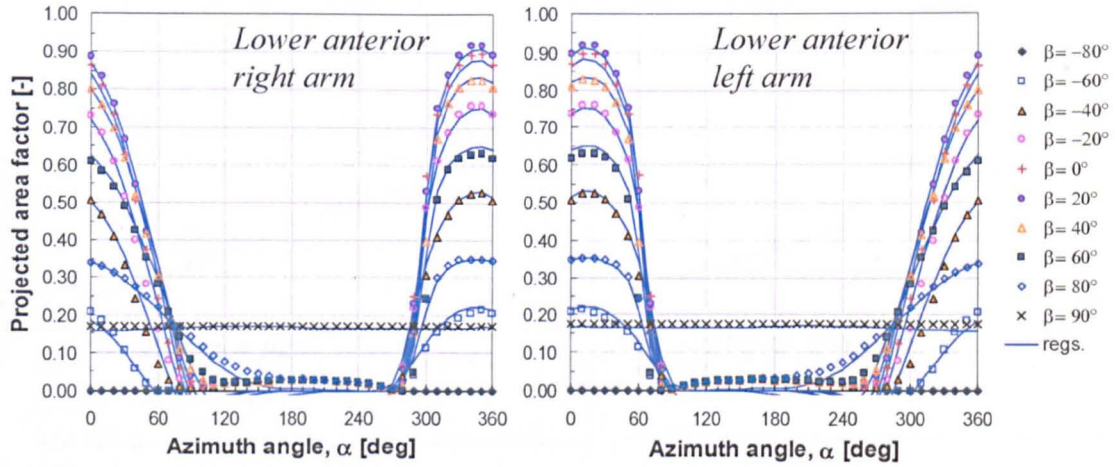

Figure 4.11 Projected area factors of the right and left lower anterior arm predicted for a standing posture.

Finally, six examples for projected area factors with respect to diffuse solar radiation are shown in Figure 4.12, indicating a linear relationship between f_p and the ground albedo, ρ_g, however with variable slopes. As in case of $f_{p,dif}$, there was little effect of the body posture for some body sectors (e.g. face in Figure 4.12). For other body parts, however, significant discrepancies occurred caused by changes in the orientation of individual body parts (e.g. anterior upper legs in *Figure 4.12*) and/or shadowing effects through other body parts (anterior abdomen in *Figure 4.12*).

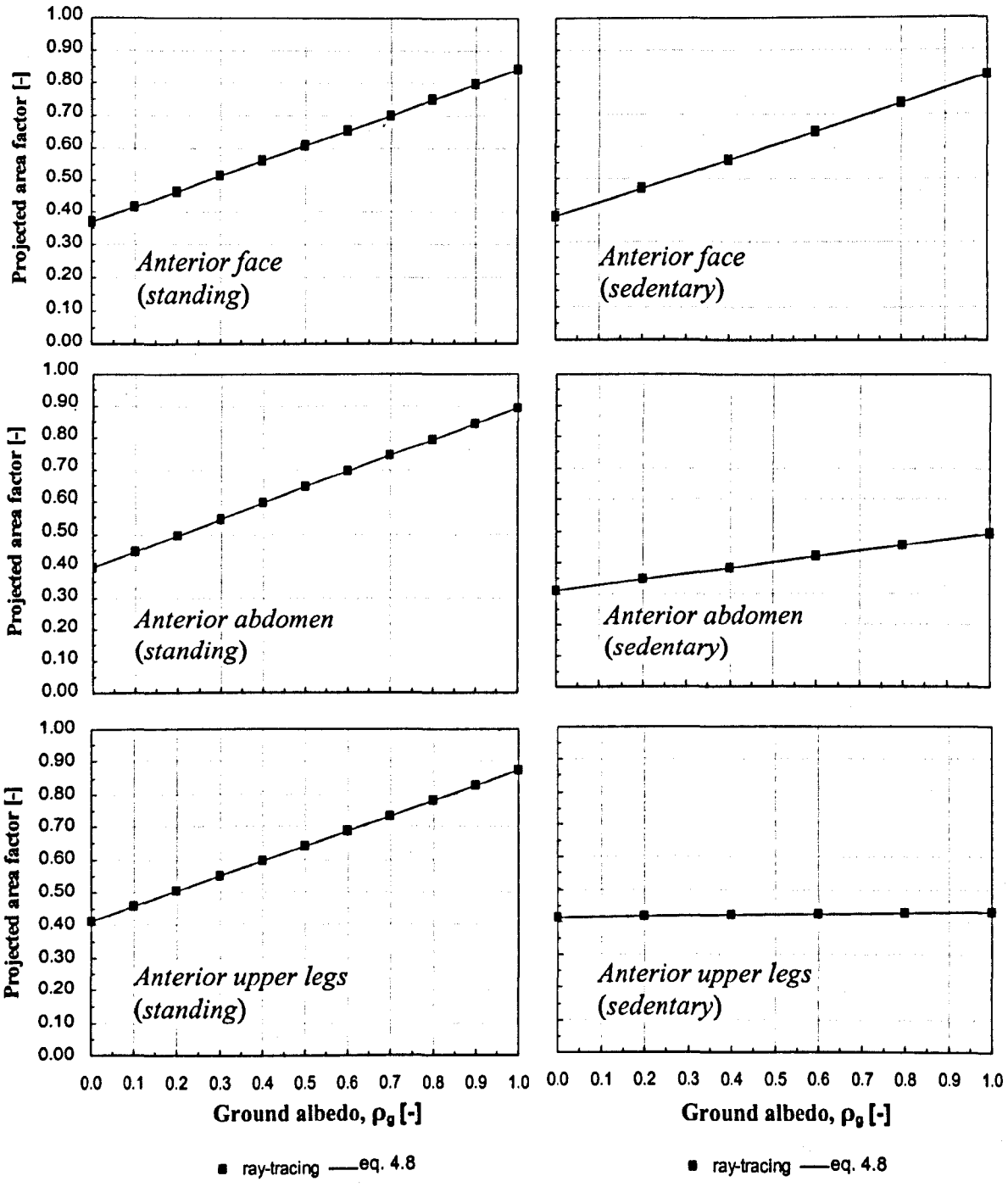

Figure 4.12 Projected area factor curves for diffuse solar radiation of the anterior face (standing and sedentary), anterior abdomen (standing and sedentary) and upper anterior legs (standing and sedentary).

4.5 Validation and discussion

To date, most experimental data is available just for the whole human body. To enable a comparison with measurements, the predicted results obtained for individual body sectors were therefore integrated over the whole body surface. Furthermore, in most cases, experimental f_p-factors have been presented as a ratio of the projected body area and the effective radiation area (rather than the actual surface area). For validation purposes hence also the predicted values were weighted by the effective radiation area factor of the humanoid model used in this study (f_{eff} = 0.84 and 0.78 for the standing and sedentary posture, respectively).

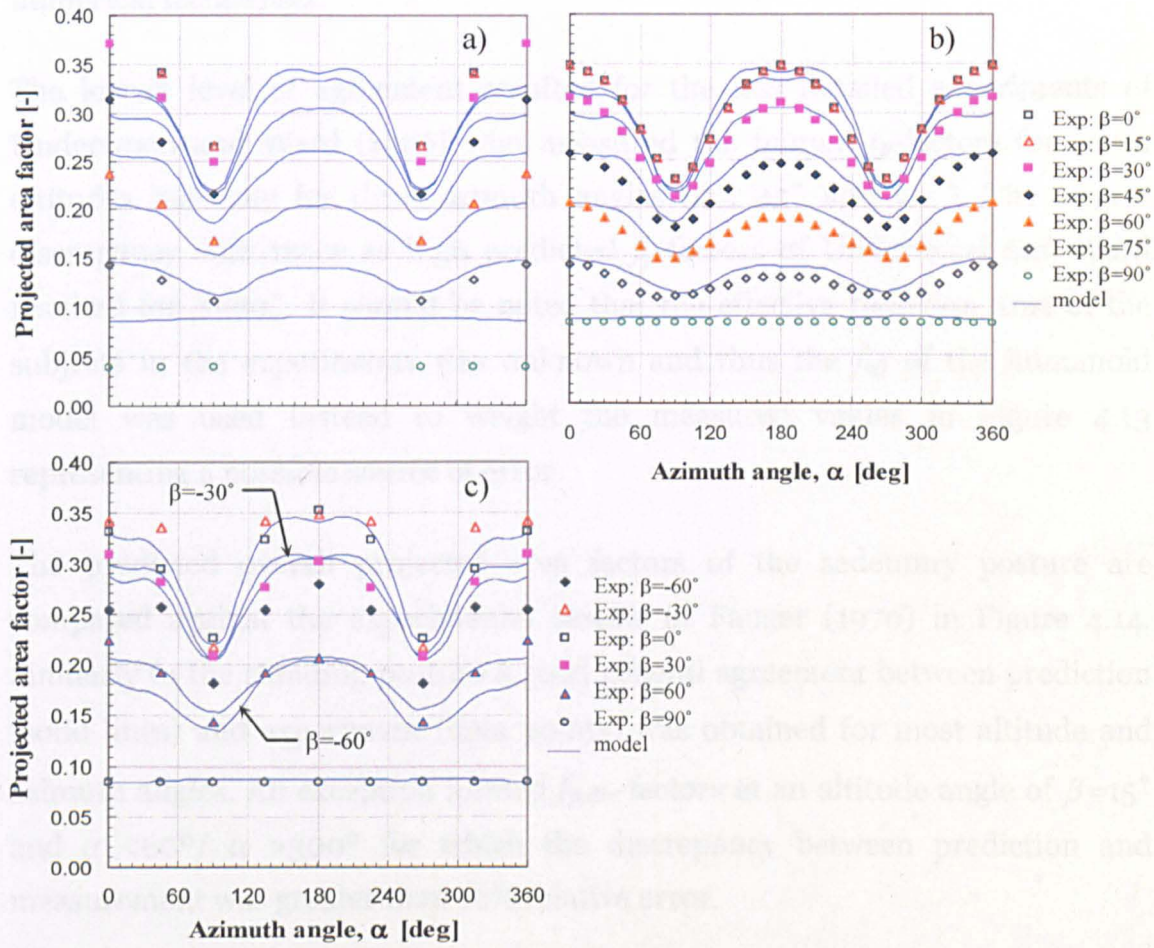

Figure 4.13 Comparison of predicted projected area factors for the whole body in standing posture with experimental results obtained by:

a) Underwood and Ward (1966); b) Fanger (1970); and

c) Jones et al. (1998).

The results for the standing posture are compared with measured data obtained by Underwood and Ward (1966), Fanger (1970) and Jones et al. (1998) in Figure 4.13. The marks indicate the experimental results whereas lines represent the predicted overall projected area factors as integrated over the humanoid's surface. Generally, the best agreement between predicted and measured values was achieved for the detailed experiments carried out by Fanger (1970). For most altitude and azimuth angles the discrepancy was typically about 5% relative error. Greater discrepancies resulted for the overall $f_{p,dir}$-factors measured by Jones et al. (1998) at β=-30° and β=-60°. For these altitude angles, however, the measured quantities were partly greater than for frontal exposures which seems less plausible and difficult to reproduce by rigorous numerical techniques.

The lowest level of agreement resulted for the less detailed experiments of Underwood and Ward (1966) who measured the human f_p-factors for seven altitudes but only for three azimuth angles (0°, 45° and 90°). The largest discrepancy with twice as high predicted f_p-factors of Underwood and Ward resulted for β=90°. It should be noted that the effective radiation area of the subjects in the experiments was unknown and thus the f_{eff} of the humanoid model was used instead to weight the measured values in Figure 4.13 representing a possible source of error.

The predicted overall projected area factors of the sedentary posture are compared against the experimental results of Fanger (1970) in Figure 4.14. Similarly to the standing posture a good general agreement between prediction (solid lines) and experiment (data points) was obtained for most altitude and azimuth angles. An exception formed $f_{p,dir}$-factors at an altitude angle of β=15° and α <60°/ α >300° for which the discrepancy between prediction and measurement was greater than 10% relative error.

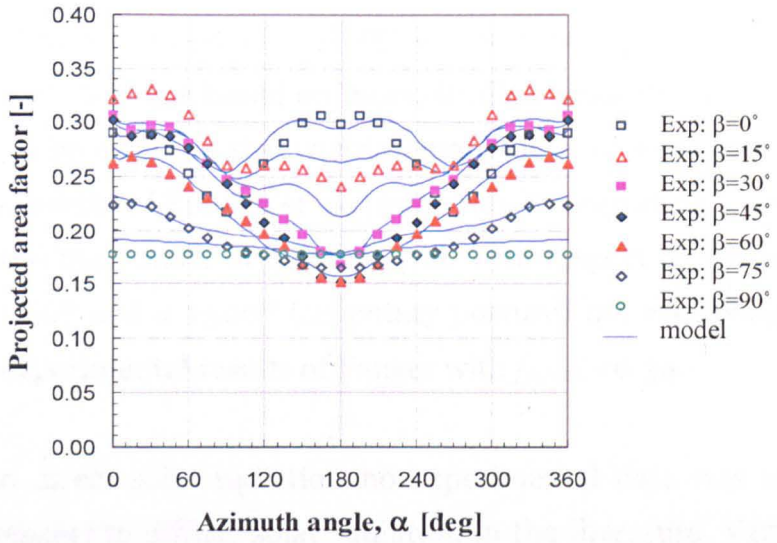

Figure 4.14 Comparison of predicted overall projected area factors for the sedentary posture with experimental results obtained by Fanger (1970).

The results of this study were also compared with the simulation results obtained by other authors. A comparison with the overall projected area factors predicted by Tanabe et al. (2000) for standing and sedentary postures is shown in Figure 4.15.

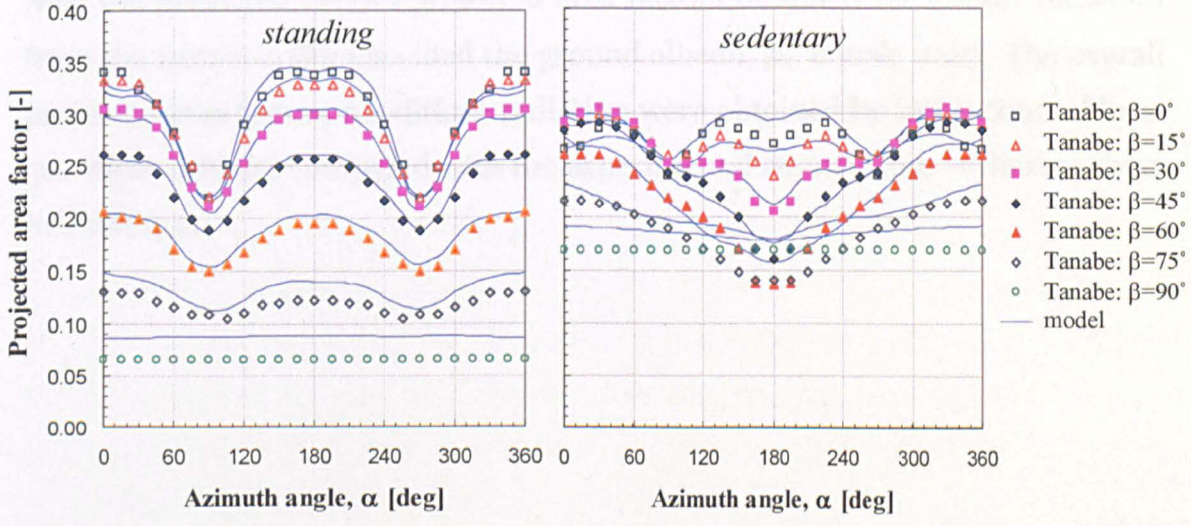

Figure 4.15 Comparison of predicted projected area factors of the whole body with simulation results obtained by Tanabe et al. (2000).

The models agreed with each other within 7% relative error. The greatest relative discrepancies occurred at β=90° for both postures where the present regression model (which is based on more detailed geometry models) predicted the f_p-factors to be closer to the experimental results of Fanger (1970) than to the numerical results of Tanabe et al. (2000). It is interesting to note that this study confirmed the results of Tanabe et al. with respect to the maximum f_p-factors for α <60° and α >300° (sedentary posture) not exceeding 0.31 which contrasts the experimental results of Fanger with $f_{p,max}$ =0.34.

In contrast to direct solar radiation no experimental data was found for f_p-factors with respect to diffuse solar radiation in the literature. Various authors (e.g. Fanger 1970; Horikoshi et al. 1990; Miyazaki et al. 1995; Tanabe et al. 2000), however, reported on measured effective radiation area factors for the human body as a whole. The effective radiation area factor is defined as the ratio between the effective radiation area and the actual surface area of the human body. Thereby, the effective radiation area is that area of the human body that is presented to the environment contributing to the radiation exchange with a diffusely radiating homogeneous enclosure. The experimentally observed human effective radiation area factors could therefore be directly compared with the predicted overall projected area factors obtained for diffuse radiation from the isotropic sky provided the ground albedo, ρ_g, equals unity. The overall projected area factors for diffuse radiation were obtained by integration of local quantities and are compared with the experimental results from various authors in Table 4.2.

Table 4.2 Comparison of predicted overall projected area factors for diffuse solar radiation with measured effective radiation area factors.

Description	Effective radiation area factor			
	Standing posture		Sedentary posture	
	nude	clothed	nude	clothed
Present study	0.84		0.78	
Bedford [a.]	0.82		0.72	
Guibert [b.]	0.73		0.65	
Fanger [c.]	0.73	0.87	0.70	0.77
Horikoshi [d.]	0.80	0.91	0.74	0.80
Miyazaki [e.]	0.83		0.78	
Tanabe [f.]	0.74		0.69	

[a.] Bedford (1935); [b.] Guiber and Taylor (1952); [c.] Fanger (1970);
[d.] Horikoshi et al. (1990); [e.] Miyazaki et al. (1995); [f.] Tanabe et al. (2000).

The results of the present study agreed well (within 5% relative error) with data obtained by Bedford, Horikoshi and Miyazaki but they are greater (13% relative error) than those obtained e.g. by Fanger and Tanabe. It is hypothesized that these discrepancies were due to differences in the body posture considered. In this study the geometry models for both the standing and sedentary posture represented relaxed, stress-free position. In contrast, other studies considered compact geometry models and subjects with extremities closely attached to each other or to the body.

While most investigations have dealt with the overall radiation characteristics of the human body, to date, also some information is available on measured local quantities. In Figure 4.16, the predicted local projected area factors of individual body parts with respect to direct radiation are compared with the corresponding measured data obtain by Jones et al. (1998). To make a comparison possible the predictions referring to individual spatial body sectors were integrated locally to obtain f_p-factors of the body parts according to the experimental set-up. Unfortunately, no experimental data was found with which to compare predicted local f_p-factors for diffuse radiation.

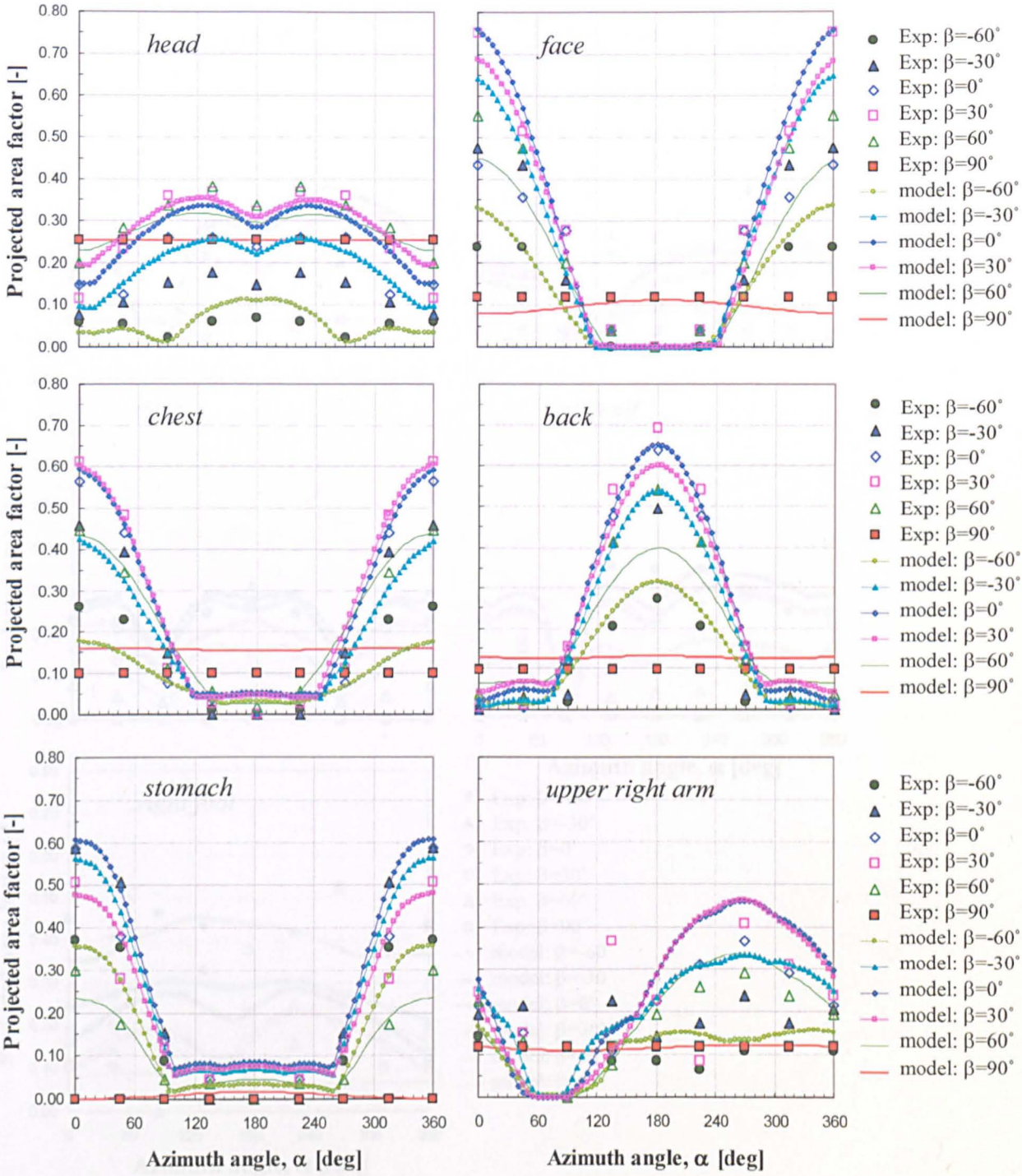

Figure 4.16 Comparison of local projected area factors predicted for individual body parts with measured data using a standing manikin, Jones et al. (1998).

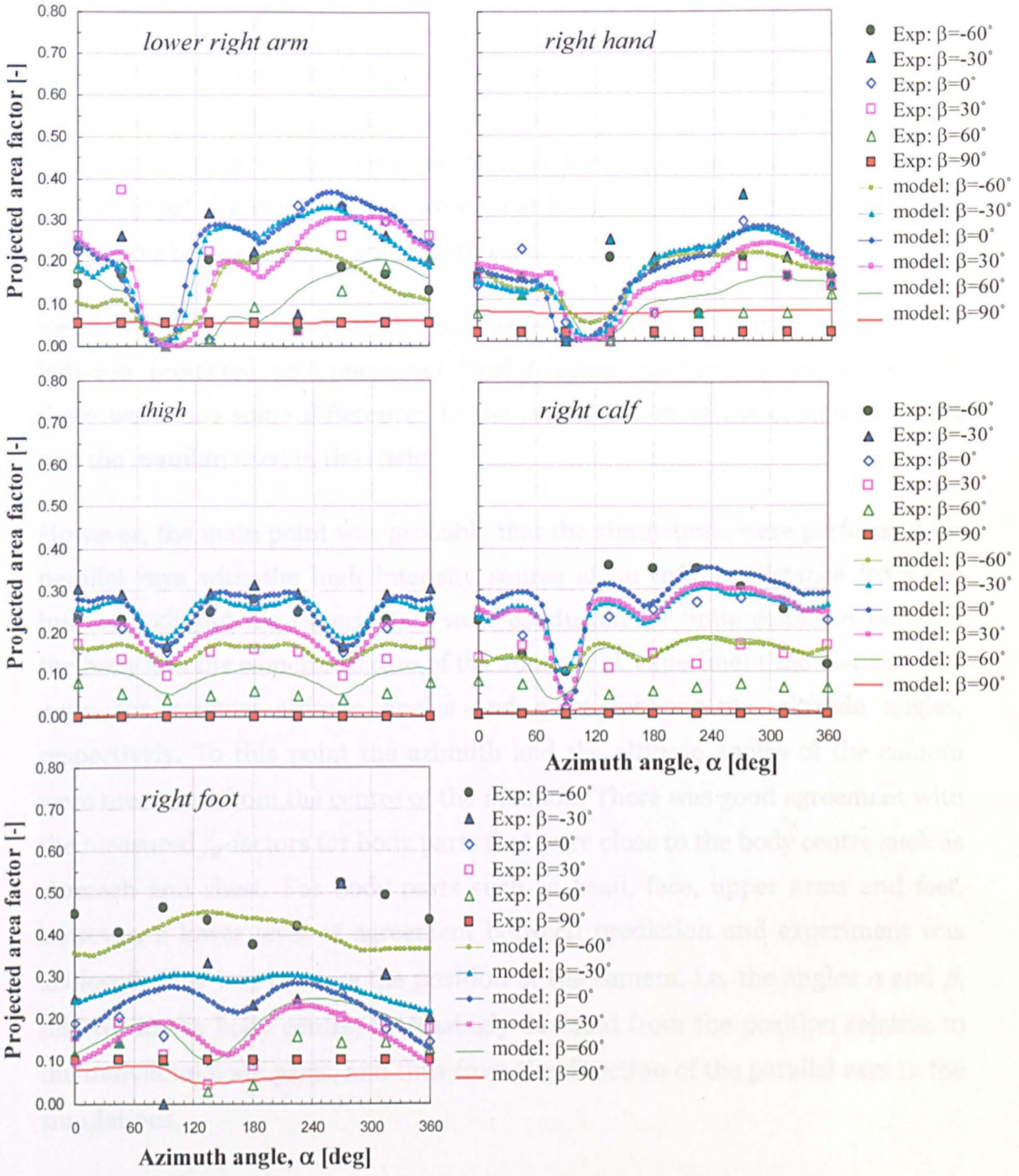

Figure 4.16 (Continued).

As in the case of overall factors, also the predicted local $f_{p,dir}$-factors agreed generally well with the measurements reproducing both the trend and absolute values for most body sectors. The average deviation including all angles and body sectors was $\Delta f_p = \pm$ 0.03. Partly large discrepancies however resulted for non-central body sectors such as feet. A thorough analysis of the results assumed that the discrepancies were most likely associated with the following differences between model and experiment.

Besides differences in posture that were suggested to cause discrepancies between predicted and measured local f_p-values particularly in extremities, there were also some differences in the segmentation of the computer model and the manikin used in the trials.

However, the main point was probably that the simulations were performed for parallel rays with the high intensity source at an infinite distance from the human body but the experiments were conducted for finite distances between the body and the camera. In case of the Jones et al. experiment the distance was 4.3m for positive altitude angles and 3.7m for negative altitude angles, respectively. To this point the azimuth and the altitude angles of the camera were measured from the centre of the manikin. There was good agreement with the measured f_p-factors for body parts that were close to the body centre such as stomach and chest. For body parts such as head, face, upper arms and feet, however, a lower level of agreement between prediction and experiment was achieved. This was because the position of the camera, i.e. the angles α and β, relative to the body centre, increasingly deviated from the position relative to the individual body parts, and thus from the direction of the parallel rays in the simulations.

4.6 Conclusions

In this study, regression equations for predicting local projected area factors of standing and sedentary persons were developed using detailed computer models of the human body geometry and numerical ray-tracing techniques. The new regression model was developed for both diffuse and direct solar radiation. Validation tests showed good general agreement with measured data for both overall and local quantities. Discrepancies between predicted and measured data appeared to be associated mainly with differences in posture and with the fact that the simulations were performed for parallel rays with the high intensity source being at an infinite distance from the body whereas the experiments were performed for finite distances.

The projected area factor equations developed in this study can be used to predict the irradiation and absorption of direct and diffuse solar radiation over the 3D surface of the human body. Bio-meteorologists and other scientists can use the equations to perform detailed analysis of the effect of solar radiation on human beings exposed to outdoor weather conditions. This information can then serve, for example, to develop bio-climatic charts and rationally derived operative temperatures which characterise the outdoor climate conditions including the effect of solar radiation on humans.

The presented equations may prove useful especially when used in conjunction with detailed, multi-segmental models of the human thermoregulatory system and thermal comfort. With these models the thermal effect of direct and diffuse solar radiation on humans and the associated physiological and perceptual implications can be quantified. Another possible application of the equations, besides any thermal effects, is the prediction of the UV-dose and the assessment of the associated health risks and possible injuries to exposed body parts.

Chapter 5

Modelling view factors for individual parts of the human body

5.1 Introduction

View factors are important figures when calculating the long-wave radiative heat exchange between humans and the surroundings. These factors incorporate the effect of body geometry, orientation and the general geometric set up of the enclosure. Literature provides two principal methods of measuring view factors for the human body. One of them is the mechanical integrator method which was used e.g. by Dunkle (1963), who worked out view factor diagrams for a single standing person. The other method used e.g. by Fanger (1970) and Horikoshi et al. (1990) is the photographic method. Most of the recent studies have been conducted using the latter procedure.

Based on measurements using the photographic method, Fanger (1970) has developed view factor diagrams for sedentary and standing persons (see Figures 2.8 to 2.11, Chapter 2) with respect to both vertical and horizontal rectangular plane surfaces. Each diagram displays the view factors of the whole human body as a function of dimensionless distances a/c and b/c between the body and the wall, where a and b are the side lengths of the rectangle and c is the normal distance between the person (his centre) and the rectangle (for more details see Chapter 2, section 2.5.1.4).

Fanger's diagrams were developed for distances between the body and the surface of $c>7$m. Horikoshi et al. (1990) discovered that for distances $c<2$m the view factors between a person and rectangular plane were underestimated by up

to 40% using the Fanger approach. Ozeki et al. (2000) who determined the view factors between the human body and rectangular planes using numerical methods, however, found a better agreement with the Fanger's experimental results for $c \leq 2.0$, as shown in Figure 5.1. The maximum discrepancy reached about 4% for standing and about 7% for sedentary subjects, respectively, Ozeki et al. (2000).

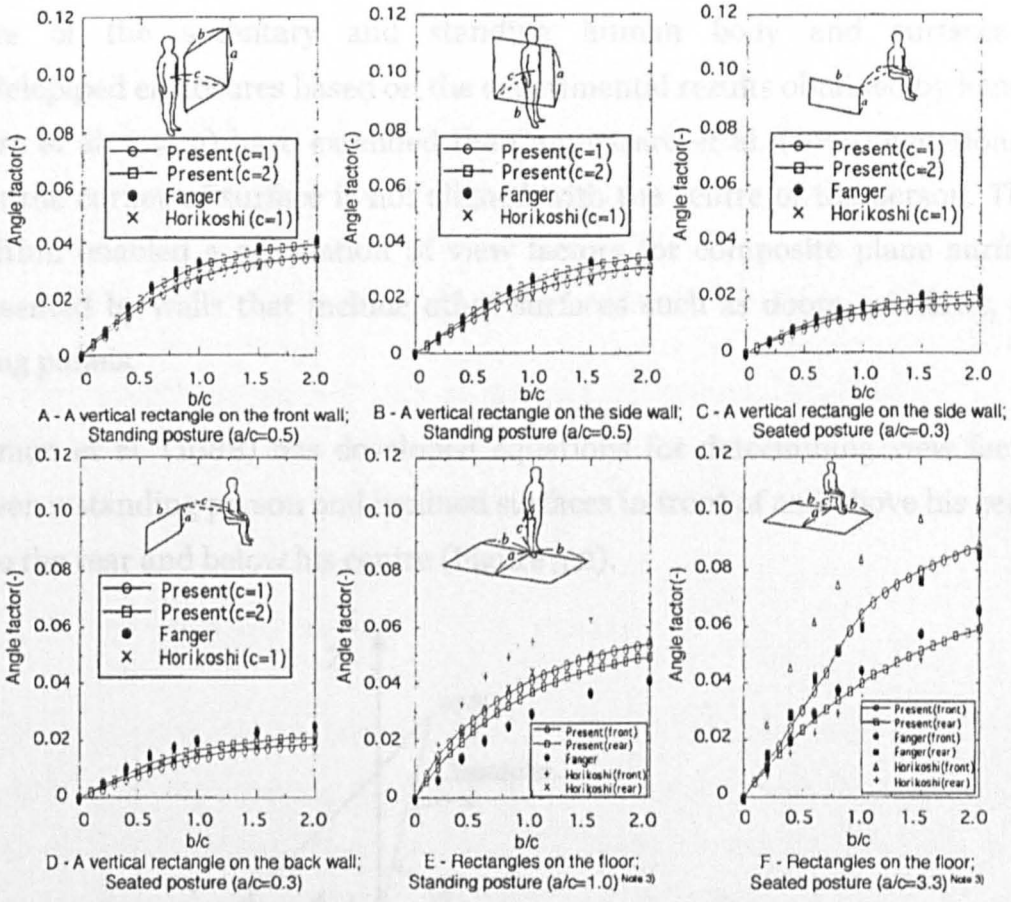

Figure 5.1 Comparison of view factors between human body (standing and seated posture) and rectangular plane surfaces obtained by different authors (Ozeki et al., 2000).

Nevertheless, it seems that human view factors depend on the distance between the human body and surrounding surfaces when defined as a function of the dimensionless distances a/c and b/c as currently used in various standards .

5.1.1 Empirical methods for estimating human view factors

Experimentally obtained view factors have usually been presented as graphs and diagrams. The disadvantage of this presentation method is that graphs or diagrams are inappropriate for computer applications. A number of empirical approaches and equations has therefore been developed by various authors. Cannistraro et al. (1992) have presented a simple algorithm for calculating view factors of the sedentary and standing human body and surfaces of parallelepiped enclosures based on the experimental results obtained by Fanger. Nucara et al. (1999) have extended the Cannistraro et al. (1992) equations in which the corner of surface is not aligned with the centre of the person. Their algorithm enabled a calculation of view factors for composite plane surfaces represented by walls that include other surfaces such as doors, windows, and heating panels.

Steinman et al. (1988) has developed equations for determining view factors between a standing person and inclined surfaces in front of and above his centre and to the rear and below his centre (Figure 5.2).

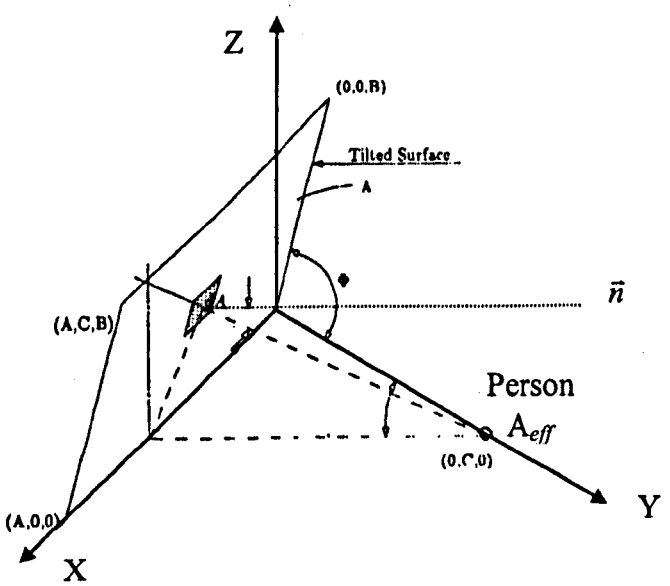

Figure 5.2 Development of view factor between a person and a rectangle at tilt angle Φ (Steinman et al., 1988).

In his work view factors appear as a function of the body's projected area factor, f_p:

$$\varphi_{PA} = \frac{1}{\pi} \int_0^{A/C} \int_0^{B/C} \frac{f_p}{[(\frac{x}{c})^2 + (\frac{z}{c})^2 + (1 - \frac{z}{c \tan \Phi})^2]^{\frac{3}{2}}} d(\frac{x}{c}) d(\frac{z}{c}) \qquad (5.1)$$

where φ_{PA} = view factor between the human body and an inclined surface,

f_p = projected area factor of the human body,

A, B, C= coordinates of the inclined surface,

x, y, z = orthogonal coordinates,

Φ = tilt angle of the inclined surface.

Steinman's equations are not only applicable to rectangular surfaces but can also be used to calculate view factors for surfaces of different shapes. Unfortunately, Steinman's equations only apply to standing persons.

5.1.2 Numerical approaches

Over many years various analytical solutions for determining view factors have been developed for a variety of simple geometries e.g. Ozisik (1973), Brewster (1992), ASHRAE (1993), Jones (2000). For complex geometries such as the human body, however, no analytical solutions have been available and thus numerical techniques have to be used.

Nowadays the availability of powerful microprocessor computers makes the use of accurate numerical techniques possible to calculate view factors of even complex geometric shapes and configurations. Ozeki et al. (2000) and Tanabe et al. (2000) used a 3D humanoid geometry models to determine view factors of the human body as whole by means of numerical simulation. The Tanabe's model, for example, divided the body into 4396 quadrilateral surface elements with a total surface area of 1.72 m² (Figure 5.3). The authors predicted whole body view factor for standing and sedentary persons with respect to vertical and

horizontal rectangular surfaces. They were able to reproduce Fanger's experimental view factors within 10% relative error using their computer simulation models.

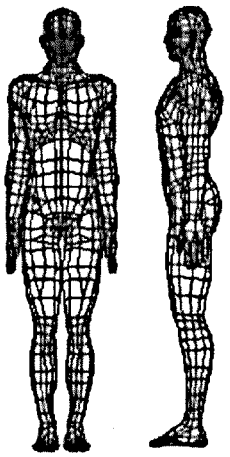

Figure 5.3
Ozeki's three-dimensional geometry model of a standing nude male, Ozeki et al. (2000).

Huizenga et al. (2001) also used a realistic 3D model of the human body to predict radiative heat losses for each of the 5000 polygons of his numerical humanoid in inhomogeneous environments. Unfortunately, neither information on predicted view factors nor information on the numerical techniques used was provided.

In most experimental as well as simulation studies, however, overall human radiation data rather than local quantities were provided. Also current national and international thermal comfort standards only provide information on human view factors for the body as a whole and only for surfaces of parallelepiped enclosures.

The aim of this study was to develop a model for predicting human view factors for individual body parts. Human local projected area factors, f_p, developed in Chapter 4, incorporate all the necessary information on the local, geometry-related radiation characteristics of the human body. The idea here was to use these f_p-factors to enable predictions of human local view factors with respect to arbitrary surfaces of the radiant enclosures.

5.2 Method of modelling

5.2.1 General considerations

In Chapter 4, a model was developed which predicts the projected area factors of individual body parts with respect to parallel rays at any azimuth and altitude angles. These f_p-factors will be used here to model view factors between individual body parts and surrounding surfaces. The geometrical parameters required to calculate the view factor between a body part and a surrounding wall are indicated in Figure 5.4.

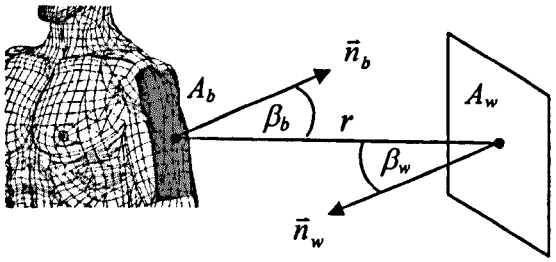

Figure 5.4 Geometrical parameters required to calculate the view factor between the upper exterior left arm body sector and a vertical wall.

The general analytical expression for calculating the view factor, $\varphi_{b,w}$ between A_b and A_w is:

$$\varphi_{b,w} = \frac{1}{\pi A_b} \int_{A_b} \int_{A_w} \frac{\cos\beta_b \cos\beta_w}{r^2} dA_b dA_w \qquad (5.2)$$

where

$\varphi_{b,w}$	=	view factor between A_b and A_w,	[-]
r	=	distance vector between dA_b and dA_w,	[m]
$\vec{n}_b$	=	normal vector of dA_b,	[-]
$\vec{n}_w$	=	normal vector of dA_w,	[-]
β_b	=	angle between normal vector $\vec{n}_b$ and distance vector $\vec{r}$,	[rad]
β_w	=	angle between normal vector $\vec{n}_w$ and distance vector $\vec{r}$,	[rad]
A_w	=	total area of the wall,	[m²]
A_b	=	total surface area of the body sector.	[m²]

The term $cos\beta_b dA_b$ is the (differential) projected area (dA_p) of the body sector A_b. The corresponding projected area factor (f_p) is then the ratio of this projected area and the corresponding actual surface area. Equation (5.2) can therefore be expressed as a function of the projected area factor, f_p, as follows:

$$\varphi_{b,w} = \frac{1}{\pi A_b} \int_{A_b} \int_{A_w} \frac{1}{r^2} f_p dA_b \cos\beta_w dA_w \qquad (5.3)$$

where f_p is the projected area factor of a surface element of dA_b with respect to a surface element dA_w.

5.2.2 Numerical model

5.2.2.1 Geometry

In the numerical model the human body is positioned in a Cartesian coordinate system as shown for a standing and sedentary person in Figure 5.5.

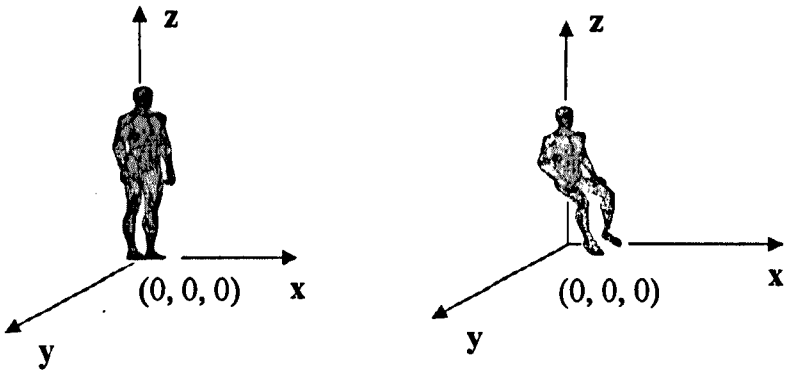

a. Standing posture *b. Sedentary posture*

Figure 5.5 Location of the geometry models in a global coordinate system.

The segmentation of the body geometry is described in Chapter 4. In the model for calculating view factors each body part is assumed to be a finite surface element which is represented by a reference point located in the centre of the respective body sector, Figure 5.6.

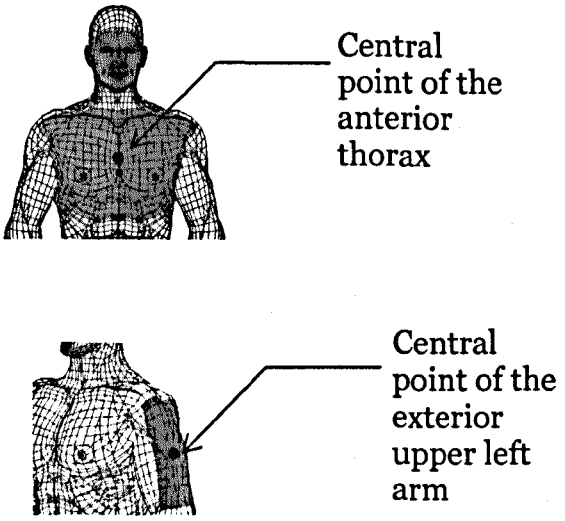

Figure 5.6 Body segments with the respective reference points.

The coordinates (x_b, y_b, z_b) of the sectors' reference points for both standing and sedentary posture are listed in Table 5.1.

Table 5.1 Coordinates of the reference points of individual body sectors for standing and sedentary postures in the global coordinate system.

Body parts	Standing posture			Sedentary posture		
	x_b	y_b	z_b	x_b	y_b	z_b
	10^{-3}m			10^{-3}m		
Head	-59	0	1719	-118	13	1358
Forehead	84	0	1666	34	0	1277
Face: Anterior	102	-3	1597	18	3	1221
Face: Left (Right) exterior	16	-65 (65)	1625	-91	-60 (60)	1227
Neck: Anterior	34	0	1510	-83	0	1111
Neck: Left (Right) exterior	4	-47 (47)	1522	-144	-51 (51)	1153
Neck: Posterior	-67	-1	1533	-186	0	1149
Shoulder: Left (Right)	-32	-131 (131)	1465	-150	-163 (163)	1080
Thorax: Anterior	105	-1	1355	14	0	990
Thorax: Left (Right) inferior	-11	-147 (147)	1241	-109	-150 (150)	920
Thorax: Posterior	-125	0	1358	-238	0	986
Abdomen: Anterior	101	0	1075	13	0	777
Abdomen: Left (Right) inferior	-4	-138 (138)	1070	-73	-136 (136)	761
Abdomen: Posterior	-61	0	1064	-153	0	763
Arm: Left (Right)Upper anterior	32	-193 (193)	1288	-65	-184 (184)	916
Arm: Left (Right) upper exterior	-29	-235 (235)	1322	-111	-231 (231)	946
Arm: Left (Right) upper inferior	-25	-178 (178)	1215	-119	-149 (149)	869
Arm: Left (Right) upper posterior	-94	-203 (203)	1279	-180	-231 (231)	895
Arm: Left (Right) lower anterior	44	-226 (226)	1072	2	-168 (168)	708
Arm: Left (Right) lower exterior	14	-272 (272)	1068	20	-221 (221)	718
Arm: Left (Right) lower inferior	-11	-193 (193)	1062	64	-204 (204)	687
Arm: Left (Right) lower posterior	-45	-255 (255)	1057	-52	-254 (254)	697
Hand: Left (Right) handback	79	-255 (255)	876	131	-192 (192)	641
Hand: Left (Right) palm	55	-226 (226)	846	152	-180 (180)	608
Leg: Left (Right) upper anterior	87	-108 (108)	720	163	-134 (134)	597
Leg: Left (Right) upper exterior	-4	-174 (174)	713	133	-200 (200)	549
Leg: Left (Right) upper inferior	-5	-30 (30)	697	163	-58 (58)	533
Leg: Left (Right) upper posterior	-82	-73 (73)	696	81	-91 (91)	472
Leg: Left (Right) lower anterior	15	-115 (115)	291	401	-149 (149)	302
Leg: Left (Right) lower exterior	-34	-167 (167)	319	348	-199 (199)	296
Leg: Left (Right) lower inferior	-21	-63 (63)	326	363	-103 (103)	308
Leg: Left (Right) lower posterior	-100	-101 (101)	323	292	-138 (138)	287
Foot: Left (Right) instep	22	-120 (120)	57	433	-122 (122)	76
Foot: Left (Right) sole	37	-109 (109)	5	434	-128 (128)	4

Note: *Values in parentheses are the coordinated of the right hand side body parts.*

5.2.2.2 Integration procedure

The new model uses a numerical form of equation (5.3) to calculate view factors between body sectors and surrounding surfaces. The wall surfaces are positioned within the coordinate system described above. In order to perform the numerical integration each surface is subdivided into small surface elements $A_{w_{i,j}}$ (*Figure 5.7*).

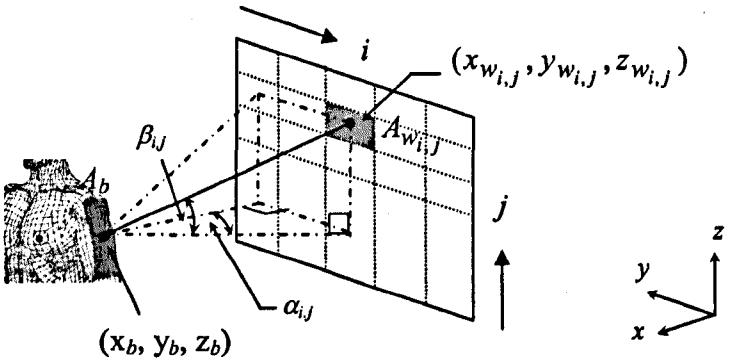

Figure 5.7 Geometric parameters used in the numerical model.

The view factor between the body sector and a finite surface element $A_{w_{i,j}}$ is obtained by:

$$\varphi_{b,A_{w_{i,j}}} = \frac{1}{\pi r_{i,j}^2} f_{p_{i,j}} \cos\beta_{w_{i,j}} \Delta A_{w_{i,j}} \qquad (5.4)$$

where $r_{i,j}$ = distance vector $\vec{r}$ between the body sector and the surface element $A_{w_{i,j}}$, [m]

$\beta_{w_{i,j}}$ = angle between the normal vector of the surface element and the distance vector $\vec{r}$, [rad]

$f_{p_{i,j}}$ = projected area factor of the body sector with respect to $A_{w_{i,j}}$. [-]

The model predicts the projected area factors $f_{p_{i,j}}$ in equation (5.4) for each finite surface element $A_{w_{i,j}}$ by calculating the corresponding azimuth and altitude angles (α and β) as follows:

$$\alpha_{i,j} = \tan^{-1}\left(\frac{y_b - y_{w_{i,j}}}{x_b - x_{w_{i,j}}}\right) \tag{5.5}$$

and

$$\beta_{i,j} = \tan^{-1}\left[\frac{z_{w_{i,j}} - z_b}{\sqrt{(x_b - x_{w_{i,j}})^2 + (y_b - y_{w_{i,j}})^2 + (z_b - z_{w_{i,j}})^2}}\right]. \tag{5.6}$$

The parameters $r_{i,j}$ and $\beta_{w_{i,j}}$ are calculated from the geometrical configuration indicated in Figure 5.8.

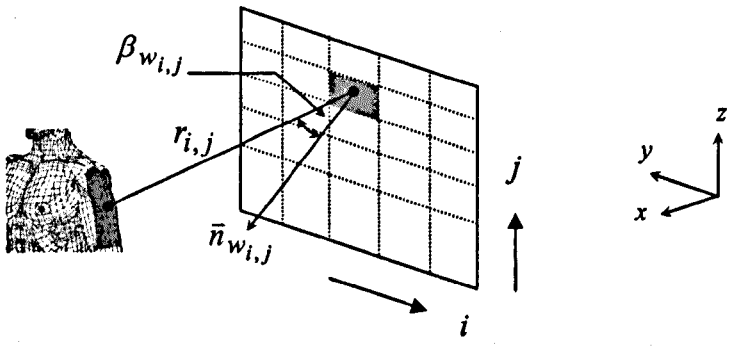

Figure 5.8 Distance vector $\vec{r}$ and altitude angle (β) of each surface element of the wall with respect to the body sector.

The angle, $\beta_{w_{i,j}}$, between $r_{i,j}$ and the normal vector, $\vec{n}_{w_{i,j}}$, of the plane element, i, is determined by:

$$\cos\beta_{w_{i,j}} = \frac{\vec{n}_{w_{i,j}} \cdot \vec{r}_{i,j}}{|\vec{r}_{i,j}|} \tag{5.7}$$

where the normal vector $\vec{n}_{w_{i,j}}$ of the plane element is defined as:

$$\vec{n}_{w_{i,j}} = \begin{bmatrix} n_{x_{i,j}} \\ n_{y_{i,j}} \\ n_{z_{i,j}} \end{bmatrix}; \ \vec{n}_{x_{i,j}} = \begin{bmatrix} \sin\Phi\cos\alpha \\ 0 \\ 0 \end{bmatrix}; \ \vec{n}_{y_{i,j}} = \begin{bmatrix} 0 \\ -\sin\alpha \\ 0 \end{bmatrix}; \ \vec{n}_{z_{i,j}} = \begin{bmatrix} 0 \\ 0 \\ \cos\Phi \end{bmatrix} \tag{5.8}$$

where Φ and α is tilt and azimuth angle of the plane, respectively.

The distance vector $\vec{r}$ is defined as:

$$\vec{r}_{i,j} = \begin{bmatrix} r_{x_{i,j}} \\ r_{y_{i,j}} \\ r_{z_{i,j}} \end{bmatrix} = \begin{bmatrix} x_b - x_{w_{i,j}} \\ y_b - y_{w_{i,j}} \\ z_b - z_{w_{i,j}} \end{bmatrix} \tag{5.9}$$

with $$\left|\vec{r}_{i,j}\right| = \sqrt{r_{x_{i,j}}^2 + r_{y_{i,j}}^2 + r_{z_{i,j}}^2} \tag{5.10}$$

being the length of $\vec{r}$.

With the above information, the view factor between A_b and A_w is obtained by numerical integration of equation (5.6) in the i^{th} and j^{th} direction over A_w (Figure 5.8):

$$\varphi_{b,w} = \frac{1}{\pi} \sum_{i=1}^{m} \sum_{j=1}^{n} \frac{1}{r_{i,j}^2} f_{p_{i,j}} \cos\beta_{w_{i,j}} \Delta A_{w_{i,j}} \tag{5.11}$$

5.2.2.3 Model extension for arbitrary azimuth angles

The calculations of the azimuth and altitude angles for individual body sectors using equations (5.5) and (5.6) are valid between $-\frac{\pi}{2} < \alpha < \frac{\pi}{2}$ and $-\frac{\pi}{2} < \beta < \frac{\pi}{2}$. The equation (5.6) covers the whole range β-angles considered. To obtain a universal model also for any α, i.e. between 0 to 2π, the following concept was proposed.

Consider Figure 5.9 which subdivides the scene into four quadrants (A, B, C and D). The extended model calculates the resultant α based on the identification of the 'active' quadrant in which a wall surface element is located relatively to the body sector considered.

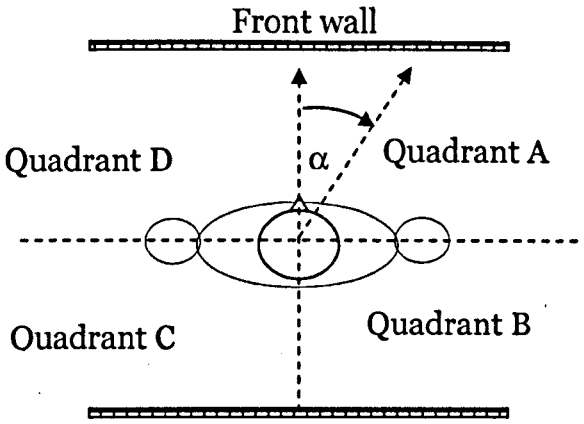

Figure 5.9 Subdivision of the scene into four quadrants to determine the relative position of the wall-surface elements.

The following observations can be made:

1) A surface element A_w is located in the quadrant A when its x- and y-coordinates are greater than the corresponding coordinates of the reference point of the considered body sector: i.e. $x_w > x_b$ and $y_w > y_b$. In this case the azimuth angle is between $0 < \alpha < \frac{\pi}{2}$ and equation (5.5) applies.

2) The surface element A_w is located in the quadrant B when its x-coordinate is smaller and y-coordinate is greater than the corresponding coordinates of the reference point of the considered body sector: $x_w < x_b$ and $y_w > y_b$. In this case the azimuth angle is between $\frac{\pi}{2} < \alpha < \pi$. Therefore, equation (5.5) has to be modified as follows:

$$\alpha_i = \pi - tan^{-1}\left(\left|\frac{y_b - y_{w_{i,j}}}{x_b - x_{w_{i,j}}}\right|\right) \qquad (5.12)$$

3) The surface element A_w is located in the quadrant C when its x- and y-coordinates are smaller than the corresponding coordinates of the reference point of the considered body sector: i.e. $x_w < x_b$ and $y_w < y_b$. In this case the azimuth angle is between $\pi < \alpha < \frac{3\pi}{2}$. The adapted equation (5.5) results in equation (5.13):

$$\alpha_i = \pi + tan^{-1}\left(\left|\frac{y_b - y_{w_{i,j}}}{x_b - x_{w_{i,j}}}\right|\right) \tag{5.13}$$

4) A_w is located in the quadrant D when its x-coordinate is greater and y-coordinate is smaller than the corresponding coordinates of the reference point of the considered body sector: $x_w > x_b$ and $y_w < y_b$. In this case the azimuth angle is between $\frac{3\pi}{2} < \alpha < 2\pi$, and equation (5.5) becomes:

$$\alpha_i = 2\pi - tan^{-1}\left(\left|\frac{y_b - y_{w_{i,j}}}{x_b - x_{w_{i,j}}}\right|\right) \tag{5.14}$$

5.3 Verification of predicted view factors

The numerical procedure was implemented in a spreadsheet software which calculates human local view factors for the required boundary conditions including body posture, the position and the azimuth angle of the person, the dimensions of the surrounding surfaces and the resolution of the surfaces as user-defined inputs into the calculation.

For verification purposes the predicted local view factors were initially compared with results obtained by the voxel-based ray tracing technique, (ThermoAnalytics, 2001). The comparisons were performed for both sedentary and standing subjects exposed to vertical (front and side wall) and horizontal surfaces (floor and ceiling).

The surfaces were subdivided into 2500 small surface elements (50 in i direction and 50 in j direction). The view factors were computed by varying the dimensionless distance a/c and b/c between 0.2 and 10, whereby a and b is the width and the height of the plane, respectively and c is the distance between the centre of the body (1.0m and 0.6m above the floor for the standing and the sedentary posture, respectively) and the surface (see e.g. *Figure 5.10* top). The distance between the body and the surfaces was chosen to be 1m, 5m, and 10m.

5.3.1 Vertical surfaces

These simulations were performed for frontal and spatial walls and both for standing and sedentary posture. The distances, c chosen for the analysis were 1m and 10m for the standing posture and 1m and 5m for the sedentary posture.

In Figures 5.10 to 5.13 the model results (for two exposed body parts) are compared with the corresponding voxel-based ray tracing technique results. The local view factors of a standing and sedentary person with respect to a front wall are plotted in Figure 5.10 and 5.11, respectively. Solid lines represent the predicted view factors obtained using the new model and marks represent voxel-based ray tracing technique results. The results obtained for other body sectors are presented in Appendix C.1 and C.5.

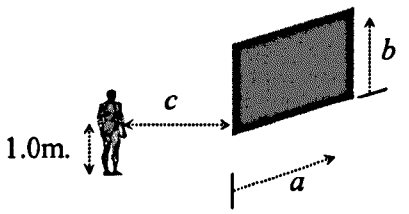

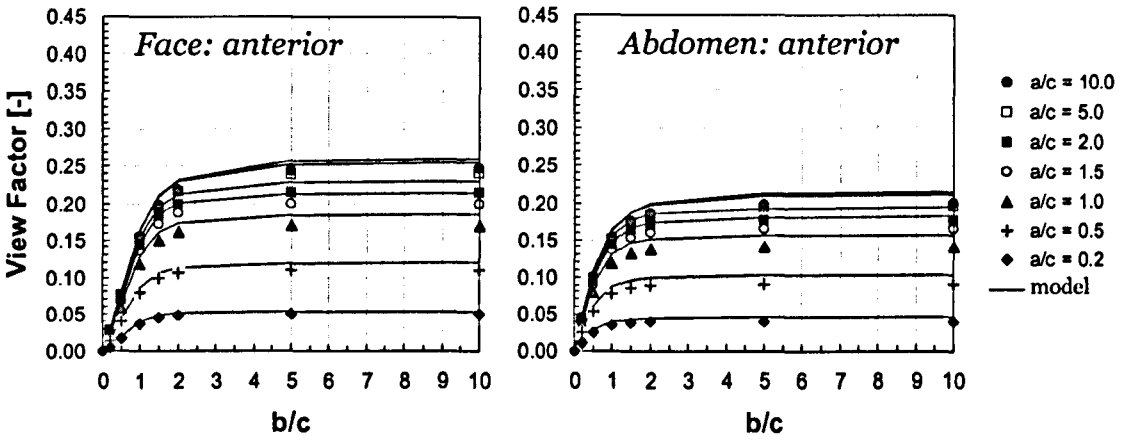

i) Subject close to the front wall (c=1.0 m)

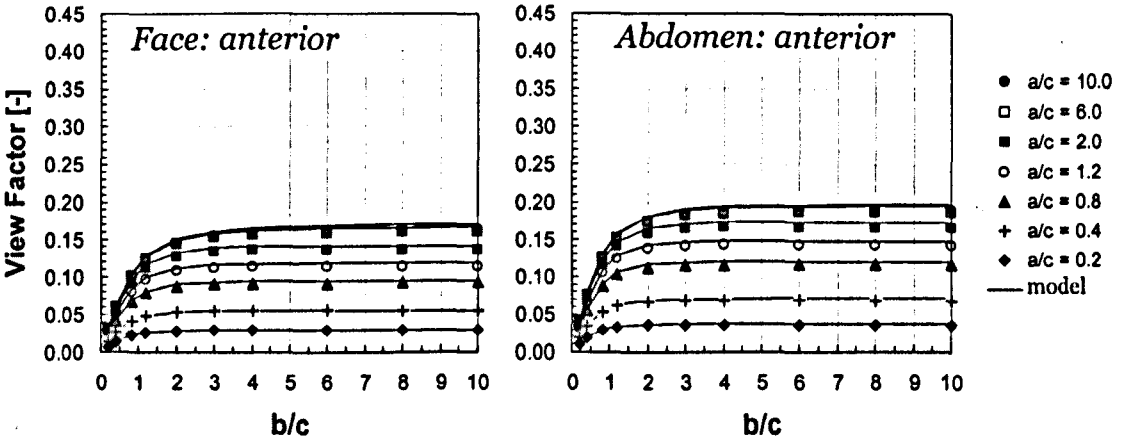

ii) Subject far from the wall (c=10.0 m)

Figure 5.10 View factors of two exposed body parts of a standing person with respect to a vertical front wall when the body is located (i) close to (ii) far from the wall.

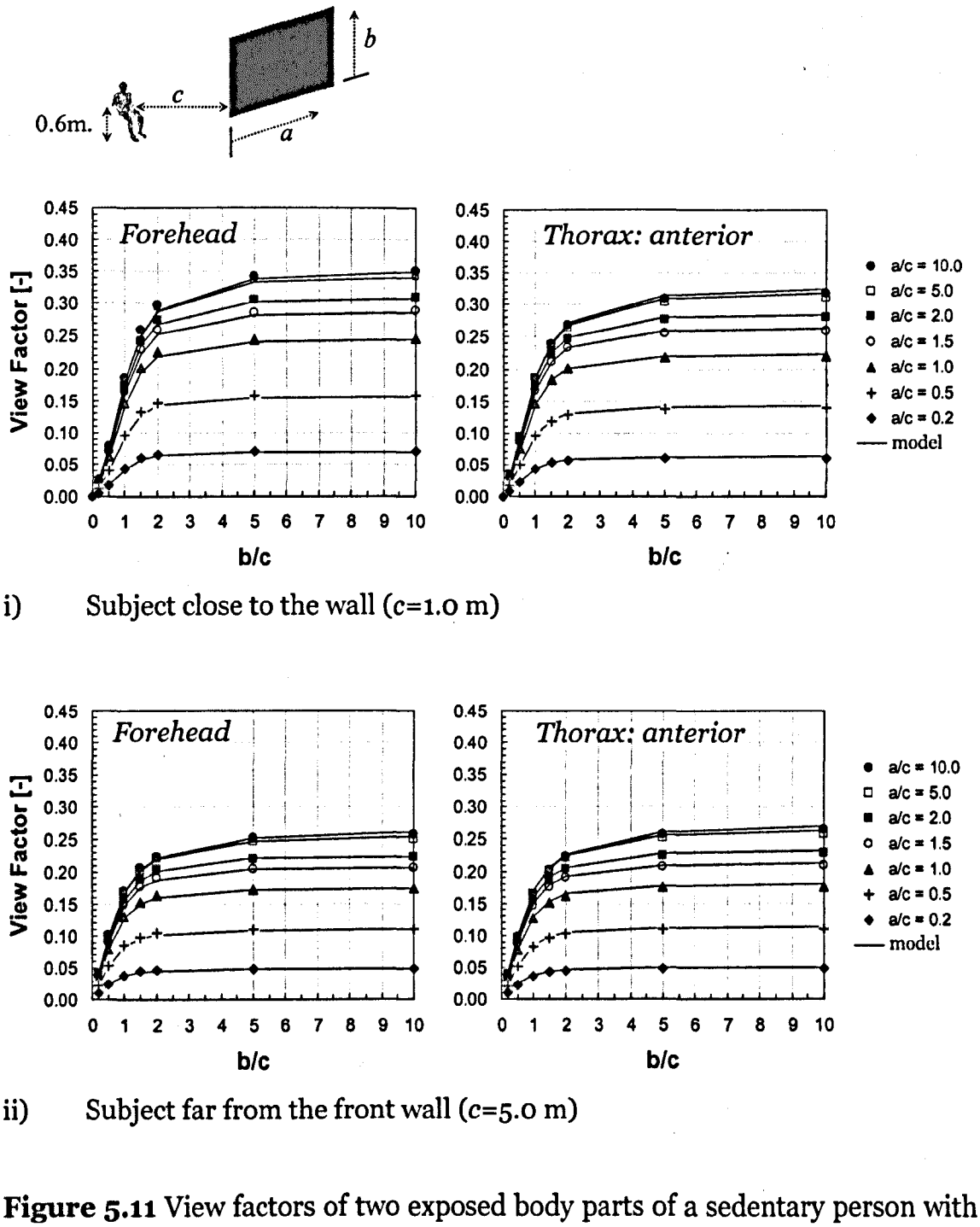

i) Subject close to the wall (c=1.0 m)

ii) Subject far from the front wall (c=5.0 m)

Figure 5.11 View factors of two exposed body parts of a sedentary person with respect to a vertical front wall when the body is located (i) close to (ii) far from the wall.

It can be observed that the view factors both for standing and sedentary posture strongly rose with the increasing the dimensionless distance a/c for $b/c<2$, but reaching saturation for $b/c>5$.

Generally, the predictions agreed well with the results of the voxel-based ray tracing techniques for all distances. The accuracy of the predictions, however, did depend on the distance c between the subject and the wall. The average relative error (see details in Chapter 3) between the new model and RadTherm (voxel-based ray tracing techniques) was 2.72% and 5.58% for 10m (standing) and 5m (sedentary), respectively, compared to 3.13% (standing) and 9.81% (sedentary) obtained for c=1m distance.

The explanation for this phenomenon is the fact that in the model the body sectors are represented by singular points rather than 3D surfaces which plays an increasingly important role for small distance from the surface. Nevertheless with the above relative errors the results predicted by the new model were considered to be acceptable.

The view factors of two exposed body parts with respect to a side wall are plotted for the standing and sedentary posture in Figure 5.12 and 5.13, respectively.

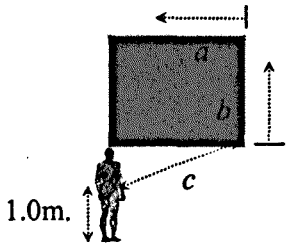

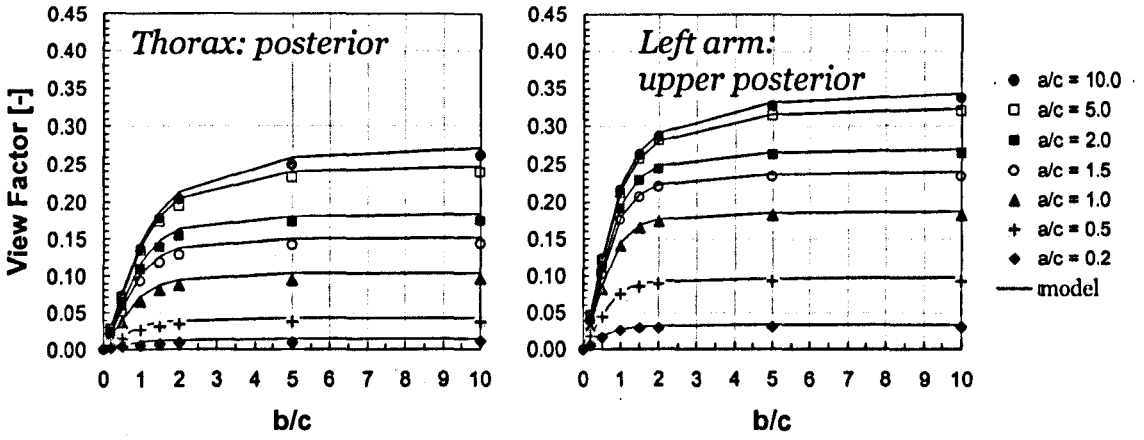

i) Subject close to the side wall (c=1.0 m)

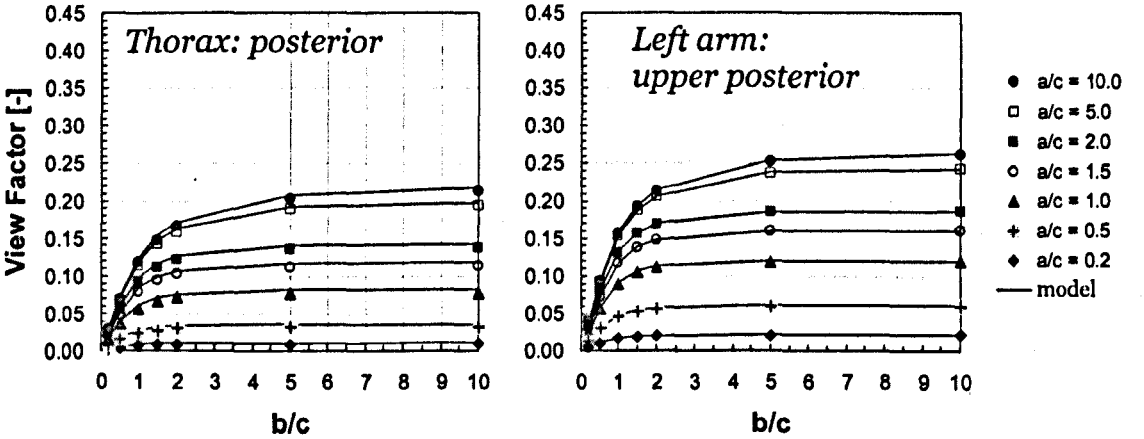

ii) Subject far from the side wall (c=10.0 m)

Figure 5.12 View factors of two exposed body parts of a standing person with respect to a vertical side wall when the body is located (i) close to and (ii) far from the wall.

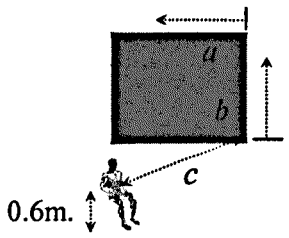

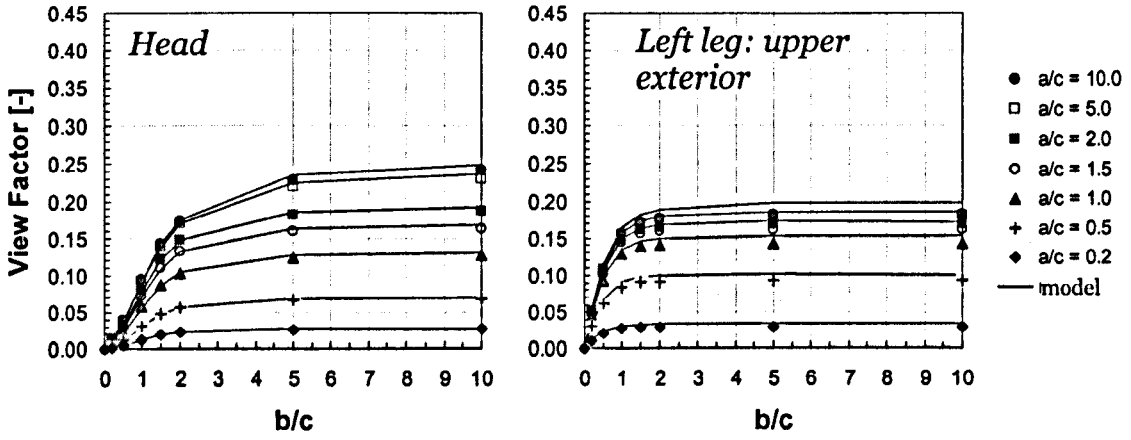

i) Subject close to the side wall (c=1.0 m)

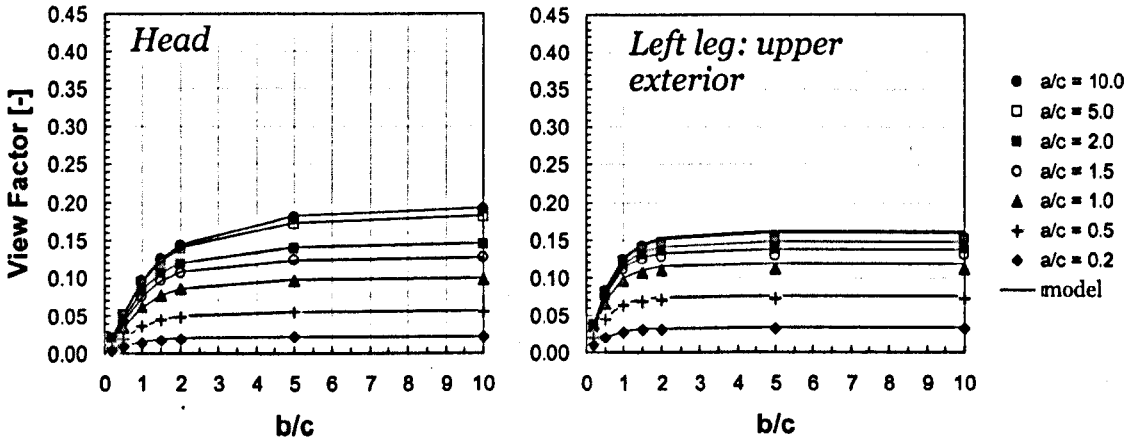

ii) Subject far from the side wall (c=5.0 m)

Figure 5.13 View factors of two body parts of a sedentary person with respect to a vertical side wall when the body is located (i) close to and (ii) far from the wall.

Similarly to the front wall, the predicted view factors obtained using the developed model (solid lines) agreed well with the results of the voxel-based ray

tracing techniques (data points) both for standing and sedentary postures over the whole range of *a/c* and *b/c*. Here too, there was a tendency of slightly over predicting view factors obtained by RadTherm for close distances c. With 4.25% (standing) and 8.45% (sedentary) the average relative error was generally smaller compared to the front wall. In Appendix C2 and C6 are provided the results for other body parts.

5.3.2 Floor

A comparison of view factors as predicted by the new model and RadTherm for the floor is provided in Figure 5.14. Here, the body sectors selected represent body parts whose view factors strongly depend on the body posture.

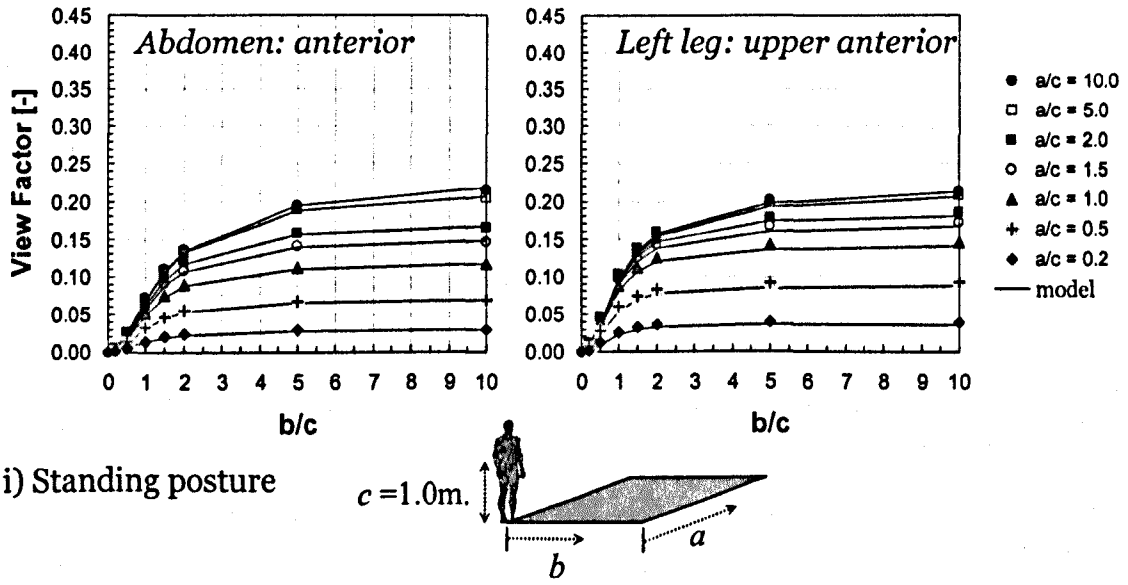

i) Standing posture

Figure 5.14 View factors of the anterior abdomen and the anterior upper left leg with respect to a floor for (i) standing and (ii) sedentary posture.

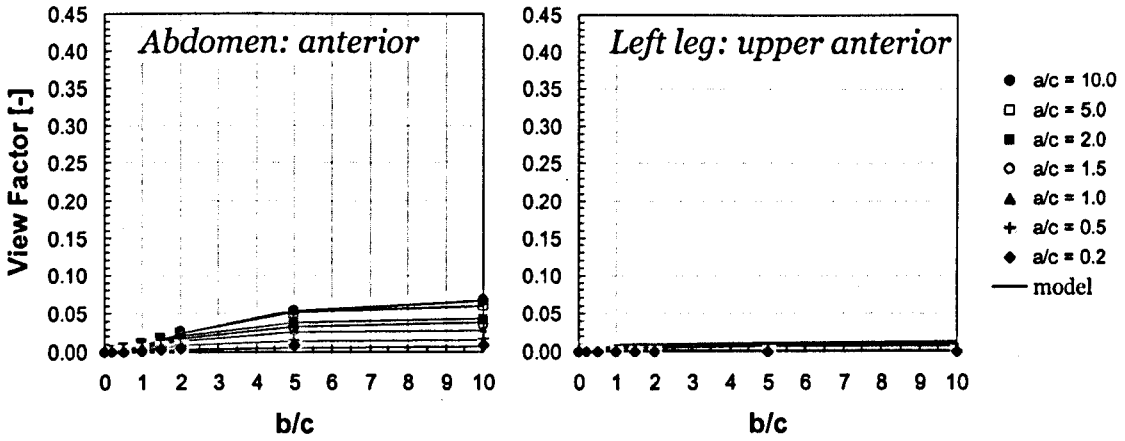

ii) Sedentary posture

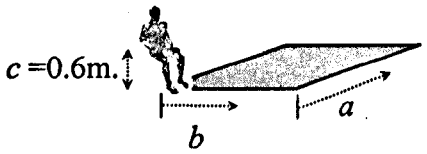

Figure 5.14 (Continued).

Figure 5.14 demonstrates the importance of the body posture on the local view factors of some body parts. For the case of sedentary posture, the anterior abdomen was partly hidden by the upper legs. These view factors are therefore considerably lower than those obtained for the standing posture. The upper anterior legs of a sedentary person are not exposed to the floor resulting in view factors close to zero. The results obtained for other body parts are provided in Appendix C.4 and C.8. The average relative error of local view factor with respect to the floor ranged between 8.0% and 9.3% for standing and sedentary posture, respectively. The maximum total error did not exceed 28.5%.

5.3.3 Ceiling

Figure 5.15 shows the results obtained for the ceiling.

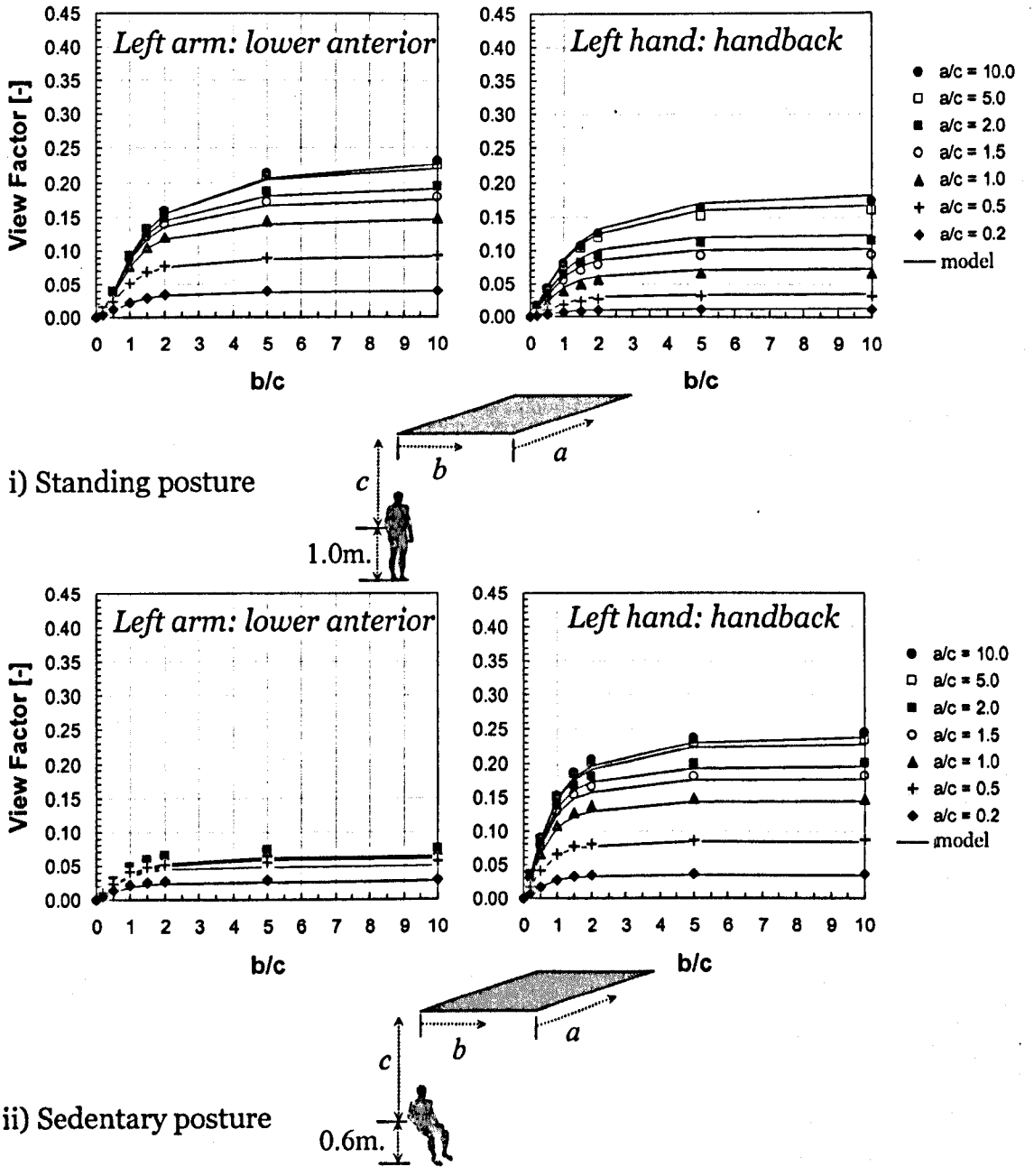

Figure 5.15 View factors of the lower left arm (anterior) and the left handback with respect to the ceiling for (i) standing and (ii) sedentary posture.

Also figures 5.15 demonstrate the impact of the body posture on local view factors. For other body parts (see Appendix C.3 and C.7), however, only a marginal effect of the body posture was observed.

The predictions agreed very well with the results obtained using the ray tracing technique both for standing and sedentary posture for all *a/c* and *b/c* values. The average relative error was evaluated to be 7.8% and 7.9 % for standing and sedentary posture, respectively. The maximum relative was about 22.7%.

5.3.4 Sensitivity analysis

To investigate how the accuracy of the predicted view factors is affected by the resolutions of the plane, a simplified geometry was defined featuring a vertical wall of 10x10m in front of the person both standing and sedentary. The front wall was subdivided into a different number of surface elements representing four resolution levels: low, medium, high and very high resolution. In case of low resolution, the area of the surface elements was about 4m² (2 x 2m) whereas for the medium resolution 1m². The surface area of the element in case of high and very high resolution was 0.25 m² (0.5 x 0.5m) and 0.04m² (0.2 x 0.2m), respectively (*Table 5.2*).

The humanoid was placed centred to the middle of the wall at the distance *c* (Figure 5.16). The view factors were predicted for the following distances between the subject and the wall, *c*: 1, 2, 3, 5 and 10m. The predicted view factors were compared with results obtained by voxel-based ray tracing technique (RadTherm) for both standing and sedentary postures.

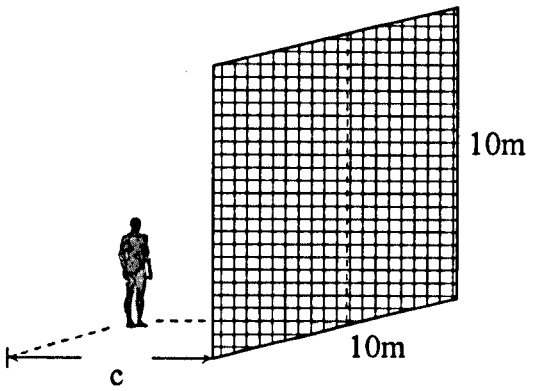

Figure 5.16 Geometrical configuration used in the sensitivity study.

Table 5.2 The four resolutions of the plane analysed in the study.

Resolution of plane	Number of surface elements	Area of each surface element (m^2)
Low	25 (5x5)	4.00
Medium	100 (10x10)	1.00
High	400 (20x20)	0.25
Very high	2500 (50x50)	0.04

The results obtained for some body parts are shown graphically in Figure 5.17. Data points are the view factors predicted by the new model, solid lines represent the results obtained by the voxel-based ray tracing technique.

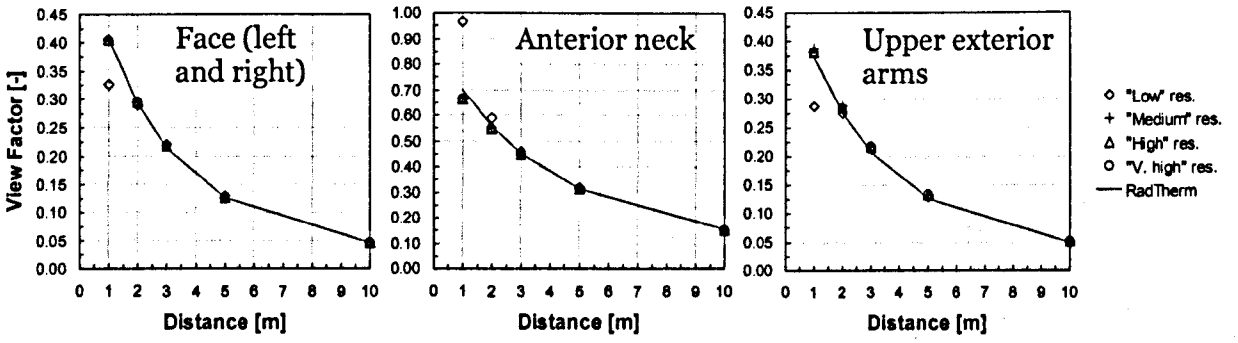

a. Standing posture

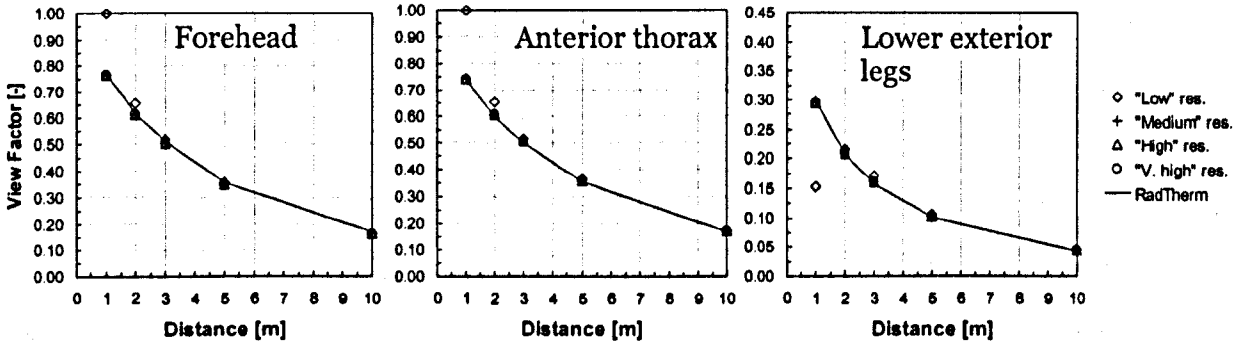

b. Sedentary posture

Figure 5.17 Comparison of predicted view factors of some body parts with the results obtained by the voxel-based ray tracing technique.

The predictions were in very good agreement with RadTherm results when the distance between the body and the wall was greater than 2m for all resolutions. However, partly significant discrepancies occurred for c=1m in which case the view factors predicted using the low resolution deviated by 20% and more from the results obtained using the ray tracing technique.

In this study, it was also interesting to obtain information on the overall relative error, i.e. the relative error referring to the overall view factor for the human body as a whole. For this purpose, the local values were integrated over the whole body surface. The results are listed in Table 5.3.

Table 5.3 The average relative error of the whole-body view factors.

Distance [m]	Relative error [%]							
	Standing posture				Sedentary posture			
	Low Res.	Med. Res.	High Res.	V. high Res.	Low Res.	Med. Res.	High Res.	V. high Res.
1	20.41	9.97	8.57	8.44	30.86	11.68	10.09	10.22
2	5.25	4.25	4.40	4.55	9.47	8.85	8.82	8.92
3	5.00	4.69	4.91	4.97	5.43	5.36	5.47	5.65
5	4.85	4.95	4.91	4.97	3.79	3.83	3.89	3.98
10	2.60	2.64	2.65	2.64	3.22	3.23	3.37	3.40

As can be seen the largest discrepancies occurred for the lowest resolution when the body was close to the wall (c=1m). The relative error dramatically decreased for higher resolutions and distances c>1m.

Although a large number of surface elements provided improved accuracy when the body was close to the wall, there was a rather little effect to the wall resolution for distances c = 5m and more. For all three cases, a 'medium' resolution was felt to be the best compromise between accuracy, computational time and hardware requirements for most practical applications.

5.4 Validation of predicted view factors and discussions

In this section, the new model was validated against available experimental results obtained by Fanger (1970) and Horikoshi et al. (1990). Four geometrical configurations were analysed: front wall (FW), sidewall (SW), ceiling (CE), and floor (FL) which were all chosen to match the experimental design (Figure 5.18). As described in section 5.3 the view factors were calculated by varying the dimensionless distances a/c and b/c. Each surface was subdivided into 100 (10 x 10 elements) surfaces elements which referred, approximately, to a 'medium' resolution described in section 5.3.5. The view factors of individual body sectors were predicted for both standing and sedentary posture.

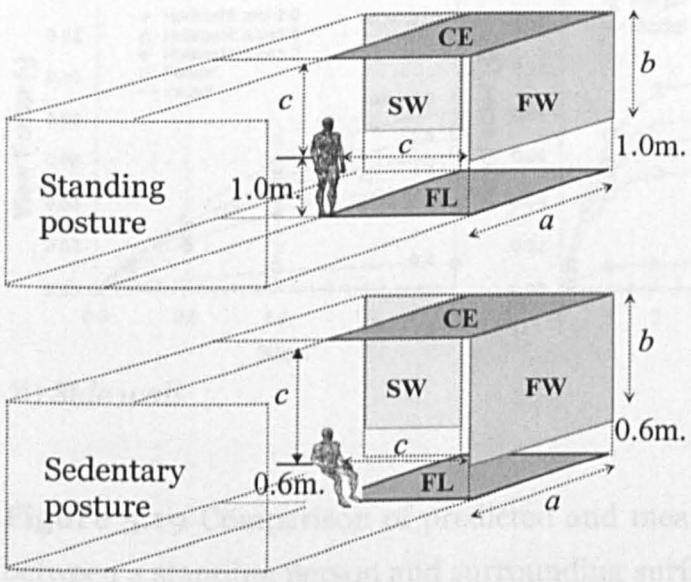

Figure 5.18 Geometrical configuration used in the study.

To date, there are no experimental results available for individual body sectors. For validation purposes, therefore, the predicted results obtained for the individual body sectors were integrated over the whole body to enable a comparison with experimental results. The analysis was performed for two distances: 1) close distance corresponding to the experiment of Horikoshi et al. (1990) in which c was set to 1m and 2) a distance of c=10m according to the experiments of Fanger (1970). In case of ceiling, the view factors were predicted for a height of 3.0m above the floor (Fanger, 1970). The predicted results

obtained for the standing posture are plotted together with the corresponding measured data in Figures 5.19 and 5.20.

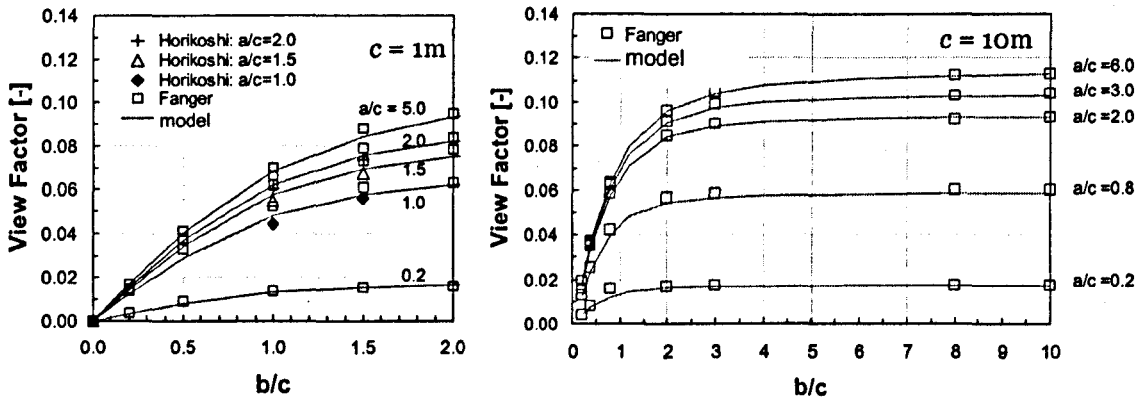

i) *Front wall*

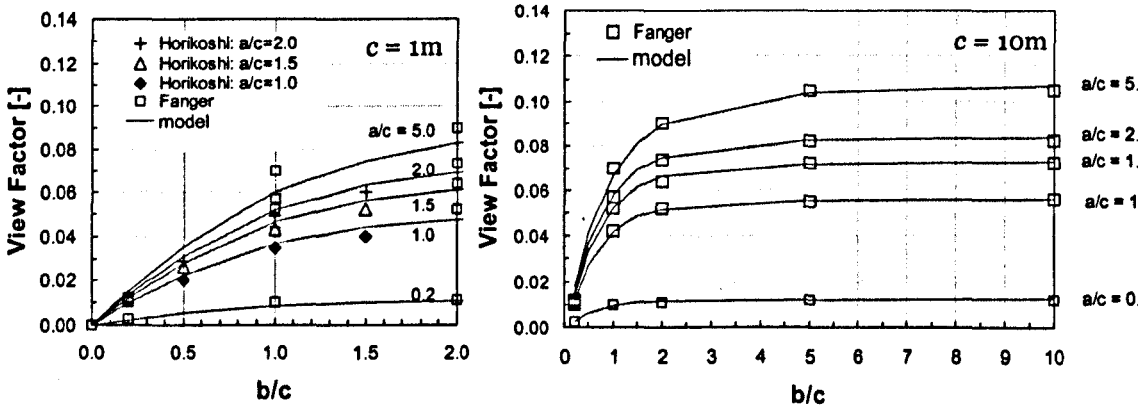

ii) *Side wall*

Figure 5.19 Comparison of predicted and measured whole-body view factors between a standing person and surrounding surfaces at the distance c=1m (left) and c=10m (right).

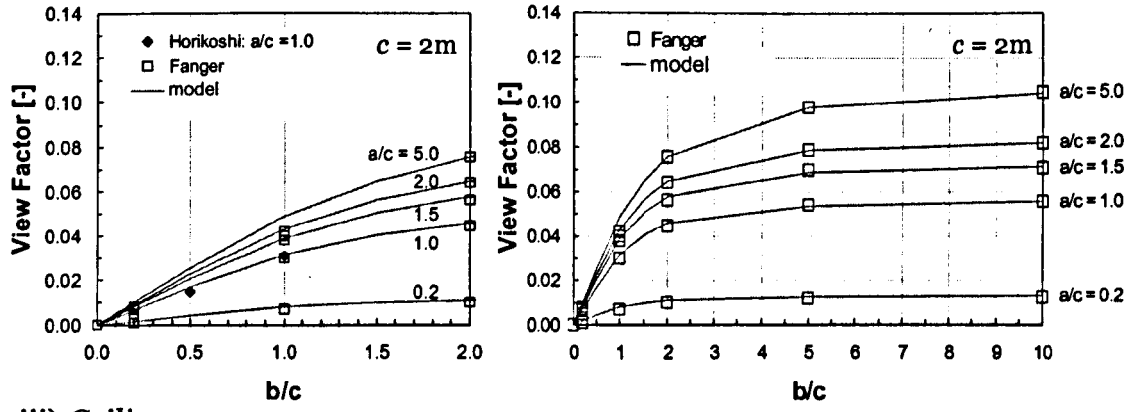

iii) *Ceiling*

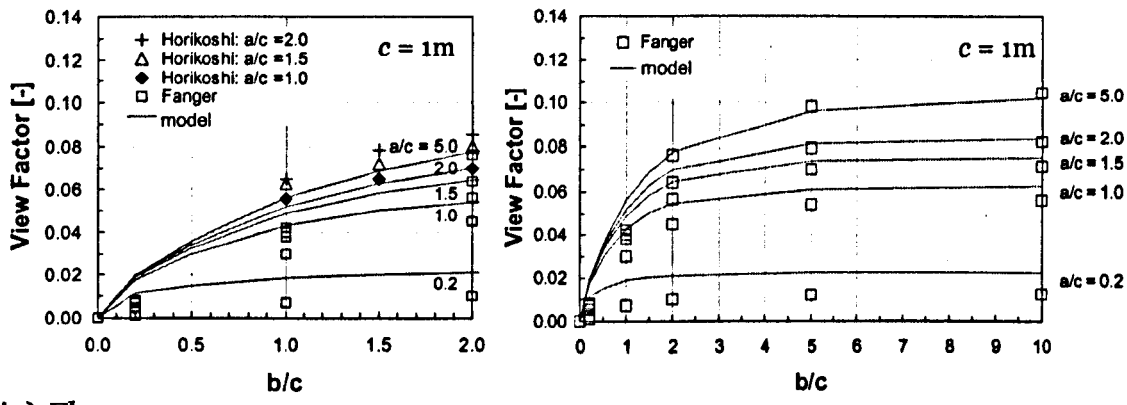

iv) *Floor*

Figure 5.19 (Continued).

Left hand side diagrams include view factors for subjects in close proximity of the panel (c=1m, except Fanger's results) whereas the right hand side figures display view factors for c=10m (front and side wall).

Generally, there was good agreement between predictions and experimental values for most a/c and b/c values at both distances c. An exception formed view factors with respect to the floor which were predicted to be greater than in the experiments of Fanger but lower than in the experiments of Horikoshi. Figure 5.19 demonstrates that the new model is able (in contrast to the Fanger data) to reproduce measured view factor reasonably well also for the close distances between a person and surfaces of the surrounding.

The results obtained for the sedentary posture are plotted in Figure 5.20. Here too, left hand side diagrams of Figure 5.20 show view factors of subjects in the close proximity to the panel (except Fanger's results) while the right hand side diagrams show view factors for c=5m (vertical wall).

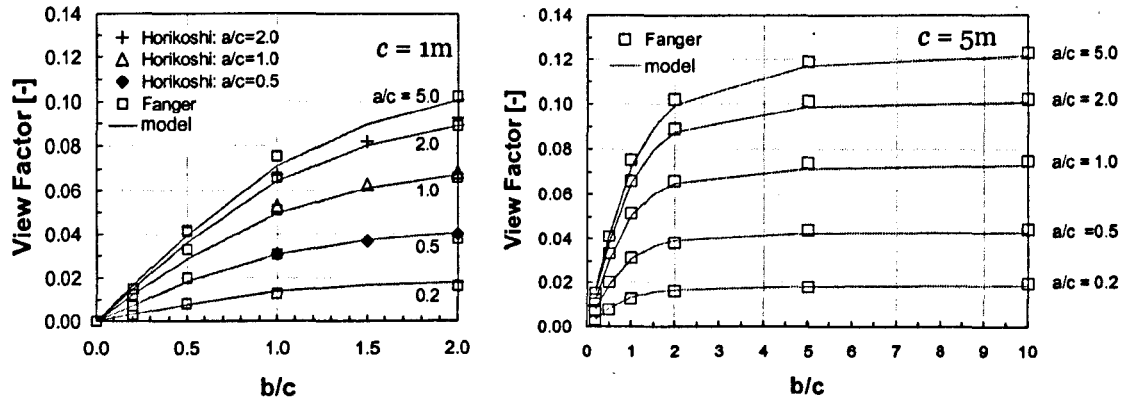

i) *Front wall*

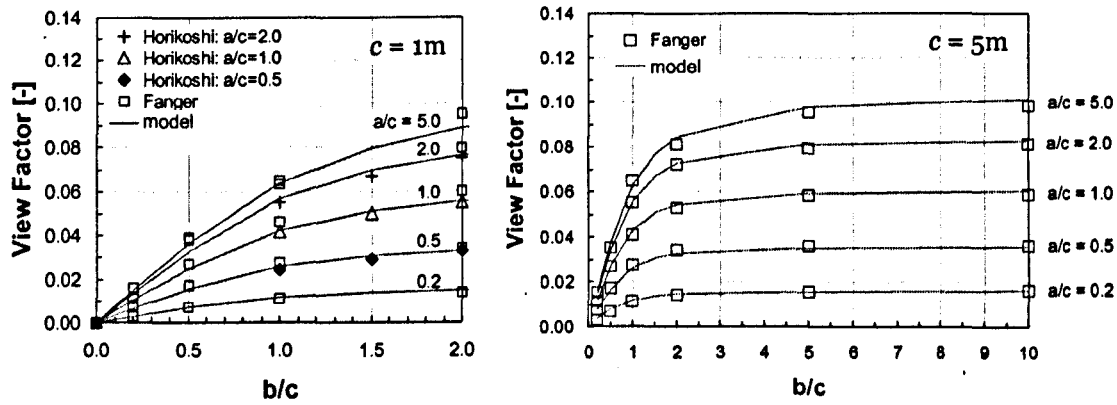

ii) *Side wall*

Figure 5.20 Comparison of predicted and measured whole-body view factors between a sedentary person and surrounding surfaces at the distance c=1m (left) and c=5m (right).

The predictions (solid lines) agreed well with the experimental values including close distances. Again, an exception formed view factors obtained for the floor which were predicted to be higher than the results of Fanger but lower than the experimental results of Horikoshi.

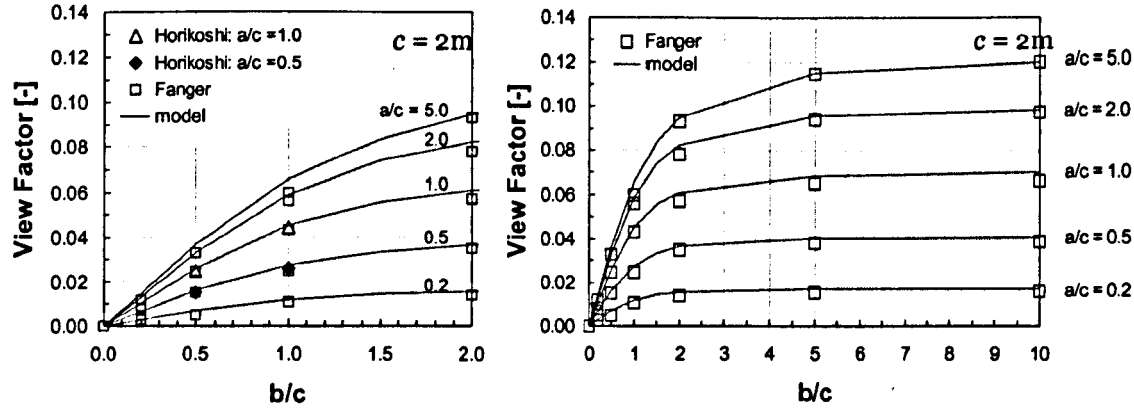

iii) *Ceiling*

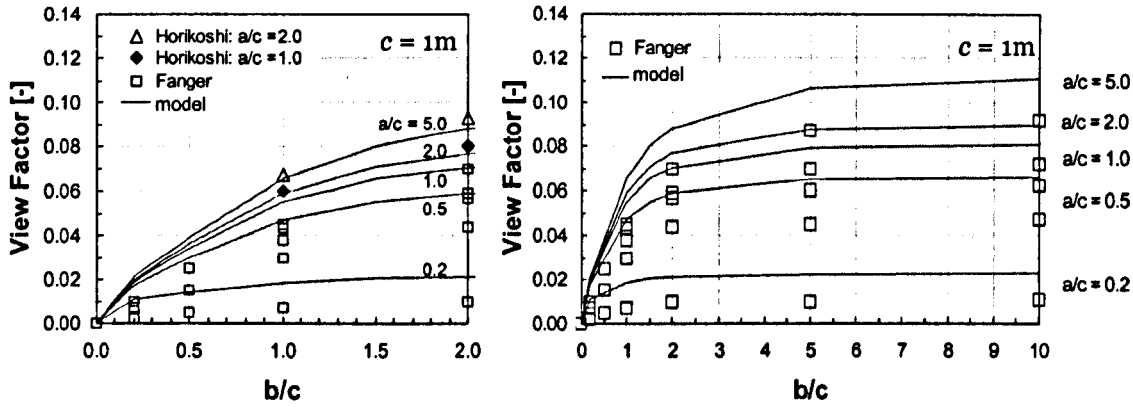

iv) *Floor*

Figure 5.20 (Continued).

Some reasons for the discrepancies between predictions and measurements are: a) the humanoid body simulated could differ in both geometry and posture from the subjects in the experiments, and b) the Fanger's results are known for not performing well for close distances between a person and a surface. This might be the reason why the predictions agreed better with the experimental data of Horikoshi than with the results of Fanger.

5.5 Conclusions

In this chapter a finite element method was used to model human local view factors. The new model enables predicting view factors of individual parts of the human body with respect to any arbitrary surrounding surface. It is therefore hoped that the model will be a useful tool for detailed human radiation analysis in inhomogeneous environments.

The model showed good general agreement with available experimental results for both standing and sedentary posture. Some discrepancies between predicted and measured data appeared for close distances between the body and surrounding surfaces which is because of the limitation of considering body sectors as singular finite elements. Nevertheless, the results obtained using the new model reproduced measured data obtained for close distances much better than the Fanger approach.

Scientists and engineers can use the view factors to perform detailed radiation calculations for building occupants. Together with a detailed thermal comfort model these factors can assist architects, designers, building simulation vendors, and researchers to quantify the comfort performance of buildings and HVAC systems, as well as individual built constructions such as windows, heated floor, radiators and etc. The combined model could also have value in analysing the health and safety critical thermal environments.

Chapter 6

Predicting human thermal responses to asymmetric radiation

6.1 Introduction

In the past, various multi-segmental models of human thermoregulation have been developed (e.g. Stolwijk 1971, Konz et al. 1977, and Wissler 1985) many of which have been valuable tools contributing to a better understanding of human thermoregulatory processes. More recent models enable environmental heat losses to be calculated in detail predicting dynamically body temperatures, local skin temperature and thermoregulatory responses over a wide range of thermal circumstances (e.g. Fiala et al. 2001, Huizenga et al. 2001). Todate, however no work has been done to validate such models under asymmetric radiation conditions.

In this chapter projected area factors (f_p) and view factors (φ) described in Chapter 4 and Chapter 5 were used with IESD-Fiala model (Fiala et al., 1999) to enable detailed radiation calculations and to predict human thermal responses to asymmetric radiation environments. This multi-segmental model has been shown to provide good agreement with measured physiological and perceptual responses over a wide range of steady state and transient conditions (Fiala et al., 2001 and 2003). The model has found applications, e.g. in medical engineering to predict temperature and regulatory responses of anaesthetised patients, in the car industry to predict passengers' responses to the transient and asymmetric boundary conditions found inside car cabins (Fiala et al. 2004), in

meteorology to quantify human physiological and comfort responses to outdoor weather conditions (e.g. Fiala et al. 2001), some military applications, and the thermal comfort analysis in buildings and individual built components (Fiala et al. 1999 and Martinez et al. 2000).

A number of experiments on physiological responses useful to validate the extended model for asymmetric radiation environments has been found in the literature. Fanger et al. (1980 and 1985) conducted series of experiments on human physiological responses to various asymmetric radiation configurations. Fourteen local skin temperatures across the body and rectal temperature (as well as thermal sensation) of the subjects were recorded.

Hall and Klemm (1967 and 1969) studied physiological responses of subjects in extreme environments with radiant asymmetry of over 100 K. They measured rectal temperatures and seventeen skin temperature across the body of the subjects every five minutes.

Hodder (2002) exposed seated subjects to simulated direct solar radiation intensities of 200, 400 and 600 Wm^{-2} and measured local skin temperatures at six body parts.

The aim of this part of the study was to predict human physiological responses to asymmetric radiation environments and validate the simulation results against the above experimental trials. Of special interest were predictions of local skin temperatures which are important signal of human local thermal reception and comfort (Hensel, 1979 and 1981) and thus for this research the main objective is to develop a physiologically based thermal comfort model for predicting human local perceptual responses to asymmetric radiation.

6.2 The IESD-Fiala model of the human thermoregulatory system

The mathematical model of human thermoregulation and thermal comfort used in this research is IESD-own development. This multi-node, dynamic model incorporates two interacting systems of thermoregulation: the controlling, active system (i.e. thermoregulatory system) and the controlled passive system. The IESD-Fiala model incorporates a physiological based thermal comfort model which predicts overall thermal sensation responses in steady state and transient environments.

6.2.1 Passive System

The passive system of the IESD-Fiala model is a multi-segmental, multi-layered representation of the human body with spatial subdivisions (*Figure 6.1*) and detailed information on anatomic and geometrical body properties. The body is idealised as 19 spherical and cylindrical elements built of annular concentric tissue layers with the appropriate thermophysical properties and physiological functions. Individual tissue layers are subdivided into spatial sectors to enable detailed modelling of environmental asymmetries. Tissue layers are further discretised into (a total of 317) tissue nodes. The model represents an average person with a body weight of 73.5 kg, body fat content of 14%wt, Dubois-area of 1.86 m^2, basal metabolism of 87 W, basal evaporation from the skin of 18W, and basal cardiac output of 4.9 L min^{-1}. The passive system is described in detail in Fiala et al. (1999).

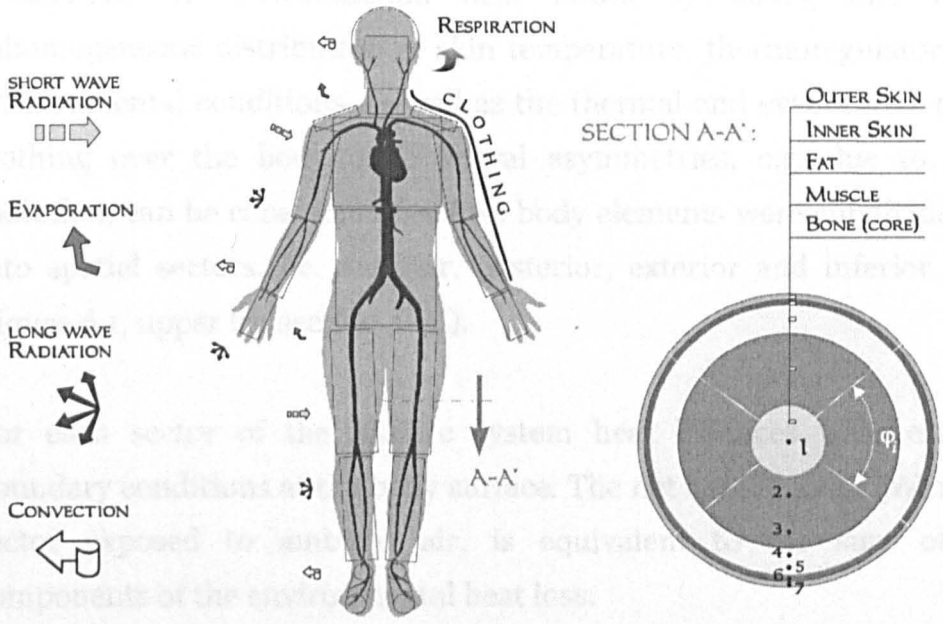

Figure 6.1 The passive system of the IESD-Fiala model (Fiala et al., 1999).

The model predicts the dynamic heat transport within the body taking into account the metabolic heat production, blood perfusion, heat conduction from warmer to colder tissue locations and heat storage. The model uses the Pennes' (1948) *bioheat equation* of heat transfer occurring in the living tissue, equation (6.1):

$$k\left(\frac{\partial^2 T}{\partial r^2}+\frac{\omega}{r}\frac{\partial T}{\partial r}\right)+q_m+\rho_{bl}w_{bl}c_{p,bl}\left(T_{bla}-T\right)=\rho_{ts}c_{p,ts}\frac{\partial T}{\partial t} \qquad (6.1)$$

where k [W m^{-1} K^{-1}] is tissue conductance; T [°C] tissue temperature; r [m] radius; ω geometry factor: ω=1 for polar co-ordinates, ω=2 for spherical co-ordinates; q_m [W m^{-3}] metabolism; ρ_{bl} [kg m^{-3}] density of blood; w_{bl} [m^3 s^{-1} m^{-3}] blood perfusion rate; $c_{p,bl}$ [J kg^{-1} K^{-1}] heat capacitance of blood; T_{bla} [°C] arterial blood temperature; ρ_{ts} [kg m^{-3}] tissue density; $c_{p,ts}$ [J kg^{-1} K^{-1}] tissue heat capacitance; and t [s] time.

In the passive system model provisions were made to enable detailed predictions of environmental heat losses by taking into account the inhomogeneous distribution of skin temperature, thermoregulatory responses, environmental conditions, as well as the thermal and evaporative properties of clothing over the body. Also lateral asymmetries, e.g. due to direct solar radiation, can be considered because body elements were subdivided thermally into spatial sectors, i.e. anterior, posterior, exterior and inferior sectors (see *Figure 6.1*, upper leg section A-A').

For each sector of the passive system heat balances were established as boundary conditions at the body surface. The net heat loss, q_{sk} [Wm^{-2}], of a skin sector exposed to ambient air, is equivalent to the sum of individual components of the environmental heat loss:

$$q_{sk} = q_c + q_e + q_r - q_{sR} \tag{6.2}$$

where q_c [W m^{-2}] is the heat exchange by convection with the air, q_r [Wm^{-2}] the thermal radiation exchange with surrounding surfaces, q_{sR} [Wm^{-2}] the absorption of direct and diffuse solar irradiation, and q_e [Wm^{-2}] the latent heat loss from the skin due to moisture evaporation. The calculation of q_c and q_e is detailed in Fiala et al. (1999).

The original IESD-Fiala model was enhanced for purposes of this research to enable detailed predictions of the long-wave and short-wave radiative heat exchange. The long-wave radiation between the body sector, i, and surrounding surfaces can be calculated as equation (6.3).

$$q_{r,i} = \sigma \sum_{j=1}^{n} \varepsilon_{b,i} \varepsilon_{sr,j} \varphi_{b,i-sr,j} (T_{b,i}^4 - T_{sr,j}^4) \tag{6.3}$$

where σ = Stefan-Bolzmann constant = 5.67 x 10^{-8}, [Wm^{-2}K^{-4}]

ε_b = the emissivity of the body sector, [-]

ε_{sr} = the emissivity of the surrounding surface, [-]

$\varphi_{b\text{-}sr}$ = view factor of the body sector with respect to the surrounding surface, [-]

T_b = absolute temperature of body sector, [K]

T_{sr} = absolute temperature of body sector, [K]

i = the running number indicated body sector from 1 to 59, [-]

j = the running number indicated surrounding surface from 1 to n. [-]

In case of short-wave radiation, the radiative heat transfer (direct and diffuse irradiation) at the body sector, i, can be expressed to apply for the humanoid of 59 body parts as shown in equation (6.4).

$$q_{sR,i} = \alpha_{b,i}(f_{p,dir,i}S_{dir} + f_{p,dif,i}S_{dif}) \tag{6.4}$$

where $\alpha_{b,i}$ = short wave absorptivity of (naked or clothed) the body sector i, [-]

$f_{p,dir,i}$ and $f_{p,dif,i}$ = direct and diffuse projected area factor of body sector i, [-]

S_{dir} and S_{dif} = direct and diffuse short wave radiation. [Wm^{-2}]

The radiative heat exchange in asymmetric environments of above equations (q_r and q_{sR}) are described in section 6.3.

6.2.2 Active System

The active system of the IESD-Fiala model simulates responses of the human thermoregulatory system, i.e. suppression (vasoconstriction) and elevation (vasodilatation) of the skin blood flow, sweat moisture excretion and changes in the metabolic heat production by shivering thermogenesis. The individual thermoregulatory responses were modelled by means of statistical regression using measured data obtained from various physiological experiments covering steady state and transient cold stress, cold, moderate, warm and hot stress conditions, and activity levels of up to heavy exercise. The development and validation of IESD-Fiala active system model is described in detailed in Fiala et al. (2001). A block diagram of the active system model is shown in *Figure 6.2*.

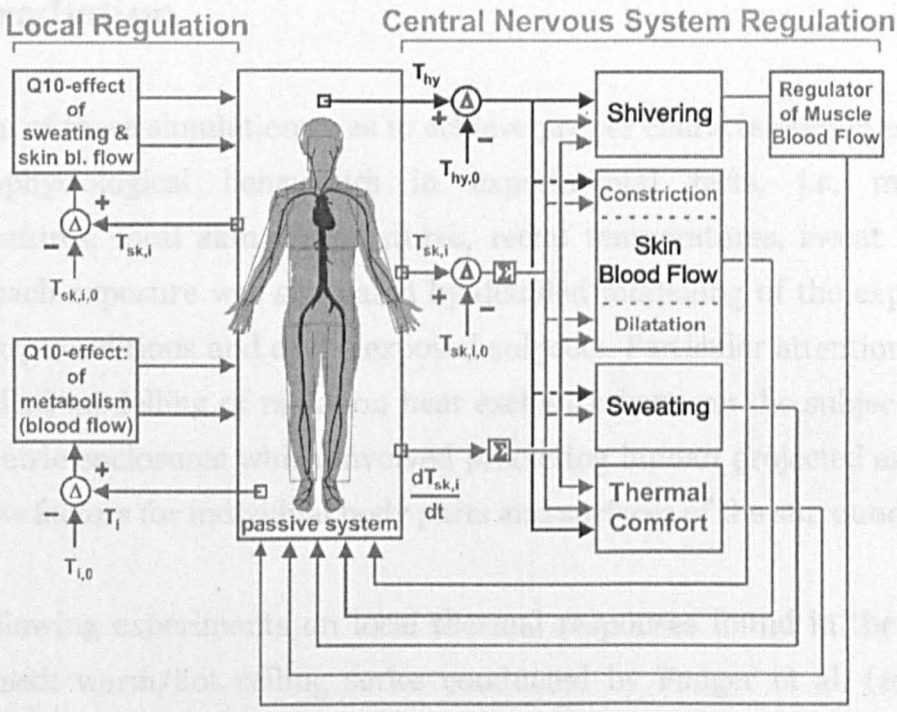

Figure 6.2 Block diagram of the active system, Fiala et al. (2001). *The central nervous system thermoregulation (CNS) accounts for overall changes in muscle metabolism via shivering (and the corresponding changes in muscle blood flow), skin blood flow via dilatation and constriction, and skin moisture extraction via sweating. The model uses temperatures of the skin (T_{sk}) and of the head core (hypothalamus, T_{hy}) as well as the rate of change of skin temperature ($dT_{sk,i}/dt$) as input signals into the regulatory centre. The local autonomic regulation utilises local skin and tissue temperatures, $T_{sk,i}$ and T_i, to modify local sweat rates, blood flows, and tissue metabolic rates.*

The IESD-Fiala model predicts perceptual responses from the physiological states of the human body, Fiala et al. (2003). Extensive comfort experiments involving over 2000 male and female subjects, and covering a wide range of static and transient environmental temperatures, relative humidities, and activity levels were used to derive the Dynamic Thermal Sensation (DTS) model (using the seven-point ASHRAE scale) running from -3 for cold to +3 for hot).

The comfort model was also validated against experimental data and showed good general agreement with measured thermal sensation votes obtained for a wide range of boundary conditions, Fiala et al. (2003).

6.3 Simulating human thermal responses to asymmetric radiation

The aim of these simulations was to achieve proper characterisation of subjects' thermophysiological behaviours in experimental tests, i.e. mean skin temperatures, local skin temperatures, rectal temperatures, sweat rates, etc. Thus, each exposure was simulated by detailed modelling of the experimental boundary conditions and of the exposed subjects. Particular attention was paid to detailed modelling of radiation heat exchange between the subjects and the asymmetric enclosures which involved predicting human projected area factors and view factors for individual body parts and surfaces of the surroundings.

The following experiments on local thermal responses found in the literature were used: warm/hot ceiling series conducted by Fanger et al. (1980), cool ceiling series of Fanger et al. (1985), warm and cool wall series of Fanger et al. (1985). Other available experiments, i.e. human responses to extreme asymmetric radiation conditions conducted by Hall and Klemm (1967 and 1969), and experiments investigating human responses to simulated solar radiation conducted by Hodder (2002) were simulated to validate the model for non-moderate global environment conditions.

6.3.1 Warm/hot ceiling

6.3.1.1 Experiments

Fanger et al. (1980) measured physiological responses of sedentary subjects exposed to a warm/hot ceiling panel at six different radiant temperature asymmetries. The experiments were conducted in a chamber with a dimension of 4.7 x 6.0 x 2.4m. Sixteen subjects (8 males and 8 females) were seated in a chair (with the seat and back composed of plastics strips) exposed to the centre of a warm/hot ceiling placed at a height of 2 m above the floor. The dimensions of the warm/hot ceiling were 2.20 x 2.20 and 2.00 m (*Figure 6.3*). The authors estimated the view factor between the subject and the warm/hot ceiling as 0.11. The subjects were clad in the standard KSU-uniform consisting of underwear, long trousers, long sleeve shirt and socks in which the overall clo-values of this ensemble was 0.6 clo.

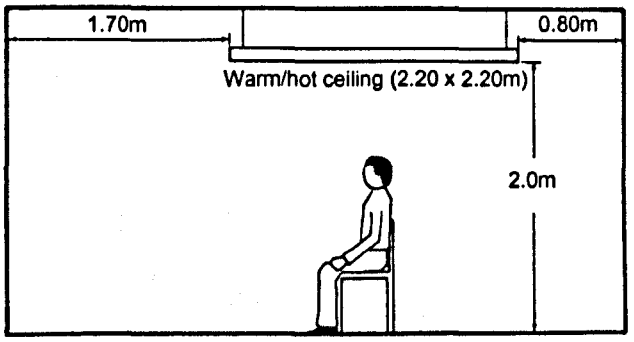

Figure 6.3 Experimental set up for the warm/hot ceiling exposure, Fanger et al. (1980).

At the start of the experiment the air temperature was set at 25°C which was estimated to be the temperature which most likely would keep a seated person clothed at 0.6 clo thermally neutral, Fanger et al. (1980). During the first hour the ceiling was unheated. In the following five half-hour periods the subjects were exposed to five different ceiling temperatures as listed in Table 6.1. When the ceiling temperature was increased, the air temperature in the chamber was lowered accordingly to provide a constant operative temperature, calculated to maintain thermal neutrality for the subject. The air velocity was less than 0.1 ms^{-1} and the relative humidity was approximately at 50%.

Table 6.1 Temperatures of the warm/hot ceiling and surrounding temperatures used in the experimental trials of Fanger et al. (1980).

Time [min]	Ceiling temp. [°C]	MRT [°C]	Ta [°C]	Operative temp. [°C]	Radiant temp. asymmetry [°C]
0-60	24.1	24.1	24.1 ± 1.6	24.1	0
60-90	34.0	25.2	24.0 ± 1.5	24.6	4.5
90-120	43.0	25.7	23.0 ± 1.7	24.3	9.2
120-150	52.0	26.4	22.3 ± 1.3	24.3	14.1
150-180	63.0	27.2	21.4 ± 1.1	24.2	20.4
180-210	69.0	27.5	20.6 ± 1.5	24.0	23.6

Every 30 minutes, rectal temperatures, local skin temperatures of the subjects were measured at different positions across the body (*Figure 6.4*). Other physiological measurements included.

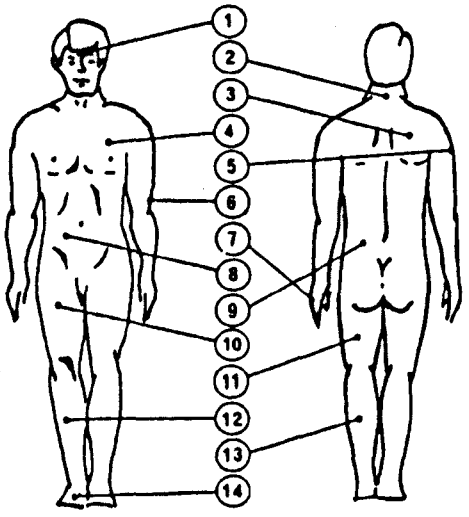

Figure 6.4 Position of skin temperature measurements on the subjects, Fanger et al. (1980).

6.3.1.2 Simulations

In the simulation the environmental conditions were chosen to match the experimental set-up (*Table 6.1*). The temperature of surrounding surfaces (front wall, back wall, side wall and floor) were calculated from the experimental mean

radiant temperature and the ceiling temperature using the whole body view factor determined by Fanger. A typical uniform emissivity of 0.95 was assumed for wall surfaces and for the ceiling. The simulations were performed for time steps of Δt=5min with a constant air velocity 0.09 ms^{-1} and a constant relative humidity of 50%. Figure 6.5 presents the environmental temperatures used in the simulation of the warm/hot ceiling series.

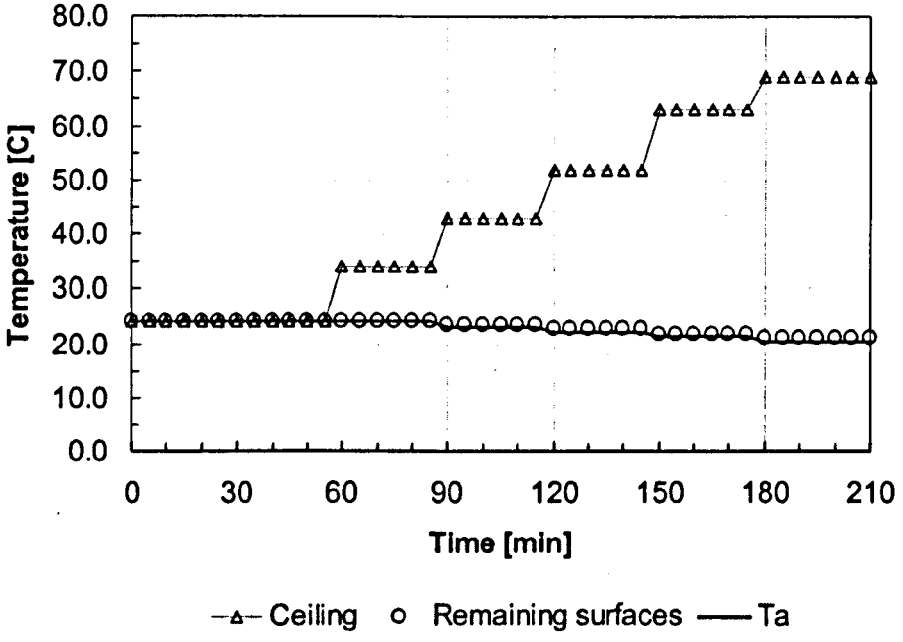

Figure 6.5 Environmental temperatures used in the simulation.

In the simulations the subject was assumed to be quietly seated corresponding to an activity level of 1.0 met. Local view factors were calculated for the scenario outlined in Figure 6.3 for each of the 59 body parts of the IESD-Fiala model. The view factors were predicted with respect to the warm/hot ceiling and the rest of the surrounding surfaces using the numerical procedure described in Chapter 5. An integration of the local quantities revealed a whole body view factor for the ceiling of 0.11 which was also the experimental value. The predicted local view factors indicated that the head and the shoulders were the most exposed body parts in the scenario. The results are listed in Table 6.2.

Table 6.2 Local view factors between individual body sectors and (i) warm/hot ceiling and (ii) the rest of the chamber.

Body parts	Warm/ hot ceiling	Rest of chamber	Body parts	Warm/ hot ceiling	Rest of chamber
Forehead	0.256	0.723	L. Leg: Up. Inferior	0.070	0.494
Head	0.346	0.618	L. Leg: Up. Exterior	0.068	0.708
Face: Anterior	0.167	0.657	L. Leg: Lo. Anterior	0.074	0.926
L. Face	0.216	0.668	L. Leg: Lo. Posterior	0.038	0.671
R. Face	0.216	0.669	L. Leg: Lo. Inferior	0.040	0.701
Neck: Anterior	0.141	0.626	L. Leg: Lo. Exterior	0.070	0.854
Neck: Posterior	0.248	0.695	L. Foot: Instep	0.108	0.778
Neck: L. Exterior	0.253	0.578	L. Foot: Sole	0.000	0.897
Neck: R. Exterior	0.253	0.581	R. Shoulder	0.318	0.568
L. Shoulder	0.318	0.567	R. Arm: Up. Anterior	0.075	0.389
Thorax: Anterior	0.208	0.705	R. Arm: Up. Posterior	0.161	0.839
Thorax: Posterior	0.150	0.839	R. Arm: Up. Inferior	0.045	0.561
Thorax: L. Inferior	0.038	0.418	R. Arm: Up. Exterior	0.204	0.750
Thorax: R. Inferior	0.038	0.426	R. Arm: Lo. Anterior	0.072	0.353
Abdomen: Anterior	0.095	0.395	R. Arm: Lo. Posterior	0.062	0.938
Abdomen: Posterior	0.095	0.905	R. Arm: Lo. Inferior	0.023	0.590
Abdomen: L. Inferior	0.067	0.601	R. Arm: Lo. Exterior	0.163	0.701
Abdomen: R. Inferior	0.067	0.600	R. Hand: Handback	0.147	0.565
L. Arm: Up. Anterior	0.075	0.400	R. Hand: Palm	0.023	0.236
L. Arm: Up. Posterior	0.161	0.839	R. Leg: Up. Anterior	0.106	0.322
L. Arm: Up. Inferior	0.045	0.552	R. Leg: Up. Posterior	0.000	0.936
L. Arm: Up. Exterior	0.204	0.750	R. Leg: Up. Inferior	0.070	0.493
L. Arm: Lo. Anterior	0.072	0.353	R. Leg: Up. Exterior	0.068	0.708
L. Arm: Lo. Posterior	0.062	0.938	R. Leg: Lo. Anterior	0.074	0.926
L. Arm: Lo. Inferior	0.023	0.592	R. Leg: Lo. Posterior	0.038	0.669
L. Arm: Lo. Exterior	0.163	0.704	R. Leg: Lo. Inferior	0.040	0.697
L. Hand: Handback	0.147	0.567	R. Leg: Lo. Exterior	0.070	0.857
L. Hand: Palm	0.023	0.231	R. Foot: Instep	0.108	0.776
L. Leg: Up. Anterior	0.106	0.325	R. Foot: Sole	0.000	0.895
L. Leg: Up. Posterior	0.000	0.946	**Whole Body**	**0.109**	**0.674**

The clothing ensemble was simulated to reproduce the KSU-uniform worn by the subject in the experiment. The overall simulated *clo* value of the ensemble

resulted in 0.6 *clo*. The local thermal and evaporative resistances of individual items used in the simulation are listed in Appendix D (*Table D.1*).

6.3.1.3 Results

Predicted body and skin temperatures obtained for the warm/hot ceiling experiment of Fanger et al. (1980) are plotted in Figure 6.6.

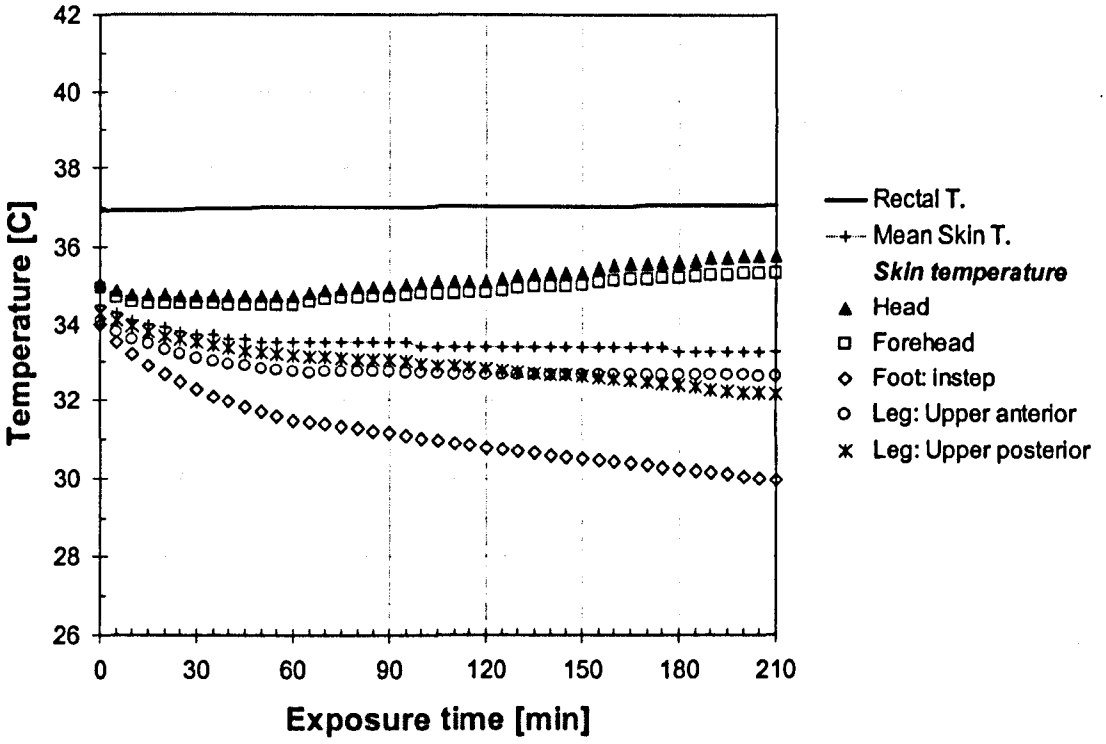

Figure 6.6 Predicted rectal, mean skin and local skin temperatures of some exposed body parts obtained for the warm/hot ceiling experiments of Fanger et al. (1980).

The simulation indicated rising skin temperature of exposed body parts (e.g. head and forehead) to the warm/hot ceiling while the opposite behaviour was predicted for skin temperatures of non-exposed body parts such as feet and legs. The mean skin and the rectal temperature, however, remained fairly constant for the whole duration of the exposure.

The predictions (local skin temperatures, mean skin temperature and rectal temperature) are plotted together with the corresponding measured data over the radiant temperature asymmetry in Figure 6.7. Also shown in Figure 6.7 are the air temperature and the mean radiant temperature in the chamber. Only those predicted local skin temperatures are plotted in Figure 6.7 which were available as measured in the experimental report, Fanger et al. (1980).

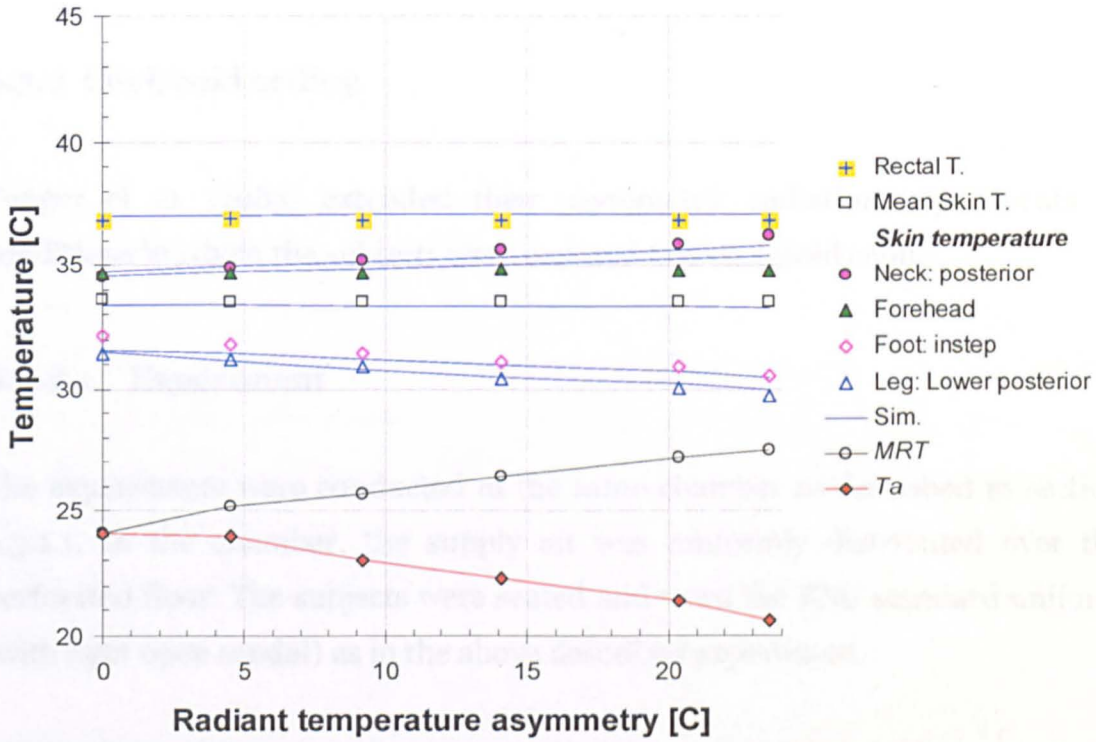

Figure 6.7 Measured and predicted local skin temperatures, mean skin temperature and rectal temperature obtained for the warm/hot ceiling series conducted by Fanger et al. (1980).

Solid lines represent predicted results and marks represent the experimental values. It can be seen that the local skin temperatures of body parts exposed to the hot surface (posterior neck and forehead) rose with increasing radiant temperature asymmetry. The opposite behaviour resulted for body parts such as hands, legs and feet, which were not directly exposed to the warm/hot ceiling.

Generally, there was very good agreement between predictions and experimental results for all physiological variables. Noticeable discrepancies

between prediction and measurement resulted for the forehead when the radiation level reached and exceeded 20K. This was presumably because of differences in body posture i.e. the position of the head. In the experiment, the subjects were allowed to read and therefore, presumably, the face and forehead were only partly exposed to radiation from the ceiling. Simulation results for all body parts are provided in Appendix E (*Table E.1*).

6.3.2 Cool/cold ceiling

Fanger et al. (1985) extended their asymmetric radiation experiments to conditions in which the subjects were exposed to a cool/cold ceiling.

6.3.2.1 Experiment

The experiments were conducted in the same chamber as described in section 6.3.1.1. In the chamber, the supply air was uniformly distributed over the perforated floor. The subjects were seated and worn the KSU standard uniform (with light open sandal) as in the above described experiment.

The seated subjects (8 males and 8 females) were exposed to the centre of a cool/cold 'ceiling' which geometry is shown in Figure 6.8. The ceiling consisted of three panels: front and back panels (each 0.9 x 2.0m) and an overhead panel (1.6 x 2.0m). The authors estimated the view factor between the test person and the ceiling to be 0.20.

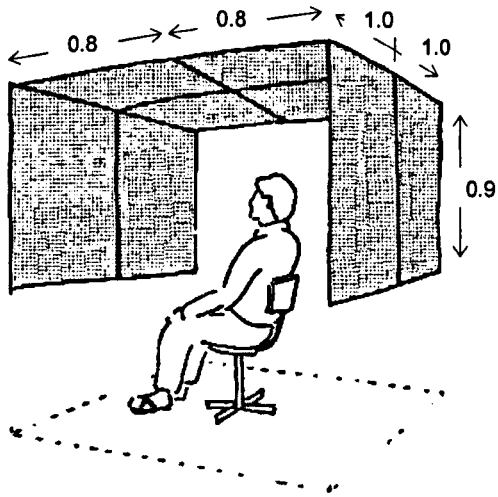

Figure 6.8 Experimental set up of the cool/cold ceiling series, Fanger et al. (1985).

During the first hour the ceiling was maintained equal to the air temperature (24°C). In the following five half-hour periods the subjects were exposed to five different ceiling temperatures. This was done by changing the temperature of the panel in steps as shown in Table 6.3. At the same time the air temperature was changed to maintain the operative temperature about 23°C through the experiment. The vapour pressure was kept constant at 1 kPa during the experiment.

Table 6.3 Environmental conditions in the cool/cold ceiling series of Fanger et al. (1985).

Time [min]	Ceiling temp. [°C]	MRT [°C]	Ta [°C]	Va [ms^{-1}]	Operative Temp. [°C]	Radiant temp. asymmetry [°C]
0-60	22.7 ± 1.9	22.7	22.7 ± 1.9	0.07	22.7	0
60-90	16.0 ± 2.3	19.9	24.1 ± 2.3	0.12	22.0	4.4
90-120	12.1± 2.6	19.0	25.8 ± 2.6	0.12	22.4	7.5
120-150	7.9 ± 2.2	18.6	27.2 ± 2.2	0.14	22.9	10.5
150-180	3.9 ± 1.5	18.1	28.7 ± 1.6	0.18	23.4	13.0
180-210	0.8 ± 0.3	17.5	29.7 ± 1.9	0.20	23.6	15.0

The subjects were measured their local skin temperatures (Figure 6.4) every 30 minutes.

6.3.2.2 Simulations

The simulations of the cool/cold ceiling series were carried out for the experimental conditions listed in Table 6.3 using time steps of Δt=5min. The resultant environmental conditions used in the simulation are plotted in Figure 6.9. The personal conditions i.e. clothing and activity level were the same as used in the simulation of the hot ceiling experiment, section 6.3.1.

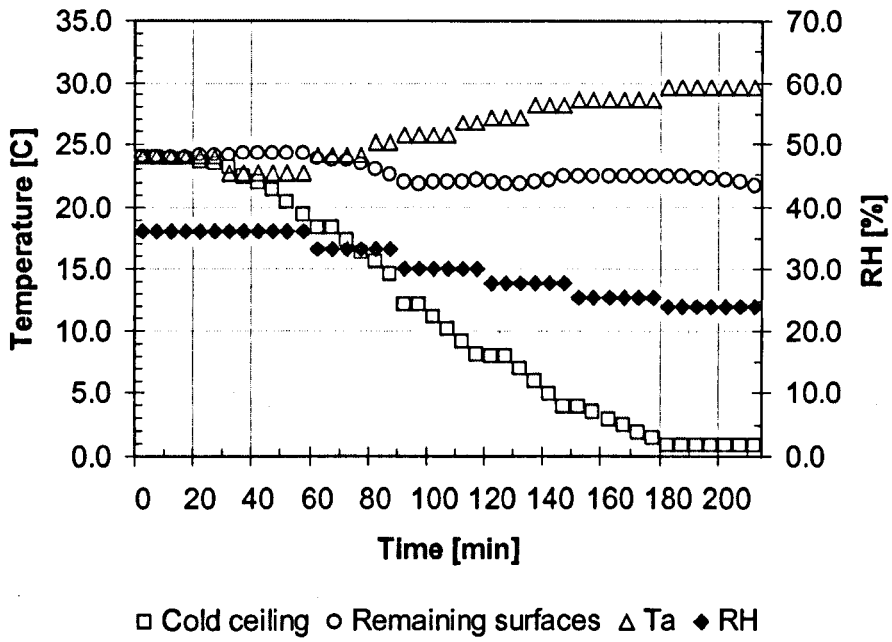

Figure 6.9 Environmental temperatures and relative humidity used in the simulation of the cool/cold ceiling series.

The predicted view factor between the whole body and the cool ceiling was 0.21 which again agreed well with the experimental value. The predicted local view factors between individual body parts and the cool ceiling are listed in Table 6.4. For this geometrical configuration the shoulders, head, posterior neck and the forehead were the most exposed body parts.

Table 6.4 Local view factors between the sedentary subject and (i) the cool/cold ceiling and (ii) the rest of the chamber.

Body parts	Cool/ cold ceiling	Rest of chamber	Body parts	Cool/ cold ceiling	Rest of chamber
Forehead	0.555	0.424	L. Leg: Up. Inferior	0.109	0.454
Head	0.603	0.361	L. Leg: Up. Exterior	0.095	0.681
Face: Anterior	0.360	0.464	L. Leg: Lo. Anterior	0.097	0.903
L. Face	0.327	0.557	L. Leg: Lo. Posterior	0.049	0.661
R. Face	0.327	0.557	L. Leg: Lo. Inferior	0.064	0.677
Neck: Anterior	0.335	0.432	L. Leg: Lo. Exterior	0.085	0.839
Neck: Posterior	0.597	0.346	L. Foot: Instep	0.134	0.752
Neck: L. Exterior	0.404	0.426	L. Foot: Sole	0.001	0.896
Neck: R. Exterior	0.404	0.426	R. Shoulder	0.673	0.212
L. Shoulder	0.673	0.212	R. Arm: Up. Anterior	0.160	0.315
Thorax: Anterior	0.429	0.484	R. Arm: Up. Posterior	0.368	0.632
Thorax: Posterior	0.421	0.568	R. Arm: Up. Inferior	0.132	0.464
Thorax: L. Inferior	0.092	0.363	R. Arm: Up. Exterior	0.366	0.588
Thorax: R. Inferior	0.092	0.363	R. Arm: Lo. Anterior	0.158	0.267
Abdomen: Anterior	0.211	0.279	R. Arm: Lo. Posterior	0.103	0.897
Abdomen: Posterior	0.207	0.793	R. Arm: Lo. Inferior	0.067	0.548
Abdomen: L. Inferior	0.120	0.549	R. Arm: Lo. Exterior	0.336	0.531
Abdomen: R. Inferior	0.120	0.549	R. Hand: Handback	0.290	0.424
L. Arm: Up. Anterior	0.160	0.315	R. Hand: Palm	0.032	0.222
L. Arm: Up. Posterior	0.368	0.632	R. Leg: Up. Anterior	0.200	0.231
L. Arm: Up. Inferior	0.132	0.464	R. Leg: Up. Posterior	0.000	0.945
L. Arm: Up. Exterior	0.366	0.588	R. Leg: Up. Inferior	0.109	0.454
L. Arm: Lo. Anterior	0.158	0.267	R. Leg: Up. Exterior	0.095	0.681
L. Arm: Lo. Posterior	0.103	0.897	R. Leg: Lo. Anterior	0.097	0.903
L. Arm: Lo. Inferior	0.067	0.548	R. Leg: Lo. Posterior	0.049	0.661
L. Arm: Lo. Exterior	0.336	0.531	R. Leg: Lo. Inferior	0.064	0.677
L. Hand: Handback	0.290	0.424	R. Leg: Lo. Exterior	0.085	0.839
L. Hand: Palm	0.032	0.222	R. Foot: Instep	0.134	0.752
L. Leg: Up. Anterior	0.200	0.231	R. Foot: Sole	0.001	0.896
L. Leg: Up. Posterior	0.000	0.945	**Whole body**	**0.210**	**0.572**

6.3.2.3 Results

Predictions of some physiological parameters resulting for the cool/cold ceiling experiment of Fanger et al. (1985) are presented in Figure 6.10.

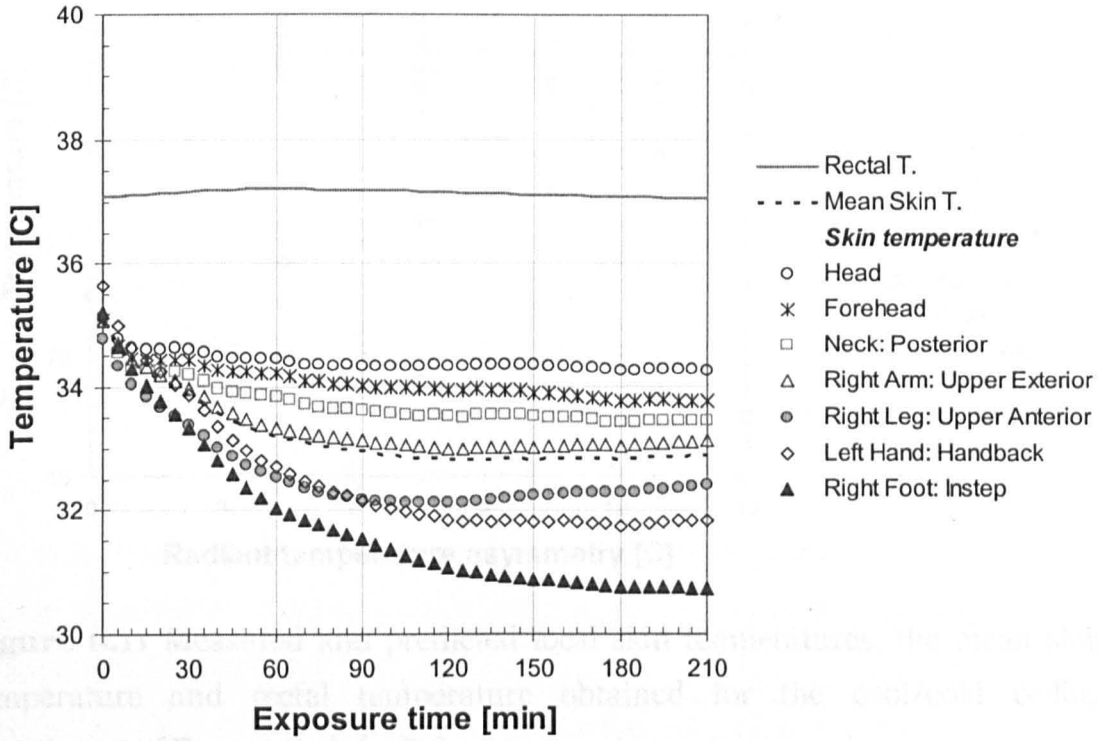

Figure 6.10 Predicted rectal, mean skin and local skin temperatures of some exposed and non-exposed.

For this type of exposure the extended model predicted most local skin temperatures to decrease slightly with time, for example, head, forehead, upper anterior right arm, handbacks and insteps. The skin temperature of the upper anterior legs initially fell from 34.7°C to 32.5°C before it started to rise slightly after 90 minutes of the exposure. During the exposure the rectal temperature was quite constant while the mean skin temperature decreased by about 2.5°C for t<90 min but rose moderately thereafter.

The simulation results are plotted together with the corresponding measured data over the radiant temperature asymmetry in Figure 6.11. The air

temperature and the mean radiant temperature in the chamber are also presented in the Figure 6.11.

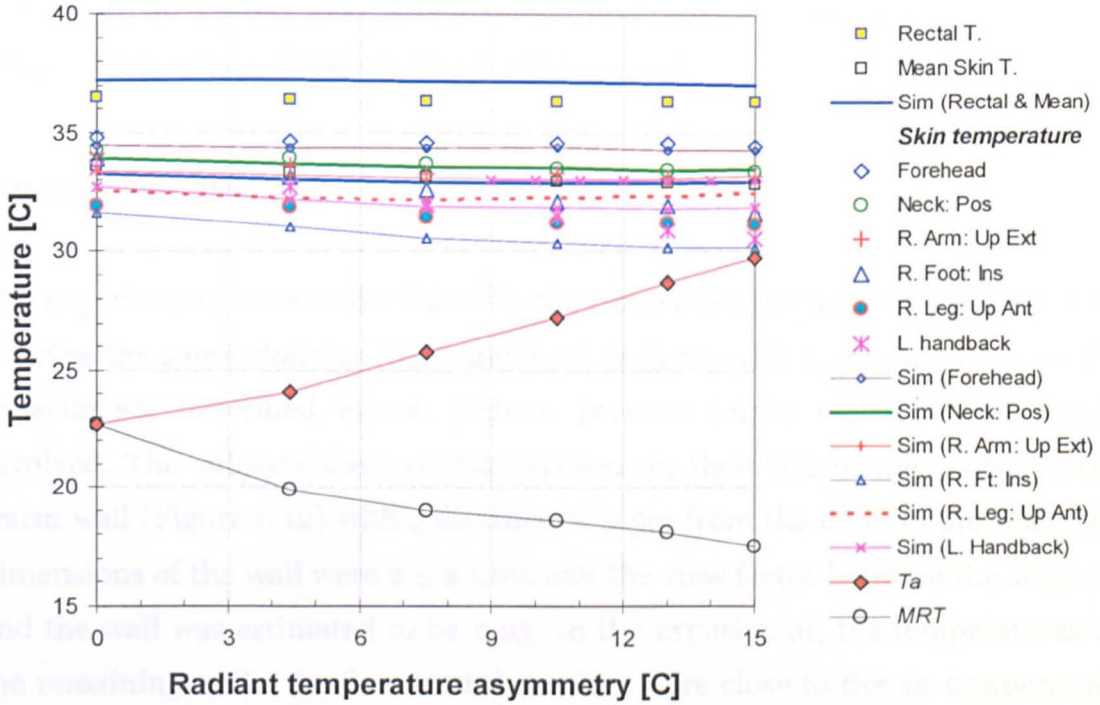

Figure 6.11 Measured and predicted local skin temperatures, the mean skin temperature and rectal temperature obtained for the cool/cold ceiling experiment of Fanger et al. (1985).

Generally, there were no significant differences between predictions (solid lines) and experimental results (data points). As can be seen, the predicted skin temperatures of forehead, posterior neck, upper exterior right arm and mean skin temperature were in good agreement with the experiments, i.e. an average within 0.8°C. An exception formed the instep of the right foot, the upper anterior right leg and left handback where the prediction deviated from measurements by about 1.4°C at the end of the exposure, i.e. at a radiant temperature asymmetry of 15°C. A possible explanation could be the fact that the simulation was performed using a fixed posture whereas in the experiments the subjects might have moved their extremities, e.g. because of perceiving locally cold discomfort. The skin temperatures predicted for all body sectors are provided in Appendix E (*Table E.2*).

6.3.3 Warm/hot wall

Fanger et al. (1985) also investigated physiological responses of sedentary subjects exposed, to their left, to a warm/hot wall.

6.3.3.1 Experiment

The experiments were under taken in the same chamber and the subjects were wearing the same clothing (KSU-standard uniform with open sandal) as in the experiments described above. Sixteen persons (eight males/females) were involved. The subjects were seated exposed on their left to the centre of the warm wall (Figure 6.12) with a distance of 0.5m from the body to the wall. The dimensions of the wall were 2.0 x 1.6m and the view factor between the subjects and the wall was estimated to be 0.25. In the experiment, the temperatures of the remaining walls, the floor and the ceiling were close to the air temperature in the room. The air velocity was maintained under 0.1 ms^{-1} and the vapour pressure was kept constant at 1 kPa.

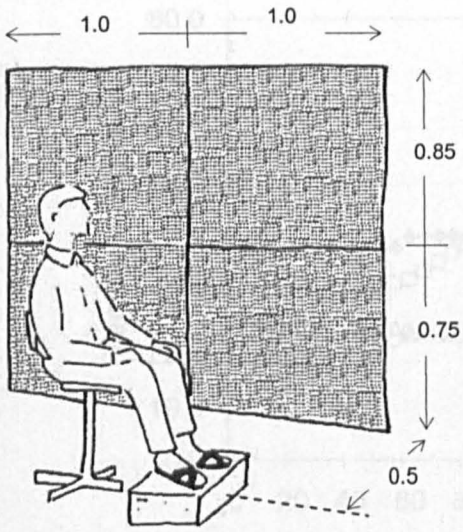

Figure 6.12 Experimental set up for warm/hot wall experiment, Fanger et al. (1985).

Similarly to the previous experiments, during the first hour the wall was unheated. In the following five half-hour periods the temperatures of heated wall was increased in steps from about 23°C to 70°C (*Table 6.5*).

Table 6.5 Experimental setting of the warm/hot wall experiment of Fanger et al. (1985).

Time [min]	Warm/hot wall temp. [°C]	MRT [°C]	T_a [°C]	Operative temp. [°C]	Radiant temp. asymmetry [°C]
0-60	23.2 ± 2.0	23.2	23.1 ± 2.0	23.4	-0.2
60-90	32.6 ± 2.0	25.3	21.9 ± 1.9	23.6	6.6
90-120	42.0 ± 1.9	26.5	20.7 ± 1.9	23.6	13.3
120-150	51.6 ± 1.6	27.5	19.3 ± 1.6	23.4	20.7
150-180	61.1 ± 1.8	29.3	17.9 ± 1.8	23.6	28.0
180-210	70.1 ± 3.3	30.5	16.7 ± 1.8	23.6	35.1

The local skin temperatures (Figure 6.4) were recorded every five minutes.

6.3.3.2 Simulations

The environmental conditions used in the simulations are plotted in Figure 6.13. The simulations were run with time steps of Δt=5min and assuming (as in other simulations) a typical emissivity of indoor surfaces of 0.95.

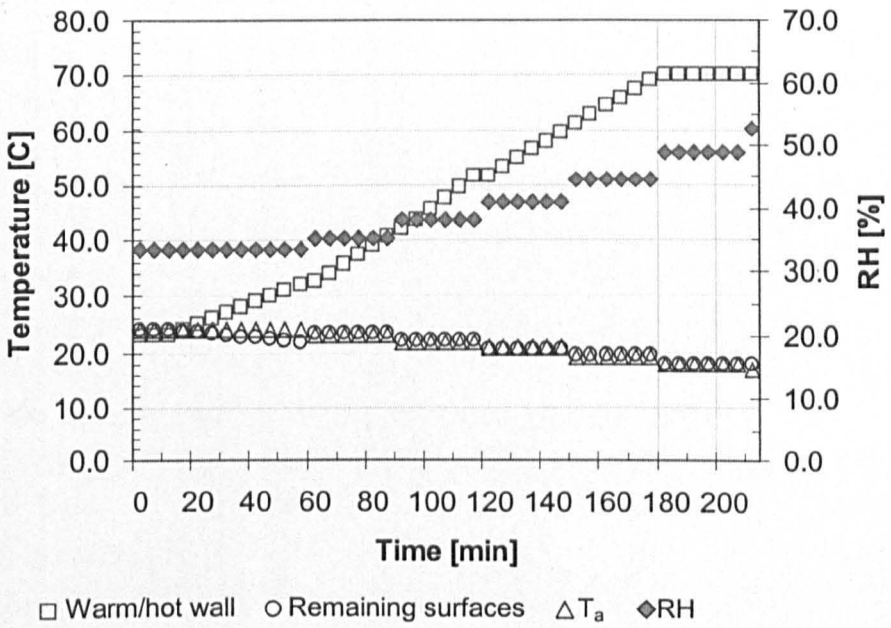

Figure 6.13 Environmental conditions in the simulation of the warm wall.

The predicted overall view factor between the subject and the heated wall panel resulted in $\varphi_{12} = 0.26$. The radiation calculations were performed using local view factors between body parts and the warm/hot panel and the rest of the chamber as listed in Table 6.6. For this geometrical configuration, e.g. the left face, exterior left neck, upper exterior left arm, lower posterior left arm, upper exterior left leg and lower exterior left leg were the most exposed body parts.

The subject was simulated as being seated (1.0 met) and wearing the KSU-uniform (Appendix D, *Table D.1*).

Table 6.6 Local view factors between the sedentary subject and (i) the warm/hot wall and (ii) the rest of the chamber.

Body parts	Warm /hot wall	Rest of chamber	Body parts	Warm /hot wall	Rest of chamber
Forehead	0.219	0.760	L. Leg: Up. Inferior	0.000	0.563
Head	0.184	0.780	L. Leg: Up. Exterior	0.589	0.186
Face: Anterior	0.239	0.585	L. Leg: Lo. Anterior	0.169	0.831
L. Face	0.688	0.196	L. Leg: Lo. Posterior	0.222	0.488
R. Face	0.000	0.885	L. Leg: Lo. Inferior	0.000	0.741
Neck: Anterior	0.201	0.566	L. Leg: Lo. Exterior	0.562	0.362
Neck: Posterior	0.172	0.770	L. Foot: Instep	0.245	0.641
Neck: L. Exterior	0.535	0.295	L. Foot: Sole	0.011	0.886
Neck: R. Exterior	0.000	0.833	R. Shoulder	0.035	0.851
L. Shoulder	0.235	0.650	R. Arm: Up. Anterior	0.067	0.397
Thorax: Anterior	0.245	0.667	R. Arm: Up. Posterior	0.056	0.944
Thorax: Posterior	0.216	0.773	R. Arm: Up. Inferior	0.254	0.352
Thorax: L. Inferior	0.263	0.192	R. Arm: Up. Exterior	0.001	0.952
Thorax: R. Inferior	0.007	0.457	R. Arm: Lo. Anterior	0.260	0.166
Abdomen: Anterior	0.114	0.376	R. Arm: Lo. Posterior	0.000	1.000
Abdomen: Posterior	0.269	0.731	R. Arm: Lo. Inferior	0.106	0.507
Abdomen: L. Inferior	0.471	0.198	R. Arm: Lo. Exterior	0.033	0.831
Abdomen: R. Inferior	0.000	0.667	R. Hand: Handback	0.086	0.625
L. Arm: Up. Anterior	0.193	0.282	R. Hand: Palm	0.043	0.217
L. Arm: Up. Posterior	0.452	0.548	R. Leg: Up. Anterior	0.161	0.268
L. Arm: Up. Inferior	0.043	0.553	R. Leg: Up. Posterior	0.087	0.849
L. Arm: Up. Exterior	0.604	0.349	R. Leg: Up. Inferior	0.295	0.268
L. Arm: Lo. Anterior	0.003	0.423	R. Leg: Up. Exterior	0.000	0.776
L. Arm: Lo. Posterior	0.721	0.279	R. Leg: Lo. Anterior	0.241	0.759
L. Arm: Lo. Inferior	0.110	0.504	R. Leg: Lo. Posterior	0.198	0.509
L. Arm: Lo. Exterior	0.399	0.467	R. Leg: Lo. Inferior	0.395	0.342
L. Hand: Handback	0.263	0.451	R. Leg: Lo. Exterior	0.000	0.927
L. Hand: Palm	0.141	0.113	R. Foot: Instep	0.205	0.679
L. Leg: Up. Anterior	0.040	0.391	R. Foot: Sole	0.004	0.892
L. Leg: Up. Posterior	0.225	0.721	**Whole body**	**0.254**	**0.528**

6.3.3.3 Results

Predictions of some physiological parameters resulting for the warm/hot wall experiment of Fanger et al. (1985) are shown in Figure 6.14.

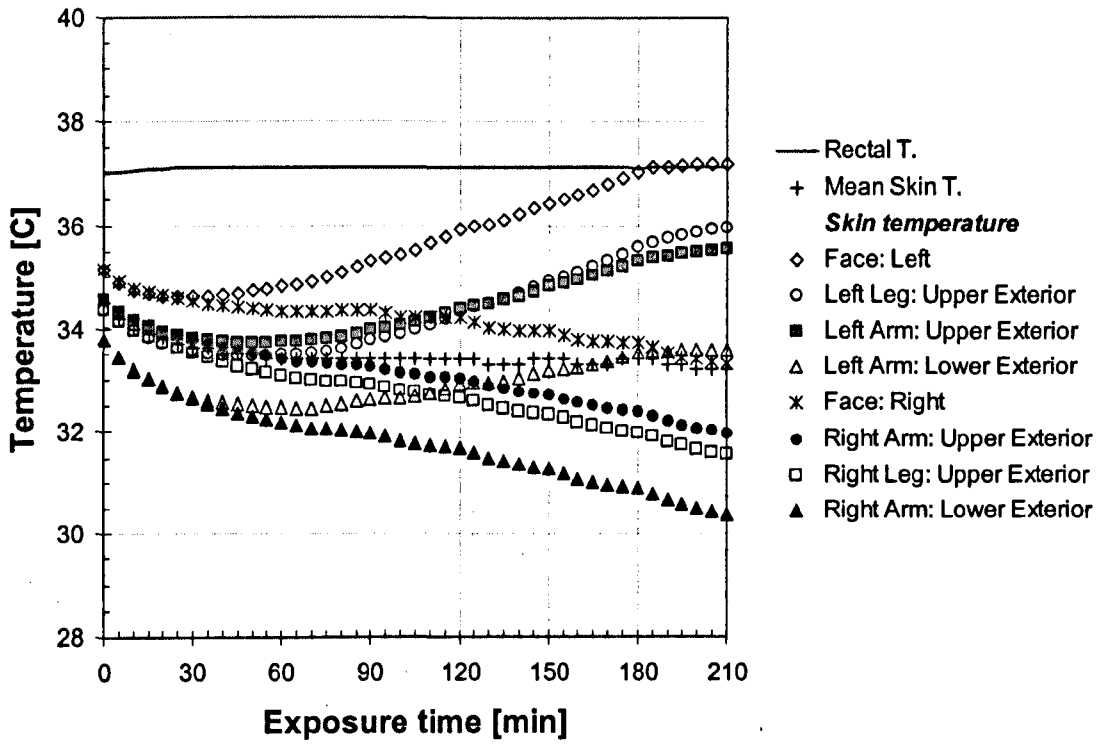

Figure 6.14 Predicted rectal, mean skin and local skin temperatures of some exposed and non-exposed body parts.

For the warm/hot wall exposure the predicted local skin temperature of those body parts that were exposed to the heated panel rose significantly with time, e.g. left face, upper exterior left leg, upper exterior left arm and lower exterior left arm. The highest local skin temperature of 37.2°C was predicted for the left exterior part of the face. On the other hand the skin temperatures of the right face, upper exterior right leg, upper exterior right arm and lower exterior right arm were predicted to fall with time. The mean skin and the rectal temperature, however, remained fairly constant until the end of the experiment indicating thermoneutral overall conditions.

The predicted and measured body temperatures (local skin temperatures, mean skin temperature and rectal temperature) are plotted over the horizontal radiant temperature asymmetry in Figure 6.15.

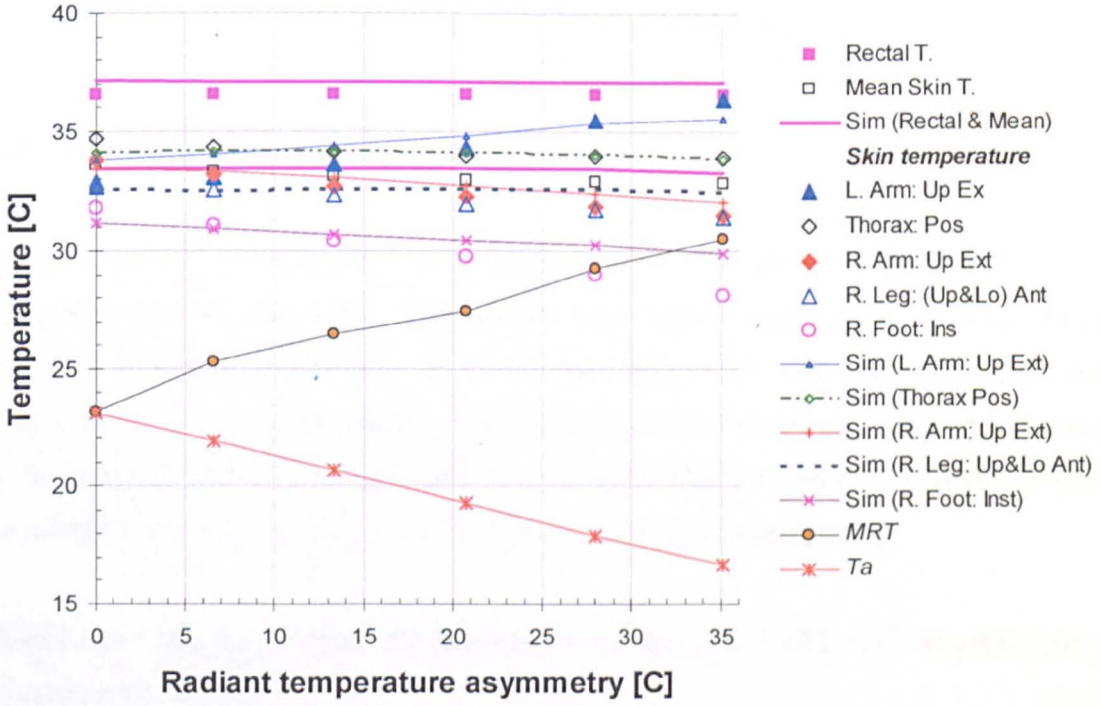

Figure 6.15 The predicted and measured (Fanger et al. 1985) skin temperatures and rectal temperature of subjects exposed spatially to a warm/hot wall panel.

The predictions (solid lines) showed good agreement with experimental results (data points) for skin temperatures of the upper exterior left arm, posterior thorax, upper exterior right arm, upper and lower anterior right leg, upper exterior right arm and the mean skin temperature. The average discrepancy was about 0.6°C. An exception formed the predicted skin temperature of the instep of the right foot which was about 1.8°C higher than the measured value. The predicted and measured rectal and mean skin temperatures were constant for all radiant temperature asymmetries. The average discrepancies ranged at about 0.1°C and 0.5°C for the mean skin and the rectal temperature, respectively. Further simulation results are provided in Appendix E (*Table E.3*).

6.3.4 Cool/cold wall

Fanger et al. (1985) also investigated physiological responses of sedentary subjects exposed to theirs left to a cool/cold vertical panel.

6.3.4.1 Experiment

In these experimental series participated thirty two persons (16 males and 16 females). The geometrical configuration (see Figure 6.12), experimental design and the clothing of the test persons were identical with the warm/hot wall series, section 6.3.3. The surface temperature of the panel was however lowered in steps from 24°C down to 0.4°C (*Table 6.7*). The air velocity and the relative humidity were kept constant at <0.1 ms^{-1} and 1 kPa, respectively.

Table 6.7 Environmental temperatures in the cool/cold wall experiment of Fanger et al. (1985).

Time [min]	Cool/cold wall temp. [°C]	MRT [°C]	T_a [°C]	Operative temp. [°C]	Radiant temp. asymmetry [°C]
0-60	24.1 ± 1.5	24.1	24.3 ± 1.5	24.2	0.4
61-90	17.8 ± 1.5	23.7	25.9 ± 1.5	24.8	5.3
91-120	13.3 ± 1.5	22.9	27.1 ± 1.5	25.0	8.6
121-150	8.7 ± 1.5	22.3	28.1 ± 1.5	25.2	12.8
151-180	4.1 ± 1.7	21.4	29.0 ± 1.7	25.2	16.6
181-210	0.4 ± 0.5	21.4	29.6 ± 1.8	25.5	18.2

Local skin temperatures of the subjects were measured every 30 minutes across the body (*Figure 6.4*).

6.3.4.2 Simulations

The simulations were run for the environmental conditions provided in Figure 6.16 with Δt=5min. The radiation calculations were performed using local view factors listed in Table 6.6 and an emissivity of the surrounding surfaces which was assumed to be 0.95.

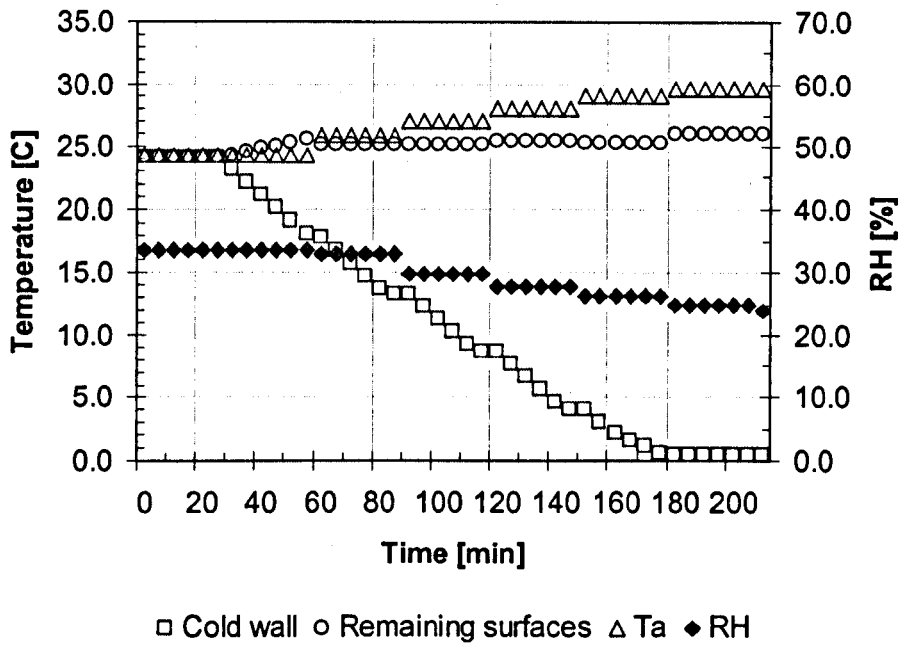

Figure 6.16 Environmental conditions used in the simulations of the cool/cold wall experiment (Fanger et al., 1985).

Similarly to the previous simulations, the subject was simulated as being seated (1.0 met) and wearing the KSU-uniform (*Appendix D, Table D.1*).

6.3.4.3 Results

Predicted local skin temperatures of selected body parts are plotted in Figure 6.17. Also shown in Figure 6.17 are the predicted rectal and mean skin temperature.

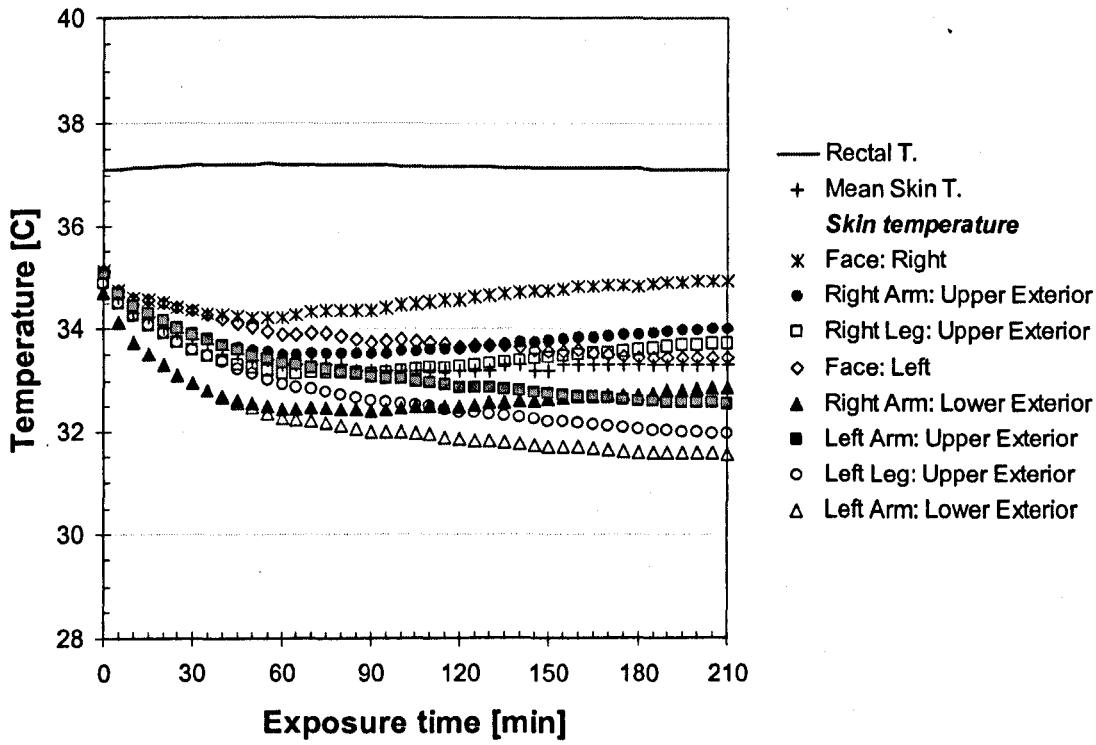

Figure 6.17 Predicted rectal, mean skin and some local skin temperatures obtained for the cool/cold wall exposure (Fanger et al. 1985).

The skin temperature of body parts exposed to the chilled panel (i.e. left face, upper exterior left leg, upper exterior left arm and lower exterior left arm) slightly fell with time. Because the subjects were exposed to temporal increasing air temperatures the skin temperature of most body parts rose with time (in Figure 6.17, e.g. right face, upper exterior right leg, upper exterior right arm and lower exterior right arm). Nevertheless the mean skin and the rectal temperature were maintained at constant levels.

The predicted rectal, mean skin and local skin temperatures are compared with available measured data as a function of the radiant temperature asymmetry in

Figure 6.18. Also plotted in Figure 6.18 are the air temperature and the mean radiant temperature in the chamber.

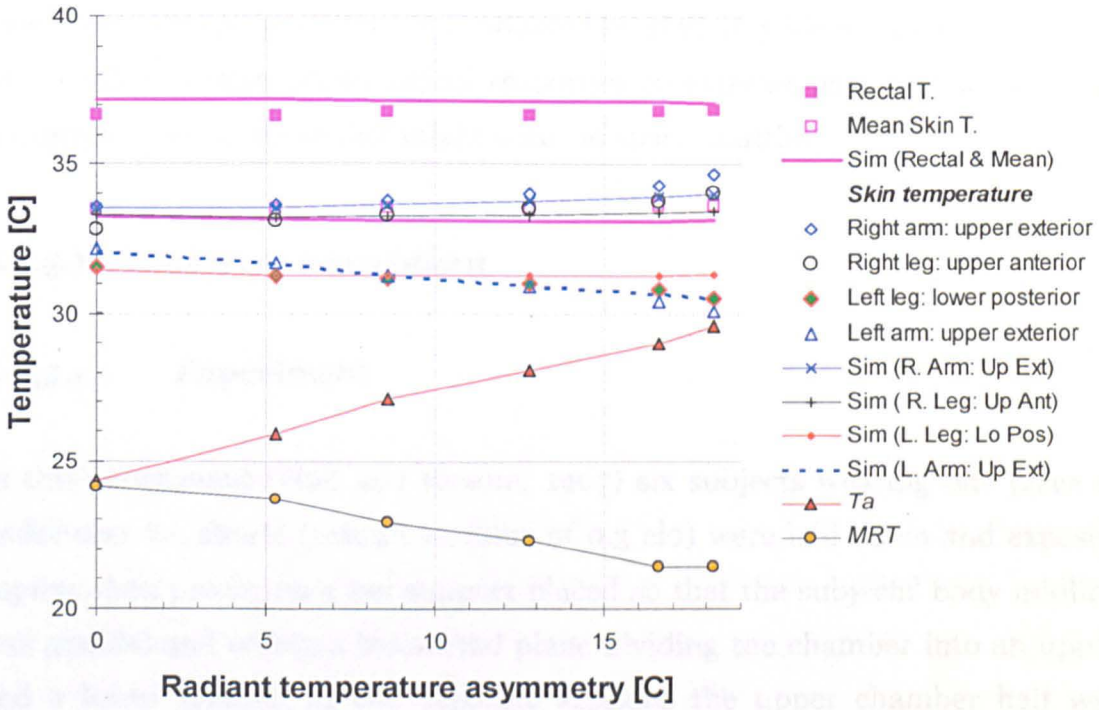

Figure 6.18 Comparison of predicted rectal and skin temperatures obtained for the cool/cold wall experiment of Fanger et al. (1985).

Generally, there were no significant differences between predictions (solid lines) and experimental results (data points) for rectal and skin temperatures. The greatest discrepancy between prediction and experiment resulted for the left lower posterior leg at a radiant temperature asymmetry of 18.2°C yielding 0.8°C. Further simulation results are provided in Appendix E (*Table E.4*).

6.3.5 Extreme asymmetric radiation conditions

Two series of experiments were conducted by Hall and Klemm (1967 and 1969) who studied human physiological responses to extreme asymmetric radiation conditions such as those that might occur in space shuttles.

6.3.5.1 Transient experiment

6.3.5.1.1 Experiment

In this experiment (Hall and Klemm, 1967) six subjects wearing one piece of underwear i.e. shorts (overall I_{cl}-value of 0.3 clo) were laid down and exposed supine, then prone, on a net support placed so that the subjects' body midline was parallel and within a horizontal plane dividing the chamber into an upper and a lower section. In two separate sessions the upper chamber half was maintained at 82.2 and 93.3°C while the lower half was kept commonly at -6.7°C. Air temperatures in the chamber varied from -6.7 to 82 and 93°C, respectively, with a range of 15-30°C in the close proximity of the subjects. The subjects were exposed first supine for 30 minutes and then prone for 45 minutes while lying on the net support. Rectal temperature and 17 skin temperature (forehead, neck, scapula, kidney, nipple, abdomen, rump, upper right arm, lower left arm, right and left hand, upper right anterior leg, upper left posterior leg, lower right posterior leg, lower left anterior leg, right and left foot) were measured across the body of the subjects every five minutes. The measured mean skin temperature were determined from the 17 local skin temperatures and weighted on a surface area basis. The air velocity and the water vapour pressure in the chamber were constant at 0.08 ms^{-1} and 0.3-0.4 kPa, respectively.

6.3.5.1.2 Simulations

This transient exposure was simulated by exposing the anterior and posterior body parts to the hot and cold half of the chamber, respectively, for the initial 30minutes. The environmental conditions were then 'swapped' to simulate the 'turning around' the subjects in the experiment. The environmental conditions used in the simulation are provided in Table 6.8. The simulations were performed for time steps, Δt=5min.

Table 6.8 Environmental conditions used in the simulation of the transient exposure experiment of Hall and Klemm (1967).

Series no.	Time [min]	Anterior body parts			Posterior body parts			V_a [ms^{-1}]
		Surf. temp. [°C]	T_a [°C]	RH [%]	Surf. temp. [°C]	T_a [°C]	RH [%]	
1	0-30	93.0	31.0	7.4	-6.7	17.0	17.2	0.08
	30-75	-6.7	17.0	17.2	93.0	31.0	7.4	0.08
2	0-30	82.0	25.0	10.5	-6.7	14.0	20.9	0.08
	30-75	-6.7	14.0	20.9	82.0	25.0	10.5	0.08

The human local view factors for each of the 59 body parts of the subject with respect to the upper half and lower half of the chamber are listed in Table 6.9. The emissivity of the chamber was assumed to be 0.95. The clothing file with local clothing characteristics used in the simulations is provided in Appendix D (*Table D.2*).

Table 6.9 Local view factors between the subject and the lower and upper section of the climate chamber used in Hall and Klemm (1967) experiment.

Body parts	U. half chamber	L. half chamber	Body parts	U. half chamber	L. half chamber
Forehead	0.953	0.033	L. Leg: Up. Inferior	0.320	0.149
Head	0.257	0.708	L. Leg: Up. Exterior	0.282	0.597
Face: Anterior	0.769	0.073	L. Leg: Lo. Anterior	0.920	0.008
L. Face	0.507	0.384	L. Leg: Lo. Posterior	0.014	0.925
R. Face	0.507	0.384	L. Leg: Lo. Inferior	0.443	0.283
Neck: Anterior	0.775	0.004	L. Leg: Lo. Exterior	0.415	0.565
Neck: Posterior	0.005	0.938	L. Foot: Instep	0.369	0.491
Neck: L. Exterior	0.425	0.432	L. Foot: Sole	0.568	0.328
Neck: R. Exterior	0.425	0.432	R. Shoulder	0.291	0.614
L. Shoulder	0.291	0.614	R. Arm: Up. Anterior	0.735	0.019
Thorax: Anterior	0.904	0.027	R. Arm: Up. Posterior	0.022	0.905
Thorax: Posterior	0.002	0.957	R. Arm: Up. Inferior	0.101	0.235
Thorax: L. Inferior	0.186	0.254	R. Arm: Up. Exterior	0.405	0.577
Thorax: R. Inferior	0.186	0.254	R. Arm: Lo. Anterior	0.877	0.000
Abdomen: Anterior	0.892	0.001	R. Arm: Lo. Posterior	0.042	0.922
Abdomen: Posterior	0.011	0.878	R. Arm: Lo. Inferior	0.218	0.289
Abdomen: L. Inferior	0.199	0.434	R. Arm: Lo. Exterior	0.601	0.396
Abdomen: R. Inferior	0.199	0.434	R. Hand: Handback	0.577	0.307
L. Arm: Up. Anterior	0.735	0.019	R. Hand: Palm	0.226	0.154
L. Arm: Up. Posterior	0.022	0.905	R. Leg: Up. Anterior	0.874	0.002
L. Arm: Up. Inferior	0.101	0.235	R. Leg: Up. Posterior	0.003	0.934
L. Arm: Up. Exterior	0.405	0.577	R. Leg: Up. Inferior	0.320	0.149
L. Arm: Lo. Anterior	0.877	0.000	R. Leg: Up. Exterior	0.282	0.597
L. Arm: Lo. Posterior	0.042	0.922	R. Leg: Lo. Anterior	0.920	0.008
L. Arm: Lo. Inferior	0.218	0.289	R. Leg: Lo. Posterior	0.014	0.925
L. Arm: Lo. Exterior	0.601	0.396	R. Leg: Lo. Inferior	0.443	0.283
L. Hand: Handback	0.577	0.307	R. Leg: Lo. Exterior	0.415	0.565
L. Hand: Palm	0.226	0.154	R. Foot: Instep	0.369	0.491
L. Leg: Up. Anterior	0.874	0.002	R. Foot: Sole	0.568	0.328
L. Leg: Up. Posterior	0.003	0.934	**Whole Body**	**0.402**	**0.434**

6.3.5.1.3 Results

In the experiment, the measured local skin temperatures were used to calculate the average skin temperature separately for the anterior and for the posterior body side (rather than providing the local quantities). Accordingly, the anterior and posterior average skin temperatures were calculated using the predicted local skin temperatures. The results are presented in Figure 6.19. Also shown are the predicted and measured body average skin temperature and rectal temperature.

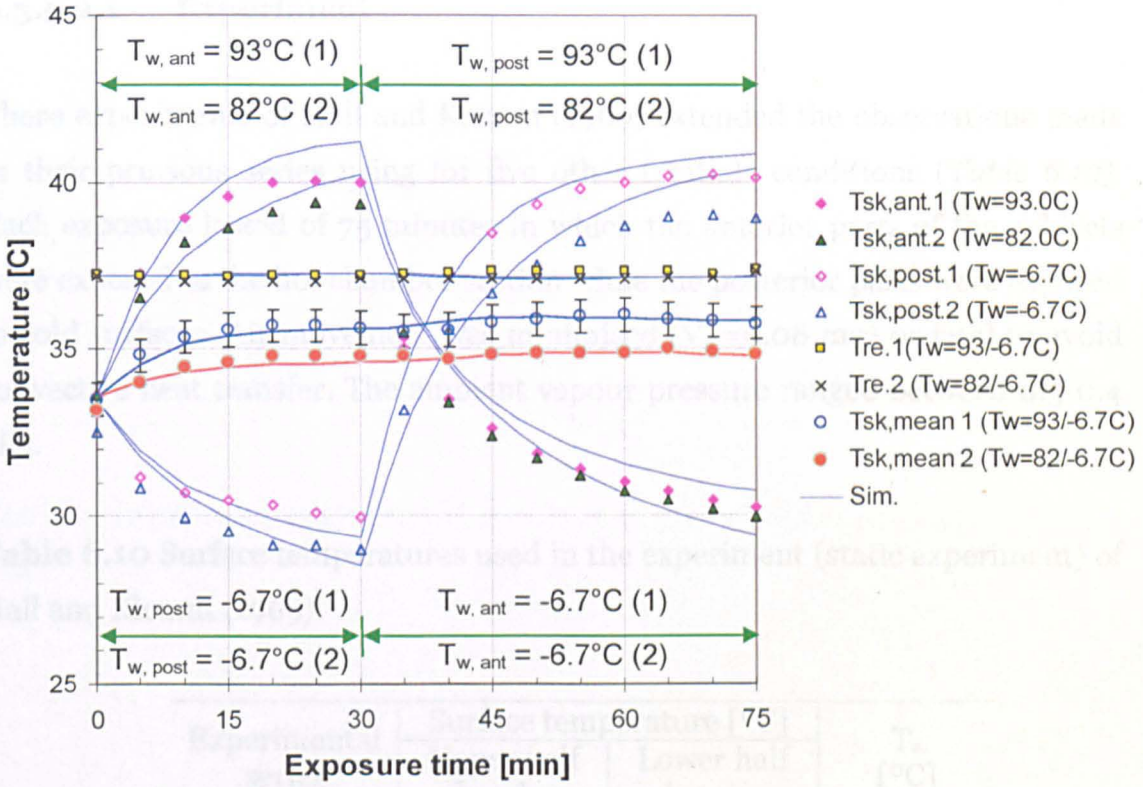

Figure 6.19 Measured and predicted rectal, mean skin, mean anterior and mean posterior skin temperature of subjects exposed to extreme radiant asymmetry conditions (Hall and Klemm, 1967).

During the first 30 minutes, the measured mean anterior skin temperatures rose considerably reaching about 39.5°C and 40°C at T_w=82°C and 93°C, respectively. The opposite behaviour was observed for the average skin temperature of the posterior body site. It fell from its initial value of 33.5°C

under 30°C after 30minutes. The maximum discrepancy between experiment and prediction reached about 1.2°C ($T_{w,\,post}$ at 93°C) and 1.36°C ($T_{w,\,post}$ at 82°C) here. Rectal temperatures were constant while the mean skin temperatures slightly increased during the whole experiments. It can be seen from Figure 6.19 that both quantities were predicted reasonably well, i.e. within the range of experimental error.

6.3.5.2 Static experiment

6.3.5.2.1 Experiment

These experiments of Hall and Klemm (1969) extended the observations made in their previous series using for five other (static) conditions (*Table 6.10*). Each exposure lasted of 75 minutes in which the anterior parts of the subjects were exposed to the hot chamber section while the posterior parts were exposed to cold surfaces. Air movement was minimised (V_a =0.08 ms^{-1} or less) to avoid convective heat transfer. The ambient vapour pressure ranged between 0.3-0.4 kPa.

Table 6.10 Surface temperatures used in the experiment (static experiment) of Hall and Klemm (1969).

Experimental series	Surface temperature [°C]		T_a [°C]
	Upper half chamber	Lower half chamber	
1	104	-6.7	24.0
2	92	-6.7	17.0
3	83	-6.7	14.0
4	65	-11	17.0
5	53	-11	11.0

6.3.5.2.2 Simulations

The simulations were conducted for the environmental settings listed in Table 6.11 and time steps of Δt=5 min. The radiation calculations were performed using local view factors listed in Table 6.9 (*section 6.3.5.1.2*) and a surface emissivity of the chamber walls of 0.95.

Table 6.11 Environmental conditions used in the simulation of the static experiments.

Series no.	Time [min]	Upper half chamber		Lower half chamber		V_a [ms^{-1}]
		Surf. Temp. [°C]	Ta [°C]	Surf. Temp. [°C]	T_a [°C]	
1	0-75	104.0	42.0	-6.7	24.0	0.08
2	0-75	92.0	33.0	-6.7	17.0	0.08
3	0-75	83.0	28.0	-6.7	14.0	0.08
4	0-75	65.0	29.0	-11.0	17.0	0.08
5	0-75	53.0	22.0	-11.0	11.0	0.08

The clothing ensemble used in the simulations is provided in Appendix D (*Table D.2*).

6.3.5.2.3 Results

As in the previous experiment the measured mean skin temperature were determined from 17 local skin temperatures. A comparison of the predicted mean skin temperatures and rectal temperatures with the corresponding experimental values obtained for the five exposures is presented in Figure 6.20.

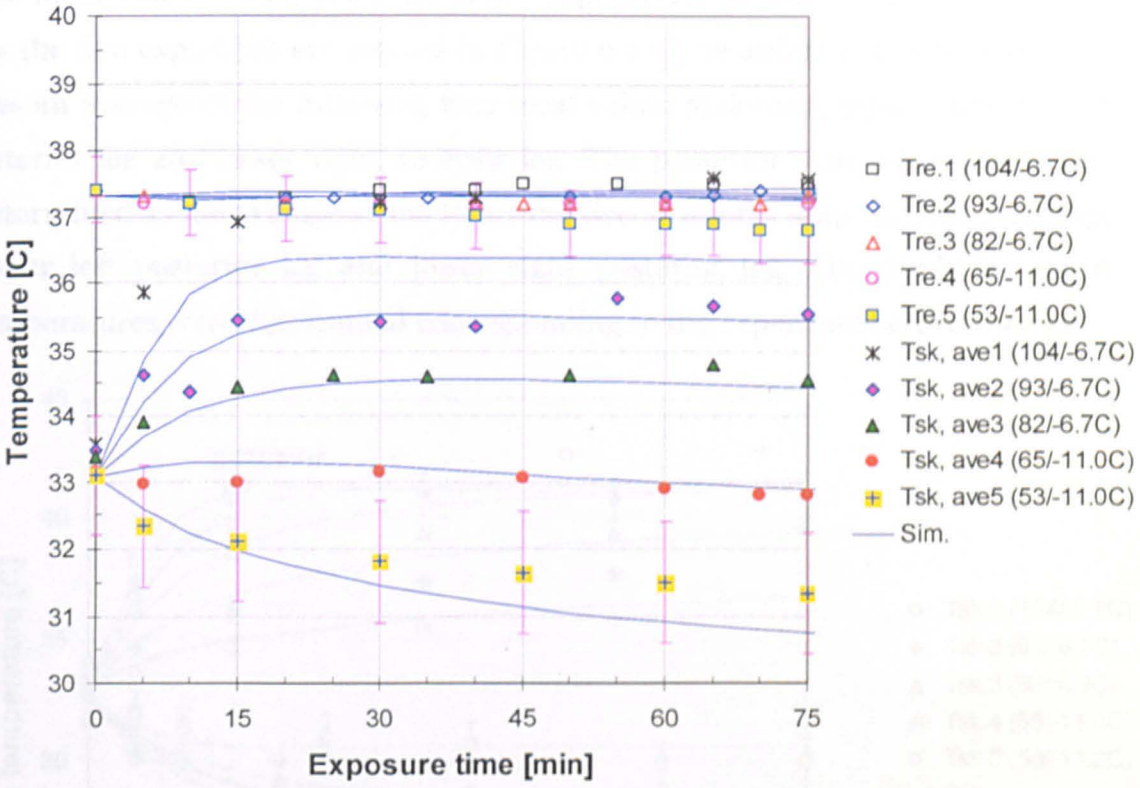

Figure 6.20 Rectal and average skin temperatures of the subjects exposed to five different-radiant asymmetries, Hall and Klemm (1969).

For exposures 1-3 (i.e. T_w=104/-6.7°C, 93/-6.7°C and 82/-6.7°C) the mean skin temperatures rose quickly during the first 15 minutes reaching about 37.0, 35.5 and 34.4°C. Equilibrium temperatures were obtained after about 30minutes for these exposures. Relatively constant and decreasing skin temperatures resulted for exposures 4 and 5, i.e. T_w=65.0/-11.0°C and 53.0/-11.0°C.

The average deviation between prediction and measured result was 0.4 K considering all five exposures. The maximum discrepancy reached about 1.24°C

for exposure 1, i.e. T_w=104/-6.7°C. The rectal temperatures were relatively constant throughout exposures. An exception formed the exposure to T_w=53/-11.0°C when the measured rectal temperature fell by about 36.8 K. It can be seen from Figure 6.20 that the predicted values (solid lines) were generally in good agreement with the experimental data.

The mean anterior and posterior skin temperatures as measured and predicted for the five exposures are plotted in Figure 6.21. The anterior skin temperature was an average of the following four local value: abdomen, nipple, upper right anterior leg and lower right anterior leg. The posterior skin temperature was determined as the average of the following five locations: scapula, kidney, rump, upper left posterior leg and lower right posterior leg. The predicted mean temperatures were determined corresponding to the experimental procedure.

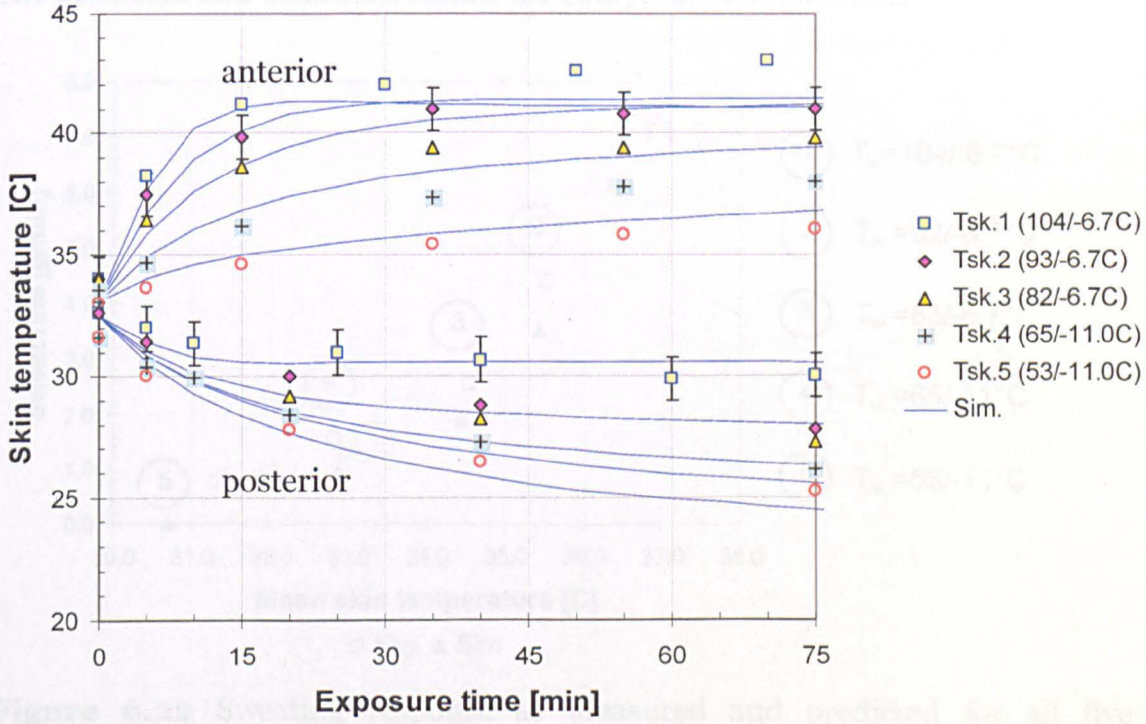

Figure 6.21 Measured and predicted mean anterior and mean posterior skin temperatures of the subjects exposed to five different radiant asymmetries (Hall and Klemm, 1969).

The measured anterior skin temperatures increased considerably while the posterior skin temperatures significantly decreased during the first 15 minutes. After 15 minutes, the anterior skin temperature rose slightly and on the other hand the posterior skin temperatures slightly declined until the end on the experimental time. Generally, the predictions agreed well with the experiments for both anterior skin temperatures and posterior skin temperatures. The average deviation between prediction and measured result was 0.7 °C. The maximum discrepancy of 1.9°C resulted for exposure 1 (T_w =104/-6.7 °C) which was greater than the experimental error (±1.1 °C) indicated as bars in Figure 6.21.

For the static-exposure experiment of Hall and Klemm also provided information on measured sweat rates as a function of mean skin temperature. The predicted and measured results are compared in Figure 6.22.

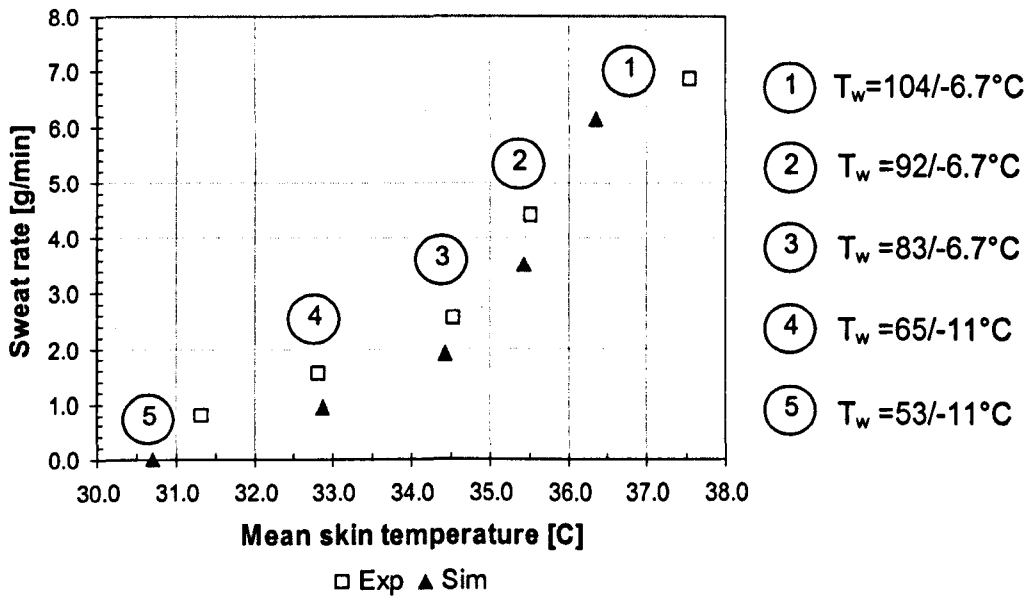

Figure 6.22 Sweating response as measured and predicted for all five exposures (Hall and Klemm, 1969) as a function of the mean skin temperature.

Rectangular marks represent measured data and triangles the predicted sweat rates. As can be seen both measured and predicted quantities significantly increased with raising skin temperatures. The predictions agreed generally well with the experimental results, i.e. within 0.7 g/min average deviation.

6.3.6 Exposure to simulated solar radiation

In this example, the performance of the model was examined for conditions in which human subjects were exposed to simulated direct solar radiation, Hodder (2002).

6.3.6.1 Experiment

Eight healthy male subjects participated in the experiment of Hodder (2002). The subjects were taken into a preparation room with a neutral ambient temperature. After 30 minutes (solar simulation lamp were turned on for at least 30 minutes prior to the start of the experiment to allow them to reach their steady state operating conditions), the subjects were then moved to sit in a car seat directly facing to a 1000W solar simulation lamp in a test chamber (*Figure 6.23*). The lamp was fitted behind a clear glass window (which transmission coefficient was assumed to be 0.96). The subjects were exposed to three radiation levels: 200, 400 and 600 Wm^{-2}. Each exposure lasted 30 minutes.

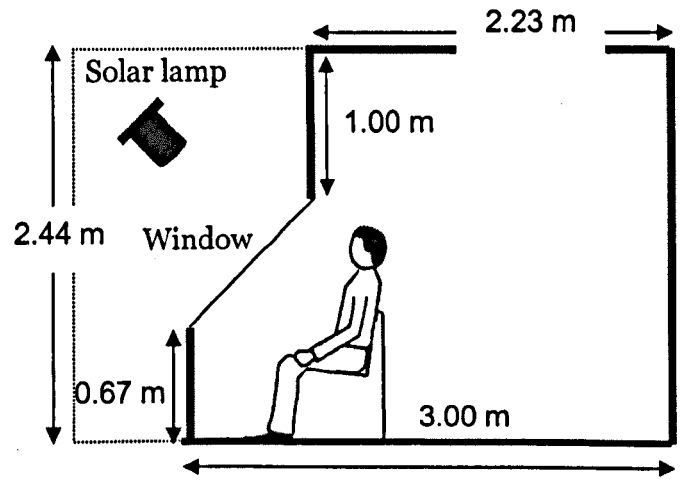

Figure 6.23 Experimental set up of short-wave radiation in the experiment of Hodder (2002).

The environmental chamber was controlled in order to maintain constant 'neutral' environmental conditions within PMV=0±0.5. In this study only the exposures with the lowest and the highest radiation level were considered, i.e. 200 and 600 Wm^{-2}. The experimental boundary conditions for these exposures are provided in Table 6.12. The subjects were clothed in white cotton/polyester long sleeve shirt, beige cotton/polyester trousers, undergarments and shoes. The overall clo-value of this ensemble was estimated to be 0.7 clo.

Table 6.12 Environmental conditions of the experiment of Hodder (2002).

Solar radiation level [Wm^{-2}]	T_{window} [°C]	T_a [°C]	MRT [°C]	V_a [ms^{-1}]	RH [%]
200	33.51	23.44	37.70	0.05	51.47
600	37.32	24.09	44.40	0.06	49.65

Skin temperatures were recorded every 10 seconds at six different body sides: forehead, exterior upper arm, exterior lower arm, chest, thigh (exterior upper leg) and calf (exterior lower leg). The measured mean skin temperatures in the experiments were determined as a function of four local skin temperature, Ramanathan (1964).

6.3.6.2 Simulations

As above mentioned, only the lowest and highest radiation levels (200 and 600 Wm^{-2}) were chosen for simulation purposes. The simulations were run with time steps of Δt=2min assuming a typical emissivity of indoor surface at 0.95. The emissivity of clothing was assumed as 0.95. Absorptivity of white cotton shirt and trousers was assumed to be 0.5 and 0.7, respectively. Details of clothing ensembles used in the simulations are provided in Appendix D (*Table D.3*). The environmental conditions used in the simulation are listed in Table 6.13.

Table 6.13 Environmental conditions used to simulate the Hodder (2002) experiments.

Solar radiation level [Wm^{-2}]	Time [min]	Window temp. [°C]	Rest of chamber [°C]	MRT [°C]	T_a [°C]	V_a [ms^{-1}]
200	0-30	33.51	18.16	37.70	23.44	0.05
600	0-30	37.32	24.21	44.40	24.09	0.06

The predicted view factor of the whole body with respect to the front window was 0.05. Detailed view factors of 59 body parts used in the simulation are listed in Table 6.14.

Table 6.14 Local view factors of the subject with respect to the front window and the rest of the chamber.

Body parts	Front panel	Rest of chamber	Body parts	Front panel	Rest of chamber
Forehead	0.680	0.299	L. Leg: Up. Inferior	0.012	0.552
Head	0.085	0.878	L. Leg: Up. Exterior	0.008	0.768
Face: Anterior	0.471	0.353	L. Leg: Lo. Anterior	0.000	1.000
L. Face	0.166	0.718	L. Leg: Lo. Posterior	0.000	0.709
R. Face	0.166	0.719	L. Leg: Lo. Inferior	0.000	0.740
Neck: Anterior	0.359	0.408	L. Leg: Lo. Exterior	0.000	0.924
Neck: Posterior	0.000	0.943	L. Foot: Instep	0.000	0.886
Neck: L. Exterior	0.086	0.744	L. Foot: Sole	0.000	0.897
Neck: R. Exterior	0.086	0.747	R. Shoulder	0.031	0.854
L. Shoulder	0.031	0.854	R. Arm: Up. Anterior	0.125	0.338
Thorax: Anterior	0.277	0.635	R. Arm: Up. Posterior	0.000	1.000
Thorax: Posterior	0.000	0.989	R. Arm: Up. Inferior	0.000	0.606
Thorax: L. Inferior	0.018	0.437	R. Arm: Up. Exterior	0.059	0.894
Thorax: R. Inferior	0.018	0.446	R. Arm: Lo. Anterior	0.060	0.366
Abdomen: Anterior	0.100	0.390	R. Arm: Lo. Posterior	0.006	0.994
Abdomen: Posterior	0.000	1.000	R. Arm: Lo. Inferior	0.000	0.613
Abdomen: L. Inferior	0.002	0.667	R. Arm: Lo. Exterior	0.103	0.761
Abdomen: R. Inferior	0.002	0.666	R. Hand: Handback	0.040	0.672
L. Arm: Up. Anterior	0.125	0.350	R. Hand: Palm	0.001	0.259
L. Arm: Up. Posterior	0.000	1.000	R. Leg: Up. Anterior	0.022	0.407
L. Arm: Up. Inferior	0.000	0.597	R. Leg: Up. Posterior	0.000	0.936
L. Arm: Up. Exterior	0.059	0.894	R. Leg: Up. Inferior	0.012	0.551
L. Arm: Lo. Anterior	0.060	0.366	R. Leg: Up. Exterior	0.008	0.767
L. Arm: Lo. Posterior	0.006	0.994	R. Leg: Lo. Anterior	0.000	1.000
L. Arm: Lo. Inferior	0.000	0.614	R. Leg: Lo. Posterior	0.000	0.707
L. Arm: Lo. Exterior	0.103	0.763	R. Leg: Lo. Inferior	0.000	0.737
L. Hand: Handback	0.040	0.675	R. Leg: Lo. Exterior	0.000	0.927
L. Hand: Palm	0.001	0.254	R. Foot: Instep	0.000	0.884
L. Leg: Up. Anterior	0.022	0.409	R. Foot: Sole	0.000	0.895
L. Leg: Up. Posterior	0.000	0.945	**Whole Body**	**0.048**	**0.734**

For short-wave radiation, projected area factors of 59 individual body sectors are required. The corresponding local projected area factors of the subjects facing to the solar lamp in the simulations at altitude angle of 45° are provided

in Table 6.15. The transmittance of a clear glass window was assumed to be 0.96.

Table 6.15 Local projected area factors of the subject using in the simulation.

Body parts	fp-factor	Body parts	fp-factor
Forehead	0.624	L. Leg: Up. Inferior	0.059
Head	0.251	L. Leg: Up. Exterior	0.048
Face: Anterior	0.375	L. Leg: Lo. Anterior	0.748
L. Face	0.134	L. Leg: Lo. Posterior	0.028
R. Face	0.134	L. Leg: Lo. Inferior	0.226
Neck: Anterior	0.323	L. Leg: Lo. Exterior	0.155
Neck: Posterior	0.000	L. Foot: Instep	0.341
Neck: L. Exterior	0.206	L. Foot: Sole	0.000
Neck: R. Exterior	0.206	R. Shoulder	0.402
L. Shoulder	0.402	R. Arm: Up. Anterior	0.335
Thorax: Anterior	0.724	R. Arm: Up. Posterior	0.000
Thorax: Posterior	0.001	R. Arm: Up. Inferior	0.002
Thorax: L. Inferior	0.011	R. Arm: Up. Exterior	0.298
Thorax: R. Inferior	0.011	R. Arm: Lo. Anterior	0.447
Abdomen: Anterior	0.462	R. Arm: Lo. Posterior	0.000
Abdomen: Posterior	0.000	R. Arm: Lo. Inferior	0.016
Abdomen: L. Inferior	0.030	R. Arm: Lo. Exterior	0.700
Abdomen: R. Inferior	0.030	R. Hand: Handback	0.472
L. Arm: Up. Anterior	0.335	R. Hand: Palm	0.007
L. Arm: Up. Posterior	0.000	R. Leg: Up. Anterior	0.422
L. Arm: Up. Inferior	0.002	R. Leg: Up. Posterior	0.000
L. Arm: Up. Exterior	0.298	R. Leg: Up. Inferior	0.059
L. Arm: Lo. Anterior	0.447	R. Leg: Up. Exterior	0.048
L. Arm: Lo. Posterior	0.000	R. Leg: Lo. Anterior	0.748
L. Arm: Lo. Inferior	0.016	R. Leg: Lo. Posterior	0.028
L. Arm: Lo. Exterior	0.700	R. Leg: Lo. Inferior	0.226
L. Hand: Handback	0.472	R. Leg: Lo. Exterior	0.155
L. Hand: Palm	0.000	R. Foot: Instep	0.341
L. Leg: Up. Anterior	0.422	R. Foot: Sole	0.000
L. Leg: Up. Posterior	0.000		

For this experimental exposure, forehead, anterior thorax, lower exterior arms and lower anterior legs were the most exposed body parts.

6.3.6.3 Results

The prediction of body and local skin temperatures of some exposed and non-exposed body parts to the solar radiation source are plotted in Figure 6.24.

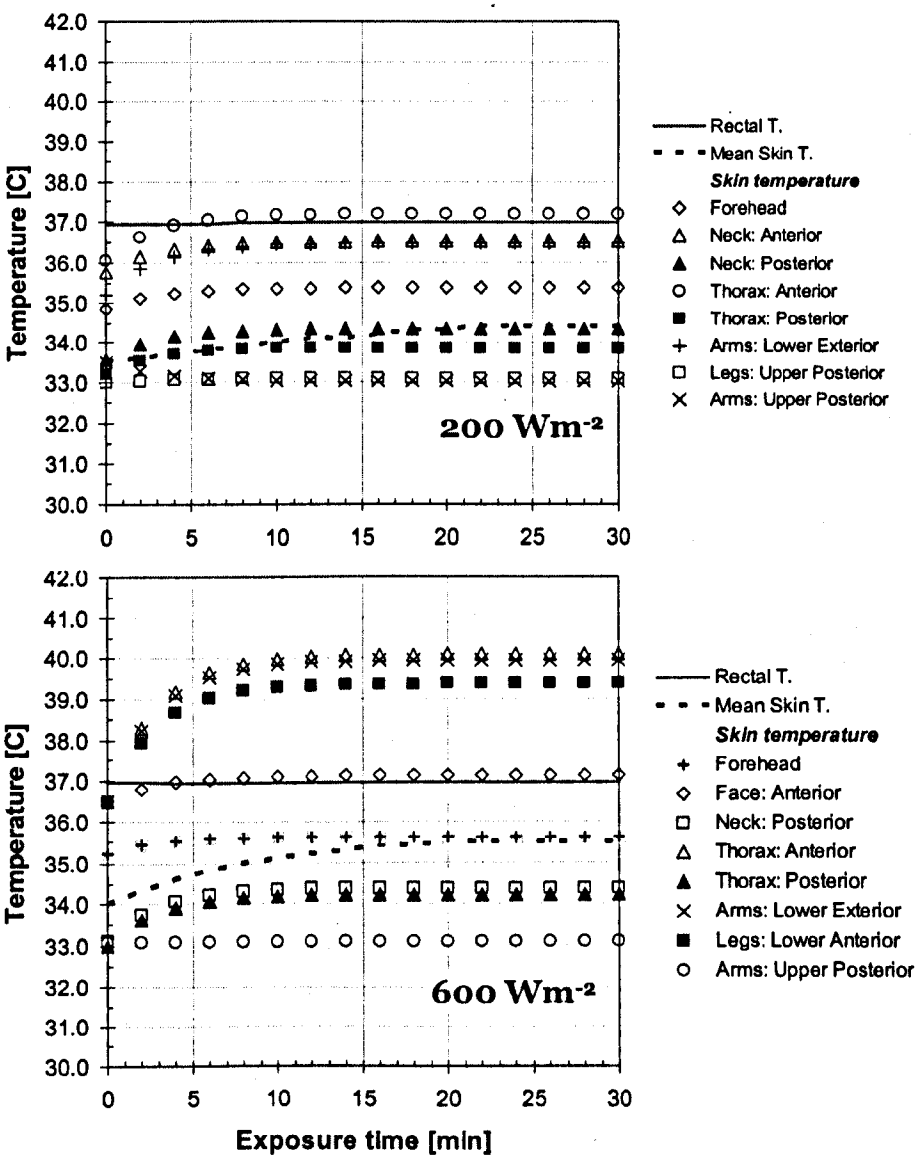

Figure 6.24 Example of predicted temporal trend of mean and local skin temperatures of the subjects exposed to radiation level of 200 and 600 Wm^{-2} obtained for the experiments of Hodder (2002).

It can be seen that the predicted local skin temperature of body parts that exposed to the radiation source significantly increased with time both for radiation level of 200 and 600 Wm^{-2}, for example, forehead, anterior face, anterior neck, anterior thorax, lower exterior arms and lower anterior legs. The predicted skin temperature of anterior thorax seemed the warmest body part in which reached to about 37.2°C in case of radiation level at 200 Wm^{-2} and about 40.1°C at 600 Wm^{-2}, respectively. The skin temperature of non-exposed body parts, e.g. upper posterior arms and upper posterior legs were virtually constant during the exposure. The predicted mean skin temperature notably increased during the first 20 minutes of both exposures and remained constant thereafter. The rectal temperature was fairly constant until the end of the experiment. Predicted body and local skin temperatures for all body parts are provided in Appendix E (*Table E.14*).

The predictions: local skin temperature of five body parts (forehead, exterior upper arms, exterior lower arms, chest and thigh) and mean skin temperatures ($T_{sk,m}$) are compared against experimental results in Figure 6.25 and 6.26. The comparisons are available only exposure time of 30 minutes. Also shown in the Figure 6.25 and Figure 6.26 are the measured local skin temperatures of the persons in the experiments of Hodder (subject A, B, C, D, E, F, G and H) and the average local skin temperatures obtained for the eight subjects.

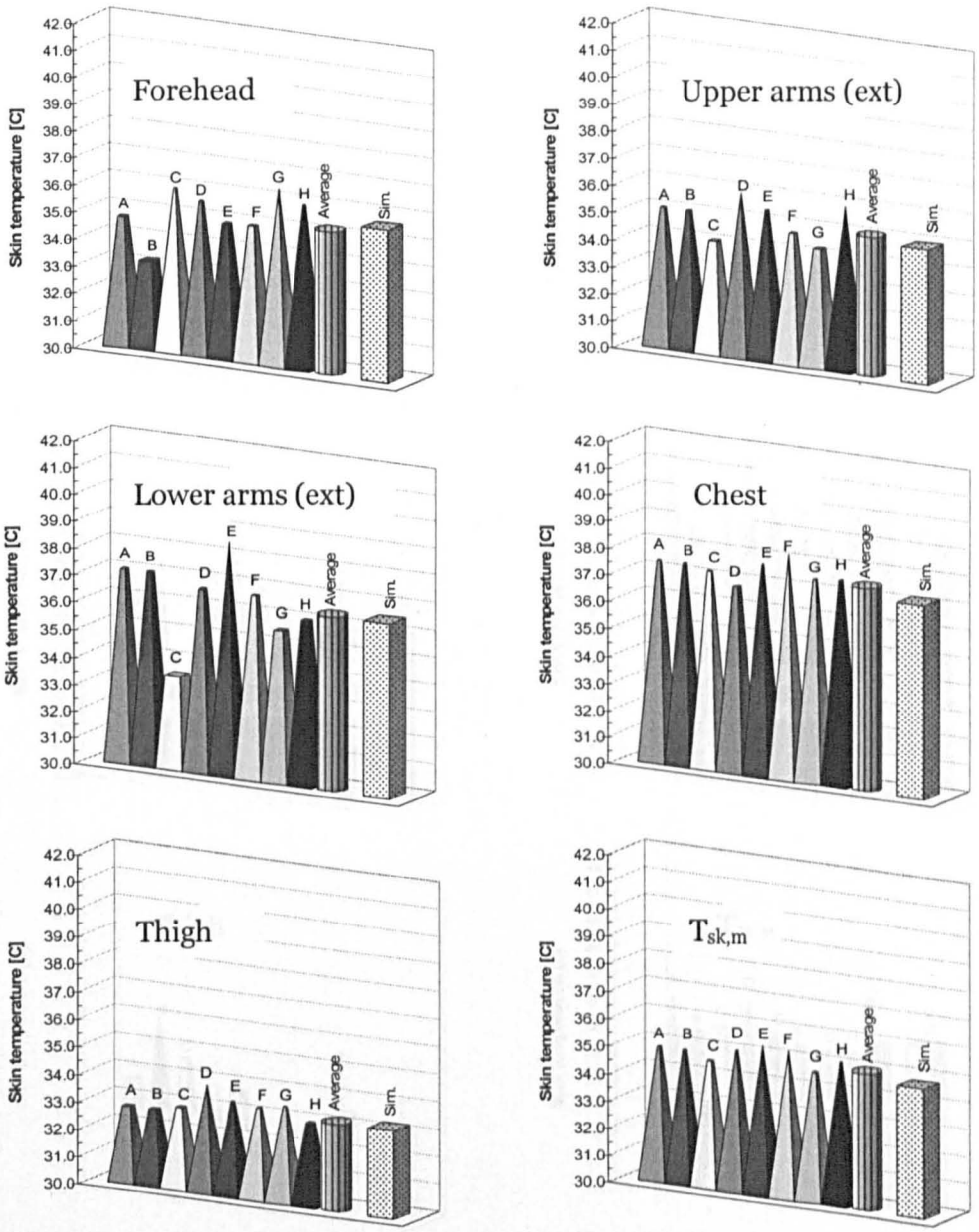

Figure 6.25 A comparison of predicted and measured local skin temperatures after 30 minutes exposure of 200 Wm^{-2} simulated direct solar radiation.

The predicted values (rectangular shapes) were in good general agreement compared with the average values of the measurement (cylinder) for all five local skin temperatures. The maximum discrepancy between the measurements and predictions reached about 0.3°C at chest. The predicted mean skin temperature ($T_{sk,m}$) of the subjects agreed well with the experiment in which slight discrepancy (0.15°C) can be observed.

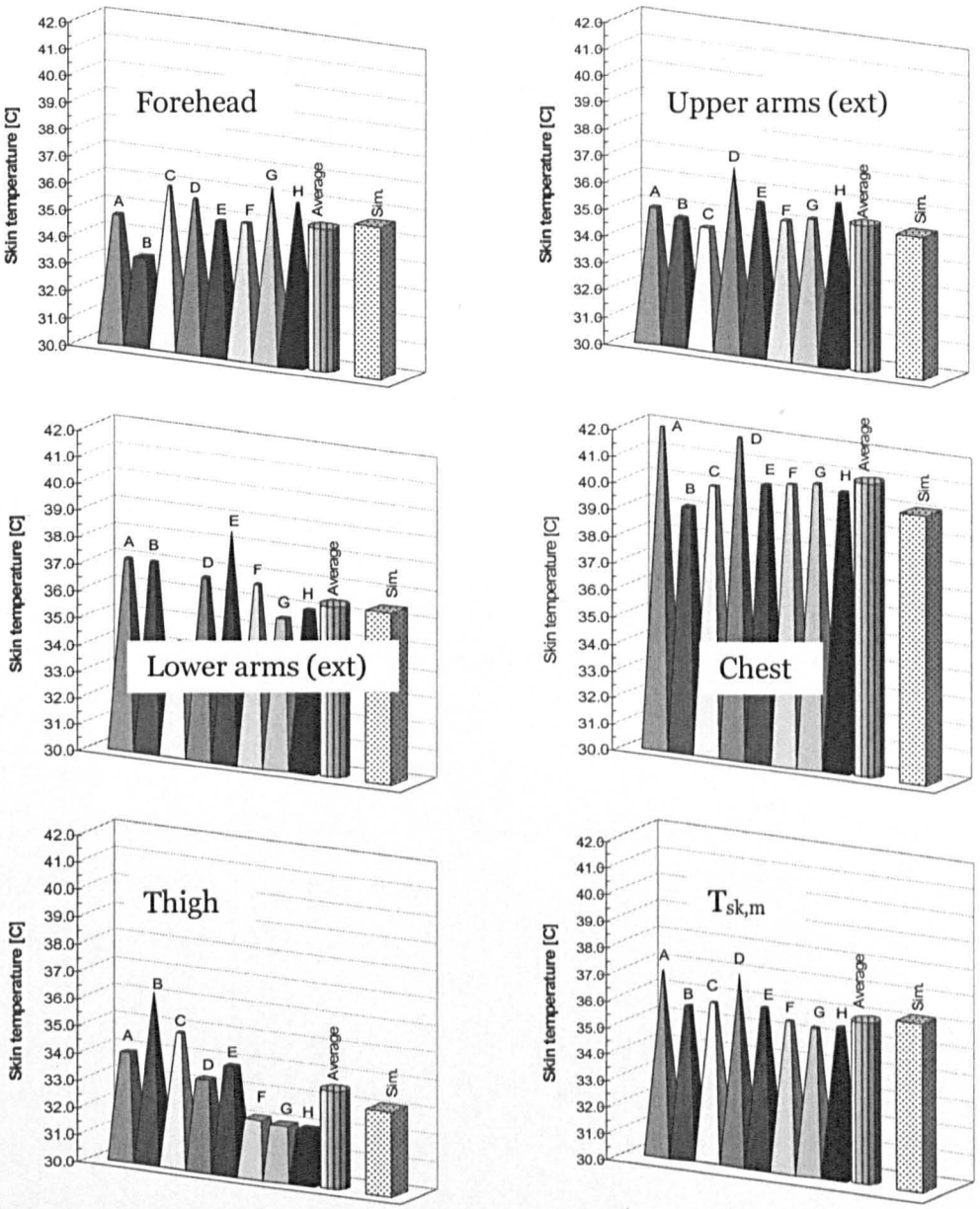

Figure 6.26 A comparison of predicted and measured local skin temperatures after 30 minutes exposure of 600 Wm^{-2} simulated direct solar radiation.

Similar to the exposure of 200 Wm^{-2}, the predicted local skin temperatures agreed well with the averaged-experimental results, e.g. forehead, upper arms, lower arms and thigh. Also the predicted mean skin temperature was in good agreement with the measured data. The maximum discrepancy can be observed at chest in which the prediction was lower than the measured value about 0.9°C.

The main reason was probably that differences in posture in the simulation and experiments. The driving posture subjects, obviously, upper main body parts (e.g. abdomen and thorax) were slightly inclined backward which cause discrepancies found in some body part that directly exposed to the short-wave source, i.e. chest.

6.4 Conclusions

In this chapter detailed projected area factors (f_p) and view factors (φ)were used with IESD-Fiala to enable detailed radiation calculations and to predict human thermal responses to asymmetric radiation environments. The extended model was simulated corresponding to available experimental series found in literature, e.g. experimental series of Fanger et al. (1980 and 1985), experiments of Hall and Klemm (1967 and 1969) and experiments of Hodder (2002). The predicted physiological responses obtained using the model showed generally good agreement with the above experimental results.

Although, a good level of agreement with experimental results was achieved considering deviation figure (i.e. within acceptable average deviation value). However, a large discrepancies between the predictions and the measurements can be observed in some exposures, e.g. static exposure in extreme asymmetric radiation of Hall and Klemm (1969). The main point was differences in posture that were suggested to cause discrepancies between the predicted and measured physiological responses, i.e. local skin temperature particularly in extremities.

A special interest of the simulation is to use local skin temperatures which are important signal of human local thermal reception and comfort (Hensel, 1979 and 1981). Thus the main objective of this research to develop a physiologically based thermal comfort model to predict human local perceptual responses to asymmetric radiation is feasible. Details of development for the new comfort model are described in Chapter 7.

Chapter 7

Modelling human local thermal comfort responses to asymmetric radiation

7.1 Introduction

Human thermal comfort under asymmetric radiation conditions has been subjected to experimental investigation for over five decades. Well known examples include Chrenko (1953), McNall and Biddison (1970), McIntyre and Griffiths (1972), Olesen et al. (1972), Fanger et al. (1980), Fanger et al. (1985), and Berglund and Fobelets (1987). Most of the experiments were carried out in climate chambers under well controlled boundary conditions for vertical and/or horizontal radiant asymmetry situations.

Some of the above experiments formed the basis of current national and international standards such as ASHRAE Standard 55 (2004) and ISO 7730 (1994). The limitations of current standard comfort models regarding asymmetric radiation and the validity of the environmental asymmetry limits are discussed in Chapter 1.

Modelling human perceptual responses to asymmetric radiation has ever since been an important challenge in thermal comfort research. The main purpose of modelling is to interpolate available measured data to conditions for which no experimental results exist. The aim of this chapter is to develop and validate a more universally applicable model for predicting human local perceptual responses to asymmetric radiation. A possible route for obtaining such a model

is to predict local comfort responses based on physiological principles rather than considering environmental limits. This approach is elaborated in this chapter.

7.2 Physiological basis of thermal comfort

The local sensation of temperature and comfort has been linked to the local cutaneous thermoreception. Several excellent studies, e.g. Hensel (1979 and 1981) have shown the dominant role of skin temperature and cutaneous thermoreceptors in the human local perceptual responses.

Studies on physiological implications of human thermal comfort have been conducted by various authors over many decades. Yaglou (1927), for example, exposed subjects to ambient temperatures between 20°C and 40°C at 30% and 70% RH. The experimental results revealed that the mean skin temperature was a good indicator of thermal comfort, Figure 7.1, as well as subjects sensations of cold and warmth.

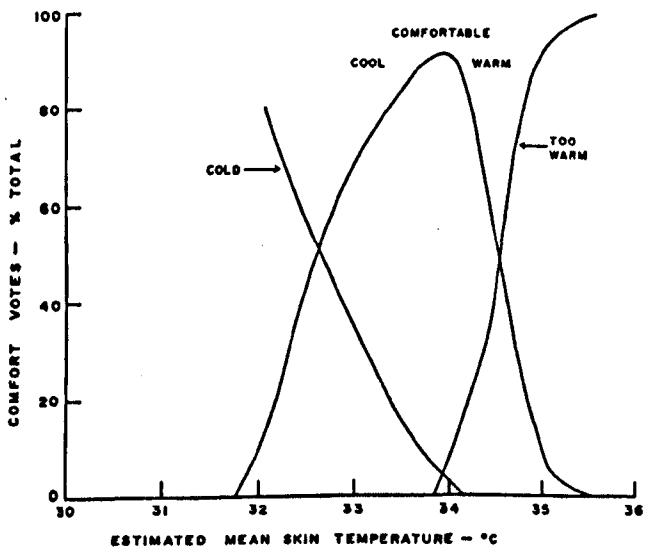

Figure 7.1 Percentage of people expressing discomfort as related to the mean skin temperature, (Yaglou, 1927).

More comprehensive studies on the relationship between thermal comfort and skin temperature were conducted by Gagge et al. (1937). Clothed and unclothed male subjects were exposed to thermally controlled environments in which the

wet- and dry-bulb temperatures, air velocity and wall temperatures were varied. The subjects were asked to report on their subjective feelings using a five category scale: (1) very pleasant, (2) pleasant, (3) indifferent, (4) unpleasant, and (5) very unpleasant. The mean skin temperature showed a good correlation with the perceived unpleasantness for both clothed and unclothed subjects in both cold and warm environment, Figure 7.2, (Gagge et al., 1937).

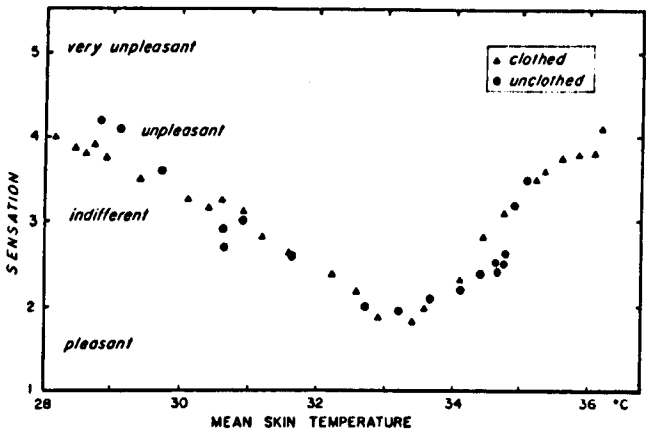

Figure 7.2 The sensations of thermal pleasantness as a function of the mean skin temperature (Gagge et al., 1937).

Cold discomfort has been found to be governed by skin temperature, Gagge et al. (1967), Gonzalez and Gagage (1973), and Hardy (1970), and also warm discomfort has been related to skin temperature (Gagge et al., 1967; Gonzalez et al., 1973; and Gagge, 1979). Reports of warm discomfort due to elevated skin temperature have been made even though no appreciable increase in body core temperature occurred (Gagge et al., 1967).

More recently, the work of Fiala et al. (2003) confirmed the mean skin temperature to be an important signal involved in the human sensation of temperature. The authors used a detailed model of the human thermoregulatory system to resimulate available thermal comfort experiments and to perform statistical regression analyses of predicted physiological states and measured perceptual responses. They found that the mean skin temperature is the best predictor of cold discomfort but is also an important punitive signal affecting the human sensation of warmth in sedentary subjects.

Cold and warm cutaneous receptors are distributed inhomogeneously over the body surface resulting in regionally different thermal sensitivity of the human skin, Nadel et al. (1973), Steven et al. (1973), and Crawshaw et al. (1975). The cutaneous receptors respond to thermal stimuli by periodic electrical impulses of about 50 mV, Hensel (1981). Both types of receptors have a static discharge frequency at a constant skin temperature but perform a dynamic overshoot in frequency during temporal changes in skin temperature, Hensel (1981).

Wyon (e.g. Wyon et al. 1989, Wyon and Sandberg, 1990) proposed an Equivalent Homogeneous Temperature (EHT) to predict acceptable range of temperature for individual body parts. The EHT is defined as the temperature in a uniform environment where the heat loss from a person (or a body part) is the same as his/her heat loss in an actual environment. The EHT was derived using the measured heat loss of a thermal manikin in which e.g. wearing the same clothing, seated in the same posture. Their finding in which obtained from 72 human subjects indicated that an optimum EHT was 25.1°C for the whole body (for mean thermal vote at 0). Also an empirical equation to predict the EHT was provided, for example, for head to thighs regions is equal to 14.10 + 0.428T, where T is air temperature.

Significant experimental work on local thermal sensation and comfort perception has recently been conducted by Zhang (2003). Zhang observed local perceptual responses of sedentary subjects in a well controlled climatic chamber which temperature was varied between 20 to 32 °C. Local skin temperature (of 19 different body parts) was controlled independently by applying air-sleeves with defined air temperature directly to the body parts. Although, the experiments were not concerned with the effect of asymmetric radiation on human thermal comfort and are thus not directly relevant to this work, they again demonstrated the dominant role of skin temperature on the local sensation of temperature and comfort.

7.3 Method of modelling

In this chapter, a first principle model for predicting human comfort responses to asymmetric radiant fields is developed using available experimental knowledge sampled over the past 30 years. According to the results of thermophysiological research the perception of local 'cold' and 'warm' discomfort is associated with local cutaneous thermoreceptions, Hensel (1979 and 1981). Following this principle local perceptual responses could be predicted using local skin temperatures as the physiological origin of local thermal (dis)comfort (Issing and Hensel, 1982). From the thermophysical point of view, skin temperature represents a cumulative quantity that integrates the partial thermal influences from the environment, personal circumstances (e.g. clothing), and thermoregulatory effects (sweating and skin blood flow). Using this physiological principle it should thus be possible to extrapolate available measured data to conditions for which no experimental results exist and enable predictions of human local comfort responses even for the complex radiation regimes to which humans are exposed in their daily lives.

The IESD-Fiala multi-segmental model (Fiala et al., 1999) of human thermoregulation is used to simulate the above experiments for asymmetric radiation. The experiments were simulated by accurately modelling the experimental boundary conditions and the radiative heat exchanges between individual parts of the human body and the asymmetric enclosure. The IESD-Fiala model predicted local skin temperatures, local sweat rates, body core temperatures, and other physiological variables dynamically for the duration of over exposure. The predicted local physiological variables were correlated with experimentally observed local comfort responses (expressed as a percentage of subjects dissatisfied with the asymmetric radiation conditions) to obtain the required functional relationships.

Regression analysis was employed to develop the model for predicting local comfort responses. The two-tailed population *t*-test was applied to determine the significance level of the regression coefficients.

7.4 Simulating thermal comfort experiments for asymmetric radiation

The aim of the simulations was to achieve proper characterisation of subjects' thermophysiological states. The boundary conditions and the simulation of some experiments below are described in Chapter 6. In this section, further experiments are described, additional information relevant to thermal comfort are provided, and simulation results for each experiment are presented.

7.4.1 Exposure to a warm/hot ceiling

7.4.1.1 Experiment

These experiments were conducted by Fanger (Fanger et al., 1980). A description of the experimental design and the boundary conditions is provided in Chapter 6. During each half-hour period (during which the temperature of the ceiling panel was kept constant), each subject was asked every five minutes whether he/she felt warm or cold on any part of the body and whether he/she regarded this as uncomfortable. Only the last three responses (20, 25 and 30 min after the beginning of each condition) were considered in the analysis. For these times any transient discomfort due to the sudden change from one experimental condition to the next was assumed to have disappeared. It was decided to regard a certain radiation asymmetry level as uncomfortable for a given subject if he/she indicated local discomfort at least twice of three responses. In the experiment, local discomfort was felt either in the head region (uncomfortable warm) or at the feet (uncomfortable cool) or at both places at the same time. Table 7.1 summarises the results indicating the level of local

discomfort in dependence on the measured vertical radiant temperature asymmetry.

Table 7.1 Percentage of subjects who experienced local thermal discomfort due to vertical radiant temperature asymmetry (Fanger et al. 1980).

Body sector	Radiant temperature asymmetry (°C)				
	4.5	9.2	14.1	20.4	23.6
Head	0.0	12.5	25.0	56.3	62.5
Feet	6.3	12.5	37.5	50.0	43.8
Total	6.3	25.0	43.8	75.0	68.8

It is interesting to note that local discomfort due to cold feet occurred almost as frequently as local discomfort due to a warm head.

7.4.1.2 Simulation

Details of the simulation are described in Chapter 6, section 6.3.1.2 and a comparison of predicted and measured skin temperatures is shown in Figure 6.7 (*Chapter 6*). The predicted local skin temperature of the main body parts are listed in Table 7.2.

Table 7.2 Predicted local skin temperatures of the main body parts as a result of an exposure to a vertical radiant temperature asymmetry (Fanger et al. 1980).

Body sector	Radiant temperature asymmetry (°C)				
	4.5	9.2	14.1	20.4	23.6
Head	35.0	35.1	35.3	35.6	35.8
L. Face	34.7	34.8	34.9	35.0	35.1
R. Face	34.7	34.8	34.9	35.0	35.1
Neck: L. exterior	34.5	34.6	34.8	35.1	35.2
Neck: R. exterior	34.5	34.6	34.8	35.0	35.2
L. Shoulder	33.9	34.2	34.5	34.9	35.1
Thorax: Anterior	34.7	34.9	35.0	35.2	35.3
Thorax: Posterior	34.7	34.7	34.8	34.9	34.9
Abdomen: Anterior	34.2	34.2	34.3	34.3	34.3
Abdomen: Posterior	33.9	33.9	33.8	33.8	33.8
L. Arm: Upper exterior	33.6	33.6	33.7	33.8	33.8
L. Arm: Lower exterior	32.4	32.3	32.3	32.4	32.3
L. Hand: Handback	33.0	32.8	32.7	32.7	32.6
L. Leg: Upper exterior	33.2	33.1	33.0	32.9	32.8
L. Leg: Lower exterior	32.4	32.2	32.1	31.9	31.8
L. Foot: Instep	31.2	30.8	30.5	30.2	30.0
R. Shoulder	33.9	34.2	34.5	34.9	35.1
R. Arm: Upper exterior	33.6	33.6	33.7	33.8	33.8
R. Arm: Lower exterior	32.4	32.3	32.3	32.4	32.3
R. Hand: Handback	33.0	32.8	32.7	32.7	32.6
R. Leg: Upper exterior	33.2	33.1	33.0	32.9	32.8
R. Leg: Lower exterior	32.4	32.2	32.1	31.9	31.8
R. Foot: Instep	31.2	30.8	30.5	30.3	30.0

The skin temperature distribution differs from the distribution experienced in a homogeneous thermo-neutral environment. However, the mean skin temperature was kept constant at about 33.4°C and the body core temperature at about 37.0°C (see *Table E.1, Appendix E*) both indicating overall thermo-neutral physiological conditions.

In order to obtain information on which body parts were cooled or warmed in the asymmetric radiation conditions, the local skin temperatures can be related to their respective setpoints (*Appendix E, Table E.1*). The local skin temperature differences ($\Delta T_{sk,i}=T_{sk,i}-T_{sk,l,o}$) in which defined as the difference of local skin temperature ($T_{sk,i}$) and local skin temperature setpoint ($T_{sk,l,o}$) are ranked from the 'coldest' to the 'warmest' body parts in Table 7.3.

Table 7.3 Local skin temperature differences ($\Delta T_{sk,i}$) obtained for the warm/hot ceiling exposure (Fanger et al., 1980).

Body sector	Radiant temperature asymmetry (°C)				
	4.5	9.2	14.1	20.4	23.6
L. Foot: Instep	-2.21	-2.58	-2.87	-3.12	-3.41
R. Foot: Instep	-2.20	-2.58	-2.87	-3.11	-3.40
L. Hand: Handback	-2.12	-2.29	-2.35	-2.35	-2.47
R. Hand: Handback	-2.12	-2.29	-2.35	-2.35	-2.47
L. Leg: Lower Exterior	-1.29	-1.45	-1.58	-1.71	-1.89
R. Leg: Lower Exterior	-1.30	-1.46	-1.58	-1.71	-1.89
L. Leg: Upper Exterior	-0.95	-1.08	-1.17	-1.26	-1.40
R. Leg: Upper Exterior	-0.95	-1.08	-1.17	-1.26	-1.40
L. Arm: Lower Exterior	-0.76	-0.83	-0.82	-0.79	-0.83
R. Arm: Lower Exterior	-0.76	-0.82	-0.82	-0.78	-0.82
L. Face	-1.00	-0.93	-0.81	-0.65	-0.61
R. Face	-1.00	-0.93	-0.81	-0.65	-0.61
Abdomen: Posterior	-0.31	-0.37	-0.39	-0.41	-0.46
Neck: L. Exterior	-0.70	-0.57	-0.38	-0.14	-0.04
Neck: R. Exterior	-0.70	-0.57	-0.38	-0.15	-0.04
Thorax: Posterior	-0.21	-0.15	-0.08	0.01	0.05
Head	-0.74	-0.58	-0.36	-0.09	0.07
Abdomen: Anterior	0.02	0.00	0.03	0.07	0.07
L. Arm: Upper Exterior	-0.04	-0.04	0.02	0.11	0.13
R. Arm: Upper Exterior	-0.04	-0.04	0.02	0.11	0.13
Thorax: Anterior	-0.14	-0.02	0.12	0.30	0.41
L. Shoulder	-0.30	-0.05	0.27	0.65	0.90
R. Shoulder	-0.30	-0.05	0.27	0.65	0.90

These simulation results confirmed the experimental findings, i.e. the body parts that were predicted as coldest and warmest were the feet and the head region (including shoulders, Fanger et al., 1980), respectively.

7.4.2 Exposure to cool/cold ceiling

7.4.2.1 Experiment

In the cool/cold ceiling series of Fanger et al. (1985), the sixteen subjects (eight male and eight female) voted on their local discomfort using a procedure similar to the warm/hot ceiling, section 7.4.1.1. The experimental set up and boundary conditions are described in Chapter 6 (*section 6.3.2.1*). Table 7.4 shows the percentage of subjects in the experiment indicating local discomfort perceived in the head region and/or warm feet, Fanger et al. (1985).

Table 7.4 Percentage of subjects who experienced local discomfort in the cool/cold ceiling series of Fanger et al. (1985).

Body sector	Radiant temperature asymmetry (°C)				
	4.4	7.5	10.5	13.0	15.0
Head	0.0	0.0	0.0	6.3	6.3
Feet + ankles	0.0	0.0	0.0	0.0	0.0
Total	0.0	0.0	0.0	6.3	6.3

The experimental findings showed only a few complaints of local discomfort indicating the comfort limits for this type of asymmetric radiation are based on a relatively weak data basis, Fanger et al. (1985).

7.4.2.2 Simulation

The simulation procedure and the predicted results obtained for this experiment are detailed in Chapter 6 (*section 6.3.2.2 and 6.3.2.3*). The predicted local skin temperatures of the main body parts are listed in Table 7.5 (*details of all local skin are presented in Appendix E, Table E.2*).

Table 7.5 Local skin temperatures of the main body parts predicted for the cool/cold ceiling series of Fanger et al. (1985).

Body sector	Radiant temperature asymmetry (°C)				
	4.4	7.5	10.5	13.0	15.0
Head	34.3	34.3	34.4	34.3	34.3
L. Face	33.9	33.9	33.9	33.9	33.9
R. Face	33.9	33.9	33.9	33.9	33.9
Neck: L. exterior	33.8	33.7	33.7	33.6	33.7
Neck: R. exterior	33.8	33.7	33.7	33.6	33.7
L. Shoulder	33.0	33.1	33.3	33.3	33.4
Thorax: Anterior	34.3	34.2	34.1	34.1	34.1
Thorax: Posterior	34.4	34.3	34.3	34.3	34.3
Abdomen: Anterior	33.9	33.7	33.7	33.7	33.7
Abdomen: Posterior	33.7	33.5	33.5	33.5	33.5
L. Arm: Upper exterior	33.2	33.0	33.0	33.1	33.1
L. Arm: Lower exterior	31.9	31.6	31.6	31.6	31.6
L. Hand: Handback	32.2	31.9	31.8	31.8	31.9
L. Leg: Upper exterior	32.9	32.9	33.0	33.1	33.2
L. Leg: Lower exterior	32.2	32.1	32.2	32.2	32.3
L. Foot: Instep	31.0	30.5	30.3	30.2	30.1
R. Shoulder	33.0	33.1	33.3	33.3	33.4
R. Arm: Upper exterior	33.2	33.0	33.0	33.1	33.1
R. Arm: Lower exterior	31.9	31.6	31.6	31.6	31.6
R. Hand: Handback	32.2	31.9	31.8	31.8	31.9
R. Leg: Upper exterior	32.9	32.9	33.0	33.1	33.2
R. Leg: Lower exterior	32.2	32.1	32.2	32.2	32.3
R. Foot: Instep	31.0	30.5	30.3	30.2	30.1

The corresponding local skin temperature differences, $\Delta T_{sk,i}$, are listed in Table 7.6.

Table 7.6 Local skin temperature differences, $\Delta T_{sk,i}$ obtained for the cool/cold ceiling exposure (Fanger et al. 1985).

Body sector	Radiant temperature asymmetry (°C)				
	4.4	7.5	10.5	13.0	15.0
L. Hand: Handback	-2.91	-3.22	-3.25	-3.32	-3.22
L. Foot: Instep	-2.37	-2.87	-3.07	-3.20	-3.22
R. Hand: Handback	-2.91	-3.22	-3.24	-3.32	-3.22
R. Foot: Instep	-2.37	-2.86	-3.07	-3.20	-3.22
L. Face	-1.77	-1.84	-1.77	-1.84	-1.79
R. Face	-1.77	-1.84	-1.77	-1.84	-1.79
Neck: L. Exterior	-1.43	-1.51	-1.49	-1.59	-1.54
Neck: R. Exterior	-1.43	-1.51	-1.49	-1.59	-1.54
L. Arm: Lower exterior	-1.28	-1.51	-1.56	-1.59	-1.53
R. Arm: Lower exterior	-1.28	-1.51	-1.56	-1.59	-1.53
Head	-1.36	-1.36	-1.35	-1.43	-1.43
L. Leg: Lower exterior	-1.48	-1.58	-1.49	-1.42	-1.32
R. Leg: Lower exterior	-1.48	-1.58	-1.50	-1.42	-1.32
L. Leg: Upper exterior	-1.25	-1.30	-1.19	-1.08	-0.96
R. Leg: Upper exterior	-1.25	-1.30	-1.18	-1.08	-0.96
L. Shoulder	-1.18	-1.10	-0.94	-0.89	-0.81
R. Shoulder	-1.18	-1.10	-0.94	-0.89	-0.81
Thorax: Anterior	-0.60	-0.71	-0.75	-0.80	-0.80
Abdomen: Posterior	-0.55	-0.72	-0.75	-0.75	-0.71
Thorax: Posterior	-0.51	-0.59	-0.58	-0.59	-0.56
Abdomen: Anterior	-0.35	-0.48	-0.50	-0.54	-0.51
L. Arm: Upper exterior	-0.50	-0.64	-0.62	-0.59	-0.51
R. Arm: Upper exterior	-0.50	-0.64	-0.62	-0.59	-0.51

The simulation results indicated that the coldest body parts would be hands, if $\Delta T_{sk,i}$ would be based as criterion. This result would not correspond to the experimental findings in which the head region was perceived as coldest body part (although the experimental results were not statistically significant, Fanger et al., 1985).

7.4.3 Expose to warm/hot vertical panel

7.4.3.1 Experiment

In the warm/hot wall series of Fanger et al. (1985), the sixteen subjects (eight male and eight female) voted on their local discomfort using a procedure similar to the warm/hot ceiling, section 7.4.1.1. The experimental set up and boundary conditions are described in Chapter 6 (*section 6.3.3.1*). Table 7.7 lists the percentage of subjects in the experiment indicating local discomfort due to cold right body parts and/or warm left body parts, Fanger et al. (1985).

Table 7.7 Percentage of subjects who experienced local discomfort in the warm/hot wall series of Fanger et al. (1985).

Body sector	Radiant temperature asymmetry (°C)				
	6.6	13.3	20.7	28.0	35.1
Left	0.0	0.0	6.3	6.3	6.3
Right	0.0	6.3	6.3	0.0	6.3
Total	0.0	6.3	12.5	6.3	12.5

Similar to the experimental findings of the cool/cold ceiling series, only a few number of the subjects complained about local discomfort. The researchers found that the experimental results obtained were based on a weak data basis, Fanger et al. (1985).

7.4.3.2 Simulation

The simulation procedure and the predicted results obtained for this experiment are described in Chapter 6 (*section 6.3.3.2 and 6.3.3.3*). The predicted local skin temperatures of the main body parts are listed in Table 7.8. Details of all local skin , mean and rectal temperature are presented in Appendix E, Table E.3.

Table 7.8 Local skin temperatures of main body parts predicted for the warm /hot wall series of Fanger et al. (1985).

Body sector	Radiant temperature asymmetry (°C)				
	6.6	13.3	20.7	28.0	35.1
Head	34.9	34.9	34.9	34.9	34.7
L. Face	35.3	35.9	36.4	37.1	37.2
R. Face	34.4	34.2	34.0	33.7	33.3
Neck: L. exterior	34.9	35.4	35.8	36.3	36.4
Neck: R. exterior	34.1	33.9	33.6	33.4	33.1
L. Shoulder	33.9	34.1	34.1	34.2	34.2
Thorax: Anterior	34.7	34.9	35.0	35.1	35.1
Thorax: Posterior	34.6	34.7	34.8	34.9	34.9
Abdomen: Anterior	34.2	34.2	34.1	34.1	34.0
Abdomen: Posterior	34.0	34.1	34.2	34.4	34.4
L. Arm: Upper exterior	34.0	34.4	34.8	35.3	35.6
L. Arm: Lower exterior	32.6	32.9	33.2	33.5	33.6
L. Hand: Handback	32.9	33.0	33.0	33.1	32.9
L. Leg: Upper exterior	33.8	34.3	34.9	35.6	36.0
L. Leg: Lower exterior	32.9	33.4	33.9	34.6	34.9
L. Foot: Instep	31.0	30.8	30.7	30.6	30.3
R. Shoulder	33.7	33.5	33.3	33.1	32.8
R. Arm: Upper exterior	33.3	33.0	32.7	32.4	32.0
R. Arm: Lower exterior	32.0	31.7	31.3	30.9	30.4
R. Hand: Handback	32.5	32.2	31.9	31.5	30.9
R. Leg: Upper exterior	32.9	32.7	32.3	32.0	31.6
R. Leg: Lower exterior	32.1	31.8	31.4	31.0	30.5
R. Foot: Instep	30.9	30.7	30.4	30.3	29.9

The local skin temperature differences, $\Delta T_{sk,i}$, for this type of asymmetric radiation are listed in ascending order in Table 7.9 as an indication of body parts which were likely to be perceived as uncomfortable.

Table 7.9 Local skin temperature differences, $\Delta T_{sk,i}$ obtained for the warm/hot vertical wall exposure (Fanger et al., 1985).

Body sector	Radiant temperature asymmetry (°C)				
	6.6	13.3	20.7	28.0	35.1
R. Hand: Handback	-2.53	-2.83	-3.22	-3.54	-4.13
R. Foot: Instep	-2.47	-2.69	-2.93	-3.09	-3.47
R. Leg: Lower exterior	-1.59	-1.89	-2.29	-2.68	-3.15
L. Foot: Instep	-2.39	-2.53	-2.68	-2.73	-3.02
R. Arm: Lower exterior	-1.15	-1.46	-1.86	-2.24	-2.75
R. Leg: Upper exterior	-1.23	-1.49	-1.82	-2.16	-2.59
R. Face	-1.32	-1.48	-1.74	-1.96	-2.36
L. Hand: Handback	-2.16	-2.10	-2.09	-1.97	-2.21
Neck: R. Exterior	-1.11	-1.29	-1.55	-1.76	-2.09
R. Arm: Upper exterior	-0.39	-0.63	-0.95	-1.26	-1.67
R. Shoulder	-0.54	-0.66	-0.89	-1.13	-1.45
Head	-0.85	-0.82	-0.85	-0.84	-0.97
Abdomen: Anterior	-0.06	-0.07	-0.11	-0.11	-0.22
L. Shoulder	-0.27	-0.13	-0.06	0.04	-0.02
Thorax: Posterior	-0.23	-0.12	-0.06	0.04	0.01
Abdomen: Posterior	-0.24	-0.13	-0.04	0.13	0.14
Thorax: Anterior	-0.17	-0.02	0.09	0.24	0.25
L. Arm: Lower exterior	-0.51	-0.22	0.04	0.39	0.45
Neck: L. Exterior	-0.28	0.23	0.63	1.14	1.20
L. Leg: Lower exterior	-0.73	-0.23	0.29	0.92	1.24
L. Face	-0.38	0.25	0.75	1.36	1.49
L. Leg: Upper exterior	-0.38	0.18	0.76	1.43	1.82
L. Arm: Upper exterior	0.33	0.75	1.17	1.67	1.90

In accordance with the experiment, the $\Delta T_{sk,i}$–data would indicate the right-hand side body parts likely to be perceived as cold and the left-hand side body parts as warm. Thereby, the right handback, right foot and the lower exterior right leg were predicted to be the coldest body parts whereas left face, upper exterior left leg and the upper exterior left arm were predicted to be the warmest body regions when compared to their thermo-neutral states.

7.4.4 Exposures to a hot spatial wall

7.4.4.1 Experiment

In this experimental series carried out by McNall and Biddison (1970), seventy subjects (35 males and 35 females) were employed. In each exposure, five sedentary subjects were positioned along a warm/hot wall on their left hand side. The dimensions of the wall were 2.4m (height) x 7.3m (width). The average view factor between the subjects and the wall was estimated to be about 0.16. The experiments were conducted for seven different combinations of wall and air temperatures (*Table 7.10*). The air velocity varied between 0.10-0.15 m/s and the vapour pressure was kept constant at 1.47 kPa. The subjects were clothed in the KSU uniform (with cotton sweat socks but no shoes) with insulation value of 0.59 clo.

Table 7.10 Environmental conditions of the warm/hot wall series conducted by McNall and Biddison (1970).

Condition No.	Warm/hot wall (°C)	Other walls (°C)	Air temperature (°C)
1	54.4	12.8	25.6
2	54.4	12.8	28.9
3	54.4	16.7	25.6
4	54.4	21.7	23.3
5	54.4	24.4	32.2
6	54.4	29.4	27.8
7	54.4	16.1	21.1

Each testing session lasted three hours. The subjects voted on their thermal comfort sensations through each exposure but only the first four votes (0-90 min) were included in the analysis which results were published in their paper. Even when extremes were excluded and not published (condition 5 and 6), a significant number, i.e. 40.5% of the subjects were found to be thermally uncomfortable in the experiments. A significant number of them, i.e. 75% (or

30% in total) indicated that the sole, or at least a contributing cause of their warmth discomfort was due to "uneven body temperatures", i.e. local discomfort, McNall and Biddison (1970).

7.4.4.2 Simulation

The simulations were performed for (the five) environmental boundary conditions listed in Table 7.10. A typical emissivity of 0.95 was assumed for the chamber surfaces. A constant air velocity and vapour pressure of 0.12 m/s and 1.47 kPa, respectively, were used in the simulations. Each of the five test-conditions were simulated separately as three hour exposures using time steps of Δt=5min.

The human thermal simulations were performed for several positions along the warm/hot wall. For simplification, however, only three positions (*Figure 7.3*) were considered (leaving out the two positions inbetween).

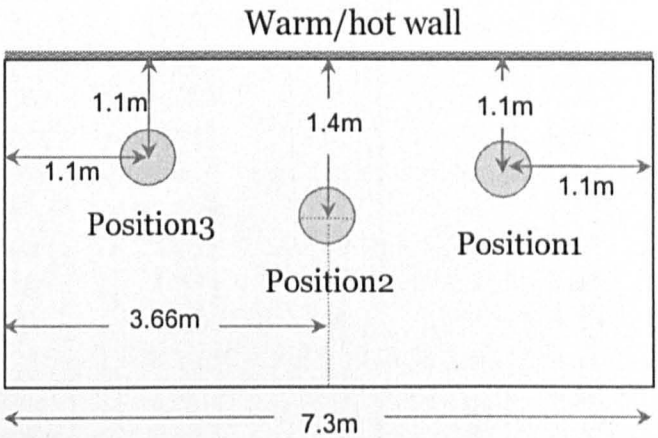

Figure 7.3 Simulated positions of the subjects in the experiment of McNall and Biddison (1970).

The environmental conditions used in the simulations of the spatial warm/hot wall series are indicated graphically in Figure 7.4.

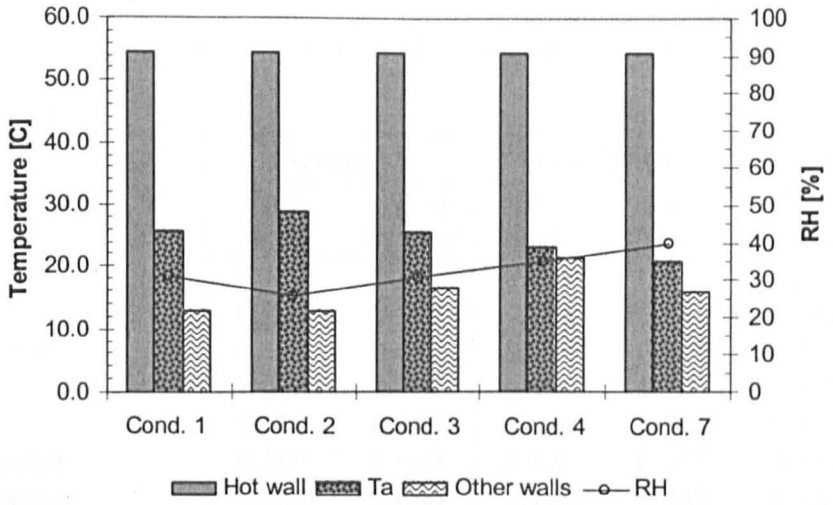

Figure 7.4 Environmental conditions used in the simulations.

The predicted view factors between the whole body and the spatial warm/hot wall at the position 1, 2 and 3 were 0.170, 0.159 and 0.164, respectively. The view factors for individual body sectors for each of the three positions are provided in Table 7.11.

Table 7.11 Local view factors between the subject and the spatial warm/hot wall series and the rest of the chamber (McNall and Biddison, 1970).

Body part	Position 1		Position 2		Position 3	
	Hot wall	Rest of chamber	Hot wall	Rest of chamber	Hot wall	Rest of chamber
Forehead	0.172	0.807	0.213	0.766	0.280	0.699
Head	0.244	0.719	0.208	0.755	0.208	0.756
Face: Anterior	0.182	0.642	0.212	0.612	0.270	0.554
L. Face	0.596	0.288	0.589	0.295	0.652	0.233
R. Face	0.000	0.885	0.000	0.885	0.001	0.884
Neck: Anterior	0.107	0.660	0.170	0.597	0.231	0.536
Neck: Posterior	0.257	0.686	0.190	0.753	0.143	0.800
Neck: L. Exterior	0.512	0.319	0.504	0.326	0.536	0.295
Neck: R. Exterior	0.000	0.833	0.000	0.833	0.000	0.833
L. Shoulder	0.249	0.635	0.222	0.662	0.225	0.660
Thorax: Anterior	0.167	0.745	0.212	0.700	0.278	0.635
Thorax: Posterior	0.277	0.712	0.210	0.779	0.170	0.818
Thorax: L. Inferior	0.193	0.262	0.197	0.259	0.203	0.253
Thorax: R. Inferior	0.012	0.452	0.005	0.459	0.002	0.462
Abdomen: Anterior	0.067	0.424	0.101	0.390	0.137	0.353
Abdomen: Posterior	0.274	0.726	0.206	0.794	0.171	0.829
Abdomen: L. Inferior	0.388	0.281	0.333	0.336	0.318	0.351
Abdomen: R. Inferior	0.004	0.664	0.000	0.667	0.000	0.667
L. Arm: Up. Anterior	0.082	0.393	0.126	0.349	0.170	0.305
L. Arm: Up. Posterior	0.438	0.562	0.359	0.641	0.318	0.682
L. Arm: Up. Inferior	0.058	0.539	0.036	0.561	0.012	0.585
L. Arm: Up. Exterior	0.426	0.527	0.445	0.508	0.491	0.462
L. Arm: Lo. Anterior	0.000	0.425	0.003	0.422	0.009	0.416
L. Arm: Lo. Posterior	0.499	0.501	0.465	0.535	0.456	0.544
L. Arm: Lo. Inferior	0.065	0.549	0.042	0.572	0.022	0.592
L. Arm: Lo. Exterior	0.274	0.593	0.312	0.555	0.374	0.492
L. Hand: Handback	0.206	0.508	0.206	0.508	0.225	0.490
L. Hand: Palm	0.100	0.155	0.083	0.172	0.069	0.185
L. Leg: Up. Anterior	0.027	0.404	0.031	0.400	0.040	0.391
L. Leg: Up. Posterior	0.123	0.822	0.104	0.841	0.108	0.838
L. Leg: Up. Inferior	0.000	0.563	0.000	0.563	0.000	0.563
L. Leg: Up. Exterior	0.423	0.353	0.395	0.381	0.384	0.391
L. Leg: Lo. Anterior	0.146	0.854	0.177	0.823	0.228	0.772
L. Leg: Lo. Posterior	0.188	0.522	0.144	0.566	0.077	0.632
L. Leg: Lo. Inferior	0.000	0.741	0.001	0.740	0.005	0.736
L. Leg: Lo. Exterior	0.432	0.492	0.412	0.512	0.381	0.543
L. Foot: Instep	0.228	0.658	0.212	0.674	0.185	0.701
L. Foot: Sole	0.012	0.886	0.013	0.884	0.011	0.886
R. Shoulder	0.058	0.828	0.048	0.838	0.050	0.836
R. Arm: Up. Anterior	0.019	0.445	0.061	0.403	0.095	0.369

Table 7.11 (Continued)

R. Arm: Up. Posterior	0.132	0.868	0.088	0.912	0.062	0.938
R. Arm: Up. Inferior	0.280	0.326	0.215	0.391	0.196	0.410
R. Arm: Up. Exterior	0.000	0.953	0.001	0.952	0.003	0.950
R. Arm: Lo. Anterior	0.225	0.201	0.247	0.178	0.302	0.124
R. Arm: Lo. Posterior	0.003	0.997	0.000	1.000	0.000	1.000
R. Arm: Lo. Inferior	0.108	0.505	0.073	0.540	0.045	0.568
R. Arm: Lo. Exterior	0.030	0.834	0.049	0.815	0.077	0.787
R. Hand: Handback	0.091	0.621	0.091	0.621	0.117	0.595
R. Hand: Palm	0.043	0.217	0.030	0.229	0.021	0.239
R. Leg: Up. Anterior	0.159	0.269	0.152	0.277	0.177	0.251
R. Leg: Up. Posterior	0.045	0.891	0.027	0.909	0.036	0.900
R. Leg: Up. Inferior	0.223	0.340	0.218	0.345	0.270	0.293
R. Leg: Up. Exterior	0.000	0.776	0.000	0.776	0.000	0.776
R. Leg: Lo. Anterior	0.261	0.739	0.271	0.729	0.338	0.662
R. Leg: Lo. Posterior	0.184	0.523	0.142	0.565	0.100	0.607
R. Leg: Lo. Inferior	0.359	0.378	0.330	0.407	0.332	0.405
R. Leg: Lo. Exterior	0.000	0.927	0.000	0.926	0.003	0.923
R. Foot: Instep	0.215	0.669	0.196	0.688	0.176	0.708
R. Foot: Sole	0.004	0.891	0.004	0.891	0.004	0.892
Whole body	**0.170**	**0.613**	**0.159**	**0.623**	**0.164**	**0.618**

As an example, Figure 7.5, shows the temporal trends of body temperatures predicted for some different body sides for subject at position 1 and exposure 1.

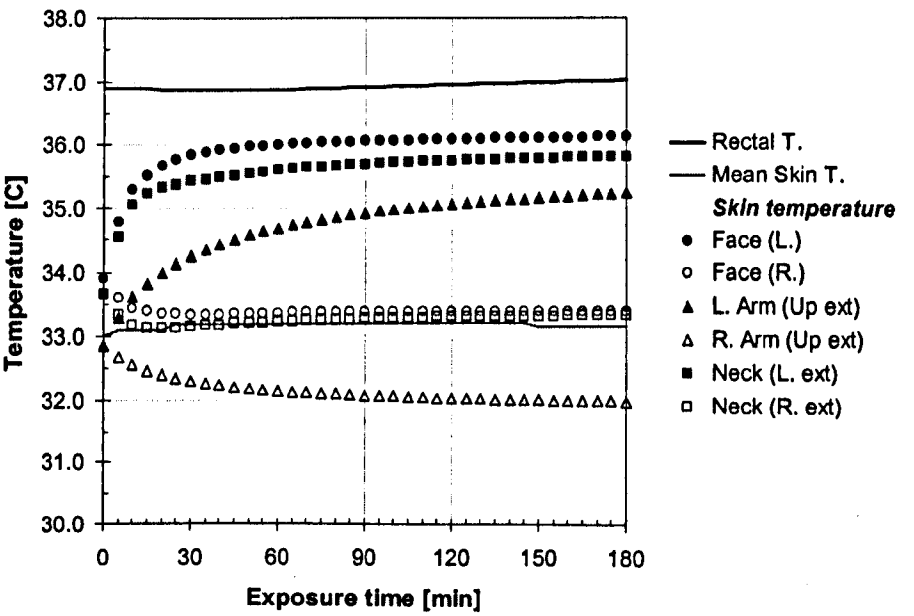

Figure 7.5 Example of predicted temporal trend of body and skin temperatures for exposure 1 (position 1) of McNall and Biddison (1970).

It can be seen that the predicted local skin temperature ($T_{sk,i}$) of body parts that were exposed to the hot wall rose with time, for example, left face, left neck (exterior) and upper exterior left. The opposite behaviour was observed for the right face, right neck (exterior) and lower exterior right arm. The mean skin and the rectal temperature, however, remained fairly constant until the end of the experiment.

The average local skin temperatures of exposures 1, 2, 3, 4, and 7 obtained for some main body parts for the three positions along the hot wall are listed in Table 7.12 (see *Appendix E, Table E.10-E.12 for all body sectors*).

Table 7.12 Local skin temperatures of the main body parts predicted at the exposure time 90 min for the spatial warm/hot wall experiments of McNall and Biddison (1970).

Body sector	Simulated position		
	1	2	3
Head	35.0	34.9	34.7
L. Face	36.1	36.0	36.0
R. Face	33.7	33.6	33.6
Neck: L. exterior	35.7	35.6	35.5
Neck: R. exterior	33.5	33.5	33.5
L. Shoulder	34.7	34.5	34.3
Thorax: Anterior	34.6	34.7	35.0
Thorax: Posterior	34.8	34.5	34.1
Abdomen: Anterior	34.2	34.4	34.5
Abdomen: Posterior	34.5	34.4	34.2
L. Arm: Upper exterior	35.0	34.8	34.9
L. Arm: Lower exterior	32.9	32.9	33.3
L. Hand: Handback	33.1	33.1	33.3
L. Leg: Upper exterior	35.1	34.9	35.0
L. Leg: Lower exterior	33.6	33.6	33.9
L. Foot: Instep	30.9	31.1	31.2
R. Shoulder	33.3	33.2	33.1
R. Arm: Upper exterior	32.4	32.4	32.5
R. Arm: Lower exterior	30.6	30.7	30.9
R. Hand: Handback	31.8	31.9	32.0
R. Leg: Upper exterior	32.5	32.5	32.5
R. Leg: Lower exterior	30.2	30.2	30.2
R. Foot: Instep	30.0	30.2	30.2

The corresponding local skin temperature differences ($\Delta T_{sk,i}$) are shown in Table 7.13.

Table 7.13 Local skin temperature differences, $\Delta T_{sk,i}$, obtained for the spatial warm/hot wall exposure by McNall and Biddison (1970).

Body sector	Simulated position		
	1	2	3
R. Leg: Lower exterior	-3.45	-3.45	-3.42
R. Foot: Instep	-3.33	-3.11	-3.11
R. Hand: Handback	-3.23	-3.18	-3.03
R. Arm: Lower Exterior	-2.56	-2.41	-2.27
L. Foot: Instep	-2.44	-2.29	-2.21
R. Face	-2.03	-2.05	-2.06
L. Hand: Handback	-1.94	-1.99	-1.80
Neck: R. Exterior	-1.70	-1.71	-1.72
R. Leg: Upper exterior	-1.63	-1.64	-1.64
R. Arm: Upper exterior	-1.24	-1.21	-1.18
R. Shoulder	-0.92	-1.00	-1.08
Head	-0.73	-0.85	-0.98
Thorax: Posterior	-0.05	-0.32	-0.78
Thorax: Anterior	-0.28	-0.14	0.08
L. Arm: Lower exterior	-0.23	-0.22	0.15
L. Leg: Lower Exterior	-0.04	-0.01	0.20
Abdomen: Anterior	0.03	0.14	0.26
Abdomen: Posterior	0.32	0.17	-0.06
L. Shoulder	0.51	0.25	0.13
L. Face	0.38	0.27	0.28
Neck: L. Exterior	0.52	0.41	0.27
L. Leg: Upper exterior	0.94	0.78	0.81
L. Arm: Upper exterior	1.31	1.15	1.21

The 'warmest' body parts with the highest $\Delta T_{sk,i}$ values were those sectors of the extremities which were directly exposed to the hot wall, i.e. the exterior sector of the left upper arm and leg. The simulation results indicated position 1 to be the most critical of the three positions analysed regarding to radiant asymmetry and possible local discomfort, although, there were no really significant differences between the three positions.

7.4.5 Exposure to a cool/cold vertical panel

7.4.5.1 Experiment

In this experiment conducted by Fanger et al. (1985), thirty two subjects were employed. The sedentary subjects were exposed to a cool/cold vertical panel on their left hand side. A more detailed description of the experimental procedure is provided in Chapter 6 (*section 6.3.4*). The subjects voted on their local thermal sensation and local discomfort, i.e. whether they felt warm or cool on any part of the body and whether they regarded this as uncomfortable every five minutes. Table 7.14 summaries the results provided as a percentage of subjects feeling local cold and/or warm discomfort on their left/right side.

Table 7.14 Percentage of subjects who experienced cold and warm discomfort, Fanger et al. (1985).

Body part	Radiant temperature asymmetry (°C)				
	5.3	8.6	12.8	16.6	18.2
Left	3.1	0.0	9.4	28.1	37.5
Right	0.0	0.0	0.0	0.0	9.3
Total	3.1	0.0	9.4	28.1	43.8

The experimental results indicated that local cold discomfort perceived at the left body side was the dominant figure in this type of exposure. Local warm discomfort was perceived only by a small number of subject at the highest radiant asymmetry.

7.4.5.2 Simulation

Details of the simulation are described in Chapter 6, section 6.3.4.2. A comparison of predicted and measured skin temperature is presented in Figure 6.18. The predicted local skin temperature of the main body parts are provided in Table 7.15.

Table 7.15 Predicted local skin temperatures of the main body parts as a result of an exposure to a cool/cold vertical panel (Fanger et al., 1985).

Body sector	Radiant temperature asymmetry (°C)				
	5.3	8.6	12.8	16.6	18.2
Head	34.6	34.7	34.8	34.8	34.9
L. Face	33.8	33.7	33.6	33.5	33.5
R. Face	34.4	34.6	34.7	34.8	34.9
Neck: L. exterior	33.7	33.6	33.5	33.4	33.4
Neck: R. exterior	34.2	34.3	34.5	34.6	34.6
L. Shoulder	33.3	33.5	33.7	33.8	33.9
Thorax: Anterior	34.5	34.5	34.5	34.5	34.5
Thorax: Posterior	34.4	34.5	34.5	34.5	34.6
Abdomen: Anterior	34.0	34.0	34.1	34.1	34.2
Abdomen: Posterior	33.7	33.6	33.6	33.6	33.6
L. Arm: Upper exterior	33.1	32.9	32.7	32.6	32.6
L. Arm: Lower exterior	32.0	31.9	31.7	31.6	31.6
L. Hand: Handback	32.4	32.3	32.2	32.2	32.3
L. Leg: Upper exterior	32.6	32.4	32.2	32.1	32.0
L. Leg: Lower exterior	31.9	31.7	31.5	31.3	31.2
L. Foot: Instep	31.1	30.8	30.5	30.3	30.2
R. Shoulder	33.4	33.7	34.0	34.3	34.5
R. Arm: Upper exterior	33.5	33.6	33.8	33.9	34.0
R. Arm: Lower exterior	32.4	32.5	32.6	32.7	32.9
R. Hand: Handback	32.6	32.7	32.8	32.9	33.0
R. Leg: Upper exterior	33.1	33.3	33.4	33.6	33.7
R. Leg: Lower exterior	32.4	32.5	32.7	32.8	32.9
R. Foot: Instep	31.1	30.8	30.6	30.4	30.4

The local skin temperature differences ($\Delta T_{sk,i}$) for this asymmetric radiation exposure are listed in Table 7.16.

Table 7.16 Local temperature differences ($\Delta T_{sk,i}$) obtained for the vertical cold panel of Fanger et al. (1985).

Body sector	Radiant temperature asymmetry (°C)				
	5.3	8.6	12.8	16.6	18.2
L. Foot: Instep	-2.27	-2.61	-2.86	-3.08	-3.17
R. Foot: Instep	-2.22	-2.52	-2.73	-2.92	-2.98
L. Hand: Handback	-2.68	-2.79	-2.83	-2.85	-2.76
L. Leg: Lower exterior	-1.75	-1.98	-2.18	-2.36	-2.46
L. Face	-1.94	-2.03	-2.12	-2.24	-2.24
L. Leg: Upper exterior	-1.55	-1.76	-1.94	-2.10	-2.18
R. Hand: Handback	-2.43	-2.41	-2.31	-2.21	-2.04
Neck: L. Exterior	-1.53	-1.61	-1.69	-1.79	-1.78
L. Arm: Lower exterior	-1.13	-1.29	-1.43	-1.55	-1.57
L. Arm: Upper exterior	-0.59	-0.77	-0.91	-1.04	-1.09
Head	-1.13	-1.02	-0.93	-0.88	-0.81
R. Face	-1.33	-1.14	-0.96	-0.87	-0.77
R. Leg: Lower exterior	-1.21	-1.11	-0.97	-0.86	-0.73
Abdomen: Posterior	-0.53	-0.60	-0.64	-0.67	-0.66
Neck: R. Exterior	-1.02	-0.87	-0.72	-0.64	-0.55
R. Leg: Upper exterior	-1.01	-0.88	-0.71	-0.57	-0.43
Thorax: Anterior	-0.43	-0.40	-0.39	-0.39	-0.37
L. Shoulder	-0.94	-0.75	-0.55	-0.42	-0.31
Thorax: Posterior	-0.42	-0.38	-0.35	-0.35	-0.31
R. Arm: Lower exterior	-0.72	-0.64	-0.51	-0.41	-0.27
Abdomen: Anterior	-0.21	-0.20	-0.15	-0.10	-0.04
R. Shoulder	-0.77	-0.48	-0.18	0.06	0.25
R. Arm: Upper exterior	-0.12	-0.02	0.12	0.23	0.35

The left foot showed the highest negative temperature difference of body parts while only very small positive $\Delta T_{sk,i}$ difference (right arm upper exterior and right shoulder) were predicted for this type of exposure. These results would seem to confirm the experimental findings of Fanger et al. (1985) in which significant local discomfort at the left body side but only slightly warm discomfort at the right body side was observed in this experiment.

7.4.6 Exposures to a cold spatial wall

7.4.6.1 Experiment

One hundred (50 male and 50 female) subjects were employed in the experiment of McNall and Biddison (1970). Similar to the experimental series of the same authors (section 7.4.4), in each exposure, five sedentary subjects were positioned along a cold wall on their left hand side. The dimensions of the wall were 2.4 m height and 7.3 m width. The experiments were conducted for ten different combinations of environmental conditions (*Table 7.17*). The air velocity varied between 0.10-0.15 m/s and the vapour pressure was kept constant at 1.47 kPa. Similar to their hot wall experiment, the subjects were clothed in the KSU uniform (with cotton sweat socks but no shoes) with insulation value of 0.59 clo.

Table 7.17 Environmental conditions of the cold spatial wall series conducted by McNall and Biddison (1970).

Condition No.	Cold wall (°C)	Rest walls (°C)	Air temperature (°C)
1	15.6	26.7	28.9
2	18.9	30.0	23.3
3	18.3	30.0	32.2
4	14.4	25.6	21.1
5	13.3	24.4	25.6
6	24.4	35.6	27.8
7	16.1	27.2	25.6
8	8.9	21.1	25.6
9	8.9	21.1	28.9
10	18.3	29.4	32.2

Each testing session lasted three hours. The subjects voted on their thermal comfort sensation through the experiment but only the first four votes (0-90 min) were included in the analysis which results were published. Excluding extremes (condition 3, 4, 6, 8, and 10), it was found that 12.9% of the subjects were thermally uncomfortable in these experiments but none of them due to

local discomfort. These experiments were simulated in order to determine the physiological strain due to asymmetric radiation in which human beings can be exposed without perceiving any local discomfort.

7.4.6.2 Simulation

The simulations were performed for the experimental boundary conditions listed in Table 7.17 with an air velocity and vapour pressure of 0.12 m/s and 1.47 kPa. A typical emissivity 0.95 was assumed for all chamber surfaces. Each of the five test-conditions considered were simulated separately as a three hour exposures using time steps of Δt=5min.

The spatial cold wall series of McNall and Biddison were simulated considering only one position of the subjects in the room (*Figure 7.6*). The considered position was chosen of the five positions in the experiment to represent an "average" exposure. The view factor predicted between the whole body and the spatial cold wall had a value of 0.170.

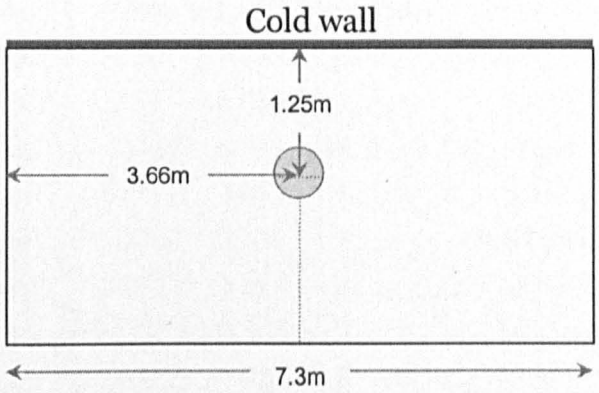

Figure 7.6 Simulated position of the subject for the cold wall experimental series of McNall and Biddison (1970).

The environmental conditions used in the simulation of the spatial cold wall series in which excluded the extreme conditions of cases 3, 4, 6, 8 and 10 (*Table 7.17*) are presented in Figure 7.7.

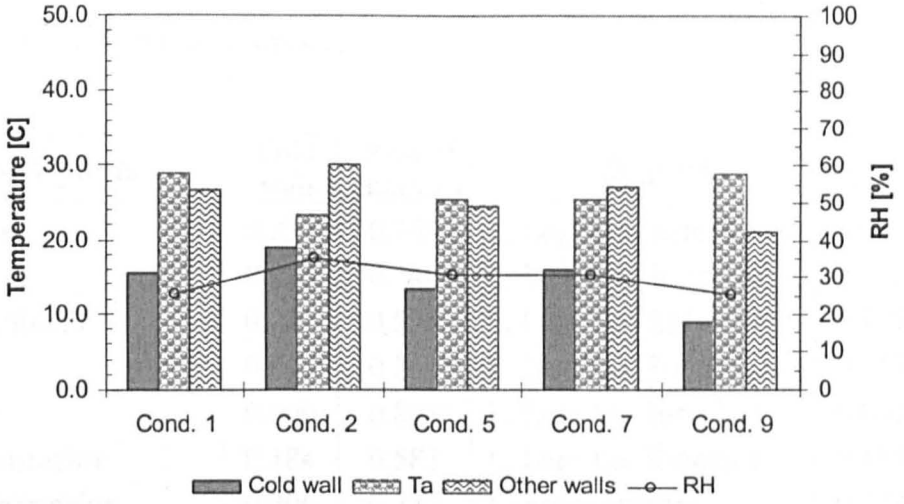

Figure 7.7 Environmental conditions in the simulation of the spatial cold wall (McNall and Biddison, 1970).

The predicted view factors between individual body sectors of the exposed subject and (i) the cold spatial wall and (ii) the rest of the chamber are provided in Table 7.18.

Table 7.18 Local view factors between the subject and the spatial vertical cold wall and the rest of the chamber.

Body parts	Cold wall	Rest of chamber	Body parts	Cold wall	Rest of chamber
Forehead	0.230	0.749	L. Leg: Up. Inferior	0.000	0.563
Head	0.224	0.740	L. Leg: Up. Exterior	0.415	0.360
Face: Anterior	0.227	0.597	L. Leg: Lo. Anterior	0.189	0.811
L. Face	0.624	0.261	L. Leg: Lo. Posterior	0.153	0.557
R. Face	0.000	0.885	L. Leg: Lo. Inferior	0.001	0.739
Neck: Anterior	0.184	0.583	L. Leg: Lo. Exterior	0.431	0.493
Neck: Posterior	0.206	0.737	L. Foot: Instep	0.223	0.663
Neck: L. Exterior	0.532	0.299	L. Foot: Sole	0.013	0.884
Neck: R. Exterior	0.000	0.833	R. Shoulder	0.054	0.832
L. Shoulder	0.238	0.647	R. Arm: Up. Anterior	0.068	0.396
Thorax: Anterior	0.228	0.684	R. Arm: Up. Posterior	0.098	0.902
Thorax: Posterior	0.226	0.763	R. Arm: Up. Inferior	0.232	0.374
Thorax: L. Inferior	0.208	0.247	R. Arm: Up. Exterior	0.002	0.952
Thorax: R. Inferior	0.007	0.457	R. Arm: Lo. Anterior	0.263	0.163
Abdomen: Anterior	0.109	0.381	R. Arm: Lo. Posterior	0.001	0.999
Abdomen: Posterior	0.222	0.778	R. Arm: Lo. Inferior	0.081	0.532
Abdomen: L. Inferior	0.352	0.317	R. Arm: Lo. Exterior	0.056	0.808
Abdomen: R. Inferior	0.001	0.667	R. Hand: Handback	0.099	0.613
L. Arm: Up. Anterior	0.136	0.339	R. Hand: Palm	0.033	0.226
L. Arm: Up. Posterior	0.381	0.619	R. Leg: Up. Anterior	0.162	0.267
L. Arm: Up. Inferior	0.040	0.557	R. Leg: Up. Posterior	0.032	0.904
L. Arm: Up. Exterior	0.471	0.482	R. Leg: Up. Inferior	0.233	0.329
L. Arm: Lo. Anterior	0.004	0.421	R. Leg: Up. Exterior	0.000	0.776
L. Arm: Lo. Posterior	0.490	0.510	R. Leg: Lo. Anterior	0.288	0.712
L. Arm: Lo. Inferior	0.047	0.568	R. Leg: Lo. Posterior	0.152	0.555
L. Arm: Lo. Exterior	0.331	0.536	R. Leg: Lo. Inferior	0.349	0.388
L. Hand: Handback	0.218	0.496	R. Leg: Lo. Exterior	0.001	0.926
L. Hand: Palm	0.088	0.166	R. Foot: Instep	0.206	0.678
L. Leg: Up. Anterior	0.033	0.398	R. Foot: Sole	0.005	0.891
L. Leg: Up. Posterior	0.112	0.834	**Whole Body**	**0.170**	**0.612**

As an example, Figure 7.8 shows the temporal trends of body temperatures predicted for some body sides of the subject in exposure 2.

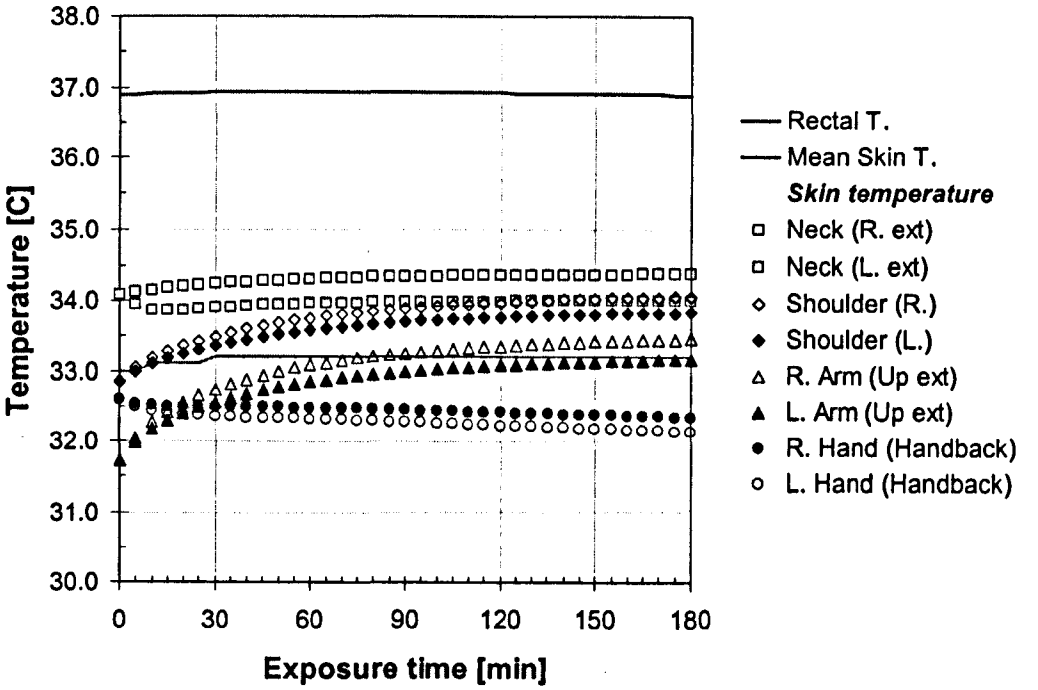

Figure 7.8 Example of predicted temporal trends of body and skin temperatures for the spatial cold wall series (exposure 2) of McNall and Biddison (1970).

The mean skin temperature and the rectal temperature were virtually constant over the whole exposure. It is interesting to note that the predicted local skin temperature of both exposed and non-exposed body parts to the cold wall did not perform significantly different trend as expectation e.g. left and right shoulder, left and right hand, and exterior sector of upper left and right arm, respectively. An exception only neck in which the predicted skin temperature of the left hand side (exposed) body part was significant higher than the right hand side (non-exposed) body part about 0.9 °C.

The predicted local skin temperatures of some main body parts obtained as averages of the five exposures (condition 1, 2, 5, 7, and 9) are presented in Table 7.19. The results for all body sectors are provided in Appendix E, Table E.13.

Table 7.19 Average local skin temperatures of the main body parts obtained for the five environmental conditions at the exposure time of 90 min for the spatial cold wall of McNall and Biddison (1970).

Body sector	$T_{sk,i}$ (°C)
Head	35.0
L. Face	34.4
R. Face	35.0
Neck: L. exterior	34.1
Neck: R. exterior	34.6
L. Shoulder	34.1
Thorax: Anterior	34.8
Thorax: Posterior	34.8
Abdomen: Anterior	34.5
Abdomen: Posterior	34.7
L. Arm: Upper exterior	33.2
L. Arm: Lower exterior	31.6
L. Hand: Handback	32.9
L. Leg: Upper exterior	33.4
L. Leg: Lower exterior	31.7
L. Foot: Instep	31.1
R. Shoulder	34.4
R. Arm: Upper exterior	33.9
R. Arm: Lower exterior	32.2
R. Hand: Handback	33.2
R. Leg: Upper exterior	34.1
R. Leg: Lower exterior	32.6
R. Foot: Instep	31.3

The corresponding local skin temperature differences are listed in Table 7.20.

Table 7.20 Local skin temperature differences, $\Delta T_{sk,i}$ averaged for the five exposures of the spatial cold wall exposure of McNall and Biddison (1970).

Body sector	$\Delta T_{sk,i}$ (°C)
L. Foot: Instep	-2.24
L. Hand: Handback	-2.18
R. Foot: Instep	-2.03
L. Leg: Lower Exterior	-1.97
R. Hand: Handback	-1.89
L. Arm: Lower Exterior	-1.53
L. Face	-1.29
R. Leg: Lower Exterior	-1.09
Neck: L. Exterior	-1.08
R. Arm: Lower Exterior	-0.94
R. Face	-0.74
Head	-0.73
L. Leg: Upper Exterior	-0.73
Neck: R. Exterior	-0.55
L. Arm: Upper Exterior	-0.46
Thorax: Anterior	-0.13
L. Shoulder	-0.11
Thorax: Posterior	-0.11
R. Leg: Upper Exterior	-0.10
R. Shoulder	0.20
R. Arm: Upper Exterior	0.20
Abdomen: Anterior	0.31
Abdomen: Posterior	0.42

The 'coldest' body parts with the lowest $\Delta T_{sk,i}$ values were those sectors of the extremities which were directly exposed to the cold wall, i.e. the left foot (instep) and the left hand (handback). The simulation results indicated that abdomen would be the warmest body part in which the highest $\Delta T_{sk,i}$ values were predicted.

7.5 Developing the local comfort model

The physiological simulations of subjects exposed to asymmetric radiation as described in Chapters 6 and 7.4 showed good agreement with the experimental results investigated. The simulations provided all the physiological parameters which might be important for modelling human local perceptual responses. These included local and mean skin temperatures, local sweat rates and blood flow rates, body core temperatures, the general thermo-regulatory states, etc. The simulations provided a first indication of possible strategies how to model the experimentally observed local thermal comfort responses. This initial analysis indicated that ranking the local skin temperature signals might provide useful information on (i) the location of the body, and (ii) potentially, on the magnitude of local discomfort perceived under given boundary conditions.

In this section, local thermal comfort responses to asymmetric radiation are modelled by correlating experimentally observed local perceptual responses (in term of the percentage of dissatisfied) with predicted physiological responses using statistical regression analysis methods. According to thermophysiological research, the perception of local cold and warm discomfort seems to be based on different physiological mechanisms involving signals from 'cold' and 'warm' cutaneous thermoreceptors, e.g. Hensel (1981). Correspondingly, the modelling approach should use punitive signals from the skin which are defined as the difference between the actual local skin temperature, $T_{sk,i}$, and the corresponding reference value:

$$\Delta T_{sk,i} = T_{sk,i} - T_{sk,\,ref} \qquad (7.1)$$

The $T_{sk,ref}$ reference values refer e.g. to local skin temperatures under thermo-neutral boundary conditions ($T_a<T_R<30°C$, still air, 40% of RH, 0.8 met activity level and no clothing) listed in Appendix E (*Table E.1*) or other thermophysiological conditions at the skin. Negative $\Delta T_{sk,i}$-signals represent

'cold' thermoreceptors, positive $\Delta T_{sk,i}$-signals represent 'warm' cutaneous thermoreceptors.

For each exposure, the cold and warm signals are to be determined for each body part then ranked, and the most extreme positive and/or negative signals selected to be plotted against the experimentally observed local comfort responses. Local cold discomfort can then be modelled as a function of negative $\Delta T_{sk,i}$-signals and the local warm discomfort as a function of positive $\Delta T_{sk,i}$-signals.

7.5.1 Local cold discomfort (LCD)

The experimental series of Fanger et al. (1980 and 1985) and the spatial cold wall series of McNall and Biddison (1970) were used to develop the model for predicting local cold discomfort responses. The analysis of the $\Delta T_{sk,i}$–signals obtained from simulations described in section 7.4 (i.e. using local skin temperature setpoints $T_{sk,l,o}$ as reference values) indicated that the location at the body where local cold discomfort was perceived in the experiments was not always coincident with the lowest $\Delta T_{sk,i}$–signals. The predicted $\Delta T_{sk,i}$–signals are collected together with information on the corresponding body parts, and the percentage of dissatisfied due to LCD in Table 7.21.

Table 7.21 $\Delta T_{sk,i}$-signals obtained for various asymmetric radiation exposures, Fanger et al. (1980 and 1985) and McNall and Biddison (1970).

Type of exposure	Author of experiments		Exposure time [min]				
			90 (30)#	120 (60)#	150 (90)#	180	210
warm/hot ceiling	Fanger et al. (1980)	%LCD	6.3	12.5	37.5	50.0	43.8
		$\Delta T_{sk,i}$ [K]	-2.230	-2.580	-2.870	-3.120	-3.410
			-2.210	-2.480	-2.700	-2.940	-3.210
		Body part	Legs (lo pos)	Feet (inst)	Feet (inst)	Feet (inst)	Feet (inst)
			Feet (inst)	Legs (lo pos)	Legs (lo pos)	Legs (lo pos)	Legs (lo pos)
cool/cold ceiling	Fanger et al. (1985)	%LCD	0.0	0.0	0.0	6.3	6.3
		$\Delta T_{sk,i}$ [K]	-2.910	-3.220	-3.250	-3.320	-3.220
			-2.370	-2.870	-3.070	-3.200	-3.220
		Body part	Hands (Hnbck)	Hands (Hnbck)	Hands (Hnbck)	Hands (Hnbck)	Hands (Hnbck)
			Feet (Inst)	Feet (Inst)	Feet (Inst)	Feet (Inst)	Feet (Inst)
warm/hot wall	Fanger et al. (1985)	%LCD	0.0	0.0	0.0	0.0	6.3
		$\Delta T_{sk,i}$ [K]	-2.530	-2.830	-3.220	-3.540	-4.130
			-2.470	-2.690	-3.130	-3.090	-3.470
		Body part	R. Hand (Hnbck)	R. Hand (Hnbck)	R. Hand (Hnbck)	R. Hand (Hnbck)	R. Hand (Hnbck)
			R. foot (Inst)	R. foot (Inst)	R. foot (Inst)	R. foot (Inst)	R. foot (Inst)
cool/cold vertical panel	Fanger et al. (1985)	%LCD	3.1	0.0	9.4	28.1	37.5
		$\Delta T_{sk,i}$ [K]	-2.680	-2.790	-2.860	-3.080	-3.170
			-2.430	-2.610	-2.830	-2.920	-2.980
		Body part	L. Hand (Hnbck)	L. Hand (Hnbck)	L. foot (Inst)	L. foot (Inst)	L. foot (Inst)
			L. Leg (lo pos)	L. foot (Inst)	L. Hand (Hnbck)	R. foot (Inst)	R. foot (Inst)
cold wall	McNall and Biddison (1970)	%LCD	0.0	0.0	0.0	-	-
		$\Delta T_{sk,i}$ [K]	-2.46	-2.24	-2.34	-	-
			-2.18	-2.18	-2.11	-	-
		Body part	L. Hand (Hndbck)	L. Foot (Inst)	L. Foot (Inst)	-	-
			R. Hand (Hnbck)	L. Hand (Hnbck)	R. Foot (Inst)	-	-

Note: # denotes the exposure time for the experiments of McNall and Biddison (1970).

According to Table 7.21, the affected body parts would only be hands, lower legs and feet. In the experiments, however, local cold discomfort was also sensed at other region of the exposed body side, Fanger et al. (1980 and 1985).

Plotting the percentage of subjects feeling local cold discomfort in the experiments over the corresponding $\Delta T_{sk,i}$–signals from Table 7.21 reveal a rather poor correlation between the LCD-responses and these signals (*Figure 7.9*).

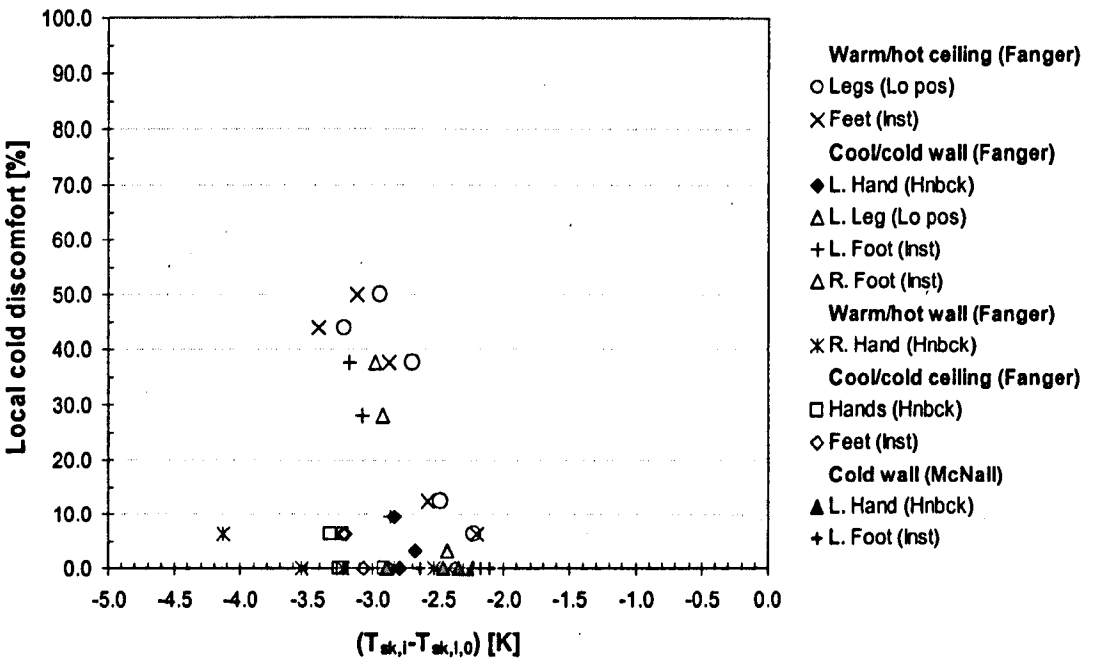

Figure 7.9 Percentage of subjects feeling local cold discomfort as a function of the $\Delta T_{sk,i}$–signals from Table 7.21.

The analysis of the experimental and simulated data revealed that the following aspect need to be considered when modelling LCD.

Firstly, using $\Delta T_{sk,i}$–signals which incorporate local setpoints ($T_{sk,l,o}$) would suggest that local cold discomfort is perceived when $\Delta T_{sk,i} < 0$ K, i.e. when a local skin temperature is lower than the corresponding local value in an environment of T_a= 30°C. However, experimental observations as well as daily experience show that local discomfort is not necessary perceived in any environments that are cooler than the thermophysiologically neutral conditions of T_a= 30°C.

Rather, various experiments, e.g. Gagge et al. (1967), Gonzalez and Gagage (1973), and Hardy (1970), have shown that the perception of local cold discomfort is related in some way to the overall thermal state of the body. The 'normal' distribution of skin temperature varies with the ambient temperature. Thereby, the local skin temperature can fall, especially in extremities, well below its thermo-neutral value. Only if the local $T_{sk,i}$ deviates from the average body skin temperature, $T_{sk,m}$, to a certain degree than LCD is perceived (Wyon and Sandberg, 1990). A widely applicable LCD model has to account for this effect. This was accomplished by redefining the local punitive signal from the skin as the difference between the local skin temperature, $T_{sk,i}$, and the mean skin temperature, $T_{sk,m}$:

$$\Delta T_{sk,i} = T_{sk,i} - T_{sk,m}. \qquad (7.2)$$

Secondly, the analysis of the data clearly indicated that there is a further physiological quantity that influences the human sensation of local cold discomfort, i.e. the local skin sensitivity. Nadel et al. (1973), Steven et al. (1973), and Crawshaw et al. (1975) measured local sensitivity coefficients for cold stimuli at different parts of the human body including face, chest, upper back, abdomen, upper legs, lower legs, upper arms and lower arms. Their results are summarised in Appendix E (*Table E.15*).

These results were used to obtain local sensitivity coefficients for each of the 59 skin sectors of the humanoid. For this purpose, any area-weighting factors were eliminated from the original data and the coefficients were recalculated to obtain a total of unity keeping the relative local proportions equal to the measured data. For some body sectors (head, shoulders, hands and feet) no information was available. In these cases the local sensitivities were obtained as averages of coefficients of the closest body parts for which measured data was available.

The area-weighting was removed from the original data based on the findings of Steven et al. (1974) who discovered that the human local sensation of thermal

(dis)comfort is independent of the skin area to which a thermal stimulus is applied, provided the affected skin area is $A_{sk} > 60$ cm². For $A_{sk} < 60$ cm² the magnitude of discomfort decreased proportionally to the decrease of stimulated A_{sk}. In the model, the sensitivity coefficients of sectors which surface area was less than 60 cm² (forehead and anterior neck) were recalculated to include the effect of reduced skin area on the perceptual response. The local cold sensitivity coefficients used in this study are listed in Table 7.22.

Table 7.22 Model's coefficients of sensitivity to cold stimuli.

Body sector	Body part	Cold sensitivity	Body sector	Body part	Cold sensitivity
Head	forehead	0.0310	upper arms (L & R)	anterior	0.0152
	head	0.0389		posterior	0.0152
Face	anterior	0.0389		inferior	0.0151
	left exterior	0.0389		exterior	0.0151
	right exterior	0.0389	lower arms (L & R)	anterior	0.0151
Neck	anterior	0.0214		posterior	0.0151
	posterior	0.0274		inferior	0.0108
	L. exterior	0.0274		exterior	0.0108
	R. exterior	0.0274	Hands (L & R)	hand back	0.0108
Shoulders	left	0.0228		palm	0.0108
	right	0.0228	upper legs (L & R)	anterior	0.0171
Thorax	anterior	0.0202		posterior	0.0171
	posterior	0.0228		inferior	0.0171
	L. inferior	0.0228		exterior	0.0171
	R. inferior	0.0228	lower legs (L & R)	anterior	0.0107
Abdomen	anterior	0.0228		posterior	0.0107
	posterior	0.0152		inferior	0.0107
	L. inferior	0.0152		exterior	0.0107
	R. inferior	0.0152	Feet (L & R)	instep	0.0107
				sole	0.0107

With the above modification, the local cold stimulus, LCS, used to develop the *LCD*-model is calculated as follows:

$$LCS = (T_{sk,i}-T_{sk,m})*C_{sk,c,i} \quad (7.3)$$

where
- LCS = local cold stimulus, [K]
- $T_{sk,i}$ = local skin temperature of a body sector, [°C]
- $T_{sk,m}$ = mean skin temperature of the body, [°C]
- $C_{sk,c,i}$ = skin sensitivity coefficient of body sector *i* with respect to local stimuli. [-]

The predicted *LCS*-signals obtained for all analysed exposures are presented together with the corresponding measured LCD-responses and information on the affected body parts in Table 7.23.

Table 7.23 Sensitivity-weighted local cold stimuli and LCD responses obtained for the 'coldest' body parts in the experimental series of Fanger et al. (1980 and 1985) and McNall and Biddison (1970).

Type of exposure	Author of experiments		Exposure time [min]				
			90 (30)#	120 (60)#	150 (90)#	180	210
warm/hot ceiling	Fanger et al., (1980)	%LCD	6.3	12.5	37.5	50.0	43.8
		LCS	-2.506	-2.794	-3.104	-3.370	-3.530
			-2.186	-2.357	-2.709	-3.221	-3.487
		Body part	Feet (inst)	Feet (inst)	Feet (inst)	Feet (inst)	Feet (inst)
			Legs (lo pos)	Legs (lo pos)	Legs (lo pos)	Legs (lo pos)	Legs (lo pos)
cool/cold ceiling	Fanger et al. (1985)	%LCD	0.0	0.0	0.0	6.3	6.3
		LCS	-2.250	-2.570	-2.890	-3.029	-3.050
			-1.909	-1.770	-2.890	-1.781	-1.824
		Body part	Hands (Hnbck)	Hands (Hnbck)	Hands (Hnbck)	Hands (Hnbck)	Hands (Hnbck)
			Feet (Inst)	Feet (Inst)	Feet (Inst)	Feet (Inst)	Feet (Inst)
warm/hot wall	Fanger et al. (1985)	%LCD	0.0	0.0	0.0	0.0	6.3
		LCS	-2.677	-2.912	-3.168	-3.338	-3.583
			-1.723	-2.150	-2.679	-3.208	-3.530
		Body part	R. Arm (Lo. pos)	R. Arm (Lo. pos)	R. Arm (Lo. pos)	R. Arm (Lo. pos)	R. Arm (Lo. pos)
			L. Leg (Up ant)	L. Leg (Up ant)	L. Leg (Up ant)	L. Leg (Up ant)	L. Leg (Up ant)
cool/cold vertical panel	Fanger et al. (1985)	%LCD	3.1	0.0	9.4	28.1	37.5
		LCS	-2.250	-2.613	-2.880	-3.221	-3.317
			-2.197	-2.517	-2.741	-3.050	-3.114
		Body part	L. Foot (Inst)	L. Foot (Inst	L. Foot (Inst)	L. Foot (Inst)	L. Foot (Inst)
			L. Leg (Lo pos)	L. Arm (Lo. Ext)	L. Arm (Lo. Ext)	L. Arm (Lo. Ext)	L. Arm (Lo. Ext)
cold wall	McNall and Biddison (1970)	%LCD	0.0	0.0	0.0	0.0	-
		LCS	-2.65	-2.57	-2.53	-2.40	
			-2.12	-2.47	-2.75	-2.86	
			-2.45	-2.32	-2.26	-2.12	-
		Body part	L. Arm (Lo pos)	L. Arm (Lo pos)	L. Arm (Lo pos)	L. Arm (Lo pos)	L. Arm (Lo pos)
			L. Foot (Inst)	L. Foot (Inst)	L. Foot (Inst)	L. Foot (Inst)	L. Foot (Inst)
			L. Arm (Lo ext)	L. Arm (Lo ext)	L. Arm (Lo ext)	L. Arm (Lo ext)	L. Arm (Lo ext)

Note: # denotes the exposure time for the experiments of McNall and Biddison (1970).

There was a good agreement regarding the location on the body where local discomfort was perceived in the experiments and the body parts predicted as being the 'coldest' using the new 'sensitivity-weighted' punitive signals. Only for exposures in which the percentage of dissatisfied was insignificant (i.e. cool/cold ceiling) there were still discrepancies regarding the predicted and observed location on the body where LCD was perceived.

The percentage of subjects who perceived local cold discomfort due to asymmetric radiation in the experiments of Fanger et al. (1980 and 1985) and McNall and Biddison (1970) are plotted against the sensitivity-weighted *LCS*-signals in Figure 7.10. The trend of the data was modelled using an exponential function that asymptotically approaches the lower and upper limit assumed to be at 0 and 100% of dissatisfied:

$$LCD = \frac{100}{1 + \exp(a \cdot LCS + b)} \tag{7.4}$$

where *LCS* is the local cold stimulus according to equation 7.3 and a and b are coefficients to be determined from available measured and simulated data.

Equation (7.4) can be performed linearization for purposes of regression analysis as follows:

$$\ln\left(\frac{100}{LCD} - 1\right) = a \cdot LCS + b \tag{7.5}$$

The analytical solution was then performed with $Y = \ln(\frac{100}{LCD} - 1)$ and $X = LCS$ and where a and b is regression coefficient to be determined by regression analysis. The LCD responses correlated well with the sensitivity weighted LCS signals with a correlation coefficient R^2=0.791. The regression analysis[1] revealed a= 3.390 ± 0.091 and b= 11.511 ± 0.277.

[1] The experimental data from the hot wall series of Fanger et al. (1985) showed a large discrepancy from the general trend of all other experiments and was thus excluded for the analysis.

With the regression results the final equation of the percentage of people being dissatisfied due to local cold discomfort (LCD) becomes:

$$LCD = \left\{ \frac{1}{1+\exp(3.390 \times LCS + 11.511)} \right\} \times 100 \qquad (7.6)$$

where LCD = Percentage of dissatisfied due to local cold discomfort, [%]

LCS = Local cold stimulus

= $(T_{sk,i}-T_{sk,m})^{*}C_{sk,c,i}$. [K]

Equation 7.6 can also be written as:

$$LCD = \frac{100}{1+9.981^{*}10^{4}\, e^{3.39LCS}} \qquad (7.7)$$

The regression line is drawn together with the experimental data in Figure 7.10.

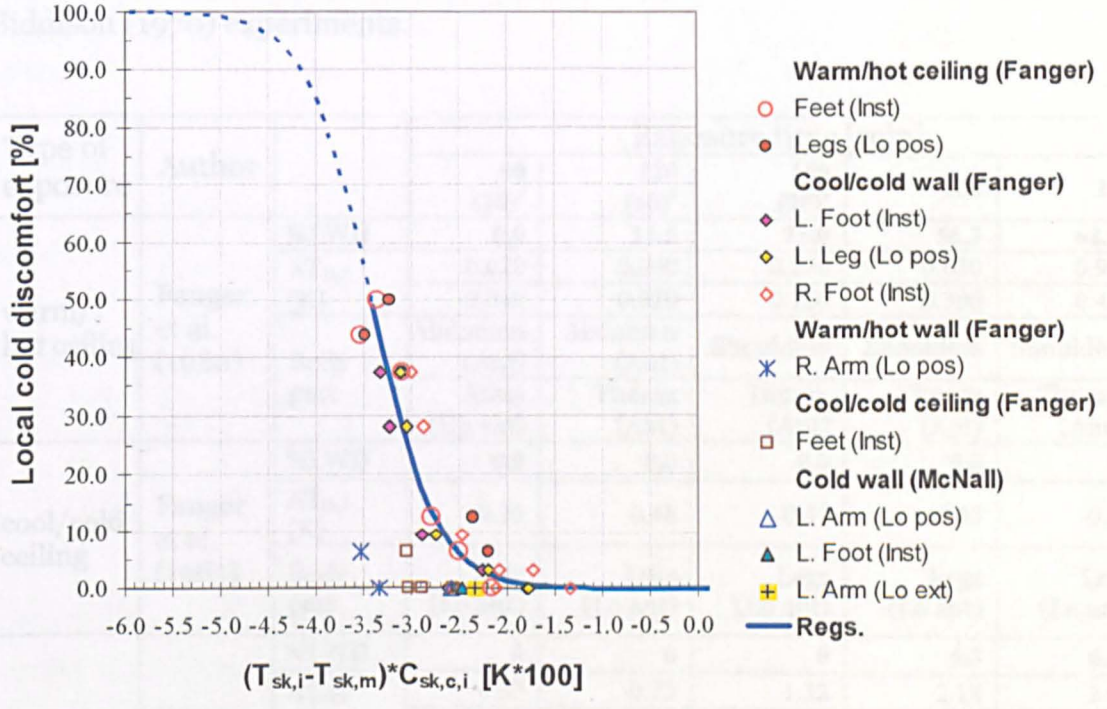

Figure 7.10 Percentage of dissatisfied due to LCD as a function of sensitivity-weighted LCS-signals.

7.5.2 Local warm discomfort (LWD)

As mentioned in section 7.5, LWD, i.e. the percentage of dissatisfied due to local warm discomfort, modelled as separate perceptual response. As with LCD, the first step of the analysis was to evaluate the $\Delta T_{sk,i}$- signals defined as the difference between the actual local skin temperature, $T_{sk,i}$ and the corresponding temperature setpoint, $T_{sk,l,o}$.

The local signals $\Delta T_{sk,i}=T_{sk,i}-T_{sk,l,o}$ obtained for the 'warmest' body parts from the simulations of the experimental series of Fanger et al. (1980 and 1985) and the experimental series of McNall and Biddison (1970) described in section 7.4.1 to 7.4.6 are sorted in ascending order and listed together with measured LWD-responses in Table 7.24.

Table 7.24 $\Delta T_{sk,i}$- signals of the 'warmest' body parts and the percentage of dissatisfied due to LWD for the Fanger et al. (1980 and 1985) and McNall and Biddison (1970) experiments.

Type of exposure	Author		Exposure time [min]				
			90 (30)#	120 (60)#	150 (90)#	180	210
warm/ hot ceiling	Fanger et al. (1980)	%LWD	0.0	12.5	25.0	56.3	62.5
		$\Delta T_{sk,i}$ [K]	0.020	0.000	0.270	0.650	0.90
			-0.040	0.020	0.120	0.300	0.41
		Body part	Abdomen (Ant)	Abdomen (Ant)	Shoulders	Shoulders	Shoulders
			Arms (Up ext)	Thorax (Ant)	Thorax (Ant)	Thorax (Ant)	Thorax (Ant)
cool/cold ceiling	Fanger et al. (1985)	%LWD	0.0	0.0	0.0	0.0	0
		$\Delta T_{sk,i}$ [K]	-0.35	0.48	-0.48	-0.45	-0.40
		Body part	Legs (Lo ant)	Legs (Lo ant)	Legs (Lo ant)	Legs (Lo ant)	Legs (Lo ant)
warm/ hot wall	Fanger et al. (1985)	%LWD	0	0	0	6.3	6.3
		$\Delta T_{sk,i}$ [K]	0.33	-0.75	1.32	2.18	2.60
			-0.06	-0.60	1.17	1.67	1.90
		Body part	L. Arm (Up ext)	L. Arm (Up ext)	L. Arm (Up pos)	L. Arm (Up pos)	L. Arm (Up pos)
			Abdomen (L)	L. Arm (Up pos)	L. Arm (Up ext)	L. Arm (Up ext)	L. Arm (Up ext)

Table 7.24 (continued)

Type of exposure	Author		Exposure time [min]				
			90 (30)#	120 (60)#	150 (90)#	180	210
hot wall	McNall and Biddison (1970)	%LWD	-	-	30.38	-	-
		$\Delta T_{sk,i}$ [K] (1)	0.61	1.07	1.31	-	
			0.19	0.70	0.97	-	
		Body part (1)	L. Arm (Up ext)	L. Arm (Up ext)	L. Arm (Up ext)	-	-
			Neck (L)	L. Arm (Up pos)	L. Arm (Up pos)	-	-
		$\Delta T_{sk,i}$ [K] (2)	0.51	0.93	1.15	-	
			0.42	0.70	0.78	-	
		Body part (2)	L. Arm (Up ext)	L. Arm (Up ext)	L. Arm (Up ext)	-	-
			L. Leg (Up ext)	L. Leg (Up ext)	L. Leg (Up ext)	-	-
		LWS (3)	0.55	0.99	1.21	-	-
			0.45	0.74	0.81	-	-
		Body part (3)	L. Arm (Up ext)	L. Arm (Up ext)	L. Arm (Up ext)	-	-
			L. Leg (Up ext)	L. Leg (Up ext)	L. Leg (Up ext)	-	-
cool/cold vertical panel	Fanger et al. (1985)	%LWD	0.0	0.0	0.0	0.0	9.3
		$\Delta T_{sk,i}$ [K]	-0.12	0.02	0.12	0.23	0.35
			-0.21	0.20	-0.15	0.06	0.25
		Body part	R. Arm (Up. Ext)	R. Arm (Up. Ext)	R. Arm (Up. Ext)	R. Arm (Up. Ext)	R. Arm (Up. Ext)
			Abdomen (Ant)	Abdomen (Ant)	Abdomen (Ant)	R. Shoulder	R. Shoulder
cold wall	McNall and Biddison (1970)	%LWD	0.0	0.0	0.0	-	-
		$\Delta T_{sk,i}$ [K]	-0.11	0.21	0.42	-	-
		Body part	Feet (Inst)	Abdomen (pos)	Abdomen (pos)	-	-

Note: (1) is $\Delta T_{sk,i}$ -signal regarding to the position 1,
(2) is $\Delta T_{sk,i}$ -signal regarding to the position 2 and
(3) is $\Delta T_{sk,i}$ -signal regarding to the position 3 and
# denotes exposure time for the experiments of McNall and Biddison (1970).

The results in Table 7.24 showed relatively good agreement with experimental results regarding the location at the body where LWD was perceived. For the warm/hot ceiling series, in which the subjects perceived local warm discomfort in the 'head region' (without specifying the exact position), the simulations revealed the shoulders to be the 'warmest' body parts. This exactly agrees with the experimental findings of McIntyre and Griffiths (1972) who found that

shoulders are the most affected body parts of subjects exposed to a hot ceiling. In the warm/hot vertical panel series, the upper arm was the warmest body part in both simulation and experiment. No body parts were predicted to be 'warm', i.e. $\Delta T_{sk,i} > 0$ K, in the cool-ceiling series of Fanger et al. (1985).

The signals listed in Table 7.24 are plotted against the corresponding percentage of people dissatisfied due to local warm discomfort in Figure 7.11.

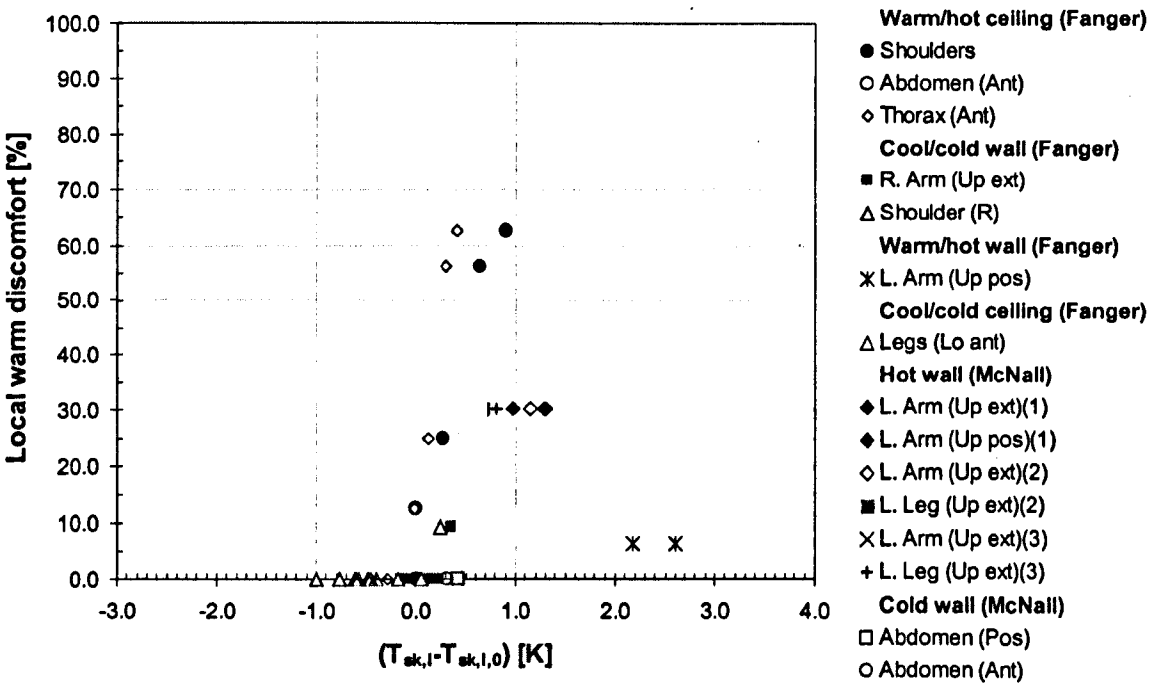

Figure 7.11 Percentage of dissatisfied due to local warm discomfort drawn over the local temperature difference $T_{sk,i}$-$T_{sk,l,o}$ obtained for the experimental series of Fanger et al. (1980 and 1985) and McNall and Biddson (1970).

In contrast to cold discomfort the local warm discomfort responses observed in the experiments already correlated quite well with the $(T_{sk,i}$-$T_{sk,l,o})$–signal. Exception formed the results of Fanger's warm/hot-wall series which deviated vastly from the general trend of the data. A similar observation has also been made by the authors of the experiments in their paper. This data was therefore excluded from further analysis.

A thorough analysis of measured and predicted data indicated that local warm discomfort responses are best predicted using local skin temperature differences ($T_{sk,i}$-$T_{sk,l,o}$) as input signals when weighted by the corresponding local sensitivity coefficients, $C_{sk,w,i}$:

$$LWS = (T_{sk,i}-T_{sk,l,o})*C_{sk,w,i} \quad (7.8)$$

where
- LWS = local warm stimulus, [K]
- $T_{sk,i}$ = local skin temperature of a body sector, [°C]
- $T_{sk,l,o}$ = local skin temperature set point of a body sector, [°C] (see *Appendix E, Table E.1*)
- $C_{sk,w,I}$ = local warm sensitivity coefficient of a body sector. [-]

The $C_{sk,w,i}$ coefficients are listed in Table 7.25. They were obtained from data of Crawshaw et al. (1975) using as similar method described for cold sensitivity coefficients in section 7.5.1.

The analysis also showed that the use of mean skin temperature, $T_{sk,m}$, as reference value in the LWS-signals for modelling the LWD-response would be less appropriate. There were two reasons for this. Firstly, in warm environments the mean skin temperature is subject to much smaller changes than in cooler environments. This is a result of the cooling effect of sweat evaporation which is activated in the warmth and which causes $T_{sk,m}$ to be maintained fairly constant over a relatively wide range of warm environments. The effect of changes in $T_{sk,m}$ on LWD would therefore be small compared to its effect on LCD and thus difficult to quantify by means of statistical regression analysis.

Secondly, using $T_{sk,m}$ in the LWS-signals, would mean that, in environments which are cooler than the thermophysiologically neutral condition of 30°C, local warm discomfort would be predicted for any $T_{sk,i} > T_{sk,m}$, i.e. even if $T_{sk,i}$ was lower than it's thermo-neutral setpoint $T_{sk,l,o}$ (because $T_{sk,m}$ in the actual environment was decreased compared to $T_{sk,m}$ at T_a=30°C). There is no experimental evidence known to the author of this work which would indicate

such a response. In opposite, various experiments (Hensel 1981, Gagge et al. 1967 and Mover 1976) have shown that warming the skin towards thermal neutrality is perceived as pleasant/comfortable rather than uncomfortable.

Table 7.25 Model's coefficients of sensitivity to warm stimuli.

Body sector	Body part	Warm sensitivity
Head	forehead	0.0545
	head	0.0682
Face	anterior	0.0682
	left exterior	0.0682
	right exterior	0.0682
Neck	anterior	0.0292
	posterior	0.0373
	left exterior	0.0373
	right exterior	0.0373
Shoulders	left and right	0.0222
Thorax	anterior	0.0202
	posterior	0.0222
	left & right inferior	0.0222
Abdomen	anterior	0.0222
	posterior	0.0172
	left & right inferior	0.0172
upper arms	anterior	0.0172
	posterior	0.0172
	inferior	0.0112
	exterior	0.0112
lower arms	anterior	0.0112
	posterior	0.0112
	inferior	0.0043
	exterior	0.0043
Hands	hand back	0.0043
	palm	0.0043
upper legs	anterior	0.0170
	posterior	0.0170
	inferior	0.0170
	exterior	0.0170
lower legs	anterior	0.0045
	posterior	0.0045
	inferior	0.0045
	exterior	0.0045
Feet	instep	0.0045
	sole	0.0045

The calculated local weighted LWS-signals obtained for all analysed experiments are gathered together with the corresponding LWD-responses in Table 7.26.

Table 7.26 Sensitivity-weighted local skin temperature signals of the 'warmest' body parts and LWD-responses obtained for the Fanger et al. (1980 and 1985) and McNall and Biddison (1970) experiments.

Type of exposure	Author		Exposure time [min]				
			90 (30)#	120 (60)#	150 (90)#	180	210
warm/ hot ceiling	Fanger et al. (1980)	%LWD	**0.0**	**12.5**	**25.0**	**56.3**	**62.5**
		LWS	0.03	0.00	0.60	1.44	2.00
			-0.06	-0.06	0.24	0.61	0.83
		Body part	Abdomen (Ant)	Abdomen (Ant)	Shoulders	Shoulders	Shoulders
			Thorax (Ant)	Thorax (Ant)	Thorax (Ant)	Thorax (Ant)	Thorax (Ant)
cool/cold ceiling	Fanger et al. (1985)	%LWD	**0.0**	**0.0**	**0.0**	**0.0**	**0**
		LWS	-0.53	-0.73	-0.76	-0.82	-0.77
		Body part	Arms (Lo inf)	Arms (Lo inf)	Arms (Lo inf)	Arms (Lo inf)	Arms (Lo inf)
warm/ hot wall	Fanger et al. (1985)	%LWD	**0**	**0**	**0**	**6.3**	**6.3**
		LWS	0.37	1.70	5.11	9.27	10.16
			-0.09	0.86	2.35	4.25	4.48
		Body part	L. Arm (Up ext)	L. Face	L. Face	L. Face	L. Face
			Abdomen (L. inf)	Neck (L. ext)	Neck (L. ext)	Neck (L. ext)	Neck (L. ext)
hot wall	McNall and Biddison (1970)	%LWD	-		**30.38**	-	-
		LWS (1)	0.67	1.17	1.49	-	
			0.82	0.99	1.12	-	
		Body part (1)	L. Face	L. Face	L. Face	-	-
			Neck (L. ext)	Neck (L. ext)	Neck (L. ext)	-	-
		LWS (2)	0.00	0.46	0.78	-	-
			0.56	0.72	0.85	-	-
		Body part (2)	L. Face	L. Face	L. Face	-	-
			L. Leg (Up. ext)	Neck (L. ext)	Neck (L. ext)	-	-
		LWS (3)	0.08	0.53	0.86	-	-
			0.60	0.76	0.89	-	-
		Body part (3)	L. Face	L. Face	L. Face	-	-
			L. Leg (Up. ext)	L. Leg (Up. ext)	L. Arm (Up. ext)	-	-

Table 7.26 (Continued)

Type of exposure	Author		Exposure time [min]				
			90 (30)#	120 (60)#	150 (90)#	180	210
cool/cold vertical panel	Fanger et al. (1985)	%LWD	0.0	0.0	0.0	0.0	9.3
		LWS	-0.18	-0.03	0.13	0.26	0.56
			-0.32	-0.30	-0.23	0.13	0.39
		Body part	R. Arm (Up. Ext)	R. Arm (Up. Ext)	R. Arm (Up. Ext)	R. Arm (Up. Ext)	R. Shoulder
			Abdomen (ant)	Abdomen (ant)	Abdomen (ant)	R. Shoulder	R. Arm (Up. Ext)
cold wall	McNall and Biddison (1970)	%LWD	0.0	0.0	0.0	-	-
		LWS	0.36	0.72	0.96	-	-
		Body part	Abdomen (pos)	Abdomen (pos)	Abdomen (pos)	-	-

Note: (1) is LWS -signal regarding to the position 1,
(2) is LWS -signal regarding to the position 2 and
(3) is LWS -signal regarding to the position 3 and
# denotes exposure time for the experiments of McNall and Biddison (1970).

For the warm/hot-ceiling and the cool/cold-vertical panel series of Fanger et al. (1980 and 1985), shoulders were predicted to be the warmest body parts whereas the left face was the warmest body region in the warm/hot wall series of Fanger et al (1985) and McNall and Biddison (1970). For the cool/cold ceiling series of Fanger et al (1985), the local stimuli were negative indicating that the subjects would perceive local cold rather than warm discomfort. It should be noted, however, in the experiment none of the subjects perceived LWD. For the experimental series of McNall and Biddison, the left face was predicted to be the warmest body part in the hot wall series whereas the posterior abdomen was the warmest body part in the cold wall series.

The percentage of subjects who perceived local warm discomfort in all experiments analysed are plotted against the sensitivity-weighted LWS-signal in Figure 7.12. Similar to the local cold discomfort, the trend of the data was modelled using an exponential equation that approached asymptotically its lower and upper limit set at 0 and 100% LWD:

$$LWD = \frac{100}{1+\exp(a \cdot LWS + b)} \tag{7.9}$$

where LWS is the local warm stimulus according to equation 7.8 and a and b are coefficients to be determined from available measured and simulated data. Equation (7.9) can be performed linearization for purposes of regression analysis as follows:

$$\ln\left(\frac{100}{LWD} - 1\right) = a \cdot LWS + b \tag{7.10}$$

The analysis was then presented with $Y = \ln(\frac{100}{LWD} - 1)$ and X=LWS and with a and b being regression coefficients to be determine by regression analysis. The LWD responses correlated well with the sensitivity weighted LWS signals with a correlation coefficient R^2=0.806. The regression analysis[1] revealed a= -1.730 ± 0.048 and b= 2.663 ± 0.121.

With the regression results the final equation of the percentage of people being dissatisfaction due to local warm discomfort (LWD) becomes:

$$LWD = \left\{\frac{1}{1+\exp(-1.730 \times LS + 2.663)}\right\} \times 100 \tag{7.11}$$

where LWD= Percentage of dissatisfied due to local warm discomfort, [%]

LWD= local warm discomfort, [%]

= $(T_{sk,i}-T_{sk,l,o})^*C_{sk,w,i}$. [-]

Equation 7.11 can also be written as:

$$LWD = \frac{100}{1+14.33e^{-1.73LWS}} \tag{7.12}$$

[1] The experimental data from the hot-wall series of Fanger et al. (1985) showed a large discrepancy from the general trend of all other experiments and was thus excluded from the analysis.

The regression line is drawn together with the experimental data in Figure 7.12.

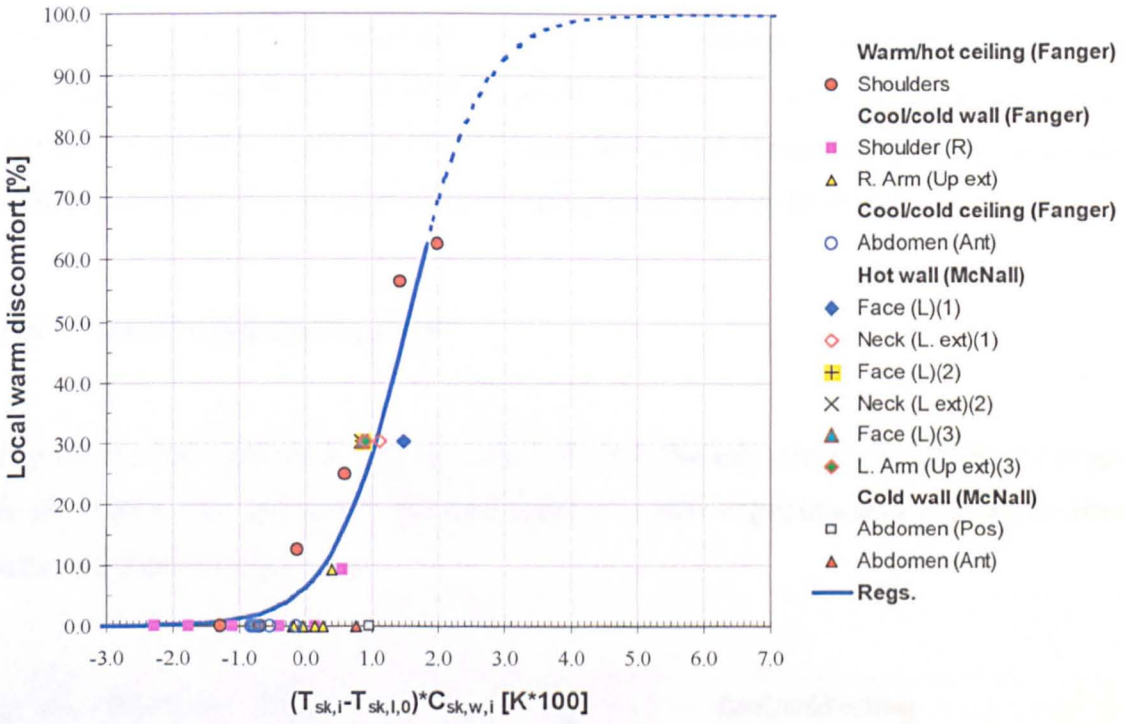

Figure 7.12 Percentage of dissatisfied due to LWD as a function of sensitivity-weighted LWS-signals.

7.6 Verification

The experiments which were used in the model development were used to verify the complete model. The interesting point here was to see to what degree would the new regression models (which were developed using various experiments) would reproduce the human perceptual responses in individual exposures.

7.6.1 Local cold discomfort

The local cold comfort responses predicted for the experimental series of Fanger et al. (1980 and 1985) are plotted together with experimental results as time series in Figure 7.13.

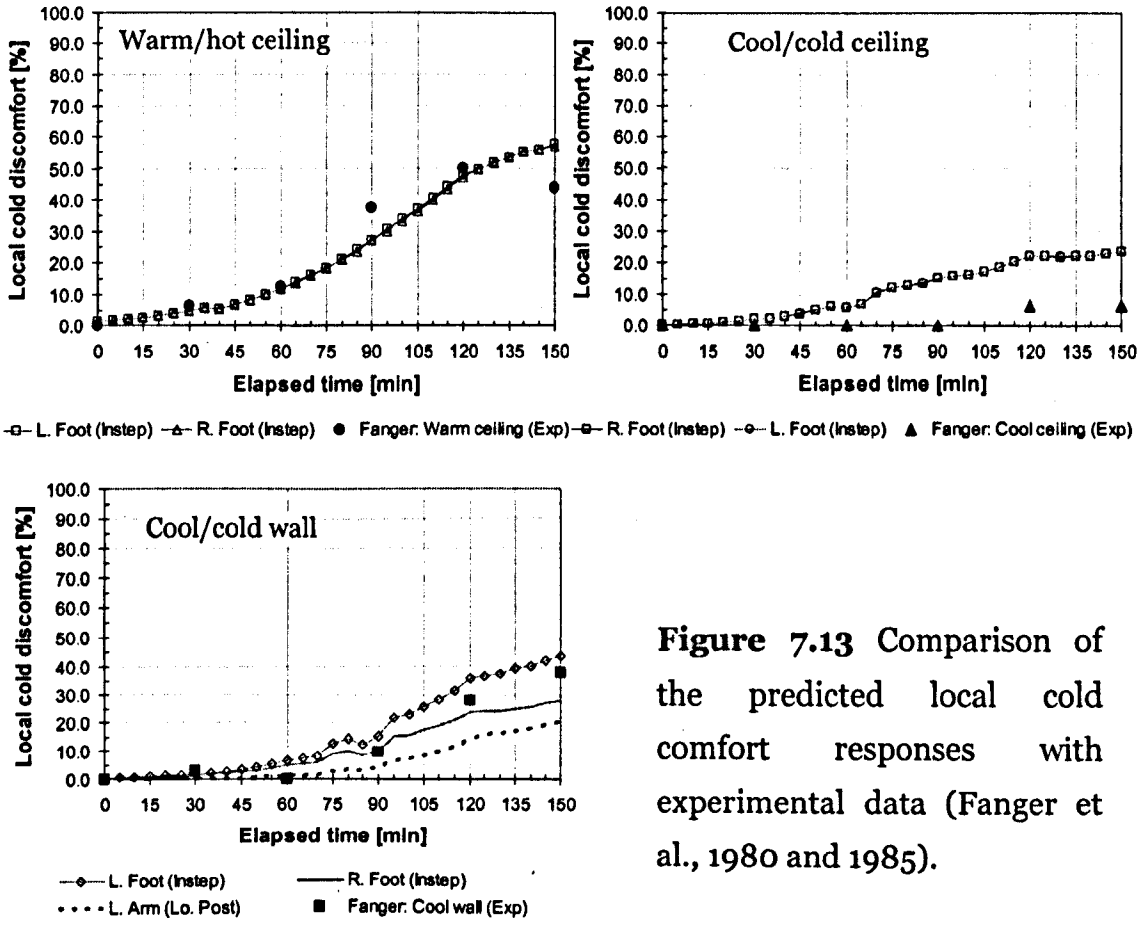

Figure 7.13 Comparison of the predicted local cold comfort responses with experimental data (Fanger et al., 1980 and 1985).

Solid lines represent predictions using regression equation (7.4). Data points indicate experimental results of Fanger et al. (1980 and 1985). Generally, there was good agreement between the predictions and the experimental results. The greatest relative error resulted for the cool/cold ceiling exposure. On average however LCD was predicted within 6.4% of experimentally observed responses.

A comparison of the local cold comfort responses predicted for the experimental series of McNall and Biddison is plotted together with experimental results in Figure 7.14.

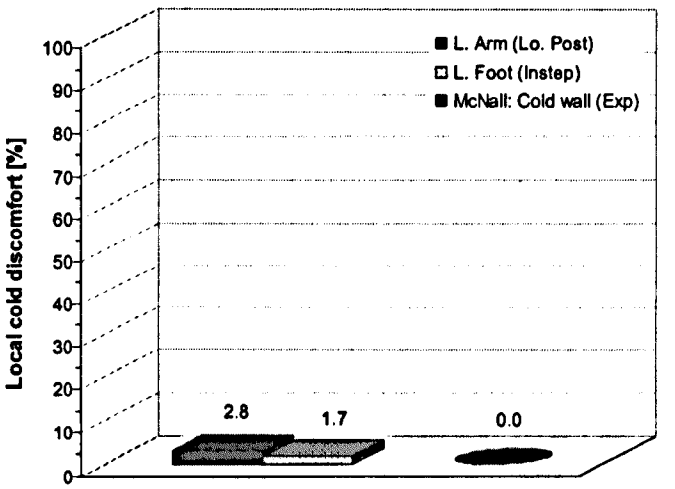

Figure 7.14 Predicted and measured percentage of dissatisfied due to local cold discomfort in the cold-wall series of McNall and Biddison (1970).

For the cold-wall series of McNall and Biddison (1970), the predictions reproduced well the experimental results (circular shape), i.e. indicated negligible percentage of subjects feeling local cold discomfort.

7.6.2 Local warm discomfort

Predicted LWD responses are compared with the experimental results of Fanger et al. (1980 and 1985) in Figure 7.15.

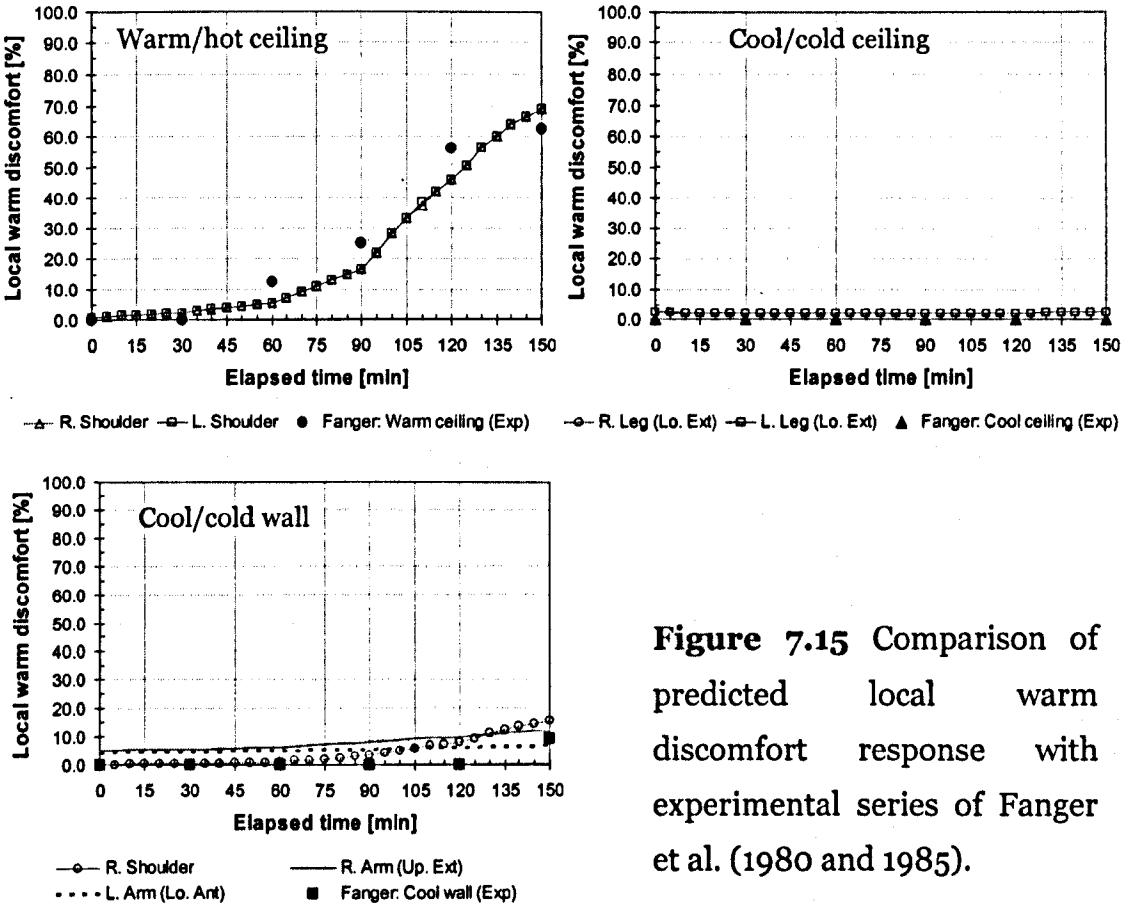

Figure 7.15 Comparison of predicted local warm discomfort response with experimental series of Fanger et al. (1980 and 1985).

Generally, the predictions (lines) agreed very well with the experimental results of Fanger et al. (data points). The average deviation was 4.2%. The model also predicted well the time of the onset of warm discomfort in the warm-ceiling and cold-wall series.

A comparison of predicted local warm discomfort responses with the experimental results of McNall and Biddison (1970) is illustrated in Figure 7.16.

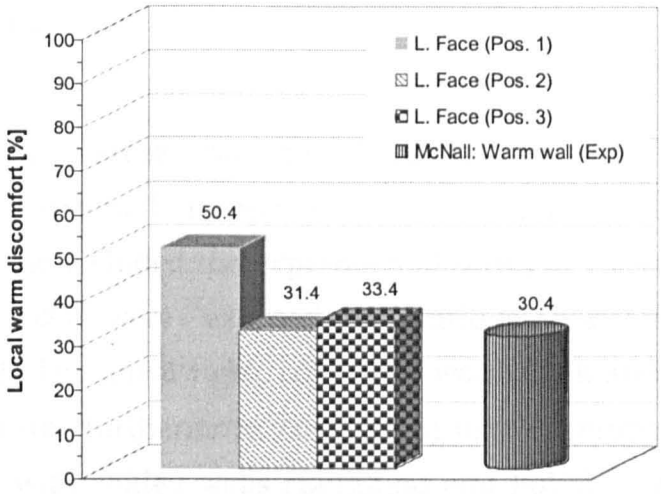

Figure 7.16 Comparison of the predicted local warm discomfort and experimental series of McNall and Biddison (1970).

The predicted percentage of dissatisfied due to local warm discomfort (rectangular bars) reproduced the experimental results of McNall and Biddson with 8% of average error. The greatest discrepancy resulted for the warm-wall(1) scenario where the model overpredicted the percentage of dissatisfied by about 20%.

7.7 Validation

In the validation exercise the model predictions were compared with independent experimental results which were not used in the model development. These included the experimental series of Olesen et al. (1972) in which the subjects were exposed to various horizontal temperature asymmetries: cold left-warm right, cold front-warm back and warm front-cold back. The model was furthermore validated against experiments conducted in spaces equipped with chilled walls (Burglund and Fobelets, 1987) and chilled ceilings (Loveday et al., 1998 and 2002). Unfortunately, no experiments were found in the literature investigating thermal comfort implications of short-wave radiation asymmetries.

Each experiment mentioned above was simulated using the IESD-Fiala model to obtain the required local and global physiological responses and the corresponding thermal comfort responses. The environmental and personal conditions were set according to the experimental conditions. The radiative heat exchanges with the environment were predicted by the IESD-Fiala model for each body sector using local view factors developed in Chapter 5.

7.7.1 Exposure to cold left-warm right vertical wall

Thirty two subjects (8 females and 24 males) were employed in the experiment of Olesen et al. (1972). The subjects (with light clothing of 0.1 clo, males wore cotton briefs and shorts while females wore bikini) were exposed on their left hand side to vertical-cold wall and on their right hand side to vertical-warm/hot wall, simultaneously. In the experiment, the air temperature was constant at 28°C. The mean radiant temperature of the chamber was maintained the same as the air temperature. Temperature of the vertical plane was changed in opposite increment of 5°C every 30 minutes (by decreasing the temperature in one of the end walls and simultaneously increasing the temperature of the opposite wall). The plane radiant temperature asymmetries investigated were 5, 10, 15 and 20°C. Details of the environmental conditions in the experiment and simulation are presented in Appendix D (*Figure D.1*). The experimental results of the subjects experiencing local discomfort are shown in Table 7.27.

Table 7.27 Percentage of subjects who experienced local thermal discomfort in the cold left-warm right exposure of Olesen et al. (1972).

	Exposed time (min)			
	30 (5°C-level)	60 (10°C-level)	90 (15°C-level)	120 (20°C-level)
Discomfort (%)	3.1	6.3	15.6	52.2

In the experiment no distinction was made between the sensation of warm and cold discomfort, i.e. the authors did not provided any information on where the subjects perceived local discomfort and no detailed information on what type of discomfort (cold or warm) they perceived. The information provided was the total percentage of subjects dissatisfied due to asymmetric radiation.

The predicted local comfort responses are compared with observed responses in Figure 7.17.

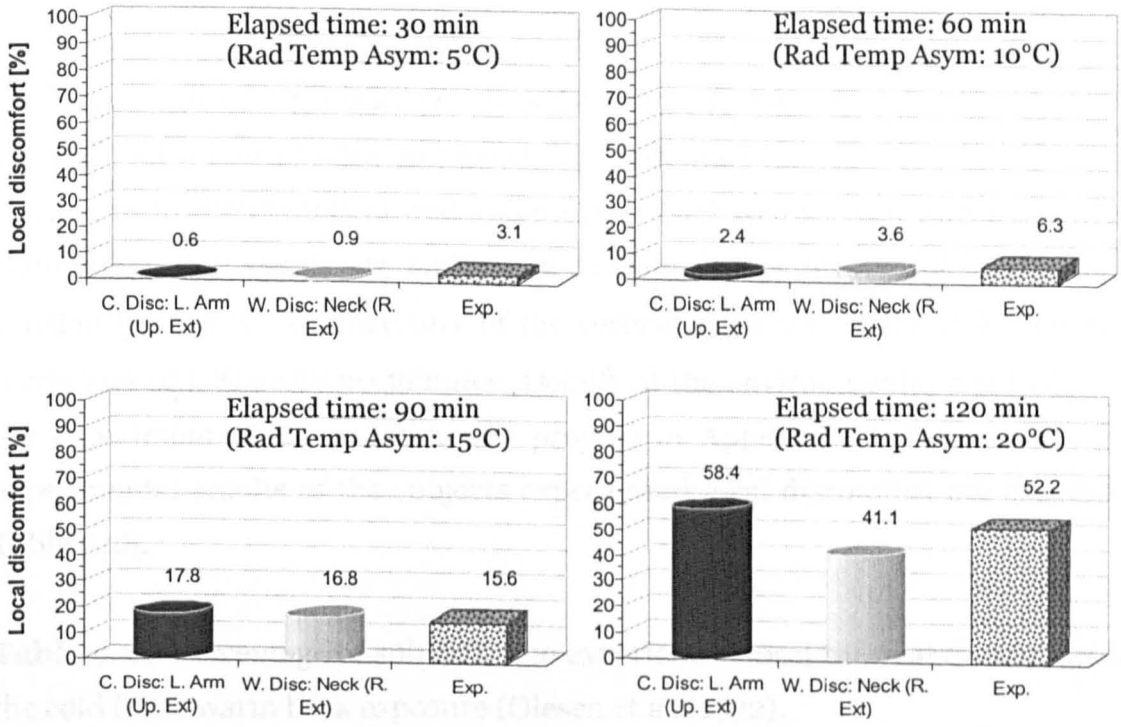

Figure 7.17 Comparison of predicted local cold and warm discomfort responses with experimental results of Olesen et al. (1972).

Circular bars represent the predictions using regression equations (Eq. 7.4 and 7.8) and rectangular bars are the experimental results of Olesen et al. (1972) obtained for the cold left-warm right asymmetry. For local cold discomfort, the predictions (left circular bars in Figure 7.17) agreed within 6.2% with the experimental data. The model predicted lower levels of local warm discomfort which agreed with Olesen et al. (1972) findings that in the experiments most of the subjects complained about cold rather than warm local discomfort.

7.7.2 Exposure to cold front-warm back vertical wall

In the cold front-warm back series of Olesen et al. (1972), sixteen subjects (8 females and 8 males) were employed. The sedentary subjects were exposed on their front to a vertical cold wall and on their back to a vertical warm/hot wall, simultaneously. Again, air and mean radiant temperature was maintained constantly at 28°C. Temperature of the vertical walls was changed in opposite increment of 5°C every 30 minutes. Details of the environmental conditions in the experiment and simulation are provide in Appendix D, Figure D.1. The experimental results of the subjects experienced local discomfort are shown in Table 7.28.

Table 7.28 Percentage of subjects who experienced local thermal discomfort in the cold front-warm back exposure (Olesen et al., 1972).

	Exposed time (min)			
	30 (5°C-level)	60 (10°C-level)	90 (15°C-level)	120 (20°C-level)
Discomfort (%)	0.0	0.0	0.0	14.3

Similar to the cold left–warm right series, the experimental results only provided for the total percentage of dissatisfied due to asymmetric radiation. It is interesting to note that the level of discomfort in this type of exposure was significantly lower compared to the left-right asymmetric conditions.

A comparison of predicted and observed local discomfort responses for the cold front-warm back asymmetric scenario (Olesen et al., 1972) is shown in Figure 7.18.

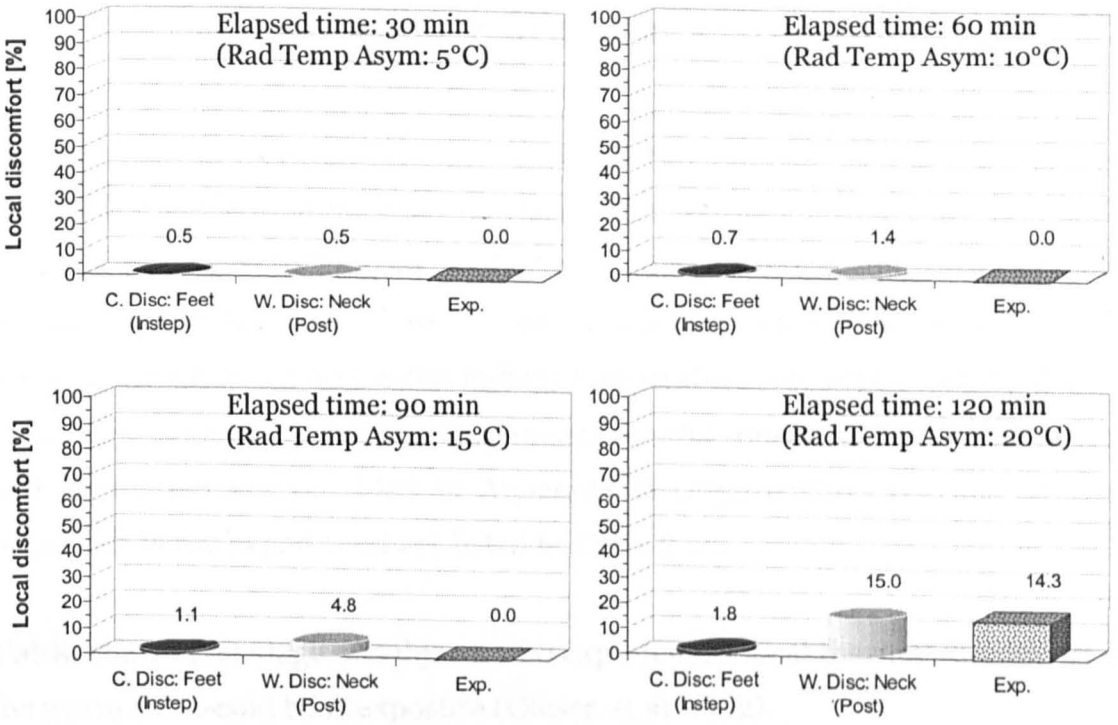

Figure 7.18 Comparison of predicted local cold and warm discomfort obtained for the cold front-warm back series with experimental results of Olesen et al. (1972).

For the cold front-warm back series, it can be observed that cold discomfort was predicted for the feet while warm discomfort arose for the posterior neck. The main cause of complains however was predicted to be local warm discomfort in this exposure. The model reproduced the level of local discomfort observed in the experiment very well.

7.7.3 Exposure to warm front-cold back vertical wall

Sixteen subjects (8 females and 8 males) were employed in this experimental series. The subjects were exposed facing the warm/hot wall with their back exposed to the vertical cold wall. As same as the foregoing experiments, temperature of the vertical walls was changed in opposite increment of 5°C every 30 minutes. Air and mean radiant temperature was kept constant at 28°C as in the previous experiments. The environmental conditions of the experiment and simulation are provided in Appendix D (*Figure D.1*). Thermal comfort responses in the experiment are listed in Table 7.29.

Table 7.29 Percentage of subjects who experienced local thermal discomfort in the warm front-cold back exposure (Olesen et al. 1972).

	Exposed time (min)			
	30 (5°C-level)	60 (10°C-level)	90 (15°C-level)	120 (20°C-level)
Discomfort (%)	0.0	8.9	13.3	33.3

The experiment indicated that facing a warm/hot surface with the back being exposed to a cold surface is more uncomfortable than the opposite exposure (Table 7.28).

A comparison of predicted and observed local discomfort responses for the warm front-cold back series (Olesen et al., 1972) is shown Figure 7.19.

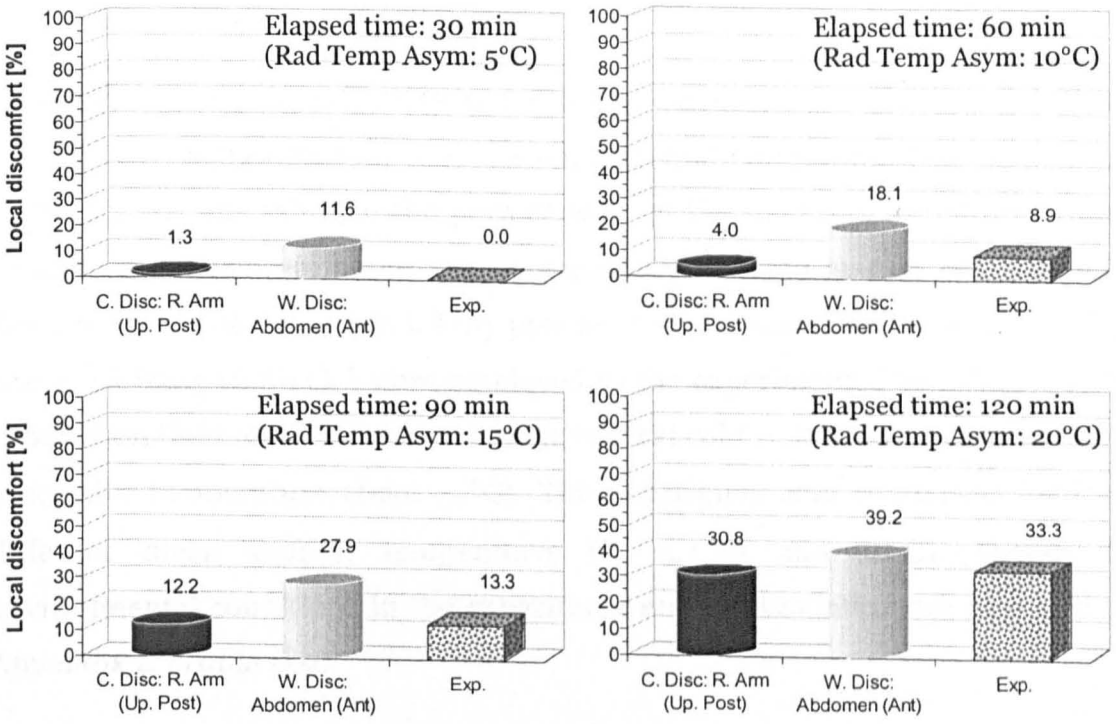

Figure 7.19 Comparison of predicted local cold and warm discomfort obtained for the warm front-cold back series with experimental results of Olesen et al. (1972).

For this exposure the model predicted some cold discomfort at the upper right-exterior arm and warm discomfort at the anterior abdomen. While the predicted level of cold discomfort was similar to the experimentally observed percentage of dissatisfied the warm discomfort overpredicted the experimental level temporarily by up to 15% (at t= 90 min).

7.7.4 Exposure to a cold wall in a cool environment

Most experiments investigating the effect of asymmetric radiation on human comfort were conducted for global environmental conditions close to thermal neutrality. In this example the performance of the model is tested for overall conditions which were about 3°C cooler than a thermo-neutral environment, Berglund and Fobelets (1987). Fifty persons (25 males and 25 females) wearing winter clothing (0.86 clo) were employed in the experiment. The subjects were exposed on their left hand side to a large vertical cold wall in a cool environment (operative temperature about 19°C). The experiment was conducted for four different mean radiant temperature (0, 5, 10 and 18°C). Details of environmental conditions in the experiment and in simulation are provided in Appendix D (*Table D.9*).

A comparison of predicted and observed local discomfort responses for the cold-wall series of Berglund and Fobelets (1987) is presented in Figure 7.20.

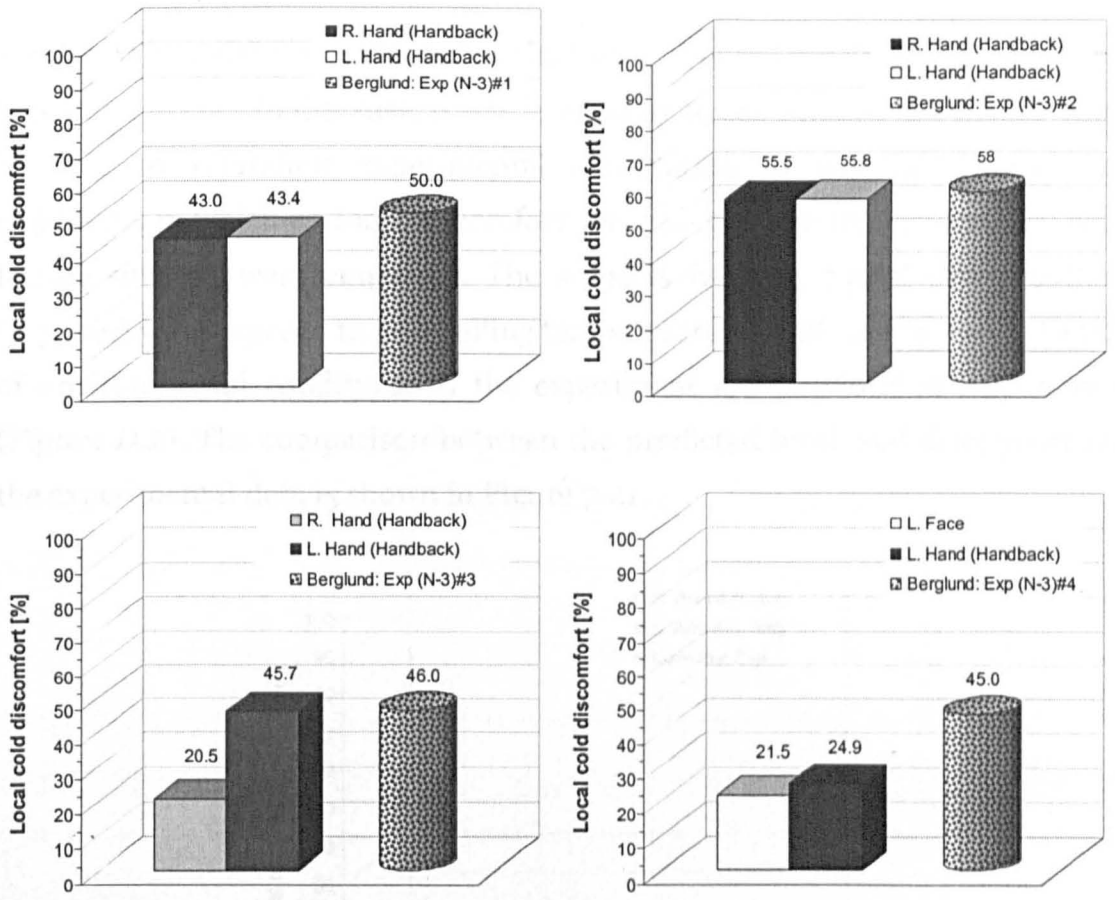

Note: *#1, #2, #3, and #4 represented MRT of 0, 5, 10, and 18 ℃, respectively.*

Figure 7.20 Comparison of predicted local cold discomfort obtained for the cold wall series with experimental results of Berglund and Fobelets (1987).

The model predicted the coldest body parts to be hands in all exposures. This confirmed the findings of Berglund and Fobelets (1987) in which the cold perception was associated with hands. A large discrepancy resulted for the series #4 (MRT of 18°C) where LCD was underpredicted by about 20%. Nevertheless, generally, there was a good general agreement between the predictions and the experimental data (*Figure 7.20*).

7.7.5 Chilled ceiling experiment

Finally, the model was validated against experimental results of Loveday et al. (1998 and 2002). In this case, it was interesting to see whether the model would be able to reproduce experimental observation in asymmetric radiation conditions in which no local discomfort was observed. In the experiment, eight female subjects were employed. The subjects wearing typical office clothing (0.75 clo) were exposed to four ceiling temperature (22, 18, 14 and 12°C). Details of environmental conditions in the experiment are provided in Appendix D (*Figure D.2*). The comparison between the predicted local cold discomfort and the experimental data is shown in Figure 7.21.

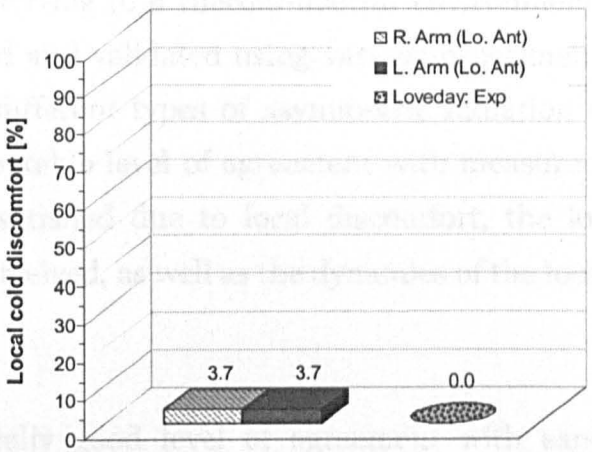

Figure 7.21 Comparison of predicted local cold discomfort response obtained for the chilled ceiling experiments of Loveday et al. (1998 and 2002).

The predictions (rectangular bars) agreed well with the experiment data (circular bar) which indicated no local discomfort (*Figure 7.21*). The low percentage of 3.7% was predicted for the lower anterior arms. In the geometry model used to simulate this exposure (*Chapter 4, Figure 4.1*), these body sectors were oriented permanently towards the cool/cold ceiling which might not have been the case in the experiment and which might be the reason for the slight difference between prediction and measurement.

7.8 Summary

In this chapter, a new comfort model for predicting local cold discomfort (LCD) and local warm discomfort (LWD) responses to asymmetric radiation conditions were developed using available thermal comfort experiments of the past 30 years. LCD and LWD – which are based on different physiological principles – were modelled as two separate responses. LCD was found to be a function of the sensitivity-weighted local skin temperature as related to the actual general thermal state of the human body described by the mean skin temperature. LWD was modelled as an exclusive function of local influences, i.e. the (sensitivity-weighted) local skin temperature and the corresponding local setpoint value (referring to a thermo-neutral environment of 30°C). The new model was verified and validated using various experiments in which subjects were exposed to different types of asymmetric radiation conditions. The test showed good/acceptable level of agreement with measured data regarding the percentage of dissatisfied due to local discomfort, the location on the body discomfort was perceived, as well as the dynamics of the local response (i.e. time dependence).

Although a generally good level of agreement with experimental data was achieved, the level of reproducibility of measured local responses by prediction turned out to be comparably lower than for global responses. Reasons for this are associated with the complexity of the problem regarding geometry (exact body posture and position), physiology (e.g. individual differences in non-uniformity of thermoregulatory responses, local anthropometric body data, local sensitivity), as well as the physics (e.g. local differences in micro-climatic conditions, clothing inhomogeneity) involved. Nevertheless, in contrast to existing methods using environmental parameters, the new model will allow the users to predict human comfort implications for a variety of different asymmetric radiation situations and environmental conditions.

Chapter 8

Predicting thermal comfort responses in buildings

8.1 Introduction

Thermal simulation is an established technique for analysing the dynamic behaviour of whole buildings including heating demands, cooling loads, and solar gains. This technique has enabled the cost-effective development of optimum solutions regarding building design, low energy concepts, and heating, ventilation and air-conditioning (HVAC) strategies. Current state-of-the-art building simulation programs (BSP's) such as ESP-r (ESRU 1998) provide comprehensive predictions of indoor air temperature, humidity, and interior surface temperatures for specified weather and site data and HVAC system performance. Many BSP's predict the thermal and radiation transport in buildings in detail taking into account the effect of obstructions and diverse shading devices. Other computer tools provide the necessary information on the thermal and optical properties of glazing systems and other transparent constructions e.g. Pformmer et al. (1994) and Window 5.0 (2001).

BSP's have been subject to analytical, inter-model and empirical validation exercises, e.g. Lomas et al. (1997). They are a credible tool for determining the boundary conditions to which building occupants are exposed.

In this chapter, a computerised procedure is developed which links the new comfort model predicting both global and local responses with a state-of-the-art building simulation program (BSP). The work describes the way the thermal

simulations should be conducted to obtain dynamic predictions of human heat transfer and thermal comfort.

8.2 Choice of building simulation program

One of the most well known, sophisticated BSPs which has a large national and international user community both in academia and consultancy is ESP-r (ESRU, 1998). ESP-r is an integrated modelling tool for the simulation of the thermal, visual and acoustic performance of buildings and the assessment of the energy use associated with the environmental control systems and constructional materials. ESP-r has been validated for a number of various buildings and has been used to explore e.g. the implications of shading, type of glazing, internal gains, thermal mass, rate of ventilation on indoor temperatures under summer and winter climate conditions, Strachan (2000). A list of the various validation exercises is provided in ESRU (2002). In this study, ESP-r is used as an example to demonstrate the linkage of a BSP with the new comfort model.

8.3 Procedure of linking and postprocessing

A computerised procedure developed here is concerned with linking ESP-r with the new comfort model rather than 'coupling' these two tools. In confined space, such as car cabins, the thermal interactions between the occupants and the immediate environment must be considered to enable adequate predictions of the indoor climate and occupant comfort conditions. This is usually accomplished by coupling thermal models of the car indoor environment and of the cars occupants. In buildings, the indoor spaces are much larger and so the impact of the occupancy on the indoor climate conditions does not necessarily need to be predicted using detailed models of the human heat transfer.

In ESP-r the impact of occupancy is dealt with user-defined casual/internal gains. The strategy here was therefore to link (rather than couple) ESP-r with the new comfort model allowing these two tools to be executed subsequently with ESP-r providing the necessary indoor climate conditions as input into the new comfort model. The linking procedure was accomplished and implemented as a Microsoft Excel spreadsheet tool with incorporated graphical and statistical analysis postprocesing.

The linking procedure consists of three stages: (1) generation and preparation of data needed for comfort simulations, (2) prediction of occupant physiological responses, and (3) data postprocessing. Figure 8.1 shows a schematic diagram of the linking procedure.

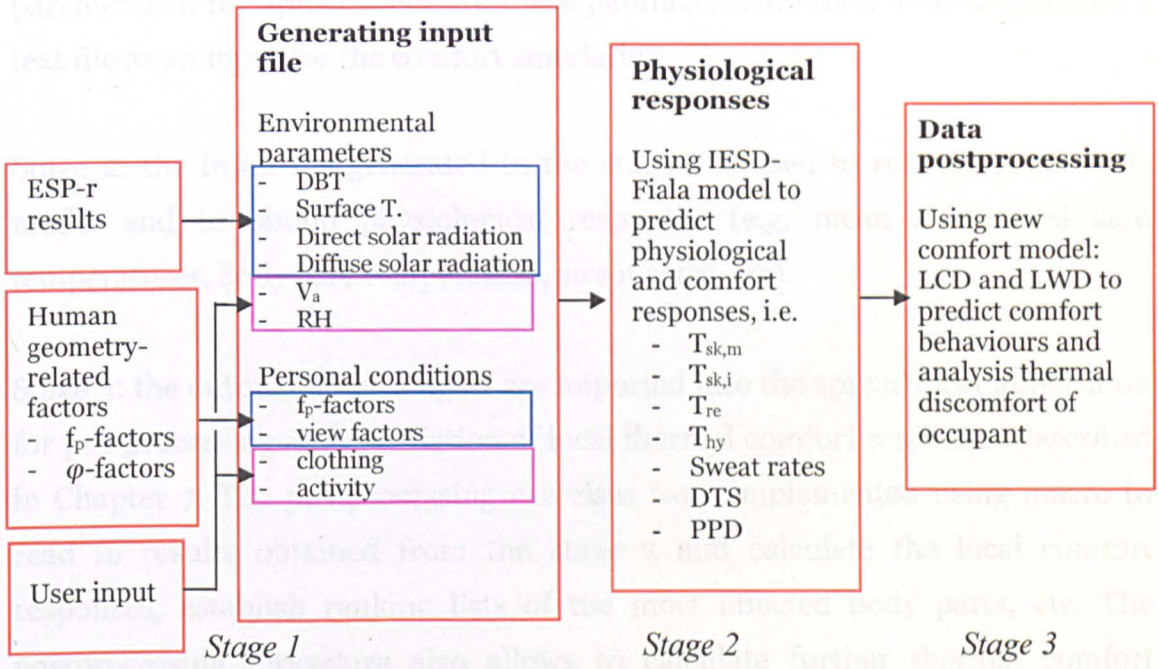

Figure 8.1 Schematic diagram of the linking procedure.

In stage 1, various environmental parameters and four personal parameters (as shown in Figure 8.1) are collected to create the input file needed to run the comfort model. Thereby the following environmental parameters are obtained from the ESP-r: DBT, surface temperatures, direct and diffuse solar radiation. Depending on the detail of the building model in ESP-r the air velocity (V_a) and

the relative humidity (RH) can either be predicted/estimated by ESP-r or defined by the user of the link (in case only thermal effects are considered in ESP-r).

Four 'personal' parameters are: (i) local projected area factors, (ii) view factors between body parts and individual surrounding surfaces of the occupied zone, (iii) clothing and (iv) activity level of subject. The calculation of the human geometry-related factors described in Chapter 4 and 5 is implemented for the user-defined geometry in the spreadsheet software. The position of the sun (azimuth and altitude angles) is thereby calculated time-depending to obtain the projected area factors for each time-step of the simulation. The clothing properties (from a data base) and the activity level are simple user-defined parameter in the spreadsheet. All these parameters are then used to generate a text file as an input for the comfort simulation.

Stage 2: the input file generated in the stage 1 is used to run the IESD-Fiala model and to obtain physiological responses (e.g. mean skin, local skin temperatures, body core temperature, sweat rates, etc).

Stage 3: the outputs of the stage 2 are imported into the spreadsheet application for postprocessing and calculation of local thermal comfort responses described in Chapter 7. The postprocessing exercises were implemented using macro to read in results obtained from the stage 2 and calculate the local comfort responses, establish ranking lists of the most affected body parts, etc. The postprocessing procedure also allows to calculate further thermal comfort analysis is carried out corresponding the above statistical analysis figures including seasonal averages, standard deviations, monthly and daily, minimum and maximum values for both local and global thermal discomfort.

8.4 Simulation demonstration

8.4.1 The building

An existing building, the Brockshill Environment Centre (BHEC), was chosen as an example to demonstrate the predictive capabilities of the link. The BHEC building is located on the southern edge of the city of Leicester, UK. It was opened to the public in April 2001 as a facility owned and operated by a small council with the objective of promoting energy and environmental awareness to the surrounding communities. The building (Figure 8.2) consists of three main thermal zones, i.e. a restaurant, a conservatory and a large exhibition hall with a classroom where educational activities are based for visiting school groups.

Figure 8.2 Brockshill Environment Centre.

The building is a mechanically ventilated building which was also claimed as a super low energy building. The ventilation rate into the occupied spaces was defined as 0.25 air change per hour. Wall, floor, ceiling, and window were fabricated of composite elements: (1) external wall was 100 mm brick, 100 mm thermal insulation and 100 mm exposed concrete block ($U=0.34\ Wm^{-2}K^{-1}$), (2) suspended ceiling/floor was 80 mm cement screed, 150 mm heavy mix concrete, 350 mm air cavity and 10 mm plasterboard, (3) roof was insulated metal panels

with U-value of 0.20 $Wm^{-2}K^{-1}$, and (4) window was low-e double glazing (U= 2.0 $Wm^{-2}K^{-1}$).

In the study, the restaurant was selected for the thermal comfort analysis. This zone features three large windows at the south façade (Figure 8.2). The thermal comfort analysis was performed for two locations within the restaurant zone with:

1) the subject located in close proximity (1m distance) to a window in the south façade and
2) the subject located at the middle of the occupied zone (Figure 8.3).

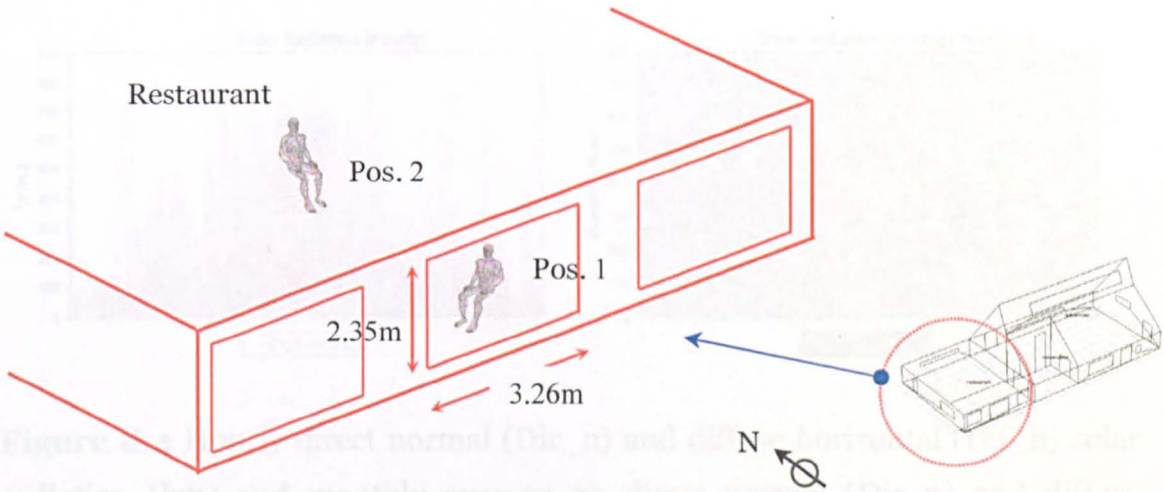

Figure 8.3 Location of the occupant for thermal comfort analysis.

8.4.2 ESP-r simulations

The BSP-simulations were performed as whole-year simulations using the CIBSE Design Summer Year weather data and time step of 15 minutes. Three cases were simulated:

- low-e double glazing with U-value = 2.0 $Wm^{-2}K^{-1}$, case A (DG),
- low-e double glazing with external shading, case B (DG+S), and
- triple glazing with U-value of 1.8 $Wm^{-2}K^{-1}$, case C (TG).

For simplicity, all simulations were run assuming the restaurant being heated for room air temperature of 21°C, but, as in the real building no cooling of the zone was assumed for air temperatures exceeding this value.

8.4.2.1 Weather data

The simulations were carried out using the CIBSE Design Summer Year recommended for detailed summer overheating analysis purposes. The hourly solar radiation data and the monthly averages including the corresponding standard deviations for solar radiation, relative humidity and wind are plotted in Figure 8.4 and 8.5.

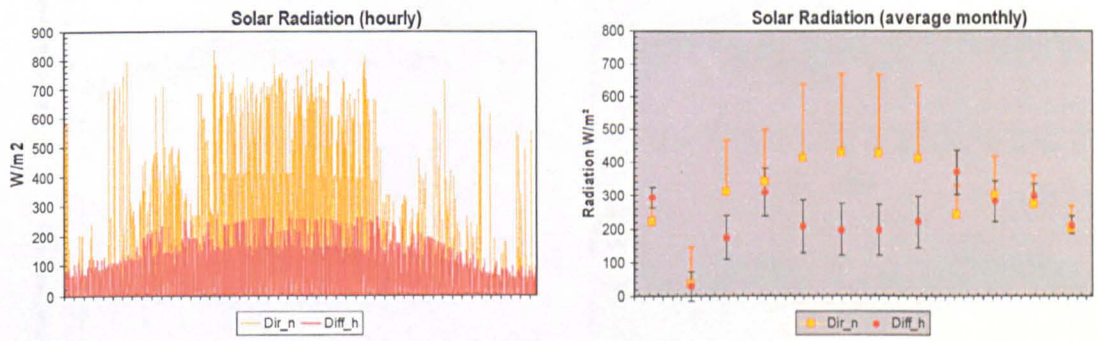

Figure 8.4 Hourly direct normal (Dir_n) and diffuse horizontal (Dif_h) solar radiation (left) and monthly average on direct normal (Dir_n) and diffuse horizontal (Dif_h) solar radiation (right).

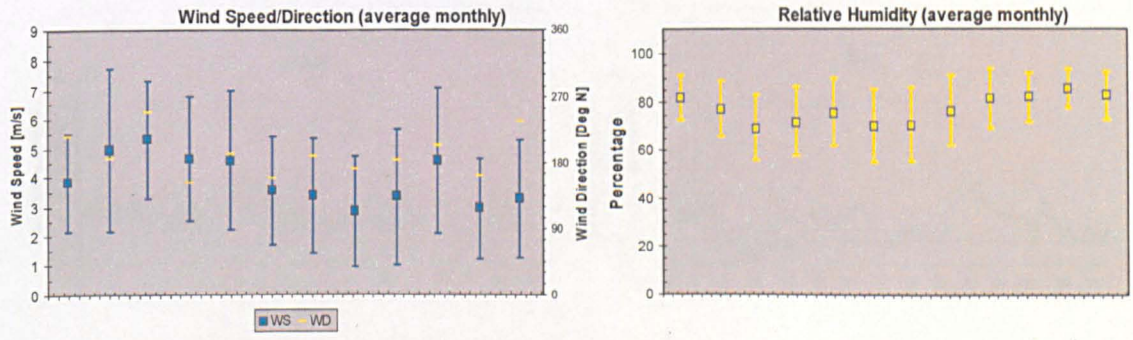

Figure 8.5 Monthly averages on wind speed (WS), wind direction (WD), and relative humidity.

The hourly ambient temperature of the whole year is presented in Figure 8.6.

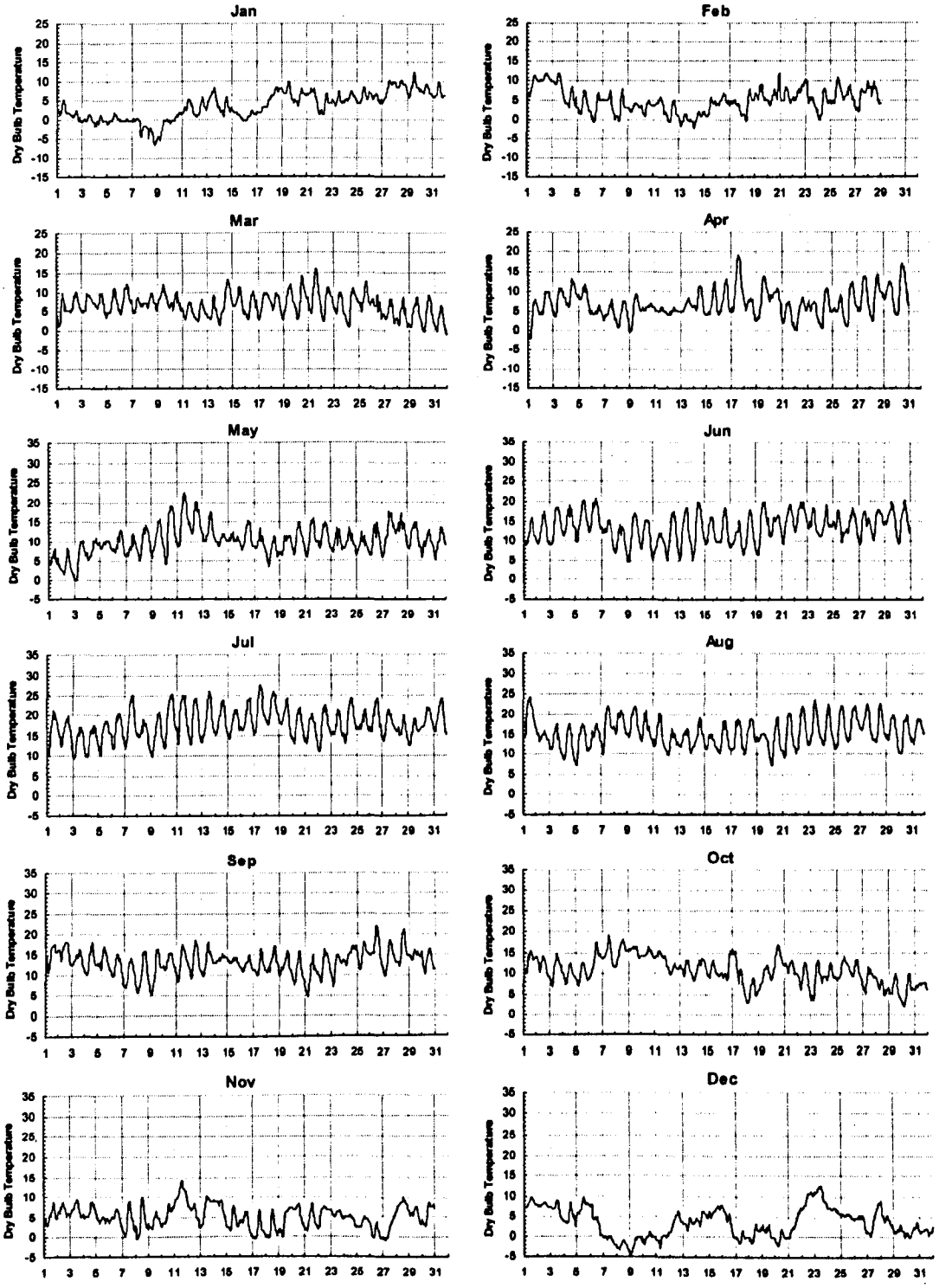

Figure 8.6 Ambient temperature (DBT).

8.4.2.2 Predicted indoor climate conditions

The annual indoor climate in the restaurant predicted by ESP-r for the three cases noted above are plotted in Figures 8.7 to 8.9.

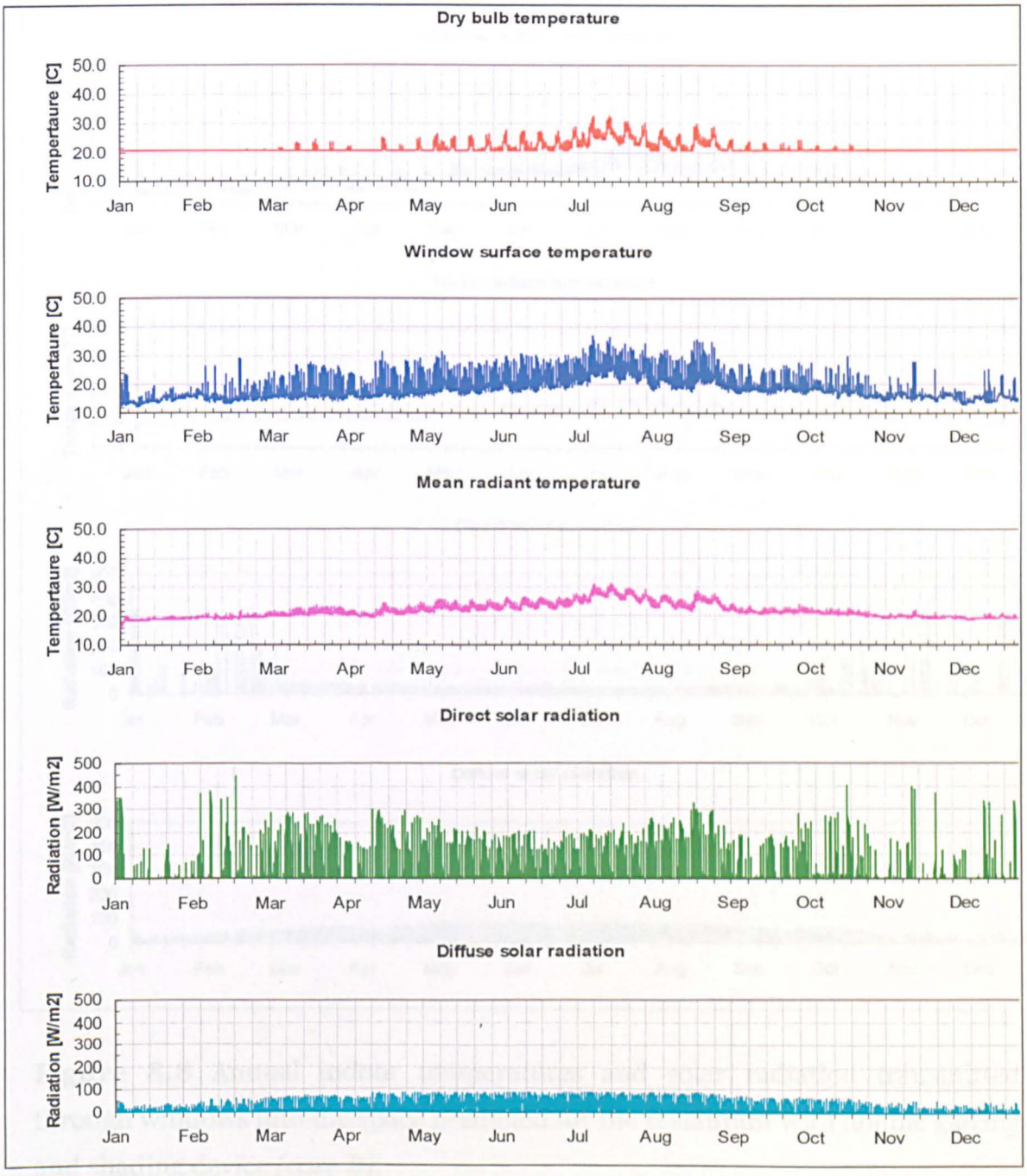

Figure 8.7 Annual indoor temperatures and solar radiation transmitted through windows into the space predicted for the restaurant with double glazing (*case A*).

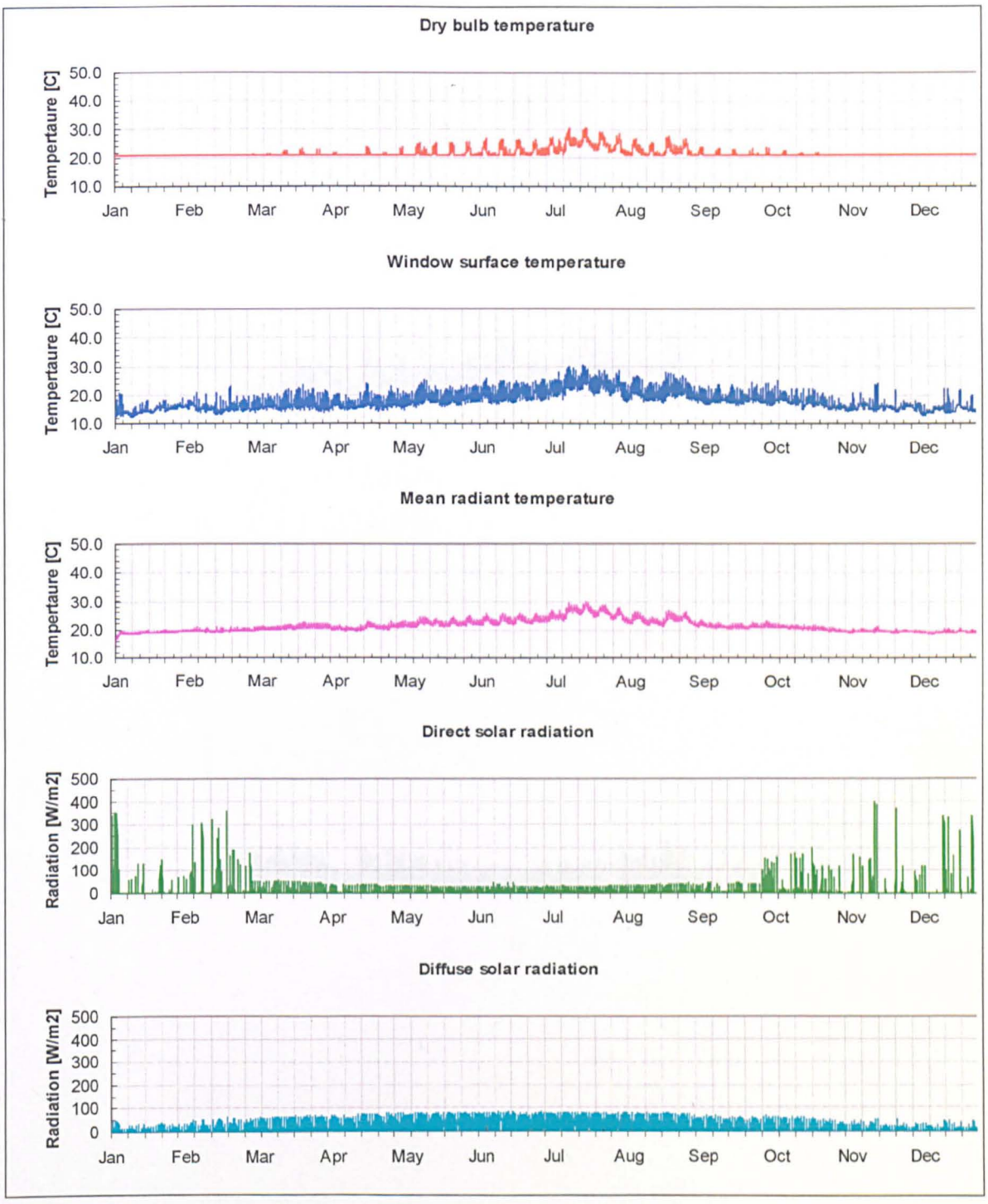

Figure 8.8 Annual indoor temperatures and solar radiation transmitted through windows into the space predicted for the restaurant with double glazing and shading device *(case B)*.

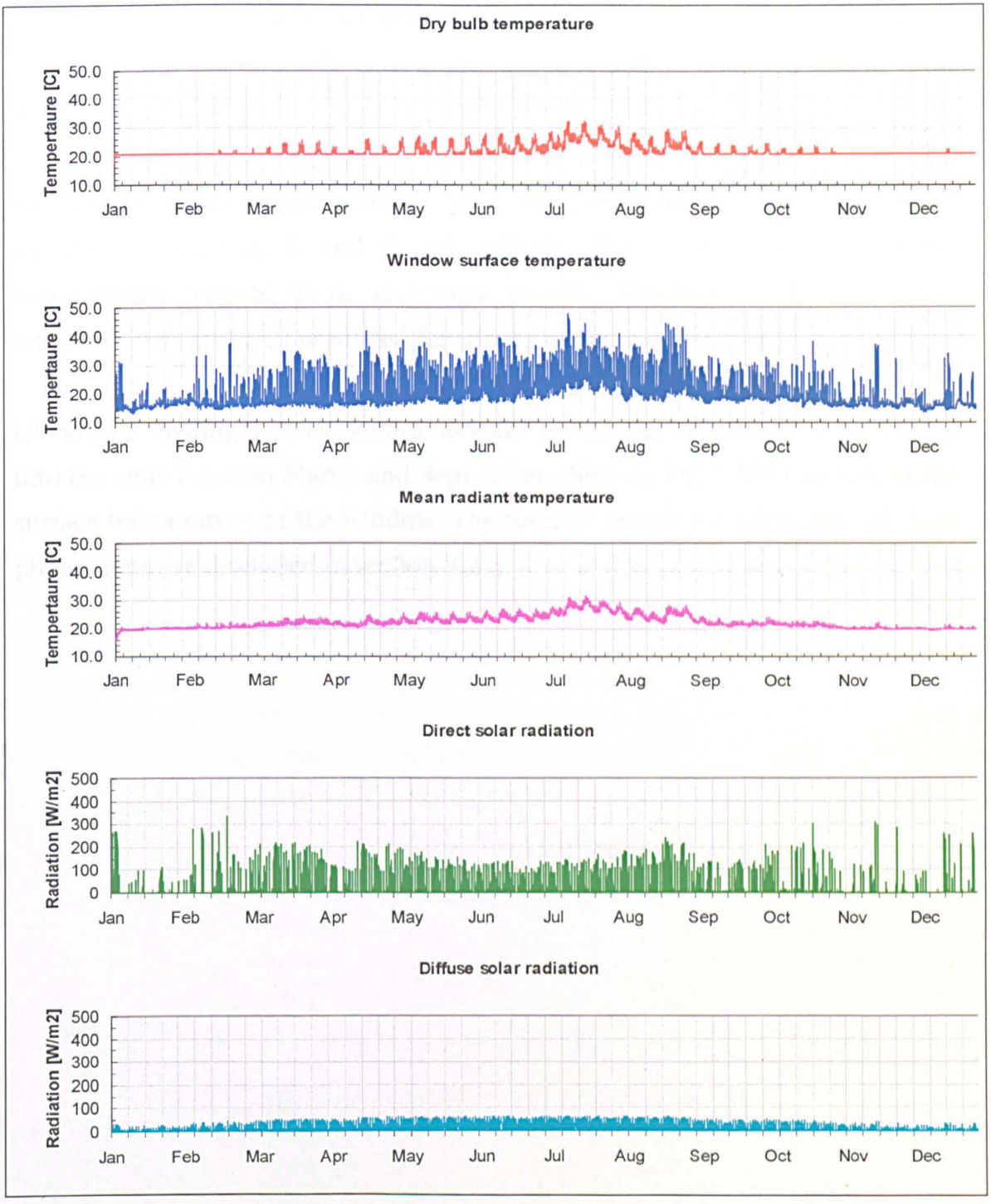

Figure 8.9 Annual indoor temperatures and solar radiation transmitted through windows into the space predicted for the restaurant with triple glazing *(case C)*.

As can be observed in all three cases the hottest conditions occurred during June to August whereas the lowest (surface) temperatures were predicted for

the period between November and February. A summary statistics with average, minimum and maximum for each month are provided for analysed case in Table 8.1.

In July, the average zone air temperature was predicted to be 25.57, 24.70 and 25.78°C for case A, B and C, respectively. The corresponding maximum temperatures reached 32.11, 30.57 and 32.34°C. The highest window surface temperatures (47.59°C) predicted for triple glazing in July.

Obviously, shading devices can dramatically reduce the incoming solar radiation into the zone between March and September affecting DBT, MRT as well as the surface temperature of the window. The thermal comfort implications of these phenomena are discussed in section 8.4.4.

Table 8.1 Summary statistics of predicted indoor temperatures and solar gains for the months January, July and August.

		DBT [°C]	MRT [°C]	Window Surface T. [°C]	Direct Sol. [Wm^{-2}]	Diffuse Sol. [Wm^{-2}]
Double glazing (case A)						
Jan	Min	17.61	14.93	12.17	0.00	0.00
	Max	21.35	19.97	23.74	349.73	44.86
	Avg	21.00	19.04	14.93	8.16	5.54
Jul	Min	21.00	23.16	18.97	0.00	0.00
	Max	32.11	31.13	36.64	237.38	87.15
	Avg	25.57	26.94	25.27	35.48	34.82
Aug	Min	21.00	21.55	17.23	0.00	0.00
	Max	29.94	29.01	35.49	326.75	87.63
	Avg	23.38	24.76	23.14	41.50	29.26
Double glazing with shading (case B)						
Jan	Min	17.61	14.93	12.17	0.00	0.00
	Max	21.35	19.93	20.77	349.73	44.86
	Avg	21.00	19.01	14.87	8.16	5.54
Jul	Min	21.00	22.63	18.48	0.00	0.00
	Max	30.57	29.68	30.23	36.36	82.24
	Avg	24.70	25.89	23.72	7.53	34.08
Aug	Min	21.00	21.32	17.10	0.00	0.00
	Max	28.53	27.68	28.84	43.83	80.22
	Avg	22.64	23.77	21.59	8.09	28.36
Triple glazing (case C)						
Jan	Min	17.61	14.98	13.32	0.00	0.00
	Max	21.37	20.68	31.27	266.46	32.49
	Avg	21.00	19.82	16.29	6.16	3.97
Jul	Min	21.10	23.44	18.48	0.00	0.00
	Max	32.34	31.16	47.59	164.45	62.10
	Avg	25.78	27.15	27.01	23.55	24.73
Aug	Min	21.00	21.94	17.14	0.00	0.00
	Max	30.25	29.15	44.75	235.80	62.70
	Avg	23.62	25.04	24.79	28.95	20.88

For further comparison three days were selected representing the worst conditions predicted for the three cases in the restaurant. The statistical analysis implemented in the linking and postprocessing procedure revealed the 1st of January to be the coldest and 11 July and 21 August the hottest indoor climate conditions. The indoor conditions are plotted for these three days in Figure 8.10.

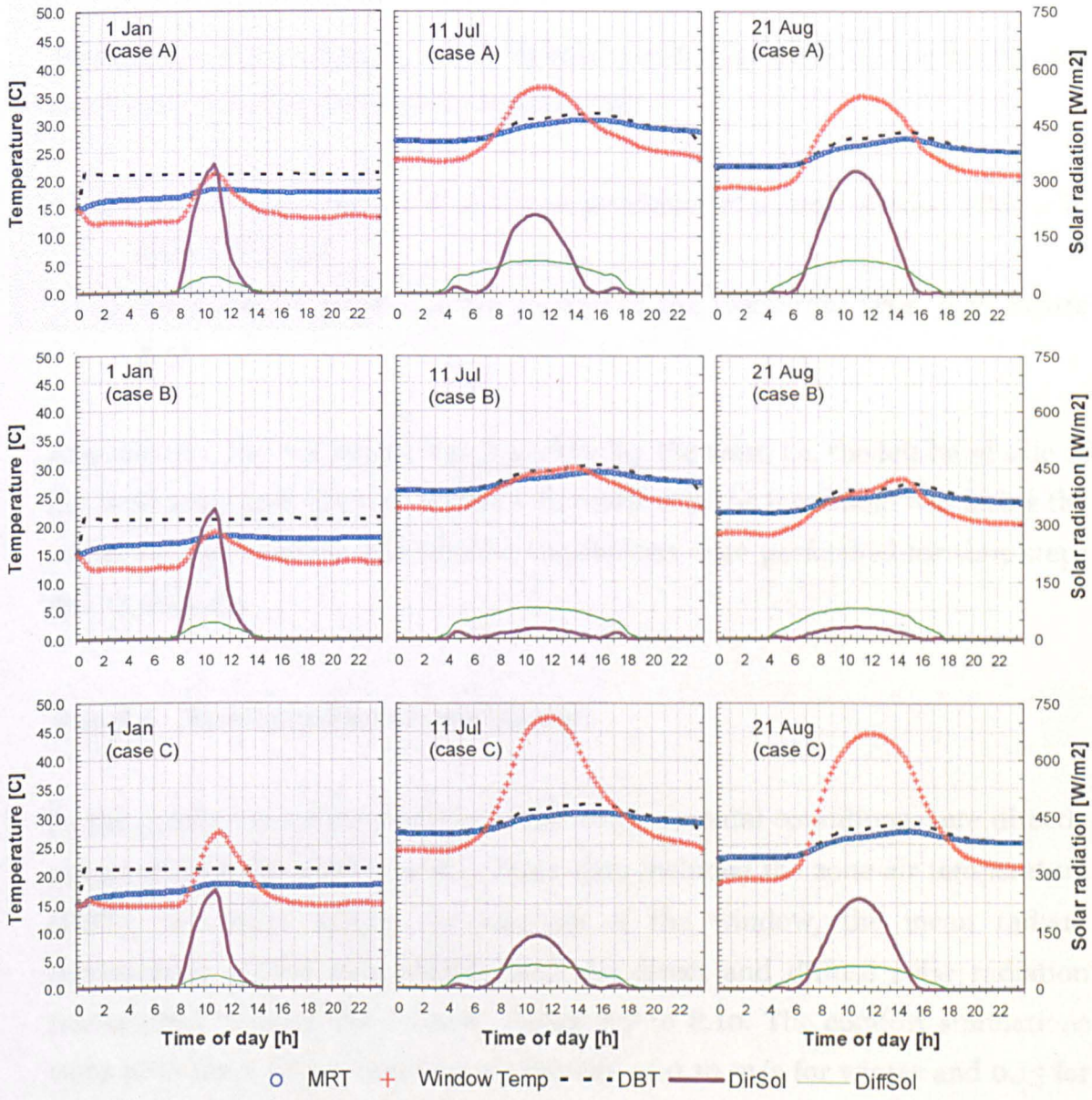

Figure 8.10 Predicted indoor climate conditions in the restaurant during the coldest and the hottest days of the year.

Blue marks represent the mean radiant temperature, MRT, whereas red marks are the inner surface temperatures of the window. Dotted lines are the dry bulb temperature, DBT, in the zone. Dark grey and green lines indicate the direct and the diffuse radiation transmitted through glazing, respectively.

8.4.3 Thermal comfort simulation

As mentioned in section 8.4.1, the thermal comfort analysis was performed for two locations within the restaurant zone with:

1) the occupant located in the close proximity of a large window (Pos. 1 in Figure 8.3) and
2) the occupant located in the middle of the restaurant (Pos. 2 in Figure 8.3).

At position 1, the humanoid was placed facing the west, i.e. the left hand side of the body was exposed to the window. In position 2, the humanoid was facing the south, i.e. the window. The comfort simulations were performed for time steps Δt= 15 minutes.

8.4.3.1 Environmental conditions

In the comfort simulations most of the environmental conditions were directly obtained from the ESP-r results. These data included the zone air temperature (DBT), the inner surface temperature of the window, the mean radiant temperature of the zone (MRT), and the direct and diffuse solar radiation transmitted through the window, Figure 8.7 to 8.10. The comfort simulations were performed with a constant air velocity of 0.10 m/s for winter and 0.15 for the summer season, respectively. The relative humidity was assumed to be constant at 50% through the year.

8.4.3.2 Radiation modelling

The human radiative heat transfer calculations were carried out taking into account both the long- and short-wave radiation in the occupied zone. To simplify the calculation the long-wave radiation heat exchanges from individual body parts were calculated with respect to (i) the window and (ii) the rest of the room. The corresponding local view factors for Pos. 1 and Pos. 2 are listed in Table 8.2 and 8.3. The view factor of the whole body with respect to window at the position 1 and 2 in Figure 8.3 was 0.16 and 0.01, respectively. The temperature of the rest of the room was calculated from the zone mean radiant temperature predicted for each time step by ESP-r using the whole body view factors obtained for Pos. 1 and 2. A typical long-wave emissivity of 0.95 was assumed for all surfaces of the envelope in the calculations. The emissivity of the body surface varied locally depending on the covering material (see clothing file in Appendix D, *Table D.5*)

The short-wave radiation calculations were performed with respect to both direct and diffuse solar radiation in the space. For Pos. 1, the amount of direct solar radiation incident at individual body parts was computed from the amount of direct radiation transmitted through the glazing as predicted by ESP-r and using local projected area factors which were predicted dynamically for the position of the sun at the given time, season, and location of the building. For Pos. 2, it was assumed that no body part was irradiated by a direct beam. The level of diffuse radiation was estimated separately for Pos. 1 and Pos. 2 from the total amount of solar radiation transmitted through the windows into the zone assuming an even distribution of solar rays in the perimeter zone of the restaurant (Pos. 1) and within the entire zone (Pos. 2). The short-wave radiation calculations were performed using an average short-wave absorptivity of 0.7 for the clothing (skin: 0.67).

Table 8.2 View factors of individual body sectors predicted for a sedentary person located at the close proximity to the window (Pos. 1 in Figure 8.3).

Body parts	View factor		Body parts	View factor	
	Window	Rest of room		Window	Rest of room
Forehead	0.210	0.769	L. Leg: Up. Inferior	0.000	0.563
Head	0.212	0.752	L. Leg: Up. Exterior	0.456	0.320
Face: Anterior	0.215	0.610	L. Leg: Lo. Anterior	0.145	0.855
L. Face	0.653	0.232	L. Leg: Lo. Posterior	0.158	0.551
R. Face	0.000	0.885	L. Leg: Lo. Inferior	0.000	0.741
Neck: Anterior	0.165	0.602	L. Leg: Lo. Exterior	0.442	0.482
Neck: Posterior	0.164	0.779	L. Foot: Instep	0.213	0.673
Neck: L. Exterior	0.538	0.292	L. Foot: Sole	0.009	0.888
Neck: R. Exterior	0.000	0.833	R. Shoulder	0.037	0.849
L. Shoulder	0.255	0.629	R. Arm: Up. Anterior	0.041	0.423
Thorax: Anterior	0.209	0.704	R. Arm: Up. Posterior	0.046	0.954
Thorax: Posterior	0.182	0.807	R. Arm: Up. Inferior	0.187	0.419
Thorax: L. Inferior	0.218	0.237	R. Arm: Up. Exterior	0.001	0.953
Thorax: R. Inferior	0.002	0.462	R. Arm: Lo. Anterior	0.220	0.205
Abdomen: Anterior	0.092	0.398	R. Arm: Lo. Posterior	0.000	1.000
Abdomen: Posterior	0.194	0.806	R. Arm: Lo. Inferior	0.060	0.553
Abdomen: L. Inferior	0.374	0.294	R. Arm: Lo. Exterior	0.027	0.837
Abdomen: R. Inferior	0.000	0.667	R. Hand: Handback	0.079	0.632
L. Arm: Up. Anterior	0.146	0.329	R. Hand: Palm	0.028	0.232
L. Arm: Up. Posterior	0.395	0.605	R. Leg: Up. Anterior	0.147	0.281
L. Arm: Up. Inferior	0.027	0.569	R. Leg: Up. Posterior	0.032	0.904
L. Arm: Up. Exterior	0.533	0.420	R. Leg: Up. Inferior	0.220	0.343
L. Arm: Lo. Anterior	0.001	0.425	R. Leg: Up. Exterior	0.000	0.776
L. Arm: Lo. Posterior	0.550	0.450	R. Leg: Lo. Anterior	0.203	0.797
L. Arm: Lo. Inferior	0.055	0.560	R. Leg: Lo. Posterior	0.137	0.570
L. Arm: Lo. Exterior	0.351	0.516	R. Leg: Lo. Inferior	0.298	0.438
L. Hand: Handback	0.233	0.481	R. Leg: Lo. Exterior	0.000	0.927
L. Hand: Palm	0.098	0.156	R. Foot: Instep	0.177	0.707
L. Leg: Up. Anterior	0.033	0.398	R. Foot: Sole	0.003	0.893
L. Leg: Up. Posterior	0.122	0.824	**Whole Body**	**0.161**	**0.621**

Table 8.3 View factors of individual body sectors predicted for a sedentary person located in the middle of the room (Pos. 2 in Figure 8.3).

Body parts	View factor		Body parts	View factor	
	Window	Rest of room		Window	Rest of room
Forehead	0.049	0.930	L. Leg: Up. Inferior	0.008	0.555
Head	0.007	0.957	L. Leg: Up. Exterior	0.003	0.773
Face: Anterior	0.039	0.786	L. Leg: Lo. Anterior	0.063	0.937
L. Face	0.013	0.871	L. Leg: Lo. Posterior	0.000	0.709
R. Face	0.013	0.872	L. Leg: Lo. Inferior	0.019	0.722
Neck: Anterior	0.051	0.716	L. Leg: Lo. Exterior	0.015	0.909
Neck: Posterior	0.000	0.943	L. Foot: Instep	0.015	0.871
Neck: L. Exterior	0.009	0.821	L. Foot: Sole	0.002	0.896
Neck: R. Exterior	0.009	0.824	R. Shoulder	0.005	0.880
L. Shoulder	0.005	0.879	R. Arm: Up. Anterior	0.036	0.428
Thorax: Anterior	0.050	0.863	R. Arm: Up. Posterior	0.000	1.000
Thorax: Posterior	0.000	0.989	R. Arm: Up. Inferior	0.000	0.606
Thorax: L. Inferior	0.003	0.453	R. Arm: Up. Exterior	0.013	0.941
Thorax: R. Inferior	0.003	0.462	R. Arm: Lo. Anterior	0.019	0.406
Abdomen: Anterior	0.035	0.455	R. Arm: Lo. Posterior	0.001	0.999
Abdomen: Posterior	0.000	1.000	R. Arm: Lo. Inferior	0.000	0.613
Abdomen: L. Inferior	0.000	0.669	R. Arm: Lo. Exterior	0.035	0.829
Abdomen: R. Inferior	0.000	0.667	R. Hand: Handback	0.016	0.696
L. Arm: Up. Anterior	0.036	0.439	R. Hand: Palm	0.000	0.259
L. Arm: Up. Posterior	0.000	1.000	R. Leg: Up. Anterior	0.010	0.419
L. Arm: Up. Inferior	0.000	0.597	R. Leg: Up. Posterior	0.004	0.933
L. Arm: Up. Exterior	0.013	0.940	R. Leg: Up. Inferior	0.008	0.555
L. Arm: Lo. Anterior	0.019	0.406	R. Leg: Up. Exterior	0.003	0.773
L. Arm: Lo. Posterior	0.001	0.999	R. Leg: Lo. Anterior	0.063	0.937
L. Arm: Lo. Inferior	0.000	0.614	R. Leg: Lo. Posterior	0.000	0.707
L. Arm: Lo. Exterior	0.035	0.832	R. Leg: Lo. Inferior	0.019	0.718
L. Hand: Handback	0.016	0.698	R. Leg: Lo. Exterior	0.015	0.911
L. Hand: Palm	0.000	0.254	R. Foot: Instep	0.015	0.869
L. Leg: Up. Anterior	0.010	0.421	R. Foot: Sole	0.002	0.894
L. Leg: Up. Posterior	0.004	0.942	**Whole Body**	**0.014**	**0.768**

8.4.3.3 Personal conditions

In order to account to some degree for seasonal changes in clothing, two different indoor ensembles were used in the simulations. From May to September, the subject was assumed to wear a long sleeve ensemble comprising long sleeve shirt, trousers, underwear, sweat sock and shoes. The overall clo value of this clothing is about 0.6 clo. A jacket was added to this ensemble resulting in an overall clo-value of 1.1 clo to simulate the clothing of the occupant between October and April. The local thermal and evaporative resistances of the both ensembles used in the simulations are listed in Table D.5 (*Appendix D*). Throughout the year the activity level was assumed to be 1.2 met which corresponds to a typical indoor sedentary activity.

8.4.4 Thermal comfort analysis

The thermal comfort predictions under the double glazing scenario (case A) for both locations (i.e. close to the window and in the middle of the zone) are described in section 8.4.4.1 to 8.4.4.2. The comparison of the three different scenarios thermal discomfort according to three worst days is presented in section 8.4.4.4.

8.4.4.1 Zone perimeter: case A

The percentage of dissatisfied due to both global and local discomfort predicted for the occupant located close to the window during the course of a year is plotted in Figure 8.11.

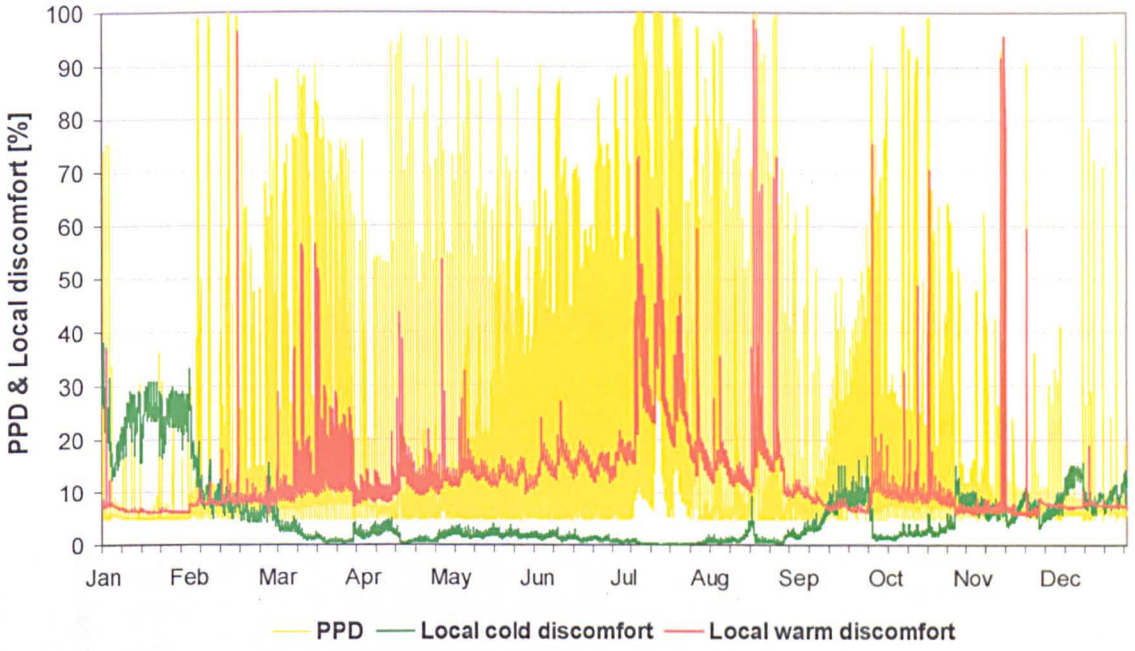

Figure 8.11 Global and local thermal discomfort predicted for a person located at close to the window.

The yellow line is the predicted PPD whereas green and red lines represent the local cold (LCD) and warm discomfort (LWD) of the person, respectively. For most of the year the thermal dissatisfaction was mainly due to global discomfort (PPD). The local cold discomfort was a major concern only in January. Significant local warm discomfort occurred mainly in March and July. Local warm discomfort was also the main cause of thermal dissatisfaction in August and occasionally in October and November.

The course of predicted local discomfort of the 'coldest' body parts is plotted for the month 'January' and 'August' in Figure 8.12.

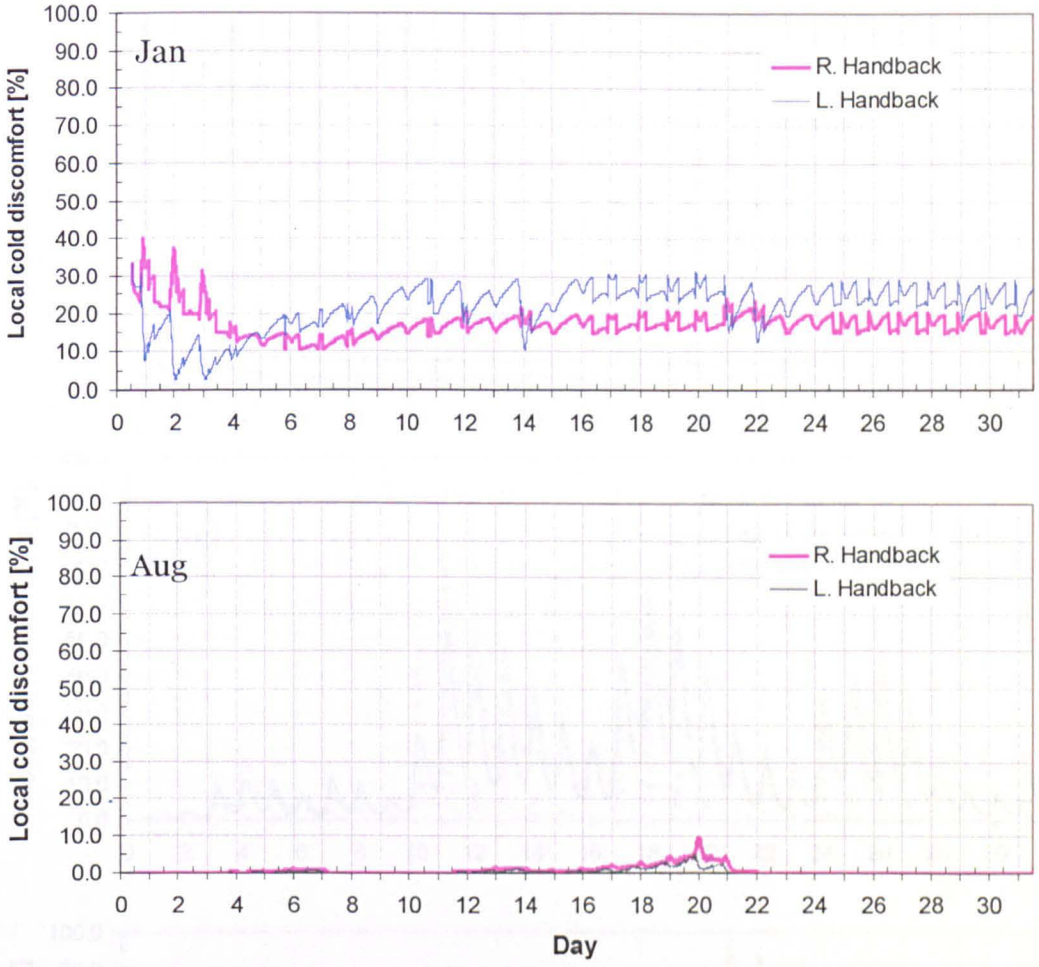

Figure 8.12 Local cold discomfort in January and August.

As can be seen LCD exceeding 20% occurred in January. The most affected body part was the left hand (handback) which was exposed to the cold window. In August LCD did not exceed 10%. There was no LCD for the whole month of July. Local warm discomfort (LWD) predicted for the above three months is plotted in Figure 8.13.

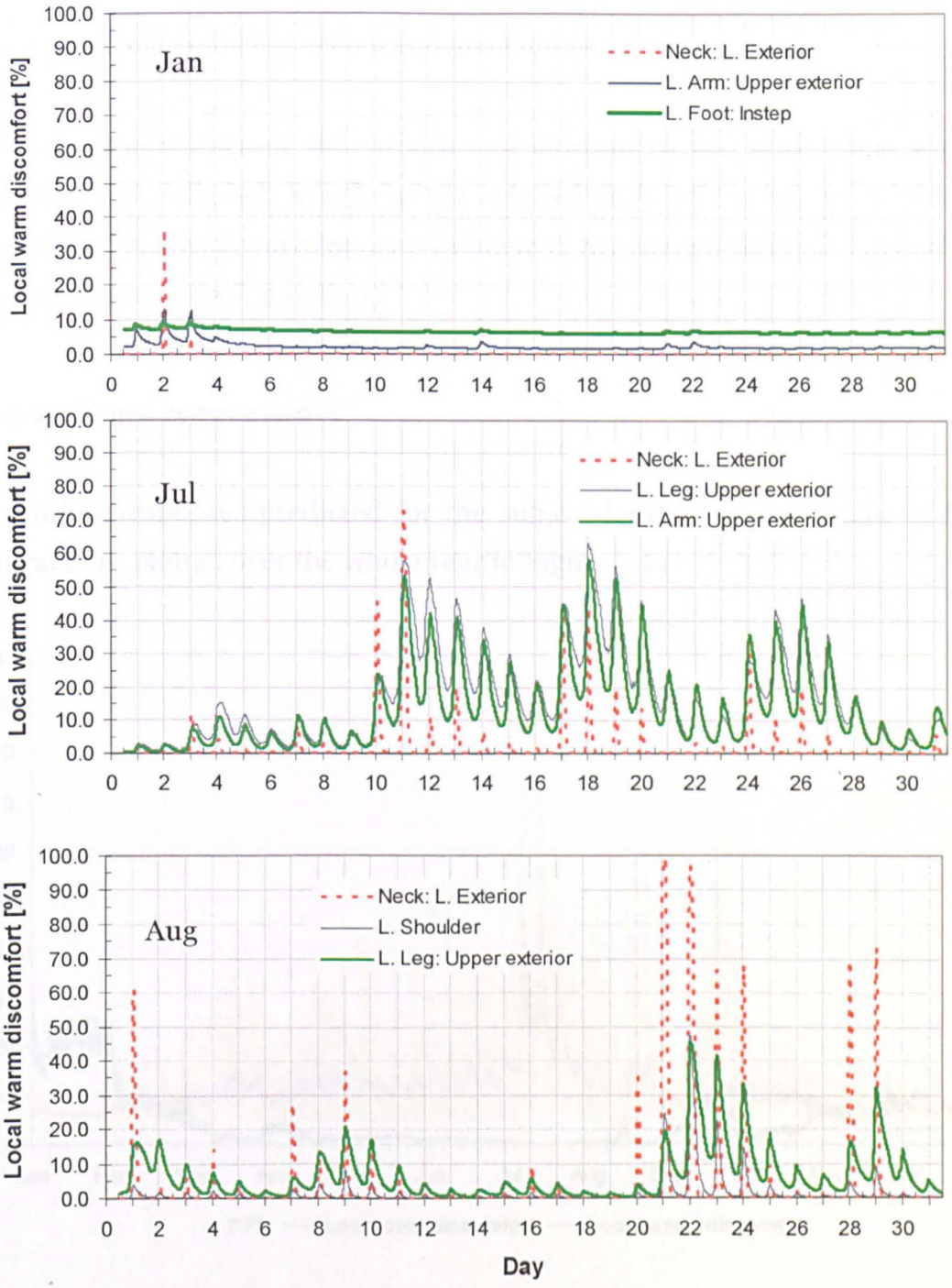

Figure 8.13 Local warm discomfort predicted for January, July and August.

Considerable LWD was predicted for the neck (left exterior) during July and August. This body part was directly exposed to solar radiation and the hot glass surface therefore exceeding 90% on 21 and 22 August. In January, local warm

discomfort occasionally occurred at the neck as a result of direct radiation from the sun which elevation did not exceed 30° on this day (Figure 8.13, top).

In the close proximity of the window in addition to the neck, local warm discomfort was perceived mainly at the exposed parts of the upper and lower extremities. This local warming also influenced the overall thermal discomfort of the body (shown in Figure 8.11).

8.4.4.2 Zone core: case A

The comfort responses predicted for the subject located in the middle of the restaurant are plotted over the whole year in Figure 8.14.

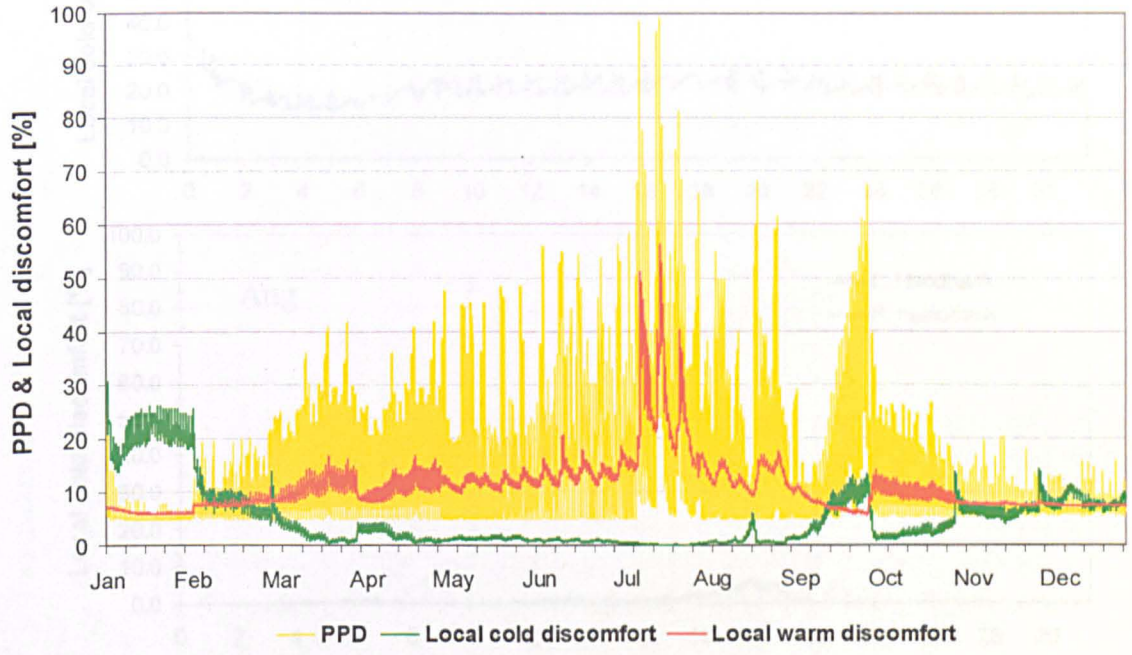

Figure 8.14 Global and local thermal discomfort predicted for a person located in the middle of the restaurant.

Similar to the person located close to the window, for most of the year (except January) the thermal dissatisfaction was mainly due to global discomfort (PPD). Local cold discomfort was of some concern in January, and occasionally in

September, October, November and December. In contrast to the perimeter some noticeable LWD, with values exceeding 50%, only occurred in July.

The local cold discomfort predicted for the subject located in the middle of the zone is presented for January and August in Figure 8.15. The observations are very similar to those made for the subject in the zone perimeter. Noticeable LCD, i.e. about 20% on average, occurred only in January. In August LCD did not exceed the level of 6%. Again, no LCD occurred in July. Similarly to the zone perimeter, the body parts most affected by LCD were the handbacks.

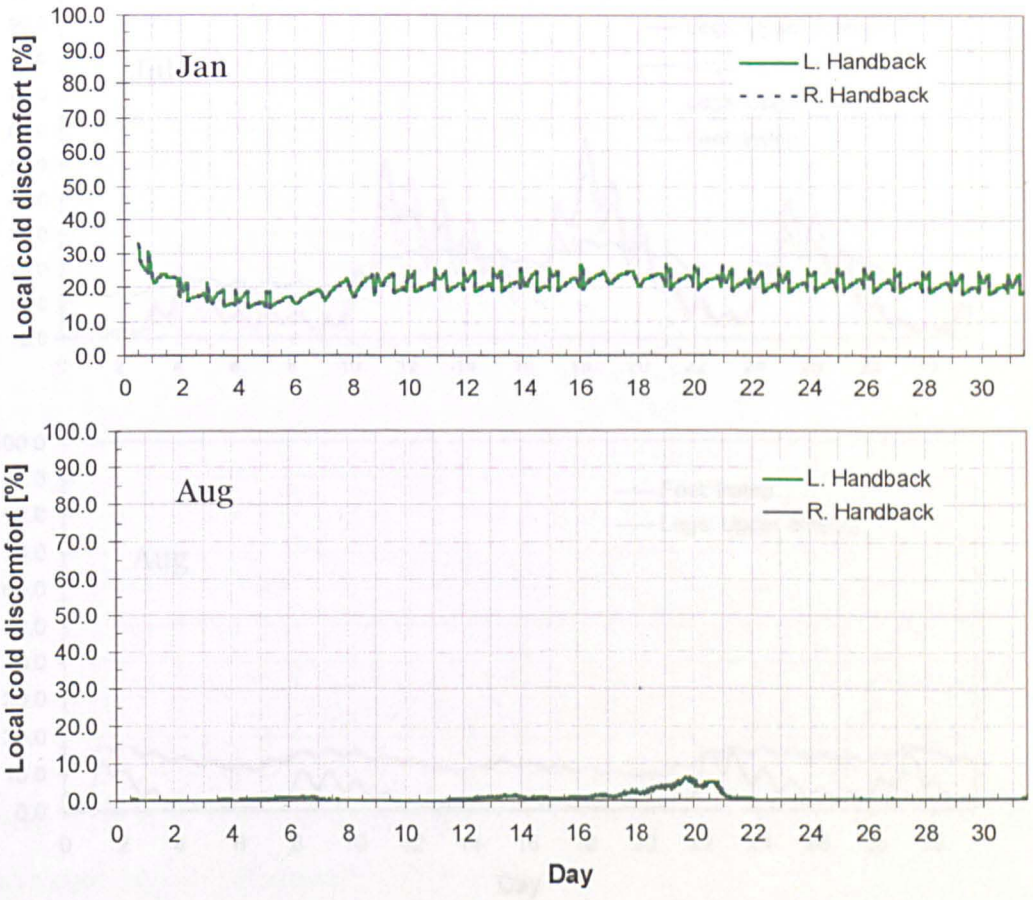

Figure 8.15 Local cold discomfort for January and August predicted for a person seated in the middle of the restaurant.

LWD predicted for the middle of the zone during January, July and August are plotted in Figure 8.16.

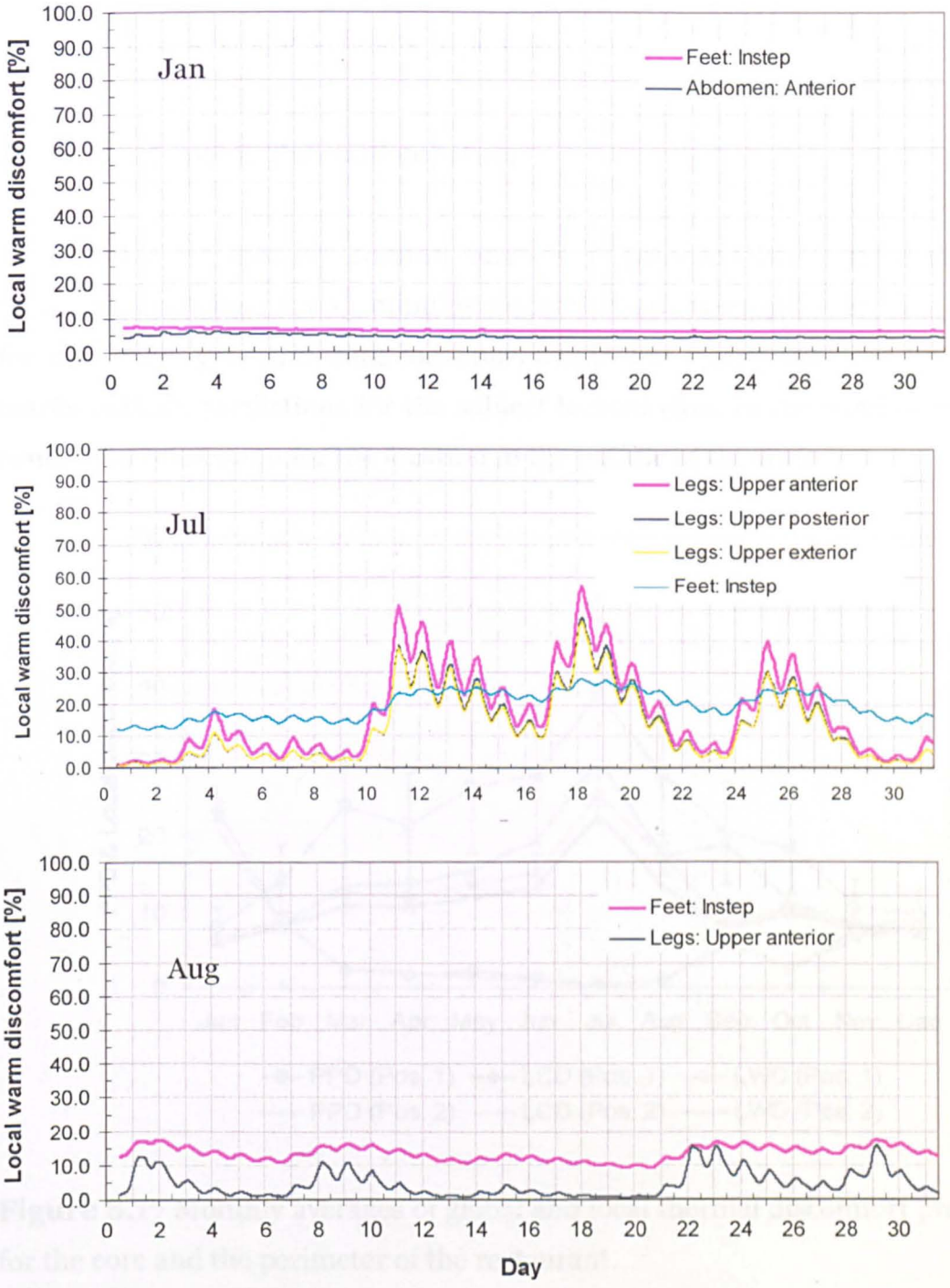

Figure 8.16 Local warm discomfort predicted for January, July and August in the middle of the restaurant.

The subject was predicted to perceive considerable local warm discomfort reaching up to 58% in July at upper legs. Some LWD was perceived at feet in

August (about 18%) and in January effectively no local warm discomfort occurred, i.e. LWD <10% (Figure 8.16, top).

8.4.4.3 Monthly thermal comfort

An example for monthly comfort analysis is provided in Figure 8.17. The predictions obtained for 15 minutes intervals were averaged over each month for the whole year and both locations within the restaurant. The lines with marks indicate predictions for the subject located close to the window whereas condensed lines stand for the location in the middle of the zone.

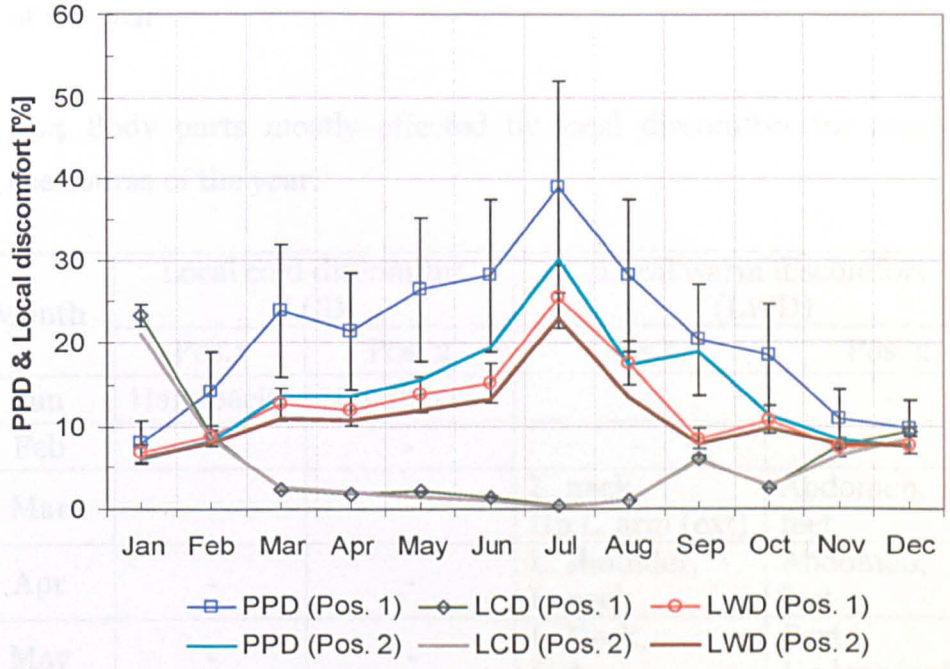

Figure 8.17 Monthly averages of global and local thermal discomfort predicted for the core and the perimeter of the restaurant.

The highest monthly average PPD resulted for July for the perimeter. With 38.9 ± 33.3% this value was clearly higher than the corresponding PPD obtained for the middle of the room (30.1 ± 23.7%). Both PPD values were higher than the corresponding local warm discomfort responses (25.5 ± 10.6% for Pos. 1 and 22.9 ± 9.4% for Pos. 2). In January, local cold discomfort was the main reason

for dissatisfaction with 23.4 ± 4.2% and 21.0 ± 2.7% for the subject close to the window and at the middle of the zone, respectively.

The average PPD for the whole year was 20.8 ± 24.9% for the subject in the close proximity to the window but only 14.2 ± 13.7% for the subject located in the middle of the zone. Only a small number (an average about 5%) of occupants would perceive local cold discomfort at both locations. However, a higher percentage of occupants would suffer from local warm discomfort (12.2 ± 7.7%: close to the window and 10.9 ± 5.3%: at the middle of room). More detailed information is provided in Tables F.1 to F.3 (*Appendix F*). Table 8.4 lists those body parts predicted to be mostly affected by local discomfort (>10%) for each month of the year.

Table 8.4 Body parts mostly affected by local discomfort for each month during the course of the year.

Month	Local cold discomfort (LCD)		Local warm discomfort (LWD)	
	Pos.1	Pos. 2	Pos.1	Pos. 2
Jan	Handbacks	Handbacks	-	-
Feb	-	-	-	-
Mar	-	-	L. neck, Up L. arm (ext)	Abdomen, feet
Apr	-	-	L. shoulder, L. neck	Abdomen, feet
May	-	-	L. Neck, feet	Feet, Up legs (ant)
Jun	-	-	Up legs (ant), L. neck	Up legs (ant), feet
Jul	-	-	L. neck, Up L. leg (ext), Up L. arm (ext)	Up legs (ant, ext and pos), Feet
Aug	-	-	L. Neck, L. shoulder	Feet, Up legs (ant)
Sep	Handbacks	Handbacks	-	-
Oct	-	-	L. Neck, L. shoulder	-
Nov	-	-	-	-
Dec	Handbacks	Handbacks	-	-

The person was predicted to perceive noticeable (>10%) local cold discomfort in January, September and December both in Pos. 1 and Pos. 2. The only body parts affected were hands. This was associated with the general thermoregulatory state of the body (vasoconstriction in the hands) rather than any radiant asymmetries.

The comfort analysis using the new model revealed LWD to be the main cause of thermal dissatisfaction due to local effects in the restaurant. In contrast to LCD, however, several body parts were affected depending on the thermoregulatory states of the body, the clothing worn, and the asymmetric radiation conditions in the space. In the zone perimeter, body parts directly exposed to the window and incoming solar radiation i.e. left neck, left shoulders and left leg were the most affected body parts whereas warm feet and warm legs were frequently predicted to be the cause of local warm discomfort in the middle of the zone.

8.4.4.4 Analysis of seasonal thermal comfort

As an example for seasonal comfort analysis, the seasonal averages of PPD, LCD and LWD (with the corresponding standard deviations) are compared for the person located close to the window and in the middle of the restaurant for case A in Figure 8.18.

During the summer season (June, July and August) global thermal discomfort (PPD) was clearly the major cause of thermal dissatisfaction both at the perimeter and in the middle of the restaurant with 31.8 ± 31.2% and 22.3 ± 19.7%, respectively. Local warm discomfort reached 19.4 ± 10.0 % near the window and 16.6 ± 7.2% in the middle of the room. In the winter season (December, January and February), although the level of local cold discomfort was not negligible, global discomfort (PPD) was the main reason of complaints both in the zone core and perimeter. This is lower reproduced by the seasonal averages rather by the corresponding standard deviations.

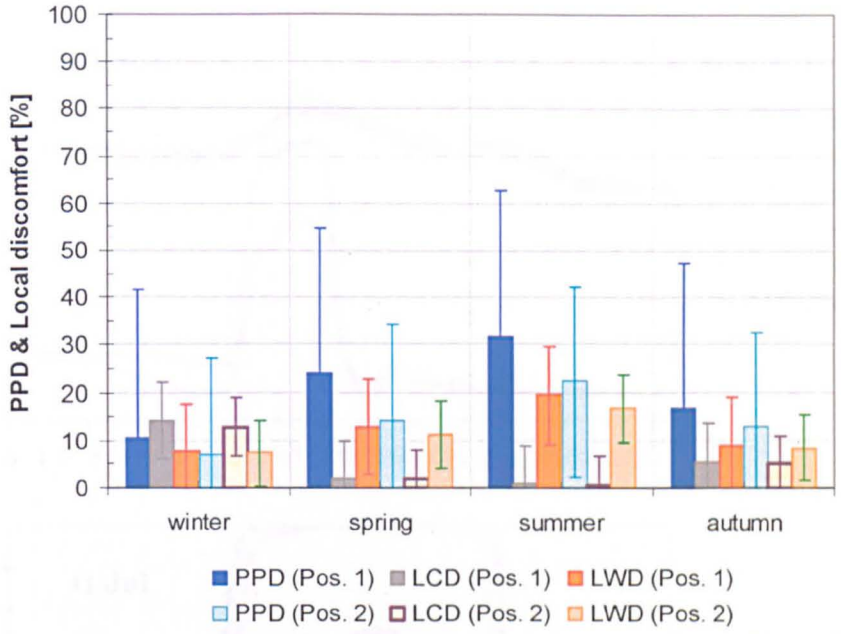

Figure 8.18 Seasonal average values of global and local discomfort of occupants at Pos. 1 and Pos. 2.

In the spring (March, April and May) the subject would feel overall significantly warmer near the window (23.9 ±26.7%) than in the middle of the room (14.2 ± 10.8%). For autumn conditions (September, October and November) both types of local discomfort, i.e. warm and cold, were predicted to be at similar levels for both the core and the perimeter of the zone (see also Table F4 to F6, Appendix F). During this season occupant discomfort was dominated by the global response especially in the zone perimeter.

8.4.4.5 Comparison of different design scenarios

These comparisons were carried out for the person located close to the window (Pos. 1) for the following three days: 1st January, 11th July and 21st August as mentioned in section 8.3.2.2. The results obtained for the three design scenarios investigated, i.e. double glazing (case A), double glazing with external shading (case B) and triple glazing (case C) are plotted together in Figure 8.19.

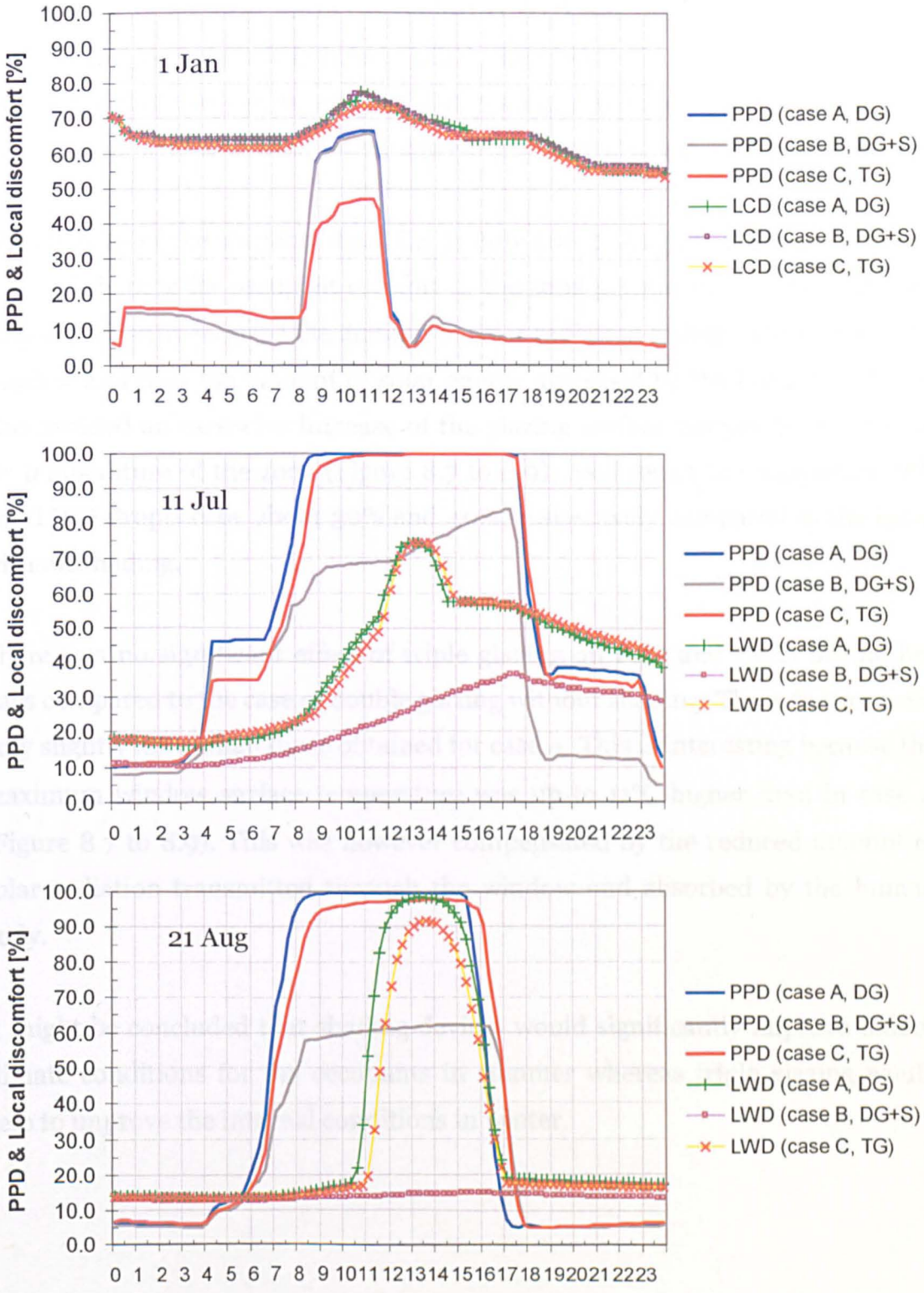

Figure 8.19 Predicted PPD, LCD and LWD on three days for the person located in close proximity of the window.

On 1st January no local warm discomfort (LWD) was predicted for either case. Considering local cold discomfort (LCD), there were no significant differences among the three scenarios analysed. Interestingly, in case of triple glazing PPD was significantly lower than for double glazing with and without shading device.

The analysis of the warmest days, i.e. 11 July and 21 August, indicated that the value of shading for occupant comfort in the zone perimeter. This measure not only significantly reduced the amount of solar radiation transmitted through the window and thus the amount of solar energy absorbed by the human body but also avoided an excessive increase of the glazing surface temperatures and the air temperature of the zone (Figure 8.7 to 8.9). As a result the maximum PPD and LWD dropped by about 30% and 40%, respectively compared to the cases without shading.

There was no significant effect of triple glazing on PPD and LWD during hot days compared to the case of double glazing without shading. These figures were only slightly lower than those obtained for case A. This is interesting because the maximum window surface temperature was up to 11°C higher than in case A (Figure 8.7 to 8.9). This was however compensated by the reduced amount of solar radiation transmitted through the window and absorbed by the human body.

It might be concluded that shading devices would significantly improve indoor climate conditions for the occupants in summer whereas triple glazing would help to improve the internal conditions in winter.

8.5 Summary

In this chapter the new comfort model was linked with the dynamic building simulation program ESP-r to predict thermal comfort conditions in buildings and to demonstrate the predictive abilities of the new thermal comfort model for practical applications. Researchers and engineers can use such a link to quantify the thermal comfort implications of different building designs and constructions, optimise low energy concepts, heating systems/or ventilation and air-conditioning (HVAC) strategies.

Chapter 9

Conclusions and recommendations

This chapter concludes the main outcomes of the work conducted for this thesis. It also presents recommendations that might be considered for future research work.

9.1 Summary and conclusions

A more universal, physiologically based, model for predicting human local thermal comfort responses in asymmetric radiation environments was developed. The model includes detailed calculations of the human long-wave and short-wave radiative heat exchange for individual parts of the human body represented by 3D computational humanoids.

9.1.1 Choice of simulation tools

A numerical simulation tool, RadTherm, which is capable of dealing with highly complex geometries (such as the human body) and complex boundary conditions was used in this study. The software incorporates advanced, voxel-based ray tracing techniques to enable fast and accurate radiation predictions. The technique produced sufficiently accurate results of view factors compared with available analytical solutions as presented in Chapter 3.

9.1.2 Local projected area factors

The 3D humanoids consisting of 59 body sectors were used to model local projected area factors for individual body parts. The projected area factors were modelled for both direct and diffuse short-wave radiation using regression analysis methods.

A validation study of the projected area factor showed good agreement with experimental results of Underwood and Ward (1966), (Fanger (1970), Jones et al. (1998) and Tanabe et al. (2000), as described in Chapter 4. Discrepancies between predicted and measured data appeared to be associated mainly with differences in posture and with the fact that the simulations were performed for parallel rays with the high intensity source being at an infinite distance from the body whereas the experiments were performed for finite distances.

The projected area factor equations developed in this study can be used to predict the irradiation and absorption of direct and diffuse solar radiation over the 3D surface of the human body. Bio-meteorologists and other scientists can use the equations to perform detailed analysis of the effect of solar radiation on human beings exposed to outdoor weather conditions. This information can then serve, for example, to develop bio-climatic charts and rationally derived operative temperatures which characterise the outdoor climate conditions including the effect of solar radiation on humans. Another possible application of the equations, besides any thermal effects, is the prediction of the UV-dose and the assessment of the associated health risks and possible injuries to exposed body parts.

9.1.3 Local view factors

In this study, a finite element method was used to model view factors between individual body sectors and surrounding surfaces. The model was developed as a function of the projected area factors resulted in Chapter 4. Good agreement was shown for both standing and sedentary posture when compared with available experimental results of Fanger (1970), and Horikoshi et al. (1990) as presented in Chapter 5. Good agreement was achieved also for close distance between the body and the surfaces although some discrepancies between predicted and measured data appeared. These were associated with the limitations of the method used in which each body sector was represented by a point in the centre of each sector.

The new model enables predicting view factors of individual parts of the human body with respect to any arbitrary surrounding surface and can thus be for detailed human radiation analysis of inhomogeneous environments.

9.1.4 Human physiological responses to asymmetric radiation

The developed models for predicting human local geometry-related characteristics, i.e. projected area and view factors of individual body sectors were incorporated in the IESD-Fiala multi-segmental mathematical model of human heat transfer and thermal comfort. The extended physiological model was then validated against available experimental data specifically for local physiological responses to asymmetric radiation. The validation showed good general agreement with measured data on local skin, body core and mean skin temperature, i.e. Fanger et al. (1980 and 1985), Hall and Klemm, (1967 and 1969), and Hodder (2002).

9.1.5 New local comfort model

The new comfort model for predicting local perceptual responses was developed based on experiments conducted by Fanger (1980 and 1985) and the extensive experiments of Mcnall and Biddison (1970). The verification exercise showed that the new comfort model reproduced well experimental data of those authors. Validations showed that the model also reproduced well independent experiments which were not used to develop the model, i.e. Olesen et al. (1972), and Loveday et al. (1998 and 2002). The model also showed good general agreement with experimental results obtained for non-neutral overall indoor climate conditions (Berglund and Fobelets, 1987).

The model was linked with a state-of-the-art dynamic building simulation program (BSP) to predict both global and local thermal discomfort in buildings. Sample simulations were carried out for an existing building and using the CIBSE Design Summer Year recommend for summer overheating analysis purposes. Using the link of the new comfort model with BSP it is possible to quantify the thermal comfort implications of different building designs and constructions and to perform daily, weekly, monthly, seasonal and annual statistical thermal comfort analysis.

The new comfort model predicting both local and global responses is intended to assist architects, designers, engineers, building simulation vendors, and researchers when quantifying the comfort performance of buildings, HVAC systems or individual built constructions such as windows, radiator heated floor or chilled ceilings. For example, new high-performance windows reduce the energy cost of heating, cooling and electrical lighting. However, while the energy-related issues of windows are well understood, the thermal comfort implications are not. The model will provide the necessary information to understand human comfort implications and will help to differentiate between products on the basis of their comfort qualities in different climates and building types.

Thermal and solar radiation is also a substantial issue for human comfort inside cars, aircraft cabins and other artificial environments. Some experimental investigations have been conducted in this regard. At present, however, there are no strategies for heating, ventilating and air-conditioning that would adequately take into account and compensate for the impact of solar and thermal radiation on their occupants. The new model would facilitate the integration of such effects into control strategies for these specific indoor climates.

9.2 Suggestions for future research work

9.2.1 Human body geometry models

The human body geometry models developed for purposes of this project represent an unclothed 'average' sedentary and standing male person. For future studies similar models can be developed to represent a female person which would take into account the gender-specific body characteristics in the human radiant heat transfer.

In future, predicting physiological and perceptual responses of indíviduals using 'personalised' models might become an important issue in a number of research areas. In addition, to average persons there might thus be need for geometry models that consider individual differences in antropometric and body-composition data such as body weight, body size and age of person (adult/child). The application of the latest computer simulation technology and mesh manipulation tools would facilitate the creation of such personalised body geometry models. These tools will enable creating radiation geometry models also for specific body postures and clothed-body-contours such as car-driving, walking/running, or humans wearing protective clothing. These models will be of importance in diverse industrial, sport research, and heath and safety applications.

9.2.2 Modelling local perceptual responses

The new comfort model predicts the percentage of dissatisfied due to local discomfort using local skin temperatures as the only punitive signals and the local sensitivity to 'cold' and 'warm' stimuli of the human skin. The model was developed using available experimental trials conducted mainly under overall conditions that referred to thermal neutrality. The validation work carried out as part of this project showed that the new model is able to predict local discomfort also under overall conditions that are colder than thermoneutral environments. Further work will be required to validate the model also for warm and hot overall conditions. This work could not be accomplished due to the lack of adequate experimental data.

The next step in the development of a more universal thermal comfort model would be to model human perceptual responses to draughts, (Fanger et al., 1977). The sensation of draughts involves a strong dynamic component (de Dear et al., 1989) caused by fluctuations of air flows (turbulent intensity) which are not presented in the sensation of local discomfort due to asymmetric radiation. This research would suggest extending the existing comfort model for a specifically dynamic component based on simulation and analysis of available experimental investigation on the sensation of draughts, i.e. Fanger and Pedersen (1977), Fanger et al. (1988), and Mayer and Schwab (1990).

Future work might also concentrate on including further punitive signals in addition to local skin temperatures and its time-related derivatives. For example, the sensation of local thermal discomfort of humans involved in higher than sedentary (and quietly-standing) activities and/or exposed to non-neutral overall environmental conditions is likely to be affected by further signals from the body core i.e. the hypothalamus temperature (and associated efferent signals such as skin wettedness, Gagge et al., 1986). The availability of adequate experimental investigation would make this modelling research possible.

9.2.3 Further experimental investigations

The experiments used to develop the local thermal comfort model referred to asymmetric thermal radiation conditions and, in most cases, thermoneutral overall environmental conditions. Future investigations might concentrate on studies of thermal comfort in warm and hot conditions including intense solar radiation. In addition, local comfort responses of humans exercising at activity levels higher than sedentary should be considered for future experiments.

More detailed experiments are needed on the local skin sensitivity to cold and warm stimuli for use with higher resolution models. Experimental data on local sensitivities is still missing for some body parts such as neck, shoulders etc.

Furthermore, experiments used in this project provided information on percentage of dissatisfied due to local discomfort. Future experiments should also provide information on the actual comfort and thermal sensation votes. Thereby, the asymmetric radiation conditions investigated should also include IR-radiation and solar radiation.

References

ASHRAE Handbook Fundamentals (1993), Physiological Principles and Thermal Comfort. American society of heating, refrigerating and air-conditioning engineer, Inc., Atlanta. pp. 8.1-8.27.

ASHRAE Handbook Fundamentals (1996), Infrared Radiant Heating. American society of heating, refrigerating and air-conditioning engineer, Inc., Atlanta, pp. 15.1-15.8.

ASHRAE Standard 55 (2004), The environmental conditions for human occupancy. American Society of Heat, Refrigerating and Air-conditioning Engineers, Atlanta.

Bedford T. (1935), The effective radiating surface of the human body. J Hyg Camb 35: 303-306.

Berglund L.G. and Fobelets A.P.R. (1987), Subjective human response to low-level air currents and asymmetric radiation. ASHRAE Transaction, pp. 497-523.

Berglund P.E. and D.J. Cunningham. (1986), Parameters of human discomfort in warm environments. ASHRAE Transaction, Vol. 92, part 2B, pp. 732-746.

Blazejczyk K. (1996), Assessment of solar radiation absorbed by man based on simple meteorological parameters In: Shaparo Y, Moran DS, Epstein Y (eds) 7th International Conference on Environmental Ergonomics, Israel, Conference proceedings. Freund Publ House Ltd, London: 190-193.

Blazejczyk K., H. Nilsson, and I. Holmer (1992), A modified equation for the calculation of solar heat load in man. In: Lotens W.A., Hanenith G. (eds) 5th

International Conference on Environmental Ergonomics, Maastricht, Conference proceedings. The Library, Soesterberg, Netherlands: 82-83.

Blum E.K. (1972), Numerical Analysis and Computation: Theory and practice. Reading (Mass.); Addison-Wesley, London. 1972.

Bøje O., M. Nielsen and J. Olesen (1948), Studied on the effect of unilateral cooling by radiation, contribution No. 9 from Committee for the Study of Domestic Heating, University of Copenhagen, Copenhagen.

Breckenridge J.R. and R.F. Goldman (1972), Human solar heat load. ASHRAE Trans 78(1):110-119.

Brewster M.Q. (1992), Thermal Radiative Transfer & Properties. John Wiley & Sons, Inc.

Bullard R.W., M.R. Banerjee, F. Chen, R. Elizondo and B. MacInTyre (1970), Skin temperature and thermoregulatory sweating: a control systems approach. In Physiological and behavioural temperature regulation, Thomas pp. 597-610.

Cannistraro G., G. Franzitta, C. Giaconia, and G. Rizzo (1992), Algorithms for the calculation of the view factors between human body and rectangular surfaces in parallelepiped environment. Energy and Buildings, Vol. 19, 1992, pp. 51-60

Chrenko F.A. (1953), Heated ceiling and comfort. Journal of the Inst. Heating and Ventilating Engineers, 21: 145-154.

Clark J.P. and D. McLean (1988), ESP – A building and plant energy simulation system. Version 6, release 8, Energy simulation Research Unit, University of Strathclyde and ABACUS Simulations Ltd., Glasgow, UK.

Clark R.P. (1981), Human skin temperature and convective heat loss, Studies in environmental science Vol. 10, Bioengineering, thermal physiologu and comfort, Elsevier Scientific Publishing Company ISBN 0-444-99761-X.

Crawshaw L. I., E. R. Nadel, J. A. J. Stolwijk, and B. A. Stamford (1975), Effect of local cooling on sweating rate and cooling sensation. Pfügers Arch. 354, pp. 19-27.

Curious Labs (2000), POSER4: The Premier 3D Character Animation and Figure Design Tool. Curious Labs Inc, Santa Cruz, California, USA.

Curran A. R. et al. (1995), Automated radiation modeling for vehicle thermal management, 1995 SAE International Congress and Exposition, Cobo Center, Detroit, USA, March, 1995.

de Dear R. J., J. W. Ring, and P. O. Fanger (1993), Thermal sensation resulting from sudden ambient temperature changes. Indoor Air, Vol. 3, pp. 181-192.

DuBois D. and E. F. DuBois (1916), A formula to estimate approximate surface area, if height and weight are known. Archives of Internal Medicine 17: 863-871.

Duffie J. A. and W. A. Beckman (1991), Solar engineering and thermal processes (2nd ed.), New York, Chichester: Wiley-Interscience.

ESRU (1998), ESP- a building and plant simulation system. User Guide. Energy Systems Research Unit, University of Strathclyde, Glasgow.

ESRU (2002), The ESP-r System for Building Energy Simulation User Guide Version 10 Series, Energy Systems Research Unit, University of Strathclyde, Glasgow.

Fanger P.O. (1970), Thermal Comfort - Analysis and Applications in Environmental Engineering, Technical University of Denmark, Laboratory of Heating and Air Conditioning, McGraw-Hill Book Company.

Fanger P. O. and C. J. K. Pedersen. (1977), Discomfort due to air velocities in spaces. Proc. Meeting of Commission EI (Air conditioning) of the International Institute of Refrigeration, Belgrade.

Fanger P. O., B. M. Ipsen, G. Langkilde, B. W. Olesen, N. K. Christensen, and S. Tanabe (1985), Comfort limits for asymmetric thermal radiation. Energy and Buildings, Vol. 8, pp. 225-236.

Fanger P. O., L. Banhidi, B. W. Olesen, and G. Langkilde (1980), Comfort limits for heated ceilings. ASHRAE Transactions Vol. 6, pp. 141-155.

Fiala D. (1991), Bestimmung von Einstrahizahlen zwischen rotationssymmetrischen Körpern und parallelen Rechteckflächen mit Analyse eines Halbraum-strahlungssensors. Diplomarbeit im Studiengang Grundlagen und Bauphysik an der Fachhochschule für Technik in Stuttgart vom 15. Januar 1991.

Fiala D., A. Bunzl, K. J. Lomas, P. C. Cropper, and D. Schlenz (2004), A new simulation system for predicting human thermal and perceptual responses in vehicles. PKW-Klimatisierung III: Klimakonzepte, Regelungsstrategien und Entwickluungsmethoden. Haus der Technik Fachbuch Band 27, Expert Verlag, pp. 147-162, 2004.

Fiala D., K. J. Lomas and M. Stohrer. (1999), A computer model of human thermoregulation for a wide range of environmental conditions: the passive system. The American Physiological Society, Vol. 87(5), pp. 1957-1972.

Fiala D., K. J. Lomas, and M. Stohrer (2001), Computer prediction of human thermoregulatory and temperature responses to a wide range of environmental

conditions. International Journal of Biometeorology, Volume 45 (2001), pp. 143-159.

Fiala D., K. J. Lomas, and M. Stohrer (2003), First Principles Modelling of Thermal Sensation Responses in Steady State and Transient Boundary Conditions. ASHRAE Transactions, Vol. 109 (1), pp. 179-186.

Fishman G. S. (1996), Monte Carlo: concepts, algorithms, and applications, Springer-Verlag, NewYork.

Gagge A. P. (1979), The role of humidity during warm discomfort. Proceeding of Indoor Climate Conference, Copenhagen, Danish Building Research Institute, Vol. 2, pp. 527-538.

Gagge A. P., A. P. Fobelets, and L. G. Berglund. (1986), A standard predictive index of human response to the thermal environment. ASHRAE Trans. 92(2), pp. 709-731.

Gagge A. P., J. A. J. Stolwijk and J. D. Hardy (1967), Comfort and thermal sensations and associated physiological responses at various ambient temperatures. Environmental Research, Vol. 1, pp. 1-20.

Gagge A.P. and J.D. Hardy (1967), Thermal radiation exchange of the human by partitional calorimetry, Journal of Applied Physiology, Vol. 23(2), pp. 248-258.

Gagge A.P., L.P. Herrington and C.E.A. Winslow (1937), Thermal interchanges between the human body and its atmosphere environment. Am. Jour Hygiene, 26: 84-102.

Gaage A. P. and Y. Nishi (1977), Heat exchange between human skin surface and the thermal environment. In Handbook of physiology, section 9, Reaction to environmental agents, American Physiological Society.

Gonzalez R. R. and A. P. Gagage. (1973), Magnitude estimates of thermal discomfort during transient of humidity and operative temperature and their relation to the new ASHRAE effective temperature (ET*). ASHRAE Trans., Vol. 79, pp. 88-96.

Gonzalez R. R., K. B. Pandolf, and A. P. Gagage. (1973), Physiological responses and warm discomfort during heat strain. Arch. Sci. Physigl. Vol. 27 (1973), pp. A563-A571.

Griffiths I. and D. McIntyre (1974), Subjective response to overhead thermal radiation, Human Factors, Vol. 16 (4), pp. 415-422.

Guibert A. and C. L. Taylor (1952), Radiation area of the human body. Journal of Applied Physiology, Vol. 5, pp. 24-37.

Haghighat F., F. Allard, and A. C. Megri (1998), Thermal comfort and indoor air quality inforty-three flights. EPIC (17)2, pp. 439-444.

Haghighat F., F. Allard, and A. C. Megri (1998), Measurement of thermal comfort and indoor air quality abroad 43 flights on commercial airlines. Indoor Built Environment, (8), pp. 58-66.

Hall J. F. and F. K. Klemm. (1967), Thermoregulatory responses in disparate thermal environments. Journal of Applied Physiology, Vol.23, No.4, pp. 540-544.

Hall J. F. Jr. and Klemm F. K. (1969), Thermal comfort in disparate thermal environments. Journal of Applied Physiology, Vol.27, No.5, pp. 601-606.

Hammersley J. M. and D. C. Handscomb (1964), Monte Carlo Methods, Methuen, London.

Hardy J. D. (1970), Thermal comfort: skin temperature and physiological thermoregulation. In "Physiological and Behavioural Temperature Regulation", Hardy, Gagge & Stolwijk, Springfield, pp. 856-873.

Hensel H. (1979), Thermoreception and human comfort. In "Indoor Climate", eds. P.O. Fanger and O. Valbjorn, Danish Building Research Institute, Copenhagen, pp. 426-440.

Hensel H. (1981), Thermoreception and temperature regulation. (Monographs of the physiological society; no.38), Academic Press, London.

Hodder S. G. (2002), Thermal comfort in vehicles: The effects of solar radiation. Doctoral Thesis, Loughborough University, UK

Hodder S. G., D. L. Loveday, K. C. Parson and A. H. Taki (1998), Thermal comfort in chilled ceiling and displacement ventilation environments: vertical radiant temperature asymmetry effects. Energy and Building, Vol. 27, pp. 167-173.

Holman J. P. (1981), Heat Transfer (5^{th} ed.) McGraw-Hill.

Horikoshi T., T. Tsuchikawa, Y. Kobayashi, E. Miwa, Y. Kurazumi and K. Hirayama (1990), The effective radiation area and angle factor between man and a rectangular plane near him. ASHRAE Transaction, Vol. 96, 1990, pp. 60-66.

Huizenga C., Z. Hui, and E. Arens (2001), A model of human physiology and comfort for assessing complex thermal environments. Building and Environment 36: 691-699.

ISO 7730 (1994), Moderate thermal environments- Determination of the PMV and PPD indices and specification of the conditions for thermal comfort, British Standard, London.

Issing K. and H. Hensel (1982), Temperaturempfindung und thermischer Komfort bei statischen Temperaturreizen. Z. Phys. Med. Baln. Med. Klim., Vol. 11, pp. 354-365.

Jacquez J. A, J. Huss, W. McKeehan, J. M. Dimitroff and H. F. Kuppenheim (1955). Spectral reflectance of human skin in the region 0.7 to 2.6μm. Journal of Applied Physiology, Vol. 8, pp. 297-299.

Jones H.R.N. (2000), Radiation Heat Transfer. Oxford Science Publication.

Jones B. W., S. Hong, and E. A. McCullough (1998), Detailed projected area data for the human body. ASHRAE Trans 104(2): 1327-1339.

Kimlin M., A. Prisi, B. Carter, and D. Turnbull (2002), Comparison of the solar spectral ultraviolet irradiance in motor vehicles with windows in an open and closed position. International Journal of Biometeorology, Vol. 46: (3), pp. 150-156.

Konz S., C. Hwang, B. Dhiman, J. Duncan, and A. Masud (1977), An experimental validation of mathematical simulation of human thermoregulation. Comput. Biol. Med., Vol. 7, pp. 71-82.

Kubaha K., D. Fiala, J. Toftum, and A. H. Taki (2004), Human projected area factor for detailed direct and diffuse solar radiation analysis. International Journal of Biometeorology, Vol. 49 (2), pp. 113-129.

Kubaha K., D. Fiala, and K. J. Lomas (2003), Predicting human geometry-related factors for detailed radiation analysis in indoor spaces, Eighth International IBPSA Conference, Building Simulation 2003, Eindhoven, Netherlands, Vol. 2, pp. 681-688.

Leduc G., F. Monchoux, and F. Thellier (2001), Analysis of human's radiative exchange in a complex enclosure. Moving Thermal Comfort Standards into the 21st Century, Conference Proceedings, Cumberland Lodge, Windsor, UK, April 2001, pp. 385-392.

Lomas K. J., H. Eppel, C. J. Martin, and D.P. Bloomfield. (1997), Empirical validation of thermal building simulation programs. Energy and Buildings, Vol. 26(3), pp. 253-275.

Loveday D. L., K. C. Parsons, A. H. Taki, S. G. Hodder, and L. D. Jeal. (1998), Designing for thermal comfort in combined chilled ceiling/displacement ventilation environments. ASHRAE Transaction, Vol. 104, part 1.

Loveday D. L., K. C. Parson, A. H. Taki, and S. G. Hodder (2001), Thermal comfort design of chilled ceiling/ displacement ventilation environments based on ISO 7730: Validation, adaptive context and influence on system configurations. Moving Thermal Comfort Standards into the 21st Century, Conference Proceedings, Cumberland Lodge, Windsor, UK, pp. 323-334.

Loveday D. L., K. C. Parsons, A. H. Taki, and S. G. Hodder (2002), Displacement ventilation environments with chilled ceiling: thermal comfort design within the context of BS EN ISO7730 versus adaptive debate. Energy and Buildings 34 (2002), pp. 573-579.

Martinez D., D. Fiala, M. J. Cook, and K. J. Lomas (2000), Predicted comfort envelopes for office buildings with passive downdraught evaporative cooling. Proceeding of the 7th International Conference on Air Distribution in Rooms, Ventilation for Health and Sustainable Environment (Roomvent 2000), Reading, UK, 9-12 July 2000, Vol. 1, pp. 53-58.

Mayer E. and R. Schwab (1990), Untersuchungen der physikalischen Ursachen von Zugluft. Gesundheitsingenieur 111, Heft 1, pp. 17-30.

McAdams H. M. (1954), Heat transmission, McGraw-Hill.

McIntyre D. A. (1980), Indoor Climate. Applied Science Publishers Ltd, London, 1980.

McIntyre D. A. and I. D. Griffiths. (1972), Radiant temperature and comfort. Proceeding of CIB Symposium on Thermal Comfort, Building Research Station, London, pp. 113-132.

McNall P. E. Jr., and R. E. Biddison (1970), Thermal and comfort sensations of sedentary persons exposed to asymmetric radiant fields. ASHRAE Transaction Vol. 76, part 1, pp. 123-136.

Mitchell D. (1970), Measurement of the thermal emissivity of human skin in vivo. In J. D. Hardy: Physiological and behavioural temperature regulation, Charles C. Thomas, Illinois.

Miyazaki Y, M. Saito, and Y. Seshimo (1995), A study of evaluation non-uniform environments by human body model. Journal of Human and Living Environment 2(1): 92-100.

Nadel E. R., J. W. Mitchell and J. A. J. Stolwijk (1973), Differential thermal sensitivity in the human skin. Pflügers Arch. 340, pp 71.76.

Nevins R. G., R. R. Gonzalez, Y. Nishi, and A. P. Gagge (1975), Effect of changes in ambient temperature and level of humidity on comfort and thermal sensation. ASHRAE Transactions, Vol. 81 (2), pp.169-182.

Nucara A., M. Pietrafesa, G. Rizzo and G. Rodono (1999), Human body view factors for composite plane surfaces. Indoor Air 99, The International Academy of Indoor Air Sciences (IAIAS), 1999, Vol. 1, pp. 650-655.

Olesen S., P. O. Fanger, P. B. Jensen and O. J. Nielsen (1972), Comfort limits for man exposed to asymmetric thermal radiation. Proc. of CIB Symposium on Thermal Comfort, Building Research Station, London, pp. 133-150.

Olsen B. W. and P. O. Fanger (1973), The skin temperature distribution for resting man in comfort, Arch. Sci. Physiol., 27(4): A383-A393.

Olesen B. W., M. Schöler, and P. O. Fanger (1979), Discomfort cause by vertical air temperature. Indoor climate, ed. P. O. Fanger and O. Valbjorn, Danish Building Research Institute, Copenhagen, pp. 561-579.

Ozeki Y., M. Konishi, C. Narita, and S. Tanabe (2000), Numerical calculation of angle factors between human body and rectangular planes. Air distribution in rooms, Ventilation for Health and Sustainable Environment (Roomvent 2000), Proceeding of the 7th International Conference on Air Distribution in Rooms, July 2000, Vol. I, pp. 27-33.

Ozisik M. N. (1973), Radiative Transfer and Interactions with Conduction and Convection. John Wiley & Sons, Inc.

Pennes H. H. (1948), Analysis of tissue and arterial blood temperatures in the resting human forearm. Journal of Applied Physiology, Vol. 1, pp. 93-121.

Pformmer P. (1995), Thermal modelling of highly glazed spaces. PhD-thesis, chap. 8: Internal solar radiation distribution, Institute of Energy and Sustainable Development, De Montfort University, Leicester.

Pformmer P., K. J. Lomas and C. Kupke (1994), The radiation transfer through coated and tinted glazing. Solar Energy, Vol. 54(5), pp. 287-299.

Ramanathan N. L. (1964), A new weighting system for men surface temperature of the human body. Journal of Applied Physiology, Vol. 19, pp. 531-533.

Rizzo G., G. Franzitta, and G. Cannistraro (1991), Algorithms for the calculation of the mean projected area of seated and standing persons. Energy and Buildings 17:221-230.

Rohles F. H., and R. G. Nevins (1971), The nature of thermal comfort for sedentary man. ASHRAE Trans. 77:1, pp. 239-246.

Siegel, R. and J. R. Howell (1992), Thermal Radiation Heat Transfer. 2nd ed., Taylor & Francis, New York.

Steinman M, L. N. Kalisperis, and L. H. Summers (1988), Angle factor determination from a person to inclined surfaces. ASHRAE Trans 94(1): 1809-1823.

Stevens J. C., L. E. Marks, and D. C. Simonson (1974), Regional sensitivity and spatial summation in the warmth sense. Physiology and Behavior, Brain Research Publications Inc, Vol. 13, pp. 825-836.

Stevens J. C., W. C. Okulicz, and L. E. Marks (1973), Temporal summation at the warmth threshold. Percept. Psychophys. 14, pp. 307-312.

Stolwijk J. A. J. (1970), Mathematical model of thermoregulation, Physiological and behavioural temperature regulation, chapter 48, Charles C. Thomas Pub., pp. 730-721.

Stolwijk J. A. J. (1971), A mathematical model of physiological and behavioural temperature regulation in man. NASA contractor report CR-1855. Washington DC.

Stolwijk J. A. J. (1979), Physiological responses and thermal comfort in changing environment temperature and humidity. In "Indoor Climate", eds. P.O. Fanger & O. Valbjorn, Danish Building Research Institute, Copenhagen, pp. 491-505.

Strachan P. (2000), ESRU Technical Report. Energy Systems Research Unit, University of Strathclyde, Glasgow.

Tanabe S., C. Narita, Y. Ozeki and M. Konishi (2000), Effective radiation area of human body calculated by a numerical simulation. Energy and Buildings, Vol. 32(2), pp. 205-215.

ThermoAnalytics (2001), RadTherm Technical Documentation. ThermoAnalytics Inc, Calumet, Michigan, USA.

Underwood C. R. and E. J. Ward (1966), The solar radiation area of man. Ergonomics 9:155-168.

Wagner J. A., and S. M. Horvath (1985), Influences of age and gender on human thermoregulatory responses to cold exposures. Journal of Applied Physiology, Vol. 58, pp.180-186.

Window 5.0 (2001), A PC Program for Analysis Window Thermal Performance, Window & Daylighting Group, Building Technologies Program, Environmental Energy Technologies Department, Lawrence Berkeley National Laboratory, Berkeley, California, USA.

Wissler E. H. (1985), Mathematical simulation of human thermal behaviour using whole body models. In: Shitzer A., and R. C. Eberhart: Heat Transfer in Medicine and Biology Analysis and Application, Vol. 1, chap 13, pp. 325-373, Plenum Press, New York and London.

Wyon D. P. and M. Sandberg (1990), Thermal manikin prediction of discomfort due to displacement ventilation. ASHRAE Transaction (1990), 96: I, pp. 67-75.

Yaglou C. P. (1927), The thermal zone for men at rest and stripped to the waist. Tran. Am. Soc. Heating and Ventilating Engineers, 33:165-179.

Zhang H. (2003), Human thermal sensation and comfort in transient and non-uniform thermal environment, Doctoral Thesis, University of California, Berkeley, USA.

Appendix A

Comparison of view factors obtained using numerical simulation technique (voxel-based ray tracing) with analytical results

Table A.1 Comparison of numerically calculated view factors between two parallel plates with the corresponding analytical results.

		Distance c [m]										
		0.5		1		1.5		2				
Analytical solution		0.41525		0.19982		0.11071		0.06859				
Numerical solution			Δe [%]		Δe [%]		Δe [%]		Δe [%]	Δe [%]		
										Min	Average	Max
Low resolution	1ray	0.41680	0.37	0.19596	1.93	0.10987	0.75	0.06620	3.48	0.37	1.63	3.48
	2rays	0.41971	1.07	0.19794	0.95	0.10884	1.69	0.06998	2.03	0.95	1.43	2.03
	3rays	0.41845	0.77	0.19916	0.33	0.10857	1.93	0.06796	0.92	0.33	0.99	1.93
	4rays	0.42192	1.61	0.20117	0.67	0.11099	0.25	0.06790	1.01	0.25	0.89	1.61
	5rays	0.42051	1.27	0.20165	0.91	0.11097	0.23	0.06736	1.79	0.23	1.05	1.79
Min			0.37		0.33		0.23		0.92	0.23		
Average			1.02		0.96		0.97		1.84		1.20	
Max			1.61		1.93		1.93		3.48			3.48
Medium resolution	1ray	0.41493	0.08	0.20049	0.33	0.11081	0.09	0.06636	3.25	0.08	0.94	3.25
	2rays	0.41478	0.11	0.20120	0.69	0.11092	0.19	0.06804	0.81	0.11	0.45	0.81
	3rays	0.41560	0.08	0.20045	0.31	0.11009	0.55	0.06792	0.97	0.08	0.48	0.97
	4rays	0.41657	0.32	0.19982	0.00	0.11029	0.38	0.06822	0.54	0.00	0.31	0.54
	5rays	0.41669	0.35	0.19920	0.31	0.11105	0.31	0.06800	0.85	0.31	0.46	0.85
Min			0.08		0.00		0.09		0.54	0.00		
Average			0.19		0.33		0.31		1.28		0.53	
Max			0.35		0.69		0.55		3.25			3.25
High resolution	1ray	0.41493	0.08	0.19888	0.47	0.10873	1.79	0.06615	3.55	0.08	1.47	3.55
	2rays	0.41517	0.02	0.19911	0.36	0.10948	1.11	0.06726	1.94	0.02	0.86	1.94
	3rays	0.41486	0.09	0.19967	0.08	0.10965	0.95	0.06744	1.68	0.08	0.70	1.68
	4rays	0.41610	0.20	0.19938	0.22	0.11044	0.24	0.06771	1.29	0.20	0.49	1.29
	5rays	0.41586	0.15	0.19984	0.01	0.11038	0.30	0.06790	1.01	0.01	0.36	1.01
Min			0.02		0.01		0.24		1.01	0.01		
Average			0.11		0.23		0.88		1.89		0.78	
Max			0.20		0.47		1.79		3.55			3.55
Very high resolution	1ray	0.41440	0.20	0.19981	0.01	0.10928	1.29	0.06722	2.00	0.01	0.87	2.00
	2rays	0.41486	0.09	0.19968	0.07	0.10956	1.04	0.06722	1.99	0.07	0.80	1.99
	3rays	0.41483	0.10	0.19971	0.06	0.11016	0.49	0.06798	0.88	0.06	0.38	0.88
	4rays	0.41553	0.07	0.19959	0.12	0.11025	0.41	0.06786	1.06	0.07	0.41	1.06
	5rays	0.41506	0.05	0.19963	0.10	0.11018	0.47	0.06816	0.63	0.05	0.31	0.63
Min			0.05		0.01		0.41		0.63	0.01		
Average			0.10		0.07		0.74		1.31		0.56	
Max			0.20		0.12		1.29		2.00			2.00

Table A.2 Comparison of numerically calculated view factors between two perpendicular plates with the corresponding analytical results.

		Length a [m]								Δe [%]		
		0.5		1		1.5		2				
Analytical solution		0.29237		0.20004		0.14822		0.11643				
Numerical solution			Δe [%]		Δe [%]		Δe [%]		Δe [%]	Min	Average	Max
Low resolution	1ray	0.29060	0.61	0.20103	0.49	0.14504	2.14	0.11564	0.67	0.49	0.98	2.14
	2rays	0.29595	1.22	0.20054	0.25	0.14863	0.28	0.11668	0.22	0.22	0.49	1.22
	3rays	0.29324	0.30	0.20023	0.09	0.14748	0.50	0.11695	0.45	0.09	0.33	0.50
	4rays	0.29393	0.53	0.19973	0.16	0.14709	0.76	0.11630	0.11	0.11	0.39	0.76
	5rays	0.29345	0.37	0.19961	0.22	0.14647	1.18	0.11609	0.29	0.22	0.51	1.18
Min			0.30		0.09		0.28		0.11	0.09		
Average			0.61		0.24		0.97		0.35		0.54	
Max			1.22		0.49		2.14		0.67			2.14
Medium resolution	1ray	0.29601	1.24	0.19990	0.07	0.14842	0.14	0.11637	0.05	0.05	0.38	1.24
	2rays	0.29206	0.11	0.19972	0.16	0.14764	0.39	0.11593	0.42	0.11	0.27	0.42
	3rays	0.29137	0.34	0.19991	0.07	0.14775	0.31	0.11605	0.33	0.07	0.26	0.34
	4rays	0.29238	0.00	0.20007	0.01	0.14824	0.02	0.11643	0.00	0.00	0.01	0.02
	5rays	0.29282	0.15	0.20022	0.09	0.14849	0.18	0.11656	0.11	0.09	0.13	0.18
Min			0.00		0.01		0.02		0.00	0.00		
Average			0.37		0.08		0.21		0.18		0.21	
Max			1.24		0.16		0.39		0.42			1.24
High resolution	1ray	0.28503	2.51	0.20030	0.13	0.14812	0.06	0.11640	0.03	0.03	0.68	2.51
	2rays	0.28460	2.66	0.20024	0.10	0.14823	0.01	0.11648	0.05	0.01	0.70	2.66
	3rays	0.28471	2.62	0.20011	0.03	0.14817	0.03	0.11644	0.01	0.01	0.67	2.62
	4rays	0.28426	2.78	0.20018	0.07	0.14833	0.08	0.11649	0.06	0.06	0.75	2.78
	5rays	0.28422	2.79	0.20006	0.01	0.14832	0.07	0.11642	0.00	0.00	0.72	2.79
Min			2.51		0.01		0.01		0.00	0.00		
Average			2.67		0.07		0.05		0.03		0.70	
Max			2.79		0.13		0.08		0.06			2.79
Very high resolution	1ray	0.29284	0.16	0.20007	0.01	0.14812	0.07	0.11624	0.16	0.01	0.10	0.16
	2rays	0.29271	0.11	0.20010	0.03	0.14824	0.02	0.11643	0.00	0.00	0.04	0.11
	3rays	0.29251	0.05	0.20009	0.03	0.14822	0.00	0.11642	0.00	0.00	0.02	0.05
	4rays	0.29260	0.08	0.20013	0.04	0.14825	0.02	0.11646	0.03	0.02	0.04	0.08
	5rays	0.29256	0.06	0.20012	0.04	0.14823	0.01	0.11644	0.01	0.01	0.03	0.06
Min			0.05		0.01		0.00'		0.00	0.00		
Average			0.09		0.03		0.02		0.04		0.05	
Max			0.16		0.04		0.07		0.16			0.16

Table A.3 Comparison of numerically calculated view factors between cylinder and plate with the corresponding analytical results (*case a*).

		Distance *a* [m]										
		0.5		1		1.5		2				
Analytical solution		0.23772		0.09678		0.04804		0.02769				
Numerical solution			Δe [%]		Δe [%]		Δe [%]		Δe [%]	Δe [%]		
										Min	Average	Max
Low resolution	1ray	0.23893	0.51	0.09643	0.35	0.04767	0.77	0.02781	0.44	0.35	0.52	0.77
	2rays	0.23935	0.69	0.09638	0.41	0.04818	0.29	0.02717	1.87	0.29	0.81	1.87
	3rays	0.24006	0.99	0.09646	0.33	0.04788	0.33	0.02727	1.53	0.33	0.79	1.53
	4rays	0.24023	1.06	0.09687	0.10	0.04756	0.99	0.02729	1.46	0.10	0.90	1.46
	5rays	0.24027	1.07	0.09654	0.24	0.04778	0.55	0.02763	0.22	0.22	0.52	1.07
Min			0.51		0.10		0.29		0.22	0.10		
Average			0.86		0.28		0.58		1.10		0.71	
Max			1.07		0.41		0.99		1.87			1.87
Medium resolution	1ray	0.23953	0.76	0.09638	0.41	0.04785	0.39	0.02802	1.19	0.39	0.69	1.19
	2rays	0.23921	0.63	0.09719	0.43	0.04791	0.26	0.02779	0.36	0.26	0.42	0.63
	3rays	0.23905	0.56	0.09694	0.17	0.04780	0.50	0.02763	0.21	0.17	0.36	0.56
	4rays	0.23891	0.50	0.09682	0.05	0.04799	0.11	0.02760	0.32	0.05	0.24	0.50
	5rays	0.23898	0.53	0.09645	0.34	0.04797	0.14	0.02776	0.25	0.14	0.32	0.53
Min			0.50		0.05		0.11		0.21	0.05		
Average			0.60		0.28		0.28		0.47		0.41	
Max			0.76		0.43		0.50		1.19			1.19
High resolution	1ray	0.23348	1.78	0.09649	0.30	0.04754	1.03	0.02776	0.25	0.25	0.84	1.78
	2rays	0.23343	1.80	0.09687	0.10	0.04806	0.04	0.02766	0.11	0.04	0.51	1.80
	3rays	0.23798	0.11	0.09655	0.23	0.04805	0.02	0.02756	0.46	0.02	0.21	0.46
	4rays	0.23796	0.10	0.09677	0.01	0.04780	0.51	0.02756	0.48	0.01	0.27	0.51
	5rays	0.23800	0.12	0.09672	0.06	0.04801	0.07	0.02770	0.04	0.04	0.07	0.12
Min			0.10		0.01		0.02		0.04	0.01		
Average			0.78		0.14		0.33		0.27		0.38	
Max			1.80		0.30		1.03		0.48			1.80
Very high resolution	1ray	0.23811	0.16	0.09680	0.02	0.04775	0.60	0.02742	0.97	0.02	0.44	0.97
	2rays	0.23805	0.14	0.09645	0.34	0.04793	0.24	0.02745	0.86	0.14	0.40	0.86
	3rays	0.23802	0.13	0.09688	0.10	0.04807	0.06	0.02772	0.12	0.06	0.10	0.13
	4rays	0.23799	0.11	0.09666	0.12	0.04804	0.01	0.02754	0.53	0.01	0.19	0.53
	5rays	0.23799	0.11	0.09680	0.03	0.04803	0.03	0.02770	0.03	0.03	0.05	0.11
Min			0.11		0.02		0.01		0.03	0.01		
Average			0.13		0.12		0.19		0.50		0.24	
Max			0.16		0.34		0.60		0.97			0.97

Table A.4 Comparison of numerically calculated view factors between cylinder and plate with the corresponding analytical results (*case b*).

		Distance *a* [m]										
		0.5		1		1.5		2				
Analytical solution		0.29482		0.16765		0.10228		0.06688				
Numerical solution			Δe [%]		Δe [%]		Δe [%]		Δe [%]	Δe [%] Min	Δe [%] Average	Δe [%] Max
Low resolution	1ray	0.29437	0.15	0.16619	0.87	0.10223	0.05	0.06543	2.17	0.05	0.81	2.17
	2rays	0.29155	1.11	0.16534	1.37	0.10246	0.17	0.06587	1.52	0.17	1.04	1.52
	3rays	0.29288	0.66	0.16674	0.54	0.10152	0.74	0.06665	0.34	0.34	0.57	0.74
	4rays	0.29339	0.49	0.16729	0.21	0.10138	0.88	0.06625	0.94	0.21	0.63	0.94
	5rays	0.29383	0.34	0.16666	0.59	0.10152	0.74	0.06609	1.19	0.34	0.71	1.19
Min			0.15		0.21		0.05		0.34	0.05		
Average			0.55		0.72		0.52		1.23		0.75	
Max			1.11		1.37		0.88		2.17			2.17
Medium resolution	1ray	0.29462	0.07	0.16842	0.46	0.10165	0.62	0.06570	1.76	0.07	0.73	1.76
	2rays	0.29494	0.04	0.16723	0.25	0.10236	0.08	0.06656	0.49	0.04	0.21	0.49
	3rays	0.29426	0.19	0.16751	0.08	0.10236	0.08	0.06650	0.57	0.08	0.23	0.57
	4rays	0.29486	0.01	0.16745	0.12	0.10236	0.08	0.06675	0.20	0.01	0.10	0.20
	5rays	0.29470	0.04	0.16733	0.19	0.10224	0.04	0.06643	0.68	0.04	0.24	0.68
Min			0.01		0.08		0.04		0.20	0.01		
Average			0.07		0.22		0.18		0.74		0.30	
Max			0.19		0.46		0.62		1.76			1.76
High resolution	1ray	0.29558	0.26	0.16728	0.22	0.10195	0.32	0.06671	0.26	0.22	0.26	0.32
	2rays	0.29529	0.16	0.16750	0.09	0.10181	0.46	0.06761	1.09	0.09	0.45	1.09
	3rays	0.29489	0.02	0.16771	0.04	0.10216	0.12	0.06699	0.16	0.02	0.09	0.16
	4rays	0.29490	0.02	0.16739	0.16	0.10223	0.05	0.06679	0.13	0.02	0.09	0.16
	5rays	0.29487	0.02	0.16746	0.11	0.10205	0.23	0.06701	0.20	0.02	0.14	0.23
Min			0.02		0.04		0.05		0.13	0.02		
Average			0.10		0.12		0.24		0.37		0.21	
Max			0.26		0.22		0.46		1.09			1.09
Very high resolution	1ray	0.29522	0.13	0.16813	0.29	0.10174	0.53	0.06669	0.28	0.13	0.31	0.53
	2rays	0.29478	0.02	0.16717	0.28	0.10233	0.05	0.06659	0.44	0.02	0.20	0.44
	3rays	0.29488	0.02	0.16744	0.12	0.10217	0.11	0.06670	0.27	0.02	0.13	0.27
	4rays	0.29498	0.05	0.16739	0.15	0.10237	0.09	0.06691	0.03	0.03	0.08	0.15
	5rays	0.29489	0.02	0.16762	0.01	0.10228	0.00	0.06689	0.01	0.00	0.01	0.02
Min			0.02		0.01		0.00		0.01	0.00		
Average			0.05		0.17		0.16		0.21		0.15	
Max			0.13		0.29		0.53		0.44			0.53

Appendix B

Regression coefficients of projected area factor

Table B.1 Polynomial of the coefficient A of the basic cosine function $f_{p,dir}$ (eq. 4.2), $A = \sum_{j=0}^{4} a_j \beta^j$ and the corresponding correlation coefficient, R.

Body sectors	Standing posture						Sedentary posture					
	a_0	a_1	a_2	a_3	a_4	R	a_0	a_1	a_2	a_3	a_4	R
Head	0.1429	-0.0284	-0.0668	0.0169	0.0000	1.00	0.1486	-0.0300	-0.0682	0.0180	0.0000	1.00
Forehead	0.5055	0.0366	-0.2348	0.0000	0.0000	1.00	0.5144	0.0453	-0.2363	0.0000	0.0000	1.00
Face (*anterior*)	0.3178	-0.1671	0.0000	0.0891	-0.0695	0.97	0.3296	-0.1260	-0.0581	0.0720	-0.0455	0.99
Face (*R & L*)	0.8526	-0.0115	-0.4797	0.0294	0.0387	1.00	0.8551	-0.0012	-0.4913	0.0263	0.0440	1.00
Neck (*anterior*)	0.6988	-0.4388	-0.3071	0.1816	0.0000	0.99	0.7272	-0.4806	-0.4488	0.2446	0.0403	1.00
Neck (*R & L*)	0.6325	0.3031	-0.5492	-0.1331	0.1299	0.99	0.6251	0.3191	-0.5370	-0.1369	0.1287	0.99
Neck (*posterior*)	0.5749	0.0429	-0.2468	0.0000	0.0000	0.98	0.6137	0.0391	-0.2692	0.0000	0.0000	0.99
Shoulder (*R & L*)	0.1568	0.1954	-0.0481	-0.0925	0.0000	0.98	0.1591	0.1594	-0.0591	-0.0635	0.0000	0.98
Thorax (*anterior*)	0.5050	0.1582	-0.3273	-0.0674	0.0525	1.00	0.5334	0.2031	-0.3729	-0.0792	0.0667	1.00
Thorax (*inferior*)	0.3660	-0.0140	-0.1465	0.0000	0.0000	0.97	0.3728	-0.0251	-0.1467	0.0000	0.0000	0.97
Thorax (*posterior*)	0.5196	0.0257	-0.3047	-0.0157	0.0423	1.00	0.5371	0.0117	-0.3084	-0.0064	0.0414	1.00
Abdomen (*anterior*)	0.7090	-0.1368	-0.3400	0.0436	0.0268	1.00	0.4966	0.2208	-0.4061	-0.0978	0.0915	0.99
Abdomen (*inferior*)	0.5141	0.0000	-0.2865	0.0000	0.0335	1.00	0.6135	-0.0953	-0.2806	0.0528	0.0000	0.99
Abdomen (*posterior*)	0.4876	0.0406	-0.2671	-0.0241	0.0349	1.00	0.4521	-0.0384	-0.1954	0.0203	0.0000	1.00
Upper arm (*anterior*)	0.5678	-0.0414	-0.3145	0.0000	0.0445	1.00	0.6135	-0.0953	-0.2806	0.0528	0.0000	0.99
Upper arms (*exterior*)	0.5773	0.1176	-0.3420	-0.0377	0.0398	1.00	0.4444	-0.0907	-0.2156	0.0532	0.0000	0.99
Upper arms (*inferior*)	0.2508	-0.2750	0.0000	0.1247	-0.0516	0.99	0.5607	0.0515	-0.2528	0.0000	0.0000	1.00
Upper arms (*posterior*)	0.5043	0.0159	-0.2148	0.0000	0.0000	1.00	0.4584	-0.2358	-0.2009	0.1005	0.0000	0.99
Lower arms (*anterior*)	0.7318	0.0920	-0.3252	-0.0212	0.0000	1.00	0.5710	0.0575	-0.2563	0.0000	0.0000	0.99
Lower arms (*exterior*)	0.7677	0.0213	-0.4289	0.0000	0.0425	1.00	0.4736	0.4902	-0.4472	-0.2134	0.1180	0.95
Lower arms (*inferior*)	0.4570	0.0000	-0.2861	0.0000	0.0405	0.98	0.4773	0.2919	-0.2749	-0.1198	0.0393	1.00
Lower arms (*posterior*)	0.6152	-0.1644	-0.3402	0.0655	0.0350	1.00	0.3652	-0.2153	-0.2808	0.0915	0.0553	0.99
Hands (*handback*)	0.3494	-0.0305	-0.1566	0.0215	0.0000	0.99	0.7875	-0.1788	-0.5674	0.0709	0.1011	1.00
Hands (*palm*)	0.2782	0.0000	-0.1165	0.0000	0.0000	0.98	0.1195	0.0135	-0.0542	0.0000	0.0000	0.97
Upper legs (*anterior*)	0.7597	0.0251	-0.4238	0.0000	0.0378	1.00	0.1071	-0.0388	-0.0725	0.0108	0.0161	0.81
Upper legs (*exterior*)	0.6963	-0.0291	-0.3991	0.0000	0.0515	1.00	0.0730	0.1876	0.0000	-0.0877	0.0000	0.93
Upper legs (*inferior*)	0.6902	-0.0509	-0.4351	0.0000	0.0759	0.99	0.7209	0.0000	-0.5094	0.0000	0.0867	1.00
Upper legs (*posterior*)	0.5509	-0.0317	-0.2739	0.0124	0.0200	1.00	0.6481	0.0402	-0.2499	-0.0124	-0.0050	0.95
Lower legs (*anterior*)	0.6848	0.0000	-0.3028	0.0000	0.0000	0.96	0.1749	-0.2020	-0.0804	0.0917	0.0000	0.98
Lower legs (*exterior*)	0.7382	0.0000	-0.3711	0.0000	0.0259	1.00	0.6267	0.0869	-0.4192	-0.0285	0.0690	1.00
Lower legs (*inferior*)	0.6504	-0.0328	-0.2575	0.0000	0.0000	0.99	0.6792	0.0000	-0.3568	0.0000	0.0323	1.00
Lower legs (*posterior*)	0.4285	0.0258	-0.2241	-0.0132	0.0238	1.00	0.5785	0.0000	-0.3114	0.0000	0.0348	0.99
Feet (*instep*)	0.1720	0.1009	0.1104	-0.0441	-0.0715	0.88	0.3552	-0.0665	-0.2435	0.0208	0.0449	1.00
Feet (*sole*)	0.0472	-0.0304	-0.0219	0.0138	0.0000	0.98	0.1832	-0.0557	-0.0835	0.0303	0.0000	0.99

Table B.2 Polynomial of the coefficient B of the basic cosine function $f_{p,dir}$ (eq. 4.2), $B = \sum_{j=0}^{4} b_j \beta^j$ and the corresponding correlation coefficient, R.

Body sectors	Standing posture						Sedentary posture					
	b_0	b_1	b_2	b_3	b_4	R	b_0	b_1	b_2	b_3	b_4	R
Head	0.2575	0.1362	-0.0322	0.0000	0.0000	1.00	0.2573	0.1335	-0.0319	0.0000	0.0000	1.00
Forehead	0.2667	0.0005	-0.1139	0.0196	0.0059	1.00	0.2728	0.0000	-0.1037	0.0248	0.0000	1.00
Face (*anterior*)	0.2852	0.0000	-0.2266	0.0000	0.0474	0.98	0.2782	-0.0430	-0.1675	0.0386	0.0123	1.00
Face (*R & L*)	0.0689	-0.0528	-0.0336	0.0285	0.0000	0.92	0.0692	-0.0416	-0.0350	0.0245	0.0000	0.92
Neck (*anterior*)	0.1264	0.0394	-0.2067	0.0780	0.0000	0.98	0.1203	0.1017	-0.1350	0.0000	0.0000	0.96
Neck (*R & L*)	0.1690	0.1343	-0.0636	-0.0515	0.0000	0.97	0.1470	0.0989	-0.0128	-0.0292	-0.0233	0.98
Neck (*posterior*)	0.3219	0.2376	-0.1510	-0.0897	0.0000	0.95	0.2891	0.2264	-0.1319	-0.0879	0.0000	0.96
Shoulder (*R & L*)	0.1891	0.4127	0.0883	-0.0722	0.0000	0.99	0.1839	0.4316	0.0890	-0.0796	0.0000	0.99
Thorax (*anterior*)	0.2421	0.0703	-0.0625	0.0000	0.0000	0.97	0.2586	0.0996	-0.0914	0.0000	0.0000	0.92
Thorax (*inferior*)	0.1350	-0.1850	-0.0336	0.0591	0.0000	0.93	0.1427	-0.1661	-0.0346	0.0499	0.0000	0.94
Thorax (*posterior*)	0.3539	0.0000	-0.1895	0.0000	0.0390	0.98	0.3694	0.0000	-0.1842	0.0000	0.0342	1.00
Abdomen (*anterior*)	0.1325	0.0000	-0.1112	0.0000	0.0251	0.95	0.0889	0.0000	-0.0635	0.0000	0.0144	0.96
Abdomen (*inferior*)	0.1807	0.0180	-0.0843	0.0000	0.0000	0.98	0.1055	-0.0215	-0.0287	0.0000	0.0000	0.89
Abdomen (*posterior*)	0.2934	0.0000	-0.1057	-0.0088	0.0000	0.99	0.3658	-0.1778	-0.0899	0.0312	0.0000	1.00
Upper arm (*anterior*)	0.2420	-0.0387	-0.1203	0.0321	0.0000	1.00	0.1862	-0.0851	-0.0806	0.0373	0.0000	0.97
Upper arms (*exterior*)	0.2090	0.1402	-0.0391	-0.0286	0.0000	0.98	0.1924	0.1567	-0.0923	-0.0405	0.0234	0.99
Upper arms (*inferior*)	0.1625	-0.1908	0.0000	0.0550	-0.0123	0.99	0.2044	-0.1471	-0.0362	0.0279	0.0000	0.98
Upper arms (*posterior*)	0.3284	0.0180	-0.2176	0.0000	0.0445	0.99	0.2732	0.0531	-0.0837	0.0000	0.0000	0.98
Lower arms (*anterior*)	0.1510	0.1367	-0.0819	0.0000	0.0000	0.99	0.2673	0.2509	-0.1383	0.0000	0.0000	0.97
Lower arms (*exterior*)	0.0838	0.0282	0.0000	-0.0106	0.0000	0.84	0.1616	0.1856	0.0286	-0.0175	0.0000	1.00
Lower arms (*inferior*)	0.2240	-0.0755	-0.1289	0.0146	0.0274	1.00	0.2541	-0.2631	0.0000	0.0449	0.0000	0.98
Lower arms (*posterior*)	0.3051	-0.1363	-0.1757	0.0164	0.0479	1.00	0.1338	-0.2768	0.0505	0.0538	0.0000	0.99
Hands (*handback*)	0.1967	-0.0477	-0.0151	0.0000	0.0000	0.98	0.2414	0.2629	0.0265	-0.0413	0.0000	0.99
Hands (*palm*)	0.1613	0.0000	-0.0431	0.0000	0.0000	0.97	0.0880	-0.0659	-0.0055	0.0143	0.0000	0.97
Upper legs (*anterior*)	0.1033	-0.0419	-0.0271	0.0139	0.0000	0.95	0.0801	0.2316	0.1675	-0.0261	-0.0406	1.00
Upper legs (*exterior*)	0.1742	-0.0153	-0.1061	0.0000	0.0170	0.99	0.0430	-0.1042	0.0317	0.0199	0.0000	0.98
Upper legs (*inferior*)	0.0834	-0.0889	-0.0220	0.0300	0.0000	0.94	0.0230	-0.1424	0.1064	0.0691	-0.0413	0.98
Upper legs (*posterior*)	0.3457	-0.0614	-0.1973	0.0133	0.0210	1.00	0.1455	-0.4860	0.1043	0.0533	0.0000	0.97
Lower legs (*anterior*)	0.1902	0.0000	-0.0991	0.0000	0.0000	0.78	0.2683	0.1251	-0.0696	-0.0290	-0.0052	0.98
Lower legs (*exterior*)	0.1408	0.0000	-0.0531	0.0000	0.0000	0.94	0.1497	-0.0352	-0.0863	0.0075	0.0222	0.99
Lower legs (*inferior*)	0.1772	0.0000	-0.1455	0.0000	0.0301	0.98	0.1916	0.0331	-0.0783	0.0000	0.0000	0.98
Lower legs (*posterior*)	0.3663	0.0173	-0.1646	-0.0094	0.0097	1.00	0.3262	-0.0605	-0.2212	0.0117	0.0451	1.00
Feet (*instep*)	0.2021	0.1090	-0.0354	-0.0407	0.0000	0.91	0.3302	0.2096	-0.0540	-0.0506	0.0000	1.00
Feet (*sole*)	0.1144	-0.4391	0.3484	0.0802	-0.0973	1.00	0.1187	-0.4389	0.3513	0.0789	-0.1010	1.00

Table B.3 Polynomial of the coefficients C_o, C_1 (order 1) of the basic cosine function $f_{p,dir}$ (eq. 4.2) and the corresponding correlation coefficient, R.

Body sectors	Standing posture						Sedentary posture					
	c_{00}	c_{01}	R	c_{10}	c_{11}	R	c_{00}	c_{01}	R	c_{10}	c_{11}	R
Head	3.2183	-0.0758	0.35	-1.0279	0.0107	0.19	3.2715	-0.1356	0.53	-1.0446	0.0386	0.57
Forehead	0.1762	-0.1081	0.75	0.9432	0.0086	0.79	0.1730	-0.1101	0.74	0.9583	0.0119	0.89
Face (*anterior*)	0.1034	0.0510	0.82	0.9705	-0.0137	0.66	0.0946	0.0424	0.67	0.9811	0.0101	0.33
Face (*R & L*)	1.4099	-0.0276	0.73	-0.9990	0.0053	0.42	1.4096	-0.0142	0.40	-1.0014	-0.0033	0.66
Neck (*anterior*)	0.1090	-0.3044	0.89	0.9757	0.0795	0.81	0.0866	-0.2052	0.65	0.9928	0.0828	0.74
Neck (*R & L*)	1.5495	0.0568	0.88	-0.9948	-0.0115	0.88	1.5796	-0.0166	0.45	-1.0032	-0.0037	0.51
Neck (*posterior*)	3.9317	-0.1531	0.85	-1.2544	0.0485	0.82	3.9576	-0.2507	0.92	-1.2604	0.0763	0.93
Shoulder (*R & L*)	2.5542	-0.7017	0.87	-1.0917	0.1903	0.92	2.6405	-0.4897	0.89	-1.1059	0.1347	0.91
Thorax (*anterior*)	0.2254	-0.0646	0.36	0.9257	0.0371	0.41	0.1823	-0.0260	0.19	0.9414	0.0525	0.77
Thorax (*inferior*)	1.7660	-0.3226	0.99	-0.9774	-0.0199	0.62	1.8870	-0.3064	0.92	-1.0093	-0.0095	0.53
Thorax (*posterior*)	3.9443	-0.1067	0.72	-1.2474	0.0362	0.73	3.9725	-0.0702	0.55	-1.2560	0.0241	0.57
Abdomen (*anterior*)	0.0311	0.0496	0.99	0.9939	-0.0167	0.98	0.3130	-0.3398	0.93	0.9141	0.0886	0.96
Abdomen (*inferior*)	-1.7722	0.0630	0.49	0.9964	-0.0219	0.66	-1.9072	-0.0314	0.28	1.0295	0.0327	0.63
Abdomen (*posterior*)	3.7547	0.1105	0.75	-1.1960	-0.0328	0.74	3.8124	0.2800	0.99	-1.2112	-0.0954	0.98
Upper arm (*anterior*)	0.0441	-0.0360	0.88	0.9534	-0.0223	0.65	0.1824	-0.0975	0.96	0.9441	-0.0530	0.75
Upper arms (*exterior*)	1.5181	-0.0275	0.81	-0.9852	0.0289	0.99	1.3042	0.0558	0.93	-1.0017	-0.0010	0.18
Upper arms (*inferior*)	4.6367	0.0735	0.36	-1.0185	-0.0479	0.69	4.1611	0.2058	0.61	-1.0783	-0.0700	0.53
Upper arms (*posterior*)	3.4855	-0.2381	0.91	-1.2105	0.0413	0.87	2.8236	-0.1378	0.97	-1.1151	0.0588	0.80
Lower arms (*anterior*)	0.3282	0.0110	0.34	0.9847	-0.0029	0.42	1.4804	-0.0573	0.27	1.0000	0.0000	1.00
Lower arms (*exterior*)	1.3362	-0.0522	0.83	-0.9997	-0.0128	0.65	-0.5190	-0.1895	0.92	0.9314	0.0814	0.87
Lower arms (*inferior*)	4.4719	0.1082	0.89	-0.9886	0.0041	0.54	3.7753	0.6461	0.66	-0.8937	-0.0363	0.11
Lower arms (*posterior*)	3.2771	0.2552	0.91	-1.1789	-0.0927	0.92	1.8367	0.0566	0.71	-1.0269	-0.0412	0.86
Hands (*handback*)	1.2449	-0.1577	0.98	-1.0007	-0.0336	0.86	1.9315	-0.8627	0.95	-1.0090	0.0238	0.62
Hands (*palm*)	-4.4198	0.0184	0.26	1.0311	-0.0200	0.58	2.5396	0.7663	0.73	-1.0254	-0.1099	0.86
Upper legs (*anterior*)	0.2113	0.0786	0.93	0.9631	-0.0282	0.80	1.4677	-0.3523	0.88	0.8350	0.1600	0.92
Upper legs (*exterior*)	1.7822	-0.0052	0.08	-1.0133	0.0123	0.41	1.6596	0.0132	0.56	-1.0160	-0.0485	0.97
Upper legs (*inferior*)	-4.8471	-0.0048	0.09	1.0007	0.0033	0.77	-4.9084	0.0289	0.15	0.9945	-0.0067	0.41
Upper legs (*posterior*)	3.9764	0.1252	0.93	-1.2570	-0.0607	0.98	1.9333	0.2783	0.87	-0.9937	-0.2803	0.95
Lower legs (*anterior*)	0.1308	-0.0273	0.40	0.9623	-0.0080	0.55	0.2054	0.0719	0.73	0.9737	-0.0359	0.90
Lower legs (*exterior*)	1.5518	0.0207	0.42	-1.0029	-0.0221	0.71	1.4865	0.0171	0.77	-1.0068	-0.0269	0.82
Lower legs (*inferior*)	-4.9174	0.0436	0.65	1.0060	-0.0066	0.61	-4.8470	-0.0235	0.64	0.9991	0.0051	0.60
Lower legs (*posterior*)	3.7871	-0.0460	0.56	-1.1793	0.0035	0.14	3.6365	0.3189	0.88	-1.1438	-0.1025	0.86
Feet (*instep*)	2.3696	-0.9467	0.97	-0.7118	0.2209	0.98	2.5856	-0.0340	0.22	-0.8540	-0.0271	0.28
Feet (*sole*)	-0.6806	-0.4498	0.92	1.2242	0.3524	0.99	1.6781	0.4033	0.70	-1.2942	-0.3012	0.59

Table B.4 Polynomial of the coefficient D_l of the shading function S_h (eq. 4.7), $D_l = \sum_{j=0}^{4} d_{lj}\beta^j$ and the corresponding correlation coefficient, R.

Body sectors	Standing posture						Sedentary posture					
	d_{l0}	d_{l1}	d_{l2}	d_{l3}	d_{l4}	R	d_{l0}	d_{l1}	d_{l2}	d_{l3}	d_{l4}	R
Head	0.0000	0.0000	2.1243	-1.4816	0.0000	0.98	0.0000	0.0000	2.2067	-1.5336	0.0000	0.99
Forehead	0.0000	0.0000	0.0000	0.0000	0.0000	1.00	0.6670	0.0000	-3.7470	3.2480	-0.6164	0.98
Face (*anterior*)	0.0000	0.0000	0.0000	0.0000	0.0000	1.00	4.6866	0.0000	-2.7218	5.3366	-2.5000	0.99
Face (*R & L*)	0.1494	0.0000	-0.3568	1.5754	-0.9315	0.99	0.2106	0.0000	-0.8538	1.6030	-0.7353	0.99
Neck (*anterior*)	0.0000	0.0000	0.0000	0.0000	0.0000	1.00	2.6061	0.0000	-2.5611	4.4336	-1.9472	0.99
Neck (*R & L*)	2.5379	16.0755	10.2256	0.0000	0.0000	1.00	3.4391	20.0344	12.6911	0.0000	0.0000	0.97
Neck (*posterior*)	0.0000	0.0000	0.0000	0.0000	0.0000	1.00	0.0000	0.0000	0.0000	0.0000	0.0000	1.00
Shoulder (*R & L*)	-1.0723	-1.9802	3.7159	-4.7018	2.1357	0.68	-1.0341	-3.3306	6.8021	-7.1132	2.7330	0.89
Thorax (*anterior*)	0.0000	0.0000	0.0000	0.0000	0.0000	1.00	0.4153	-0.2248	-1.5944	1.0646	0.0000	0.98
Thorax (*inferior*)	-3.0367	0.0000	1.1617	0.0000	0.0000	0.90	-2.9529	0.7515	-0.0939	-0.5965	0.6697	0.94
Thorax (*posterior*)	0.0000	0.0000	0.0000	0.0000	0.0000	1.00	0.0000	0.0000	0.0000	0.0000	0.0000	1.00
Abdomen (*anterior*)	0.0000	0.0000	0.0000	0.0000	0.0000	1.00	1.3969	2.0986	-9.7482	5.2014	0.0000	0.99
Abdomen (*inferior*)	-3.0206	-1.7748	3.3451	1.9516	-2.4985	0.86	1.4574	0.0000	-1.5620	-0.7419	0.0000	0.99
Abdomen (*posterior*)	0.0000	0.0000	0.0000	0.0000	0.0000	1.00	0.0000	0.0000	0.0000	0.0000	0.0000	1.00
Upper arm (*anterior*)	-1.8501	2.7489	-4.4776	-3.1264	3.4099	0.86	-0.9564	1.1929	-1.6068	0.0000	0.0000	0.97
Upper arms (*exterior*)	0.0000	0.0000	0.0000	0.0000	0.0000	1.00	-0.6502	0.1639	0.0000	0.0000	0.0000	0.32
Upper arms (*inferior*)	-6.9680	-9.0647	-3.9213	9.8125	0.0000	0.91	-3.9473	0.9995	0.4234	-0.5652	0.6601	0.91
Upper arms (*posterior*)	0.0000	0.0000	0.0000	0.0000	0.0000	1.00	0.0000	0.0000	0.0000	0.0000	0.0000	1.00
Lower arms (*anterior*)	-3.1354	-1.7318	1.1750	0.4795	0.0000	0.97	-0.5390	-0.5152	-0.5088	0.0000	0.0000	0.74
Lower arms (*exterior*)	0.0000	0.0000	0.0000	0.0000	0.0000	1.00	3.4530	-0.9880	-2.1862	0.6503	0.3333	0.99
Lower arms (*inferior*)	-4.9677	-1.3673	-2.7141	0.9911	1.8224	0.84	-2.3530	-1.0638	-0.8040	0.0000	0.0000	0.84
Lower arms (*posterior*)	0.1584	1.0956	-2.0176	0.0000	0.0000	0.83	0.0000	0.0000	0.0000	0.0000	0.0000	1.00
Hands (*handback*)	0.0502	-0.1554	-0.2115	0.5317	-0.2105	0.99	-1.0267	-0.3723	-1.5312	0.0000	0.9131	0.93
Hands (*palm*)	-2.9380	-0.9203	-0.7716	0.5989	0.7053	0.90	0.0000	0.0000	0.0000	0.0000	0.0000	1.00
Upper legs (*anterior*)	0.0000	0.0000	0.0000	0.0000	0.0000	1.00	-2.1922	-2.8941	2.5620	0.0000	0.0000	0.75
Upper legs (*exterior*)	-2.0042	0.0000	0.0000	-3.7234	2.6851	0.94	0.0000	0.0000	0.0000	0.0000	0.0000	1.00
Upper legs (*inferior*)	-3.1402	0.6251	0.4658	0.0000	0.0000	0.50	1.9956	0.0723	-1.5393	0.0000	0.0000	0.57
Upper legs (*posterior*)	0.0000	0.0000	0.0000	0.0000	0.0000	1.00	-0.1230	-2.9899	3.0351	1.9843	-1.2342	0.91
Lower legs (*anterior*)	4.5282	18.1753	15.9558	0.0000	0.0000	1.00	0.0000	0.0000	0.0000	0.0000	0.0000	1.00
Lower legs (*exterior*)	0.0000	0.0000	0.0000	0.0000	0.0000	1.00	0.0000	0.0000	0.0000	0.0000	0.0000	1.00
Lower legs (*inferior*)	-6.4414	-2.7161	5.0126	1.7925	-3.2889	0.91	-3.4430	1.7018	-1.1214	-1.1578	1.3723	0.82
Lower legs (*posterior*)	-8.4381	-1.4005	3.5985	0.0000	0.0000	0.85	-1.7804	-6.3434	-3.5564	0.0000	0.0000	0.99
Feet (*instep*)	-1.6535	-0.0277	0.4633	0.0000	0.0000	0.82	-0.8878	-0.5349	0.1774	0.0000	0.0000	0.99
Feet (*sole*)	0.0000	0.0000	0.0000	0.0000	0.0000	1.00	-0.2624	-0.0139	0.0982	0.0000	0.0000	0.73

Table B.5 Polynomial of the coefficient D_o of the shading function S_h (eq. 4.7), $D_0 = \sum_{j=0}^{4} d_{0j}\beta^j$ and the corresponding correlation coefficient, R.

Body sectors	Standing posture						Sedentary posture					
	d_{00}	d_{01}	d_{02}	d_{03}	d_{04}	R	d_{00}	d_{01}	d_{02}	d_{03}	d_{04}	R
Head	10.3361	0.0000	-3.5647	7.9337	-3.7827	1.00	10.4314	0.0000	-4.3398	7.9768	-3.4768	1.00
Forehead	10.0000	0.0000	0.0000	0.0000	0.0000	1.00	10.4341	0.0000	-1.3449	4.0352	-2.1992	0.99
Face (*ant*)	9.4813	0.0000	0.0000	1.9329	-1.1810	0.99	10.5145	0.0000	-2.1120	3.8723	-1.7547	0.99
Face (*R & L*)	9.8010	0.0000	-2.1483	2.5356	-0.6751	0.99	9.7467	0.0000	-1.7072	2.5111	-0.8491	1.00
Neck (*ant*)	10.0000	0.0000	0.0000	0.0000	0.0000	1.00	10.5755	0.0000	-2.5097	4.0732	-1.7210	0.99
Neck (*R & L*)	11.4732	17.9303	12.2371	0.0000	0.0000	0.95	10.6149	14.1602	9.8892	0.0000	0.0000	0.99
Neck (*post*)	10.0000	0.0000	0.0000	0.0000	0.0000	1.00	10.0000	0.0000	0.0000	0.0000	0.0000	1.00
Shoulder (*R & L*)	10.3034	-26.4505	56.1918	-38.1416	6.9506	0.74	4.1224	6.3639	-6.0508	9.1870	-5.2962	0.89
Thorax (*anterior*)	10.0000	0.0000	0.0000	0.0000	0.0000	1.00	11.6820	-0.7202	-6.6952	4.3811	0.0000	0.99
Thorax (*inferior*)	3.8386	1.5992	-2.7123	-0.7325	1.2644	0.90	3.7794	-0.0232	-1.9355	0.6206	0.7007	0.96
Thorax (*posterior*)	10.0000	0.0000	0.0000	0.0000	0.0000	1.00	10.0000	0.0000	0.0000	0.0000	0.0000	1.00
Abdomen (*anterior*)	10.0000	0.0000	0.0000	0.0000	0.0000	1.00	10.8156	3.0347	-9.1398	4.5321	0.0000	0.99
Abdomen (*inferior*)	2.7049	2.1210	-3.2983	-1.9899	2.6563	0.92	-1.3787	0.0000	2.3163	0.0000	0.0000	0.93
Abdomen (*posterior*)	10.0000	0.0000	0.0000	0.0000	0.0000	1.00	10.0000	0.0000	0.0000	0.0000	0.0000	1.00
Upper arm (*anterior*)	6.0537	-10.8155	13.1404	9.7346	-9.8565	0.87	2.4926	-3.2681	3.9089	0.0000	0.0000	0.98
Upper arms (*exterior*)	10.0000	0.0000	0.0000	0.0000	0.0000	1.00	2.6426	0.7729	0.7735	0.0000	0.0000	0.88
Upper arms (*inferior*)	29.6416	33.2135	15.4305	-34.8845	0.0000	0.88	18.0169	-6.1854	-2.9952	4.2138	-1.2817	0.85
Upper arms (*posterior*)	10.0000	0.0000	0.0000	0.0000	0.0000	1.00	10.0000	0.0000	0.0000	0.0000	0.0000	1.00
Lower arms (*anterior*)	5.2125	2.4462	-1.4207	0.0000	0.0000	0.90	0.3278	0.8296	3.0252	0.0000	0.0000	0.90
Lower arms (*exterior*)	10.0000	0.0000	0.0000	0.0000	0.0000	1.00	1.0322	4.2261	3.3716	0.0000	0.0000	0.96
Lower arms (*inferior*)	21.6965	3.6908	4.7572	-2.7104	-4.2297	0.68	9.0887	4.2082	4.5331	0.0000	0.0000	0.86
Lower arms (*posterior*)	10.0379	-3.1011	3.8970	0.0000	0.0000	0.73	10.0000	0.0000	0.0000	0.0000	0.0000	1.00
Hands (*handback*)	11.0207	0.0960	-7.5119	1.7539	4.5080	0.79	2.2893	1.6263	2.0569	0.0000	0.0000	1.00
Hands (*palm*)	11.0700	3.0451	1.0763	-1.8525	-1.4769	0.73	10.0000	0.0000	0.0000	0.0000	0.0000	1.00
Upper legs (*anterior*)	10.0000	0.0000	0.0000	0.0000	0.0000	1.00	7.8801	-9.0053	6.7207	0.0000	0.0000	0.91
Upper legs (*exterior*)	0.9293	0.0000	0.0000	-5.3392	4.7304	0.95	10.0000	0.0000	0.0000	0.0000	0.0000	1.00
Upper legs (*inferior*)	12.5772	-6.6444	-5.6097	0.0000	0.0000	0.88	-9.9710	0.2150	10.8661	0.0000	0.0000	0.77
Upper legs (*posterior*)	10.0000	0.0000	0.0000	0.0000	0.0000	1.00	1.2488	5.7338	2.7077	-1.6714	0.0000	0.98
Lower legs (*anterior*)	24.2222	21.2884	0.0000	0.0000	0.0000	0.99	10.0000	0.0000	0.0000	0.0000	0.0000	1.00
Lower legs (*exterior*)	10.0000	0.0000	0.0000	0.0000	0.0000	1.00	10.0000	0.0000	0.0000	0.0000	0.0000	1.00
Lower legs (*inferior*)	28.0742	12.2207	-19.8894	-8.2236	12.679	0.90	16.0125	-10.1503	-2.2190	5.4286	-0.7394	0.77
Lower legs (*posterior*)	37.8126	5.1634	-12.9276	0.0000	0.0000	0.80	9.8134	5.4458	17.6432	0.0000	0.0000	1.00
Feet (*instep*)	5.1013	0.1025	-1.0893	0.0000	0.0000	0.79	2.0440	1.5734	-0.3840	0.0000	0.0000	0.99
Feet (*sole*)	1.9893	0.0000	3.8397	0.0000	0.0000	0.93	1.2304	-4.4256	2.8276	0.0000	0.0000	0.99

Table B.6 Polynomial of the coefficient E_1 of the shading function S_h (eq. 4.7), $E_1 = \sum_{j=0}^{4} e_{1j}\beta^j$ and the corresponding correlation coefficient, R.

Body sectors	Standing posture						Sedentary posture					
	e_{10}	e_{11}	e_{12}	e_{13}	e_{14}	R	e_{10}	e_{11}	e_{12}	e_{13}	e_{14}	R
Head	0.0000	0.0000	0.0000	0.0000	0.0000	1.00	0.0000	0.0000	0.0000	0.0000	0.0000	1.00
Forehead	0.0000	0.0000	0.0000	0.0000	0.0000	1.00	-0.4162	0.0000	1.5095	-3.4811	1.7460	0.99
Face (*ant*)	0.0000	0.0000	0.0000	0.0000	0.0000	1.00	-2.3848	0.0000	1.5508	-2.9470	1.3599	0.99
Face (*R & L*)	-0.1427	0.0000	0.7756	-0.7405	0.1746	0.98	-0.1022	0.0000	0.4464	-0.7221	0.3045	0.99
Neck (*ant*)	0.0000	0.0000	0.0000	0.0000	0.0000	1.00	-0.3483	0.0000	1.3525	-2.7572	1.3150	0.99
Neck (*R & L*)	1.0987	-6.3795	-5.0699	0.0000	0.0000	0.97	0.4877	-9.0637	-6.7416	0.0000	0.0000	1.00
Neck (*post*)	0.0000	0.0000	0.0000	0.0000	0.0000	1.00	0.0000	0.0000	0.0000	0.0000	0.0000	1.00
Shoulder (*R & L*)	0.0210	6.8935	-7.1246	2.2240	-0.2474	0.98	1.9987	-5.1473	26.6276	-28.0890	8.1664	1.00
Thorax (*ant*)	0.0000	0.0000	0.0000	0.0000	0.0000	1.00	-0.3641	0.1502	1.4563	-0.9504	0.0000	0.99
Thorax (*inf*)	0.8344	0.4919	2.2280	0.5675	-0.7903	1.00	0.5656	0.2764	0.7358	-0.0420	-0.4450	0.99
Thorax (*post*)	0.0000	0.0000	0.0000	0.0000	0.0000	1.00	0.0000	0.0000	0.0000	0.0000	0.0000	1.00
Abdomen (*anterior*)	0.0000	0.0000	0.0000	0.0000	0.0000	1.00	-0.3302	-0.9457	3.1923	-1.6228	0.0000	0.99
Abdomen (*inferior*)	1.1879	0.0000	0.2047	0.0000	0.0000	0.77	-0.3063	0.0000	1.5224	1.0169	0.0000	0.99
Abdomen (*posterior*)	0.0000	0.0000	0.0000	0.0000	0.0000	1.00	0.0000	0.0000	0.0000	0.0000	0.0000	1.00
Upper arm (*anterior*)	5.5679	1.9454	-1.2164	-1.8151	0.2334	1.00	6.0685	3.0772	-2.6042	0.0000	0.0000	0.72
Upper arms (*exterior*)	0.0000	0.0000	0.0000	0.0000	0.0000	1.00	0.0000	0.0000	0.0000	0.0000	0.0000	1.00
Upper arms (*inferior*)	4.8875	-1.4485	-1.6965	0.0000	0.0000	0.92	0.0000	0.0000	0.0000	0.0000	0.0000	1.00
Upper arms (*posterior*)	0.0000	0.0000	0.0000	0.0000	0.0000	1.00	0.0000	0.0000	0.0000	0.0000	0.0000	1.00
Lower arms (*anterior*)	5.9843	1.6183	-1.9134	0.0000	0.0000	0.97	4.1228	-4.0001	2.0945	0.0000	0.0000	1.00
Lower arms (*exterior*)	0.0000	0.0000	0.0000	0.0000	0.0000	1.00	0.0000	0.0000	0.0000	0.0000	0.0000	1.00
Lower arms (*inferior*)	3.2063	0.2261	3.1669	-0.1365	-1.7135	0.96	-0.3640	-0.5760	1.6984	0.0000	0.0000	0.99
Lower arms (*posterior*)	-0.2635	0.0000	0.0000	-1.2257	0.8901	0.93	0.0000	0.0000	0.0000	0.0000	0.0000	1.00
Hands (*handback*)	-0.2466	0.1938	1.6008	-1.0277	-0.5032	0.97	4.4608	1.8997	1.3831	0.0000	-1.7785	0.99
Hands (*palm*)	6.2294	4.2117	-3.6825	-3.0284	1.2923	0.94	0.0000	0.0000	0.0000	0.0000	0.0000	1.00
Upper legs (*anterior*)	0.0000	0.0000	0.0000	0.0000	0.0000	1.00	1.7368	4.8871	-3.8096	0.0000	0.0000	0.99
Upper legs (*exterior*)	2.0285	0.0000	0.0000	2.3639	-1.8052	0.93	0.0000	0.0000	0.0000	0.0000	0.0000	1.00
Upper legs (*inferior*)	4.1699	0.8301	-0.7613	0.0000	0.0000	0.74	0.0000	0.0000	0.0000	0.0000	0.0000	1.00
Upper legs (*posterior*)	0.0000	0.0000	0.0000	0.0000	0.0000	1.00	4.4658	0.0000	-4.1471	0.0000	0.0000	0.99
Lower legs (*anterior*)	0.0000	0.0000	0.0000	0.0000	0.0000	1.00	0.0000	0.0000	0.0000	0.0000	0.0000	1.00
Lower legs (*exterior*)	0.0000	0.0000	0.0000	0.0000	0.0000	1.00	0.0000	0.0000	0.0000	0.0000	0.0000	1.00
Lower legs (*inferior*)	6.3573	2.2542	-6.3098	-0.4738	2.9125	0.99	5.4745	0.6065	-4.2618	-0.3291	0.8452	0.94
Lower legs (*posterior*)	6.6866	0.7040	-2.8396	0.0000	0.0000	0.91	0.3438	1.6788	0.8795	0.0000	0.0000	0.98
Feet (*instep*)	1.2117	0.1377	0.4531	0.0000	0.0000	0.53	0.7784	-0.2893	0.3042	0.0000	0.0000	0.92
Feet (*sole*)	0.0000	0.0000	0.0000	0.0000	0.0000	1.00	0.0000	0.0000	0.0000	0.0000	0.0000	1.00

Table B.7 Polynomial of the coefficient E_o of the shading function S_h (eq. 4.7), $E_0 = \sum_{j=0}^{4} e_{0j}\beta^j$ and the corresponding correlation coefficient, R.

Body sectors	Standing posture						Sedentary posture					
	e_{oo}	e_{o1}	e_{o2}	e_{o3}	e_{o4}	R	e_{oo}	e_{o1}	e_{o2}	e_{o3}	e_{o4}	R
Head	-10.0000	0.0000	0.0000	0.0000	0.0000	1.00	-10.0000	0.0000	0.0000	0.0000	0.0000	1.00
Forehead	-10.0000	0.0000	0.0000	0.0000	0.0000	1.00	-10.3862	0.0000	1.5419	-2.9823	1.3881	0.99
Face (*ant*)	-10.0000	0.0000	0.0000	0.0000	0.0000	1.00	-10.4127	0.0000	1.6100	-3.2543	1.5461	0.99
Face (*R & L*)	-10.2218	0.0000	0.4719	-2.4400	1.4776	0.99	-10.3251	0.0000	1.3117	-2.4867	1.1462	0.99
Neck (*ant*)	-10.0000	0.0000	0.0000	0.0000	0.0000	1.00	-8.4190	0.0000	-6.4429	11.9803	-5.4684	0.99
Neck (*R & L*)	-14.1539	-21.2960	-13.2377	0.0000	0.0000	0.96	-13.0235	-16.3302	-10.1451	0.0000	0.0000	1.00
Neck (*post*)	-10.0000	0.0000	0.0000	0.0000	0.0000	1.00	-10.0000	0.0000	0.0000	0.0000	0.0000	1.00
Shoulder (*R & L*)	-10.1151	25.8754	-90.9687	92.9137	-27.7784	0.96	-10.0158	32.1237	-166.178	178.165	-53.2005	1.00
Thorax (*ant*)	-10.0000	0.0000	0.0000	0.0000	0.0000	1.00	-11.4243	0.0000	5.7636	-3.4827	0.0000	0.98
Thorax (*inf*)	-2.7918	-1.9526	-1.9129	0.0000	0.0000	0.98	-1.2320	-1.2462	-1.3267	1.1794	-1.2974	0.99
Thorax (*post*)	-10.0000	0.0000	0.0000	0.0000	0.0000	1.00	-10.0000	0.0000	0.0000	0.0000	0.0000	1.00
Abdomen (*anterior*)	-10.0000	0.0000	0.0000	0.0000	0.0000	1.00	-10.9460	-3.2629	10.1397	-5.0642	0.0000	0.99
Abdomen (*inferior*)	-1.7232	0.0000	-0.8957	0.0000	0.0000	0.80	-10.5902	0.0000	2.4067	1.5865	0.0000	0.99
Abdomen (*posterior*)	-10.0000	0.0000	0.0000	0.0000	0.0000	1.00	-10.0000	0.0000	0.0000	0.0000	0.0000	1.00
Upper arm (*anterior*)	-32.1692	-11.3790	12.9772	11.0889	-5.5058	0.99	-33.3682	-20.3675	10.4118	8.6932	0.0000	0.84
Upper arms (*exterior*)	-10.0000	0.0000	0.0000	0.0000	0.0000	1.00	-10.0000	0.0000	0.0000	0.0000	0.0000	1.00
Upper arms (*inferior*)	-27.6956	6.1865	6.2285	0.0000	0.0000	0.86	-10.0000	0.0000	0.0000	0.0000	0.0000	1.00
Upper arms (*posterior*)	-10.0000	0.0000	0.0000	0.0000	0.0000	1.00	-10.0000	0.0000	0.0000	0.0000	0.0000	1.00
Lower arms (*anterior*)	-30.6274	-8.9154	10.2034	0.0000	0.0000	0.99	-19.5739	14.3501	-5.7091	0.0000	0.0000	1.00
Lower arms (*exterior*)	-10.0000	0.0000	0.0000	0.0000	0.0000	1.00	-10.0000	0.0000	0.0000	0.0000	0.0000	1.00
Lower arms (*inferior*)	-17.8900	-0.5767	-12.7708	0.2522	6.4200	0.96	-3.9132	0.0000	-7.8159	0.0000	0.0000	0.92
Lower arms (*posterior*)	-8.8667	0.0000	0.0000	5.2726	-3.8289	0.93	-10.0000	0.0000	0.0000	0.0000	0.0000	1.00
Hands (*handback*)	-10.3122	-0.5993	2.8599	1.0495	-2.9175	0.99	-22.6841	-2.2215	-6.8150	6.3853	0.0000	0.98
Hands (*palm*)	-31.3503	-19.9270	24.5164	14.5318	-10.8305	0.94	-10.0000	0.0000	0.0000	0.0000	0.0000	1.00
Upper legs (*anterior*)	-10.0000	0.0000	0.0000	0.0000	0.0000	1.00	-8.1428	-12.4157	8.9144	0.0000	0.0000	0.86
Upper legs (*exterior*)	-1.6672	0.0000	0.0000	2.6364	-2.9436	0.97	-10.0000	0.0000	0.0000	0.0000	0.0000	1.00
Upper legs (*inferior*)	-21.8710	-4.5993	4.3609	0.0000	0.0000	0.76	-10.0000	0.0000	0.0000	0.0000	0.0000	1.00
Upper legs (*posterior*)	-10.0000	0.0000	0.0000	0.0000	0.0000	1.00	-17.6655	1.0177	2.0342	0.0000	0.0000	0.90
Lower legs (*anterior*)	-10.0000	0.0000	0.0000	0.0000	0.0000	1.00	-10.0000	0.0000	0.0000	0.0000	0.0000	1.00
Lower legs (*exterior*)	-10.0000	0.0000	0.0000	0.0000	0.0000	1.00	-10.0000	0.0000	0.0000	0.0000	0.0000	1.00
Lower legs (*inferior*)	-31.6186	-11.2602	31.7201	1.8429	-15.4226	0.99	-26.7778	-3.0897	23.5334	2.2884	-7.5920	0.90
Lower legs (*posterior*)	-38.5826	-2.3193	13.7304	0.0000	0.0000	0.81	-2.7314	0.0000	-7.6802	-3.5505	0.0000	0.97
Feet (*instep*)	-4.3581	-1.1838	-2.3067	0.0000	0.0000	0.72	-3.0855	1.3211	-0.9556	0.0000	0.0000	0.88
Feet (*sole*)	-10.0000	0.0000	0.0000	0.0000	0.0000	1.00	-10.0000	0.0000	0.0000	0.0000	0.0000	1.00

Table B.8 Polynomial of the coefficients g_0, g_1 of the $f_{p,dif}$ function for the diffuse short-wave radiation (eq. 4.8) and the corresponding correlation coefficient, *R*.

Body sectors	Standing posture			Sedentary posture		
	g_0	g_1	*R*	g_0	g_1	*R*
Head	0.6460	0.3183	1.00	0.6423	0.3211	1.00
Forehead	0.5194	0.4675	1.00	0.5295	0.4495	1.00
Face (*anterior*)	0.3701	0.4716	1.00	0.3777	0.4465	1.00
Face (*R & L*)	0.4318	0.4588	1.00	0.4354	0.4488	1.00
Neck (*anterior*)	0.3425	0.4367	1.00	0.3532	0.4137	1.00
Neck (*R & L*)	0.5441	0.3115	1.00	0.5360	0.2945	1.00
Neck (*posterior*)	0.5783	0.3650	1.00	0.5671	0.3757	1.00
Shoulder (*R & L*)	0.8119	0.0927	1.00	0.7982	0.0866	1.00
Thorax (*anterior*)	0.5603	0.3711	1.00	0.5723	0.3399	1.00
Thorax (*inferior*)	0.1365	0.2998	1.00	0.1540	0.3016	1.00
Thorax (*posterior*)	0.4850	0.4739	1.00	0.4892	0.4995	1.00
Abdomen (*anterior*)	0.3970	0.4954	1.00	0.3101	0.1801	1.00
Abdomen (*inferior*)	0.3213	0.3103	1.00	0.2879	0.3810	1.00
Abdomen (*posterior*)	0.4328	0.4558	1.00	0.4025	0.7381	1.00
Upper arm (*anterior*)	0.3505	0.4036	1.00	0.2165	0.2585	1.00
Upper arms (*exterior*)	0.6009	0.3813	1.00	0.5771	0.3760	1.00
Upper arms (*inferior*)	0.0698	0.2650	1.00	0.1745	0.4221	1.00
Upper arms (*posterior*)	0.4745	0.4576	1.00	0.5701	0.4464	1.00
Lower arms (*anterior*)	0.5132	0.3639	1.00	0.3529	0.0726	1.00
Lower arms (*exterior*)	0.5102	0.4861	1.00	0.6486	0.2182	1.00
Lower arms (*inferior*)	0.2196	0.2847	1.00	0.1281	0.4863	1.00
Lower arms (*posterior*)	0.3473	0.6165	1.00	0.3101	0.7620	1.00
Hands (*handback*)	0.3966	0.4861	1.00	0.6053	0.1090	1.00
Hands (*palm*)	0.1879	0.1894	1.00	0.0757	0.1787	1.00
Upper legs (*anterior*)	0.4106	0.4619	1.00	0.6037	0.1081	1.00
Upper legs (*exterior*)	0.3929	0.4865	1.00	0.0759	0.1838	1.00
Upper legs (*inferior*)	0.1753	0.2928	1.00	0.4142	0.0168	1.00
Upper legs (*posterior*)	0.4181	0.5203	1.00	0.3131	0.4627	1.00
Lower legs (*anterior*)	0.4374	0.4898	1.00	0.2558	0.3077	1.00
Lower legs (*exterior*)	0.4740	0.5064	1.00	0.0351	0.9104	1.00
Lower legs (*inferior*)	0.3359	0.3918	1.00	0.5861	0.4270	1.00
Lower legs (*posterior*)	0.4673	0.4728	1.00	0.4269	0.4972	1.00
Feet (*instep*)	0.5608	0.3005	1.00	0.3663	0.3743	1.00
Feet (*sole*)	0.0309	0.8656	1.00	0.2613	0.4480	1.00

Appendix C

View factors for some main body parts as predicted by developed model and voxel-based ray tracing technique

C.1 Standing posture: Front wall 1 m.

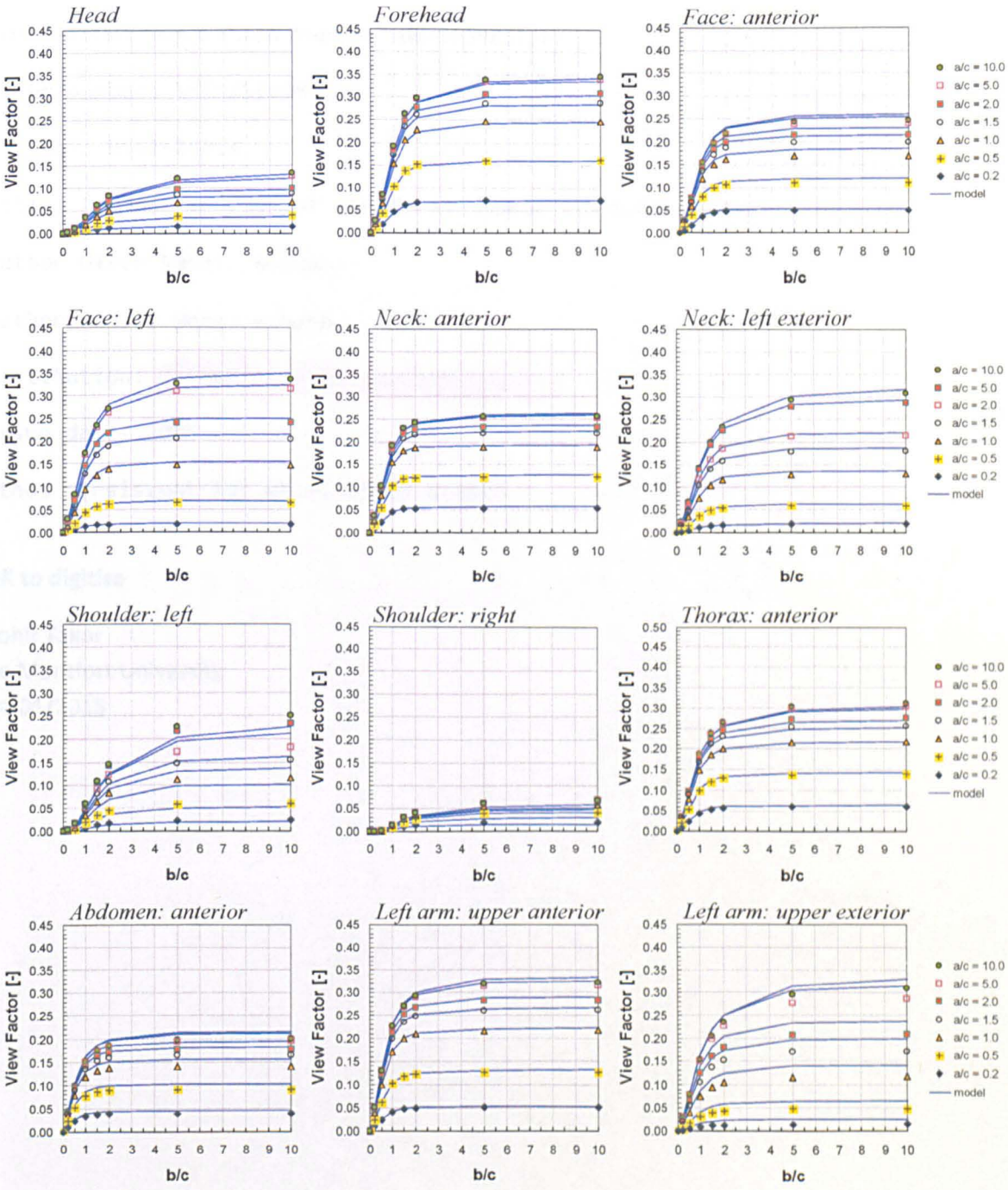

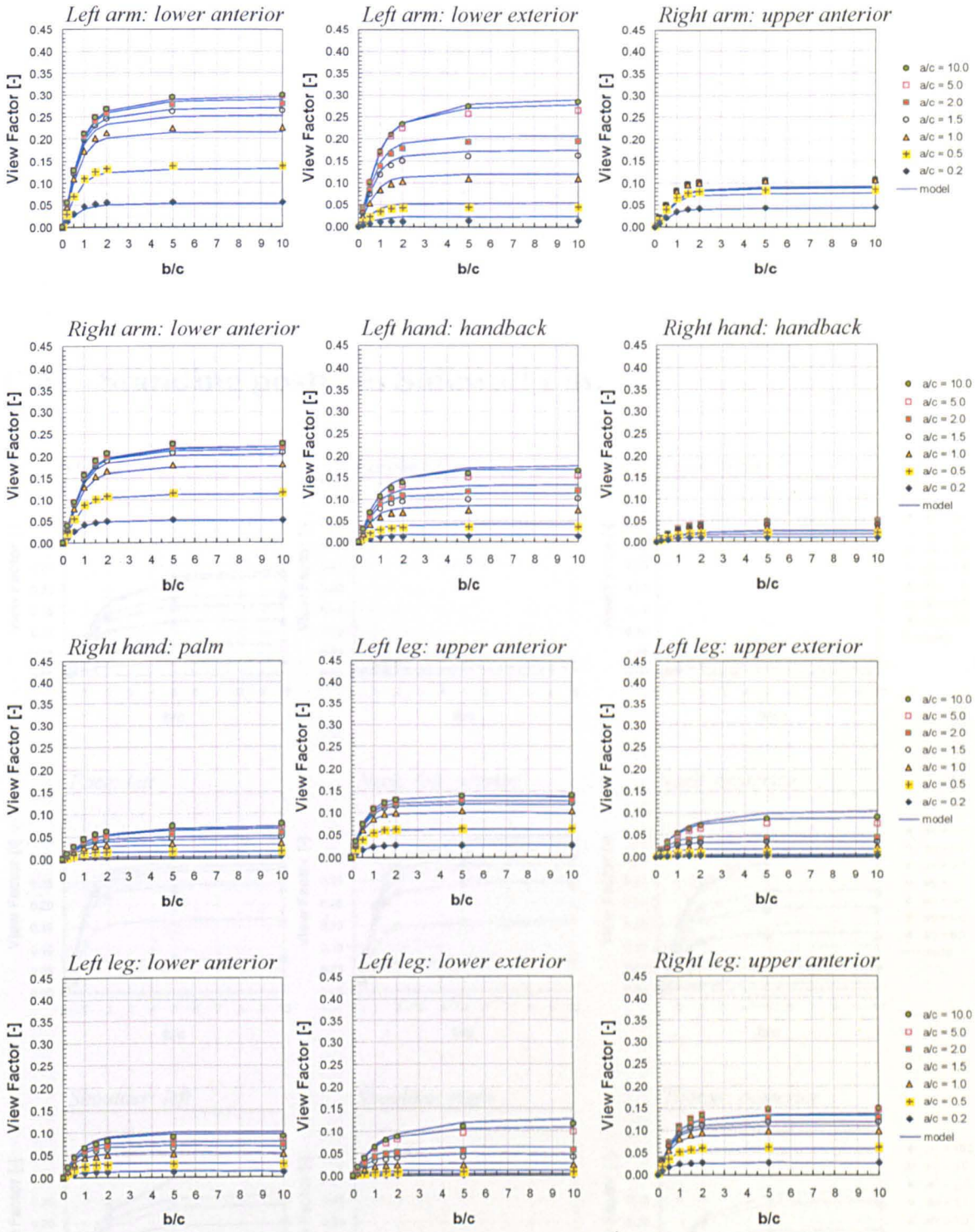
Left arm: lower anterior
Left arm: lower exterior
Right arm: upper anterior
Right arm: lower anterior
Left hand: handback
Right hand: handback
Right hand: palm
Left leg: upper anterior
Left leg: upper exterior
Left leg: lower anterior
Left leg: lower exterior
Right leg: upper anterior
View Factor [-]
b/c
a/c = 10.0
a/c = 5.0
a/c = 2.0
a/c = 1.5
a/c = 1.0
a/c = 0.5
a/c = 0.2
model

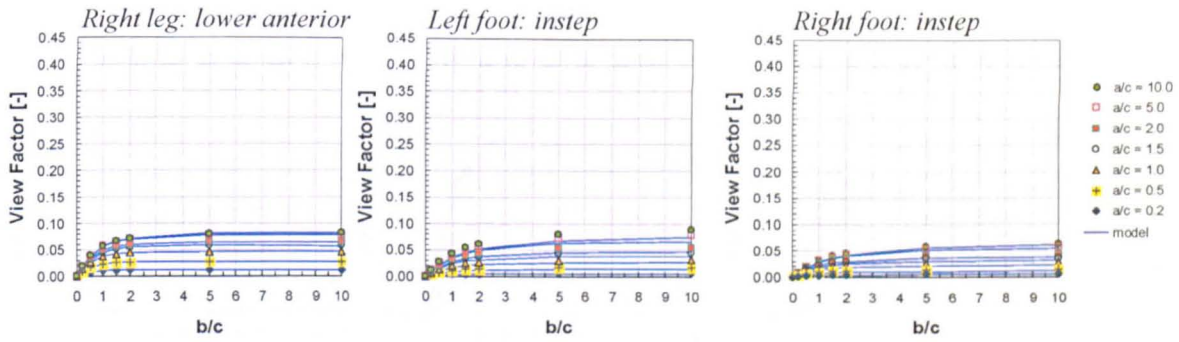

C.2 Standing posture: Sidewall 1 m.

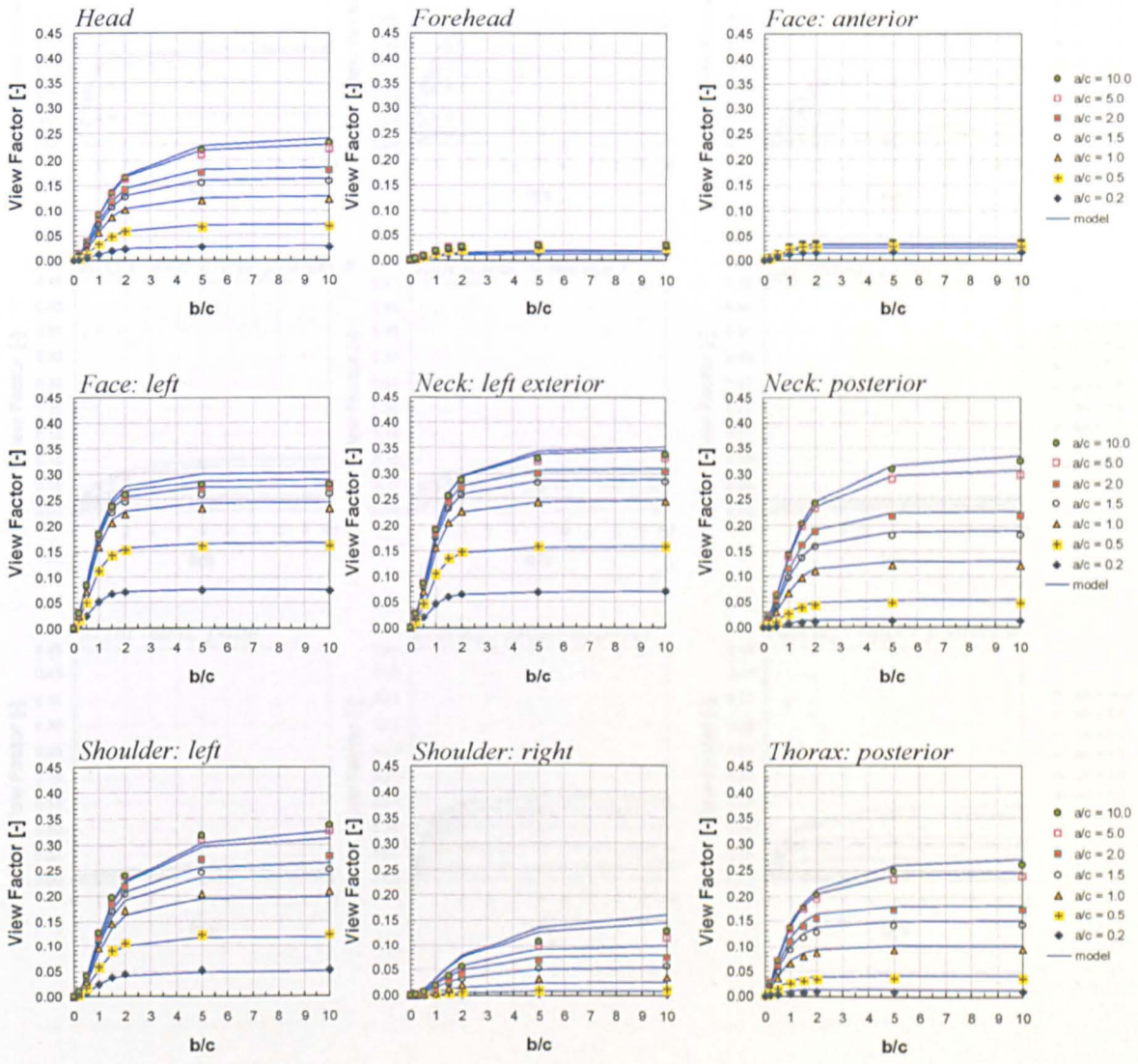

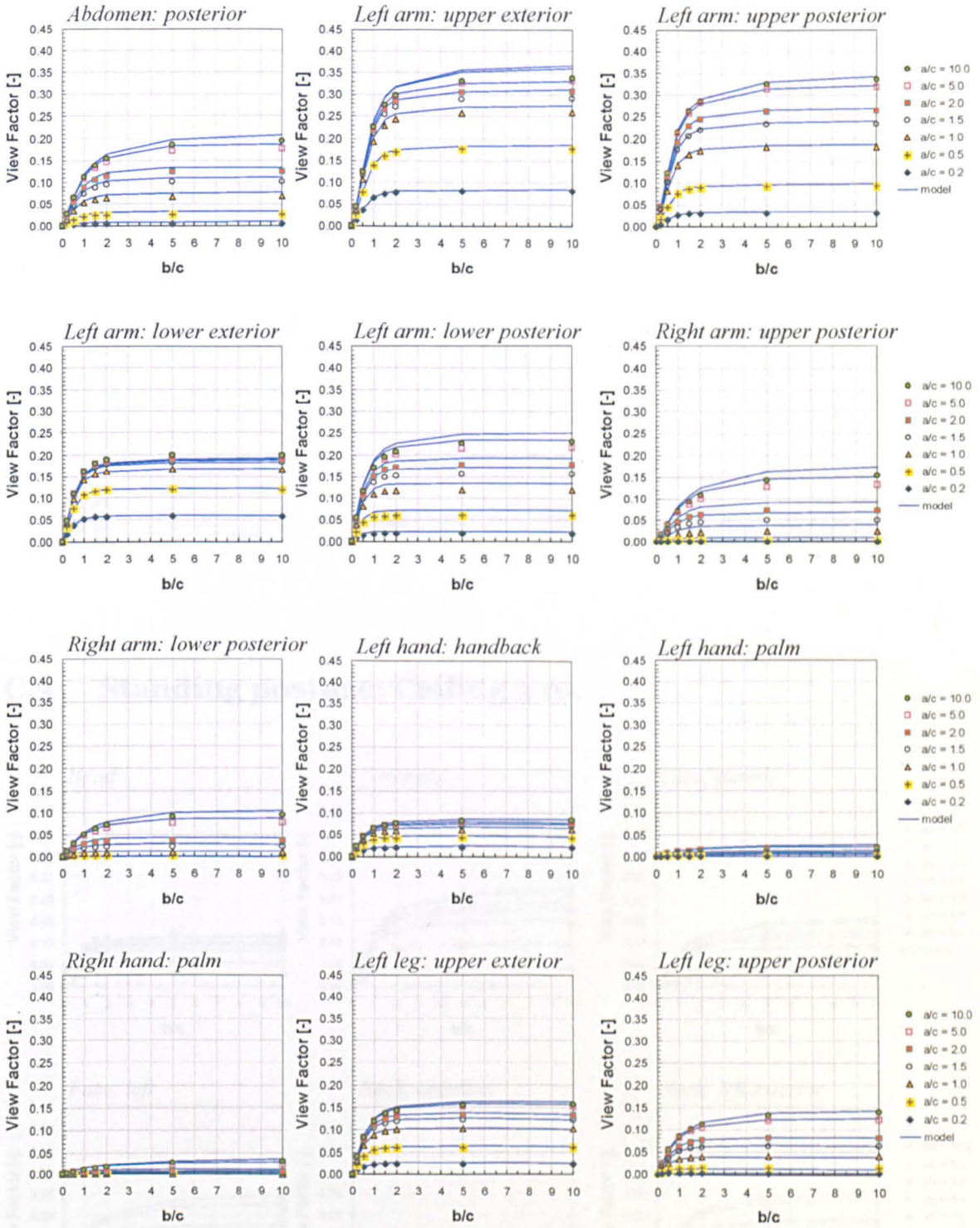
Abdomen: posterior
Left arm: upper exterior
Left arm: upper posterior
Left arm: lower exterior
Left arm: lower posterior
Right arm: upper posterior
Right arm: lower posterior
Left hand: handback
Left hand: palm
Right hand: palm
Left leg: upper exterior
Left leg: upper posterior
View Factor [-]
b/c
a/c = 10.0
a/c = 5.0
a/c = 2.0
a/c = 1.5
a/c = 1.0
a/c = 0.5
a/c = 0.2
model

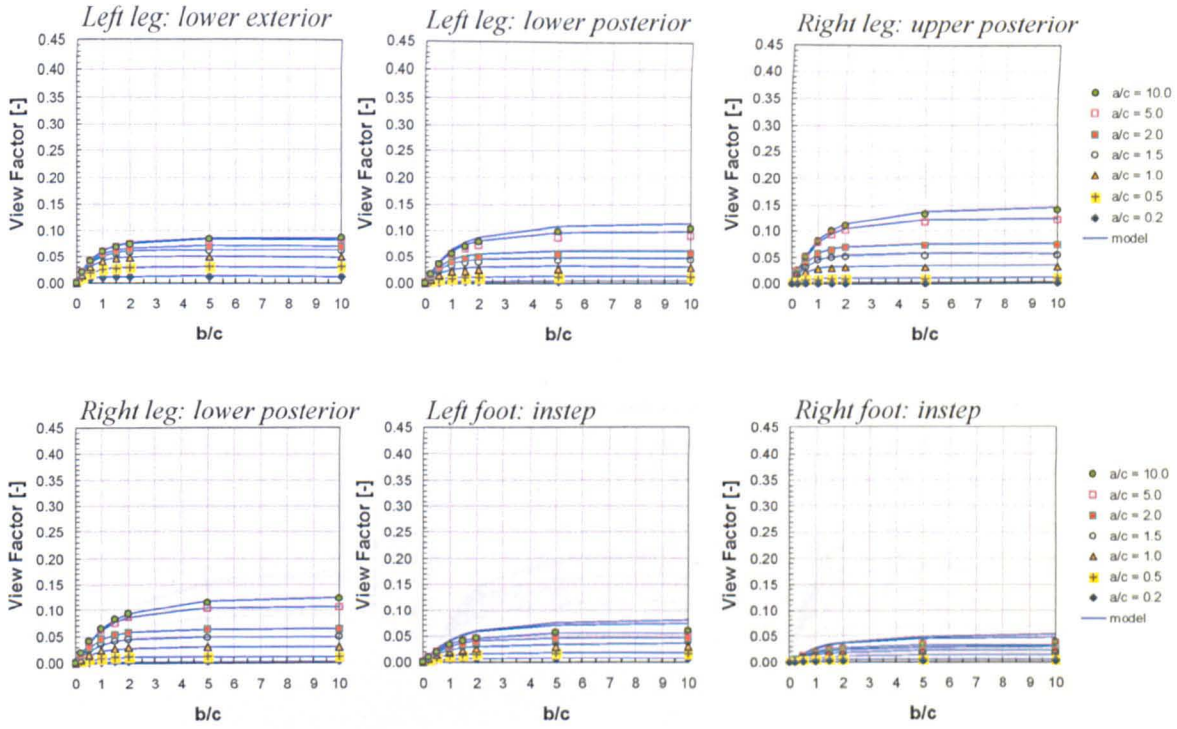

C.3 Standing posture: Ceiling 3 m.

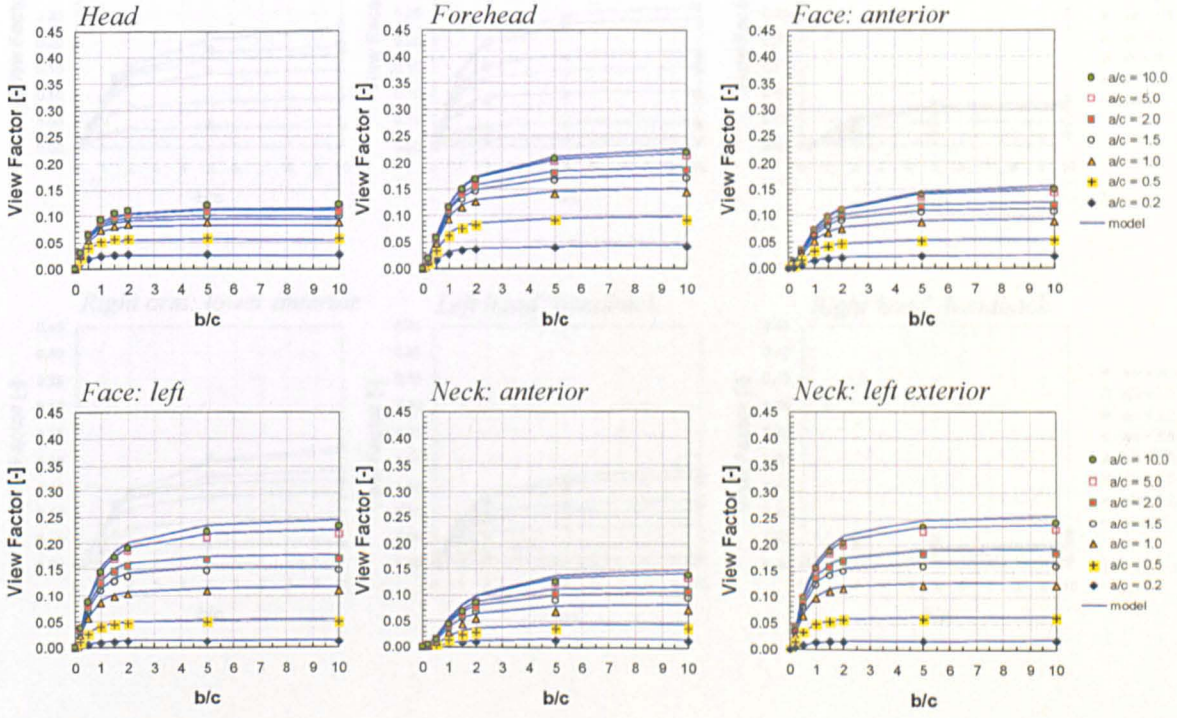

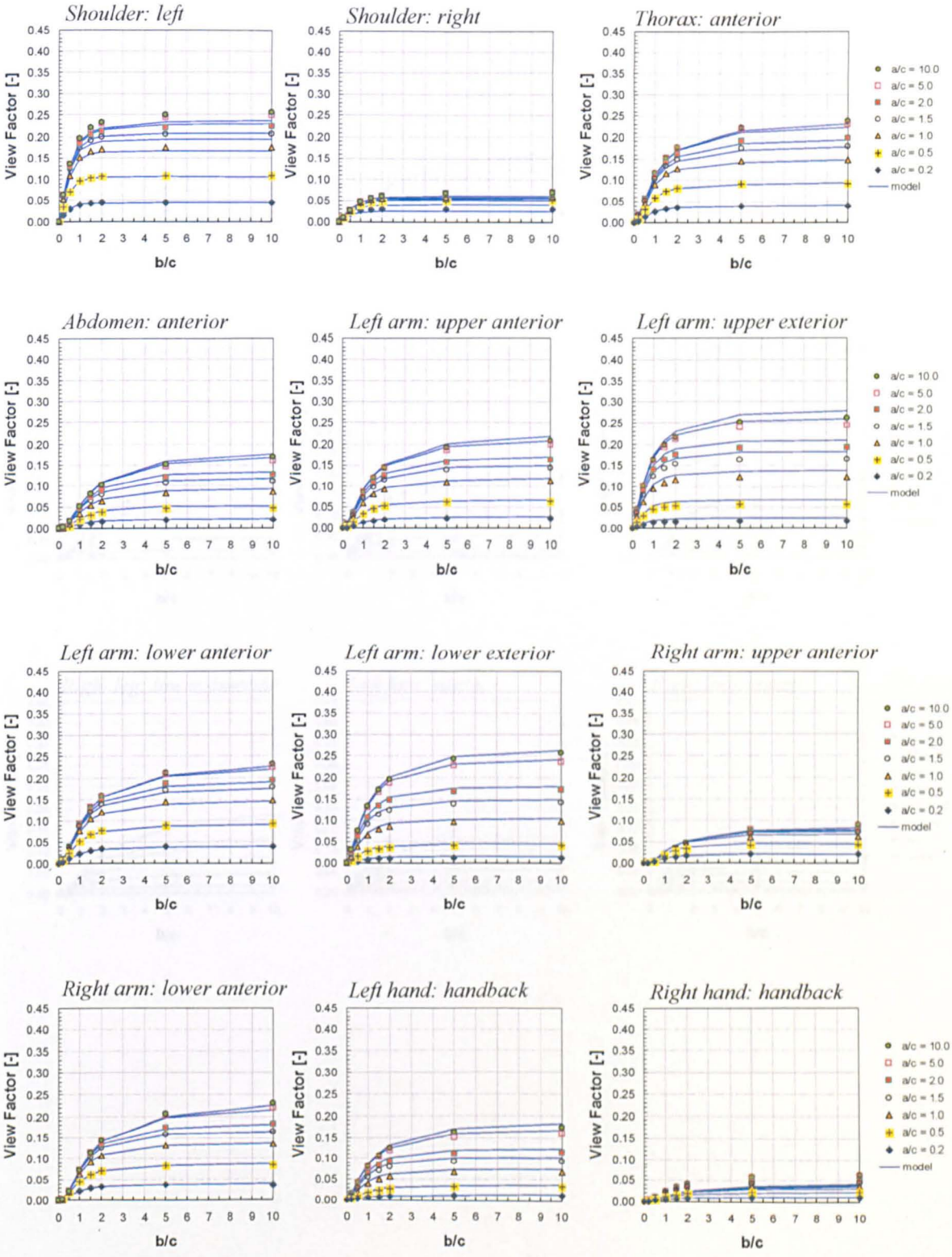
Shoulder: left
Shoulder: right
Thorax: anterior
Abdomen: anterior
Left arm: upper anterior
Left arm: upper exterior
Left arm: lower anterior
Left arm: lower exterior
Right arm: upper anterior
Right arm: lower anterior
Left hand: handback
Right hand: handback
View Factor [-]
b/c
a/c = 10.0
a/c = 5.0
a/c = 2.0
a/c = 1.5
a/c = 1.0
a/c = 0.5
a/c = 0.2
model

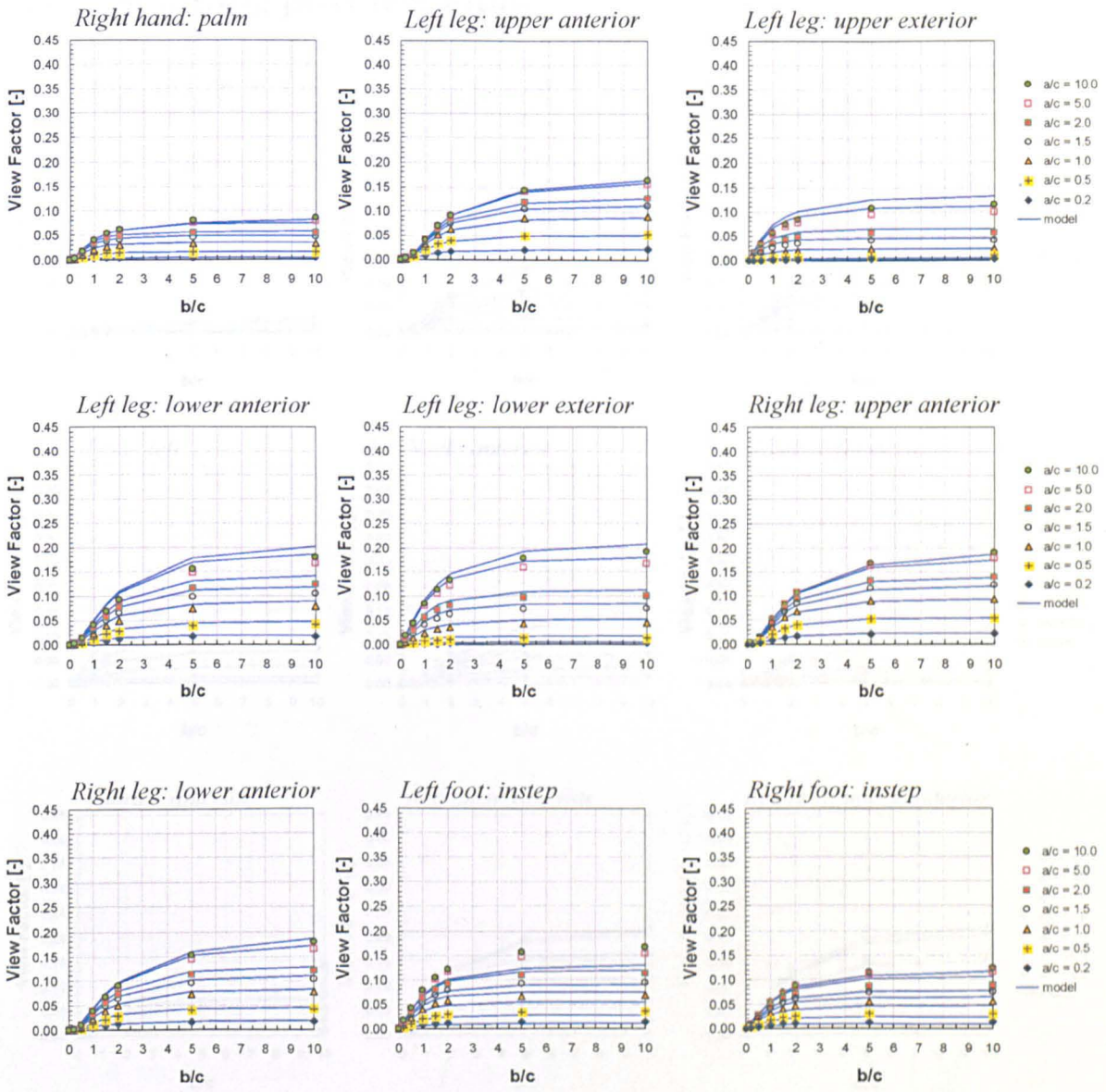
Right hand: palm
Left leg: upper anterior
Left leg: upper exterior
Left leg: lower anterior
Left leg: lower exterior
Right leg: upper anterior
Right leg: lower anterior
Left foot: instep
Right foot: instep
View Factor [-]
b/c
a/c = 10.0
a/c = 5.0
a/c = 2.0
a/c = 1.5
a/c = 1.0
a/c = 0.5
a/c = 0.2
model

C.4 Standing posture: Floor

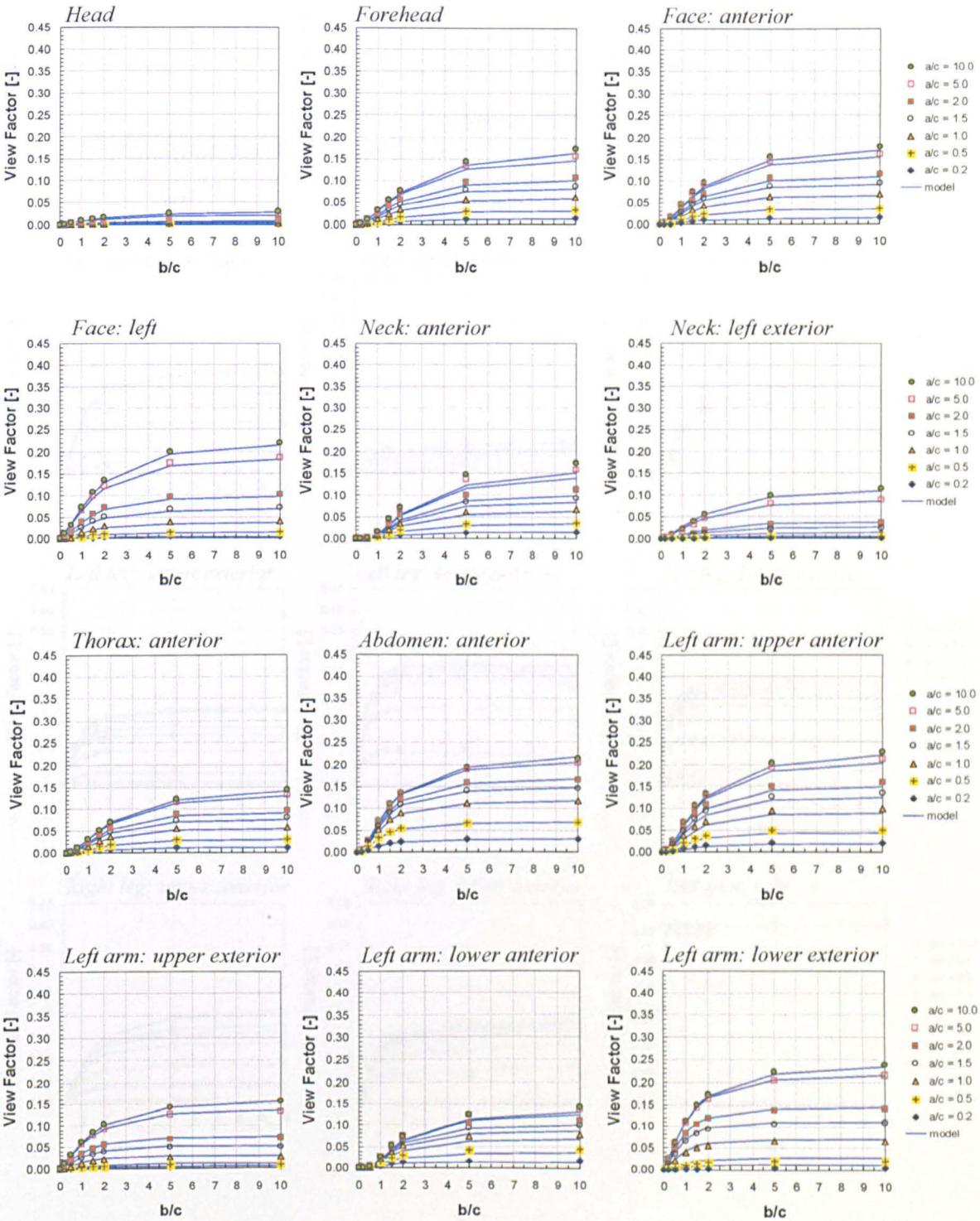

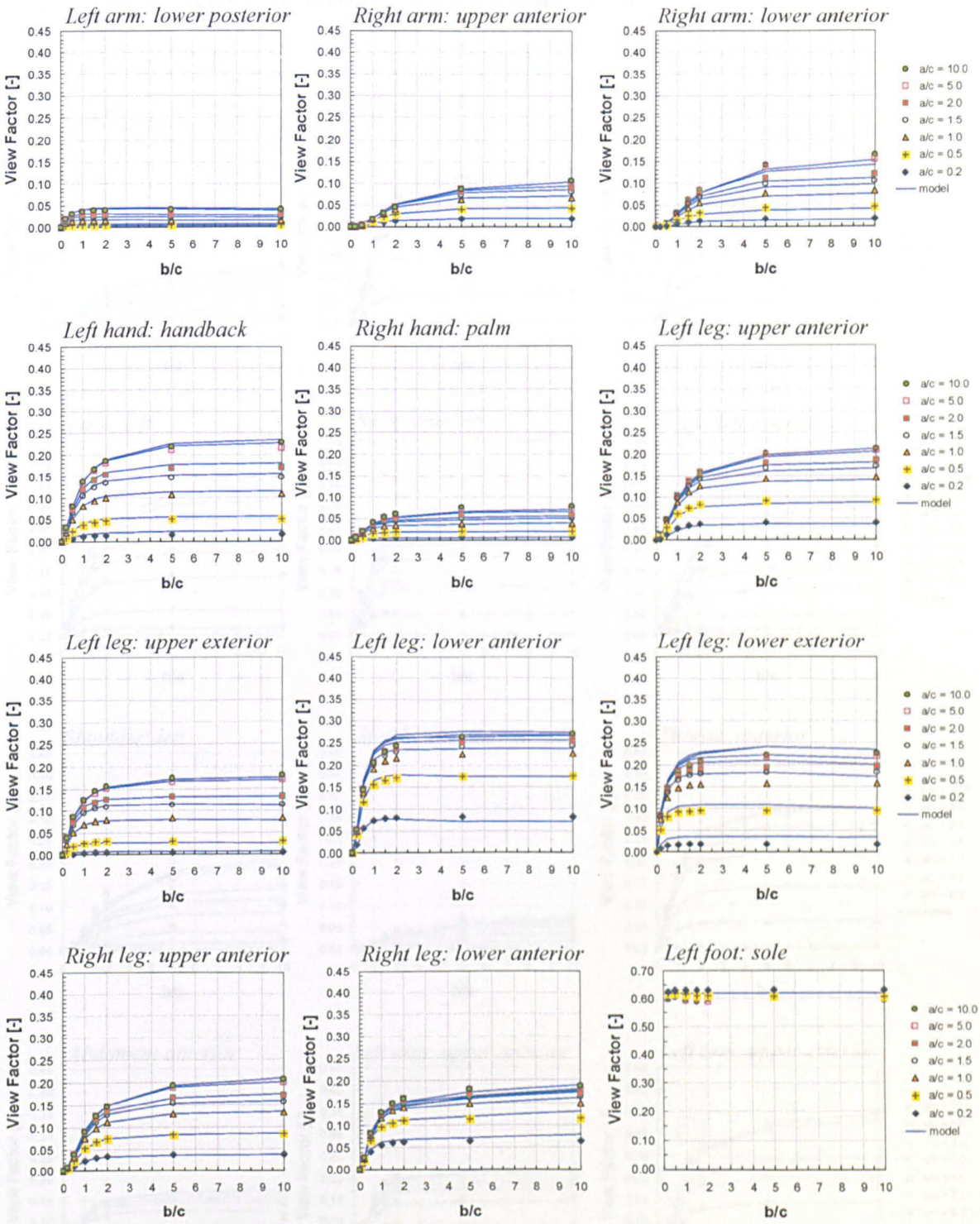
Left arm: lower posterior
Right arm: upper anterior
Right arm: lower anterior
Left hand: handback
Right hand: palm
Left leg: upper anterior
Left leg: upper exterior
Left leg: lower anterior
Left leg: lower exterior
Right leg: upper anterior
Right leg: lower anterior
Left foot: sole
View Factor [-]
b/c
a/c = 10.0
a/c = 5.0
a/c = 2.0
a/c = 1.5
a/c = 1.0
a/c = 0.5
a/c = 0.2
model

C.5 Sedentary posture: Front wall 1 m.

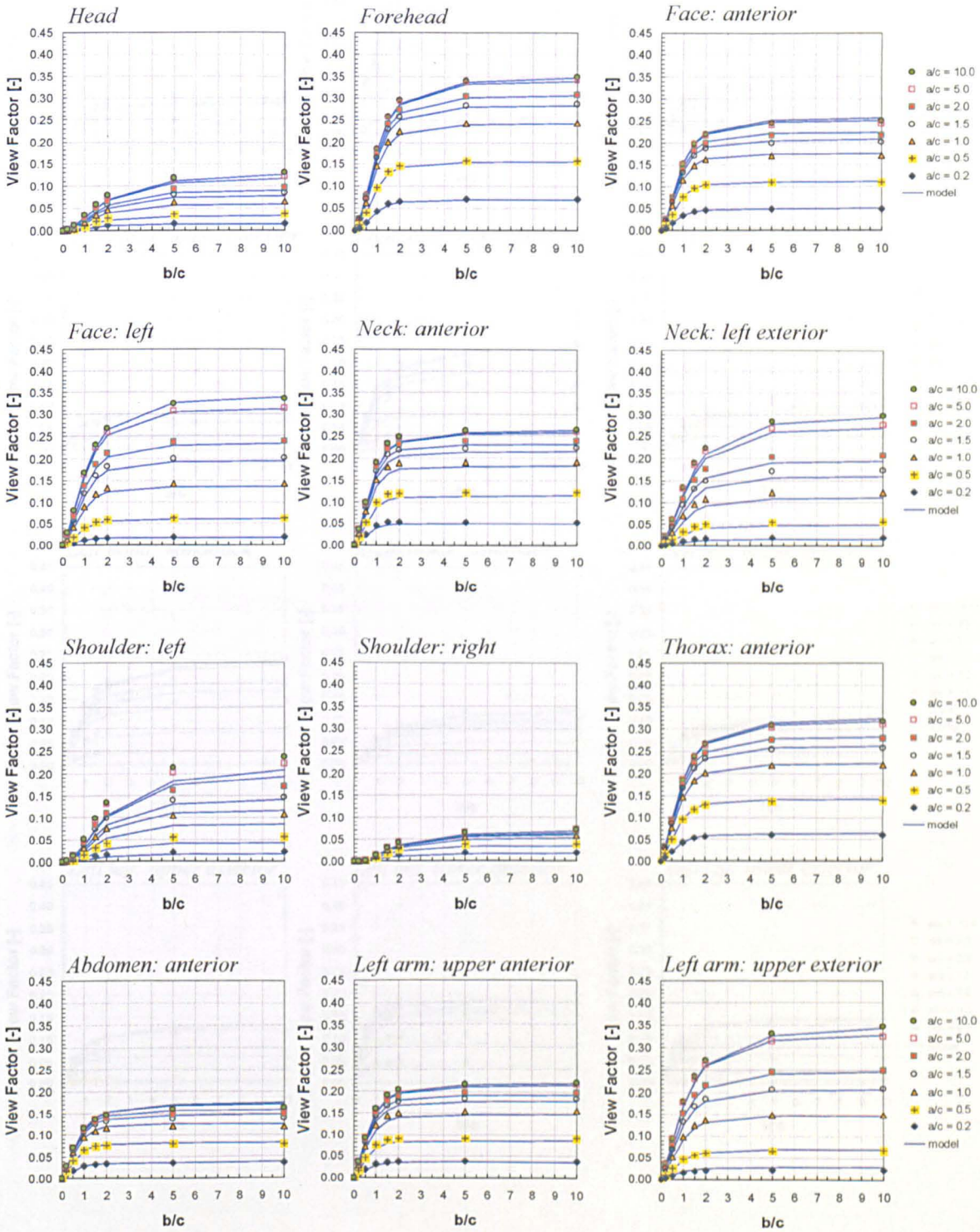

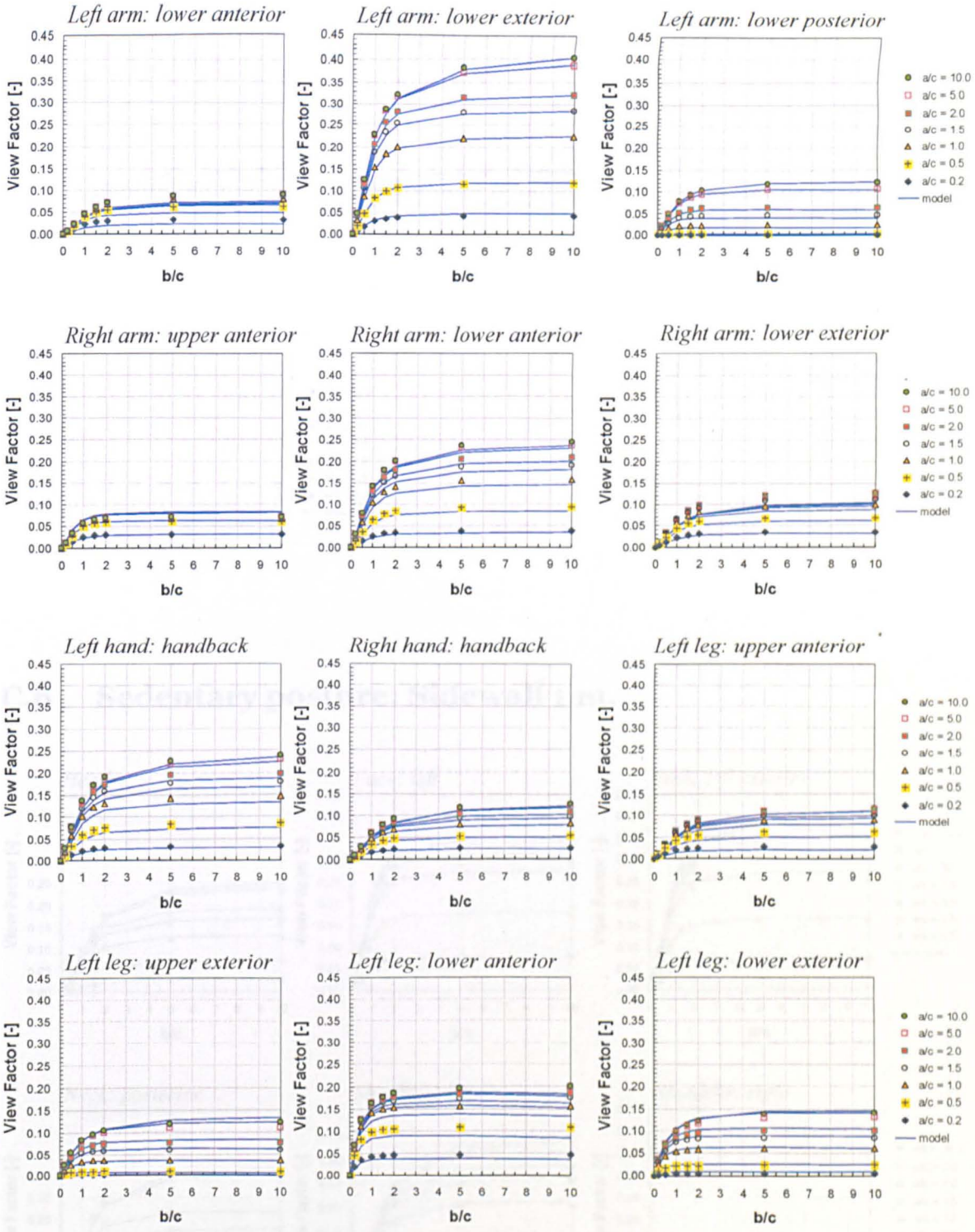
Left arm: lower anterior
Left arm: lower exterior
Left arm: lower posterior
Right arm: upper anterior
Right arm: lower anterior
Right arm: lower exterior
Left hand: handback
Right hand: handback
Left leg: upper anterior
Left leg: upper exterior
Left leg: lower anterior
Left leg: lower exterior
View Factor [-]
b/c
a/c = 10.0
a/c = 5.0
a/c = 2.0
a/c = 1.5
a/c = 1.0
a/c = 0.5
a/c = 0.2
model

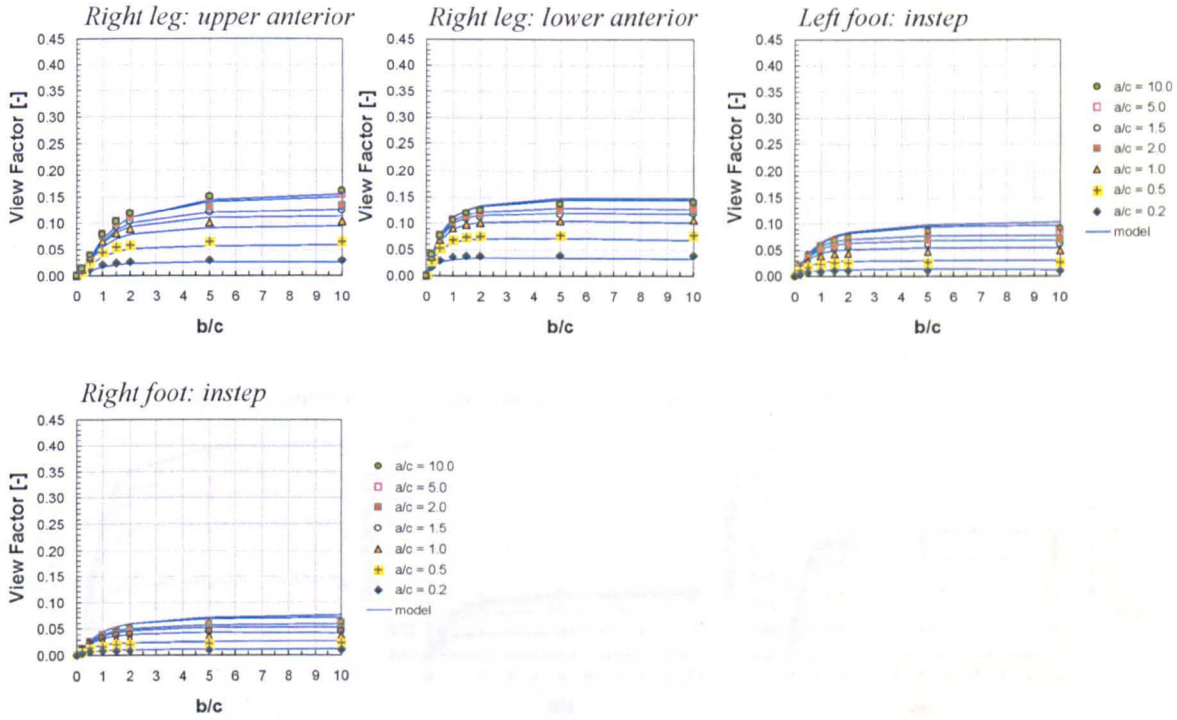

C.6 Sedentary posture: Sidewall 1 m.

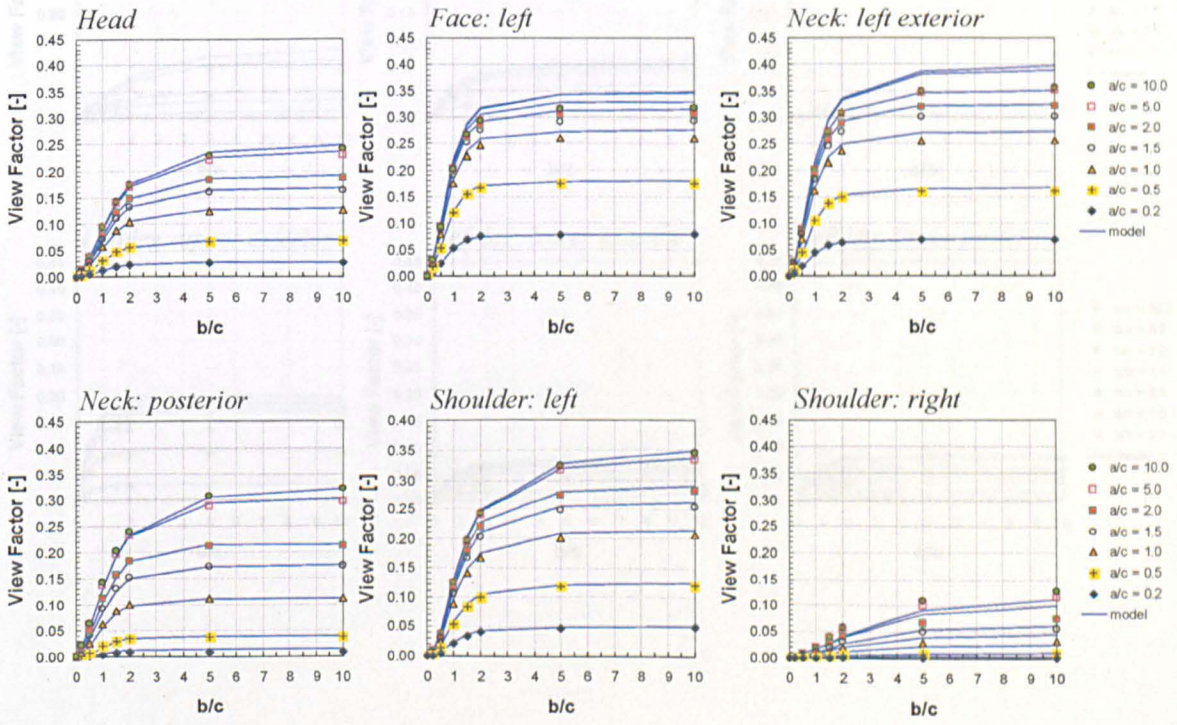

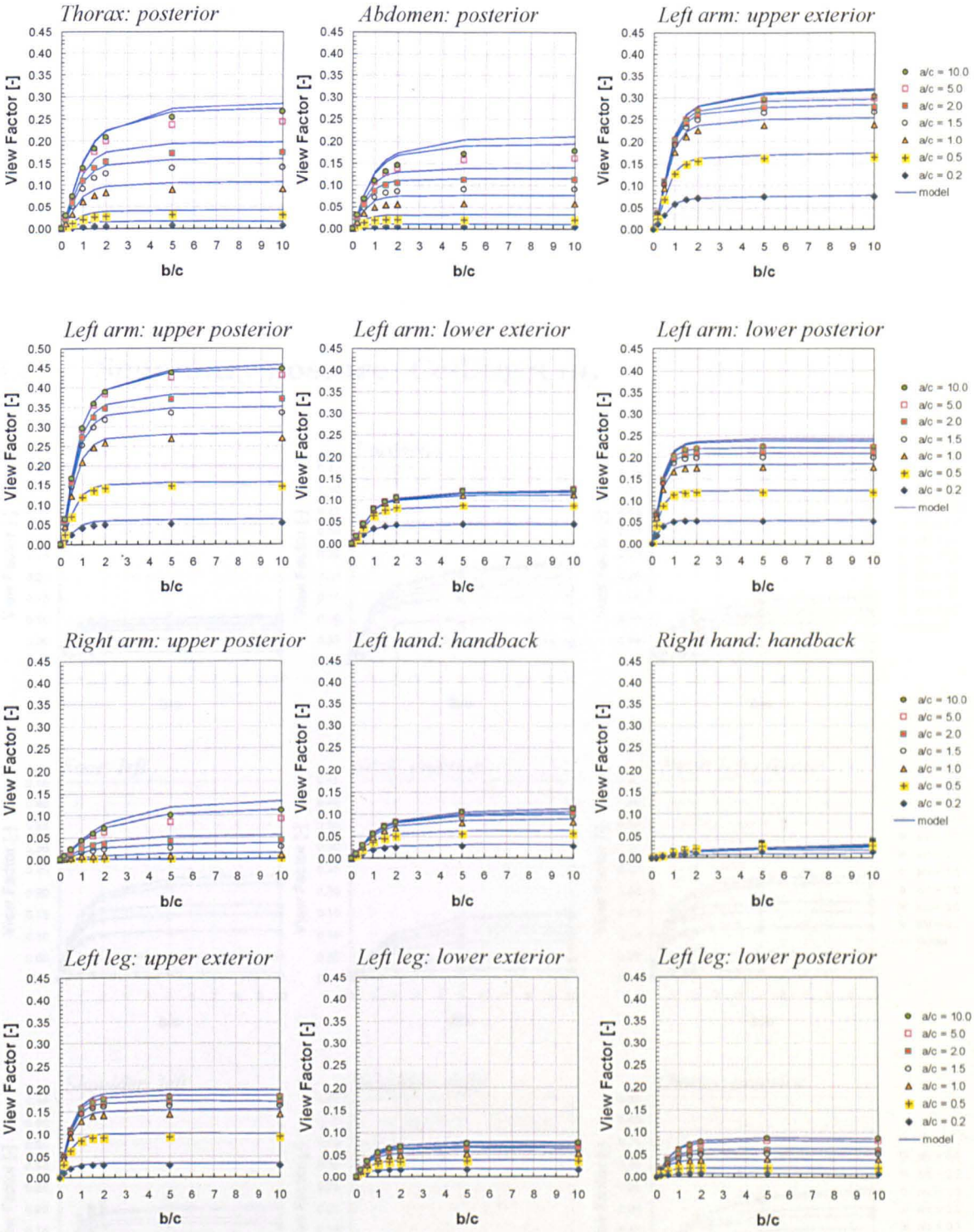
Thorax: posterior
Abdomen: posterior
Left arm: upper exterior
Left arm: upper posterior
Left arm: lower exterior
Left arm: lower posterior
Right arm: upper posterior
Left hand: handback
Right hand: handback
Left leg: upper exterior
Left leg: lower exterior
Left leg: lower posterior
View Factor [-]
b/c
a/c = 10.0
a/c = 5.0
a/c = 2.0
a/c = 1.5
a/c = 1.0
a/c = 0.5
a/c = 0.2
model

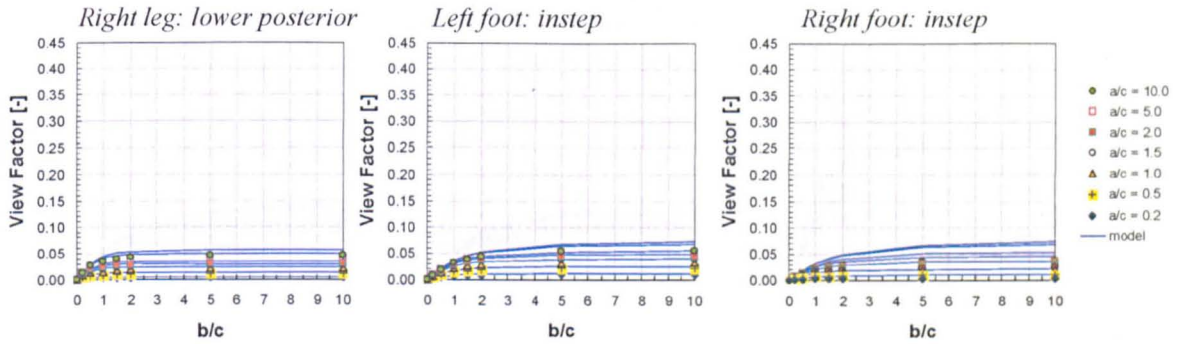

C.7 Sedentary posture: Ceiling 3 m.

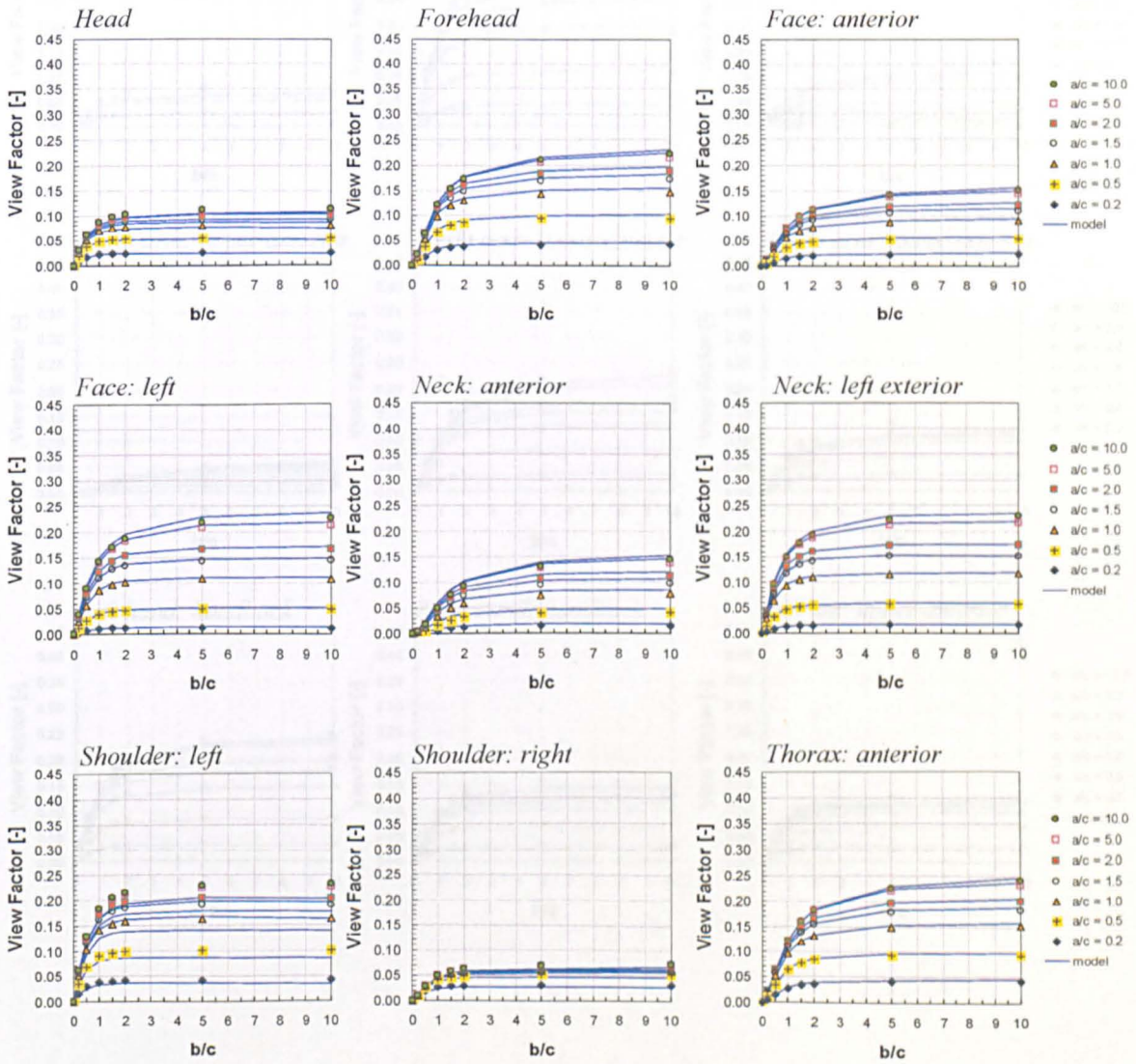

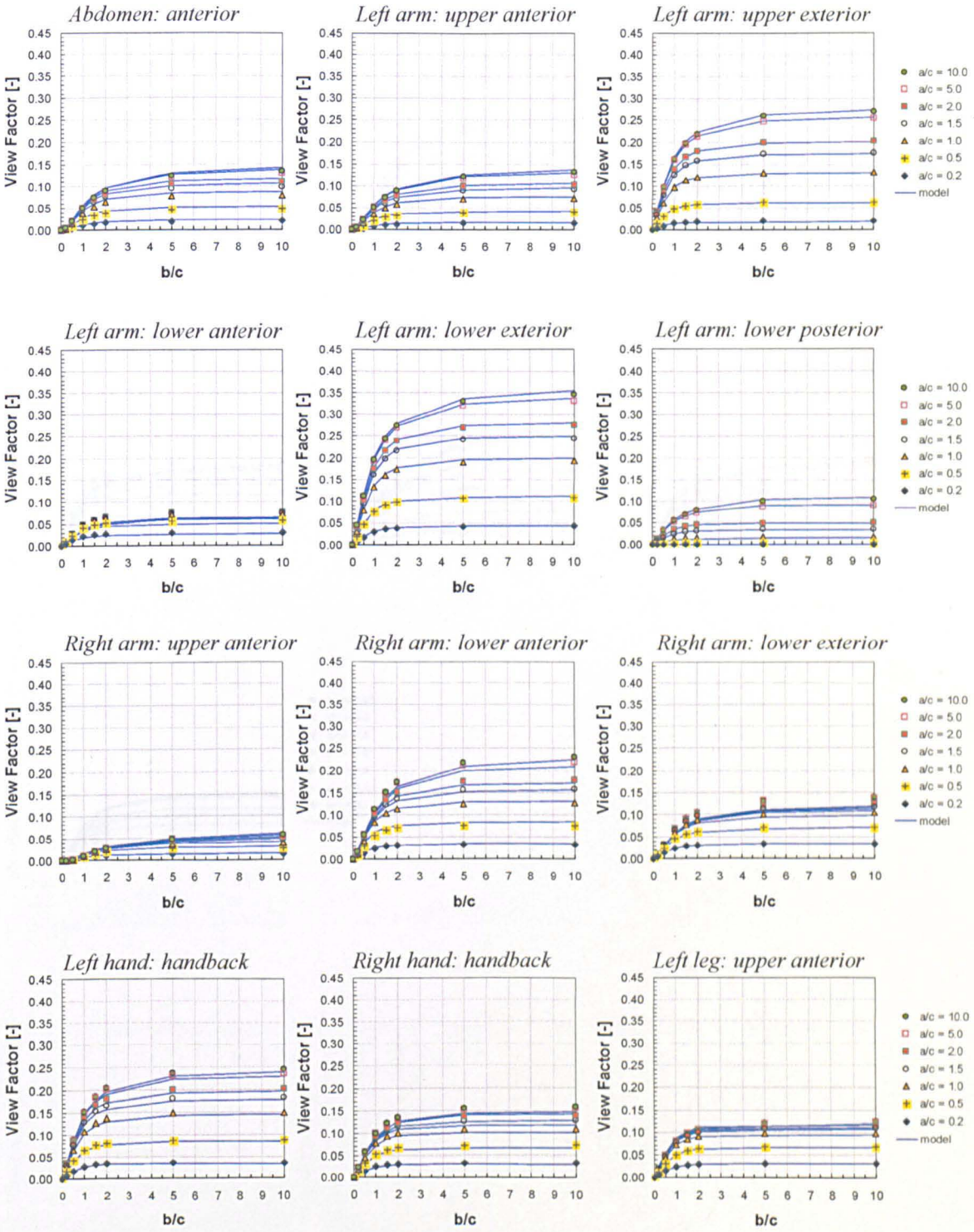
Abdomen: anterior
Left arm: upper anterior
Left arm: upper exterior
Left arm: lower anterior
Left arm: lower exterior
Left arm: lower posterior
Right arm: upper anterior
Right arm: lower anterior
Right arm: lower exterior
Left hand: handback
Right hand: handback
Left leg: upper anterior
View Factor [-]
b/c
a/c = 10.0
a/c = 5.0
a/c = 2.0
a/c = 1.5
a/c = 1.0
a/c = 0.5
a/c = 0.2
model

Left leg: upper exterior

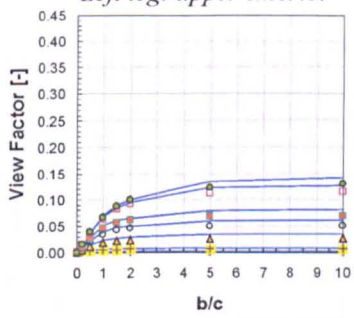

Left leg: lower anterior

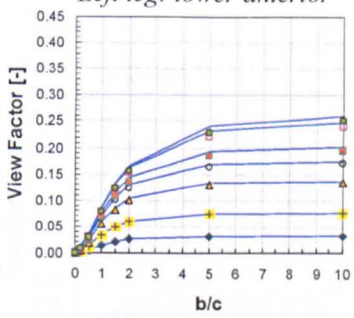

Left leg: lower exterior

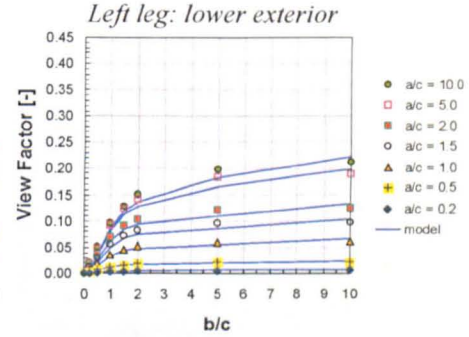

Right leg: upper anterior

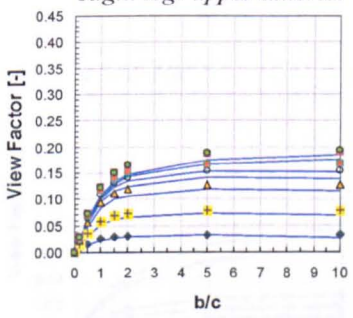

Right leg: lower anterior

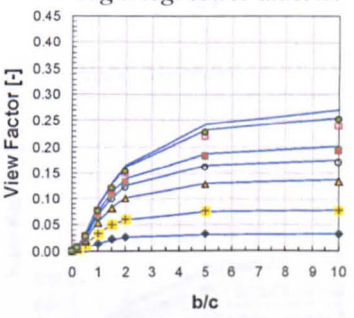

Left foot: instep

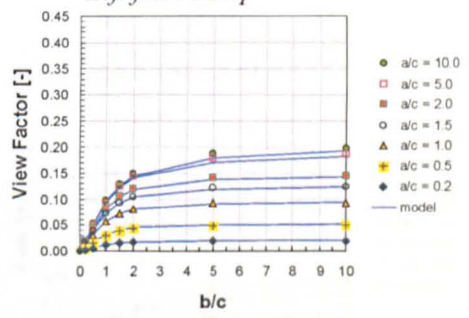

Right foot: instep

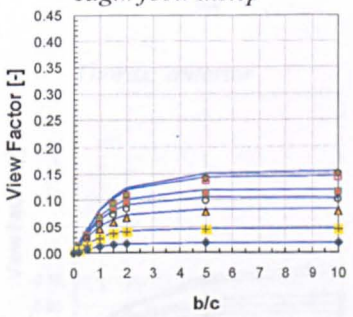

C.8 Sedentary posture: Floor

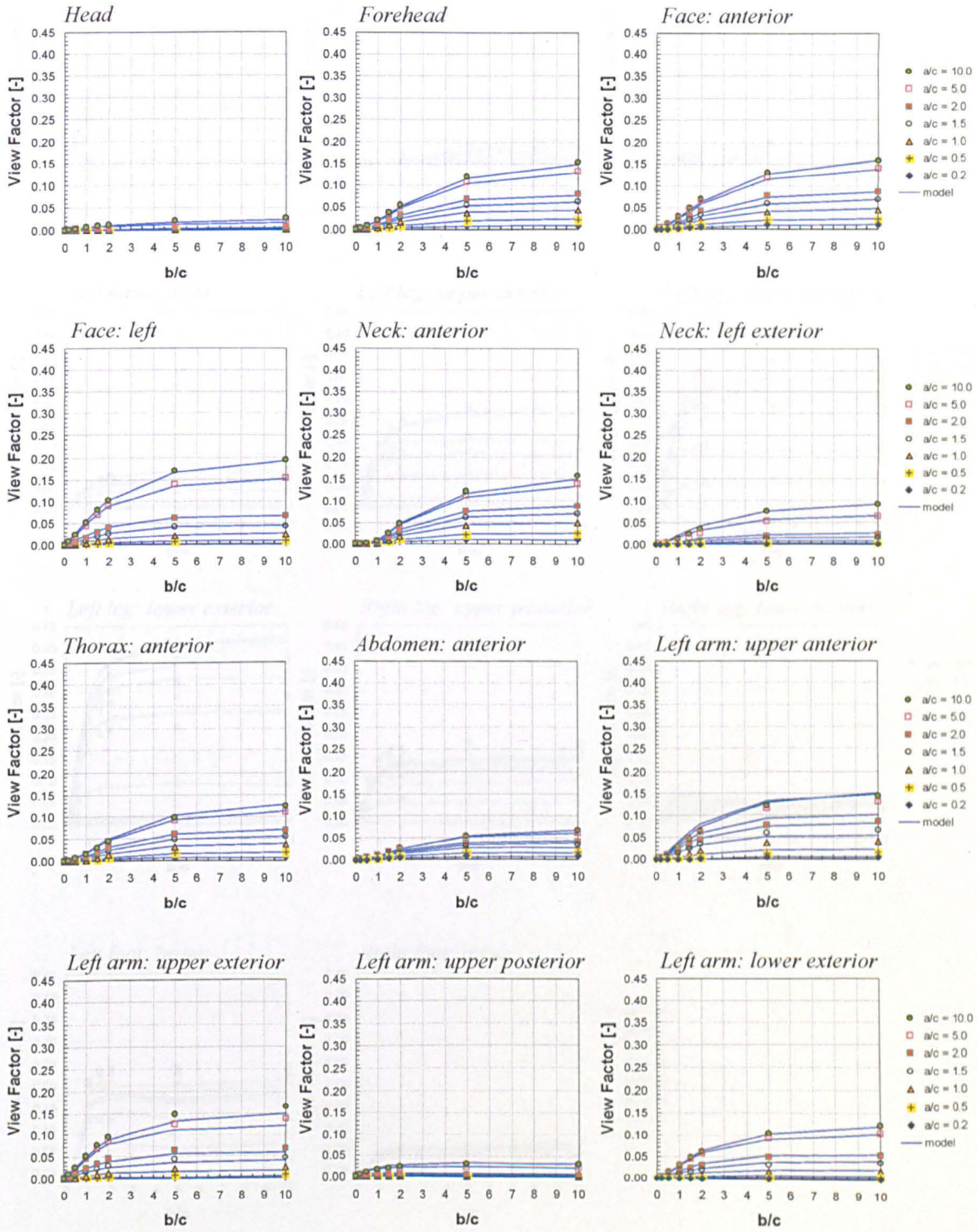

Left arm: lower posterior

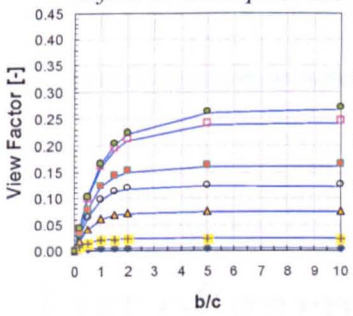

Right arm: upper anterior

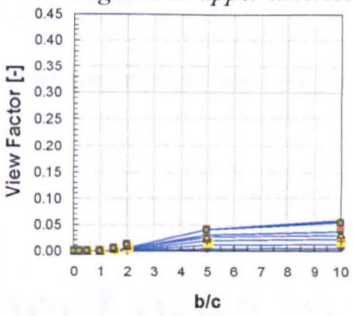

Left hand: handback

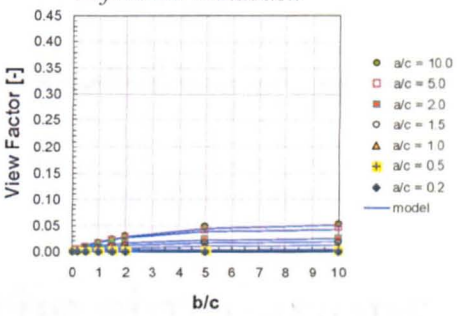

Left hand: palm

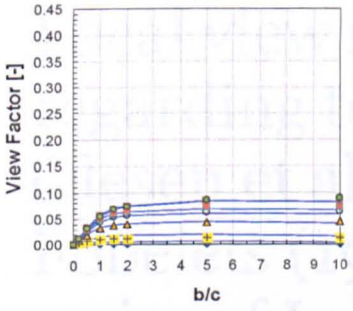

Left leg: upper exterior

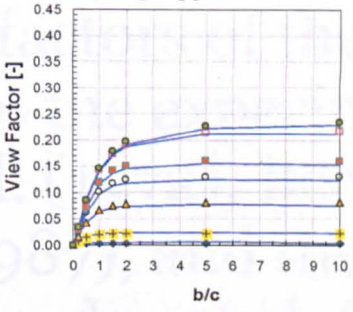

Left leg: upper posterior

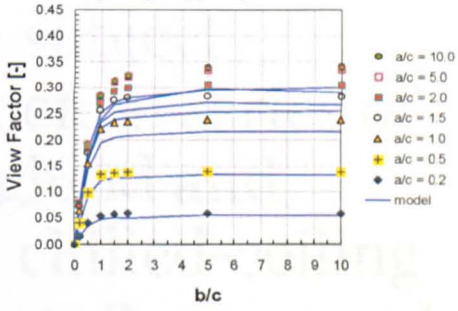

Left leg: lower exterior

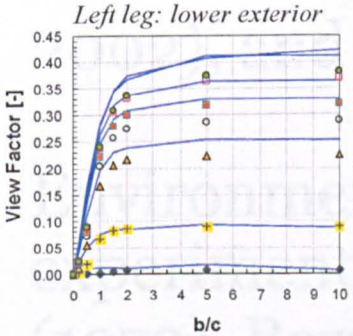

Right leg: upper posterior

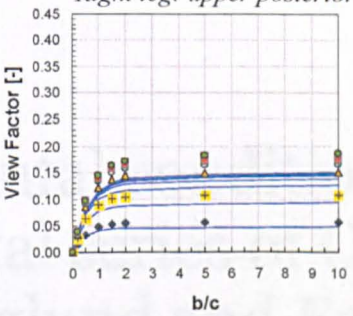

Right leg: lower posterior

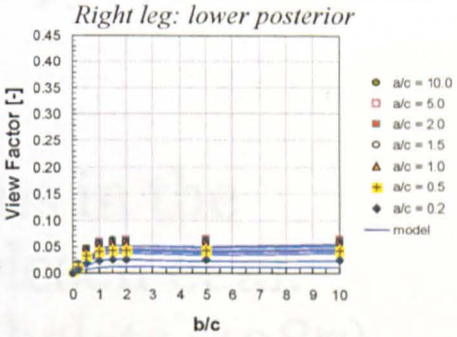

Left foot: instep

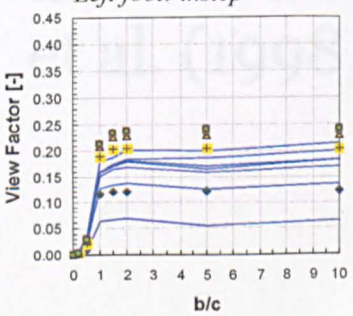

Right foot: instep

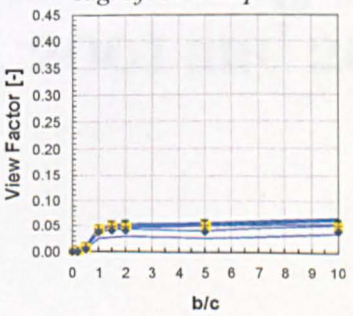

Appendix D

List of garment used in the simulations,

Local view factors of the subject regarding to the experimental series of Olesen et al. (1972), Berglund and Fobelets (1987), and the chilled-ceiling series of Loveday et al. (1998, 2001 and 2002), and

Environmental conditions in the experimental series of Olesen et al. (1972), Berglund and Fobelets (1987) and the chilled-ceiling series of Loveday et al. (1998, 2001 and 2002)

Table D.1 The local thermal and evaporative resistances of individual items used in the simulations of the heated-ceiling, cooled-ceiling, warm-wall, and cold-wall series of Fanger et al. (1980 and 1985) and in the simulations regarding to hot spatial and cold spatial-wall series of McNall and Biddison (1970).

```
11                    (number of items)
briefs (single knit)  Rf=0.0200m2K/W, Ref=  4.0 m2Pa/W
  Rcl       fcl      Recl   longwave emiss.   shortwave abs.
 [clo]      [ ]      [ ]          [ ]              [ ]
 0.216    1.018      6.1        0.950            0.700
   1                (number of body elements covered)
   6       0        (body element number, covered sector(s): 0=all)

Ankle length athletic socks (knit)  Rf=0.0360m2K/W, Ref=  4.0 m2Pa/W
  Rcl       fcl      Recl   longwave emiss.   shortwave abs.
 [clo]      [ ]      [ ]          [ ]              [ ]
 0.823    1.222     13.2        0.950            0.700
   1                (number of body elements covered)
  12       0        (body element number, covered sector(s): 0=all)

Shirt Long-sleeve, shirt collar (broadcloth)  Rf=0.0240m2K/W, Ref=
2.4 m2Pa/W
  Rcl       fcl      Recl   longwave emiss.   shortwave abs.
 [clo]      [ ]      [ ]          [ ]              [ ]
 0.127    1.222      2.0        0.950            0.700
   1                (number of body elements covered)
   3       0        (body element number, covered sector(s): 0=all)

Shirt Long-sleeve, shirt collar (broadcloth)  Rf=0.0240m2K/W, Ref=
2.4 m2Pa/W
  Rcl       fcl      Recl   longwave emiss.   shortwave abs.
 [clo]      [ ]      [ ]          [ ]              [ ]
 0.557    1.187      7.2        0.950            0.700
   1                (number of body elements covered)
   4       0        (body element number, covered sector(s): 0=all)

Shirt Long-sleeve, shirt collar (broadcloth)  Rf=0.0240m2K/W, Ref=
2.4 m2Pa/W
  Rcl       fcl      Recl   longwave emiss.   shortwave abs.
 [clo]      [ ]      [ ]          [ ]              [ ]
 0.713    1.051      9.8        0.950            0.700
   1                (number of body elements covered)
   5       0        (body element number, covered sector(s): 0=all)
```

```
Shirt Long-sleeve, shirt collar (broadcloth)  Rf=0.0240m2K/W, Ref=
2.4 m2Pa/W
  Rcl       fcl      Recl   longwave emiss.   shortwave abs.
 [clo]      [ ]      [ ]          [ ]              [ ]
 0.359    1.084     11.0        0.950            0.700
   1                (number of body elements covered)
   6       0        (body element number, covered sector(s): 0=all)

Shirt Long-sleeve, shirt collar (broadcloth)  Rf=0.0240m2K/W, Ref=
2.4 m2Pa/W
  Rcl       fcl      Recl   longwave emiss.   shortwave abs.
 [clo]      [ ]      [ ]          [ ]              [ ]
 0.577    1.432      8.3        0.950            0.700
   1                (number of body elements covered)
   7       0        (body element number, covered sector(s): 0=all)

Shirt Long-sleeve, shirt collar (broadcloth)  Rf=0.0240m2K/W, Ref=
2.4 m2Pa/W
  Rcl       fcl      Recl   longwave emiss.   shortwave abs.
 [clo]      [ ]      [ ]          [ ]              [ ]
 0.507    1.485      6.9        0.950            0.700
   1                (number of body elements covered)
   8       0        (body element number, covered sector(s): 0=all)

trousers, straight, long, fitted (tweed)  Rf=0.0490m2K/W, Ref=  5.5
m2Pa/W
  Rcl       fcl      Recl   longwave emiss.   shortwave abs.
 [clo]      [ ]      [ ]          [ ]              [ ]
 0.499    1.101     13.7        0.950            0.700
   1                (number of body elements covered)
   6       0        (body element number, covered sector(s): 0=all)

trousers, straight, long, fitted (tweed)  Rf=0.0490m2K/W, Ref=  5.5
m2Pa/W
  Rcl       fcl      Recl   longwave emiss.   shortwave abs.
 [clo]      [ ]      [ ]          [ ]              [ ]
 0.671    1.235      9.5        0.950            0.700
   1                (number of body elements covered)
  10       0        (body element number, covered sector(s): 0=all)

trousers, straight, long, fitted (tweed)  Rf=0.0490m2K/W, Ref=  5.5
m2Pa/W
  Rcl       fcl      Recl   longwave emiss.   shortwave abs.
 [clo]      [ ]      [ ]          [ ]              [ ]
 0.567    1.249      7.8        0.950            0.700
   1                (number of body elements covered)
  11       0        (body element number, covered sector(s): 0=all)
```

Notes: 1= head, 2= face, 3= neck, 4= shoulders, 5= thorax, 6= abdomen,
7= upper arms, 8= lower arms, 9= hands,
10= upper legs, 11= lower legs, and 12= feet.

Table D.2 A list of garment used in the simulations of the experimental series of Hall and Klemn (1967 and 1969).

```
2                    (number of garments)
briefs, knit (Icl=0.05, fcl=1.01, Ref=0.0052, if=0.416)
   Icli    fcli     icl     eps    swrAbsp
  [clo]     [ ]     [ ]     [ ]      [ ]
  0.211   1.043   0.413   0.950      0.70
      1                 (number of body elements covered)
      6       0         (body element number, covered side(s))

shorts  (Icl=0.600 clo, fcl=1.000, Ref=0.2400 [m2kPa/W], if=0.3000 )
  Icl*     fcl*     icl*   longwave emiss.   shortwave abs.
 [clo]      [ ]     [ ]          [ ]              [ ]
 0.548    1.000    0.300        0.950            0.700
     1                 (number of body elements covered)
     6       0         (body element number, covered side(s)
```

Table D.3 A list of garment used in the simulations of the experimental series of Hodder (2002).

```
16                    (number of items)
briefs (single knit)  Rf=0.0200m2K/W, Ref=  4.0 m2Pa/W
  Rcl       fcl      Recl   longwave emiss.   shortwave abs.
 [clo]      [ ]      [ ]          [ ]              [ ]
 0.216    1.018      6.1        0.950            0.700
   1                 (number of body elements covered)
   6       0         (body element number, covered sector(s): 0=all)

Ankle length athletic socks (knit)  Rf=0.0360m2K/W, Ref=  4.0 m2Pa/W
  Rcl       fcl      Recl   longwave emiss.   shortwave abs.
 [clo]      [ ]      [ ]          [ ]              [ ]
 0.823    1.222     13.2        0.950            0.700
   1                 (number of body elements covered)
  12       0         (body element number, covered sector(s): 0=all)

Shirt Long-sleeve, shirt collar (broadcloth). Rf=0.0240m2K/W, Ref=
2.4 m2Pa/W
  Rcl       fcl      Recl   longwave emiss.   shortwave abs.
 [clo]      [ ]      [ ]          [ ]              [ ]
 0.127    1.222      2.0        0.950            0.500
   1                 (number of body elements covered)
   3       0         (body element number, covered sector(s): 0=all)

Shirt Long-sleeve, shirt collar (broadcloth)  Rf=0.0240m2K/W, Ref=
2.4 m2Pa/W
  Rcl       fcl      Recl   longwave emiss.   shortwave abs.
 [clo]      [ ]      [ ]          [ ]              [ ]
 0.250    1.084     11.0        0.950            0.500
   1                 (number of body elements covered)
   4       0         (body element number, covered sector(s): 0=all)
```

```
Shirt Long-sleeve, shirt collar (broadcloth)  Rf=0.0240m2K/W, Ref=
2.4 m2Pa/W
  Rcl       fcl      Recl   longwave emiss.    shortwave abs.
 [clo]      [ ]      [ ]          [ ]              [ ]
 0.359    1.084     11.0        0.950             0.500
   1                 (number of body elements covered)
   5       0         (body element number, covered sector(s): 0=all)

Shirt Long-sleeve, shirt collar (broadcloth)  Rf=0.0240m2K/W, Ref=
2.4 m2Pa/W
  Rcl       fcl      Recl   longwave emiss.    shortwave abs.
 [clo]      [ ]      [ ]          [ ]              [ ]
-0.250    1.084     11.0        0.950             0.500
   1                 (number of body elements covered)
   5       0         (body element number, covered sector(s): 0=all)

Shirt Long-sleeve, shirt collar (broadcloth)  Rf=0.0240m2K/W, Ref=
2.4 m2Pa/W
  Rcl       fcl      Recl   longwave emiss.    shortwave abs.
 [clo]      [ ]      [ ]          [ ]              [ ]
 0.250    1.084     11.0        0.950             0.500
   1                 (number of body elements covered)
   6       0         (body element number, covered sector(s): 0=all)

Shirt Long-sleeve, shirt collar (broadcloth)  Rf=0.0240m2K/W, Ref=
2.4 m2Pa/W
  Rcl       fcl      Recl   longwave emiss.    shortwave abs.
 [clo]      [ ]      [ ]          [ ]              [ ]
 0.359    1.084     11.0        0.950             0.500
   1                 (number of body elements covered)
   6       0         (body element number, covered sector(s): 0=all)

Shirt Long-sleeve, shirt collar (broadcloth)  Rf=0.0240m2K/W, Ref=
2.4 m2Pa/W
  Rcl       fcl      Recl   longwave emiss.    shortwave abs.
 [clo]      [ ]      [ ]          [ ]              [ ]
 0.577    1.432      8.3        0.950             0.500
   1                 (number of body elements covered)
   7       0         (body element number, covered sector(s): 0=all)

Shirt Long-sleeve, shirt collar (broadcloth)  Rf=0.0240m2K/W, Ref=
2.4 m2Pa/W
  Rcl       fcl      Recl   longwave emiss.    shortwave abs.
 [clo]      [ ]      [ ]          [ ]              [ ]
 0.450    1.432      8.3        0.950             0.500
   1                 (number of body elements covered)
   7       0         (body element number, covered sector(s): 0=all)

Shirt Long-sleeve, shirt collar (broadcloth)  Rf=0.0240m2K/W, Ref=
2.4 m2Pa/W
  Rcl       fcl      Recl   longwave emiss.    shortwave abs.
 [clo]      [ ]      [ ]          [ ]              [ ]
-0.450    1.432      8.3        0.950             0.500
   1                 (number of body elements covered)
   11      0          (body element number, covered sector(s): 0=all)

Shirt Long-sleeve, shirt collar (broadcloth)  Rf=0.0240m2K/W, Ref=
2.4 m2Pa/W
  Rcl       fcl      Recl   longwave emiss.    shortwave abs.
```

```
 [clo]      [ ]      [ ]          [ ]              [ ]
 0.577    1.432      8.3        0.950            0.500
   1                (number of body elements covered)
   8       0        (body element number, covered sector(s): 0=all)

trousers, straight, long, fitted (tweed)  Rf=0.0490m2K/W, Ref=  5.5
m2Pa/W
  Rcl       fcl      Recl    longwave emiss.    shortwave abs.
 [clo]      [ ]      [ ]          [ ]              [ ]
 0.499    1.101     13.7        0.950            0.700
   1                (number of body elements covered)
   6       0        (body element number, covered sector(s): 0=all)

trousers, straight, long, fitted (tweed)  Rf=0.0490m2K/W, Ref=  5.5
m2Pa/W
  Rcl       fcl      Recl    longwave emiss.    shortwave abs.
 [clo]      [ ]      [ ]          [ ]              [ ]
 0.671    1.235      9.5        0.950            0.700
   1                (number of body elements covered)
  10       0        (body element number, covered sector(s): 0=all)

trousers, straight, long, fitted (tweed)  Rf=0.0490m2K/W, Ref=  5.5
m2Pa/W
  Rcl       fcl      Recl    longwave emiss.    shortwave abs.
 [clo]      [ ]      [ ]          [ ]              [ ]
 0.567    1.249      7.8        0.950            0.700
   1                (number of body elements covered)
  11       0        (body element number, covered sector(s): 0=all)

street shoes  Rf=0.1050m2K/W, Ref=  5.2 m2Pa/W
  Rcl       fcl      Recl    longwave emiss.    shortwave abs.
 [clo]      [ ]      [ ]          [ ]              [ ]
 0.921    1.371      9.0        0.950            0.700
   1                (number of body elements covered)
  12       0        (body element number, covered sector(s): 0=all)
```

Table D.4 A list of garment used in the simulations of the chilled-ceiling series of Loveday et al. (1998, 2001 and 2002).

```
     7                (number of garments worn)
 briefs, knit (Icl=0.05, fcl=1.01, Ref=0.0052, if=0.416)
   Icli    fcli     icl     eps    swrAbsp
  [clo]     [ ]     [ ]     [ ]      [ ]
  0.211   1.043   0.413   0.950     0.70
     1                (number of body elements covered)
     6       0        (body element number, covered side(s))

 undershirt
  Icl*      fcl*     icl*    longwave emiss.    shortwave abs.
 [clo]      [ ]      [ ]          [ ]              [ ]
 0.140    1.080     0.500        0.950            0.700
     4                (number of body elements covered)
     4       0        (body element number, covered side(s)
     5       0        (body element number, covered side(s)
     6       0        (body element number, covered side(s)
     7       0        (body element number, covered side(s)
```

```
twill shirt, long sleeve (Icl=0.33, fcl=1.13, Ref=0.004, if=0.541)
  Icli    fcli     icl     eps    swrAbsp
 [clo]     [ ]     [ ]     [ ]      [ ]
 0.570   1.229   0.478   0.950      0.70
     5                 (number of body elements covered)
     4       0         (body element number, covered side(s))
     5       0         (body element number, covered side(s))
     6       0         (body element number, covered side(s))
     7       0         (body element number, covered side(s))
     8       0         (body element number, covered side(s))

Shirt Long-sleeve, shirt collar (broadcloth)  Rf=0.0240m2K/W, Ref=
2.4 m2Pa/W
  Rcl       fcl      Recl   longwave emiss.    shortwave abs.
 [clo]      [ ]      [ ]          [ ]              [ ]
 0.280    1.432      0.0        0.950            0.700
   1                (number of body elements covered)
   3       0        (body element number, covered sector(s): 0=all)

trousers, straight, long, fitted (tweed)  Rf=0.0490m2K/W, Ref=  5.5
m2Pa/W
  Rcl       fcl      Recl   longwave emiss.    shortwave abs.
 [clo]      [ ]      [ ]          [ ]              [ ]
 0.671    1.235      9.5        0.950            0.700
     3                (number of body elements covered)
     6       0        (body element number, covered side(s))
    10       0        (body element number, covered side(s))
    11       0        (body element number, covered side(s))

socks, knit (Icl=0.04, fcl=1.01, Ref=0.0052, if=0.416)
   Icli    fcli     icl     eps    swrAbsp
  [clo]     [ ]     [ ]     [ ]      [ ]
  0.350   1.176   0.407   0.950      0.70
     1                 (number of body elements covered)
    12       0         (body element number, covered side(s))

warm shoes (fcl=1.04, Ref=0.047, if=0.100)
Icli      fcli       icl      eps    swrAbsp
[clo]      [ ]       [ ]      [ ]      [ ]
 1.2     1.703     0.138    0.950    0.70
   1                    (number of body elements covered)
  12       0            (body element number, covered side(s))
```

Table D.5 List of garments used in the simulations of the BHEC building (*Chapter 8*).

```
17                    (number of items)
briefs (single knit)  Rf=0.0200m2K/W, Ref=  4.0 m2Pa/W
  Rcl       fcl      Recl   longwave emiss.   shortwave abs.
 [clo]      [ ]      [ ]          [ ]              [ ]
 0.216    1.018      6.1        0.950            0.700
   1                 (number of body elements covered)
   6       0         (body element number, covered sector(s): 0=all)

Ankle length athletic socks (knit)  Rf=0.0360m2K/W, Ref=  4.0 m2Pa/W
  Rcl       fcl      Recl   longwave emiss.   shortwave abs.
 [clo]      [ ]      [ ]          [ ]              [ ]
 0.823    1.222     13.2        0.950            0.700
   1                 (number of body elements covered)
  12       0         (body element number, covered sector(s): 0=all)

Shirt Long-sleeve, shirt collar (broadcloth)  Rf=0.0240m2K/W, Ref=
2.4 m2Pa/W
  Rcl       fcl      Recl   longwave emiss.   shortwave abs.
 [clo]      [ ]      [ ]          [ ]              [ ]
 0.127    1.222      2.0        0.950            0.700
   1                 (number of body elements covered)
   3       0         (body element number, covered sector(s): 0=all)

Shirt Long-sleeve, shirt collar (broadcloth)  Rf=0.0240m2K/W, Ref=
2.4 m2Pa/W
  Rcl       fcl      Recl   longwave emiss.   shortwave abs.
 [clo]      [ ]      [ ]          [ ]              [ ]
 0.250    1.084     11.0        0.950            0.700
   1                 (number of body elements covered)
   4       0         (body element number, covered sector(s): 0=all)

Shirt Long-sleeve, shirt collar (broadcloth)  Rf=0.0240m2K/W, Ref=
2.4 m2Pa/W
  Rcl       fcl      Recl   longwave emiss.   shortwave abs.
 [clo]      [ ]      [ ]          [ ]              [ ]
 0.359    1.084     11.0        0.950            0.700
   1                 (number of body elements covered)
   5       0         (body element number, covered sector(s): 0=all)

Shirt Long-sleeve, shirt collar (broadcloth)  Rf=0.0240m2K/W, Ref=
2.4 m2Pa/W
  Rcl       fcl      Recl   longwave emiss.   shortwave abs.
 [clo]      [ ]      [ ]          [ ]              [ ]
 0.359    1.084     11.0        0.950            0.700
   1                 (number of body elements covered)
   6       0         (body element number, covered sector(s): 0=all)

Shirt Long-sleeve, shirt collar (broadcloth)  Rf=0.0240m2K/W, Ref=
2.4 m2Pa/W
  Rcl       fcl      Recl   longwave emiss.   shortwave abs.
 [clo]      [ ]      [ ]          [ ]              [ ]
 0.577    1.432      8.3        0.950            0.700
   1                 (number of body elements covered)
   7       0         (body element number, covered sector(s): 0=all)
```

```
Shirt Long-sleeve, shirt collar (broadcloth)  Rf=0.0240m2K/W, Ref=
2.4 m2Pa/W
  Rcl       fcl      Recl   longwave emiss.    shortwave abs.
 [clo]      [ ]      [ ]          [ ]              [ ]
 0.577    1.432      8.3        0.950             0.700
   1                (number of body elements covered)
   8       0        (body element number, covered sector(s): 0=all)

trousers, straight, long, fitted (tweed)  Rf=0.0490m2K/W, Ref=  5.5
m2Pa/W
  Rcl       fcl      Recl   longwave emiss.    shortwave abs.
 [clo]      [ ]      [ ]          [ ]              [ ]
 0.499    1.101     13.7        0.950             0.700
   1                (number of body elements covered)
   6       0        (body element number, covered sector(s): 0=all)

trousers, straight, long, fitted (tweed)  Rf=0.0490m2K/W, Ref=  5.5
m2Pa/W
  Rcl       fcl      Recl   longwave emiss.    shortwave abs.
 [clo]      [ ]      [ ]          [ ]              [ ]
 0.671    1.235      9.5        0.950             0.700
   1                (number of body elements covered)
  10       0        (body element number, covered sector(s): 0=all)

trousers, straight, long, fitted (tweed)  Rf=0.0490m2K/W, Ref=  5.5
m2Pa/W
  Rcl       fcl      Recl   longwave emiss.    shortwave abs.
 [clo]      [ ]      [ ]          [ ]              [ ]
 0.567    1.249      7.8        0.950             0.700
   1                (number of body elements covered)
  11       0        (body element number, covered sector(s): 0=all)

Suite Jacket (denim) Rf=0.0370m2K/W, Ref=  6.6 m2Pa/W
  Rcl       fcl      Recl   longwave emiss.    shortwave abs.
 [clo]      [ ]      [ ]          [ ]              [ ]
 0.778    1.191     13.8        0.950             0.700
   1                (number of body elements covered)
   4       0        (body element number, covered sector(s): 0=all)

Suite Jacket (denim) Rf=0.0370m2K/W, Ref=  6.6 m2Pa/W
  Rcl       fcl      Recl   longwave emiss.    shortwave abs.
 [clo]      [ ]      [ ]          [ ]              [ ]
 0.791    1.060     13.7        0.950             0.700
   1                (number of body elements covered)
   5       0        (body element number, covered sector(s): 0=all)

Suite Jacket (denim) Rf=0.0370m2K/W, Ref=  6.6 m2Pa/W
  Rcl       fcl      Recl   longwave emiss.    shortwave abs.
 [clo]      [ ]      [ ]          [ ]              [ ]
 1.089    1.181     25.6        0.950             0.700
   1                (number of body elements covered)
   6       0        (body element number, covered sector(s): 0=all)

Suite Jacket (denim) Rf=0.0370m2K/W, Ref=  6.6 m2Pa/W
  Rcl       fcl      Recl   longwave emiss.    shortwave abs.
 [clo]      [ ]      [ ]          [ ]              [ ]
 0.865    1.390     18.4        0.950             0.700
   1                (number of body elements covered)
   7       0        (body element number, covered sector(s): 0=all)
```

```
Suite Jacket (denim) Rf=0.0370m2K/W, Ref=  6.6 m2Pa/W
  Rcl       fcl      Recl   longwave emiss.   shortwave abs.
 [clo]      [ ]      [ ]          [ ]              [ ]
 0.859    1.341    17.5        0.950             0.700
   1                (number of body elements covered)
   8       0        (body element number, covered sector(s): 0=all)

street shoes  Rf=0.1050m2K/W, Ref=  5.2 m2Pa/W
  Rcl       fcl      Recl   longwave emiss.   shortwave abs.
 [clo]      [ ]      [ ]          [ ]              [ ]
 0.921    1.371     9.0        0.950             0.700
   1                (number of body elements covered)
  12       0        (body element number, covered sector(s): 0=all)
```

Table D.6 List of garments used in the simulations of the experimental series of Berglund and Fobelets (1987).

```
     7                (number of garments worn)
 briefs, knit (Icl=0.05, fcl=1.01, Ref=0.0052, if=0.416)
   Icli    fcli     icl     eps    swrAbsp
  [clo]     [ ]     [ ]     [ ]      [ ]
  0.211   1.043   0.413   0.950      0.70
     1                (number of body elements covered)
     6       0        (body element number, covered side(s))

 undershirt
  Icl*      fcl*     icl*   longwave emiss.   shortwave abs.
 [clo]      [ ]      [ ]          [ ]              [ ]
 0.140    1.080    0.500        0.950             0.700
     4                (number of body elements covered)
     4       0        (body element number, covered side(s)
     5       0        (body element number, covered side(s)
     6       0        (body element number, covered side(s)
     7       0        (body element number, covered side(s)

 twill shirt, long sleeve (Icl=0.33, fcl=1.13, Ref=0.004, if=0.541)
   Icli    fcli     icl     eps    swrAbsp
  [clo]     [ ]     [ ]     [ ]      [ ]
  0.570   1.229   0.478   0.950      0.70
     5                (number of body elements covered)
     4       0        (body element number, covered side(s))
     5       0        (body element number, covered side(s))
     6       0        (body element number, covered side(s))
     7       0        (body element number, covered side(s))
     8       0        (body element number, covered side(s))

sweater (knit) (Icl=, fcl=1., Ref=0.0, if=0.416)
    Icli    fcli    icl     eps    shortwave abs.
    [clo]   [ ]     [ ]     [ ]        [ ]
  0.600    1.20   0.03   0.950     0.700
     5                (number of body elements covered)
     4       0        (body element number, covered side(s))
     5       0        (body element number, covered side(s))
     6       0        (body element number, covered side(s))
     7       0        (body element number, covered side(s))
     8       0        (body element number, covered side(s))
```

```
trousers, loose, denim (Icl=0.30, fcl=1.09, Ref=0.004, if=0.541)
  Icli    fcli     icl     eps    swrAbsp
 [clo]     [ ]     [ ]     [ ]      [ ]
 0.596   1.181   0.485    0.95      0.70
     3                 (number of body elements covered)
     6       0         (body element number, covered side(s))
    10       0         (body element number, covered side(s))
    11       0         (body element number, covered side(s))

socks, knit (Icl=0.04, fcl=1.01, Ref=0.0052, if=0.416)
  Icli    fcli     icl     eps    swrAbsp
 [clo]     [ ]     [ ]     [ ]      [ ]
 0.350   1.176   0.407   0.950      0.70
     1                 (number of body elements covered)
    12       0         (body element number, covered side(s))

warm shoes (fcl=1.04, Ref=0.047, if=0.100)
Icli      fcli       icl      eps    swrAbsp
[clo]      [ ]       [ ]      [ ]      [ ]
 1.2     1.703     0.138    0.950    0.70
   1                    (number of body elements covered)
  12        0           (body element number, covered side(s))
```

Table D.7 Detailed local view factors of the subject regarding to the experimental series of Olesen et al. (1972)

Body part	Cold L.-warm R. (warm L.-cold R.)		Cold front-warm back (warm front-cold back)	
	L. wall	R. wall	Front wall	Back wall
Forehead	0.180	0.180	0.242	0.000
Head	0.198	0.198	0.038	0.150
Face: Anterior	0.169	0.169	0.175	0.000
L. Face	0.497	0.000	0.062	0.026
R. Face	0.000	0.497	0.062	0.026
Neck: Anterior	0.128	0.128	0.212	0.000
Neck: Posterior	0.141	0.141	0.000	0.304
Neck: L. Exterior	0.461	0.000	0.051	0.063
Neck: R. Exterior	0.000	0.463	0.051	0.063
L. Shoulder	0.302	0.043	0.045	0.140
Thorax: Anterior	0.169	0.169	0.230	0.000
Thorax: Posterior	0.151	0.151	0.000	0.301
Thorax: L. Inferior	0.194	0.001	0.020	0.057
Thorax: R. Inferior	0.001	0.197	0.020	0.059
Abdomen: Anterior	0.076	0.076	0.157	0.000
Abdomen: Posterior	0.144	0.144	0.000	0.228
Abdomen: L. Inferior	0.307	0.000	0.002	0.079
Abdomen: R. Inferior	0.000	0.307	0.002	0.079
L. Arm: Up. Anterior	0.106	0.028	0.137	0.000
L. Arm: Up. Posterior	0.329	0.040	0.000	0.255
L. Arm: Up. Inferior	0.020	0.139	0.000	0.152
L. Arm: Up. Exterior	0.495	0.001	0.075	0.043
L. Arm: Lo. Anterior	0.001	0.178	0.106	0.003
L. Arm: Lo. Posterior	0.427	0.000	0.013	0.081
L. Arm: Lo. Inferior	0.045	0.054	0.000	0.108
L. Arm: Lo. Exterior	0.336	0.026	0.207	0.000
L. Hand: Handback	0.258	0.089	0.124	0.014
L. Hand: Palm	0.062	0.017	0.002	0.031
L. Leg: Up. Anterior	0.035	0.159	0.081	0.005
L. Leg: Up. Posterior	0.112	0.023	0.016	0.030
L. Leg: Up. Inferior	0.000	0.209	0.058	0.000
L. Leg: Up. Exterior	0.369	0.000	0.029	0.026
L. Leg: Lo. Anterior	0.119	0.165	0.268	0.000
L. Leg: Lo. Posterior	0.115	0.099	0.001	0.098
L. Leg: Lo. Inferior	0.000	0.251	0.090	0.029
L. Leg: Lo. Exterior	0.369	0.000	0.075	0.023
L. Foot: Instep	0.200	0.166	0.094	0.054
L. Foot: Sole	0.329	0.107	0.144	0.066
R. Shoulder	0.043	0.303	0.045	0.140
R. Arm: Up. Anterior	0.027	0.104	0.134	0.000
R. Arm: Up. Posterior	0.040	0.329	0.000	0.255
R. Arm: Up. Inferior	0.141	0.021	0.000	0.155
R. Arm: Up. Exterior	0.001	0.495	0.075	0.043
R. Arm: Lo. Anterior	0.178	0.001	0.106	0.003
R. Arm: Lo. Posterior	0.000	0.427	0.013	0.081
R. Arm: Lo. Inferior	0.054	0.045	0.000	0.108
R. Arm: Lo. Exterior	0.026	0.335	0.207	0.000
R. Hand: Handback	0.089	0.257	0.123	0.014
R. Hand: Palm	0.018	0.064	0.002	0.032
R. Leg: Up. Anterior	0.159	0.035	0.080	0.005
R. Leg: Up. Posterior	0.023	0.111	0.016	0.030
R. Leg: Up. Inferior	0.209	0.000	0.058	0.000
R. Leg: Up. Exterior	0.000	0.368	0.029	0.026
R. Leg: Lo. Anterior	0.165	0.119	0.268	0.000
R. Leg: Lo. Posterior	0.099	0.114	0.001	0.097
R. Leg: Lo. Inferior	0.249	0.000	0.090	0.029
R. Leg: Lo. Exterior	0.000	0.371	0.075	0.023
R. Foot: Instep	0.166	0.200	0.094	0.054
R. Foot: Sole	0.107	0.328	0.144	0.066
Whole body	**0.143**	**0.143**	**0.076**	**0.068**

Table D.8 Detailed local view factors of the subject regarding to the cool-wall series of Berglund and Fobelets (1987) and the chilled-ceiling series of Loveday et al. (1998, 2001 and 2002).

Body part	Cool-wall series of Berglund and Fobelets (1987)		Chilled-ceiling series of Loveday et al. (1998, 2001 and 2002)	
	Cool wall	Rest of chamber	Chilled ceiling	Rest of chamber
Forehead	0.088	0.891	0.202	0.777
Head	0.437	0.527	0.265	0.698
Face: Anterior	0.112	0.712	0.129	0.696
L. Face	0.616	0.268	0.146	0.738
R. Face	0.029	0.855	0.146	0.739
Neck: Anterior	0.052	0.715	0.116	0.651
Neck: Posterior	0.687	0.255	0.241	0.702
Neck: L. Exterior	0.589	0.241	0.189	0.641
Neck: R. Exterior	0.079	0.754	0.189	0.644
L. Shoulder	0.437	0.447	0.289	0.596
Thorax: Anterior	0.088	0.824	0.187	0.725
Thorax: Posterior	0.721	0.268	0.168	0.821
Thorax: L. Inferior	0.282	0.173	0.032	0.424
Thorax: R. Inferior	0.097	0.367	0.032	0.432
Abdomen: Anterior	0.022	0.469	0.098	0.392
Abdomen: Posterior	0.668	0.332	0.115	0.885
Abdomen: L. Inferior	0.564	0.105	0.061	0.608
Abdomen: R. Inferior	0.108	0.560	0.061	0.606
L. Arm: Up. Anterior	0.066	0.409	0.071	0.404
L. Arm: Up. Posterior	0.911	0.089	0.175	0.825
L. Arm: Up. Inferior	0.308	0.289	0.057	0.540
L. Arm: Up. Exterior	0.542	0.411	0.169	0.784
L. Arm: Lo. Anterior	0.006	0.420	0.086	0.340
L. Arm: Lo. Posterior	0.782	0.218	0.054	0.946
L. Arm: Lo. Inferior	0.222	0.392	0.025	0.589
L. Arm: Lo. Exterior	0.205	0.662	0.170	0.697
L. Hand: Handback	0.177	0.538	0.145	0.569
L. Hand: Palm	0.154	0.100	0.023	0.231
L. Leg: Up. Anterior	0.018	0.413	0.109	0.322
L. Leg: Up. Posterior	0.191	0.755	0.000	0.946
L. Leg: Up. Inferior	0.000	0.563	0.064	0.500
L. Leg: Up. Exterior	0.420	0.356	0.059	0.717
L. Leg: Lo. Anterior	0.035	0.965	0.117	0.883
L. Leg: Lo. Posterior	0.316	0.393	0.037	0.672
L. Leg: Lo. Inferior	0.030	0.711	0.055	0.686
L. Leg: Lo. Exterior	0.352	0.572	0.074	0.850
L. Foot: Instep	0.217	0.669	0.130	0.756
L. Foot: Sole	0.009	0.889	0.000	0.897
R. Shoulder	0.198	0.688	0.289	0.597
R. Arm: Up. Anterior	0.002	0.462	0.071	0.393
R. Arm: Up. Posterior	0.466	0.534	0.175	0.825
R. Arm: Up. Inferior	0.550	0.056	0.057	0.550
R. Arm: Up. Exterior	0.046	0.908	0.169	0.784
R. Arm: Lo. Anterior	0.098	0.328	0.086	0.340
R. Arm: Lo. Posterior	0.136	0.864	0.054	0.946
R. Arm: Lo. Inferior	0.237	0.376	0.025	0.588
R. Arm: Lo. Exterior	0.000	0.864	0.170	0.694
R. Hand: Handback	0.051	0.661	0.145	0.567
R. Hand: Palm	0.090	0.169	0.023	0.236
R. Leg: Up. Anterior	0.105	0.323	0.109	0.320
R. Leg: Up. Posterior	0.101	0.835	0.000	0.936
R. Leg: Up. Inferior	0.119	0.444	0.064	0.499
R. Leg: Up. Exterior	0.028	0.748	0.059	0.717
R. Leg: Lo. Anterior	0.068	0.932	0.117	0.883
R. Leg: Lo. Posterior	0.285	0.422	0.037	0.670
R. Leg: Lo. Inferior	0.214	0.522	0.055	0.682
R. Leg: Lo. Exterior	0.022	0.905	0.074	0.853
R. Foot: Instep	0.191	0.693	0.130	0.754
R. Foot: Sole	0.004	0.891	0.000	0.895
Whole body	**0.238**	**0.544**	**0.106**	**0.676**

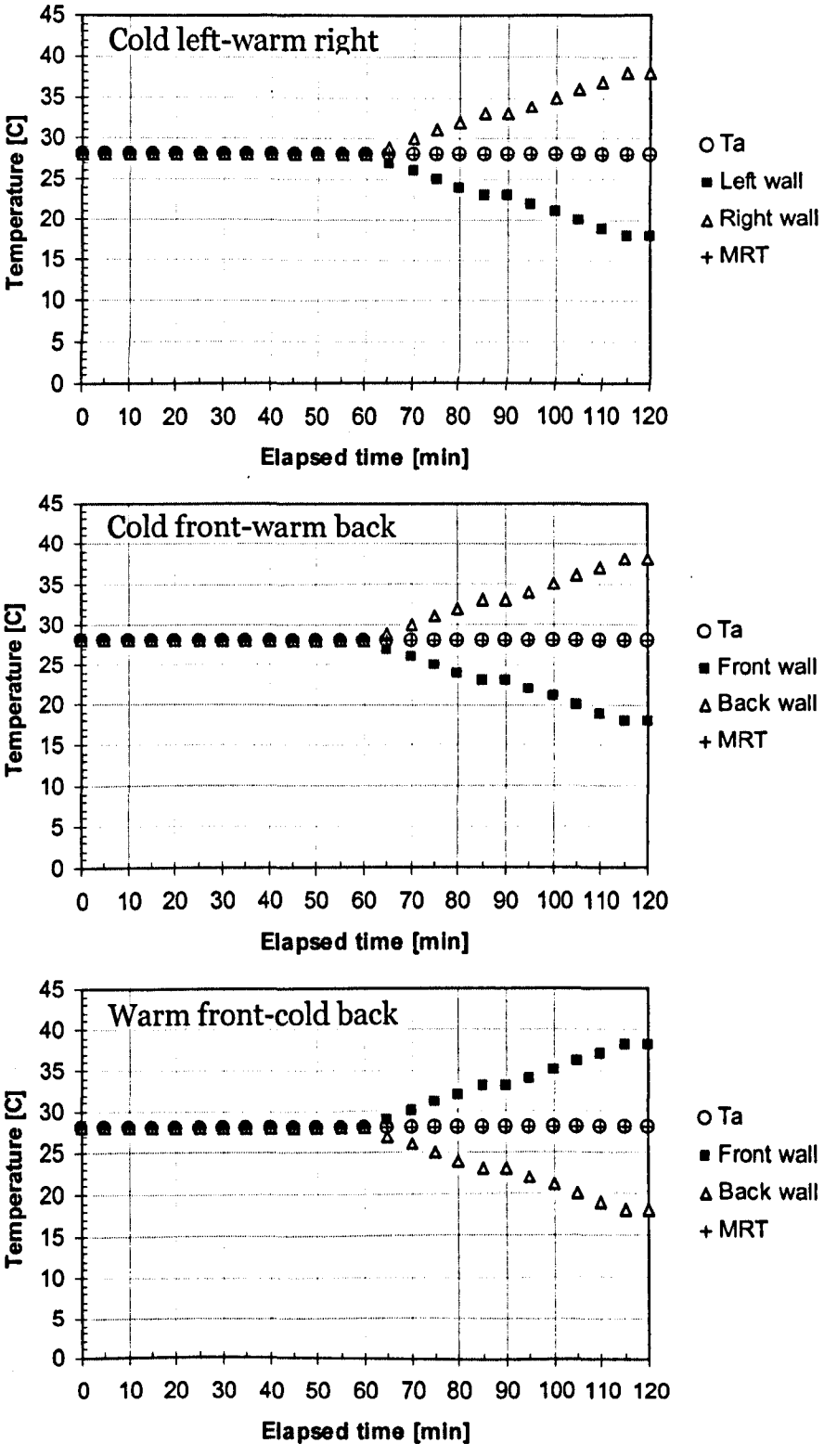

Figure D.1 Environmental conditions in the simulations regarding to experimental series of Olesen et al. (1972).

Table D.9 Environmental conditions and local discomfort results in the experimental series of Berglund and Fobelets (1987).

series	Radiant temp. asymmetry [°C]	MRT [°C]	To [°C]	Ta [°C]	Va [ms^{-1}]	RH [%]	Local discomfort [%]
(N-3)#1	0	18.74	18.46	18.09	0.07	40.90	50±7
(N-3)#2	5	18.14	18.71	19.50	0.07	38.22	58±7
(N-3)#2	10	17.53	19.05	20.75	0.06	36.84	46±7
(N-3)#2	17	16.47	19.80	22.26	0.02	31.45	45±7

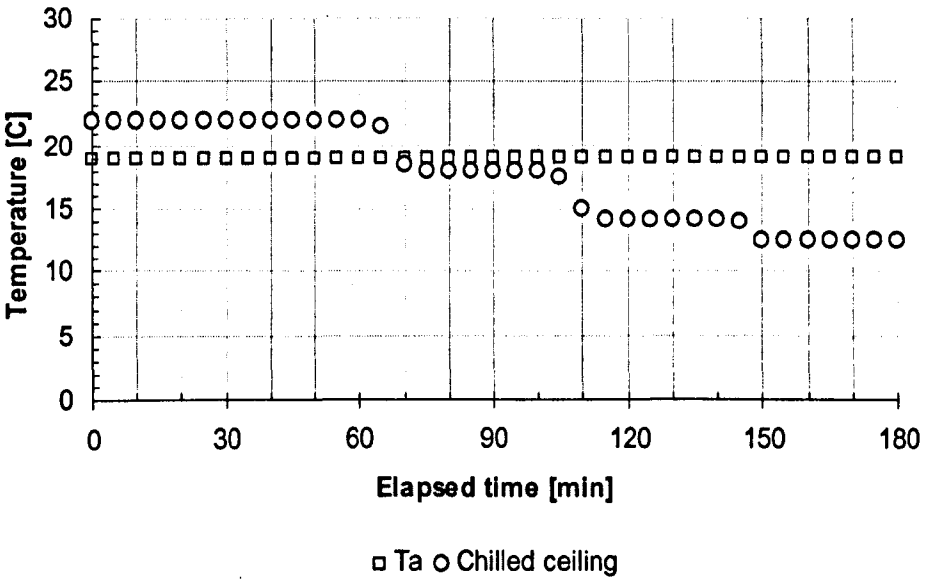

Figure D.2 Environmental conditions in the simulations regarding to chilled-ceiling series of Loveday et al. (1998, 2001 and 2002).

Appendix E

Predicted mean skin, rectal, local skin temperature and measured sensitivity coefficients

Table E.1 Predicted temperatures of subject obtained for warm/hot ceiling exposure (Fanger et al., 1980).

Body parts	$T_{sk,l,o}$	Predicted local skin temperature ($T_{sk,l}$)					
		60 (min)	90 (min)	120 (min)	150 (min)	180 (min)	210 (min)
Forehead	35.6	34.5	34.7	34.8	35.0	35.2	35.4
Head	35.7	34.7	35.0	35.1	35.3	35.6	35.8
Face: Anterior	35.7	34.5	34.7	34.7	34.8	34.9	34.9
L. Face	35.7	34.5	34.7	34.8	34.9	35.0	35.1
R. Face	35.7	34.5	34.7	34.8	34.9	35.0	35.1
Neck: Anterior	35.2	34.3	34.4	34.5	34.5	34.6	34.6
Neck: Posterior	35.2	34.2	34.4	34.5	34.7	34.9	35.0
Neck: L. Exterior	35.2	34.3	34.5	34.6	34.8	35.1	35.2
Neck: R. Exterior	35.2	34.3	34.5	34.6	34.8	35.0	35.2
L. Shoulder	34.2	33.6	33.9	34.2	34.5	34.9	35.1
Thorax: Anterior	34.9	34.6	34.7	34.9	35.0	35.2	35.3
Thorax: Posterior	34.9	34.6	34.7	34.7	34.8	34.9	34.9
Thorax: L. Inferior	35.4	34.9	34.9	34.9	34.9	34.8	34.8
Thorax: R. Inferior	35.4	34.9	34.9	34.9	34.8	34.8	34.8
Abdomen: Anterior	34.2	34.2	34.2	34.2	34.3	34.3	34.3
Abdomen: Posterior	34.2	33.9	33.9	33.9	33.8	33.8	33.8
Abdomen: L. Inferior	34.5	34.1	34.1	34.0	34.0	33.9	33.9
Abdomen: R. Inferior	34.5	34.1	34.1	34.0	34.0	33.9	33.9
L. Arm: Up. Anterior	33.8	33.4	33.3	33.2	33.1	33.0	32.9
L. Arm: Up. Posterior	33.7	33.1	33.1	33.0	33.0	33.1	33.0
L. Arm: Up. Inferior	34.2	33.3	33.2	33.0	32.9	32.7	32.6
L. Arm: Up. Exterior	33.7	33.6	33.6	33.6	33.7	33.8	33.8
L. Arm: Lo. Anterior	33.2	32.7	32.6	32.4	32.3	32.2	32.1
L. Arm: Lo. Posterior	33.2	32.3	32.2	32.0	31.8	31.6	31.4
L. Arm: Lo. Inferior	33.5	32.5	32.4	32.1	31.9	31.7	31.4
L. Arm: Lo. Exterior	33.1	32.4	32.4	32.3	32.3	32.4	32.3
L. Hand: Handback	35.1	33.0	33.0	32.8	32.7	32.7	32.6
L. Hand: Palm	35.4	33.6	33.4	33.1	32.9	32.6	32.3
L. Leg: Up. Anterior	34.2	32.7	32.7	32.7	32.7	32.7	32.6
L. Leg: Up. Posterior	34.1	33.2	33.0	32.8	32.6	32.4	32.2
L. Leg: Up. Inferior	34.5	33.4	33.3	33.2	33.2	33.1	33.0
L. Leg: Up. Exterior	34.2	33.3	33.2	33.1	33.0	32.9	32.8
L. Leg: Lo. Anterior	33.7	32.4	32.3	32.2	32.0	31.9	31.7
L. Leg: Lo. Posterior	33.7	31.6	31.5	31.2	31.0	30.7	30.5
L. Leg: Lo. Inferior	33.8	32.6	32.4	32.3	32.1	31.9	31.7
L. Leg: Lo. Exterior	33.7	32.4	32.4	32.2	32.1	31.9	31.8
L. Foot: Instep	33.4	31.5	31.2	30.8	30.5	30.2	30.0
L. Foot: Sole	33.3	32.3	31.9	31.3	30.9	30.4	29.9
R. Shoulder	34.2	33.6	33.9	34.2	34.5	34.9	35.1
R. Arm: Up. Anterior	33.8	33.4	33.3	33.2	33.1	33.0	32.9
R. Arm: Up. Posterior	33.7	33.1	33.1	33.0	33.0	33.1	33.0
R. Arm: Up. Inferior	34.2	33.3	33.2	33.0	32.9	32.7	32.5
R. Arm: Up. Exterior	33.7	33.6	33.6	33.6	33.7	33.8	33.8
R. Arm: Lo. Anterior	33.2	32.7	32.6	32.4	32.3	32.2	32.1
R. Arm: Lo. Posterior	33.2	32.3	32.2	32.0	31.8	31.6	31.4
R. Arm: Lo. Inferior	33.5	32.5	32.4	32.1	31.9	31.7	31.4
R. Arm: Lo. Exterior	33.1	32.4	32.4	32.3	32.3	32.4	32.3
R. Hand: Handback	35.1	33.0	33.0	32.8	32.7	32.7	32.6
R. Hand: Palm	35.4	33.6	33.4	33.1	32.9	32.6	32.3
R. Leg: Up. Anterior	34.2	32.7	32.7	32.7	32.7	32.7	32.6
R. Leg: Up. Posterior	34.1	33.2	33.1	32.8	32.6	32.4	32.2
R. Leg: Up. Inferior	34.5	33.4	33.3	33.2	33.2	33.1	33.0
R. Leg: Up. Exterior	34.2	33.3	33.2	33.1	33.0	32.9	32.8
R. Leg: Lo. Anterior	33.7	32.4	32.3	32.2	32.0	31.9	31.7
R. Leg: Lo. Posterior	33.7	31.6	31.5	31.2	31.0	30.7	30.5
R. Leg: Lo. Inferior	33.8	32.6	32.5	32.3	32.1	31.9	31.7
R. Leg: Lo. Exterior	33.7	32.4	32.4	32.2	32.1	31.9	31.8
R. Foot: Instep	33.4	31.5	31.2	30.8	30.5	30.3	30.0
R. Foot: Sole	33.3	32.3	31.9	31.3	30.9	30.4	29.9
Predicted mean skin temperature ($T_{sk,m}$)		33.5	33.5	33.4	33.4	33.3	33.3
Predicted rectal temperature (T_{re})		37.0	37.0	37.0	37.1	37.1	37.1

Table E.2 Predicted temperatures of subject obtained for cool/cold ceiling exposure (Fanger et al., 1985).

Body parts	Predicted local skin temperature ($T_{sk,i}$)					
	60 (min)	90 (min)	120 (min)	150 (min)	180 (min)	210 (min)
Forehead	34.2	34.0	34.0	33.9	33.8	33.8
Head	34.5	34.3	34.3	34.4	34.3	34.3
Face: Anterior	34.1	33.9	33.9	33.9	33.8	33.9
L. Face	34.1	33.9	33.9	33.9	33.9	33.9
R. Face	34.1	33.9	33.9	33.9	33.9	33.9
Neck: Anterior	34.0	33.8	33.7	33.8	33.7	33.7
Neck: Posterior	33.9	33.6	33.5	33.5	33.4	33.5
Neck: L. Exterior	34.0	33.8	33.7	33.7	33.6	33.7
Neck: R. Exterior	34.0	33.8	33.7	33.7	33.6	33.7
L. Shoulder	33.1	33.0	33.1	33.3	33.3	33.4
Thorax: Anterior	34.5	34.3	34.2	34.1	34.1	34.1
Thorax: Posterior	34.4	34.4	34.3	34.3	34.3	34.3
Thorax: L. Inferior	34.8	34.8	34.8	34.9	34.9	35.0
Thorax: R. Inferior	34.8	34.8	34.8	34.9	34.9	35.0
Abdomen: Anterior	34.1	33.9	33.7	33.7	33.7	33.7
Abdomen: Posterior	33.8	33.7	33.5	33.5	33.5	33.5
Abdomen: L. Inferior	34.0	33.9	33.8	33.8	33.8	33.9
Abdomen: R. Inferior	34.0	33.9	33.8	33.8	33.8	33.9
L. Arm: Up. Anterior	33.1	32.9	32.9	33.0	33.0	33.1
L. Arm: Up. Posterior	32.8	32.6	32.4	32.4	32.5	32.6
L. Arm: Up. Inferior	33.0	32.9	32.9	33.0	33.1	33.2
L. Arm: Up. Exterior	33.3	33.2	33.0	33.0	33.1	33.1
L. Arm: Lo. Anterior	32.5	32.3	32.2	32.3	32.3	32.4
L. Arm: Lo. Posterior	32.1	32.1	31.9	32.0	32.1	32.2
L. Arm: Lo. Inferior	32.4	32.3	32.3	32.4	32.5	32.7
L. Arm: Lo. Exterior	32.2	31.9	31.6	31.6	31.6	31.6
L. Hand: Handback	32.7	32.2	31.9	31.8	31.8	31.9
L. Hand: Palm	33.4	33.0	33.0	33.1	33.1	33.2
L. Leg: Up. Anterior	32.5	32.2	32.1	32.2	32.3	32.4
L. Leg: Up. Posterior	32.9	32.9	32.9	33.0	33.2	33.3
L. Leg: Up. Inferior	33.2	33.0	33.0	33.1	33.2	33.3
L. Leg: Up. Exterior	33.0	32.9	32.9	33.0	33.1	33.2
L. Leg: Lo. Anterior	32.3	32.1	31.9	31.9	31.9	32.0
L. Leg: Lo. Posterior	31.5	31.3	31.2	31.4	31.6	31.7
L. Leg: Lo. Inferior	32.4	32.3	32.2	32.3	32.4	32.5
L. Leg: Lo. Exterior	32.3	32.2	32.1	32.2	32.2	32.3
L. Foot: Instep	31.6	31.0	30.5	30.3	30.2	30.1
L. Foot: Sole	32.5	32.1	31.6	31.5	31.3	31.3
R. Shoulder	33.0	33.0	33.1	33.3	33.3	33.4
R. Arm: Up. Anterior	33.1	32.9	32.9	33.0	33.0	33.1
R. Arm: Up. Posterior	32.8	32.6	32.4	32.4	32.5	32.6
R. Arm: Up. Inferior	33.0	32.9	32.9	33.0	33.1	33.2
R. Arm: Up. Exterior	33.3	33.2	33.0	33.0	33.1	33.1
R. Arm: Lo. Anterior	32.5	32.3	32.2	32.3	32.3	32.4
R. Arm: Lo. Posterior	32.1	32.1	31.9	32.0	32.1	32.2
R. Arm: Lo. Inferior	32.4	32.3	32.3	32.4	32.5	32.7
R. Arm: Lo. Exterior	32.2	31.9	31.6	31.6	31.6	31.6
R. Hand: Handback	32.7	32.2	31.9	31.8	31.8	31.9
R. Hand: Palm	33.4	33.0	33.0	33.1	33.1	33.2
R. Leg: Up. Anterior	32.5	32.2	32.1	32.2	32.3	32.4
R. Leg: Up. Posterior	32.9	32.9	32.9	33.0	33.2	33.3
R. Leg: Up. Inferior	33.2	33.0	33.0	33.1	33.2	33.3
R. Leg: Up. Exterior	33.0	32.9	32.9	33.0	33.1	33.2
R. Leg: Lo. Anterior	32.3	32.1	31.9	31.9	31.9	32.0
R. Leg: Lo. Posterior	31.5	31.3	31.3	31.4	31.6	31.7
R. Leg: Lo. Inferior	32.4	32.3	32.2	32.3	32.4	32.5
R. Leg: Lo. Exterior	32.3	32.2	32.1	32.2	32.2	32.3
R. Foot: Instep	31.6	31.0	30.5	30.3	30.2	30.1
R. Foot: Sole	32.5	32.1	31.6	31.5	31.3	31.3
Predicted mean skin temperature ($T_{sk,m}$)	33.3	33.1	32.9	33.0	33.0	33.0
Predicted rectal temperature (T_{re})	37.2	37.2	37.2	37.1	37.1	37.1

Table E.3 Predicted temperatures of subject obtained for warm/hot wall exposure (Fanger et al., 1985).

Body parts	Predicted local skin temperature ($T_{sk,i}$)					
	60 (min)	90 (min)	120 (min)	150 (min)	180 (min)	210 (min)
Forehead	34.5	34.7	34.8	34.8	34.9	34.8
Head	34.7	34.9	34.9	34.9	34.9	34.7
Face: Anterior	34.6	34.8	34.9	34.9	35.1	34.9
L. Face	34.8	35.3	35.9	36.4	37.1	37.2
R. Face	34.3	34.4	34.2	34.0	33.7	33.3
Neck: Anterior	34.3	34.5	34.6	34.6	34.7	34.5
Neck: Posterior	34.1	34.3	34.3	34.2	34.3	34.1
Neck: L. Exterior	34.5	34.9	35.4	35.8	36.3	36.4
Neck: R. Exterior	34.1	34.1	33.9	33.6	33.4	33.1
L. Shoulder	33.8	33.9	34.1	34.1	34.2	34.2
Thorax: Anterior	34.6	34.7	34.9	35.0	35.1	35.1
Thorax: Posterior	34.5	34.6	34.7	34.8	34.9	34.9
Thorax: L. Inferior	34.9	35.1	35.3	35.6	35.8	35.9
Thorax: R. Inferior	34.7	34.7	34.6	34.5	34.3	34.1
Abdomen: Anterior	34.2	34.2	34.2	34.1	34.1	34.0
Abdomen: Posterior	33.9	34.0	34.1	34.2	34.4	34.4
Abdomen: L. Inferior	34.2	34.5	34.9	35.4	35.9	36.3
Abdomen: R. Inferior	33.9	33.8	33.7	33.4	33.2	32.8
L. Arm: Up. Anterior	33.4	33.3	33.4	33.4	33.4	33.3
L. Arm: Up. Posterior	33.2	33.3	33.6	33.9	34.3	34.4
L. Arm: Up. Inferior	33.1	33.0	32.8	32.5	32.2	31.9
L. Arm: Up. Exterior	33.7	34.0	34.4	34.8	35.3	35.6
L. Arm: Lo. Anterior	32.5	32.3	31.9	31.5	31.1	30.7
L. Arm: Lo. Posterior	32.6	33.0	33.8	34.5	35.4	35.8
L. Arm: Lo. Inferior	32.4	32.3	32.2	32.0	31.8	31.5
L. Arm: Lo. Exterior	32.5	32.6	32.9	33.2	33.5	33.6
L. Hand: Handback	32.9	32.9	33.0	33.0	33.1	32.9
L. Hand: Palm	33.5	33.4	33.3	33.1	33.1	32.8
L. Leg: Up. Anterior	32.6	32.4	32.1	31.8	31.5	31.1
L. Leg: Up. Posterior	33.1	33.1	33.2	33.2	33.2	33.1
L. Leg: Up. Inferior	33.2	33.1	32.8	32.5	32.2	31.8
L. Leg: Up. Exterior	33.5	33.8	34.3	34.9	35.6	36.0
L. Leg: Lo. Anterior	32.3	32.3	32.2	32.1	32.0	31.8
L. Leg: Lo. Posterior	31.6	31.6	31.7	31.7	31.8	31.7
L. Leg: Lo. Inferior	32.4	32.2	31.9	31.5	31.1	30.7
L. Leg: Lo. Exterior	32.6	32.9	33.4	33.9	34.6	34.9
L. Foot: Instep	31.2	31.0	30.8	30.7	30.6	30.3
L. Foot: Sole	31.8	31.4	30.9	30.3	29.7	29.1
R. Shoulder	33.7	33.7	33.5	33.3	33.1	32.8
R. Arm: Up. Anterior	33.3	33.1	33.0	32.7	32.5	32.2
R. Arm: Up. Posterior	32.9	32.8	32.6	32.3	32.0	31.6
R. Arm: Up. Inferior	33.3	33.3	33.4	33.5	33.6	33.5
R. Arm: Up. Exterior	33.4	33.3	33.0	32.7	32.4	32.0
R. Arm: Lo. Anterior	32.8	32.8	32.9	33.0	33.2	33.1
R. Arm: Lo. Posterior	32.0	31.9	31.5	31.0	30.6	30.0
R. Arm: Lo. Inferior	32.4	32.3	32.1	31.9	31.7	31.4
R. Arm: Lo. Exterior	32.2	32.0	31.7	31.3	30.9	30.4
R. Hand: Handback	32.7	32.5	32.2	31.9	31.5	30.9
R. Hand: Palm	33.4	33.1	32.8	32.4	32.0	31.5
R. Leg: Up. Anterior	32.7	32.7	32.7	32.7	32.7	32.5
R. Leg: Up. Posterior	33.0	32.9	32.8	32.6	32.4	32.1
R. Leg: Up. Inferior	33.4	33.5	33.7	33.9	34.2	34.2
R. Leg: Up. Exterior	33.1	32.9	32.7	32.3	32.0	31.6
R. Leg: Lo. Anterior	32.4	32.4	32.4	32.4	32.5	32.3
R. Leg: Lo. Posterior	31.5	31.5	31.6	31.6	31.6	31.4
R. Leg: Lo. Inferior	32.7	32.8	33.1	33.5	33.8	34.0
R. Leg: Lo. Exterior	32.3	32.1	31.8	31.4	31.0	30.5
R. Foot: Instep	31.2	30.9	30.7	30.4	30.3	29.9
R. Foot: Sole	31.8	31.4	30.8	30.2	29.6	29.0
Predicted mean skin temperature ($T_{sk,m}$)	33.4	33.4	33.4	33.4	33.4	33.2
Predicted rectal temperature (T_{re})	37.1	37.1	37.1	37.1	37.1	37.1

Table E.4 Predicted temperatures of subject obtained for the cool/cold wall exposure (Fanger et al., 1985).

Body parts	Predicted local skin temperature ($T_{sk,i}$)					
	60 (min)	90 (min)	120 (min)	150 (min)	180 (min)	210 (min)
Forehead	34.3	34.3	34.4	34.4	34.5	34.5
Head	34.5	34.6	34.7	34.8	34.8	34.9
Face: Anterior	34.1	34.2	34.3	34.4	34.4	34.5
L. Face	33.9	33.8	33.7	33.6	33.5	33.5
R. Face	34.2	34.4	34.6	34.7	34.8	34.9
Neck: Anterior	34.0	34.0	34.1	34.2	34.2	34.2
Neck: Posterior	33.9	33.9	34.0	34.1	34.1	34.2
Neck: L. Exterior	33.8	33.7	33.6	33.5	33.4	33.4
Neck: R. Exterior	34.0	34.2	34.3	34.5	34.6	34.6
L. Shoulder	33.1	33.3	33.5	33.7	33.8	33.9
Thorax: Anterior	34.4	34.5	34.5	34.5	34.5	34.5
Thorax: Posterior	34.4	34.4	34.5	34.5	34.5	34.6
Thorax: L. Inferior	34.6	34.6	34.6	34.6	34.6	34.6
Thorax: R. Inferior	34.7	34.8	35.0	35.1	35.2	35.2
Abdomen: Anterior	34.1	34.0	34.0	34.1	34.1	34.2
Abdomen: Posterior	33.9	33.7	33.6	33.6	33.6	33.6
Abdomen: L. Inferior	33.9	33.6	33.5	33.3	33.2	33.1
Abdomen: R. Inferior	34.0	34.0	34.1	34.2	34.3	34.4
L. Arm: Up. Anterior	33.2	33.1	33.1	33.2	33.2	33.3
L. Arm: Up. Posterior	32.9	32.7	32.5	32.4	32.3	32.3
L. Arm: Up. Inferior	33.2	33.2	33.3	33.4	33.6	33.7
L. Arm: Up. Exterior	33.3	33.1	32.9	32.7	32.6	32.6
L. Arm: Lo. Anterior	32.7	32.7	32.8	33.0	33.2	33.3
L. Arm: Lo. Posterior	32.1	31.6	31.2	30.9	30.7	30.5
L. Arm: Lo. Inferior	32.5	32.5	32.5	32.6	32.6	32.7
L. Arm: Lo. Exterior	32.3	32.0	31.9	31.7	31.6	31.6
L. Hand: Handback	32.6	32.4	32.3	32.2	32.2	32.3
L. Hand: Palm	33.3	33.1	33.1	33.1	33.2	33.3
L. Leg: Up. Anterior	32.5	32.5	32.7	32.9	33.1	33.2
L. Leg: Up. Posterior	33.0	32.9	32.9	32.9	32.9	33.0
L. Leg: Up. Inferior	33.2	33.3	33.4	33.6	33.7	33.9
L. Leg: Up. Exterior	32.9	32.6	32.4	32.2	32.1	32.0
L. Leg: Lo. Anterior	32.4	32.3	32.3	32.3	32.3	32.4
L. Leg: Lo. Posterior	31.4	31.3	31.2	31.2	31.2	31.3
L. Leg: Lo. Inferior	32.5	32.5	32.6	32.8	32.9	33.0
L. Leg: Lo. Exterior	32.2	31.9	31.7	31.5	31.3	31.2
L. Foot: Instep	31.6	31.1	30.8	30.5	30.3	30.2
L. Foot: Sole	32.6	32.2	32.0	31.8	31.7	31.6
R. Shoulder	33.2	33.4	33.7	34.0	34.3	34.5
R. Arm: Up. Anterior	33.2	33.2	33.3	33.5	33.6	33.7
R. Arm: Up. Posterior	33.0	33.0	33.1	33.2	33.3	33.4
R. Arm: Up. Inferior	33.1	33.0	32.9	32.9	32.9	33.0
R. Arm: Up. Exterior	33.5	33.5	33.6	33.8	33.9	34.0
R. Arm: Lo. Anterior	32.5	32.4	32.3	32.3	32.3	32.3
R. Arm: Lo. Posterior	32.4	32.4	32.5	32.6	32.7	32.9
R. Arm: Lo. Inferior	32.5	32.5	32.5	32.6	32.7	32.8
R. Arm: Lo. Exterior	32.4	32.4	32.5	32.6	32.7	32.9
R. Hand: Handback	32.8	32.6	32.7	32.8	32.9	33.0
R. Hand: Palm	33.3	33.3	33.3	33.5	33.6	33.7
R. Leg: Up. Anterior	32.4	32.4	32.4	32.5	32.6	32.7
R. Leg: Up. Posterior	33.1	33.0	33.1	33.2	33.3	33.4
R. Leg: Up. Inferior	33.1	33.0	32.9	32.9	32.9	32.9
R. Leg: Up. Exterior	33.1	33.1	33.3	33.4	33.6	33.7
R. Leg: Lo. Anterior	32.3	32.2	32.1	32.1	32.1	32.1
R. Leg: Lo. Posterior	31.4	31.3	31.3	31.3	31.3	31.4
R. Leg: Lo. Inferior	32.4	32.1	32.0	31.9	31.8	31.8
R. Leg: Lo. Exterior	32.5	32.4	32.5	32.7	32.8	32.9
R. Foot: Instep	31.6	31.1	30.8	30.6	30.4	30.4
R. Foot: Sole	32.6	32.2	32.0	31.8	31.7	31.7
Predicted mean skin temperature ($T_{sk,m}$)	33.3	33.2	33.2	33.2	33.3	33.3
Predicted rectal temperature (T_{re})	37.2	37.2	37.2	37.1	37.1	37.1

Table E.5 Predicted body temperatures obtained for cold left-warm right series of Olesen et al. (1972).

Body parts	Predicted local skin temperature ($T_{sk,i}$)			
	30 (min)	60 (min)	90 (min)	120 (min)
Forehead	35.0	35.1	35.1	35.1
Head	35.2	35.3	35.3	35.3
Face: Anterior	34.8	35.0	35.1	35.1
L. Face	34.8	35.0	34.9	34.7
R. Face	34.8	35.0	35.2	35.4
Neck: Anterior	34.6	34.7	34.8	34.9
Neck: Posterior	34.5	34.6	34.7	34.7
Neck: L. Exterior	34.6	34.7	34.6	34.4
Neck: R. Exterior	34.6	34.7	34.9	35.2
L. Shoulder	33.3	33.5	33.5	33.4
Thorax: Anterior	34.0	34.1	34.1	34.2
Thorax: Posterior	33.9	34.0	34.1	34.1
Thorax: L. Inferior	34.6	34.7	34.6	34.5
Thorax: R. Inferior	34.6	34.7	34.8	34.9
Abdomen: Anterior	34.1	34.3	34.4	34.4
Abdomen: Posterior	33.9	34.0	34.1	34.2
Abdomen: L. Inferior	34.1	34.2	34.2	34.1
Abdomen: R. Inferior	34.1	34.2	34.4	34.6
L. Arm: Up. Anterior	32.7	32.9	33.0	33.0
L. Arm: Up. Posterior	32.2	32.4	32.4	32.2
L. Arm: Up. Inferior	32.8	32.9	33.0	33.1
L. Arm: Up. Exterior	32.2	32.4	32.3	31.9
L. Arm: Lo. Anterior	32.0	32.3	32.6	32.8
L. Arm: Lo. Posterior	31.6	31.8	31.8	31.5
L. Arm: Lo. Inferior	32.0	32.2	32.3	32.4
L. Arm: Lo. Exterior	31.7	31.9	31.9	31.7
L. Hand: Handback	33.3	33.5	33.6	33.6
L. Hand: Palm	33.7	34.0	34.1	34.2
L. Leg: Up. Anterior	33.5	33.6	33.7	33.8
L. Leg: Up. Posterior	33.0	33.1	33.0	32.9
L. Leg: Up. Inferior	33.5	33.6	33.6	33.7
L. Leg: Up. Exterior	33.2	33.2	33.1	32.7
L. Leg: Lo. Anterior	32.6	32.6	32.6	32.6
L. Leg: Lo. Posterior	32.8	32.9	32.9	32.8
L. Leg: Lo. Inferior	32.9	32.9	33.0	33.1
L. Leg: Lo. Exterior	32.6	32.7	32.5	32.2
L. Foot: Instep	32.0	31.9	31.8	31.7
L. Foot: Sole	31.9	31.9	31.7	31.4
R. Shoulder	33.3	33.5	33.7	34.0
R. Arm: Up. Anterior	32.7	32.9	33.1	33.2
R. Arm: Up. Posterior	32.2	32.4	32.6	32.9
R. Arm: Up. Inferior	32.8	32.9	32.9	32.8
R. Arm: Up. Exterior	32.2	32.4	32.8	33.2
R. Arm: Lo. Anterior	32.0	32.3	32.4	32.3
R. Arm: Lo. Posterior	31.6	31.8	32.2	32.6
R. Arm: Lo. Inferior	32.0	32.2	32.3	32.4
R. Arm: Lo. Exterior	31.7	31.9	32.2	32.6
R. Hand: Handback	33.3	33.5	33.8	34.0
R. Hand: Palm	33.7	34.0	34.1	34.3
R. Leg: Up. Anterior	33.5	33.6	33.6	33.5
R. Leg: Up. Posterior	33.0	33.1	33.1	33.1
R. Leg: Up. Inferior	33.5	33.6	33.4	33.2
R. Leg: Up. Exterior	33.2	33.2	33.4	33.6
R. Leg: Lo. Anterior	32.6	32.6	32.6	32.5
R. Leg: Lo. Posterior	32.8	32.9	32.9	32.9
R. Leg: Lo. Inferior	32.9	32.9	32.8	32.5
R. Leg: Lo. Exterior	32.6	32.7	32.8	33.1
R. Foot: Instep	32.0	31.9	31.8	31.8
R. Foot: Sole	31.9	31.9	31.9	32.0
Predicted mean skin temperature ($T_{sk,m}$)	33.4	33.5	33.6	33.6
Predicted rectal temperature (T_{re})	36.9	36.9	36.9	36.9

Table E.6 Predicted body temperatures obtained for cold front-warm back series of Olesen et al. (1972).

Body parts	Predicted local skin temperature ($T_{sk,i}$)			
	30 (min)	60 (min)	90 (min)	120 (min)
Forehead	35.0	35.1	35.0	34.9
Head	35.2	35.2	35.3	35.4
Face: Anterior	34.8	35.0	35.0	34.9
L. Face	34.8	34.9	35.0	35.0
R. Face	34.8	34.9	35.0	35.0
Neck: Anterior	34.6	34.7	34.7	34.7
Neck: Posterior	34.5	34.6	34.8	35.0
Neck: L. Exterior	34.5	34.7	34.8	34.8
Neck: R. Exterior	34.5	34.7	34.7	34.8
L. Shoulder	33.3	33.5	33.7	33.8
Thorax: Anterior	34.0	34.1	34.0	33.9
Thorax: Posterior	34.0	34.0	34.2	34.4
Thorax: L. Inferior	34.6	34.7	34.7	34.8
Thorax: R. Inferior	34.6	34.7	34.7	34.7
Abdomen: Anterior	33.7	33.9	34.0	34.0
Abdomen: Posterior	33.6	33.7	33.8	34.0
Abdomen: L. Inferior	33.7	33.9	34.0	34.1
Abdomen: R. Inferior	33.7	33.9	34.0	34.1
L. Arm: Up. Anterior	32.7	32.9	32.9	32.9
L. Arm: Up. Posterior	32.2	32.4	32.6	32.9
L. Arm: Up. Inferior	32.8	32.9	33.0	33.2
L. Arm: Up. Exterior	32.3	32.4	32.5	32.5
L. Arm: Lo. Anterior	32.0	32.3	32.4	32.4
L. Arm: Lo. Posterior	31.6	31.8	32.0	32.1
L. Arm: Lo. Inferior	32.0	32.2	32.4	32.5
L. Arm: Lo. Exterior	31.7	31.9	32.0	31.9
L. Hand: Handback	33.3	33.5	33.6	33.6
L. Hand: Palm	33.7	33.9	34.1	34.2
L. Leg: Up. Anterior	33.5	33.6	33.6	33.5
L. Leg: Up. Posterior	33.0	33.0	33.0	33.0
L. Leg: Up. Inferior	33.5	33.5	33.5	33.4
L. Leg: Up. Exterior	33.2	33.2	33.2	33.2
L. Leg: Lo. Anterior	32.6	32.6	32.5	32.2
L. Leg: Lo. Posterior	32.8	32.9	32.9	33.0
L. Leg: Lo. Inferior	32.9	32.9	32.8	32.7
L. Leg: Lo. Exterior	32.7	32.7	32.6	32.5
L. Foot: Instep	32.0	31.9	31.8	31.6
L. Foot: Sole	32.0	31.9	31.7	31.6
R. Shoulder	33.3	33.5	33.7	33.8
R. Arm: Up. Anterior	32.7	32.9	33.0	32.9
R. Arm: Up. Posterior	32.2	32.4	32.6	32.9
R. Arm: Up. Inferior	32.8	32.9	33.0	33.2
R. Arm: Up. Exterior	32.3	32.4	32.5	32.5
R. Arm: Lo. Anterior	32.0	32.3	32.4	32.4
R. Arm: Lo. Posterior	31.6	31.8	32.0	32.1
R. Arm: Lo. Inferior	32.0	32.2	32.4	32.5
R. Arm: Lo. Exterior	31.7	31.9	32.0	31.9
R. Hand: Handback	33.3	33.5	33.6	33.6
R. Hand: Palm	33.7	33.9	34.1	34.2
R. Leg: Up. Anterior	33.5	33.6	33.6	33.5
R. Leg: Up. Posterior	33.0	33.1	33.0	33.0
R. Leg: Up. Inferior	33.6	33.5	33.5	33.4
R. Leg: Up. Exterior	33.2	33.2	33.2	33.2
R. Leg: Lo. Anterior	32.6	32.6	32.5	32.2
R. Leg: Lo. Posterior	32.8	32.9	32.9	33.0
R. Leg: Lo. Inferior	32.9	32.9	32.8	32.7
R. Leg: Lo. Exterior	32.7	32.7	32.6	32.5
R. Foot: Instep	32.0	31.9	31.8	31.6
R. Foot: Sole	32.0	31.9	31.7	31.6
Mean skin temperature ($T_{sk,m}$)	33.4	33.5	33.5	33.5
Rectal temperature (T_{re})	36.9	36.9	36.9	36.9

Table E.7 Predicted body temperatures obtained for warm front-cold back series of Olesen et al. (1972).

Body parts	Local skin temperature ($T_{sk,i}$)			
	30 (min)	60 (min)	90 (min)	120 (min)
Forehead	35.0	35.1	35.3	35.4
Head	35.2	35.3	35.2	35.2
Face: Anterior	34.8	35.0	35.2	35.3
L. Face	34.8	35.0	35.0	35.1
R. Face	34.8	35.0	35.0	35.1
Neck: Anterior	34.6	34.7	35.0	35.2
Neck: Posterior	34.5	34.6	34.4	34.3
Neck: L. Exterior	34.6	34.7	34.8	34.8
Neck: R. Exterior	34.6	34.7	34.8	34.8
L. Shoulder	33.3	33.5	33.5	33.5
Thorax: Anterior	34.0	34.1	34.4	34.7
Thorax: Posterior	33.9	34.0	33.7	33.4
Thorax: L. Inferior	34.6	34.7	34.7	34.6
Thorax: R. Inferior	34.6	34.7	34.6	34.6
Abdomen: Anterior	34.1	34.3	34.5	34.7
Abdomen: Posterior	33.9	34.0	34.0	33.9
Abdomen: L. Inferior	34.1	34.2	34.2	34.2
Abdomen: R. Inferior	34.1	34.2	34.2	34.2
L. Arm: Up. Anterior	32.7	32.9	33.2	33.5
L. Arm: Up. Posterior	32.2	32.4	32.1	31.9
L. Arm: Up. Inferior	32.8	32.9	32.7	32.6
L. Arm: Up. Exterior	32.2	32.4	32.6	32.7
L. Arm: Lo. Anterior	32.0	32.3	32.6	32.9
L. Arm: Lo. Posterior	31.6	31.8	31.9	31.9
L. Arm: Lo. Inferior	32.0	32.2	32.2	32.1
L. Arm: Lo. Exterior	31.7	31.9	32.3	32.7
L. Hand: Handback	33.3	33.5	33.8	34.0
L. Hand: Palm	33.7	34.0	34.1	34.2
L. Leg: Up. Anterior	33.5	33.6	33.7	33.8
L. Leg: Up. Posterior	33.0	33.1	33.0	32.9
L. Leg: Up. Inferior	33.5	33.6	33.6	33.6
L. Leg: Up. Exterior	33.2	33.2	33.2	33.2
L. Leg: Lo. Anterior	32.6	32.6	32.9	33.2
L. Leg: Lo. Posterior	32.8	32.9	32.8	32.6
L. Leg: Lo. Inferior	32.9	32.9	32.9	33.0
L. Leg: Lo. Exterior	32.6	32.7	32.7	32.7
L. Foot: Instep	32.0	31.9	31.9	31.8
L. Foot: Sole	31.9	31.9	31.9	31.9
R. Shoulder	33.3	33.5	33.5	33.5
R. Arm: Up. Anterior	32.7	32.9	33.2	33.5
R. Arm: Up. Posterior	32.2	32.4	32.1	31.9
R. Arm: Up. Inferior	32.8	32.9	32.7	32.6
R. Arm: Up. Exterior	32.2	32.4	32.6	32.7
R. Arm: Lo. Anterior	32.0	32.3	32.6	32.9
R. Arm: Lo. Posterior	31.6	31.8	31.9	31.9
R. Arm: Lo. Inferior	32.0	32.2	32.2	32.1
R. Arm: Lo. Exterior	31.7	31.9	32.3	32.7
R. Hand: Handback	33.3	33.5	33.8	34.0
R. Hand: Palm	33.7	34.0	34.1	34.2
R. Leg: Up. Anterior	33.5	33.6	33.7	33.8
R. Leg: Up. Posterior	33.0	33.1	33.0	33.0
R. Leg: Up. Inferior	33.5	33.6	33.6	33.6
R. Leg: Up. Exterior	33.2	33.2	33.2	33.2
R. Leg: Lo. Anterior	32.6	32.6	32.9	33.2
R. Leg: Lo. Posterior	32.8	32.9	32.8	32.6
R. Leg: Lo. Inferior	32.9	32.9	33.0	33.0
R. Leg: Lo. Exterior	32.6	32.7	32.7	32.7
R. Foot: Instep	32.0	31.9	31.9	31.8
R. Foot: Sole	31.9	31.9	31.9	31.9
Predicted mean skin temperature ($T_{sk,m}$)	33.4	33.5	33.6	33.6
Predicted rectal temperature (T_{re})	36.9	36.9	36.9	36.9

Table E.8 Predicted body temperatures obtained for spatial cold wall of Berglund and Fobelets (1987).

Body parts	Local skin temperature ($T_{sk,i}$)			
	(N-3)#1	(N-3)#2	(N-3)#3	(N-3)#4
Forehead	33.5	33.6	33.7	34.0
Head	34.0	33.7	33.8	33.7
Face: Anterior	32.8	32.5	32.8	33.2
L. Face	32.8	32.2	31.9	31.7
R. Face	32.8	32.2	32.8	33.3
Neck: Anterior	33.0	33.0	33.2	33.6
Neck: Posterior	33.0	31.9	32.0	31.7
Neck: L. Exterior	33.0	32.6	32.3	32.0
Neck: R. Exterior	33.0	32.6	33.1	33.4
L. Shoulder	33.9	33.8	33.8	33.7
Thorax: Anterior	34.4	34.5	34.6	34.8
Thorax: Posterior	34.6	34.0	33.9	33.5
Thorax: L. Inferior	34.8	34.6	34.5	34.4
Thorax: R. Inferior	34.8	34.6	34.8	34.9
Abdomen: Anterior	33.7	33.7	33.8	34.1
Abdomen: Posterior	33.7	32.9	32.9	32.5
Abdomen: L. Inferior	33.7	33.3	32.9	32.5
Abdomen: R. Inferior	33.7	33.3	33.6	33.8
L. Arm: Up. Anterior	32.8	32.8	32.9	33.2
L. Arm: Up. Posterior	32.8	32.0	31.7	31.1
L. Arm: Up. Inferior	32.9	32.3	32.6	32.6
L. Arm: Up. Exterior	32.6	32.4	32.2	31.9
L. Arm: Lo. Anterior	32.1	32.0	32.2	32.5
L. Arm: Lo. Posterior	31.9	31.4	31.0	30.5
L. Arm: Lo. Inferior	32.1	31.7	31.8	32.0
L. Arm: Lo. Exterior	31.8	31.7	31.7	31.9
L. Hand: Handback	29.4	29.0	29.3	29.7
L. Hand: Palm	30.5	29.9	30.2	30.5
L. Leg: Up. Anterior	31.9	32.1	32.4	32.8
L. Leg: Up. Posterior	31.4	31.4	31.6	31.9
L. Leg: Up. Inferior	31.8	31.9	32.3	32.7
L. Leg: Up. Exterior	31.6	31.5	31.3	31.2
L. Leg: Lo. Anterior	30.9	31.1	31.4	31.8
L. Leg: Lo. Posterior	31.3	31.0	31.1	31.0
L. Leg: Lo. Inferior	31.2	31.2	31.6	32.0
L. Leg: Lo. Exterior	31.0	31.0	30.9	30.8
L. Foot: Instep	31.7	31.3	31.4	31.5
L. Foot: Sole	31.7	31.5	31.6	31.9
R. Shoulder	33.9	33.8	34.1	34.2
R. Arm: Up. Anterior	32.8	32.8	33.0	33.3
R. Arm: Up. Posterior	32.8	32.0	32.3	32.2
R. Arm: Up. Inferior	32.9	32.3	32.2	31.8
R. Arm: Up. Exterior	32.6	32.4	32.8	33.1
R. Arm: Lo. Anterior	32.1	32.0	32.1	32.4
R. Arm: Lo. Posterior	31.9	31.4	31.8	32.1
R. Arm: Lo. Inferior	32.1	31.7	31.8	31.9
R. Arm: Lo. Exterior	31.8	31.7	32.0	32.3
R. Hand: Handback	29.4	29.0	29.6	30.3
R. Hand: Palm	30.4	29.8	30.3	30.8
R. Leg: Up. Anterior	31.9	32.1	32.2	32.5
R. Leg: Up. Posterior	31.4	31.4	31.8	32.2
R. Leg: Up. Inferior	31.8	31.9	32.1	32.4
R. Leg: Up. Exterior	31.6	31.5	32.0	32.5
R. Leg: Lo. Anterior	30.9	31.1	31.3	31.7
R. Leg: Lo. Posterior	31.3	31.0	31.1	31.1
R. Leg: Lo. Inferior	31.2	31.2	31.3	31.4
R. Leg: Lo. Exterior	31.0	31.0	31.4	31.9
R. Foot: Instep	31.7	31.3	31.4	31.5
R. Foot: Sole	31.7	31.5	31.6	31.9
Mean skin temperature ($T_{sk,m}$)	32.6	32.3	32.4	32.5
Rectal temperature (T_{re})	37.1	37.1	37.0	37.1

Table E.9 Predicted body temperatures obtained for chilled ceiling series of Loveday et al. (1998, 2001 and 2002).

Body parts	Local skin temperature ($T_{sk,i}$)			
	30 (min)	60 (min)	90 (min)	120 (min)
Forehead	34.5	34.5	34.4	34.3
Head	34.7	34.7	34.5	34.4
Face: Anterior	34.4	34.4	34.2	34.0
L. Face	34.3	34.3	34.1	33.9
R. Face	34.3	34.3	34.1	33.9
Neck: Anterior	34.1	34.1	33.9	33.7
Neck: Posterior	34.0	33.9	33.7	33.5
Neck: L. Exterior	34.0	34.0	33.8	33.6
Neck: R. Exterior	34.0	34.0	33.8	33.6
L. Shoulder	33.6	33.6	33.5	33.4
Thorax: Anterior	34.5	34.6	34.5	34.3
Thorax: Posterior	34.6	34.6	34.5	34.3
Thorax: L. Inferior	34.7	34.8	34.6	34.5
Thorax: R. Inferior	34.7	34.8	34.6	34.5
Abdomen: Anterior	33.9	34.0	34.0	33.9
Abdomen: Posterior	34.0	34.1	34.1	34.0
Abdomen: L. Inferior	34.0	34.1	34.1	34.0
Abdomen: R. Inferior	34.0	34.1	34.1	34.0
L. Arm: Up. Anterior	32.5	32.5	32.4	32.3
L. Arm: Up. Posterior	32.5	32.5	32.4	32.3
L. Arm: Up. Inferior	32.6	32.6	32.5	32.3
L. Arm: Up. Exterior	32.5	32.5	32.4	32.3
L. Arm: Lo. Anterior	31.1	31.2	31.1	30.9
L. Arm: Lo. Posterior	31.3	31.4	31.3	31.2
L. Arm: Lo. Inferior	31.3	31.3	31.2	31.1
L. Arm: Lo. Exterior	31.2	31.2	31.1	31.0
L. Hand: Handback	31.5	31.6	31.4	31.2
L. Hand: Palm	31.8	31.9	31.8	31.6
L. Leg: Up. Anterior	33.4	33.5	33.4	33.2
L. Leg: Up. Posterior	33.6	33.7	33.6	33.5
L. Leg: Up. Inferior	33.6	33.6	33.5	33.3
L. Leg: Up. Exterior	33.5	33.6	33.5	33.4
L. Leg: Lo. Anterior	33.1	33.1	33.0	32.9
L. Leg: Lo. Posterior	33.1	33.2	33.1	33.0
L. Leg: Lo. Inferior	33.1	33.2	33.1	33.0
L. Leg: Lo. Exterior	33.1	33.2	33.1	33.0
L. Foot: Instep	33.5	33.5	33.5	33.4
L. Foot: Sole	33.5	33.6	33.6	33.5
R. Shoulder	33.6	33.6	33.5	33.4
R. Arm: Up. Anterior	32.5	32.5	32.4	32.3
R. Arm: Up. Posterior	32.5	32.5	32.4	32.3
R. Arm: Up. Inferior	32.6	32.6	32.5	32.3
R. Arm: Up. Exterior	32.5	32.5	32.4	32.3
R. Arm: Lo. Anterior	31.1	31.2	31.1	30.9
R. Arm: Lo. Posterior	31.3	31.4	31.3	31.2
R. Arm: Lo. Inferior	31.3	31.3	31.2	31.1
R. Arm: Lo. Exterior	31.2	31.2	31.1	31.0
R. Hand: Handback	31.5	31.6	31.4	31.2
R. Hand: Palm	31.8	31.9	31.8	31.6
R. Leg: Up. Anterior	33.4	33.5	33.4	33.2
R. Leg: Up. Posterior	33.6	33.7	33.6	33.5
R. Leg: Up. Inferior	33.6	33.6	33.5	33.3
R. Leg: Up. Exterior	33.5	33.6	33.5	33.4
R. Leg: Lo. Anterior	33.1	33.1	33.0	32.9
R. Leg: Lo. Posterior	33.1	33.2	33.1	33.0
R. Leg: Lo. Inferior	33.1	33.2	33.1	33.0
R. Leg: Lo. Exterior	33.1	33.2	33.1	33.0
R. Foot: Instep	33.5	33.5	33.5	33.4
R. Foot: Sole	33.5	33.6	33.6	33.5
Mean skin temperature ($T_{sk,m}$)	33.3	33.4	33.3	33.2
Rectal temperature (T_{re})	37.0	37.0	37.1	37.1

Table E.10 Predicted body temperatures obtained for spatial hot wall at position 1 of McNall and Biddison (1970).

Body parts	Local skin temperature ($T_{sk,i}$)									
	Cond 1		Cond 2		Cond 3		Cond 4		Cond 7	
	60 [min]	90 [min]	60 [min]	90 [min]	60 [min]	90 [min]	60 [min]	90 [min]	60 [min]	90 [min]
Forehead	34.4	34.4	34.7	34.7	34.7	34.7	34.8	34.8	34.2	34.2
Head	34.9	34.9	35.1	35.2	35.0	35.1	35.1	35.2	34.6	34.6
Face: Anterior	*34.3*	*34.4*	34.9	35.0	34.7	34.8	34.8	34.9	33.7	33.6
L. Face	36.0	36.1	36.3	*36.4*	*36.2*	*36.2*	*36.1*	36.1	35.5	35.6
R. Face	33.4	33.4	34.0	34.2	33.9	34.0	34.2	34.3	32.7	32.5
Neck: Anterior	34.0	34.1	34.4	34.5	34.3	34.4	34.4	34.5	33.6	33.6
Neck: Posterior	34.2	34.2	34.6	34.7	34.5	34.6	34.6	34.7	33.8	33.8
Neck: L. Exterior	35.6	35.7	35.9	36.0	35.7	35.8	35.7	35.8	35.2	35.3
Neck: R. Exterior	33.2	33.3	33.7	33.8	33.6	33.7	33.8	33.9	32.8	32.8
L. Shoulder	34.5	34.6	34.9	35.1	34.7	34.9	34.7	34.9	34.0	34.1
Thorax: Anterior	34.4	34.4	34.7	34.7	34.7	34.7	34.8	34.9	34.3	34.3
Thorax: Posterior	34.6	34.7	34.9	34.9	34.9	34.9	35.0	35.1	34.5	34.6
Thorax: L. Inferior	34.8	34.8	35.1	35.1	35.0	35.0	35.0	35.0	34.6	34.6
Thorax: R. Inferior	34.4	34.3	34.6	34.6	34.5	34.5	34.6	34.6	34.2	34.1
Abdomen: Anterior	34.0	34.2	34.3	34.5	34.2	34.4	34.2	34.4	33.7	33.8
Abdomen: Posterior	34.3	34.4	34.5	34.7	34.5	34.7	34.6	34.8	34.1	34.2
Abdomen: L. Inferior	35.0	35.2	35.2	35.5	35.1	35.3	35.0	35.3	34.7	34.8
Abdomen: R. Inferior	33.6	33.6	33.9	34.0	33.8	33.9	34.0	34.1	33.3	33.3
L. Arm: Up. Anterior	33.4	33.6	34.0	34.3	33.7	33.9	33.5	33.7	32.8	32.9
L. Arm: Up. Posterior	34.3	34.6	34.8	35.1	34.5	34.8	34.5	34.7	33.8	34.0
L. Arm: Up. Inferior	32.7	32.7	33.2	33.3	33.0	33.1	33.0	33.1	32.2	32.1
L. Arm: Up. Exterior	34.7	34.9	35.2	35.5	34.9	35.1	34.7	35.0	34.2	34.3
L. Arm: Lo. Anterior	31.0	31.0	31.7	31.9	31.3	31.5	31.2	31.4	30.2	30.2
L. Arm: Lo. Posterior	33.5	33.8	34.1	34.5	33.7	34.1	33.6	33.9	32.8	33.1
L. Arm: Lo. Inferior	31.2	31.2	31.8	32.0	31.5	31.7	31.5	31.7	30.5	30.5
L. Arm: Lo. Exterior	32.6	32.8	33.2	33.5	32.8	33.1	32.8	33.0	31.9	32.1
L. Hand: Handback	32.8	32.9	33.9	34.2	33.3	33.6	33.2	33.5	31.6	31.5
L. Hand: Palm	32.7	32.8	33.9	34.2	33.1	33.4	32.9	33.1	31.3	31.2
L. Leg: Up. Anterior	33.2	33.2	33.8	33.9	33.5	33.5	33.4	33.5	32.6	32.5
L. Leg: Up. Posterior	32.9	32.7	33.4	33.3	33.3	33.2	33.5	33.4	32.5	32.3
L. Leg: Up. Inferior	32.9	32.7	33.4	33.4	33.2	33.1	33.3	33.2	32.4	32.1
L. Leg: Up. Exterior	35.0	35.1	35.5	35.6	35.1	35.3	35.0	35.1	34.4	34.4
L. Leg: Lo. Anterior	31.0	30.7	31.6	31.5	31.5	31.4	31.8	31.7	30.5	30.2
L. Leg: Lo. Posterior	31.9	31.8	32.6	32.7	32.3	32.3	32.3	32.3	31.2	31.1
L. Leg: Lo. Inferior	30.7	30.4	31.4	31.2	31.2	31.0	31.5	31.2	30.2	29.8
L. Leg: Lo. Exterior	33.5	33.5	34.2	34.2	33.8	33.8	33.8	33.8	32.8	32.7
L. Foot: Instep	30.9	30.6	31.8	31.7	31.4	31.3	31.6	31.4	30.1	29.7
L. Foot: Sole	32.7	32.4	33.1	33.1	33.0	32.8	33.1	33.0	32.4	32.1
R. Shoulder	33.1	33.1	33.5	33.5	33.4	33.5	33.6	33.7	32.8	32.7
R. Arm: Up. Anterior	32.7	32.7	33.2	33.4	33.0	33.1	33.0	33.1	32.1	32.1
R. Arm: Up. Posterior	32.3	32.4	32.9	33.0	32.8	32.9	33.0	33.1	32.0	32.0
R. Arm: Up. Inferior	32.9	32.9	33.4	33.6	33.2	33.3	33.2	33.3	32.4	32.4
R. Arm: Up. Exterior	32.2	32.1	32.7	32.8	32.6	32.6	32.8	32.9	31.9	31.7
R. Arm: Lo. Anterior	31.9	32.1	32.6	32.9	32.2	32.4	32.0	32.2	31.1	31.1
R. Arm: Lo. Posterior	29.8	29.8	30.5	30.6	30.4	30.5	30.8	30.9	29.5	29.4
R. Arm: Lo. Inferior	31.3	31.4	32.0	32.2	31.7	31.8	31.7	31.8	30.7	30.6
R. Arm: Lo. Exterior	30.2	30.2	30.9	31.0	30.8	30.9	31.0	31.1	29.8	29.7
R. Hand: Handback	31.4	31.4	32.6	33.0	32.1	32.3	32.2	32.4	30.3	30.1
R. Hand: Palm	32.4	32.5	33.6	33.9	32.9	33.1	32.7	32.9	31.1	30.9
R. Leg: Up. Anterior	33.5	33.5	34.1	34.2	33.8	33.8	33.6	33.7	32.9	32.8
R. Leg: Up. Posterior	32.4	32.1	32.9	32.8	32.8	32.7	33.1	33.0	32.1	31.8
R. Leg: Up. Inferior	33.8	33.7	34.3	34.3	34.0	34.0	34.0	33.9	33.2	33.0
R. Leg: Up. Exterior	32.4	32.2	33.0	32.9	32.9	32.8	33.1	33.0	32.1	31.8
R. Leg: Lo. Anterior	30.7	30.4	31.4	31.2	31.3	31.1	31.6	31.5	30.3	29.9
R. Leg: Lo. Posterior	31.5	31.3	32.2	32.2	31.9	31.9	32.0	32.0	30.8	30.6
R. Leg: Lo. Inferior	32.6	32.5	33.3	33.3	33.0	32.9	33.0	32.9	32.0	31.7
R. Leg: Lo. Exterior	30.1	29.7	30.8	30.5	30.8	30.5	31.1	30.9	29.7	29.3
R. Foot: Instep	30.0	29.6	30.9	30.8	30.7	30.4	30.9	30.7	29.3	28.8
R. Foot: Sole	32.6	32.3	33.0	32.9	32.9	32.7	33.0	32.9	32.4	32.0
Mean skin temperature ($T_{sk,m}$)	33.2	33.2	33.7	33.8	33.5	33.6	33.6	33.7	32.7	32.6
Rectal temperature (T_{re})	36.9	36.9	36.9	36.9	36.9	36.9	36.9	36.9	36.9	36.9

Table E.11 Predicted body temperatures obtained for spatial hot wall at position 2 of McNall and Biddison (1970).

Body parts	Local skin temperature ($T_{sk,i}$)									
	Cond 1		Cond 2		Cond 3		Cond 4		Cond 7	
	60 [min]	90 [min]	60 [min]	90 [min]	60 [min]	90 [min]	60 [min]	90 [min]	60 [min]	90 [min]
Forehead	34.5	34.6	34.8	34.8	34.8	34.8	34.9	35.0	34.3	34.3
Head	34.7	34.7	35.0	35.0	34.9	35.0	35.0	35.0	34.5	34.5
Face: Anterior	34.4	34.4	35.0	35.0	34.8	34.9	34.9	35.0	33.8	33.7
L. Face	35.9	35.9	36.2	36.3	36.1	36.1	36.0	36.1	35.4	35.4
R. Face	33.3	33.4	34.0	34.1	33.9	34.0	34.2	34.2	32.6	32.5
Neck: Anterior	34.2	34.3	34.6	34.7	34.5	34.6	34.6	34.6	33.8	33.8
Neck: Posterior	33.9	33.9	34.3	34.4	34.2	34.3	34.4	34.4	33.5	33.5
Neck: L. Exterior	35.5	35.6	35.8	35.9	35.6	35.7	35.6	35.7	35.1	35.1
Neck: R. Exterior	33.2	33.3	33.7	33.8	33.6	33.7	33.8	33.9	32.8	32.8
L. Shoulder	34.2	34.3	34.6	34.8	34.5	34.6	34.5	34.6	33.8	33.9
Thorax: Anterior	34.6	34.6	34.8	34.8	34.8	34.8	35.0	35.0	34.5	34.5
Thorax: Posterior	34.4	34.4	34.6	34.6	34.6	34.6	34.8	34.8	34.3	34.3
Thorax: L. Inferior	34.8	34.8	35.0	35.1	34.9	34.9	34.9	34.9	34.5	34.5
Thorax: R. Inferior	34.4	34.3	34.6	34.6	34.5	34.5	34.6	34.6	34.1	34.1
Abdomen: Anterior	34.1	34.3	34.4	34.7	34.3	34.5	34.3	34.5	33.8	33.9
Abdomen: Posterior	34.1	34.3	34.4	34.6	34.3	34.5	34.4	34.7	33.9	34.0
Abdomen: L. Inferior	34.8	35.0	35.1	35.3	34.9	35.2	34.9	35.1	34.5	34.6
Abdomen: R. Inferior	33.6	33.6	33.9	34.0	33.8	33.9	33.9	34.1	33.3	33.3
L. Arm: Up. Anterior	33.5	33.7	34.1	34.4	33.7	33.9	33.6	33.8	32.9	33.0
L. Arm: Up. Posterior	34.0	34.2	34.5	34.8	34.2	34.5	34.2	34.4	33.5	33.7
L. Arm: Up. Inferior	32.6	32.6	33.1	33.3	32.9	33.0	33.0	33.1	32.1	32.1
L. Arm: Up. Exterior	34.5	34.8	35.0	35.3	34.7	35.0	34.6	34.9	34.0	34.2
L. Arm: Lo. Anterior	31.0	31.0	31.7	31.9	31.3	31.5	31.2	31.4	30.2	30.2
L. Arm: Lo. Posterior	33.1	33.4	33.7	34.1	33.3	33.7	33.2	33.6	32.4	32.6
L. Arm: Lo. Inferior	31.0	31.0	31.6	31.8	31.4	31.5	31.4	31.5	30.3	30.3
L. Arm: Lo. Exterior	32.6	32.8	33.2	33.5	32.9	33.1	32.8	33.0	31.9	32.1
L. Hand: Handback	32.7	32.8	33.8	34.1	33.3	33.5	33.2	33.4	31.6	31.5
L. Hand: Palm	32.6	32.7	33.8	34.1	33.1	33.3	32.8	33.0	31.3	31.1
L. Leg: Up. Anterior	33.2	33.2	33.8	33.9	33.5	33.5	33.4	33.4	32.6	32.5
L. Leg: Up. Posterior	32.7	32.5	33.2	33.1	33.2	33.1	33.4	33.3	32.4	32.1
L. Leg: Up. Inferior	32.9	32.7	33.4	33.3	33.2	33.1	33.3	33.2	32.4	32.1
L. Leg: Up. Exterior	34.8	34.9	35.3	35.5	35.0	35.1	34.9	35.0	34.3	34.2
L. Leg: Lo. Anterior	31.5	31.3	32.2	32.1	32.0	31.9	32.3	32.1	31.0	30.7
L. Leg: Lo. Posterior	31.6	31.5	32.3	32.4	32.0	32.0	32.1	32.1	31.0	30.8
L. Leg: Lo. Inferior	30.7	30.4	31.4	31.2	31.3	31.0	31.5	31.3	30.2	29.8
L. Leg: Lo. Exterior	33.5	33.5	34.2	34.3	33.9	33.9	33.8	33.8	32.9	32.8
L. Foot: Instep	31.0	30.7	31.9	31.8	31.6	31.4	31.7	31.5	30.2	29.8
L. Foot: Sole	32.7	32.4	33.1	33.1	33.0	32.8	33.1	33.0	32.4	32.1
R. Shoulder	33.0	33.0	33.4	33.4	33.4	33.4	33.6	33.6	32.7	32.6
R. Arm: Up. Anterior	32.8	32.9	33.4	33.5	33.1	33.2	33.1	33.2	32.3	32.2
R. Arm: Up. Posterior	32.2	32.2	32.7	32.8	32.6	32.7	32.9	33.0	31.9	31.8
R. Arm: Up. Inferior	32.8	32.8	33.3	33.4	33.1	33.2	33.1	33.2	32.3	32.3
R. Arm: Up. Exterior	32.2	32.1	32.7	32.8	32.6	32.6	32.9	32.9	31.9	31.8
R. Arm: Lo. Anterior	32.3	32.4	33.0	33.3	32.5	32.7	32.2	32.4	31.4	31.5
R. Arm: Lo. Posterior	29.8	29.7	30.5	30.5	30.4	30.4	30.8	30.8	29.5	29.4
R. Arm: Lo. Inferior	31.2	31.2	31.8	32.0	31.5	31.7	31.5	31.7	30.5	30.5
R. Arm: Lo. Exterior	30.4	30.4	31.0	31.2	30.9	31.0	31.1	31.2	30.0	29.9
R. Hand: Handback	31.5	31.5	32.7	33.0	32.2	32.4	32.2	32.5	30.3	30.1
R. Hand: Palm	32.5	32.5	33.6	33.9	32.9	33.1	32.7	32.9	31.1	30.9
R. Leg: Up. Anterior	33.6	33.6	34.2	34.3	33.8	33.9	33.7	33.8	33.0	32.9
R. Leg: Up. Posterior	32.3	32.1	32.8	32.7	32.8	32.7	33.1	33.0	32.0	31.7
R. Leg: Up. Inferior	33.9	33.9	34.5	34.5	34.2	34.2	34.1	34.1	33.4	33.2
R. Leg: Up. Exterior	32.4	32.2	33.0	32.9	32.9	32.7	33.1	33.0	32.1	31.8
R. Leg: Lo. Anterior	31.4	31.1	32.0	31.9	31.9	31.7	32.2	32.0	30.9	30.6
R. Leg: Lo. Posterior	31.3	31.1	32.0	32.0	31.7	31.7	31.8	31.8	30.7	30.4
R. Leg: Lo. Inferior	33.0	32.9	33.7	33.7	33.3	33.3	33.3	33.2	32.3	32.1
R. Leg: Lo. Exterior	30.1	29.8	30.8	30.5	30.8	30.5	31.1	30.9	29.7	29.3
R. Foot: Instep	30.3	29.8	31.1	31.0	30.9	30.6	31.0	30.8	29.5	29.0
R. Foot: Sole	32.6	32.3	33.0	32.9	32.9	32.7	33.0	32.9	32.4	32.0
Mean skin temperature ($T_{sk,m}$)	33.2	33.2	33.7	33.8	33.5	33.6	33.6	33.6	32.7	32.6
Rectal temperature (T_{re})	36.9	36.9	36.9	36.9	36.9	36.9	36.9	36.9	36.9	36.9

Table E.12 Predicted body temperatures obtained for spatial hot wall at position 3 of McNall and Biddison (1970).

Body parts	Local skin temperature ($T_{sk,i}$)									
	Cond 1		Cond 2		Cond 3		Cond 4		Cond 7	
	60 [min]	90 [min]	60 [min]	90 [min]	60 [min]	90 [min]	60 [min]	90 [min]	60 [min]	90 [min]
Forehead	34.7	34.8	35.0	35.1	35.0	35.0	35.1	35.1	34.6	34.6
Head	34.6	34.6	34.9	34.9	34.8	34.8	34.9	34.9	34.4	34.4
Face: Anterior	34.6	34.6	35.1	35.2	35.0	35.0	35.0	35.1	34.0	33.9
L. Face	35.9	36.0	36.2	36.3	36.1	36.1	36.0	36.1	35.4	35.4
R. Face	33.3	33.3	34.0	34.1	33.9	34.0	34.2	34.2	32.6	32.5
Neck: Anterior	34.4	34.5	34.8	34.9	34.7	34.8	34.7	34.8	34.0	34.0
Neck: Posterior	33.3	33.4	33.8	33.9	33.7	33.8	33.9	34.0	32.9	32.9
Neck: L. Exterior	35.3	35.4	35.7	35.8	35.5	35.6	35.5	35.6	34.9	35.0
Neck: R. Exterior	33.2	33.2	33.7	33.8	33.6	33.7	33.8	33.9	32.8	32.8
L. Shoulder	34.1	34.2	34.5	34.7	34.4	34.5	34.4	34.5	33.7	33.7
Thorax: Anterior	34.8	34.8	35.0	35.1	35.0	35.0	35.1	35.2	34.7	34.7
Thorax: Posterior	33.9	33.9	34.1	34.1	34.2	34.2	34.4	34.4	33.9	33.8
Thorax: L. Inferior	34.8	34.8	35.0	35.0	34.9	34.9	34.9	34.9	34.5	34.5
Thorax: R. Inferior	34.3	34.3	34.6	34.6	34.5	34.5	34.6	34.6	34.1	34.1
Abdomen: Anterior	34.3	34.4	34.6	34.8	34.4	34.6	34.4	34.6	33.9	34.0
Abdomen: Posterior	33.9	34.0	34.2	34.3	34.1	34.3	34.3	34.5	33.7	33.8
Abdomen: L. Inferior	34.6	34.8	34.9	35.1	34.7	35.0	34.7	35.0	34.3	34.4
Abdomen: R. Inferior	33.6	33.6	33.9	34.0	33.8	33.9	33.9	34.0	33.3	33.3
L. Arm: Up. Anterior	33.8	33.9	34.3	34.6	33.9	34.1	33.8	34.0	33.1	33.2
L. Arm: Up. Posterior	33.5	33.7	34.0	34.2	33.8	34.0	33.8	34.0	33.1	33.2
L. Arm: Up. Inferior	32.5	32.5	33.1	33.2	32.9	33.0	32.9	33.0	32.1	32.0
L. Arm: Up. Exterior	34.6	34.8	35.1	35.4	34.8	35.0	34.7	34.9	34.1	34.2
L. Arm: Lo. Anterior	31.0	31.1	31.7	31.9	31.4	31.5	31.3	31.4	30.3	30.3
L. Arm: Lo. Posterior	33.0	33.3	33.6	34.0	33.3	33.6	33.2	33.5	32.4	32.6
L. Arm: Lo. Inferior	30.8	30.9	31.5	31.7	31.2	31.4	31.3	31.4	30.2	30.2
L. Arm: Lo. Exterior	32.9	33.2	33.6	33.9	33.2	33.5	33.1	33.4	32.3	32.4
L. Hand: Handback	32.9	33.1	34.0	34.3	33.4	33.7	33.3	33.6	31.8	31.7
L. Hand: Palm	32.7	32.8	33.8	34.2	33.1	33.3	32.8	33.1	31.3	31.2
L. Leg: Up. Anterior	33.3	33.3	33.9	34.0	33.6	33.6	33.5	33.5	32.7	32.6
L. Leg: Up. Posterior	32.8	32.6	33.3	33.2	33.2	33.1	33.4	33.3	32.4	32.2
L. Leg: Up. Inferior	32.9	32.7	33.4	33.4	33.3	33.1	33.3	33.2	32.4	32.1
L. Leg: Up. Exterior	34.8	34.9	35.4	35.5	35.0	35.1	34.9	35.0	34.3	34.3
L. Leg: Lo. Anterior	31.9	31.7	32.6	32.5	32.4	32.3	32.6	32.5	31.4	31.1
L. Leg: Lo. Posterior	31.3	31.2	32.0	32.0	31.8	31.7	31.9	31.8	30.7	30.5
L. Leg: Lo. Inferior	30.8	30.4	31.5	31.3	31.3	31.1	31.5	31.3	30.2	29.8
L. Leg: Lo. Exterior	33.7	33.7	34.4	34.5	34.0	34.1	34.0	34.0	33.1	33.0
L. Foot: Instep	31.1	30.8	32.0	31.9	31.6	31.5	31.7	31.6	30.3	29.9
L. Foot: Sole	32.7	32.5	33.1	33.1	33.0	32.8	33.1	33.0	32.4	32.1
R. Shoulder	32.9	32.9	33.3	33.3	33.3	33.3	33.5	33.5	32.6	32.5
R. Arm: Up. Anterior	33.0	33.0	33.5	33.7	33.2	33.3	33.2	33.3	32.4	32.4
R. Arm: Up. Posterior	32.0	32.0	32.5	32.6	32.4	32.5	32.7	32.8	31.7	31.6
R. Arm: Up. Inferior	32.6	32.6	33.1	33.2	32.9	33.0	33.0	33.1	32.1	32.0
R. Arm: Up. Exterior	32.2	32.2	32.8	32.8	32.7	32.7	32.9	32.9	31.9	31.8
R. Arm: Lo. Anterior	32.5	32.7	33.2	33.5	32.7	32.9	32.4	32.6	31.6	31.7
R. Arm: Lo. Posterior	29.8	29.7	30.5	30.5	30.4	30.4	30.8	30.8	29.5	29.3
R. Arm: Lo. Inferior	30.8	30.8	31.4	31.6	31.2	31.3	31.3	31.4	30.2	30.1
R. Arm: Lo. Exterior	30.6	30.6	31.2	31.3	31.1	31.1	31.2	31.4	30.1	30.0
R. Hand: Handback	31.6	31.7	32.8	33.1	32.3	32.5	32.4	32.6	30.5	30.3
R. Hand: Palm	32.5	32.6	33.7	34.0	33.0	33.2	32.7	32.9	31.2	31.0
R. Leg: Up. Anterior	33.8	33.8	34.4	34.5	34.0	34.1	33.8	33.9	33.1	33.1
R. Leg: Up. Posterior	32.4	32.1	32.9	32.8	32.9	32.7	33.1	33.0	32.1	31.8
R. Leg: Up. Inferior	34.2	34.2	34.7	34.8	34.4	34.4	34.3	34.3	33.6	33.5
R. Leg: Up. Exterior	32.4	32.2	33.0	32.9	32.9	32.7	33.1	33.0	32.1	31.8
R. Leg: Lo. Anterior	31.8	31.6	32.4	32.3	32.3	32.1	32.5	32.4	31.3	31.0
R. Leg: Lo. Posterior	31.1	30.9	31.8	31.7	31.5	31.5	31.7	31.6	30.5	30.2
R. Leg: Lo. Inferior	33.2	33.1	33.8	33.9	33.5	33.4	33.4	33.3	32.4	32.3
R. Leg: Lo. Exterior	30.2	29.8	30.8	30.6	30.8	30.5	31.2	30.9	29.8	29.3
R. Foot: Instep	30.3	29.8	31.2	31.0	30.9	30.6	31.0	30.8	29.5	29.0
R. Foot: Sole	32.6	32.3	33.0	32.9	32.9	32.7	33.0	32.9	32.4	32.0
Mean skin temperature ($T_{sk,m}$)	33.2	33.2	33.7	33.8	33.5	33.6	33.6	33.6	32.7	32.6
Rectal temperature (T_{re})	36.9	36.9	36.9	36.9	36.9	36.9	36.9	36.9	36.9	36.9

Table E.13 Predicted body temperatures obtained for spatial cold of McNall and Biddison (1970).

Body parts	Local skin temperature ($T_{sk,i}$)									
	Cond 1		Cond 2		Cond 5		Cond 7		Cond 9	
	60 [min]	90 [min]	60 [min]	90 [min]	60 [min]	90 [min]	60 [min]	90 [min]	60 [min]	90 [min]
Forehead	35.0	35.0	34.9	34.9	34.5	34.5	34.8	34.8	34.5	34.5
Head	35.0	35.0	34.8	34.7	34.5	34.5	34.7	34.7	34.5	34.5
Face: Anterior	35.0	35.1	34.5	34.6	34.1	34.0	34.5	34.6	34.2	34.2
L. Face	34.7	34.8	34.2	34.3	33.7	33.7	34.2	34.3	33.8	33.8
R. Face	34.9	35.0	34.5	34.6	34.0	34.0	34.5	34.5	34.1	34.1
Neck: Anterior	34.7	34.8	34.4	34.4	34.0	34.0	34.3	34.4	34.1	34.1
Neck: Posterior	34.0	34.0	33.6	33.7	33.2	33.2	33.6	33.6	33.2	33.2
Neck: L. Exterior	34.3	34.4	34.0	34.0	33.6	33.6	33.9	34.0	33.6	33.6
Neck: R. Exterior	34.6	34.7	34.3	34.3	33.9	33.9	34.3	34.3	34.0	34.0
L. Shoulder	34.0	34.1	33.6	33.7	33.3	33.4	33.6	33.7	33.3	33.4
Thorax: Anterior	34.9	34.9	34.8	34.8	34.4	34.5	34.7	34.7	34.4	34.4
Thorax: Posterior	34.3	34.3	34.2	34.2	33.8	33.9	34.1	34.1	33.7	33.7
Thorax: L. Inferior	34.9	35.0	34.6	34.7	34.6	34.6	34.7	34.7	34.6	34.7
Thorax: R. Inferior	35.1	35.1	34.8	34.8	34.7	34.7	34.8	34.9	34.8	34.8
Abdomen: Anterior	34.2	34.4	33.8	33.9	33.7	33.7	33.9	34.0	33.8	33.9
Abdomen: Posterior	33.5	33.6	33.3	33.3	32.9	32.8	33.2	33.2	32.8	32.7
Abdomen: L. Inferior	33.8	33.9	33.5	33.5	33.2	33.1	33.5	33.5	33.2	33.1
Abdomen: R. Inferior	34.1	34.3	33.8	33.9	33.6	33.6	33.8	33.9	33.6	33.6
L. Arm: Up. Anterior	33.6	33.8	32.8	32.9	32.7	32.8	33.0	33.1	33.0	33.1
L. Arm: Up. Posterior	32.5	32.6	32.0	32.1	31.6	31.6	32.0	32.1	31.6	31.6
L. Arm: Up. Inferior	33.2	33.4	32.6	32.6	32.4	32.4	32.7	32.7	32.6	32.6
L. Arm: Up. Exterior	33.3	33.5	32.9	33.0	32.5	32.6	32.9	33.0	32.5	32.6
L. Arm: Lo. Anterior	32.7	32.9	31.8	31.9	31.7	31.8	32.0	32.1	32.1	32.2
L. Arm: Lo. Posterior	31.8	31.9	31.3	31.3	30.8	30.8	31.3	31.3	30.8	30.8
L. Arm: Lo. Inferior	32.3	32.5	31.5	31.6	31.4	31.4	31.7	31.7	31.5	31.6
L. Arm: Lo. Exterior	32.3	32.5	31.7	31.8	31.4	31.4	31.8	31.9	31.4	31.5
L. Hand: Handback	33.5	33.7	32.3	32.3	31.9	31.8	32.5	32.5	32.3	32.2
L. Hand: Palm	33.9	34.1	32.5	32.4	32.5	32.4	32.9	32.9	33.1	33.1
L. Leg: Up. Anterior	33.8	33.9	32.9	32.9	32.9	32.8	33.2	33.1	33.3	33.2
L. Leg: Up. Posterior	33.8	33.9	33.4	33.4	33.0	33.0	33.4	33.4	33.0	33.0
L. Leg: Up. Inferior	34.3	34.4	33.7	33.6	33.5	33.5	33.8	33.8	33.7	33.7
L. Leg: Up. Exterior	33.7	33.8	33.2	33.2	32.9	32.8	33.2	33.2	33.0	32.9
L. Leg: Lo. Anterior	33.4	33.5	33.0	33.0	32.6	32.5	33.0	32.9	32.6	32.5
L. Leg: Lo. Posterior	32.3	32.3	31.6	31.4	31.2	31.0	31.7	31.5	31.4	31.2
L. Leg: Lo. Inferior	33.6	33.6	33.0	33.0	32.8	32.7	33.1	33.1	32.9	32.8
L. Leg: Lo. Exterior	33.0	33.1	32.6	32.6	32.2	32.1	32.6	32.5	32.2	32.1
L. Foot: Instep	31.8	31.8	31.1	30.8	30.6	30.2	31.1	30.9	30.7	30.3
L. Foot: Sole	32.5	32.6	32.0	31.8	31.6	31.3	32.0	31.8	31.6	31.3
R. Shoulder	34.1	34.3	33.8	33.9	33.5	33.5	33.8	33.9	33.5	33.6
R. Arm: Up. Anterior	33.6	33.8	32.8	32.9	32.7	32.8	33.0	33.1	33.0	33.1
R. Arm: Up. Posterior	32.8	33.0	32.4	32.5	32.0	32.0	32.4	32.5	32.0	32.0
R. Arm: Up. Inferior	32.9	33.0	32.3	32.2	32.1	32.0	32.4	32.4	32.2	32.2
R. Arm: Up. Exterior	33.5	33.8	33.1	33.3	32.8	32.9	33.1	33.3	32.8	32.9
R. Arm: Lo. Anterior	32.7	32.9	31.7	31.8	31.7	31.8	32.0	32.1	32.1	32.2
R. Arm: Lo. Posterior	32.3	32.5	31.8	31.9	31.4	31.4	31.8	31.9	31.4	31.4
R. Arm: Lo. Inferior	32.2	32.4	31.5	31.5	31.3	31.3	31.6	31.6	31.4	31.5
R. Arm: Lo. Exterior	32.4	32.7	31.8	31.9	31.5	31.5	31.9	32.0	31.5	31.6
R. Hand: Handback	33.6	33.9	32.5	32.5	32.1	32.0	32.7	32.7	32.4	32.4
R. Hand: Palm	34.0	34.2	32.6	32.5	32.6	32.5	33.0	33.0	33.2	33.2
R. Leg: Up. Anterior	33.8	33.8	32.9	32.8	32.8	32.7	33.1	33.0	33.2	33.1
R. Leg: Up. Posterior	33.9	34.0	33.5	33.5	33.1	33.1	33.5	33.5	33.1	33.1
R. Leg: Up. Inferior	34.3	34.3	33.7	33.6	33.5	33.4	33.8	33.7	33.7	33.7
R. Leg: Up. Exterior	34.1	34.2	33.6	33.6	33.3	33.2	33.6	33.6	33.4	33.3
R. Leg: Lo. Anterior	33.4	33.4	33.0	33.0	32.6	32.5	33.0	32.9	32.6	32.5
R. Leg: Lo. Posterior	32.4	32.4	31.7	31.5	31.4	31.2	31.8	31.6	31.5	31.3
R. Leg: Lo. Inferior	33.3	33.3	32.8	32.7	32.5	32.4	32.8	32.7	32.6	32.5
R. Leg: Lo. Exterior	33.4	33.5	33.0	33.0	32.6	32.5	33.0	33.0	32.6	32.6
R. Foot: Instep	31.9	31.8	31.1	30.9	30.6	30.3	31.2	30.9	30.7	30.3
R. Foot: Sole	32.6	32.6	32.0	31.8	31.6	31.3	32.0	31.8	31.6	31.3
Mean skin temperature ($T_{sk,m}$)	33.7	33.8	33.2	33.2	32.9	32.9	33.2	33.3	33.0	33.0
Rectal temperature (T_{re})	36.9	36.9	36.9	36.9	36.9	36.9	36.9	36.9	36.9	36.9

Table E.14 Predicted body temperatures at exposure time of 30 minutes obtained for experiments of Hodder (2002).

Body parts	Local skin temperature ($T_{sk,i}$)	
	200 (Wm^{-2})	600 (Wm^{-2})
Forehead	35.4	35.6
Head	35.2	35.4
Face: Anterior	36.1	37.1
L. Face	35.3	35.5
R. Face	35.3	35.5
Neck: Anterior	36.5	37.8
Neck: Posterior	34.3	34.4
Neck: L. Exterior	35.1	35.6
Neck: R. Exterior	35.1	35.6
L. Shoulder	34.5	35.0
Thorax: Anterior	37.2	40.1
Thorax: Posterior	33.9	34.2
Thorax: L. Inferior	34.6	34.9
Thorax: R. Inferior	34.6	34.9
Abdomen: Anterior	36.7	39.1
Abdomen: Posterior	33.4	33.4
Abdomen: L. Inferior	33.7	33.6
Abdomen: R. Inferior	33.7	33.6
L. Arm: Up. Anterior	36.7	39.8
L. Arm: Up. Posterior	33.0	33.1
L. Arm: Up. Inferior	33.4	33.5
L. Arm: Up. Exterior	35.0	37.5
L. Arm: Lo. Anterior	35.8	38.5
L. Arm: Lo. Posterior	33.0	33.3
L. Arm: Lo. Inferior	33.2	33.6
L. Arm: Lo. Exterior	36.5	40.0
L. Hand: Handback	34.8	36.4
L. Hand: Palm	34.4	35.1
L. Leg: Up. Anterior	34.9	36.3
L. Leg: Up. Posterior	33.1	33.0
L. Leg: Up. Inferior	33.4	33.3
L. Leg: Up. Exterior	33.2	33.1
L. Leg: Lo. Anterior	36.1	39.4
L. Leg: Lo. Posterior	33.0	33.5
L. Leg: Lo. Inferior	33.9	35.6
L. Leg: Lo. Exterior	33.2	34.5
L. Foot: Instep	33.4	35.0
L. Foot: Sole	33.0	33.8
R. Shoulder	34.5	35.0
R. Arm: Up. Anterior	36.7	39.8
R. Arm: Up. Posterior	33.0	33.1
R. Arm: Up. Inferior	33.4	33.5
R. Arm: Up. Exterior	35.0	37.5
R. Arm: Lo. Anterior	35.8	38.5
R. Arm: Lo. Posterior	33.0	33.3
R. Arm: Lo. Inferior	33.2	33.6
R. Arm: Lo. Exterior	36.5	40.0
R. Hand: Handback	34.8	36.4
R. Hand: Palm	34.4	35.1
R. Leg: Up. Anterior	34.9	36.3
R. Leg: Up. Posterior	33.1	33.0
R. Leg: Up. Inferior	33.4	33.3
R. Leg: Up. Exterior	33.2	33.1
R. Leg: Lo. Anterior	36.1	39.4
R. Leg: Lo. Posterior	33.0	33.5
R. Leg: Lo. Inferior	33.9	35.6
R. Leg: Lo. Exterior	33.2	34.5
R. Foot: Instep	33.4	35.0
R. Foot: Sole	33.0	33.8
Mean skin temperature ($T_{sk,m}$)	34.4	35.5
Rectal temperature (T_{re})	37.0	37.0

Table E.15 Measured local sensitivity coefficients for cold and warm stimuli at different parts of the human body, Crawshaw et al. (1975).

Body sector	$\overline{T}sk$ (area weighting only)	$\overline{T}sk$ (area weighting and sensitivity to warming)	$\overline{T}sk$ (area weighting and sensitivity to cooling)
Face	0.07	0.21	0.19
Chest	0.09	0.10	0.08
Upper back	0.09	0.11	0.09
Abdomen	0.18	0.17	0.12
Upper arms	0.13	0.12	0.13
Lower arms	0.12	0.06	0.12
Upper legs	0.16	0.15	0.12
Lower legs	0.16	0.08	0.15

Appendix F

Predicted LCD, LWD and PPD of subject in the BHEC building

Table F.1 Monthly minimum, maximum, and average PPD with standard deviations for a sedentary subject located in the close proximity and in the middle of zone.

	PPD (Nr. Window)				PPD (Mid. Room)			
	Max	Min	Ave	Std Dev	Max	Min	Ave	Std Dev
Jan	75.6	5.0	8.0	9.7	30.2	5.0	6.1	3.3
Feb	100.0	5.0	14.2	19.8	21.7	5.0	8.2	4.0
Mar	90.5	5.0	23.9	27.1	41.9	5.0	13.5	9.6
Apr	96.3	5.0	21.4	24.2	41.9	5.0	13.6	9.6
May	95.7	5.0	26.4	28.4	48.5	5.0	15.5	12.9
Jun	90.3	5.0	28.1	26.6	56.0	5.0	19.4	15.2
Jul	100.0	5.0	38.9	33.3	99.3	5.0	30.1	23.7
Aug	99.9	5.0	28.1	32.0	67.9	5.0	17.3	16.3
Sep	66.1	5.0	20.3	14.6	67.4	5.0	18.9	15.5
Oct	99.3	5.0	18.5	23.0	39.8	5.1	11.3	7.1
Nov	92.9	5.0	10.9	13.4	20.2	5.1	8.3	3.1
Dec	95.6	5.0	9.8	11.8	15.7	5.1	7.4	2.1
year	100.0	5.0	20.8	24.9	99.3	5.0	14.2	13.7

Table F.2 Monthly minimum, maximum, and average LCD with standard deviations for a sedentary subject located in the close proximity and in the middle of zone.

	LCD (Nr. Window)				LCD (Mid. Room)			
	Max	Min	Ave	Std Dev	Max	Min	Ave	Std Dev
Jan	40.0	12.5	23.4	4.2	34.0	13.8	21.0	2.7
Feb	33.2	4.3	8.9	4.4	25.6	3.7	8.5	2.9
Mar	15.6	0.3	2.3	2.4	13.8	0.4	2.5	2.1
Apr	5.1	0.2	1.8	1.1	4.6	0.4	2.0	1.0
May	4.1	1.0	2.1	0.5	2.1	0.6	1.4	0.3
Jun	3.2	0.5	1.4	0.5	1.6	0.5	0.9	0.2
Jul	1.1	0.0	0.3	0.2	0.8	0.0	0.2	0.2
Aug	9.3	0.2	1.0	1.0	6.2	0.2	0.9	1.0
Sep	17.6	1.1	6.1	3.5	13.3	0.7	5.8	3.6
Oct	12.5	0.8	2.5	1.5	12.1	0.8	2.7	1.3
Nov	15.1	3.4	7.6	1.9	13.8	3.8	6.5	1.3
Dec	15.6	3.3	9.4	2.7	14.2	5.8	8.4	1.4
year	40.0	0.2	5.8	6.6	34.0	0.2	5.4	5.9

Table F.3 Monthly minimum, maximum, and average LWD with standard deviations for a sedentary subject located in the close proximity and in the middle of zone.

	LWD (Nr. Window)				LWD (Mid. Room)			
	Max	Min	Ave	Std Dev	Max	Min	Ave	Std Dev
Jan	36.9	6.1	6.7	1.2	7.4	5.9	6.3	0.4
Feb	97.4	7.4	8.8	4.8	10.8	7.2	8.0	0.6
Mar	59.5	6.1	12.7	5.2	16.7	8.0	10.8	1.9
Apr	43.4	7.2	11.9	3.8	16.7	8.0	10.7	1.9
May	53.4	9.5	13.8	2.7	14.5	9.6	11.8	1.0
Jun	27.1	9.8	15.2	2.4	20.6	10.8	13.3	1.4
Jul	73.0	11.8	25.5	10.6	57.0	11.8	22.9	9.4
Aug	98.7	10.2	17.6	11.0	17.6	9.1	13.4	2.1
Sep	12.6	6.1	8.4	1.5	12.0	5.5	7.8	1.8
Oct	77.6	6.2	10.7	5.7	14.0	7.8	9.8	1.2
Nov	95.6	5.7	7.4	6.8	8.3	7.4	7.7	0.2
Dec	18.9	7.1	7.7	0.5	8.3	7.2	7.5	0.2
year	98.7	5.7	12.2	7.7	57.0	5.5	10.9	5.3

Table F.4 Seasonal minimum, maximum, and average PPD with standard deviations for a sedentary subject located in the close proximity and in the middle of zone.

	PPD (Nr. Window)				PPD (Mid. Room)			
	Max	Min	Ave	Std Dev	Max	Min	Ave	Std Dev
winter	100.0	5.0	10.5	14.5	30.2	5.0	7.2	3.3
spring	96.3	5.0	23.9	26.7	48.5	5.0	14.2	10.8
summer	100.0	5.0	31.8	31.2	99.3	5.0	22.3	19.7
autumn	99.3	5.0	16.6	18.1	67.4	5.0	12.8	10.9

Table F.5 Seasonal minimum, maximum, and average LCD with standard deviations for a sedentary subject located in the close proximity and in the middle of zone.

	LCD (Nr. Window)				LCD (Mid. Room)			
	Max	Min	Ave	Std Dev	Max	Min	Ave	Std Dev
winter	40.0	3.3	14.0	7.8	34.0	3.7	12.8	6.4
spring	15.6	0.2	2.1	1.6	13.8	0.4	2.0	1.4
summer	9.3	0.0	0.9	0.8	6.2	0.0	0.7	0.7
autumn	17.6	0.8	5.4	3.2	13.8	0.7	5.0	2.9

Table F.6 Seasonal minimum, maximum, and average LWD with standard deviations for a sedentary subject located in the close proximity and in the middle of zone.

	LWD (Nr. Window)				LWD (Mid. Room)			
	Max	Min	Ave	Std Dev	Max	Min	Ave	Std Dev
winter	97.4	6.1	7.7	2.9	10.8	5.9	7.2	0.8
spring	59.5	6.1	12.8	4.1	16.7	8.0	11.1	1.7
summer	98.7	9.8	19.4	10.0	57.0	9.1	16.6	7.2
autumn	95.6	5.7	8.9	5.4	14.0	5.5	8.4	1.6